Palynological insights into the Mid Jurassic dinoflagellate radiation

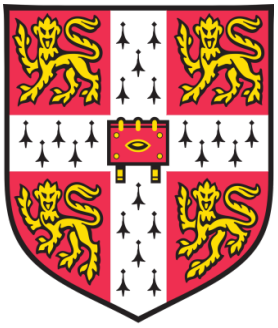

Nickolas James Wiggan

Girton College

University of Cambridge

June 2017

This dissertation is submitted for the degree of

Doctor of Philosophy

Summary: Palynological insights into the Mid Jurassic dinoflagellate radiation

Nickolas James Wiggan

Dinoflagellates are a diverse group of flagellated eukaryotes, the majority of which are marine plankton, and are one of the most important groups of primary producers in the world's oceans. The dinoflagellate fossil record is based on their zygotic resting cysts; this record indicates that the Bajocian of the Mid Jurassic (~170–168 Ma) represents a critical interval in dinoflagellate evolutionary history, marked by a rapid increase in the diversity of cysts from the family Gonyaulacaceae. From the Bajocian onwards, the Gonyaulacaceae have remained one of the most diverse and abundant groups of dinoflagellate cysts in the fossil record. Even so, Bajocian dinoflagellate cysts themselves have received relatively little study, leaving the patterns of this radiation unresolved. In this thesis, I examine the Bajocian diversification of gonyaulacacean dinoflagellate cysts in northwest Europe via quantitative palynological analysis, and relate this into a broader stratigraphic and palaeoenvironmental context. The dinoflagellate cyst record of the three key study areas demonstrates an increase in gonyaulacacean dinoflagellate cyst diversity through the Bajocian, irrespective of differing palaeoenvironmental settings. However, palynological and sedimentological data record systematic changes in lithostratigraphic composition and/or depositional environment which reflect changes in sea level. The integration of these data with biostratigraphic records indicates that the pattern of the radiation in Europe was strongly influenced by sea level, with the increase in gonyaulacacean diversity mirroring a major second-order transgression. On a finer scale, the main pulses of first appearances correlate with third-order transgressive episodes. A rise in sea level, coupled with changes in the tectonic configuration of ocean gateways, appears to have controlled the pattern of diversification in Europe. These palaeoceanographic changes may have enhanced water-mass transfer between Europe, the northwest Tethys Ocean, and the Hispanic Corridor, which promoted the floral interchange of dinoflagellates. Comparison to global data demonstrates that gonyaulacacean dinoflagellate cysts increased in diversity on a global scale through the Mid Jurassic. Whilst sea level rise and associated large-scale palaeoenvironmental shifts appear to have controlled the pattern of dinoflagellate cyst appearances in several regions (e.g. eastern Canada, Israel), there is no direct correlation between dinoflagellate cyst diversity and sea level rise on a global scale.

Within dinoflagellate cyst assemblages from Europe, the spatial and temporal distribution of key taxa can be related to differing palaeoenvironmental settings of the basins studied; but certain patterns may reflect wider palaeoenvironmental drivers. Carbon isotope records generated for this thesis, and their correlation to other European sections, demonstrate that the Early Bajocian in Europe was marked by a positive shift in $\delta^{13}C$. Previous work has linked this carbon cycle perturbation to a phase of enhanced continental weathering and associated run-off. In several European basins, the Early Bajocian was marked by an acme of the genus *Dissiliodinium*; this genus may have bloomed in response to elevated nutrient levels. Intriguingly, a similar pattern is seen within dinoflagellate cyst assemblages from Australia, indicating this interval of palaeoenvironmental change may have had a global extent.

Palaeoceanographic and palaeoclimatic changes appear to have controlled the stratigraphic pattern of the Bajocian radiation, as well as influencing palaeoecological patterns seen within dinoflagellate cyst floras, yet these factors do not appear to form the underlying driver of diversification. Although the Bajocian was transgressive in several regions, widespread flooded continental area was also present throughout the preceding Aalenian, an interval of conspicuously low gonyaulacacean diversity. Although the Mid Jurassic was an interval of major climatic cooling, there is a ~5myr gap between onset cooling and the Bajocian radiation. The Bajocian was, however, marked by a major evolutionary radiation in the pelagic realm, including coccolithophores, planktonic foraminifera, ammonites and giant suspension feeding fishes. These phenomena point to an underlying ecological driver to the Bajocian radiation, potentially an extension of the Mesozoic Marine Revolution. Within phytoplankton, the Bajocian expansion of the Gonyaulaceae marks a critical evolutionary and ecological transition in cyst-forming dinoflagellates.

Declaration of originality:

This dissertation is the result of my own work and includes nothing which is the outcome of work done in collaboration except as declared in the Preface and specified in the text. It is not substantially the same as any that I have submitted, or, is being concurrently submitted for a degree or diploma or other qualification at the University of Cambridge or any other University or similar institution except as declared in the Preface and specified in the text. I further state that no substantial part of my dissertation has already been submitted, or, is being concurrently submitted for any such degree, diploma or other qualification at the University of Cambridge or any other University or similar institution except as declared in the Preface and specified in the text

Published work arising from the dissertation:

The majority of chapters 3 and 6, and some of the interpretations in chapter 8, were presented in Wiggan et al. (2017), a peer-reviewed journal article. This is entitled "Resolving the Middle Jurassic dinoflagellate radiation: The palynology of the Bajocian of Swabia, southwest Germany". The paper was co-authored with James B. Riding and Matthias Franz, and was published in the journal Review of Palaeobotany and Palynology, volume 238, pages 55–87.

Statement of length:

This dissertation is within the prescribed length as defined by the degree committee for Earth Sciences and Geography.

"….go with the flow…."

Queens of the Stone Age

"….whiplash"

Metallica

Acknowledgements

I have been very fortunate to have received help and support from many people over the course of this project, who are too numerous to mention all by name, but I am deeply grateful to you all. My wholehearted thanks go to my two supervisors for their guidance and support. I sincerely thank Nick Butterfield, for always being willing to engage in discussion, and for driving me to challenge myself. I am greatly indebted to Jim Riding for his constant support and enthusiasm, and for guiding me through the early days of my PhD. This project was jointly funded between the British Geological Survey and the University of Cambridge, under the BUFI scheme, grant number S246. Additional financial support was kindly provided by the Cambridge Philosophical Society. Carbon isotope analysis was funded by a grant from NIGL.

I am extremely grateful to Mel Leng (BGS/NIGL) for all her assistance with carbon isotope analysis. I would also like to thank Jane Flint (BGS), for teaching me palynological processing procedures during the earliest days of this project. Special thanks also go to Matthias Franz (Geological Survey of Baden-Württemberg**)** for his incredible generosity, hospitality, and assistance, whilst undertaking fieldwork in Swabia.

I would also like to thank Mark Williams and Jan Zalasiewicz (University of Leicester) for igniting and encouraging my interest in micropalaeontology, during my time as an undergraduate. I am also forever grateful to the late Dick Aldridge, whose warm and caring nature, and inspirational teaching, have left a lasting mark on me as a person.

I extend a heartfelt thanks to various members of the department; I would particularly like to thank Charlotte Kenchington for being a valued friend, and something of my PhD mentor throughout my time in Cambridge. I am greatly indebted to Sarah Humbert, not least because she has allowed me to amass the largest collection of library books and journals of any member of the Earth Sciences Department.

I am incredibly grateful to my parents Cathy and Phil, and my sister Lucy, for always supporting me. Finally, my deepest gratitude to Áine, for all her love and support, and for being there for me when times were at their hardest, táim i ngrá leat.

Contents

List of Figures

List of Tables

Plates

Data Table Appendices

Chapter 1. General Introduction

Dinoflagellates are a diverse group of flagellated protists, the majority of which are marine plankton. Together with the diatoms and coccolithophores, they form the majority of eukaryotic phytoplankton of the world's oceans, and are important primary producers (Delwiche, 2007). Around 15% of modern dinoflagellate species produce a benthic resting cyst, and it is these cysts that form the basis of the dinoflagellate fossil record (Evitt, 1985; Head, 1996). Although molecular and biogeochemical evidence point toward a Proterozoic origin for the dinoflagellates, they are essentially a product of the post-Palaeozoic world, and underwent an adaptive radiation through the early Mesozoic (Fensome et al., 1996; Falkowski et al., 2004; van de Schootbrugge et al., 2005). The Bajocian of the Mid Jurassic (~170–168 Ma) represents a critical interval of this early Mesozoic radiation, as it was marked by a rapid increase in the species richness of dinoflagellate cysts from the family Gonyaulacaceae (Figure 1.1; Riding and Thomas, 1992; Fensome et al., 1996; Feist-Burkhardt and Monteil, 1997). From the Bajocian onwards, the Gonyaulacaceae became one of the most diverse and abundant groups of dinoflagellate cysts in the fossil record, and have remained so to the Recent. However, Bajocian dinoflagellate cysts have received relatively little study, and the pattern of this radiation has not been resolved. In this thesis, I examine the Bajocian diversification of gonyaulacacean dinoflagellate cysts in northwest Europe, via quantitative palynological analyses, and relate this into a broader stratigraphic and palaeoenvironmental context, in order to resolve the pattern of this radiation.

This chapter provides the context for the Bajocian dinoflagellate cyst diversification, including a brief overview of the dinoflagellates, and their cysts (section 1.1). I outline the nature of the dinoflagellate cyst fossil record, and review the evolutionary history of dinoflagellates, from the appearance of the first dinoflagellate cysts, to the rapid increase in species richness in the Bajocian (section 1.2.). To set the dinoflagellate cyst record within a wider framework, the geological context of the Mid Jurassic is broadly outlined (section 1.3.). Finally, I outline the aims of scope of this thesis (section 1.4).

1.1. Dinoflagellates and dinoflagellate cysts

Dinoflagellates are a diverse group of eukaryotes, represented by around 2,400 extant species, of which ~2000 are marine plankton (Fensome et al., 1996; de Vernal and Marret, 2007; Janouškovec et al., 2017). Along with the ciliates and the apicomplexans, dinoflagellates form the wider clade of the alveolates (Medlin and Fensome, 2013). Dinoflagellates are characterised by the possession of a unique nucleus, the dinokaryon, and having a stage in the life with two dissimilar flagella, one transverse and the other longitudinal, which allow the motile cell to swim (Fensome et al., 1996). Dinoflagellates can be broadly split into two morphological groups, naked and armoured/thecate. Armoured or thecate dinoflagellate have a series of cellulosic plates held within the cell wall (the amphiesma). The tabulation pattern of these plates, and its reflection on the wall of the resting cyst, provides the primary means of both thecate

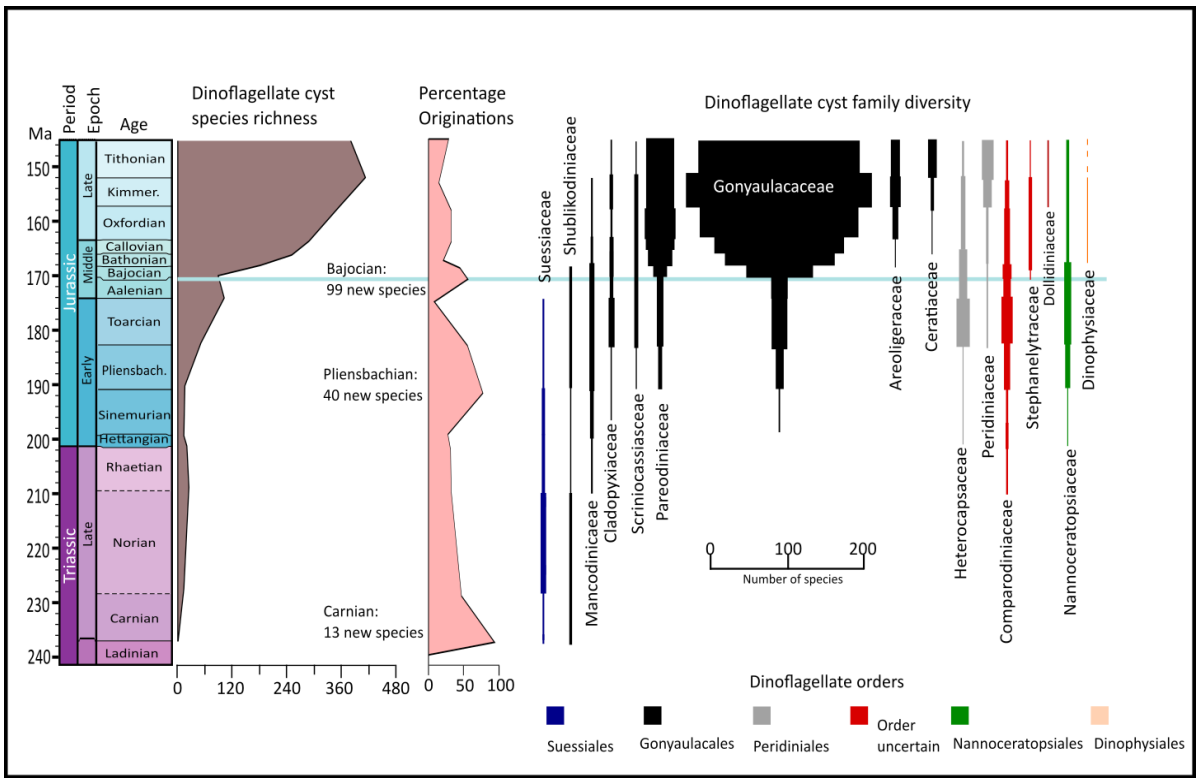

Figure 1.1. Dinoflagellate cyst richness, and family-level richness through the Mid Triassic to Jurassic. Note the diversification of the Gonyaulaceae in the Bajocian. After Wiggan et al. (2017, fig. 1), and based on data from Fensome et al. (1996) and MacRae et al. (1996).

dinoflagellate and thecate dinoflagellate cyst taxonomy (Dale, 1983; Evitt, 1985; Fensome et al., 1993; Fensome et al., 1996).

1.1.1. Dinoflagellate ecology

To correctly understand the fossil record of any group it is essential to understand the ecology, and associated taphonomy, of the subject organisms. Differing ecological strategies and preservation-potential of ancient dinoflagellates cysts may impinge on their temporal and spatial distribution in the rock record. However, high-resolution sampling, and the examination of multiple regions with differing depositional environments, can largely reduce the effects of these biases over a regional scale.

In the Recent, dinoflagellates exhibit a diverse array of ecological strategies, and inhabit marine and freshwater environments from the tropics to the poles (de Vernal and Marret, 2007). Within the marine realm, dinoflagellates are diverse and abundant in neritic environments, whilst oceanic forms are also common (de Vernal and Marret, 2007). Around half of all dinoflagellates are autotrophic or mixotrophic phytoplankton, which, together with the diatoms and coccolithophores, are responsible for a significant proportion of primary production in the world's oceans (Delwiche, 2007), whilst heterotrophic dinoflagellates are an important component of the microzooplankton (Calbet, 2008). Other ecological strategies include parasitism and symbiosis, with dinoflagellates forming mutualistic symbiotic associations with foraminifera, radiolaria, and perhaps most famously, corals (Gast and Caron, 1996; Stat et al., 2008). Many bloom-forming dinoflagellates produce toxins, which can lead to mass fish and

shellfish mortalities, making them of major economic importance (e.g. Anderson et al., 1990, 2008).

Around 13–16% of modern dinoflagellate species produce a zygotic resting cyst. For the majority of cyst-forming dinoflagellates, this cyst is composed of the complex macrobiomolecule dinosporin (Head, 1996; Bogus et al., 2014). Certain forms also produce calcareous or siliceous cysts (Sarjeant et al., 1987; Harding and Lewis, 1994). The formation of dormant resting cysts allows dinoflagellates to survive harsh conditions, and cysts can remain viable for several decades after formation (de Varnal and Marret, 2007 and references therein). In order for the motile stage to return to the photic zone, cyst formation is most viable down to depths of around 200 m, and as such, the majority of encysting dinoflagellates are neritic, although encysting oceanic forms have been recognised (Wall et al., 1977; Fensome et al., 1996; Sluijs et al., 2005). Many Recent dinoflagellates form cysts as part of a seasonal lifecycle; species which peak in abundance during the early spring bloom form cysts in the late spring/early summer, whilst species which bloom during the summer form cysts during the late summer/early autumn (Dale, 1983). Experimental and observational studies have demonstrated that declining levels of nutrients (phosphorous and nitrogen) is a key factor influencing the onset of sexual reproduction and cyst formation (Anderson et al., 1984; Coats and Tyler, 1985; Ichimi et al., 2001).

In Recent sediments, the biogeographical distribution of dinoflagellate cysts broadly reflects that of the motile stage, despite biases arising from lateral transport and preservation (Wall et al., 1977; de Vernal and Marret, 2007; Zonneveld et al., 2013). As dinoflagellates are sensitive to changes in sea surface conditions, such as temperature, salinity, and nutrient levels, dinoflagellate cyst assemblages exhibit clear inshore–offshore trends in diversity and assemblage composition, as well latitudinal diversity trends (Wall et al., 1977; de Vernal and Marret, 2007; Zonneveld et al., 2013). Moreover, several Recent dinoflagellate cyst species exhibit significant ecophenotypic variation, particularly in process morphology, in response to changes in salinity and/or temperature (e.g. Ellegaard, 2000; Ellegaard et al., 2002; Mertens et al., 2009a).

1.1.2. Dinoflagellate and dinoflagellate cyst taxonomy and classification

Analysis of evolutionary trends through time requires a robust fossil record, supported by a robust taxonomy and classification system. Within thecate (armoured) dinoflagellates, taxonomic classification is primarily based on the tabulation pattern produced by the arrangement of cellulosic plates (Evitt, 1985; Fensome et al., 1993; Fensome et al., 1996). In many dinoflagellate cyst taxa, tabulation is fully reflected, whilst in others it is only indicated by the outline of the archaeopyle (excystment aperture). Plates are arranged in latitudinal series; the number of series serves as the primary high-level taxonomic character within thecate dinoflagellates (Fensome et al., 1993). At lower ranks, differences in the number of plates within each series, and their arrangement and morphology, provides the key means of classification (Evitt, 1985; Fensome et al., 1993). In fossil cyst taxa, archaeopyle type is a key generic-level character (Fensome et al., 1993). The archaeopyle in most dinoflagellates is an opening created by the loss of

one or more plates, which can remain attached or be fully disarticulated from the cyst. However, doubt has been cast on the utility of the archaeopyle as a taxonomically-informative character, as several cyst taxa, both fossil and Recent, demonstrate intraspecific variability in archaeopyle formation (Evitt, 1985; Harding, 1986; Ellegaard et al., 2002).

Several studies have integrated morphological and molecular data to examine the phylogenetic relationships within dinoflagellates (e.g. Fensome et al., 1999; Medlin and Fensome, 2013; Janouškovec et al., 2017). Whilst naked/unarmoured dinoflagellates have been found to be a paraphyletic, recent molecular data indicates the monophyly of thecate dinoflagellates (Janouškovec et al., 2017). Moreover, the main tabulation-based thecate orders, such as the Gonyaulacales and Peridiniales, are supported by molecular data as distinct clades (Janouškovec et al., 2017).

1.2. The dinoflagellate cyst fossil record

The fossil record of any group of organisms provides a compromised view of evolution, not least because fossil species are morphologically-defined form taxa, rather than biologically-distinct reproductive populations. In the case of the dinoflagellates, this is further complicated by the fact that the motile stage is virtually never preserved, as the theca is extremely labile (Evitt, 1985). Consequently, the fossil record of dinoflagellates is based on their (refractory) resting cysts. With only 13–16% of species producing preservable cysts, the dinoflagellate cyst fossil record is inherently incomplete, as it is not known whether this has changed through geological time (Head, 1996; Fensome et al., 1996).

Dinoflagellate cysts in Quaternary sediments are primarily represented by three taxonomic groups, the Gonyaulacales, the Perdiniales, and the Gymnodiniales; the two former orders are also the most diverse and abundant groups of dinoflagellate cysts in the fossil record (Fensome et al., 1999; de Vernal and Marret, 2007). As such, the dinoflagellate cyst record is highly selective; groups such as the Gonyaulacales have a rich and extensive fossil record, whereas other extant groups such as the Dinophysiales have no appreciable fossil record (Fensome et al., 1996). The cyst is itself a phenotypic expression of only one stage of the dinoflagellate life cycle, which may reflect the morphology of the theca to varying degrees (Dale, 1983; Evitt, 1985). Even with forms that closely resemble the morphology of the theca, small morphological variations in cyst morphology which may be considered species-level characters in fossil taxa, can in Recent taxa be recognised as intraspecific variation, particularly that arising from ecophenotypism (Dale, 1983; Ellegaard et al., 2002).

Like all fossils, dinoflagellate cysts are subject to an array of taphonomic processes, which act upon the cyst from its formation in the water column, to its final burial and preservation in sediments (Zonneveld et al., 1997; Zonneveld and Brummer, 2000; Zonneveld et al., 2008). Once formed, dinoflagellate cysts behave like silt particles, and are therefore subject to lateral transport through the water column and transport by bottom-water currents (Dale, 1976; Zonneveld and Brummer, 2000). Upon final deposition, degradation from exposure to bottom-water oxygen has been widely demonstrated to affect

dinoflagellate cyst preservation in Recent sediments (Zonneveld et al., 1997, 2008; Kodrans-Nsiah et al., 2008). However, despite these biases, the biogeographical distribution of dinoflagellate cysts in Quaternary sediments appears to be broadly indicative of the motile stage (Marret and Zonneveld, 2003; Zonneveld et al., 2013).

The inherently incomplete nature of the dinoflagellate cyst fossil record has cast doubt on its utility for tracking dinoflagellate evolution through deep time (e.g. Evitt, 1985). However, molecular and biogeochemical evidence indicate that the diversification of dinoflagellate cysts through the early Mesozoic was a true evolutionary radiation (Fensome et al., 1996; Fensome et al., 1999; Janouškovec et al., 2017). The radiation of dinoflagellates through the early Mesozoic was characterised by the appearance of the main thecate dinoflagellate clades, such as the Gonyaulacales and Peridiniales, signified in the fossil record by the appearance of the gonyaulacoid-peridinoid tabulation type (Fensome et al., 1996; Janouškovec et al., 2017). Moreover, certain groups which appeared in the early Mesozoic appear to be transitionary forms between extant groups, such as the exclusively Jurassic genus *Nannoceratopsis.* The tabulation of *Nannoceratopsis* is formed from a combination of gonyaulacoid-peridinoid in the epicyst, and dinophysoid in the hypocyst. As such, *Nannoceratopsis* represent a transitionary form between the extant Gonyaulacales/Peridiniales and the Dinophysiales (Fensome et al., 1996). The increase in dinoflagellate cyst diversity through the Mesozoic was accompanied by a synchronous increase in the abundance of dinosteranes in Mesozoic sedimentary rocks (Moldowan et al., 1996). Triaromatic dinosteranes are types of lipid biomarkers derived from dinosterols, and are primarily associated with dinoflagellates (Moldowan and Talyzina, 1998). However, recent molecular phylogenetic work has revealed that the acquisition of dinosterols within the dinoflagellate lineage occurred during the Mesozoic, shedding doubt on the reliability of dinosteranes as an unequivocal biomarker for dinoflagellates in rocks of pre-Mesozoic age (Janouškovec et al., 2017). Despite this, the concomitant increase in the abundance of dinosteranes and increase in dinoflagellate cyst diversity through the Jurassic strongly suggests that dinoflagellates rose to ecological prominence in the early Mesozoic. In summary, the appearance of high-level taxa dinoflagellate taxa, which are supported by molecular data as distinct clades, and progressive innovations at lower taxonomic ranks, along with transitionary forms such as *Nannoceratopsis* and an increase in dinosterane abundance, strongly suggest that dinoflagellates underwent a true evolutionary radiation through the early Mesozoic (Fensome et al., 1996).

1.2.2. The Mid Triassic to Mid Jurassic: emergence and radiation of dinoflagellates

Dinoflagellate cysts have an unequivocal fossil record from the Mid Triassic to Recent (Fensome et al., 1996). The onset of the early Mesozoic radiation of dinoflagellates is signalled in the fossil record by the appearance of *Sahulidinium otii*, the oldest unequivocal dinoflagellate cyst, in the Middle Triassic (Ladinian) of Australia (Riding et al., 2010a). Dinoflagellate speciec richness increased through the Mid–Late Triassic with the appearances of the families Suessiaceae and the Rhaetogonyaulacaceae

(Figure 1.1; Fensome et al., 1996). The latter represents the first appearance of the order Gonyaulacales. The latest Triassic was marked by the appearance of the family Comparodiniaceae, represented solely by the genus *Valvaeodinium* (Morbey, 1975; van de Schootbrugge et al., 2013). This group is of uncertain higher taxonomic affinity but was a prominent component of Early Jurassic dinoflagellate cyst floras (Below, 1987).

Dinoflagellate cyst species richness was severely affected by the end-Triassic mass extinction (van de Schootbrugge et al., 2007). Of the Suessiaceae, the only genus to survive extinction was *Beaumontella*, similarly, the only representative to the Rhaetogonyaulcacaceae was *Dapcodinium*, whilst *Valvaeodinium* also survived the end-Triassic (van de Schootbrugge et al., 2013). Consequently, dinoflagellate species richness through the Hettangian of the Early Jurassic was represented solely by these genera (van de Schootbrugge et al., 2013). The succeeding Sinemurian was marked by the appearance, and short-lived acme, of *Liasidium variable* (van de Schootbrugge et al., 2005). The appearance of *L. variable* is significant as it appears to be the first representative of the family Peridiniaceae, which in turn marks the appearance of the order Peridiniales (van de Schootbrugge et al., 2005; Feist-Burkhardt, 2009). Moreover, *L. variable* may have had a heterotrophic habit, indicated by possible pigmentation in the cyst wall, and its short-lived acme was linked to a brief phase of warming, and a negative carbon isotope excursion (Riding et al., 2013).

The ensuing Pliensbachian was an important interval of dinoflagellate evolution, marked by the appearances of numerous genera in the Late Pliensbachian, and a significant increase in dinoflagellate cyst species richness (Figure 1.1; van de Schootbrugge et al., 2005). This interval is intriguing as dinoflagellates appear to have diversified during a time of widespread regression, and cooling temperatures; previous workers have argued this allowed newly emerging genera to invade the Tethys from the Boreal Realm (van de Schootbrugge et al., 2005, 2013). These authors argued that cooler temperatures resulted in enhanced vertical mixing of the water column, with ventilated bottom waters, which created conditions ideal for benthic-cyst forming dinoflagellates (van de Schootbrugge et al., 2005). Within the order Gonyaulacales genera belonging to several families such as *Frebolidinium* (Cladopxyiaceae), *Luenhdea* and *Mancodinium* (Mancodiniaceae), and *Scriniocassis* (Scriniocassiaceae) appeared (Morgenroth, 1970; Prauss, 1989; Feist-Burkhardt and Wille, 1992). Within the Peridiniales, the Late Pliensbachian saw the appearances of genera such as *Parvocysta* and *Reutlingia*, representing the family Heterocapsaceae (Feist-Burkhardt and Wille, 1992). *Nannoceratopsis* also appeared at this time (van de Schootbrugge et al., 2005).

Dinoflagellate cyst diversity was temporarily affected by the Early Toarcian Oceanic Anoxic Event (T-OAE) (Correia et al., 2017). Diversity declined sharply through the T-OAE, and although some taxa such as *Luehndea spinosa* went extinct, many taxa which disappeared through the T-OAE reappeared in the Late Toarcian (Bucefalo Palliani et al., 2002). The Late Toarcian was marked by a significant

increase in dinoflagellate cyst diversity and the appearance of the first gonyaulacaceans (Riding, 1984; Prauss, 1989; van de Schootbrugge et al., 2005). The appearance of *Escharisphaeridia* sp. in the Upper Toarcian of northern England, and *Sentusidinuium ringesorium* (recorded as *Escharisphaeridia rudis*) and *S. explanatum* (as *Kallosphaeridium inornatum*) in the Upper Toarcian of northern Germany (Riding, 1984; Prauss, 1989), represent the first appearance of the Gonyaulacaceae in the fossil record.

The richness of gonyaulacaceans was low through the Aalenian, and represented by the *Sentusidinium* complex of *Batiacasphaera*, *Kallosphaeridium*, and *Sentusidinium*, along with *Dissiliodinium* (Feist-Burkhardt, 1990; Feist-Burkhardt and Pross, 2010). Following this Aalenian interval of low diversity, the diversity of gonyaulacacean dinoflagellate cysts rapidly increased through the Bajocian, particularly around the Early–Late Bajocian transition (section 1.2.3). The Bajocian was characterised by the appearances of numerous gonyaulacacean genera, many of which became important components of Mid–Late Jurassic dinoflagellate cyst floras, such as *Gonyaulacysta*, *Rhynchodiniopsis*, and *Tubotuberella* (e.g. Riding, 1987; Feist-Burkhardt and Wille, 1992; Feist-Burkhardt and Monteil, 1997). Therefore, the Bajocian appears to represent a critical interval in the evolutionary history of dinoflagellates, as gonyaulacacean dinoflagellate cysts went from representing a relatively minor component of dinoflagellate cyst floras, to becoming the overwhelmingly-dominant group, in the space of a few million years. From the Bajocian onwards, gonyaulacaceans became the overwhelmingly dominant group of dinoflagellate cysts throughout the remainder of the Jurassic, with a near-continuous increase in species richness to the Cretaceous (Figure 1.1; Fensome et al., 1996). The Peridiniaceans diversified in the Cretaceous, and these two groups have dominated the dinoflagellate cyst record to the Quaternary (Fensome et al., 1996). Consequently, the Bajocian record of gonyaulacacean dinoflagellate cysts is the principal focus of this thesis.

1.2.3. Previous work on Bajocian dinoflagellate cysts

Bajocian dinoflagellate cysts have been relatively understudied in comparison to other stages of the Jurassic, and the majority of work has focused on Europe (Riding, 2012, 2013, 2014). Many works have included the stage as part of broader works on European Jurassic dinoflagellate cysts, e.g. Fensome (1979), Riding (1987), Prauss (1989), Poulsen (1996), or broad stratigraphic compilations (e.g. Riding and Thomas, 1992; Feist-Burkhardt and Wille, 1992; Poulsen and Riding, 2003). In other regions, Bajocian dinoflagellate cysts have also predominantly been examined as part of broader biostratigraphic works to develop palynozonations, e.g. eastern Canada (Bujak and Williams, 1977), Arctic Canada (Davies, 1983), Argentina (Quattrocchio and Volkheimer, 1990), North Africa and Arabia (Conway, 1990; Ibrahim et al., 2002, 2003) and Russia (Riding et al., 1999). Of any region outside of Europe, Bajocian dinoflagellate cysts have been most intensively researched from the northwest shelf of Australia (e.g. Riding et al., 2010b; Mantle and Riding, 2012). The latter authors documented numerous appearances of gonyaulacacean taxa through the Bajocian–Lower Bathonian, indicating a comparable

pattern to that seen in Europe. Moreover, these authors noted that Australian dinoflagellate cyst floras are extremely similar to Europe in their taxonomic composition, and that dinoflagellate cyst floras were largely cosmopolitan through the Bajocian–Bathonian (Mantle and Riding, 2012). Mantle and Riding (2012) suggested that a Tethyan circumglobal current drove the passive dispersal of dinoflagellate cysts between the northern and southern hemispheres, resulting in largely cosmopolitan dinoflagellate cyst associations.

Within Europe, the majority of research which has focused directly on Bajocian dinoflagellate cysts have largely been based on classic localities of the European Jurassic, such as Dorset and Yorkshire (England), the Isle of Skye (Scotland) and Normandy (France) (e.g. Fenton and Fisher, 1978; Davey, 1980; Fenton et al., 1980; Woollam, 1982; Bailey, 1987,1990; Riding et al., 1991; Feist-Burkhardt and Monteil, 1997; Butler et al., 2005). In other areas of Europe, dinoflagellate cysts have been researched from Middle Jurassic successions that lack ammonites to date them. Many studies have examined dinoflagellate cysts from the Bajocian of the Pieniny Klippen Belt of the Carpathian Mountains in southern Poland and northern Slovakia, but the data from these works largely lack independent age control (Gedl, 2008, 2013; Barski et al., 2012; Gedl and Jozsa, 2015; Segit et al., 2015).

Previous workers have also noted that in addition to the dramatic increase in gonyaulacacean dinoflagellate cyst species richness through the Bajocian, that gonyaulacaceans underwent a phase of archaeopyle experimentation (e.g. Riding, 1987; Feist-Burkhardt and Wille, 1992; Mantle and Riding, 2012; Feist-Burkhardt and Götz, 2016). These authors noted that one-plate precingular and epicystal archaeopyles appear to have been developed in gonyaulacaceans during the Bajocian, and may have been derived from earlier forms with multiplate precingular archaeopyles such as *Dissiliodinium*, which appeared during the Aalenian.

In terms of the stratigraphic pattern, previous work in Europe has highlighted the Early–Late Bajocian transition (*S. humphriesianum* and *S. niortense* ammonite zones) as a critical interval of gonyaulacacean dinoflagellate cyst evolution (Feist-Burkhardt and Wille, 1992; Riding and Thomas, 1992; Feist-Burkhardt and Monteil, 1997; Feist-Burkhardt and Götz, 2016). The most significant work directly focused on Bajocian dinoflagellate cysts is that of Feist-Burkhardt and Monteil (1997) who documented the dinoflagellate cyst record of d'Orbigny's Bajocian type section near Bayeux in Normandy, northwest France. These authors documented a fairly low number of gonyaulacacean appearances through the Early Bajocian (*W. laeviuscula* and *S. propinquans* zones) such as *Dissiliodinium giganteum*, *Durotrigia daveyi Gonylodinium erymnoteichon* and *Kallosphaeridium*? *hypornatum*. However, there was a two-step burst of first appearances around the Early–Late Bajocian transition (*S. humphriesianum* and *S. niortense* zones), with the appearances of 16 gonyaulacacean taxa (Figure 1.2). These included the first appearances of gonyaulacacean genera such as *Acanthaulax*, *Aldorfia*, *Atopodinium*, *Ctenidodinium*, *Endoscrinium*, *Gonyaulacysta*, *Korystocysta*, and *Rhynchodiniopsis*. Feist-Burlhardt and Monteil (1997)

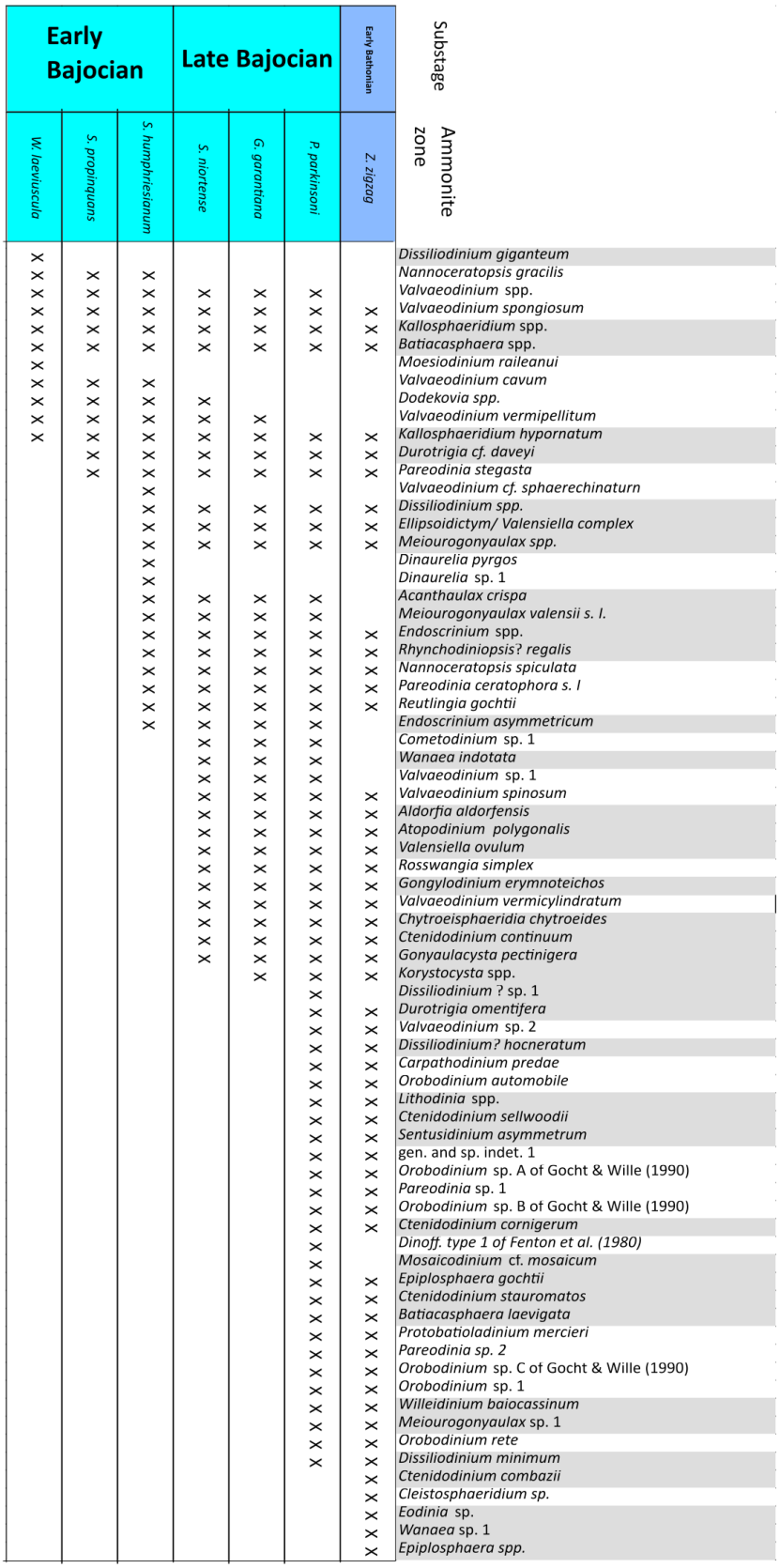

Figure 1.2. Stratigraphic ranges of dinoflagellate cysts from the historical Bajocian stratotype in Normandy, northwest France.
Based on raw data from Feist-Burkhardt and Monteil (1997).

reported a second burst of appearances in the uppermost Bajocian *P. parkinsoni* zone (Figure 1.2). However, the Bajocian succession around Bayeux is highly condensed, and the uppermost Aalenian and lowermost Bajocian is not exposed (Rioult et al., 1991). Further, the *S. humphriesianum*, *S. niortense, G. garantiana,* and lowermost *P. parkinsoni* zones are represented by ~50 cm of strata, and as such are subject to considerable time averaging, meaning that some of the occurrence data are obscured, and this emphasises the rapid, stepwise pattern of appearances through the succession. Moreover, this study reported only presence/absence data, thereby making it impossible to detect any dinoflagellate cyst abundance changes through the Bajocian radiation, and not providing any palaeoecological data.

Recently, Feist-Burkhardt and Götz (2016) provided a detailed account of dinoflagellate cyst assemblages from the uppermost Early Bajocian (*S. propinquans* and *S. humphriesianum* zones), and recorded ~12 first appearance datums of gonyaulacacean taxa from this interval. However, this study was limited in its stratigraphic coverage to these two ammonite zones. In summary, no published work has provided a quantitative dinoflagellate cyst record through an expanded Bajocian succession with ammonite zonal correlation, or related the dinoflagellate cyst record to a wider palaeoenvironmental and stratigraphic context.

1.3 Geological context for the Mid Jurassic

The Mid Jurassic was marked by major changes in tectonic configuration, climate, sea level and marine ecosystems. As dinoflagellates in the modern oceans are sensitive to environmental and climatic conditions, an understanding of the wider geological context through the Mid Jurassic is essential to set the dinoflagellate cyst record within a wider framework, and resolve how wider palaeoenvirommental and biotic changes have affected the pattern of diversification. In this section, I provide the wider context for the Mid Jurassic, with particular emphasis on Europe, as this thesis has focused on the dinoflagellate cysts from Bajocian of northwest Europe.

1.3.1 Palaeogeography

The Jurassic Period was characterised by the break-up of Pangaea, and a long-term rise in sea level, which resulted in widespread flooded continental area, and the spread of epicratonic seas. During the Mid Jurassic, Europe formed part of an extensive epicratonic sea, which has been termed the European Epicontinental Seaway (e.g. van de Schootbrugge et al., 2013) and the Laurasian Seaway (e.g. Korte et al., 2015), the former is used here. The European Epicontinetal Seaway (EES) was located on the northwest edge of the Tethys Ocean, at around 30–50°N (Figure 1.3; Callomon, 2003). The EES was bounded to the southeast by the Tethys Ocean, and by ocean gateways to the north and west (Figure 1.3). In the north, the Viking Corridor connected the EES to the Boreal Sea. During the Aalenian, thermal doming in the North Sea area largely blocked the marine connection through the Viking Corridor (Korte et al., 2015). To the west of the EES, the Hispanic Corridor provided a marine connection between Gondwana and Laurasia to the Panthalassic Ocean (Figure 1.3). The Hispanic Corridor opened during

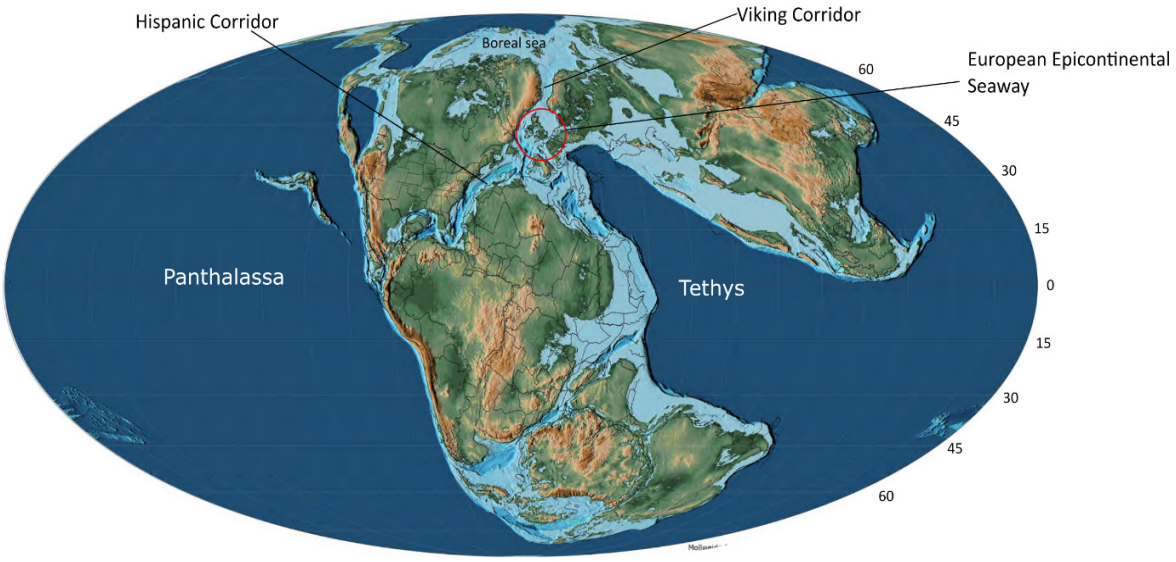

Figure 1.3. Global palaeogeographic map for the Bajocian–Bathonian.
Note that the European Epicontinental Seaway was located at the interchange of the Tethyan Ocean, the Hispanic Corridor, and the Boreal Sea via the Viking Corridor. Modified from Scotese (2014).

the Early Jurassic, but a change in plate relative motion drove a widening and deepening during the Bajocian (Aberhan, 2001; Labails et al., 2010; Dera et al., 2014).

During the Jurassic, the EES was split into two broad palaeobiogeographic regions: the Boreal and Tethyan realms (Callomon, 2003). Between these realms lay the transitional zone of the sub-Boreal province, which extended from southern France/southern Germany (~30°N) to northern Scotland (~40°N) (Figure 1.4; Callomon, 2003). The Boreal realm lay to the north of this province (e.g. East Greenland), while the Tethyan realm lay to the south and was comprised of Iberia, parts of southern France, Italy, and much of the Balkans (Figure 1,4; Callomon, 2003). Within the sub-Boreal province of Northwest Europe, three broad trends in facies distribution and palaeoenvironment can be discerned. In the south east, fine-grained siliciclastic deposition in open-marine palaeoenvironments prevailed around the Swabian Basin of southern Germany (Figure 1.4; Chapter 3). To the west of this area, covering much of Iberia, France, and southern England, was a region of shallow marine carbonate deposition, which included the Wessex and Paris basins (Figure 1.4; chapters 3 and 4). In contrast, the Cleveland Basin of northern England, the Hebrides Basin of northwest Scotland, the North Sea region were largely paralic environments (Figure 1.4; Callomon, 2003).

1.3.2 Sea level

The Jurassic period was characterised by a long-term rise in sea level (Figure 1.5; Haq et al., 1987; Hallam, 2001). In turn, this long-term rise was accompanied by five second-order (stage level) oscillations, one of which occurred through the Bajocian. In Europe, this took the form of the T7 second-order transgression, which lasted from the Late Aalenian to Early Bathonian (Jacquin et al., 1998). In

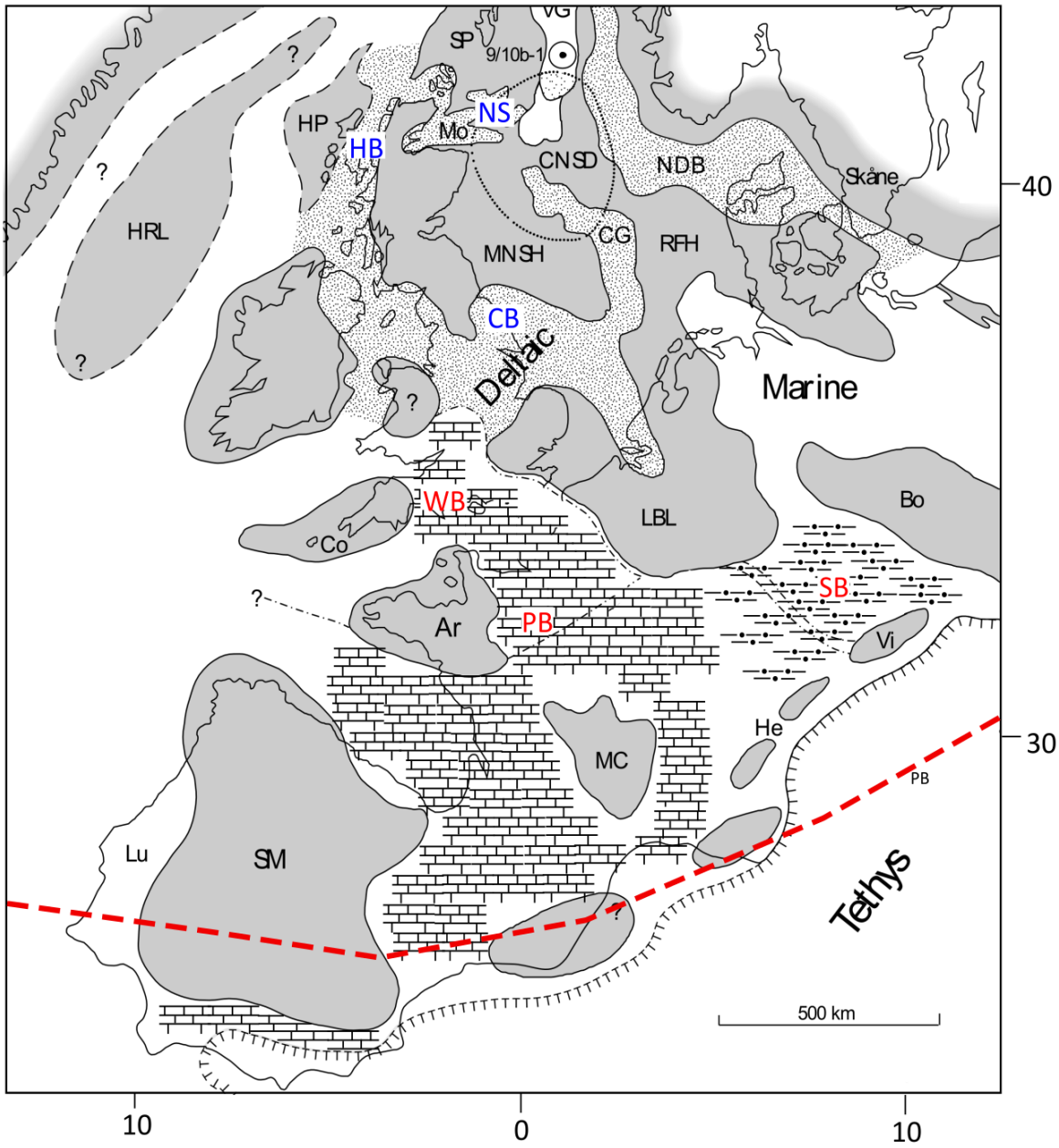

Figure 1.4. Palaeogeographic map of the European Epicontinental Seaway.
Modified from Callomon (2003) fig. 1. SB= Swabian Basin (Chapter 3), WB= Wessex Basin (Chapter 4), PB= Paris Basin (Chapter 5), HB= Hebrides Basin (text appendix A). Palaeolatitude and longitude is shown. It can be observed that there were three broad regions of facies: the paralic siliciclastic region (the North Sea, Hebrides Basin), the marine carbonate area (Wessex and Paris basins), and the marine siliciclastic area (the Swabian Basin). Dashed red line denotes the boundary between the Sub-Boreal province and the Tethyan Realm.

turn, this second-order transgression was comprised of a series of third-order cycles, which are shown in Figure 1.6. In the Boreal realm, this transgression was two pulsed, with the first pulse lasting from the Late Aalenian to Early Bajocian, and the second from the latest Early Bajocian to Early Bathonian (Figure 1.6). In the Tethyan realm, this transgression was comprised of one pulse, which lasted from the Late Aalenian to Early Bathonian (Figure 1.6). Maximum transgression of the T7 cycle as a whole corresponds to the maximum flooding surface above Bj5 of the Lower Bathonian (*Z. zigzag* zone) (Jacquin et al., 1998). Hallam (2001) argued that this transgression was eustatic, as there is evidence of

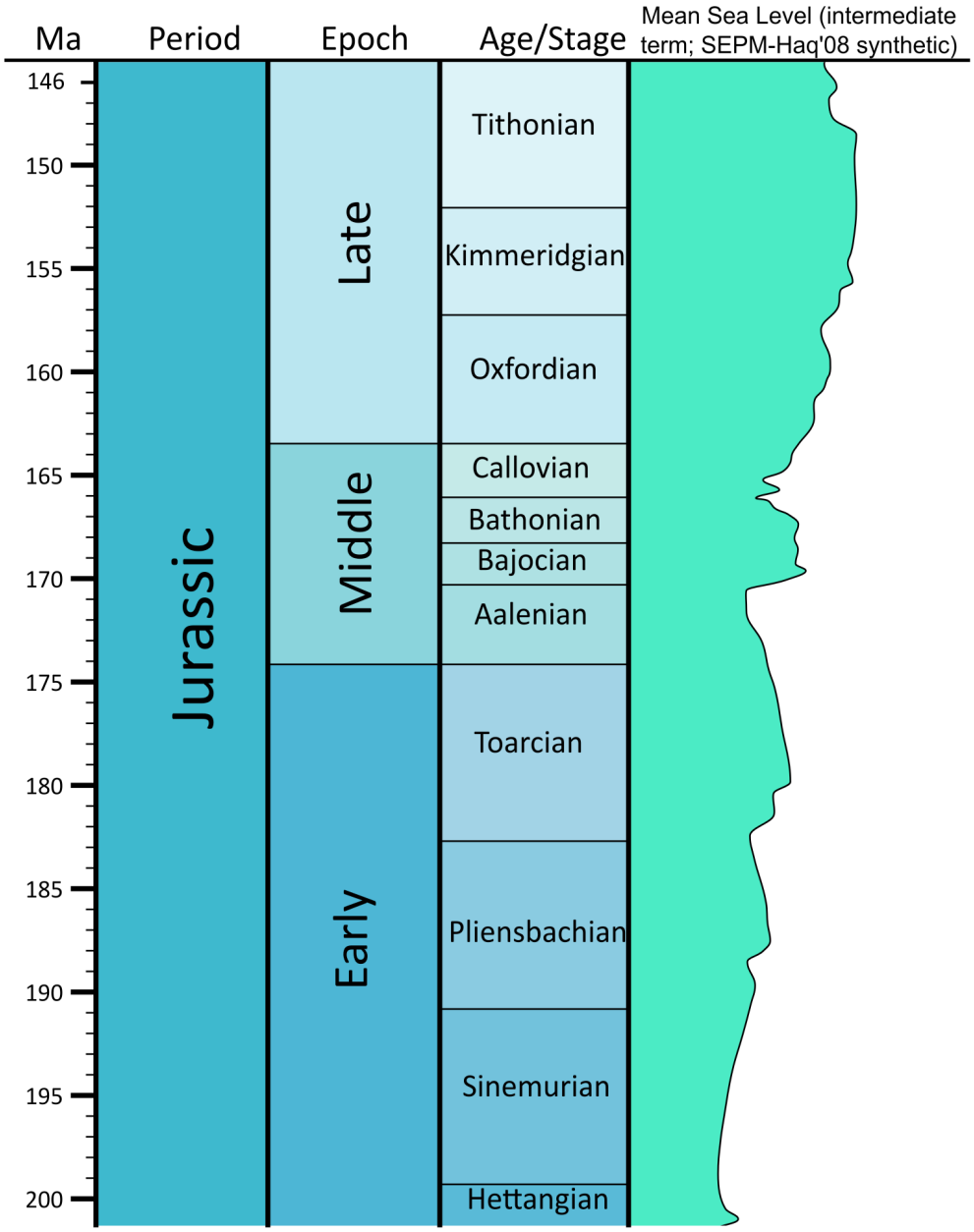

Figure 1.5. Jurassic (mean) sea level, metres relative to present.
It can be observed that there is an overall rise through the Jurassic, a pronounced transgression in the Bajocian. Generated using Timescale Creator version 6.4. Mean sea level based on Hardenbol et al. (1998).

sea level rise in Europe, South America, and the Himalayas.

Two sequence stratigraphic schemes have been used throughout this thesis. Rioult et al. (1991) devised much of the sequence stratigraphic framework for the Bajocian, based on the Jurassic of the Normandy coast. These workers used numerical ages for third-order sequence boundaries, e.g. "SB 169". Jacquin et al. (1998) used Rioult et al. (1991)'s interpretations, and synthesised data from other European basins to devise a wider sequence stratigraphic scheme for the Jurassic. The third-order boundaries recognised by these authors are numbered sequentially through each stage, e.g. "Bj1, Bj2" etc. As this scheme has been used by the Geologic Timescale (Gradstein et al., 2012), the boundary names of Jacquin et al.

(1998) are used in this thesis. Table 1.1. displays the sequence boundaries of Rioult et al. (1991) and their equivalents under the Jacquin et al. (1998) scheme.

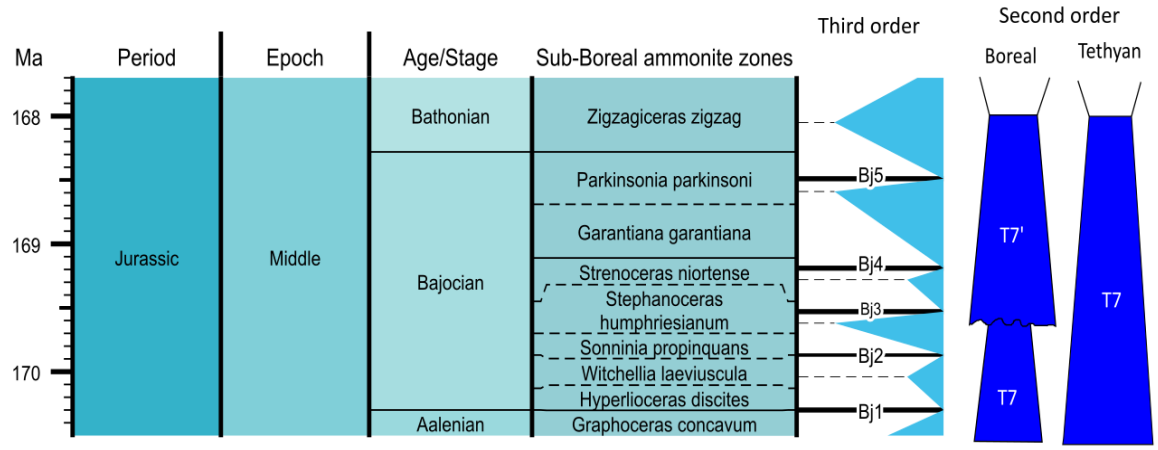

Figure 1.6. Bajocian sea level: the T7 second-order transgression, which in Europe lasted from the Late Aalenian to Early Bathonian.
In the Boreal realm, this was two-pulsed, whilst in the Tethyan realm the transgression was comprised of one main pulse (Jacquin et al., 1998). The T7 cycle was comprised of 5 to 6 third-order sequences (Jacquin et al., 1998). The Early Bajocian was marked by a particularly pronounced transgressive pulse (BJ2), and the maximum transgression of the T7 cycle was around the Bajocian–Bathonian transition, as the MFS (dashed line) above BJ5 (Jacquin et al., 1998, Hallam, 2001). Generated using Timescale Creator version 6.4, third-order sequences and second order cycles after Jacquin et al. (1998).

GTS Sequence boundaries (after Jacquin et al. 1998)	Rioult et al. 1991 sequence bounda
Bj5	SB 165.5
Bj4	-
Bj3	SB 168
Bj2	SB 169
Bj1	-

Table 1.1. Bajocian third-order sequence boundaries from Jacquin et al. (1998) and their equivalents in Rioult et al. (1991)'s scheme.

1.3.3 Palaeoclimate

The supposition that the Jurassic was a consistently warm interval of Earth history has over the last 25 years been increasingly challenged. There is a mounting body of geochemical, sedimentological and palaeontological evidence to suggest that there were cool intervals of climate during the Jurassic, which were potentially cold enough to allow polar icesheets to develop (e.g. Price, 1999; Dera et al., 2011; Korte and Hesselbo, 2011; Dera et al., 2014; Korte et al., 2015). The Mid Jurassic in particular is increasingly being recognised as a "cool mode" of the Jurassic (Korte et al., 2015). Price (1999) noted that there is a peak in the abundance of sedimentary deposits with a possible glacial affinity in the Aalenian–Bathonian, as well as a peak in the abundance of glendonite nodules at high palaeolatitudes.

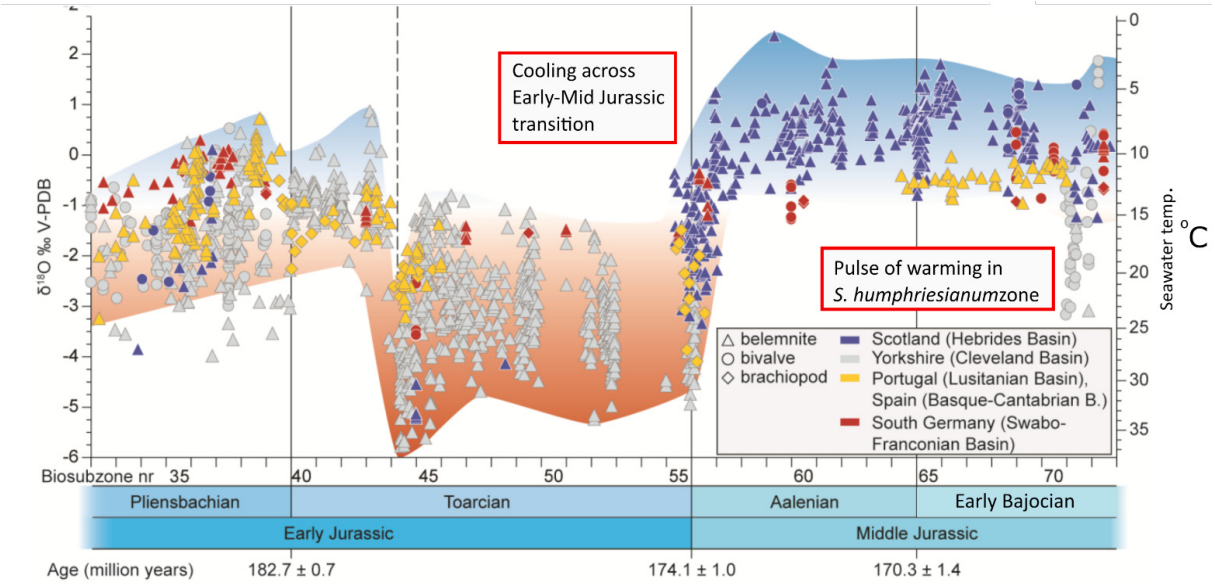

Figure 1.7. Seawater palaeotemperatures for the Early Jurassic to Early Bajocian.
Note the cooling through the Early–Mid Jurassic transition, and the brief interval of warming in the Bajocian, which corresponds to the *S. humphriesianum* zone. Modified from Korte et al. (2015, fig. 2).

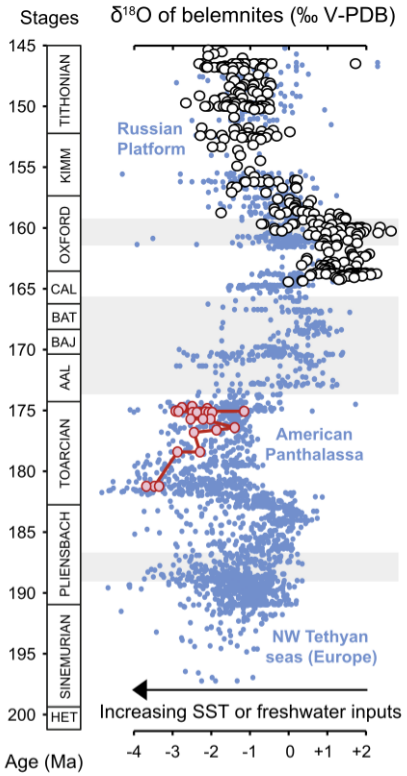

Figure 1.8. Palaeotemperatures for the Jurassic.
Note that cool temperatures persisted through the Aalenian to Bathonian. red datapoints denote samples from the Panthallasic Ocean, while black datapoints are samples from the Russian platform, blue datapoints are from Europe. Modified from Dera et al. (2014, fig. 8).

Glendonite is a low temperature polymorph of calcium carbonate, and the occurrence of nodules in high palaeolatitude localities has been suggested to reflect benthic seawater temperature close to freezing (Price, 1999). Recent geochemical evidence suggests that the glendonites in Mesozoic polar seas were formed by methane seepage at the seafloor, but the preservation of these nodules indicates benthic

seawater temperatures were below ~7°C (Morales et al., 2017).

In Europe, recently published oxygen isotope data from bivalves, brachiopods and belemnites, indicate that there was a cooling of seawater temperature recorded across the Early–Mid Jurassic transition of ~10°C (Figure 1.7; Korte et al., 2015). Cool temperatures persisted to the Bathonian, with possible short-term warm intervals the latest Early Bajocian (Figure 1.7, 1.8; see Dera et al., 2011; Korte et al., 2015). The initiation of cooling through the Early–Mid Jurassic transition is thought to have been driven by thermal doming in the North Sea, which blocked water-mass exchange through the Viking Corridor, and resulted in the thermal isolation of the Boreal Sea (Korte et al., 2015).

1.3.4. Biotic changes

The Jurassic period was characterised by the important biotic changes in marine ecosystems, with the diversification of multiple trophic levels of pelagic and benthic organisms. Escalating coevolution between predators and their prey drove persistent change in marine ecosystems, encapsulated in the concept of the Mesozoic Marine Revolution (Vermeij, 1977). The Early–Mid Jurassic was characterised by the paralleled diversifications of benthic and pelagic metazoans, including bivalves, bryozoans, cephalopods, and fishes (Figure 1.9; Hallam, 1976; Sandoval et al., 2001; Taylor and Ernst, 2008; Guinot

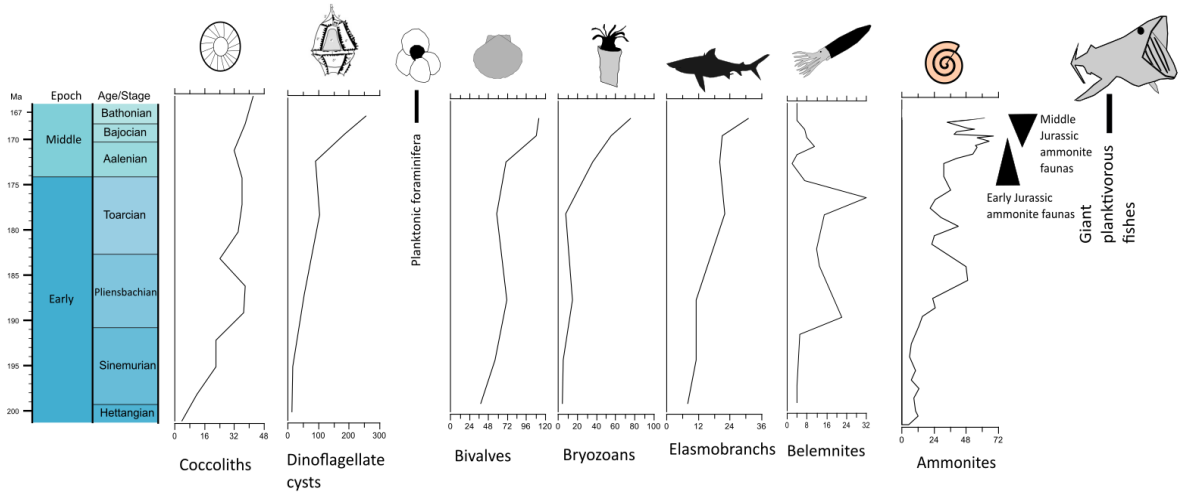

Figure 1.9. Species richnes curves and appearance of key groups of marine organisms for the Early to Mid Jurassic.
It can be observed that the richness of the coccolithophores and dinoflagellates broadly parallels that of higher trophic levels. All groups plotted per stage/substage, except where noted. Coccolith data redrawn from Bown (2005). Dinoflagellate data from MacRae et al. (1996). Planktonic foram range from Simmons et al. (1997). Bivalve data after Hallam (1976). Bryozoans from Taylor and Ernst (2008). Elasmobranch richness after Guinot and Cavin, (2015). Belemnites after Dera et al. (2016), ammonites after Sandoval et al. (2001) and O'Dogherty et al., (2006), plotted per ammonite zone. Giant suspension feeders after Friedman et al. (2010).

and Cavin, 2015). In the Bajocian, an important faunal turnover within ammonites occurred, which included the appearance of the first heteromorphs (Figure 1.9; Sandoval et al., 2001; O'Dogherty et al., 2006). Moreover, the trophic guild of giant suspension feeding fishes appeared in the Mid Jurassic, and the earliest fossil evidence for this group comes from the Bajocian (Friedman et al., 2010).

Within marine plankton, as well as the increase in dinoflagellate cyst species richness, there were important changes in other groups. Through the Aalenian–Bajocian transition the coccolith genus *Watznaueria* diversified and expanded ecologically to become the dominant coccolith genus, and remained so for the remainder of the Mesozoic (Giraud et al., 2016). As such, the Early Bajocian represents one of the most important intervals in the evolution of Mesozoic coccolithophores (Suchéras-Marx et al., 2015; Aguado et al., 2017). In the Late Bajocian, the first planktonic foraminifera appeared, represented by the meroplanktonic Conoglobogerinids (Simmons et al., 1997). Therefore, there were important ecological and evolutionary innovations during the Bajocian in plankton as a whole.

1.3.5 The stratigraphy of the Bajocian

The Bajocian Stage was originally described by d'Orbigny (1842) from a succession of limestones on the Normandy coastline, near Bayeux (Chapter 5). The Aalenian-Bajocian GSSP is located at in the Lusitanian Basin of Portugal, at Cabo Mondego (Suchéras-Marx et al., 2013). The Bajocian is subdivided

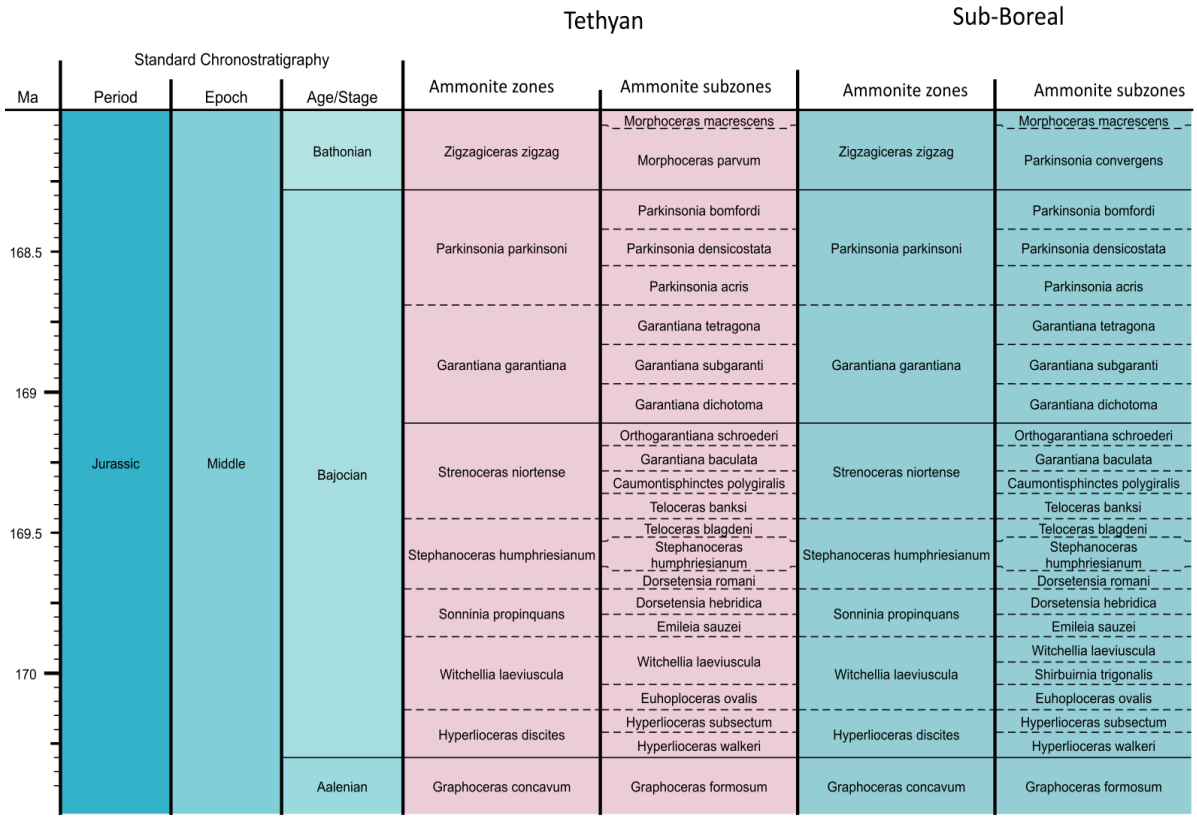

Figure 1.10. Bajocian Sub-Boreal and Tethyan ammonite zones and subzones. Generated using Timescale Creator v. 6.4.

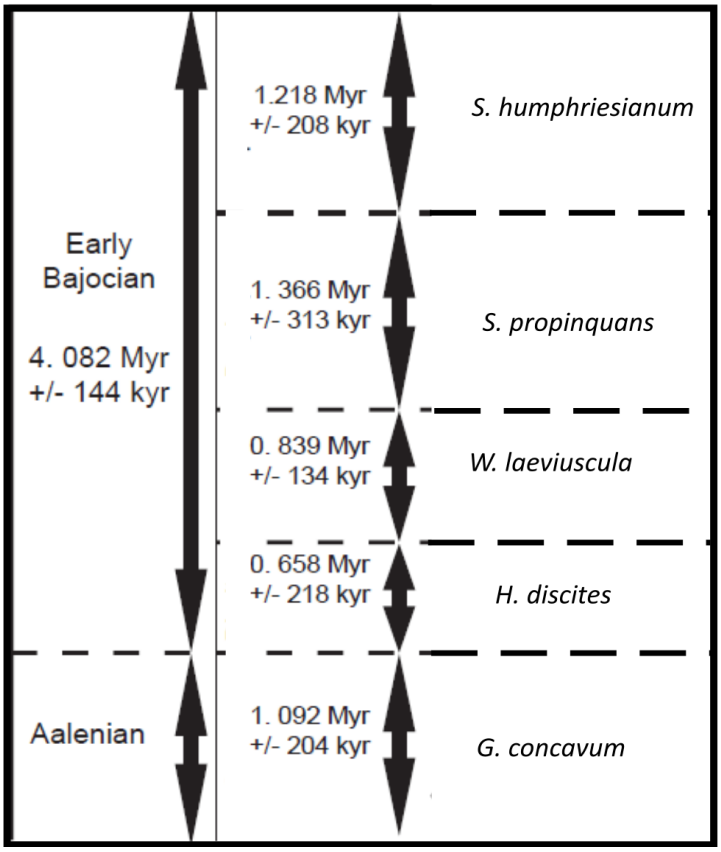

Figure 1.11. Duration of the Early Bajocian based on cyclostratigraphy. Modified from Suchéras-Marx et al. (2013) fig. 6.

into the Lower/Early and Upper/Late substages, and in both the Sub-Boreal province and the Tethyan realm the Bajocian is represented by seven ammonite zones (Figure 1.10). According to Gradstein et al. (2012) the Bajocian lasted from 170.3 Ma +/- 1.4 to 168.3 Ma +/- 1.3. However, Suchéras-Marx et al. (2013) conducted a cyclostratigraphic analysis of the Lower Bajocian in southern France, which suggests the Stage may be considerably longer, as the duration of the Early Bajocian was found to be ~4 myr (Figure 1.11).

1.4 Aims and scope of this thesis

In this thesis, I document the Bajocian record of dinoflagellate cysts from the Middle Jurassic of northwest Europe. Europe occupied a critical palaeogeographic position during the Mid Jurassic, as it lay at the interchange between the Tethyan Ocean, the Panthalassic Ocean via the Hispanic Corridor, and the Boreal Sea via the Viking Corridor (section 1.3.1). The primary aim is to unravel the stratigraphic pattern of this radiation, and relate the dinoflagellate cyst record into a wider palaeoenvironmental context, as the Mid Jurassic was a time of major oceanographic, climatic, and biotic change. This has been accomplished by the quantitative and semi-quantitative palynological analysis of dinoflagellate cysts and associated palynomorphs, and the relation of these data into a wider sedimentological and stratigraphic framework. These analyses are based on three European localities; the lithostratigraphy of each locality is correlated to the standard Sub-Boreal ammonite zonation to allow intra-regional correlation (Figure 1.10; Chapters 3–5). Although palaeobiogeographic provincialism was prevalent in ammonites during the Jurassic, leading to issues with diachroneity, this was markedly reduced during

the Aalenian–Bathonian (Callomon, 2003). Moreover, the basins studied all lay within the Sub-Boreal province, and variances in the zonation are restricted to some minor subzonal differences, which are highlighted as they arise. The sequence stratigraphic scheme of the Upper Aalenian–Lower Bathonian is also documented for the lithostratigraphic successions from each basin studied in order to relate the palynological data into a wider stratigraphic and palaeoenvironmental context.

The methods used for these palynological analyses are described in Chapter 2. The primary focus of palynological study is a suite of rock samples I collected from a borehole succession of argillaceous marine deposits from the Swabian Basin of southern Germany. This section provides a near-continuous, high resolution palynological record from the Upper Aalenian to Lower Bathonian (Chapter 3). I have also examined existing palynological slides (loaned from the British Geological Survey) from the Wessex Basin of southwest England, and Hebrides Basin of Scotland. This has allowed me to document the dinoflagellate cyst record from regions with a markedly different lithostratigraphic compositions and depositional environments to that of Swabia(Chapter 4). Additionally, I collected material from the Middle Jurassic of the Normandy coast, to provide quantitative palynological insight into the dinoflagellate cyst record documented by Feist-Burkhardt and Monteil (1997) (Chapter 5). The dinoflagellate cyst taxa I recorded during this study are fully documented in Chapter 6. To examine the relationship between the dinoflagellate cyst record, and wider palaeoenvironmental changes, I have documented the carbon isotope ($\delta^{13}C$) record of the Swabian and Wessex basins, which have been correlated to existing chemostratigraphic records (Chapter 7). The data I document in these chapters are fully synthesised in Chapter 8, to constrain the stratigraphic pattern of the dinoflagellate cyst diversification in northwest Europe, and to assess palaeoecological patterns within Bajocian dinoflagellate cysts floras, which are related into a wider palaeoceanographic and palaeoclimatic context. I have compared these records to global datasets in order to evaluate the extent and pattern of this diversification on a global scale.

The material presented in chapters 3 and 5 of this thesis is stored in the Sedgwick Muesum of Earth Sciences, Downing Street, Cambridge, CB2 3EQ, UK. The rock samples from which palynomorphs were extracted are stored in the Petrology Collections, under accession root number CAMSM 158690. The palynological residues and slides are stored in the Palaeontology Collections under accession root number CAMSM X.50293.

The palynological material presented in Chapter 4 was loaned from the micropalaeontology collections of the British Geological Survey, and the collection (MPA) number of each sample is given.

Chapter 2. Palynological Methods

2.1. Introduction

In this chapter, the procedures I have used for palynological analyses are described, including the processing of rock samples for the extraction of palynomorphs, and the counting method used to collect both the quantitative and semi-quantitative data. The palynological data from Chapter 3 and Chapter 5 are based on rock samples that I collected and processed for this thesis. The palynological data presented in Chapter 4 are based on slides loaned from the micropalaeontology collections of the British Geological Survey (BGS).

2.2. Laboratory processing

2.2.1. Introduction

In this section, the palynological processing methods used for the preparation of samples are described, which broadly follow standard palynological processing procedures (e.g. Wood et al., 1996), with several modifications. These include the use of coarse-fraction sieving for all samples, and the use of hot HCl for carbonate dissolution. The sequence of procedures is shown in Figure 2.1, and details of the procedures used for each sample are in data table appendices A.1, C.1.

2.2.2. Sample preparation

Rock samples were washed, air-dried and crushed to fine-gravel sized fragments using a hammer and anvil. The hammer and anvil were cleaned thoroughly between each sample, and dried using an air blower. If field outcrop samples were processed, the weathering crust was removed prior to crushing. The dried, crushed sample was then weighed. For siliciclastic samples, around 20 g of rock was used and for carbonate samples 40 to 80 g of rock was processed (data tables appendices A.1, C.1).

2.2.3. Addition of the Lycopodium *spore spike*

For quantitative processing, *Lycopodium* spore tablets were added after the sample was weighed, and before the addition of acid. During decantation, the supernatant was always poured through a 10 µm screen to catch any *Lycopodium* spores which may have floated to the top (Mertens et al., 2009b).

2.2.4. Removal of silicate minerals

The removal of silicate minerals was accomplished through maceration in 40% hydrofluoric acid (HF). For each sample, 50–100 ml of HF was added, and the sample left for seven days, being stirred regularly to allow the acid to fully penetrate the rock. The sample was then repeatedly topped up with water and decanted through a 10 µm screen until neutral.

2.2.5. Removal of carbonate minerals

Depending on the lithology, the removal of carbonate minerals was accomplished via two different methods. For siliciclastic samples, the carbonate minerals were removed through heating in 32% hydrochloric acid (HCl) for ten minutes. This was sufficient due to the low carbonate content of the

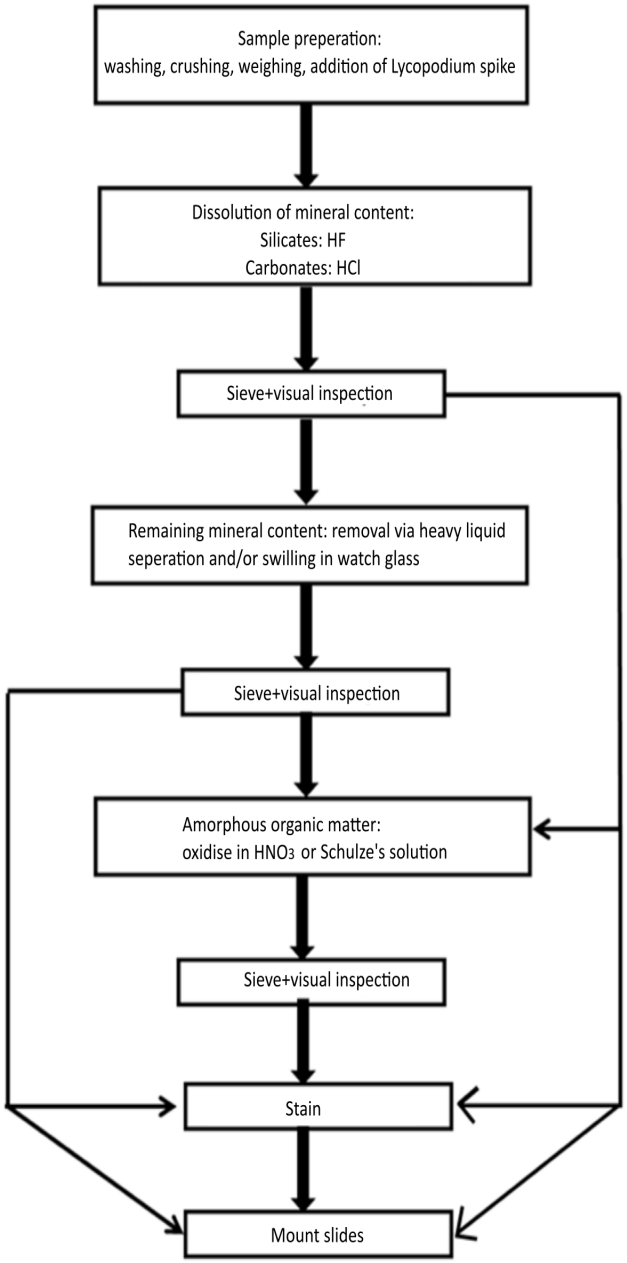

Figure 2.1. Flow chart demonstrating the procedures used for the extraction of palynomorphs from rock samples.

sediment and was carried out after the silicates had been removed with HF. This also prevented the precipitation of hydrogen fluoride gels. Alternatively, for carbonate samples, this was accomplished by macerating the crushed sample in 100–200 ml of 32 or 36% HCl for seven days, and then repeatedly topping up the sample with water and decanting through a 10 µm screen until neutral.

After acid maceration of the samples was complete, the residue was sieved at 150 µm to remove any coarse material before being sieved again at 10 µm. The sample was then visually checked under the microscope. For some samples, there were fragments of undigested rock remaining after maceration. If this was the case, these were removed, dried, weighed, and deducted from the initial weight of the sample for the absolute abundance calculations.

2.2.6. Removal of the remaining mineral component

After acid maceration, the majority of samples still contained fine mineral grains, these were removed

by heavy liquid separation or 'swirling' in a large watch glass. For heavy liquid separation, the sample was placed in a 50 ml centrifuge tube and centrifuged for one to two minutes at 4400 rpm to remove any excess water. This was passed through a 10 μm sieve to catch any *Lycopodium* spores. Thirty to fifty ml of zinc chloride ($ZnCl_2$) was then added to the sample before being centrifuged at 4400 rpm for five minutes. The $ZnCl_2$ was then sieved at 10 μm and flushed clean with water. For samples with a small amount of additional mineral content, the aqueous reside was hand-centrifuged ('swirled') in a large watch glass which allowed the mineral grains to separate into the middle of the glass, allowing the organic fraction to be pipetted off.

2.2.7. Removal of amorphous organic matter

Excessive amounts of amorphous organic matter (AOM) can hamper the visual identification of palynomorphs. If a large quantity of AOM was present, this was removed by oxidation. This was accomplished via two methods depending on the quantity of AOM present. If a sample contained excessive amounts of AOM, this was removed through oxidation in Schulze's solution which was made by mixing ~two grams of potassium chlorate ($KClO_3$) into 10–20 ml of 70% nitric acid (HNO_3). This was added to the sample and left for one to ten minutes. After being topped up with water, the sample was decanted and sieved to neutrality. If a sample contained a relatively small quantity of AOM, this was removed by placing the sample in 10 to 20 ml of 70 % HNO_3 for one to 15 minutes before being decanted and sieved. After oxidation, samples were checked under the microscope to ensure the oxidising reagent had not destroyed any of the palynomorphs. If AOM was still present after these steps, sparse mounting of slides was used to ensure minimal masking of palynomorphs rather than additional oxidation in order to ensure palynomorphs were not destroyed. Although Dodsworth (1995) demonstrated that oxidation with Schulze's solution can destroy Mesozoic gonyaulacoid dinoflagellate cysts, samples processed herein involved a much greater mass of sample (20 g compared to 5 g), a smaller volume of Schulze's solution (10–20 ml compared to 60 ml), and were only oxidised for 1 to 10 minutes.

2.2.8. Staining

Some samples were stained with Safranin to improve contrast and hence aid visual observation. This was accomplished by adding a small drop of Safranin dye to the residue before mounting.

2.2.9. Slide mounting

The completed samples were flushed thoroughly with deionised water before a small drop of 2% polyvinyl alcohol was added. This aqueous residue was pipetted onto a glass coverslip and left to dry overnight. The coverslip was then glued to a microscope slide with either a mixture of Elvacite and xylene, or Petropoxy 154, a heat setting epoxy resin.

2.3. Counting

2.3.1. Introduction

Palynomorph assemblages in marine sediments comprise a variety of terrestrial and aquatic organic-walled

microfossils. The examination of both marine-sourced and terrestrially derived palynomorphs provides a useful palaeoenvironmental tool, particularly when interpreted in the context of sedimentological data (e.g. Traverse, 1988; Tyson, 1993). In order to assess the Bajocian dinoflagellate cyst record in a broader palaeoenvironmental context, both marine and terrestrial palynomorphs were counted as part of a ~300 specimen count. The counting of 300 palynomorphs has been shown to be statistically reliable measure (Germeraad et al., 1968; Mertens et al., 2009b), and the count error according to Stockmarr (1971) is around 6%. An additional slide was scanned per sample in order to ensure that any rare palynomorphs were recorded.

Only palynomorphs were counted for the palynological analyses undertaken for this thesis. However, palynomorphs represent only one fraction of the organic matter found within sedimentary rocks. While the ratio of marine to terrestrial palynomorphs can provide a proxy for the distance from terrestrial source, this does not consider other terrestrially derived organic matter, such as wood and plant cuticle, or marine-derived amorphous organic matter. However, the aim of this thesis is to document the pattern of dinoflagellate cyst appearances through the Bajocian of northwest Europe. As such, the counting of dinoflagellate cysts and associated palynomorphs and comparison to sedimentological data allows the dinoflagellate cyst record to be assessed within a coarse palaeoenvironmental context. In turn, this allows the role of broad-scale palaeoenvirommental shifts on the stratigraphic pattern of dinoflagellate cyst appearances to be evaluated.

2.3.2. Aquatic palynomorphs

Dinoflagellate cysts are clearly the focus of this thesis, and have therefore been identified to species level as far as possible. Specimens which were too poorly preserved to allow a positive identification were grouped together as ‘dinoflagellate cysts indeterminate’. Other marine palynomorphs were also recorded, in order to accurately assess the ratio of marine to terrestrial palynomorphs, which can reflect distance for terrestrial source, and is thus a useful palaeoenvironmental indicator (Tyson, 1993). Further, the relative proportions of different microplankton groups can reflect palaeoenvironmental conditions (Tyson, 1993). Consequently, other microplankton groups were identified to generic level. In addition to dinoflagellate cysts, other microplankton encountered include the small acritarchs predominantly of the *Micrhystridium/Veryhachium* complex. Although, by definition, these palynomorphs of are of unknown affinity, these small acanthomorphs have been interpreted as the phytoplankton resting stages, and particularly were prevalent in nearshore environments (e.g. Wall, 1965; Harris and Tocher, 2003). The phycoma of prasinophyte algae such as *Tasmanites* were also encountered, and identified to generic level. Prasinophytes have been interpreted as ecological generalists, but were particularly abundant under stressed conditions during the Jurassic (e.g. van de Schootbrugge et al., 2005, 2013). Other marine palynomorphs recorded include the organic-walled linings of foraminiferal tests, and scolecodonts. The alga *Botryococcus* was also recorded at a generic level, as this group can reflect freshwater/brackish input.

2.3.3. Terrestrial palynomorphs

The relative proportion and composition of terrestrially derived palynomorphs in marine sediments can provide useful palaeoenvironmental data. Herein, sporomorphs were counted in four broad morphological groupings of bisaccate pollen, other pollen, trilete spores, and monolete spores. The proportion of sporomorphs to marine palynomorphs broadly reflects distance from terrestrial source, as the majority of the former are delivered to marine environments via fluvial input (Tyson, 1993). Within sporomorph assemblages, differential transport leads to differences in the relative abundances of each group with distance from source. In general, spores are less buoyant compared to saccate pollen, and are therefore deposited in nearshore environments, close to sources of terrigenous discharge, and are therefore abundant in deltaic settings (Tyson, 1993). In contrast, bisaccate pollen are more buoyant, and can be transported for longer distances, leading to the dominance of bisaccate pollen in sporomorph assemblages in offshore settings (Traverse, 1988). Consequently, the recording of these broad groups, and their relation to sedimentological data, allow palaeoenvironmental trends to be discerned.

Palynomorphs of unknown affinity were also encountered very sparsely. These are primarily represented by sphaeromorphs and other acritarchs, such as *Fromea*, which were counted, but excluded from marine: terrestrial ratio calculations.

2.3. Absolute abundance calculations

The relative abundances of different palynomorph groups can reflect palaeoecological signals. However, an issue with relative abundance data is that it is not clear whether an increase in the abundance of a particularly group reflects a true abundance increase, or the concomitant decrease of another group. For this reason, samples herein were spiked with tablets containing the modern spore *Lycopodium clavatum*. The majority of the tablets used are from batch 3862, manufactured by Lund University, Sweden. These have 9666 spores per tablet, with a % standard deviation of 4.91 and 3.47 for two and four tablets respectively. Sixteen samples were spiked with tablets from batch 483216 (appendix A.1, C.1), in this batch, one tablet contains 18583 spores, standard deviation was only given for 5 tablets which corresponds to a % standard deviation of 4.1, and this value has been used for the calculation of errors.

Absolute abundances of palynomorphs were calculated according to the following equation (Stockmarr, 1971; Lignum et al., 2008): $ppg = \left(\frac{pc}{lc}\right) * \left(\frac{lt}{w}\right) ppg = \left(\frac{pc}{lc}\right) * \left(\frac{lt}{w}\right)$ where: *ppg* = palynomorphs per gram of dried sediment, *pc*= palynomorphs counted, *lc*= *Lycopodium* counted, *lt*= total *Lycopodium* and *w*= dried weight of the sample in grams. The error on the calculation according to Stockmarr (1971) is $e = \sqrt{e1^2 + e2^2 + e3^2} e = \sqrt{e1^2 + e2^2 + e3^2}$ where: e1= error on number of spores in marker tablets (standard deviation), e2= error on palynomorphs counted and is: $\frac{\sqrt{cc}\sqrt{cc}}{cc \;\; cc}$ where cc is the number of palynomorphs counted, e3= error on the number of *Lycopodium* spores counted and is: $\frac{\sqrt{sc}\sqrt{sc}}{sc \;\; sc}$ where sc is the number of *Lycopodium* spores counted.

2.4. Palynomorph preservation

A qualitative assessment of the preservation of palynomorph assemblages was made for each sample, on a scale from poor to excellent (data table appendices A.1,B.1, C.1, D.1). This was primarily based on the extent of degredation/corrosion of palynomorphs present in the sample, as degradation of dinosporin can make identification of dinoflagellate cyst wall features such us tabulation and ornaments difficult, which in turn impinge on identification. The qualitative scale ranges from “excellent” which indicates minimal degradation to “poor”, which indicates a large amount of degradation. A selection of preservation states can be viewed in Figure 2.2.

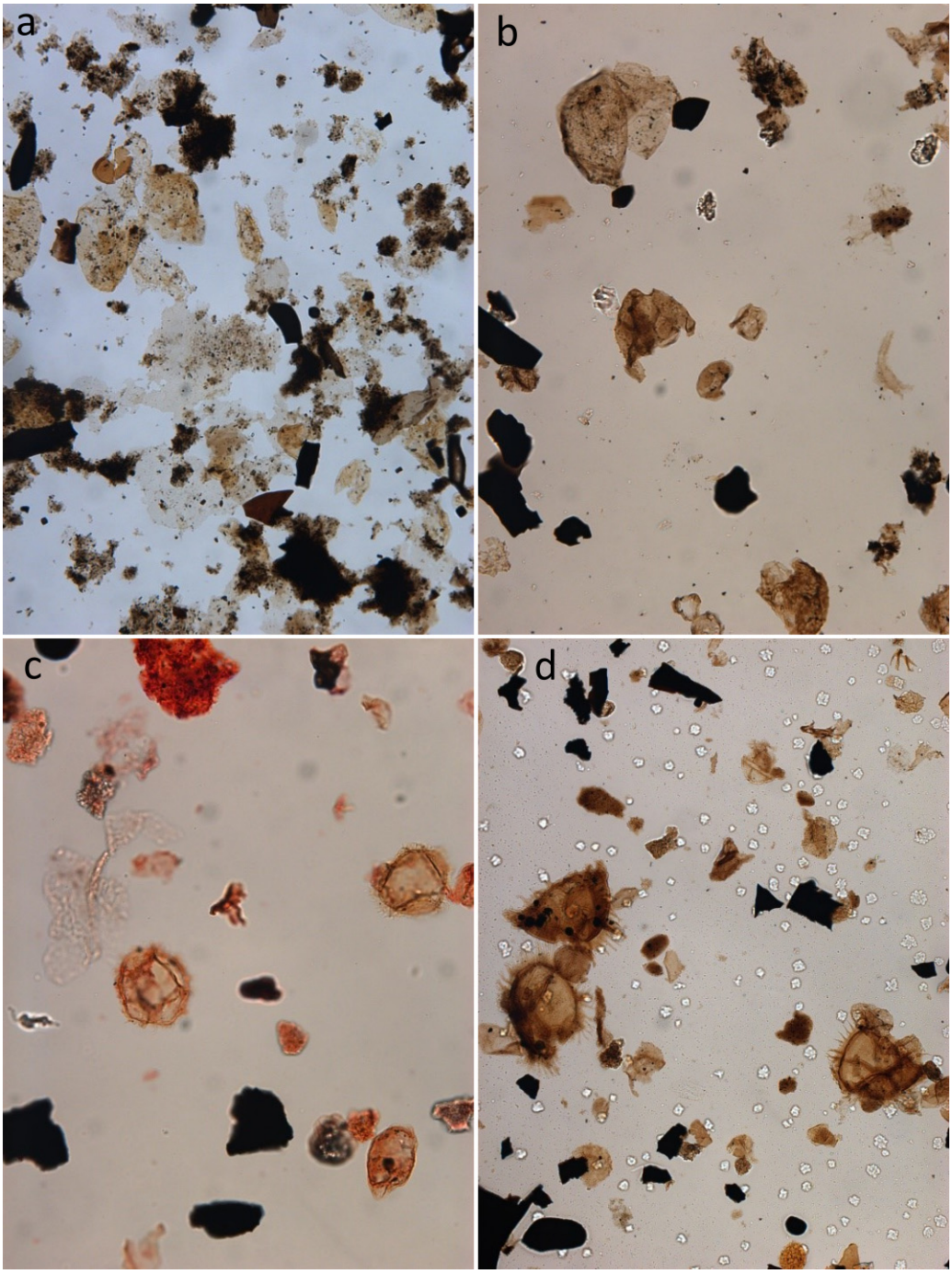

Figure 2.2. Preservation states of palynological samples.
a= poor to fair, note the large amount of degredation of palynomorphs, b=good, there is less degredation, c= very good, minimal degredation, d= excellent, extremely minimal degredation.

Chapter 3: The palynology of uppermost Aalenian to lowermost Bathonian of the Swabian Basin, southwest Germany

3.1. Introduction

The low-rising mountains of the Swabian Alb of southwest Germany have a long history of geological and palaeontological research, and the region is a classic locality of the European Jurassic (Pienkowski et al., 2008). Feist-Burkhardt and Wille (1992) provided a broad overview of the stratigraphic distributions of dinoflagellate cysts throughout the Jurassic of the Swabian Basin, and highlighted the large number of appearances in the Bajocian, particularly around the Lower–Upper Bajocian transition (*S. humphriesianum* and *S. niortense* zones). The expanded stratigraphy of the Middle Jurassic (over 280 m thick according to Pienkowski et al., 2008), and well researched ammonite zonation, make Swabia an ideal locality for examining the Bajocian dinoflagellate radiation.

3.1.1. Geological Background

During the Mid Jurassic, the Swabian Basin was located at around 30°N, in the Sub-Boreal province, at the outer region of the European Epicontinental Seaway, close to the shelf-break with the Tethyan Ocean (Figure 3.1; Callomon, 2003 fig. 1). The Swabian Basin was defined by the Tethys to the south, the northwest German Basin to the north, the eastern Paris Basin to the west and the Bohemian Massif to the east (Figure 3.1; Callomon, 2003; Pienkowski et al., 2008). During the Bajocian, the basin included the French-Swiss carbonate platform in the southwest, a mud dominated, moderately deep basin in the central area, and the Franconian iron-ooidal carbonate platform in the east (Ziegler, 1990).

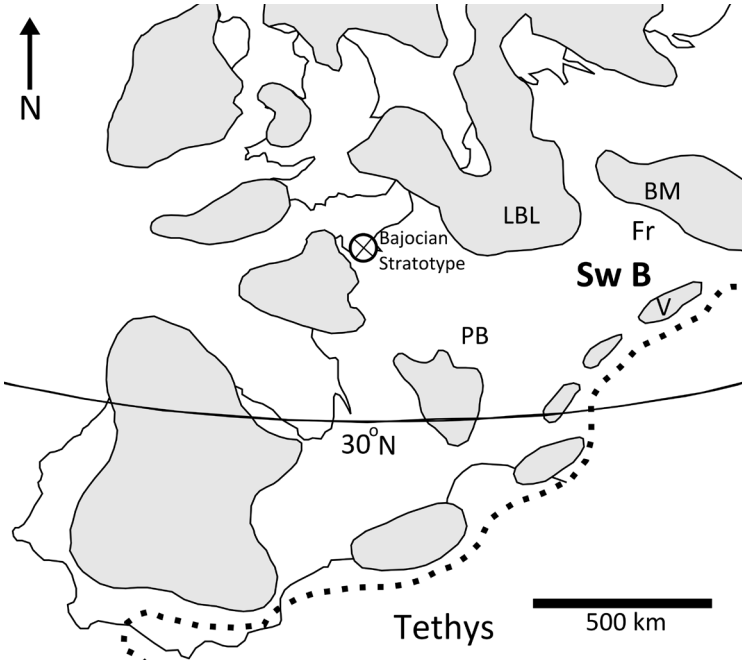

Figure 3.1. Palaeogeography for the Bajocian–Bathonian.
The location of the Swabian Basin is shown relative to the historical Bajocian stratotype in northwest France. Emergent areas (grey): LBL- London Brabant Landmass, BM- Bohemia Massif, V- Vindelecian High. Submerged areas: PB= Paris Basin, Fr= Franconian platform, SwB= Swabian Basin. After Wiggan et al. (2017) fi.g. 2 and modified from Callomon (2003) fig. 1

The majority of material analysed in this study comes from borehole B404/2, the drillsite of which is

located approximately 37 km southeast of Stuttgart (Figure 3.2, 48.59849°N, 9.61450°E) located in the eastern part of the central Swabian basin. Field outcrop samples from the Sowerbyi Oolith Member, which crops out in the southwestern part of the Swabian Basin have also been analysed. The samples were collected from a section in the western Swabian Alb, located approximately 1.5 km NW of the village of Blumberg (47.84909671°N, 8.508942429°E, Figure 2).

Figure 3.2. Locality map of the Swabian Alb.
Grey shading denotes Middle Jurassic outcrop, 1= location of borehole B404/2. 2= Sowerbyi Oolith field outcrop. locality. Modified from Dietze et al. (2009) fig. 1.

3.1.1.1. Stratigraphy

The B404/2 succession is comprised of uppermost Aalenian to lowermost Bathonian strata (Figure 3.3). The (Sub-Boreal) ammonite zonal subdivision of the succession is based on Dietl (1988, 2013) who described the ammonite biostratigraphy of the Middle Jurassic from a road cutting located 1 km from the site where the borehole was drilled. The borehole section was correlated to the road cut ammonite zonation using a combination of lithostratigraphy and ammonites present (Matthias Franz *personal communication*). With the exception of the lowermost zone (*H. discites*), which is missing due to a hiatus, the entire Bajocian Stage is present (Figure 3.3). There is some uncertainty in the recognition of the *S. propinquans* zone of the Lower Bajocian in B404/2 due to a lack of ammonites, which is herein split into the *W. laeviuscula*/*S. propinquans* and *S. propinquans*/*S. humphriesianum* zones, all other zones are accurately correlated.

An important point regarding the ammonite biozonation of the succession is the recognition of the *S. humphriesianum* zone in southern Germany, which Feist-Burkhardt and Götz (2016) have discussed in detail. In Swabia, the *D. pinguis* subzone is taken as the lowermost subzone of the *S. humphriesianum* zone (Figure 3.4). However, the *D. hebridica* subzone, which is the equivalent to the *D. pinguis* subzone in Britain and France, is included as the uppermost subzone of the *S. propinquans* zone (Figure 3.4.).

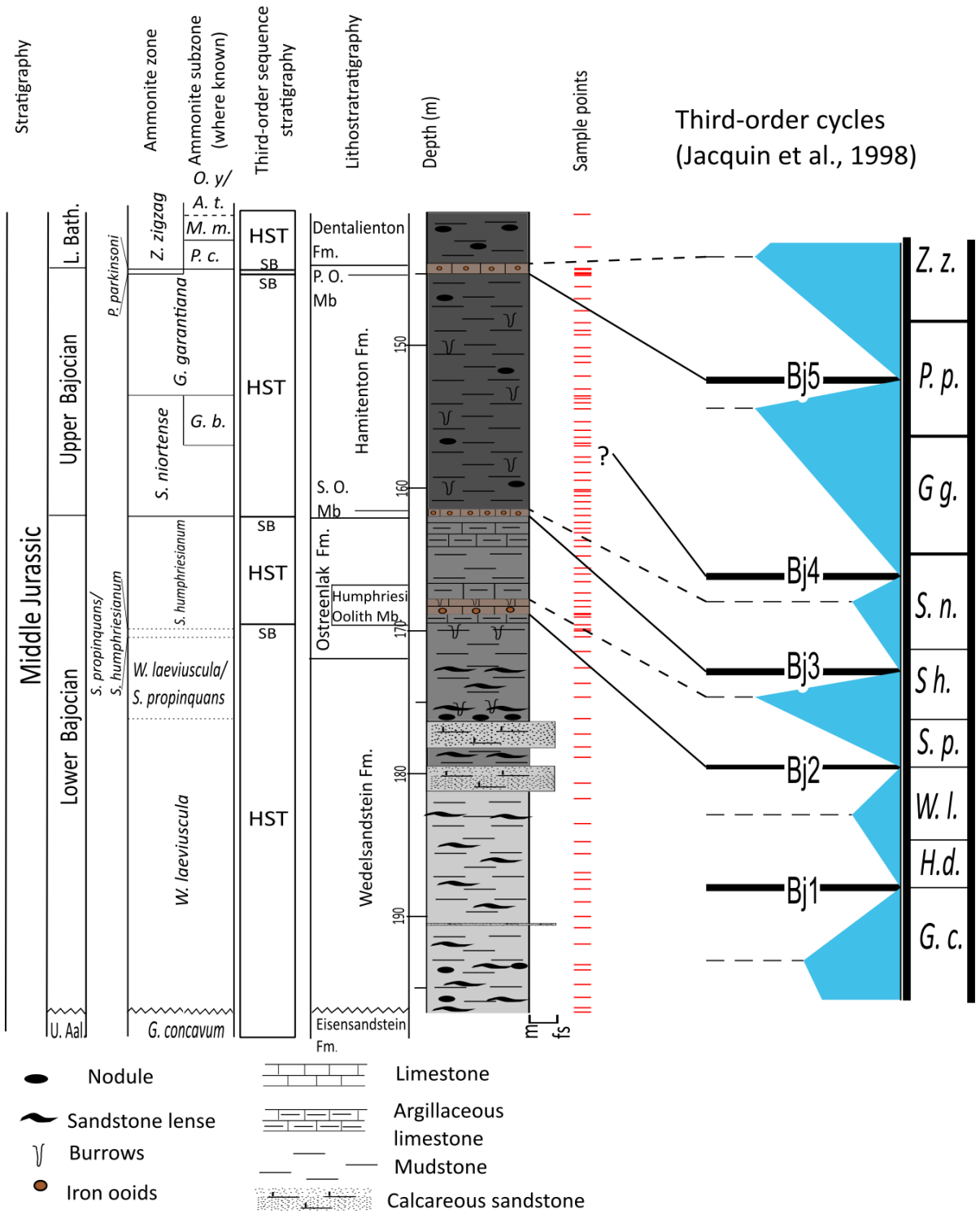

Figure 3.3. Sedimentary log of borehole B404/2. Sedimentary log of borehole B404/2.
The correlation of ammonite zones based on Dietl (1988, 2013) and sequence stratigraphy after Feist-Burkhardt and Götz (2002). Third-order sequence BJ4 cannot be recognised in Swabia. Lithostratigraphy: P.O.= Parkinsoni Oolith Member, S.O.= Subfurcaten Oolith Mb. Subzones: G.b= G. baculata, P. c= P. convergens, M.m.= M. macrascens, O.y./A.t.= O. yeovilensis/A. tenuiplicatus. Sequence stratigraphy: HST= Highstand systems tract SB= sequence boundary. Modified from Wiggan et al. (2017) fig. 4.

This means that the base of the *S. humphriesianum* zone is lower than it is in other parts of Europe. Although subzone-level ammonite biostratigraphic control is not available for the B404/2 succession, it

may be possible to determine the base of the *D. romani* subzone using sequence stratigraphy, which is discussed below.

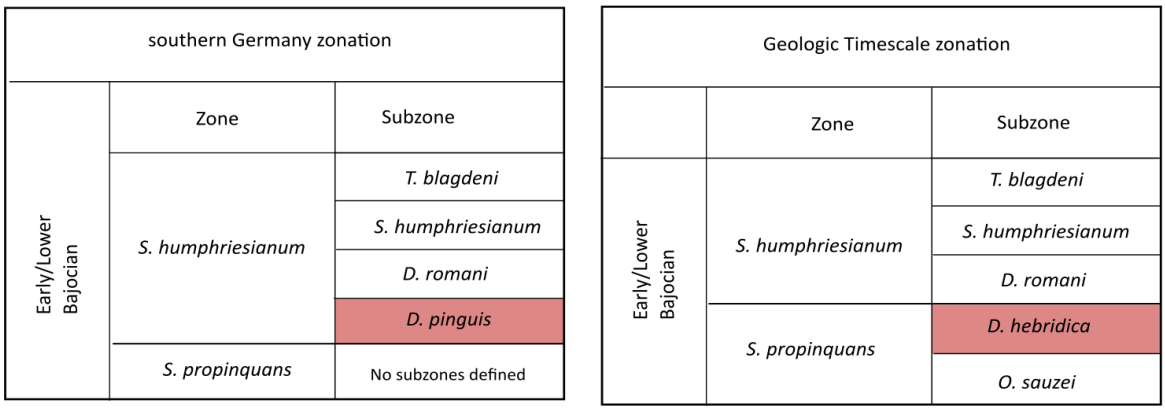

Figure 3.4. Ammonite zonation for the *S. propinquans/S. humphriesianum* zones of southern Germany and comparison to the Geologic Timescale zones.
In the global timescale, the *D. hebridica* subzone is part of the *S. propinquans* zone (red). In Germany, the lateral equivalent (the *D. pinguis* zone, red) forms the base of the *S. humphriesianum* zone. Modified from Feist-Burkhardt and Götz (2016, fig. 5.)

As the *H. discites* zone is locally missing in the B404/2 succession, outcrop samples were analysed from the *H. discites* zone of the Sowerbyi Oolith Member, a condensed unit of nodular, ferruginous oolitic limestones and marls (Figure 3.5). The Sowerbyi Oolith Member crops out in the southwestern part of

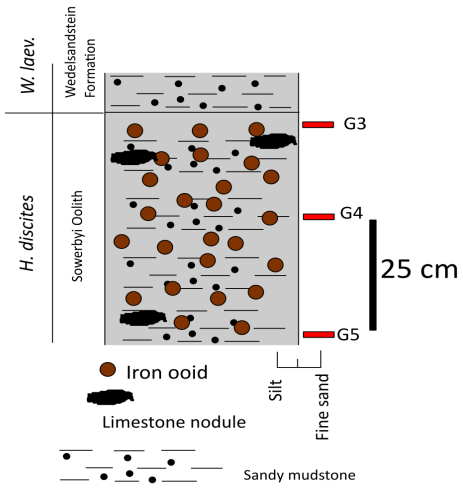

Figure 3.5. Lithological log of the Sowerbyi Oolith Member outcrop showing the distribution of palynological samples.

the Swabian Basin (Figure 3.2).

3.1.1.2 Sequence stratigraphy of the Swabian Basin and depositional environment

The lithostratigraphic succession of the Bajocian to Lower Bathonian in the Swabian Basin is comprised of four mudstone-dominated units: the Wedelsandstein, Ostreekalk, Hamitenton, and Dentalienton formations. These fine-grained silicilastics are separated by the thin condensed carbonates of the Humphriesi, Subfurcaten and Parkinsoni Oolith members (Figure 3.3). There is an overall fining-

upward trend as the Lower Bajocian Wedelsandstein Formation contains abundant sandstone lenses and interbeds whilst the overlying units are finer grained. Feist-Burkhardt and Götz (2002) proposed a sequence stratigraphic scheme for the Bajocian to Bathonian of Swabia based on the integration of palynofacies analysis and sedimentological data. This sequence stratigraphic scheme is applied to the B404/2 succession in Figure 3.2, and is described below.

The lowermost Bajocian Sowerbyi Oolith Member is a unit of ferruginous oolitic nodular limestones and marls, which was deposited as a condensed transgressive deposit over a sequence boundary (Feist-Burkhardt and Götz, 2002). The Wedelsandstein Formation (196.4 to 172.59 m in B404/2) corresponds to the *W. laeviuscula* and *W. laeviuscula/S. propinquans* zones, and was deposited as a highstand systems tract. This formation is comprised of mudstones with sandstone lenses and interbeds. The Wedelsandstein Formation transitions gradationally into the Ostreenkalk Formation (171.10 to 162.35 m), which is dominated by dark grey mudstone intercalated with argillaceous limestone. The lower part of the Ostreenkalk Formation corresponds to the *W. laeviuscula/S. propinquans* and *S. propinquans/S. humphriesianum* zones (171.90 to 170 m), with the base of the *S. humphriesianum* zone at 169.84 m. There is prominent limestone interbed at 168.95 to 167.89 m which is termed the Humphriesi Oolith Member and is comprised of carbonate-rich mudstone with abundant ferruginous ooids. The lower surface of this unit represents sequence boundary Bj2 whilst the upper surface represents a maximum flooding surface (Figure 3.3). This member is overlain by the remainder of the Ostreenkalk Formation which corresponds to a highstand systems tract, and is comprised of dark grey mudstones with limestone interbeds. The Ostreenkalk Formation contains a typical shallow-water bivalve fauna (Matthias Franz *personal communication*; Franz, 1986). The Ostreenkalk Formation is overlain by the Subfurcaten Oolith Member of the Hamitenton Formation (161.50 to 160.90 m) which marks the base of the *S. niortense* zone. The lower surface is a sequence boundary (Bj3) whilst the upper surface corresponds to a maximum flooding surface and the member is overlain by the dark grey to black mudstones of the Hamitenton Formation (160.53 to 145.05), which were deposited as a highstand systems tract. These mudstones are dark in colour and contain abundant pyrite, which indicates deposition under slightly restricted bottom water conditions (Matthias Franz *personal communication*; Dietl 1978; 2013). The heteromorphic ammonite *Spiroceras* is abundant in the Hamitenton Formation, indicating a shift to deeper, offshore conditions (Matthias Franz *personal communication*; Dietl 1978; 2013). The boundary between the *S. niortense* and *G. garantiana* zones is located at 153.50 m. The Hamitenton Formation is bounded at the top by the Parkinsoni Oolith Member (144.97 to 144.161), the lower surface of which is a sequence boundary (Bj5). The Parkinsoni Oolith Member is comprised of ferruginous oolitic marls and limestone, which was deposited as a condensed transgressive deposit, and corresponds to the *P. parkinsoni* zone and the *P. convergens* subzone of the *Z. zigzag* zone. The Bajocian/Bathonian boundary is located towards the top of this unit (~144.6 m in B404/2). The Parkinsoni Oolith Member is overlain by the Dentalienton Formation which is comprised of dark grey to back mudstone with abundant phosphorite

nodules, and was deposited as a hightstand systems tract. The Dentalienton Formation represents the Lower Bathonian *Z. zigzag* zone.

The succession represents a series of third-order stacked transgressive-regressive cycles which reflect the T7 second order transgression. The fine grained siliciclastics of the Wedelsanstein, Ostreenkalk, Hamitenton and Dentalienton formations represent highstand deposits, whilst thin-condensed carbonate units such as the Humphriesi Oolith Member, have erosive bases representing sequence boundaries and were laid down as condensed transgressive deposits (Feist-Burkhardt and Götz, 2002). The maximum flooding of the T7 cycle is represented by the contact between the Parkinsoni Oolith and Dentalienton Formation (Lower Bathonian, *Z. zigzag* zone) (Feist-Burkhardt and Götz, 2002).

3.2. Materials

The Bajocian is over 50 m thick in B404/2, which has allowed the stage to be sampled at an extremely high resolution, and in unprecedented detail. By comparison, d'Orbigy's Bajocian type section in Normnady is ~14 m thick. A total of 86 palynologically productive samples were examined, and all lithologies were sampled (Table 1.1, data table appendix A.1). All samples examined processed from B404/2 are core samples. Importantly, the Lower Bajocian *W. laeviuscula* zone is 20 m thick (compared to 3.5 m in Normandy), which has allowed 20 samples to be analysed from this understudied interval. Furthermore, the *S. humphriesianum* and *S. niortense* zones are greatly expanded with respect to Normandy, at 8 m thick each, which has allowed 35 samples to be analysed through the Lower–Upper Bajocian transition. Three rock samples were processed from the Sowerbyi Oolith Member field outcrop material (Figure

Zone	Thickness (m)	Substage	Number of (palynologically productive) samples	Lithostratigraphic unit
G. concavum (pars)	0.2	Upper Aalenian	1	Eisensandstein Formation
H. discites (pars)	1	Lower Bajocian	3	Sowerbyi Oolith
W. laeviuscula (pars)	20.26	Lower Bajocian	20	Wedelsandstein Formation
W. laeviuscual/S. propinquans	5.76	Lower Bajocian	6	Wedelsandstein Formation/Ostreenkalk Formation
S. propinquans/S. humphriesianum	0.61	Lower Bajocian	2	Ostreenkalk Formation
S. humphriesianum	7.9	Lower Bajocian	17	Ostreenkalk Formation (including Humphriesi Oolith Member)
S. niortense	8.25	Upper Bajocian	18	Hamitenton Formation (including Subfurcaten Oolith Member)
G. garantiana	8.53	Upper Bajocian	13	Hamitenton Formation
P. parkinsoni	0.35	Upper Bajocian	4	Parkinsoni Oolith Member
Z. zigzag (pars)	4.56	Lower Bathonian	3	Uppermost Parkinsoni Oolith Member/Dentalienton Formation

Table 3.1. Thicknesses of ammonite zones and number of palynologically productive samples analysed per zone.

3.5) The composite record from the B404/2 succession and the Sowerbyi Oolith Member has allowed the generation of a near-continuous palynological record from the Upper Aalenian to Lower Bathonian.

3.3. Palynology of the Swabian succession

3.3.1. Palynological composition

3.3.1.1. The B404/2 borehole

The majority of the samples examined produced abundant palynomorphs, the preservation is variable but generally good (data table appendix A.1). The specimens from the Humphriesi Oolith Member

and Ostreenkalk Formation are poorly preserved in places, and in the upper part of the Hamitenton Formation, AOM is abundant and preservation is relatively poor; four samples were excluded from further analysis after processing (data table appendix A.1). For the absolute abundance data presented below, the percentage error is <7 % (data table appendix A.3).

The assemblages are dominated by marine palynomorphs which are, in turn, dominated by dinoflagellate cysts (Figure 3.6). Acanthomorph acritarchs, largely *Micrhystridium* spp., comprise most of the remaining marine component (Figures 3.6). Other palynomorph groups include common foraminiferal test linings, sparse prasinophytes (*Tasmanites* spp.) and sphaeromorph acritarchs such as *Fromea*, rare occurrences of the freshwater alga *Botryocccus,* and occasional scolecodonts (Figure 3.6; data table appendix A.2). The terrestrial palynofloras are dominated by trilete spores, with gymnosperm pollen comprising the

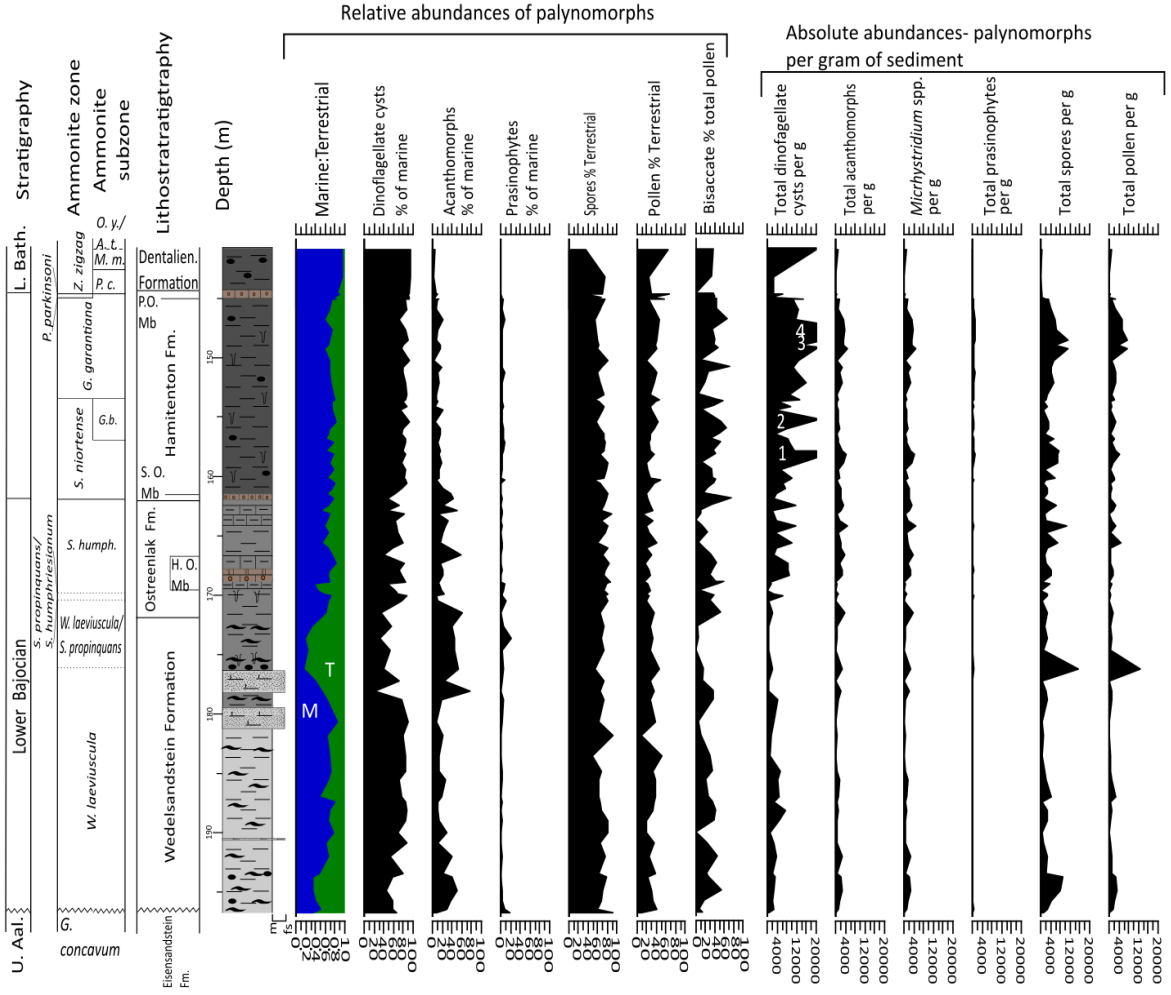

Figure 3.6. Relative and absolute abundances of main marine and terrestrial palynomorph groups for bore-hole B404/2.
There are significant terrestrial influxes in the Wedelsandstein Formation. From around 175 m upwards there is a steady but fluctuating increase in the marine:terrestrial ratio from around 175 m depth. It can clearly be seen that dinoflagellate cysts are the dominant marine palynomorph through the succession, with acantho-morphs (predominantly *Micrhystridium* spp). comprising the majority of the remaining marine component. Dinoflagellate cysts per gram- 4 values are off the scale of the graph. 1: 28717.50, 2: 21447.79, 3: 35359.88, 4:26618.93. Modified from Wiggan et al. (2017) fig. 5.

remaining component (Figures 3.6). Within the pollen floras, bisaccate pollen forms a low to moderate component of total pollen, with no trend throughout the succession (Figure 3.6).

3.3.1.2. Sowerbyi Oolith Member outcrop section

The three field outcrop samples from the Soweryi Oolith Member contain abundant, palynomorphs, and preservation is moderate (data table appendix A.1). Sporomorphs dominate, of which gymnosperm

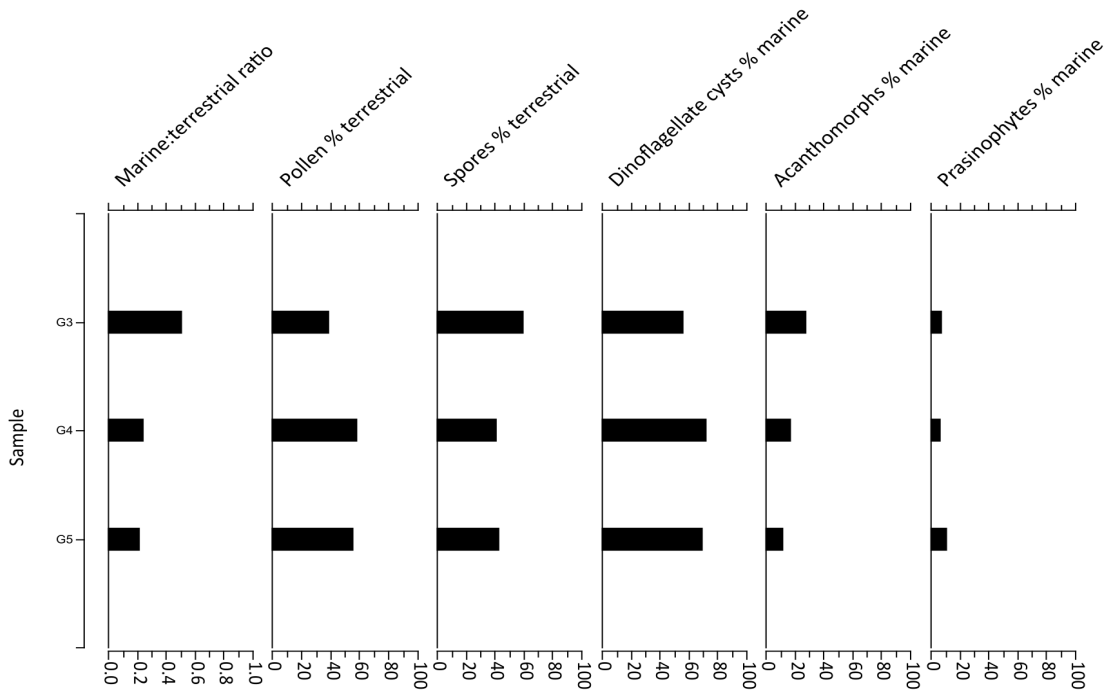

Figure 3.7. Relative abundances of main palynomorph groups for the Sowerbyi Oolith Member.

pollen is the main group (Figure 3.7). Within the marine component, dinoflagellate cysts are the dominant group (Figure 3.7).

3.3.2. Stratigraphic palynology

Eighty-one dinoflagellate cyst taxa were recorded from the Swabian succession (Table 3.2a, 3.2b). Descriptions of taxa recorded can be found in Chapter 6, and the procedure followed for taxa left in open nomenclature is shown in Table 6.1. In this study, the interval was subdivided into four components: Upper Aalenian, Lower Bajocian, Lower–Upper Bajocian transition and the Upper Bajocian–Lower Bathonian transition.

*3.3.2.1. Upper Aalenian (**G. concavum** zone)*

The single sample (S1, 196.7 m) from the Upper Aalenian (*G. convavum* zone) of B404/2 yielded five dinoflagellate cyst taxa. These are *Batiacasphaera* spp., *Dissiliodinium giganteum*, *Dissiliodinium* spp., *Nannoceratopsis ambonis* and *Pareodinia halosa*. The presence of *Dissiliodinium giganteum* is the oldest record to date. Previously *Dissiliodinium giganteum* was thought to have had a first appearance

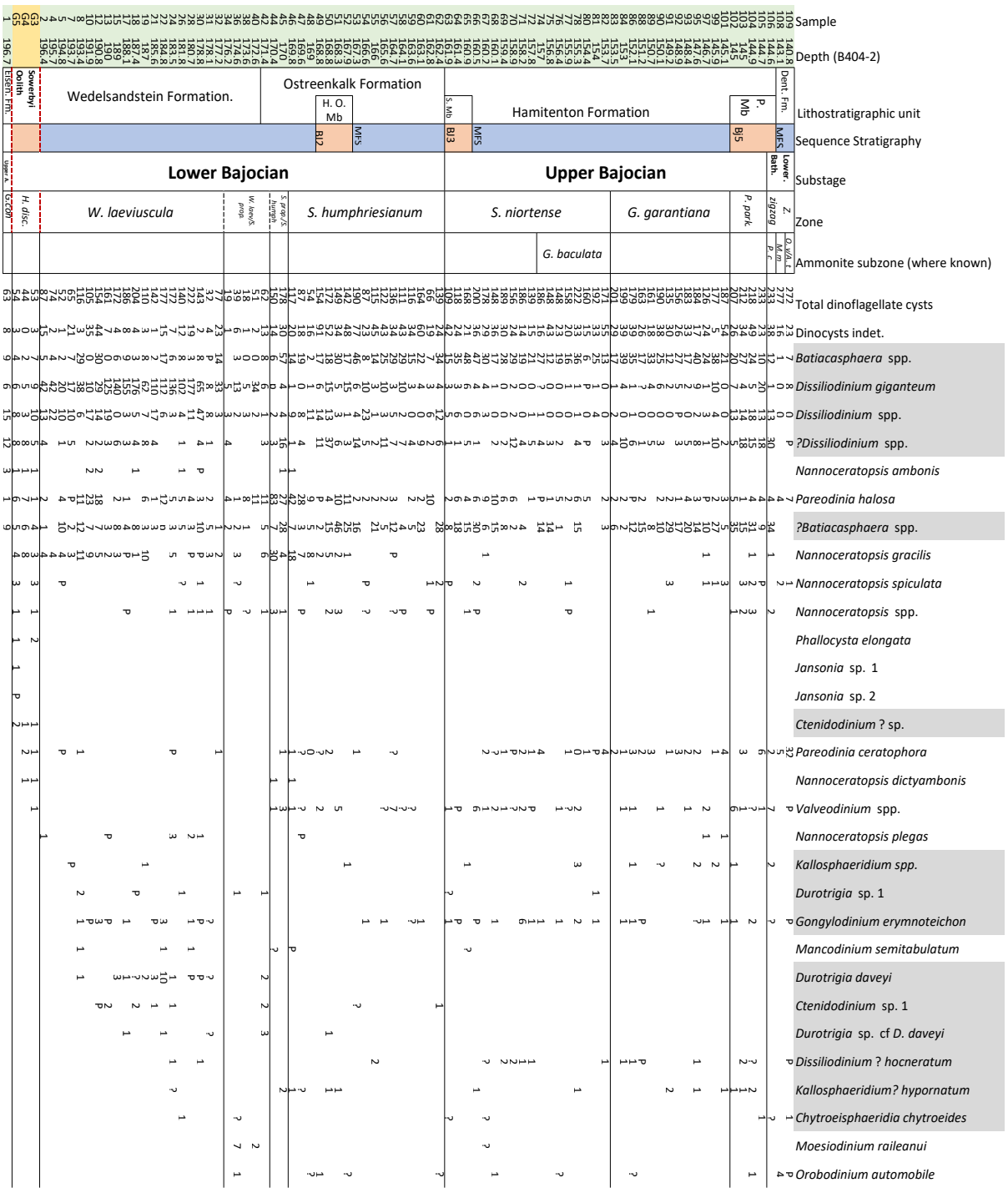

Table 3.2a. Quantitative composite dinoflagellate cyst range chart for Swabia, showing appearances from the Upper Aalenian to Lower Bajocian.

P= present outside of count,?= questionable occurrence. Taxa belonging to the family Gonyaulacaceae are highlighted in grey. Green fill denotes B404/2 samples, yellow fill denotes samples from the Sowerbyi Oolith outcrop. Lithostratigraphic units: Eisen. Fm.- Eisensandstein Formation , H. O. Mb- Humphriesi Oolith Member, S. Mb- Subfurcaten Oolith Member, P. Mb- Parkinsoni Oolith Member, Dent. Fm- Dentalienton Formation. Blue fill denotes highstand deposits, orange fill denotes transgressive deposits. Third-order sequence boundaries are shown, MFS= maximum flooding surface.

datum (FAD) in the lowermost Bajocian *H. discites* zone (Feist-Burkhardt and Monteil, 2001). The range base of *Dissiliodinium* (as *D. lichenoides*) is in the *L. murchisonae* zone of the Aalenian (Feist-Burkhardt and Pross, 2010). *Batiacasphaera* spp. and *Pareodinia halosa* have FADs in the *H. variabilis*

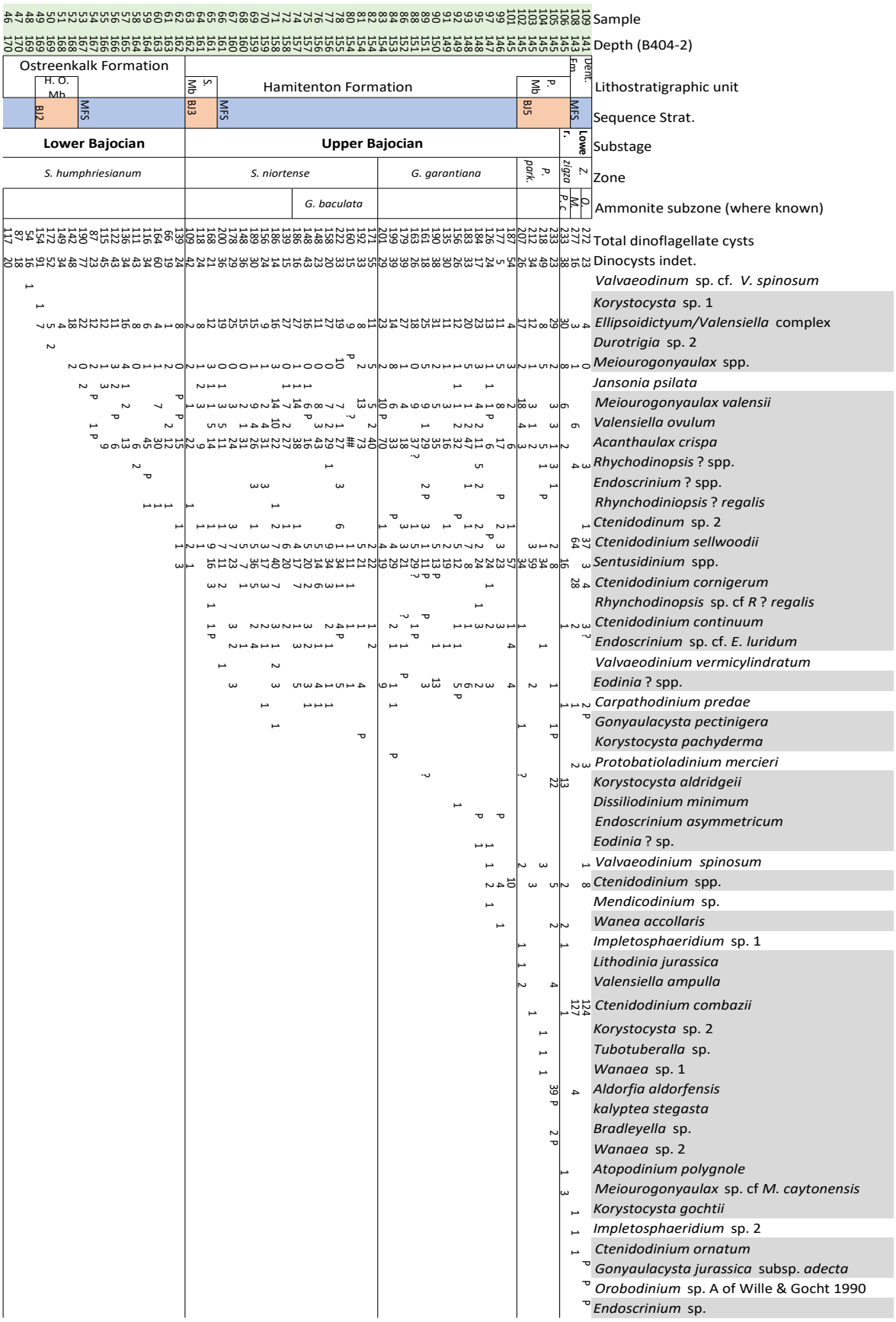

Table 3.2b. Quantitative composite dinoflagellate cyst range chart for Swabia showing appearances for the uppermost Lower Bajocian to Lower Bathonian.

Key as per Table 3.2b. Ammonite subzones- *P.c= P. convergens*, *M= M. macrescens*, *O= O. yeovilensis/A. tenuiplicatus*

and *G. thouarsense* zones respectively of the Toarcian (Riding, 1984a; de Vains, 1988). The FAD of *N. ambonis* is in the Upper Plienshachian *P. spinatum* zone (Riding, 1984b).

3.3.2.2. Lower Bajocian H. discites to S. propinquans/S. humphriesianum zones

Twenty-three dinoflagellate cyst taxa appear through the Lower Bajocian of the Sowerbyi Oolith Member and B404/2. There are several FADs of gonyaulacaceans and other taxa. In the *H. discites* zone of the Sowerbyi Oolith Member, ten dinoflagellate cyst taxa appear. The only (possible) gonyaulacacean taxon to appear is *Ctenidodinium*? sp. which is an enigmatic chorate form (Chapter 6). This morphotype may be an early representative of the genus. Other appearances include *Jansonia* sp. 1 and 2. The FAD of *Jansonia* is in the Upper Pliensbachian of Italy as *Jansonia* sp. of Bucefalo Palliani and Mattioli (1998). Several species of *Nannoceratopsis*: *N. gracilis, N. dictyambonis,* and *N. spiculata,* appear in the *H. discites* zone but are long-ranging species and have FADs in the Upper Pliensbachian and Upper Toarcian (Riding, 1984b; Prauss, 1989; Riding and Thomas, 1992). However, the range base of *N. spiculata* in Germany appears to be no lower than the *S. humphriesianum* zone (Prauss, 1989; Feist-Burkhardt and Wille, 1992) and thus this report lowers the local range base of this species to the *W. laeviuscula* zone. *Pareodinia ceratophora* appears in this zone but has a FAD in the Lower Aalenian (Prauss, 1989). Other long-ranging taxa to appear include *Phallocysta elongata* and *Valvaeodinium* spp. The FAD of the former is in the Toarcian, with a last appearance datum in the Early Bajocian (Riding, 1994), whilst *Valvaeodinium* has a FAD in the Upper Pliensbachian (*A. margaritatus* zone) as *V. armatum* (Morgenroth 1970; Riding and Thomas, 1992).

Ten dinoflagellate cyst taxa appear in the *W. laeviuscula* zone, which corresponds to 196.4 to 176.38 m in B404/2. The occurrence of *Ctenidodinium* sp. 1 in sample S12 (190.76 m) represents the first definitive appearance of this genus. Previously, this was around the Lower–Upper Bajocian transition as *Ctenidodinium continuum* (Feist-Burkhardt and Wille, 1992). The occurrence of *Dissiliodinium*? *hocneratum* in sample S24 (183.50 m) lowers the FAD of this species, which was previously in the *S. niortense* zone of the Upper Bajocian (Feist-Burkhardt and Wille, 1992). Likewise, presence of *Chytroeisphaeridia chytroeides* in sample S26 (181.75 m) represents the lowest record of this species, which was previously placed in the *S. niortense* zone of the Upper Bajocian (Feist-Burkhardt and Monteil 1997). This species is one of the earliest dinoflagellate cysts with a single-plate precingular archaeopyle. Other gonyaulacacean species to occur in the *W. laeviuscula* zone include *Durotrigia* sp. 1*, Durotrigia* sp. cf. *D. daveyi, Durotrigia daveyi* and *Gongylodinium erymnoteichon,* the latter two taxa have range bases in the *H. discites* zone (Riding and Thomas, 1992). *Kallosphaeridium*? *hypornatum* questionably occurs in sample S24 (183.50 m); the FAD of this species has previously been reported from the *W. laeviuscula* zone (Feist-Burkhardt and Monteil, 1997). *Kallosphaeridium* spp. also appear in this zone, but this group has a FAD in the *L. opalinum* zone of the Lower Aalenian (Feist-Burkhardt and Wille 1992). The non-gonyaulacaceans *Mancodinium semitabulatum* and *Nannoceratopsis plegas* appear in the *W. laeviuscula* zone but these species are long-ranging with FADs in the Upper Pliensbachian and

Upper Toarcian respectively (Morgenroth, 1970; Prauss, 1989).

As the *S. propinquans* zone cannot be accurately recognised due to a lack of ammonites in B404/2, it has been split into the *W. laeviuscula/S. propinquans* zones (176.15 to 170.98 m) and the *S. propinquans/S. humphriesianum* zones (170.41 to 170 m). In the *W. laeviuscula/S. propinquans* zone, two taxa appear, both non-gonyaulacacean, in sample S36 (174.64 m). The occurrence of *Orobodinium automobile* represents the lowest reported example of this somewhat enigmatic genus, the FAD of which has been previously placed in the Upper Bajocian *P. parkinsoni* zone (Feist-Burkhardt and Wille, 1992). In contrast, *Moesiodinium raileanui* is long-ranging with a FAD in the Upper Toarcian (Riding and Thomas, 1992). In the questionably assigned *S. propinquans*/*S. humphriesianum* zone, there are no first appearances but *Nannoceratopsis dictyambonis* is present in samples S44 (170.41 m) and also is also present in sample S46 of the lowermost *S. humphriesianum* zone (169.84 m) (Table 3.2a). The FAD of this species is in the *D. levesquei* zone of the Upper Toarcian (Riding, 1984b). However, the last appearance datum (LAD) of *N. dictyambonis* has been reported from the *W. laeviuscula* zone (Riding and Thomas, 1992; Feist-Burkhardt and Wille, 1992). As this species only occurs as two isolated specimens in B404/2, it is possible that these have been reworked, and consequently the LAD cannot be confidently raised to the *S. humphriesianum* zone.

The most striking feature of the dinoflagellate cyst abundance data through the Lower Bajocian is the prominence of *Dissiliodinium*, particularly *Dissiliodinium giganteum* in the Wedelsandstein Formation (Figures 3.8a, 9). In the B404/2 borehole, this species is highly abundant, reaching >80% of dinoflagellate cysts in the middle of the *W. laeviuscula* zone, before undergoing a decline in abundance in the *W. laeviuscula/S. propinquans* to *S. propinquans/S. humphriesianum* zones (lowermost Ostreenkalk Formation- Figures 3.8a, 9). Other taxa which occur commonly through this interval include *Batiacasphaera* spp., *Nannoceratopsis gracilis,* and *Pareodinia halosa* (Figure 3.8a).

3.3.2.3. Lower–Upper Bajocian transition: S. humphriesianum and S. niortense zones

There is a steady increase in dinoflagellate cyst appearances through *S. humphriesianum* and *S. niortense* zones in B404/2, and a number of gonyaulacacean taxa have FADs through this interval (Table 3.2a, b). In the *S. humphriesianum* zone, which corresponds to 169.84 to 162.35 m depth in B404/2, 15 dinoflagellate cyst taxa appear. Thirteen of these belong to the family Gonyaulacaceae, and many mark the FAD of each genus and/or species. *Acanthaulax crispa,* the *Ellipsoidictyum/Valensiella* complex, *Meiourogonyaulax valensii, Meiourogonyaulax* spp*., Rhynchodiniopsis*? *regalis* and *Valensiella ovulum* are known to have FADs in the *S. humphriesianum* zone, and represent the first appearances of these genera (Feist-Burkhardt and Wille, 1992; Riding and Thomas, 1992; Feist-Burkhardt and Monteil, 1997; Feist-Burkhardt and Götz, 2016). Similarly, *Korystocysta* is known to have a FAD in the *S. humphriesianum* zone as *K. gochtii* (Feist-Burkhardt and Wille, 1992), coeveal with the occurrence of *Korystocysta* sp. 1 in lower part of this zone (sample S49, 168.83 m). The appearance of *Jansonia*

psilata from sample S53 (167.31 m), is the first record of this species from Europe. The occurrence of *Ctenidodinium sellwoodii* in the uppermost part of the *S. humphriesianum* zone (sample S62, 162.35 m) places the FAD of this species close to the Lower/Upper Bajocian transition, which has previously been reported as Upper Bajocian *G. garantiana* zone (Feist-Burkhardt and Wille, 1992; Riding and Thomas, 1992). The only non-gonyaulacacean to appear in this zone is *Valvaeodinium* sp. cf. *V. spinosum* (sample S48, 169 m), *V. spinosum* has a FAD in the *S. humphriesianum* zone of Germany (Feist-Burkhardt and Wille, 1992).

Several gonyaulacacean morphotypes appear through the *S. humphriesianum* zone which may be early representatives of genera which became prominent components of Middle–Late Jurassic dinoflagellate cyst floras. *Rhynchodiniopsis*? spp., is a group of enigmatic gonyaulacaceans, which may represent early representatives of the *Gonyaulacysta* complex, and, has a first appearance in this zone (sample S58, 164.07 m). Likewise, *Endoscrinium*? spp. comprise a group with poorly developed cavation, which may be precursors of true species of this genus, although the FAD of this genus is in the *S. humphriesianum* zone as *Endoscrinium* spp. (Feist-Burkhardt and Wille, 1992). Globally, the first cavate gonyaulacacean is however, represented by the occurrence of *Cavatodissiliodinium hansgochtii* in the *W. laeviuscula* zone (Feist-Burkhardt and Monteil 2001). Thus the separation of wall layers appears to have been developed in gonyaulacaceans during the Early Bajocian.

In the *S. niortense* zone (163.40 to 154.71 m depth), nine dinoflagellate cyst taxa appear, seven of which are gonyaulacaceans (Table 3.2b). Notably, eight of the nine appearances recorded from the *S. niortense* zone occur in the lower part of the zone (161.40 to 157.37 m), which corresponds to the lowermost two subzones (*T. banksi*/*C. polygiralis*). There is only one appearance in the overlying *G. baculata* subzone (Table 3.2b).

The appearance of *Ctenidodinium cornigerum* in sample S65 (160.90 m) represents the FAD of this species, which was previously recorded from the *P. parkinsoni* zone of the Upper Bajocian (Feist-Burkhardt and Monteil, 1997; Poulsen, 1998). *Ctenidodinium continuum* and *Gonyaulacysta pectinigera* appear in this zone (sample S65/160.90 m, and sample S75/156.82 m respectively) which mark the FADs of these species. This is consistent with Feist-Burkhardt and Wille (1992). My work further refines the FADs of *C. continuum* and *G. pectinigera* to the lower half of the *S. niortense* zone (*T. banksi/C. polygiralis* subzones). The occurrence of *Korystocysta pachyderma* in the *G. baculata* subzone (sample S82, 153.71 m) represents the FAD of the species which has previously been recorded from the *P. parkinsoni* zone of the uppermost Bajocian (Prauss, 1989). *Endoscrinium* sp. cf. *E. luridum* has been reported from the Upper Bajocian–Lower Bathonian of Australia by Mantle and Riding (2012), the FAD of this morphotype herein is the confined to the *S. niortense* zone. The occurrence of *Eodinia*? spp. may be an early representative (precursor) of this genus, as *Eodinia* sp. appears in the lowermost Bathonian, *Z. zigzag* zone (Feist-Burkhardt and Monteil, 1997).

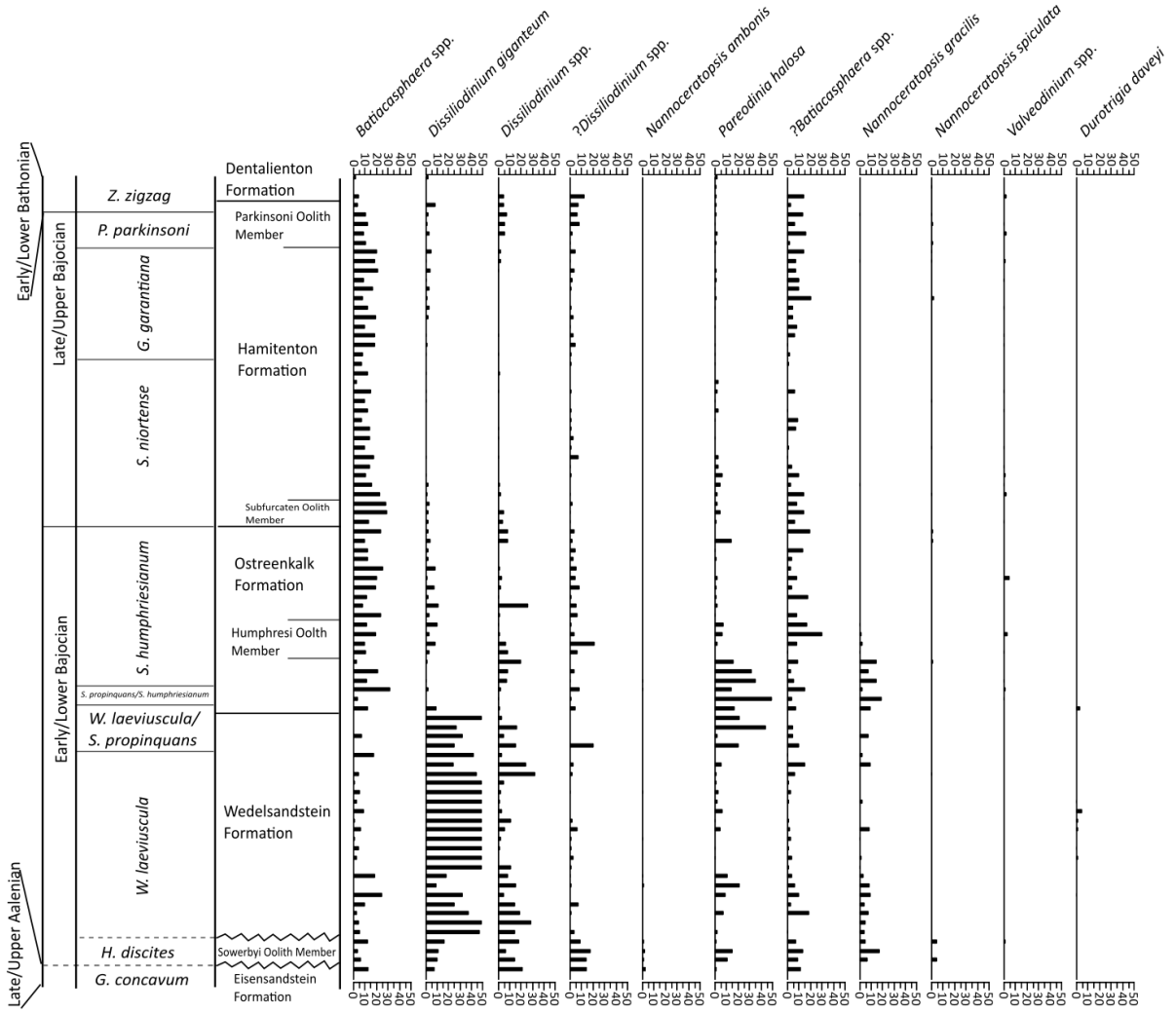

Figure 3.8a. Composite record of dinoflagellate cyst relative abundances from Swabia.
Abundances expressed as percentages of total dinoflagellate cysts, for taxa with appearances from the Upper Aalenian to Lower Bajocian. It can clearly be observed that *Dissiliodinium giganteum* is prominent through the Wedelsandstein Formation. Taxa with an abundance of <5% have been removed for clarity.

Non-gonyaulacacean taxa which occur in the *S. niortense* zone include *Valvaeodinium vermicylindratum* (sample S66, 160.53 m), the FAD of which has previously been reported from this zone (Feist-Burkhardt and Monteil, 1997). However, *Carpathodinium predae* (sample S70, 158.88 m) has a FAD in the *S. humphriesianum* zone (Feist-Burkhardt and Wille, 1992).

In terms of dinoflagellate cyst abundances, the most notable pattern of the Lower-Upper Bajocian is the moderate abundances of several gonyaulacaceans. In the *S. humphriesianum* zone (Ostreenkalk Formation) *Acanthaulax crispa, Batiacasphaera* spp., and the *Ellipsoidictyum*/*Valensiella* complex become moderately abundant, forming ~10–50% of dinoflagellate cysts (Figures 3.8a, 3.9). In the *S. niortense* zone (lower Hamitenton Formation), *Sentusidinium* spp., increase in abundance, forming ~10–30% of the dinoflagellate cysts, along with the aforementioned groups (Figures 3.8a, 3.9).

3.3.2.4. Upper Bajocian to Lower Bathonian: G. garantiana, P. parkinsoni and Z. zigzag zones

There is a continuous increase in appearances through the Upper Bajocian and lowermost Bathonian in

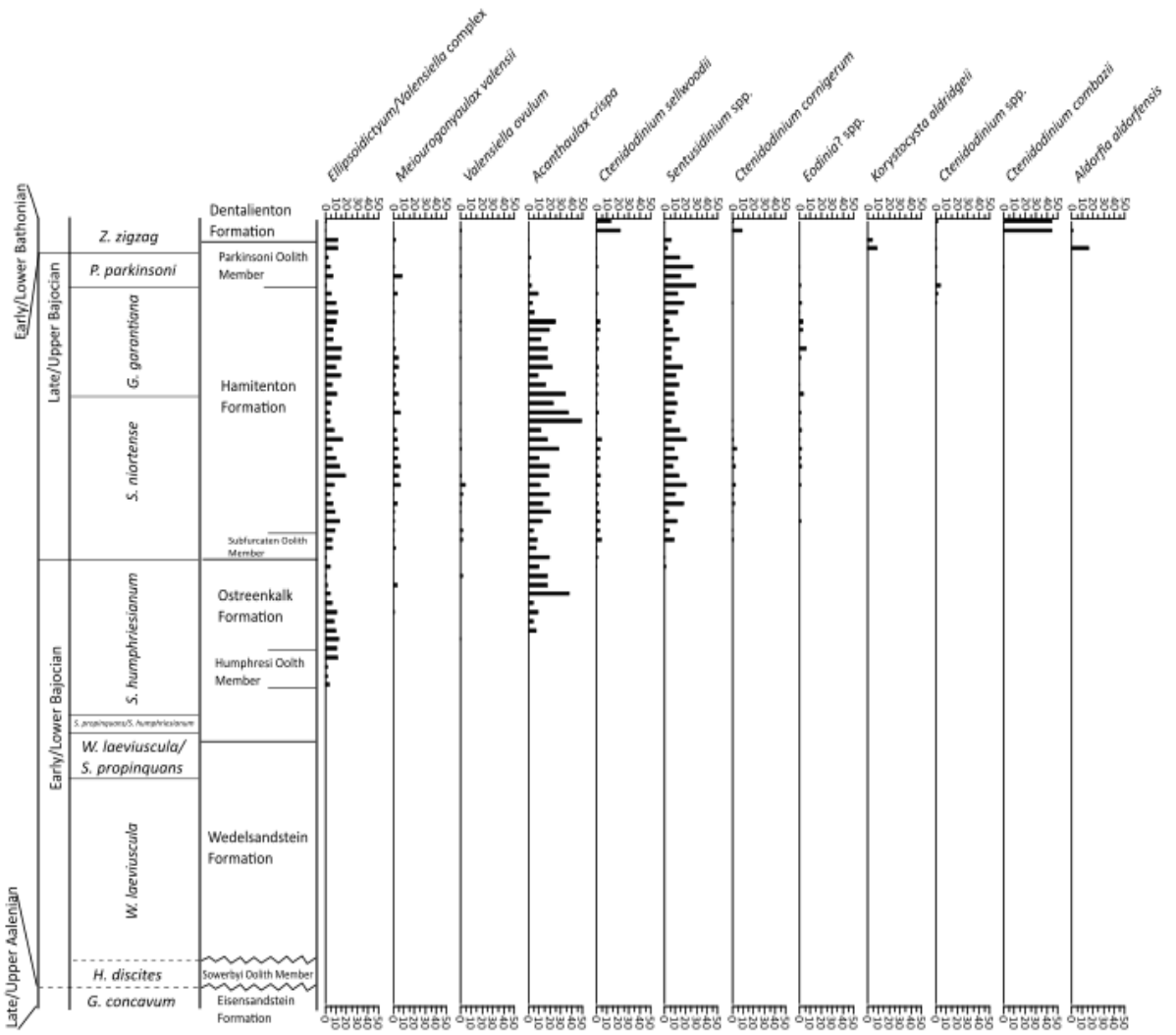

Figure 3.8b. Composite record of dinoflagellate cyst relative abundances from Swabia.
Relative abundances of taxa with appearances from the Lower Bajocian to Lower Bathonian. Through the Lower–Upper Bajocian transition and Upper Bajocian *Acanthaulax crispa*, *Batiacasphaera* spp., and *Sentusidinium* spp., are abundant, while in the Lower Bathonian, *Ctendodinium combazii* increases in abundance significant. Taxa with an abundance of <5% have been removed for clarity.

B404/2, including numerous FADs (Table 3.2b).

In the *G. garantiana* zone (153.50 to 145.05 m), eight taxa appear, seven of which are gonyaulacaceans. The appearance of *Dissiliodinium minimum* in sample S92 (148.90 m) lowers the FAD of this species, which was previously recorded from the overlying *P. parkinsoni* zone (Feist-Burkhardt and Monteil, 1997). *Endoscrinium asymmetricum* and *Wanaea acollaris* appear in the uppermost part of the *G. garantiana* zone (samples S95 and S99, 147.55 m and 145.88 m). The FADs of these species are in the *S. niortense* and *S. humphriesianum* zones (Feist-Burkhardt and Wille, 1992). *Korystocysta aldridgeii* questionably occurs due to poor preservation in sample S89 (150.74 m).

Non-gonyaulacaceans to appear include the pareodiniacean *Protobatioladinium mercieri* in sample S84 (153 m), the occurrence of which lowers the FAD from the overlying *P. parkinsoni* zone (Feist-Burkhardt

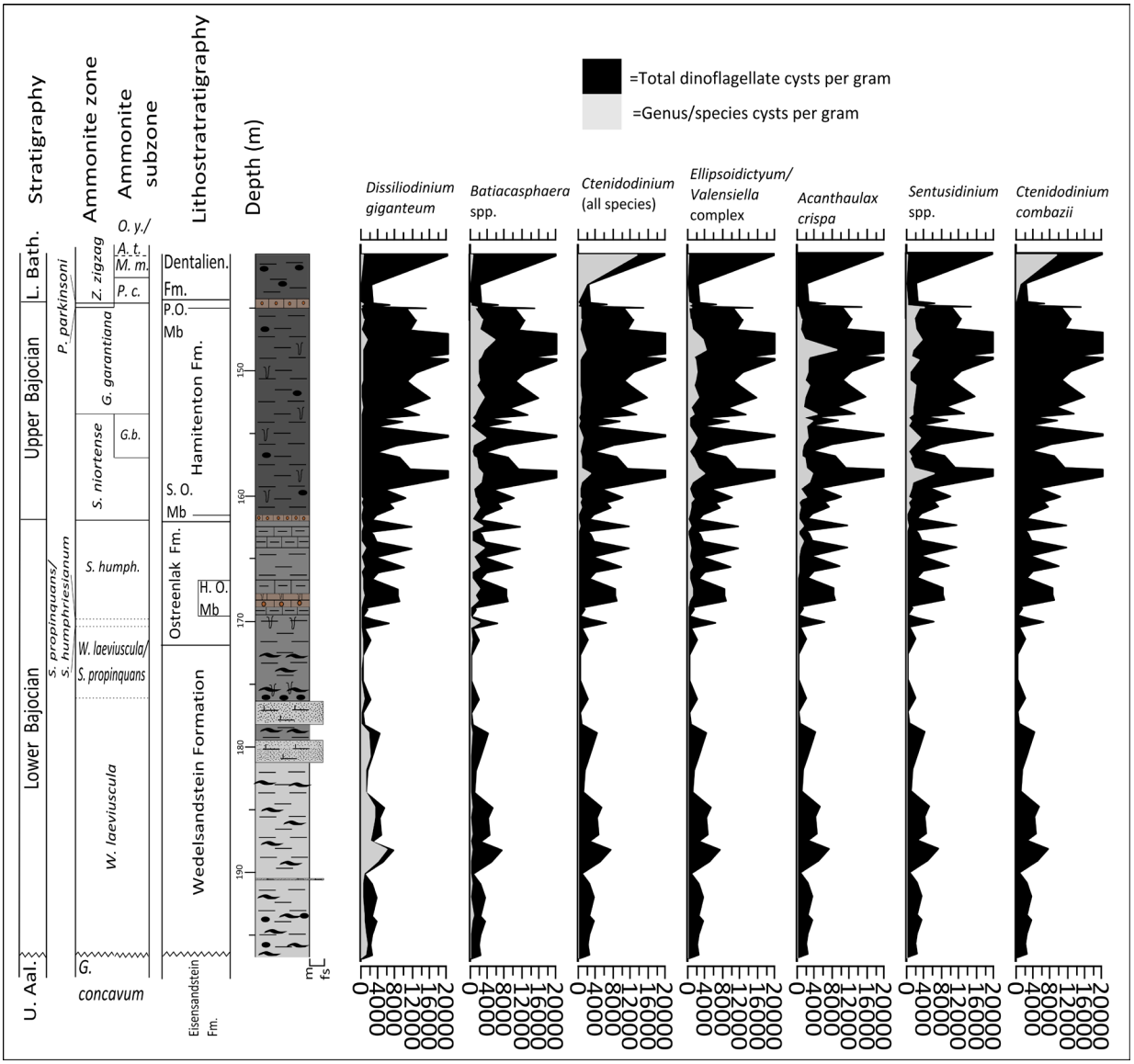

Figure 3.9. Absolute abundances of dominant groups of dinoflagellate cysts for borehole B404/2. Note the abundance of *D. giganteum* in the Lower Bajocian. This species declines in abundance through the Lower–Upper Bajocian tranisition as several other groups increase in abundance. The Lower Bathonian is marked by the increase in the abundance of *Ctenidodinium*, primarily *C. combazii*. After Wiggan et al. (2017) fig. 6.

and Pross, 1999). *Valvaeodinium spinosum* also appears in this zone (sample S97, 146.71 m) the FAD of which is in the *S. humphriesianum* zone (Feist-Burkhardt and Wille, 1992). *Mendicodinium* sp. also appears in sample S97 and is the first recorded example of this genus from the Bajocian of Germany, although it is long-ranging, with a FAD in the Pliensbachian of northern Germany as *M. reticulatum* (Morgenroth, 1970).

Eleven dinoflagellate cysts taxa, nine of which are gonyaulacaceans, appear in the *P. parkinsoni* zone (144.97 to 144.66 m). *Valensiella ampulla* appears in the lowermost sample, S102 (144.97 m), but has a FAD in the *G. garantiana* zone (Prauss, 1989). The occurrence of *Ctenidodinium combazii* in sample S103 (144.96 m) of the *P. parkinsoni* zone is consistent with the FAD of this species throughout Europe

(Feist-Burkhardt and Wille, 1992; Riding and Thomas, 1992). The occurrence of *Tubotuberella* sp. in sample S104 (144.91 m) is the lowest reported example of this genus in the Jurassic of Germany, previously recorded from the Lower Bathonian *Z. zigzag* zone as *Tubotuberalla dangeardii* (Feist-Burkhardt and Wille, 1992). However, the genus has been reported from Upper Bajocian (*G. garantiana* zone) of England by Woollam and Riding (1983) as *Tubotuberella* spp.. *Aldorfia aldorfensis* appears in sample S105 (144.66 m), though the FAD of this species is in the *S. humphriesianum* zone (Feist-Burkhardt and Wille, 1992). *Bradleyella* sp. also appears in S105, however, the FAD of this genus, as *B. adela*, is in the lowermost Bajocian (*H. discites* zone) (Riding and Thomas, 1992). *Korystocysta aldridgeii* unquestionably appears in sample S105. Other gonyaulacaceans to appear in the *P. parkinsoni* zone include *Korystocysta* sp. 2, and *Wanaea* sp. 1 and 2. These genera are known to have range bases in the *S. humphriesianum* zone (Feist-Burkhardt and Wille, 1992).

The non-gonyaulacacean forms to appear in the *P. parkinsoni* zone include the chorate *Impletosphaeridium* sp. 1 in sample S102. The pareodiniacean *Kalyptea stegasta* occurs in sample S105, the FAD of *K. stegasta* is in the *S. propinquans* zone (Feist-Burkhardt and Monteil, 1997).

Eight species appear in the *Z. zigzag* zone of the Lower Bathonian in B404/2 (144.61 to 140.8 m). Gonyaulacacean species include *Atopodinium polygonale*, *Ctenidodinium ornatum, Endoscrinium* sp.*, Gonyaulacysta jurassica* subsp. *adecta*, *Korystocysta gochtii* and *Meiourogonyaulax* sp. cf. *M. caytonensis*. The appearance of *Gonyaulacysta jurassica* subsp. *adecta* in sample S109 (140.8m) is consistent with the FAD of this species, which has previously been recorded from the *Z. zigzag* zone in southern England by Fenton et al. (1980). The FADs of *A. polygonale*, *C. ornatum* and *K. gochtii* are in the *S.humphriesianum* and *S. niortense* zones (Feist-Burkhardt and Wille, 1992). *Orobodinium* sp. A of Gocht and Wille (1990) is the only demonstrably non-gonyaulacacean taxon to appear in the *Z. zigzag* zone (sample S109). The FAD of which has been reported from the *P. parkinsoni* zone by Feist-Burkhardt and Monteil (1997).

Within dinoflagellate cyst assemblages, a similar pattern is seen through the *G. garantiana* and *P. parkinsoni* zones to that of the underlying *S. humphriesianum* and *S. niortense* zones. *Acanthaulax crispa*, *Batiacasphaera* spp.*,* the *Ellipsoidictyum/Valensiella* complex and *Sentusidinium* spp. remain the dominant groups (Figures 3.8b, 3.9). However, an abrupt change occurs in the *Z. zigzag* zone, where *Ctenidodinium* becomes superabundant, comprising 60–70% of the dinoflagellate cyst flora. This is predominantly due to a prodigious increase in the abundance of *Ctenidodinum combazii.* This species appears as a single specimen in sample S103 from the *P. parkinsoni* zone. It is also present in the lowermost *Z. zigzag* zone (*P. covergens* subzone) as a single specimen. However, in the *M. macrescens* and *A. tenuiplicatus* subzones, *Cteniodinium combazii* comprises 45% of the dinoflagellate cyst assemblage (Figures 3.8b, 3.9). A similar pattern is seen with *C. sellwoodii* and *C. cornigerum*, which both increase in abundance through the *Z. zigzag* zone.

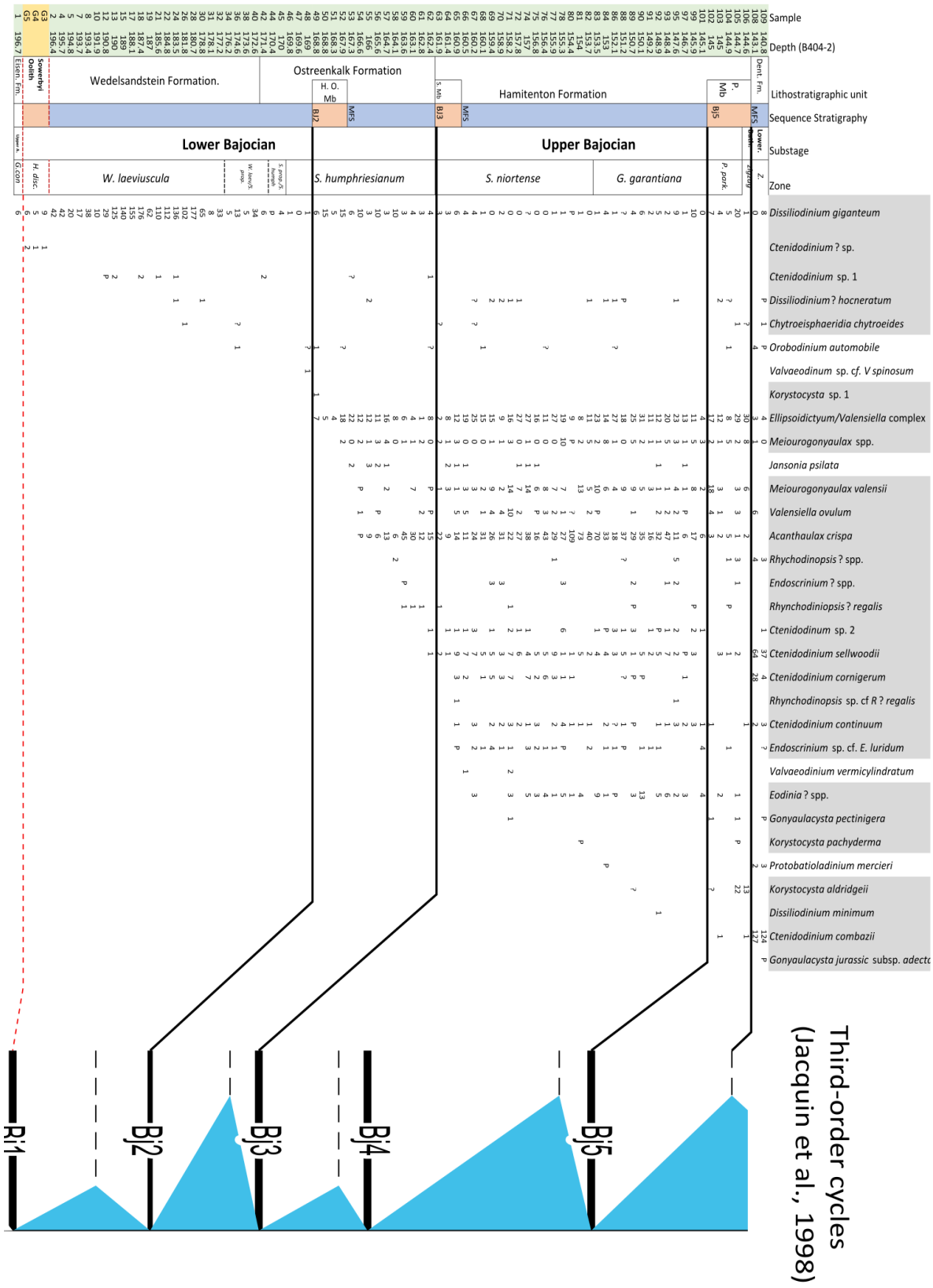

Figure 3.10. Composite range chart for Swabia with local appearances and long-ranging taxa removed. It can be observed that the majority of first appearances are recorded from the *S. humphriesianum* zone upwards. Comparison to the sequence stratigraphic record of Swabia shows that appearances in the *S. humphriesianum* zone correlate with third-order cycle Bj2. Appearances from the Upper Bajocian correlate with the third-order cycles BJ3 and BJ5.

3.3.3. The overall stratigraphic pattern of dinoflagellate cyst appearances in Swabia

At a broad scale, it can be seen that there is a relatively continuous pattern of appearances through the

Upper Aalenian to Lower Bathonian of Swabia. However, from the *S. humphriesianum* zone upwards, the newly appearing taxa are overwhelmingly dominated by the Family Gonyaulacacae, with the appearances of 44 gonyaulacacean species. When long-ranging taxa are removed from the dataset, it can be seen that the majority of gonyaulacacean first appearance datums are from the *S. humphriesinanum* zone onwards (Figure 3.10). As such, the Early–Late Bajocian transition appears to mark a critical point in the Bajocian diversification of gonyaulacacean dinoflagellate cysts.

Although confidence intervals have not been attached to the stratigraphic ranges of dinoflagellate cyst taxa, it can be observed that several ranges would have high confidence. The gonyaulacaceans *Acanthaulax crispa*, *Ctenidodinium sellwoodii, Ctenidodinium continuum, Meiourogonyaulax valensii*, the *Ellipsoidictyum/Valensiella* complex, appear through the Lower–Upper Bajocian transition (Figure 3.10). These taxa occur in almost every sample within their respective ranges (Tables 3.2a, 32.b). As such, the confidence intervals applied to these taxa would be high. In contrast, other gonyaulacaceans such as *Gonyaulacysta pectinigera*, *Korystocysta pachyderma*, and *Rhynchodiniopsis*? *regalis* have sporadic occurrences within their respective ranges, and thus lower confidence intervals. However, the high-resolution sampling of the Swabian succession should have minimised the chance of missing the first appearances of these taxa if they are significantly lower than the first appearances reported herein. Moreover, the integration of data from the Swabian Basin with others studied (Chapters 4 and 5), along with existing literature data (Chapter 8), should help negate the effects of diachroneity and localised appearances across a regional scale.

At a finer scale with the Swabian succession, comparison to the sequence stratigraphic records demonstrate the role of transgressive-regressive cycles in influencing the stratigraphic pattern of dinoflagellate cyst appearances in the Swabian Basin. Changes in relative sea level can truncate the range bases and range tops via condensation and erosion (Brett, 1995). In the B404/2 succession, appearances cluster around condensed transgressive deposits and maximum flooding surfaces at several points. Four appearances are recorded from the Humphriesi Oolith Member, which represents a condensed transgressive deposit, and overlies a sequence boundary (Table 3.2b). Furthermore, four appearances are recorded from samples in mudstone horizons (167.31 to 166.56 m) which immediately overlie the Humphriesi Oolith Member, and were deposited in association with a maximum flooding surface (Table 3.2, Figure 3.2b). Similarly, four appearances are recorded from the maximum flooding surface at the top of the Subfurcaten Oolith Member (Table 3.2b, Figure 3.3). Four appearances are also recorded from the lowermost sample of the Parkinsoni Oolith Member, which overlies a sequence boundary (Table 3.2b). Moreover, in addition to changes in sedimentation and erosion generated by fluctuations in sea level, palynological and sedimentological data record a shift to more distal palaeoenvironments through the B404/2 succession (section 3.5). This pattern may have also impinged on the pattern of dinoflagellate cyst appearances and abundances (section 3.5).

3.3.4. Recognition and correlation of the D. pinguis *and* D. romani *subzones of the* S. humphriesianum *zone in B404/2*

As previously mentioned, the base of the *S. humphriesianum* zone in southern Germany is lower than in other areas of Europe as the lowermost subzone, the *D. pinguis* subzone, is attributed to the *S. humphriesianum* zone rather than the uppermost *S. propinquans* zone (Feist-Burkhardt and Götz, 2016). In the B404/2 succession, the base of the Humphriesi Oolith Member represents sequence boundary Bj2 (Figure 3.3; Feist-Burkhardt and Götz, 2002). In the Paris Basin, Bj2 corresponds to a hiatus and consequently the *D. hebridica* subzone of the *S. propinquans* subzone is missing. The transgressive deposit which overlies Bj2 in the Paris Basin is of *D. romani* subzone age (Rioult et al., 1991). It is therefore possible that the Humphriesi Oolith Member, which overlies Bj2 in the Swabian Basin, is of equivalent age, which would place the base of the *S. humphriesianum* zone at the base of the Humphresi Oolith for the purposes of inter-regional correlation.

If the base of the *D. romani* subzone is taken at the base of the Humphesi Oolith member at 168.95 m, then the lowermost three samples (169.84 to 169 m) in the *S. humphriesianum* zone correspond to the *D. pinguis* subzone. In turn, this would correspond to the uppermost *S. propinquans* zone for regional correlation. This would mean the occurrence of *Valvaeodinium sp. cf. V. spinosum* would fall in the *S. propinquans* zone, whilst other appearances would still correspond to the *S. humphriesianum* zone.

3.4. Dinoflagellate cyst richness patterns

In terms of species richness, sample-based raw richness shows an overall steady increase through the Upper Aalenian to Lower Bathonian (Figure 3.11). It can also be observed that the increase in richness was primarily driven by the increased number of gonyaulacacean taxa. When richness per zone is plotted and taxa are allowed to range through (from their first to last occurrence in the Swabian succession), there is a similar pattern (Figure 3.12). The richness of the Swabian succession has also been analysed using sample rarefaction (Figure 3.13). Sample rarefaction allows the richness of an interval to be estimated at a lower number of samples, which in turn facilitates the richness of different intervals to be compared, independent of sampling intensity (Slater and Wellman, 2016 and references therein). Sample rarefaction was performed using PAST (Hammer et al., 2001). The sample rarefaction curves (Figure 3.13) supports an increase in richness through from the Upper Aalenian to the Lower Bathonian which is independent of sampling intensity. The richness of the Upper Bajocian and Lower Bathonian interval may however, be an underestimate, as the sample rarefaction curve has not plateaued. However, through the Swabian succession, the preservation of dinoflagellate cysts is generally poorer through the Upper Bajocian, with larger proportions of indeterminate dinoflagellate cysts recorded (Table 3.2a, b, data table appendix A.1). Poorer preservation through this interval may explain why the sample rarefaction curve indicates this interval was under-sampled, and consequently the richness through the Upper Bajocian in the Swabian Basin may be an underestimate relative to other regions. In terms of the total richness for the Bajocian, the Swabian succession is comparable to that of northern France; 74

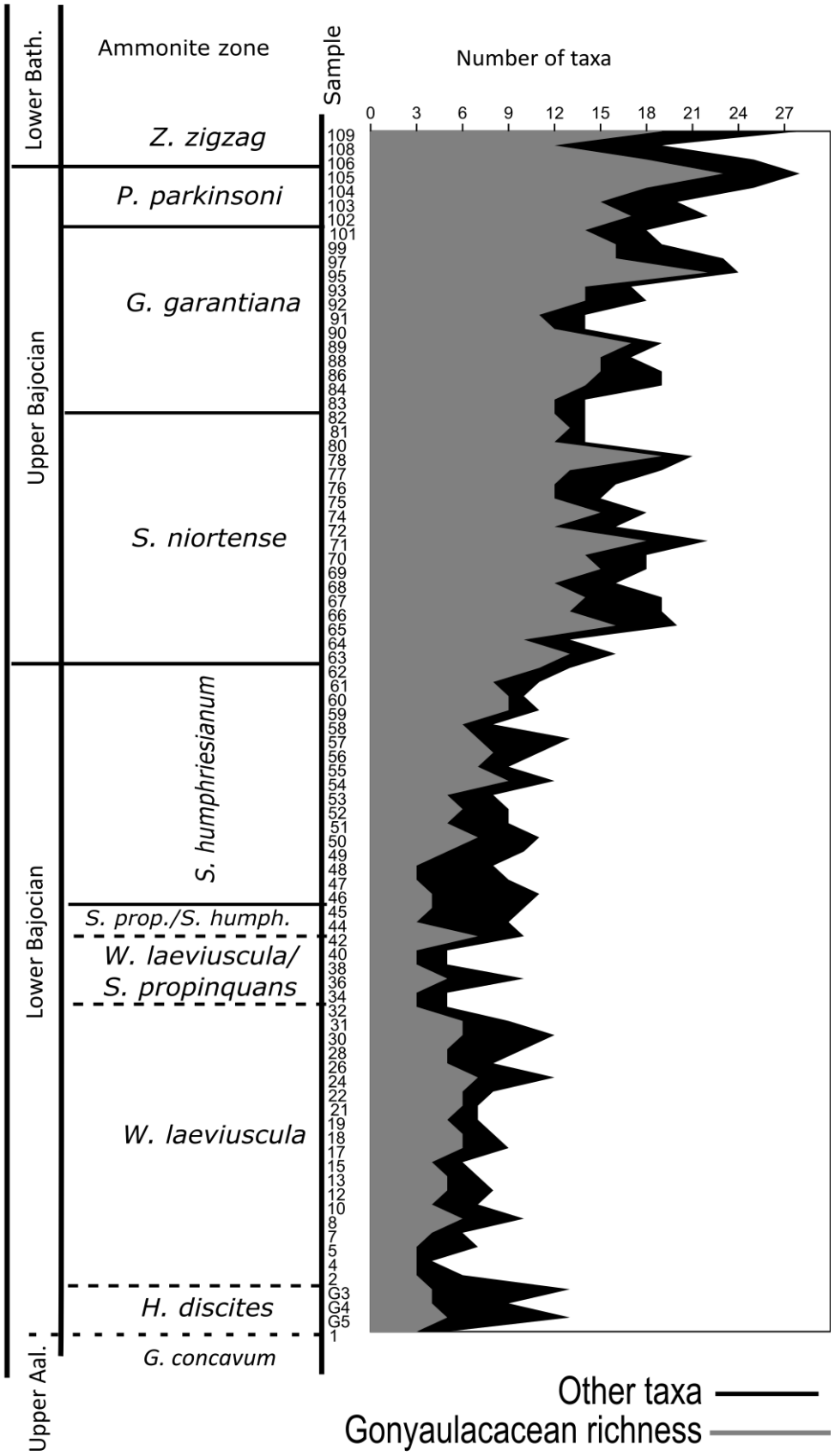

Figure 3.11. Number of taxa recorded per sample for the Swabian succession.
It can be observed that there is a gradual increase in richness which is primarily driven by an increase in the number of gonyaulacacean taxa.

Figure 3.12. Richness and percentage of gonyaulacacean taxa per zone for the Swabian succession. Grey fill denotes gonyaulacacean taxa, black denotes other taxa. Taxa have been allowed to range through from their first to last occurrence in the Swabian succession. There is an increase in the number and percentage of gonyaulacacean taxa through the Upper Aalenian to Lower Bathonian in Swabia.

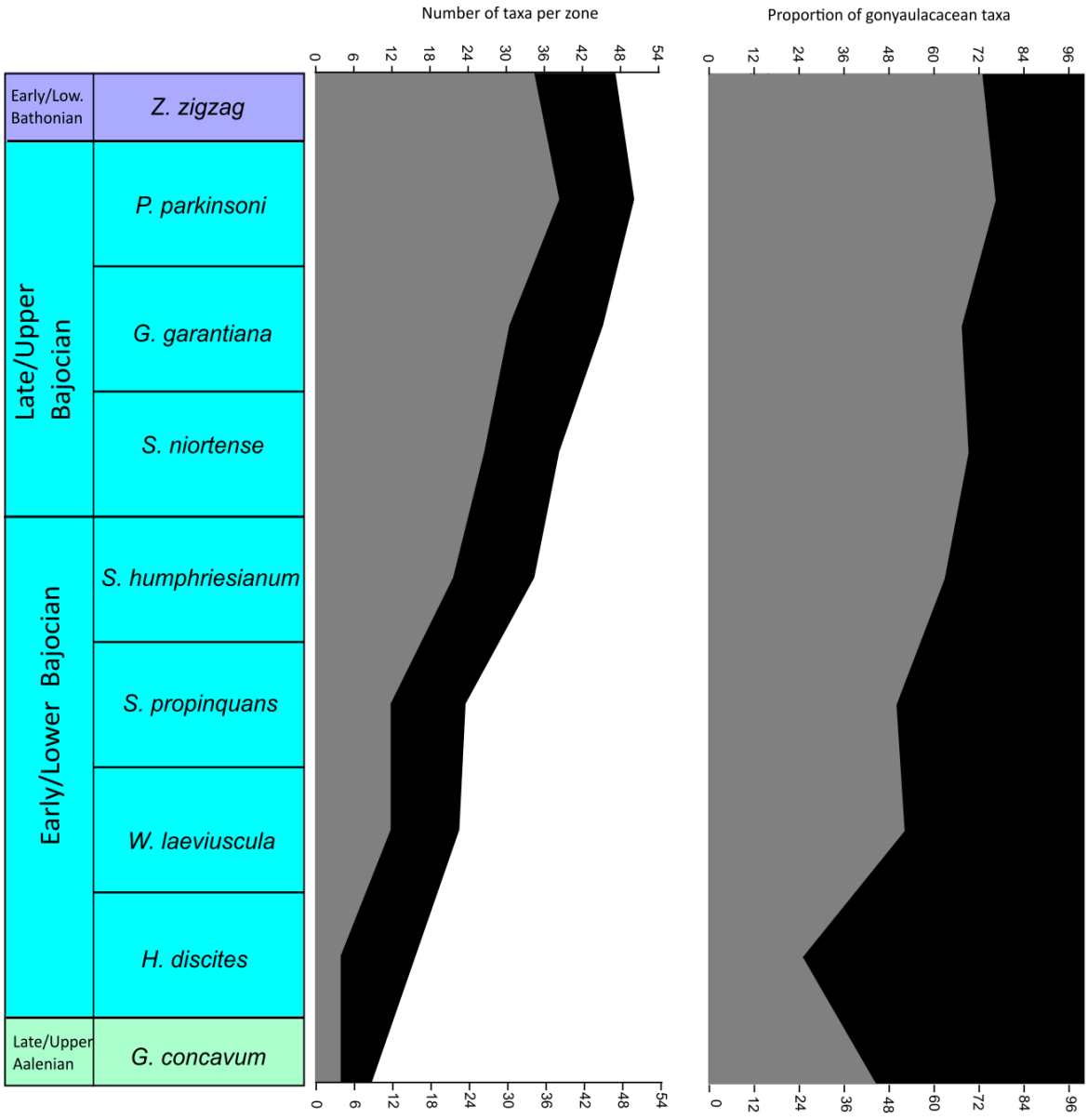

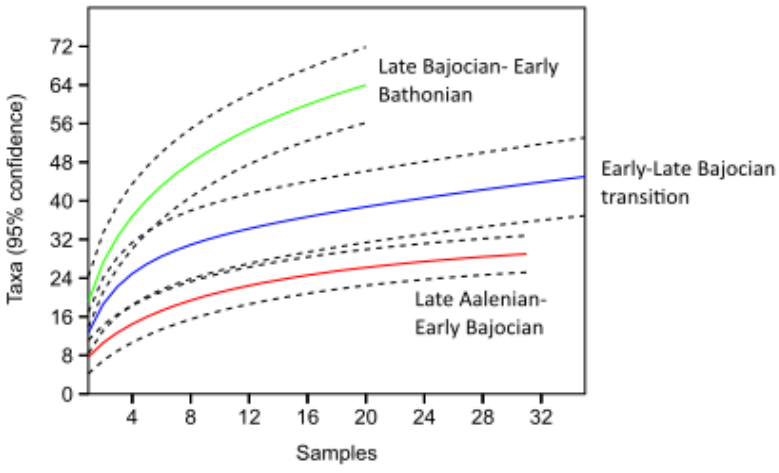

Figure 3.13. Sample rarefaction curve for the Swabian succession. There is an increase in richness from through the Bajocian regardless of number of samples examined. Dashed lines denote 95% confidence intervals.

as opposed to 76 taxa for the equivalent time slice. However, as aforementioned, poorer preservation through the Upper Bajocian may have resulted in an underestimate of richness through this interval relative to northern France.

3.5. Palaeoenvironmental interpretations from palynology

3.5.1. The B404/2 borehole

The palynomorph assemblages from the B404/2 Borehole succession record a shift to a more distal environment of deposition throughout the succession. The marine:terrestrial ratio is variable in the Lower Bajocian of B404/2, with significant terrestrial influxes in the lowermost and uppermost parts of the Wedelsandstein Formation (Figure 3.6). The latter was driven by a significant increase in the absolute abundances of spores and pollen, and is associated with an increase in the relative abundance of acanthomorph acritarchs, *Botryoccocus,* and prasinophytes (Figure 3.6; data table appendix A.2). This may indicate the influx of low-salinity surface waters, or a shift to a more proximal environment. Notably, the absolute abundance of acanthomorphs does not increase through this interval, instead, the relative abundance increase is driven by a decrease in the absolute abundance of dinoflagellate cysts (Figure 3.6).

Viewed on the microplankton-spores-pollen ternary plot, palynological assemblages from the Wedelsandstein Formation are predominantly represented by microplankton and trilete spores (Figure 3.14; data table appendix A.2). The high relative abundance of trilete spores in the Wedelsandstein Formation indicates that this unit was deposited in a relatively proximal palaeoenvironment, close to sources of terrigenous input. As the unit contains abundant trilete spores, and has numerous sandstone lenses and interbeds, it may have been deposited in a prodelta palaeoenvironment. The presence of abundant and relatively diverse dinoflagellate cysts (Figures 3.6; Table 3.2a), implies the environment of deposition was towards the distal part of the prodelta.

In the overlying Ostreenkalk Formation and succeeding units there is a trend of increasing, but fluctuating, marine influence (Figure 3.6). However, the trilete spores remain the dominant sporomorph group through the Upper Bajocian (Figure 3.6), strongly suggesting deposition in an environment in continued proximity to a source of terrigenous material. Viewed on the microplankton-spores-pollen ternary plot (Figure 3.14), the majority of samples from the Ostreenkalk Formation fall on the microplankton-dominated portion of the plot, whilst the overlying Hamitenton and Dentalienton formations fall wholly within the microplankton-dominated area. This indicates deposition in an offshore environment. Similarly, the sporomorph-acritarch-dinoflagellate cyst and acritarch-dinoflagellate cyst-prasinophyte ternary plots record a shift towards dinoflagellate cyst dominated assemblages through the Ostreenkalk, Hamitenton

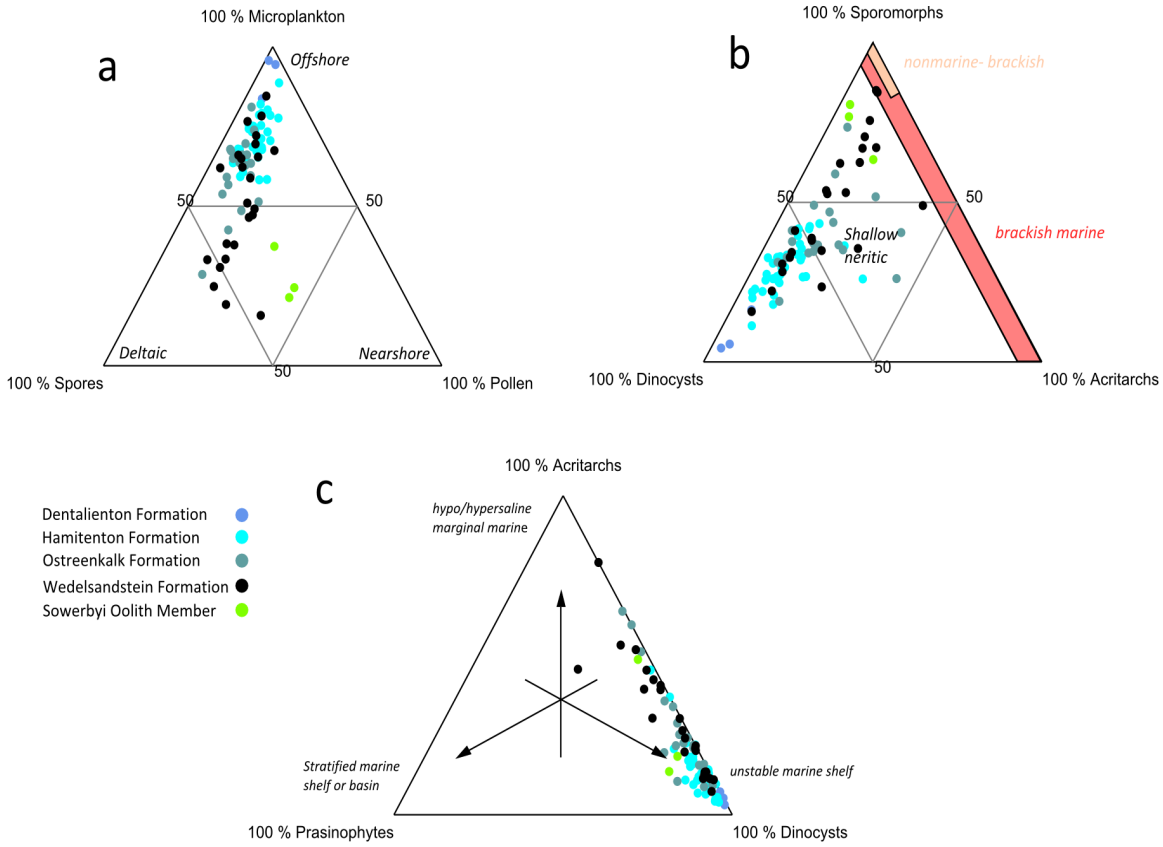

Figure 3.14. Ternary plots for Swabia.
a= microplankton-spores-pollen plot, after Federova (1977), Duringer and Doubinger (1985). b= sporomorph-acritarch-dinoflagellate cyst plot, after Burger (1980). c= phytoplankton plot, after Tyson (1993).
Plot A shows that the Lower Bajocian Wedelsandstein Formation is variably dominated by microplankton and spores. Samples from the Ostreenkalk Formation show less scatter between spores and microplankton, whilst the Upper Bajocian to Lower Bathonian Hamitenton and Dentalienton formations are microplankton dominated; samples from the Dentalienton Formation are overwhelmingly-dominated by microplankton. Similarly, plots b and c record a clear shift to dinoflagellate-cyst-dominated palynomorph assemblages in the Upper Bajocian. Dinoflagellate cysts are particularly prevalent in samples from the Lower Bathonian Dentalienton Formation.

and Dentalienton formations. Therefore, the succession overlying the Wedelsandstein Formation may reflect a deepening trend and landward shift in shelf facies over prodelta sediments, which is supported by the fining-upwards lithological trend. Macrofossils from the Ostreenkalk Formation are dominated by shallow-water bivalves whilst the overlying Hamitenton Formation contains abundant specimens of the heteromorph ammonite *Spiroceras*. Heteromorph ammonites are interpreted as reflecting deep, offshore conditions (Arkhipkin, 2014). Both palynological and macrofossil data therefore indicate a shift to a more offshore environment through the succession.

The increase in marine:terrestrial palynomorph ratio throughout B404/2 was driven by an increase in the abundance of dinoflagellate cysts. The absolute abundance of sporomorphs also increases, albeit slightly, through the Upper Bajocian. The increase in the absolute abundance of dinoflagellate cysts may be indicative of a more offshore palaeoenvironment, as the highest cyst concentrations in modern

sediments are on the continental slope (Wall et al., 1977). However, the increase in the abundance of both dinoflagellate cysts and sporomorphs may also indicate a lower sediment accumulation rate which has resulted in higher palynomorph per g concentrations. This is also consistent with a shift to a more distal environment of deposition. Alternatively, the increase in the abundances of dinoflagellate cysts and sporomorphs may be the result of the basinward transport of palynomorphs in the silt-sized sediment fraction associated with the trend to finer-grained lithologies throughout the Upper Bajocian. Sporomorphs become concentred in silty-clay sized sediments (Tyson, 1993 and references therein), whilst dinoflagellate cysts are medium to coarse silt in size, yet behave hydrodynamically like fine silt or clay (Dale, 1976). However, given the much larger increase in the abundance of dinoflagellate cysts relative to sporomorphs, it is likely the palynomorphs assemblages have recorded a primary signal of a shift to more offshore, distal palaeoenvironments. The Lower Bathonian Dentalienton Formation is marked by the maximum marine:terrestrial ratio, and a decline in the absolute abundance of terrestrial palynomorphs, which is strongly indicative of a offshore palaeoenvironment, which is likely the most distal of the succession. Acanthomorphs decline in absolute abundance in the Dentalienton Formation, whilst dinoflagellate cysts increase in abundance, this pattern indicates that acanthomorphs were less well adapted to offshore conditions compared to encysting dinoflagellates during the Mid Jurassic.

The steadily increasing, but fluctuating, marine:terrestrial ratio through the Upper Bajocian and Lower Bathonian, and the shift towards a more distal environment of deposition, is consistent with sedimentological and sequence stratigraphic interpretations, and reflects the T7 second order transgression. In particular, the maximum marine:terrestrial ratios in the lowermost Bathonian, and low abundance of sporomorphs, reflects the maximum flooding of the T7 cycle.

3.5.2. The Sowerbyi Oolith Member

The three samples from the Sowerbyi Oolith Member are dominated by terrestrial palynomorphs (Figure 3.14). The unit was probably deposited in a nearshore environment, slightly less proximal to an area of terrigenous discharge compared to the Wedelsandstein Formation due to the lower proportion of spores.

3.5.3. Dinoflagellate cyst abundance patterns

The pattern shown by the abundance data indicates that dinoflagellates were the ecologically dominant encysting organic-walled phytoplankton within the Swabian Basin, throughout most of the Late Aalenian to Early Bathonian (Figure 3.6). Within the dinoflagellate cysts, the following basic pattern can be discerned: super-abundance of *Dissiliodinium giganteum* in the Lower Bajocian Wedelsandstein Formation. This species declines in abundance in the lowermost Ostreenkalk Formation (*S. propinquans*/*S. humphriesianum* zone). This is then followed by the increase in abundance of the gonyaulacaceans *Acanthaulax crispa, Batiacasphaera* spp., the *Ellipsoidictyum*/*Valensiella* complex in the Ostreenkalk Formation (*S. humphriesianum zone*), which are accompanied by an increase in the abundance of

Sentusidinium spp. in the Hamitenton Formation (*S. niortense* to *P. parkinsoni* zones). The Lower Bathonian is marked by the increase in the abundance of *Ctenidodinium combazii* in the *Z. zigzag* zone (Figures 3.8a,b, 3.9). In broad terms, dinoflagellate cyst floras in B404-2 underwent a shift from the dominance of a single species, to more or less equal abundances of several groups, followed a shift back to the dominance of a single species.

3.5.4. Palaeenvironmetal implications for dinoflagellate cyst appearances, richness and palaeoecology

In terms of dinoflagellate appearances and richness, the steady increase in richness through the succession broadly mirrors the transgressive trend and shift to a more distal palaeoenvironment. In modern seas, there is a clear inshore-offshore trend in dinoflagellate cyst species composition and richness. There is a general increase in richness in an offshore direction, and maximum richness around the shelf-break (Wall et al., 1977). The increase in richness through the Swabian succession could therefore have been driven by a successional trend associated with a shift to a more offshore palaeoenvironment, with increased salinities. Further, the numerous appearances of gonyaulacaceans from the *S. humphriesianum* zone coincides with the pronounced transgressive pulse of third-order cycle Bj2 (Figure 3.10). This is associated with the transition from the prodelta Wedelsandstein to the shelfal palaeoenvironment of the Ostreenkalk Formation. Moreover, the transgressive trend and associated shift to a more distal palaeoenvironment through the Upper Bajocian–Lower Bathonian is associated with a significant increase in gonyaulacacean appearances and richness. As such, sea level and associated palaeoenvironmental shifts appear to be closely correlated with the increase in gonyaulacacean appearances and richness. Similarly, changes in dinoflagellate cyst abundances are clearly related to shifts in palaeoenvironmental setting, as controlled by sea level. As *D. giganteum* is abundant in the prodelta deposits of the Wedelsandstein Formation, this species may have thrived under conditions generated by terrigenous input (high nutrient levels/reduced salinities). Moreover, the decline of *D. giganteum* was coincident with the transition from prodelta to shelfal/offshore palaeoenvironments of the Ostreenkalk and Hamitenton formations. In particular, the abundance of the heteromorph ammonite *Spiroceras* in the Hamitenton Formation is indicative of a shift to a more offshore palaeoenvironment, which would have had reduced salinities. Consequently, the relatively subequal abundances of *Acanthaulax crispa*, *Batiacasphaera* spp, the *Ellipsoidictyum/Valensiella* complex, and *Sentusidinium* spp. may reflect that these groups were adapted to higher salinity conditions. The acme of *C. combazii* in the Lower Bathonian is coincident with the highstand conditions of the Dentalienton Formation, which reflects maximum flooding of the T7 second-order sea level cycle. Consequently, *C. combazii* may have been adapted to high salinity conditions. The changes in dinoflagellate cyst richness and abundances, and their relationship to palaeoenvironmental factors are explored fully in Chapter 8, with comparisons to other regions studied.

3.6. Summary

Detailed palynological analysis of the Upper Aalenian to Lower Bathonian strata of the Swabian

Basin has revealed that the stratigraphic pattern of the dinoflagellate radiation is more gradualistic and continuous in this region than the pattern observed by Feist-Burkhardt and Monteil (1997) from northern France. However, the majority of gonyaulacacean first appearances are recorded from the *S. humphriesianum* zone upwards, and taxa which appear through the Lower–Upper Bajocian transition to lowermost Bathonian are dominated by the family Gonyaulaceae. Comparison of palynological to sedimentological data demonstrates that the increase in appearances and richness through the Bajocian of Swabia broadly mirrors the transgressive trend of the T7 second-order transgression. On a fine scale appearances cluster above sequence boundaries and around maximum flooding surfaces. On a broader scale, the numerous appearances of gonyaulacaceans from the *S. humphriesianum* zone upwards is correlated with a pronounced third-order transgressive pulse, and progressive shift to a more distal depositional environment. Moreover, the abundance trends within dinoflagellate cysts clearly reflect changes in local palaeoenvironments, which reflect sea level fluctuations. The Early Bajocian was dominated by the abundance of *Dissiliodinium giganteum*, which may have thrived in the prodelta palaeoenvironments of the Wedelsandstein Formation. *Dissiliodinium giganteum* declined in abundance towards the end of the Early Bajocian as there was a shift to a more offshore palaeoenvironment in the Swabian Basin, which was associated with the broadly equal abundances of several gonyaulacacean groups. In the Early Bathonian, *Z. zigzag* zone, there was a marked increase in the abundance of *Ctenidodinium combazii*, which may have been driven by maximum transgression and associated distal offshore conditions. Although the increase in dinoflagellate cyst richness is associated with a shift to more distal palaeoenvironments throughout the Bajocian–Bathonian in the Swabian Basin, the increase in richness is comparable to that seen in northern France. During the Mid Jurassic, the northwest Paris Basin was part of an extensive carbonate ramp, and thus had a markedly different palaeoenvironment. In Chapter 8, the palynological records from the basins studied are directly compared to assess the role of local and regional palaeoenvironment shifts in controlling the stratigraphy and ecological pattern of the Bajocian dinoflagellate cyst radiation.

Chapter 4. The palynology of the uppermost Aalenian to Bajocian of the Wessex Basin, Dorset, southwest England, and the Lower Bajocian of the Isle of Skye, Scotland.

4.1. Introduction: the Wessex Basin

The Wessex Basin of southwest England contains some of the most famous and intensively studied Jurassic successions in the world. As a consequence, the Middle Jurassic of Dorset has a well-researched lithostratigraphic and biostratigraphic framework, ideal for examining the dinoflagellate cyst record. Although the palynology of the Middle Jurassic of Dorset has been relatively well studied (e.g. Davey, 1980; Fenton et al., 1980; Woollam and Riding, 1983; Bailey, 1987) there is no published work providing semi-quantitative palynological data on dinoflagellate cysts from the Bajocian. However, the Bajocian of Dorset is stratigraphically condensed, and the *S. humphriesianum* and *S. niortense* zones are poorly represented or missing in many successions (Rioult et al., 1991). Consequently, a complete stratigraphic record of the dinoflagellate cyst radiation in this region is not available. Nevertheless, the Lower Bajocian (*H. discites* to *S. propinquans* zones) is relatively complete, which provides useful stratigraphic and palaeoecological data on dinoflagellate cysts from this understudied interval, which is largely missing in the neighbouring Paris Basin. Moreover, two Bajocian successions have been studied, which has allowed the collection of spatial as well as temporal palynological data. The material presented in this chapter is based on microscope slides loaned from the British Geological Survey's micropalaeontology collections.

4.1.1. Geological Background of the Wessex Basin

Formed in the Permian from the rifting of Pangaea, the Wessex Basin was filled during the Late Permian to the Cretaceous (Lake and Karner, 1987). The depocentre is bounded by the Cornubian Massif to the west, the London-Brabant platform in the north and east and the Armorican Massif to the south (Lake and Karner, 1987) (Figure 4.1). The Aalenian to lowermost Bathonian of Dorset is represented by the Inferior Oolite Group, a unit of condensed fossiliferous micritic and oolitic limetones, deposited in a carbonate ramp environment with moderately shallow, often photic, water depths (Sellwood et al., 1991). Palynology samples were examined from one field outcrop and two borehole successions, which has allowed both temporal and spatial palynological data to be collected. The two key successions examined are the Lyme Bay and Winterborne Kingston boreholes, which span the Lower to Upper Bajocian. In these successions, the Bajocian is relatively expanded and is 12–14 m in thickness compared to sections exposed on the Dorset coast (~5 m: Sellwood et al., 1991). Additional samples were analysed from Horn Park Quarry in order to provide stratigraphic coverage of the Upper Aalenian.

4.1.2. Horn Park Quarry

Horn Park Quarry is a locality which exposes the Inferior Oolite Group, located near Beaminster in Dorset (Figure 4.2, 50.81487°N, 2.77241°W, NGR: ST 458 022). Two samples were examined to provide

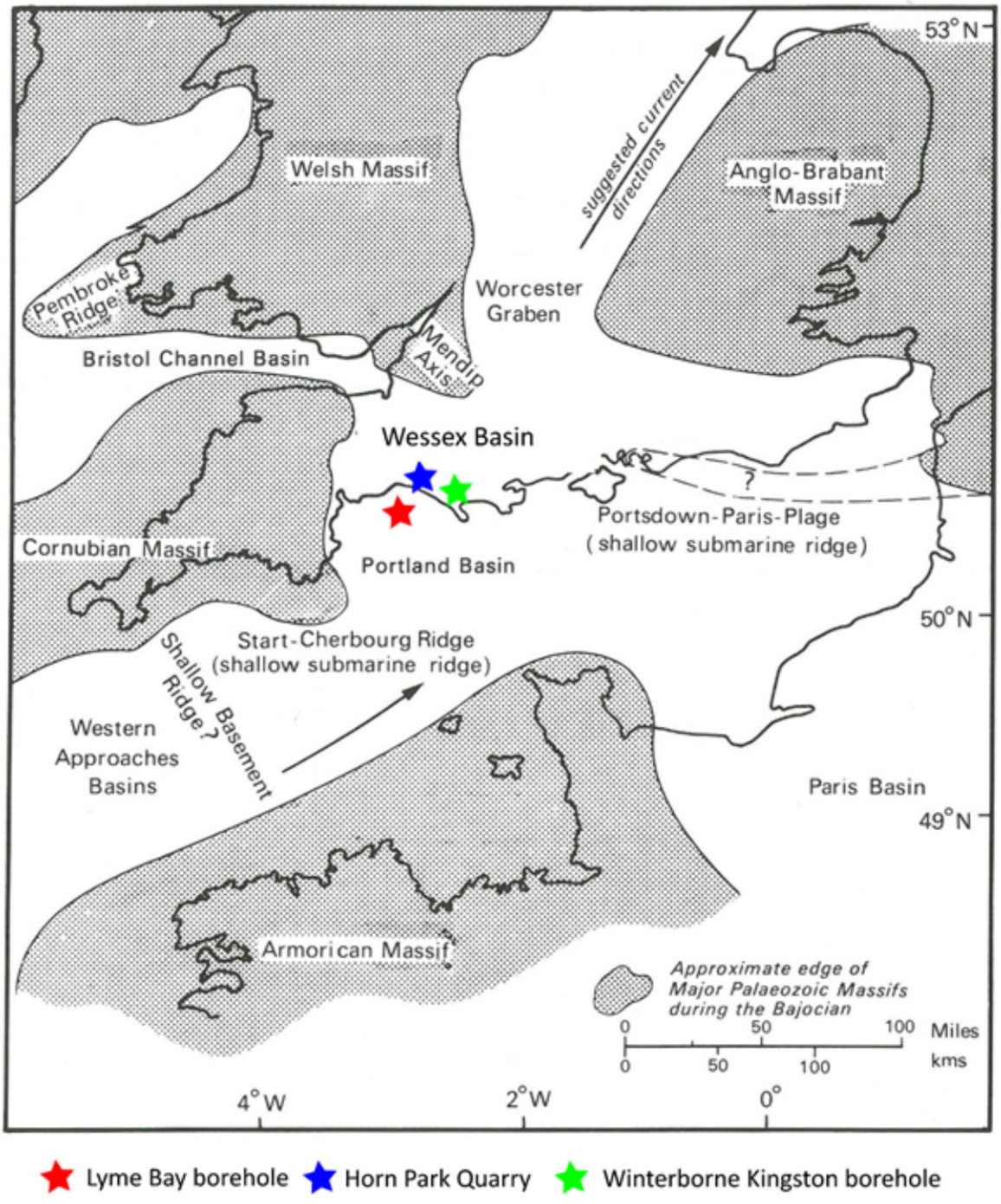

Figure 4.1. Palaeogeographic reconstruction of the Wessex Basin.
The locations of the successions examined are shown. Modified from Penn et al. (1980). Present day latitude and longitude is shown.

stratigraphic coverage of the Upper Aalenian *G. concavum* zone.

4.1.3. The Lyme Bay Borehole

The drill site of BGS offshore borehole 50/03 329 is located 10 km offshore from Lyme Regis, (Figure 4.2, 50.626428°N, 2.918189°W, NGR: SY 3515 8115). The borehole penetrated 19.30 m of ferruginous oolitic, pislithic and micritic limestones of the Inferior Oolite Group (Figure 4.3; Penn et al., 1980). The

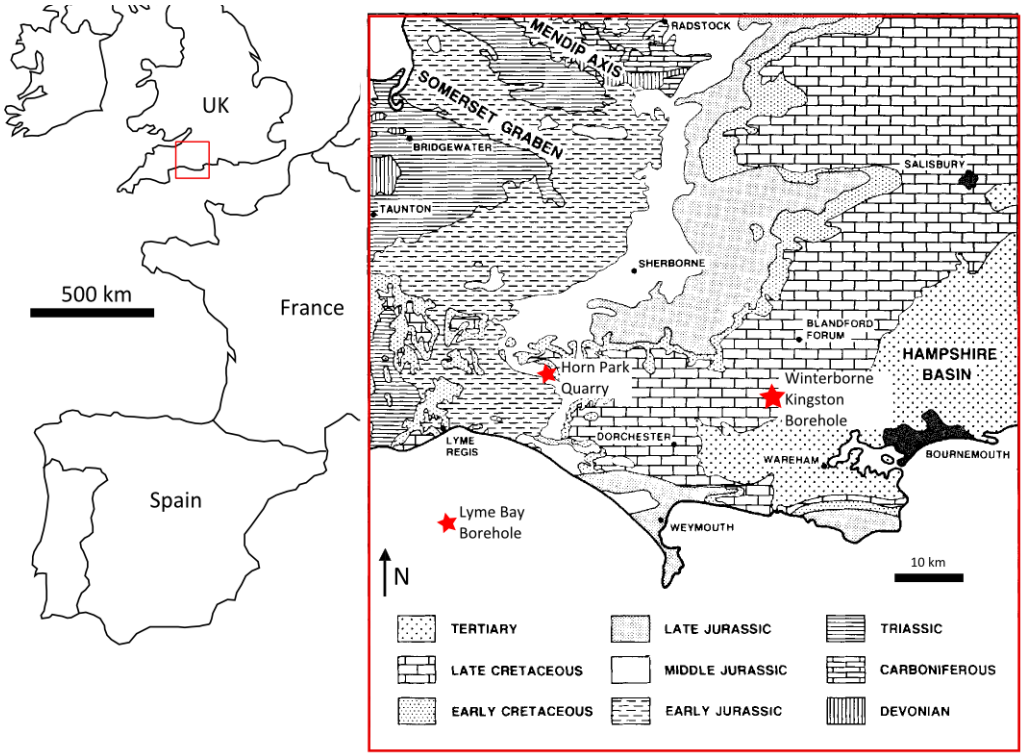

Figure 4.2. Locality map of Dorset, showing the locations of Horn Park Quarry, the Lyme Bay Borehole, and the Winterborne Kingston borehole.
Geological map modified from Bailey (1987) fig. 1.

ammonite zonation of the borehole is based on Penn et al. (1980), who used a combination of ammonites, other biostratigraphic indices and lithological correlations to onshore sections to provide a zonation for the succession. The Lower Bajocian *H. discites*, *W. laeviuscula* and *S. propinquans* zones (15.24 to 7.20 m) can be accurately recognised. The overlying *S. humphriesianum* and *S. niortense* zones are extremely thin (45 cm in total) and several subzones cannot be recognised. Only the lowermost subzone of the *S. humphriesianum* (the *T. blagdeni* subzone) can be recognised from ammonites and only the middle subzone, the *C. polygyralis*, can be recognised from the *S. niortense* zone. Core loss, and a lack of ammonites between 6.85 and 3.77 m, hamper the ammonite zonation of the Upper Bajocian. Penn et al. (1980) used the major bored horizon at 6.85 m as the base of the *G. garantiana* zone and recorded ammonites from 3.97 to 3.94 m that are indicative of the *P. acris* subzone. However, for the purpose of regional correlation, the *P. acris* subzone is treated as the lowermost subzone of the *P. parkinsoni* zone, rather than the uppermost subzone of the *G. garantiana* zone. Therefore, as no ammonites were recorded between 6.85 and 3.97 m, the *G. garantiana* zone cannot be recognised, and consequently this interval is referred to as the *G. garantiana/P. parkinsoni* zone (Figure 4.3).

The palynology samples were originally examined by Roger J. Davey, whose study of the palynology of the Lyme Bay Borehole was one of the earliest works on Bajocian dinoflagellate cysts from Europe. Davey (1980) noted the appearance and rapid diversification of gonyaulacacean dinoflagellate cysts through the Lyme Bay succession. As major advances in dinoflagellate cyst taxonomy have been made

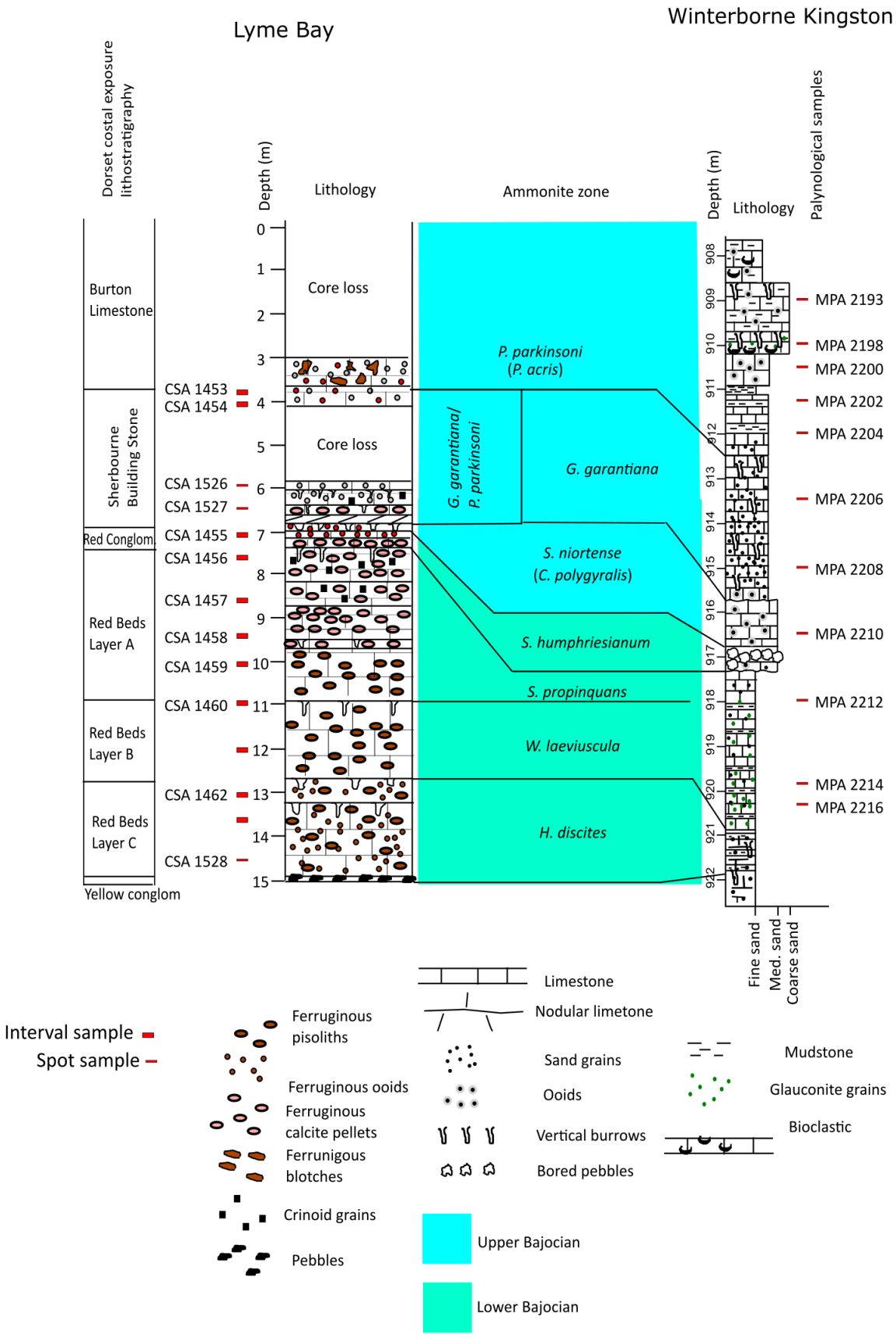

Figure 4.3. Sedimentary log and biostratigraphic correlation of the Lyme Bay and Winterborne Kingston boreholes.
Lyme Bay log modified from Penn et al. (1980). Winterborne Kingston log based on logging notes form Penn (1982). The distribution of palynological samples is shown.

since Davey (1980), the Lyme Bay succession is ideal for examining the radiation of dinoflagellates through the Bajocian of the Wessex Basin.

4.1.4. The Winterborne Kingston Borehole

The Winterborne Kingston Borehole is an onshore borehole, the drill site of which is located 20 km NE of Dorchester, Dorset (Figure 4.2, 50.780625°N, 2.075183°W, NGR: SY 9470 9796). The borehole penetrated 3000 m of ?Permian to Cretaceous strata, including the Middle Jurassic Inferior Oolite Group. The succession examined is similar in lithology to that of the Lyme Bay Borehole, and is represented by grey to green micritic, oolitic and shelly limestones (Figure 4.3, Penn, 1982). The ammonite zonation of the borehole is from Penn (1982), who based the zonation on ammonites, and other biostratigraphic indices and lithological correlation to coastal exposures. In the Lower Bajocian, the *H. discites* zone has been accurately recognised (921.65 to 920.80 m) and the base of the *S. humphriesianum* zone is marked by an erosional surface with cobbles and pebbles at 917.39 m (Figure 4.3). However, the *W. laeviuscula* and *S. propinquans* zones cannot be individually recognised so have been grouped together as the interval between the top of the *H. discites* zone and the base of the *S. humphriesianum* zone. The lowermost subzone, *D. romani*, is the only subzone recognised from the *S. humphriesianum* zone. The *S. niortense* zone is only partially recognised based on ammonites, and like Lyme Bay, is solely represented by the *C. polygyrlis* subzone. The boundary between the *S. niortense* zone and the *G. garantiana* zone is interpreted as a major lithological break at 915.84 m. The *P. acris* subzone is marked by an assemblage of ammonites at 912.84, this subzone has been taken as the base of the *P. parkinsoni* zone. Woollam (1982) gave a brief account of the dinoflagellate cyst assemblages from the Upper Bajocian and Lower Bathonian, and noted the similarity in taxonomic composition to those recorded from the Lyme Bay Borehole.

4.2. Sequence stratigraphic interpretations

Several studies have devised a sequence stratigraphic framework of the Inferior Oolite Group, which has been primarily based on outcrop exposures on the Dorset coast (Rioult et al., 1991; Jacquin et al., 1998). Using these interpretations, it may be possible to recognise sequences within the strata in the Lyme Bay and Winterborne Kingston boreholes, which provides useful palaeoenvironmental and stratigraphic data (Figure 4.4).

On the Dorset Coast, the lowermost Bajocian (*H. discites* zone) corresponds to the Yellow Conglomerate and Snuff Boxes, which are units deposited above sequence boundary Bj1 (Jacquin et al. 1998). The contact between the Snuff Boxes and the overlying Red Beds corresponds to a depostional hiatus (Figure 4.4). Rioult et al. (1991) interpreted this surface as the maximum flooding surface (MFS) of cycle Bj1, whilst Jacquin et al. (1998) interpreted this feature as sequence boundary Bj2. As this contact appears to be a depositional hiatus, rather than an erosional surface, I have used the interpretation of Rioult et al. (1991). This means that sequence boundary Bj2 (and possibly Bj3) is recognised as the erosional

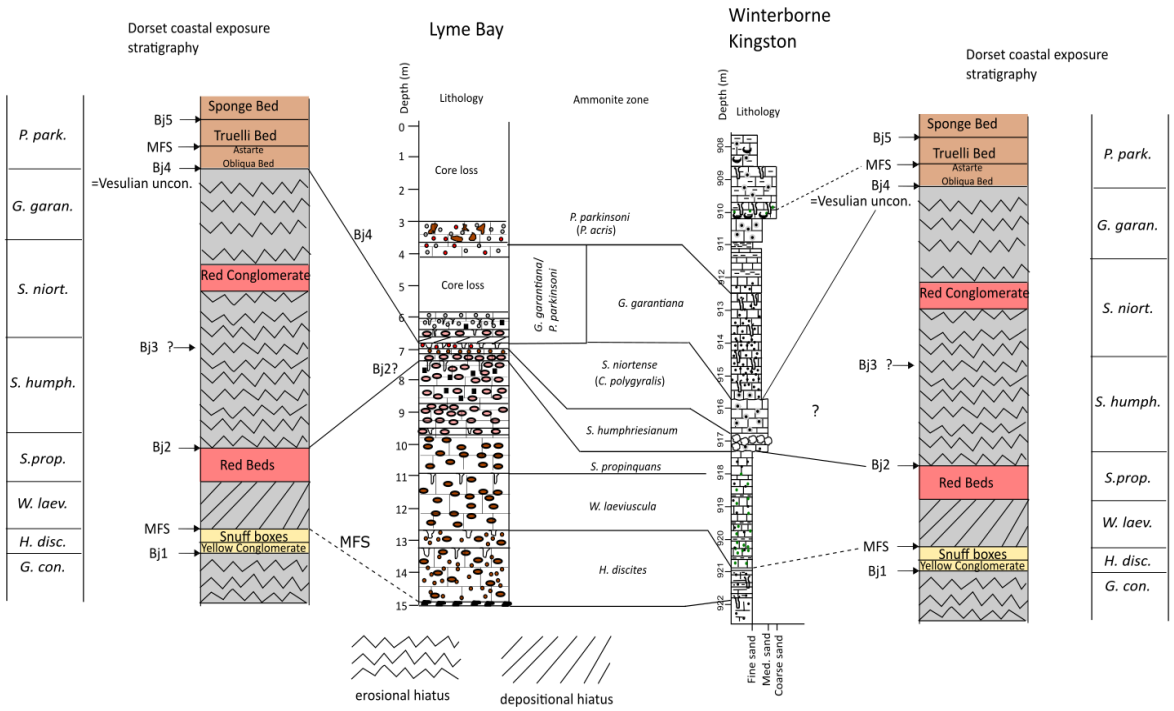

Figure 4.4. Sequence stratigraphic correlation of the Lyme Bay and Winterborne Kingston boreholes. Based on the interpretations of Rioult et al. (1991) and Jacquin et al. (1998) from coeval coastal exposure sections. Key as per Figure 4.3.

hiatus between the red beds and red conglomerate using Rioult et al. (1991)'s interpretations. In contrast, Jacquin et al. (1998) placed Bj3 as coincident with Bj4. On the Dorset coast, Bj4 corresponds to a time-gap termed the Vesulian Unconformity (equivalent of the Tarbert Unconformity in the North Sea), and is coincident with the transgressive surface (Jacquin et al., 1998). The MFS of cycle Bj4 is recognised as the contact between the Astarte Obliqua Bed and the Truelli Bed (Figure 4.4., Jacquin et al., 1998). Sequence boundary Bj5 is represented by an erosional surface between the Truelli Bed and the overlying Sponge Bed (Rioult et al., 1991).

In the Lyme Bay and Winterborne Kingston boreholes, sedimentation appears to have been more continuous than areas around the Dorset coast, as the succession is more complete, with fewer (obvious) depositional and erosional hiatuses. In Lyme Bay, the MFS of cycle Bj1 can be recognised as the contact between a conglomeratic unit at ~14.9 m and the overlying ferruginous oolitic and pisolithic limestones. The ferruginous limestones between ~14.9 and ~7.4 m are the lateral equivalent of the Red Beds. Sequence boundary Bj2 might be coincident with the maximum flooding surface, and represented by the intensely bored surface at ~7.4 m (Figure 4.4). Sequence boundary Bj3 cannot be recognised on the basis of sedimentological features in Dorset (Rioult et al. 1991). However, the fact that the lowermost subzone of the *S. niortense* zone, the *T. banksi* subzone, cannot be recognised in the Lyme Bay indicates that there is a time gap, which could represent Bj3. Similarly, the Vesulian Unconformity (Bj4) could be represented by the fact that the uppermost subzones of the *S. niortense* zone cannot be recognised in Lyme Bay.

In Winterborne Kingston, MFS of cycle Bj1 might be represented by the contact between glauconitic, and non-glauconitic limestones and mudstones at ~920.90 m, which corresponds to the boundary between the *H. discites* and *W. laeviuscula* zones. Sequence boundary Bj2 can be recognised as the sharp, erosional contact at 917.4 m. Bj3 might be represented by the fact that, as in Lyme Bay, the lowermost subzone of the *S. niortense* zone, the *T. banksi*, cannot be recognised, which may correspond to a time-gap. Bj4 can be recognised as the sharp, erosional contact at 915.8 m. As with Lyme Bay, the uppermost subzones of the *S. niortense* zone cannot be recognised, which indicate the unconformable nature of this contact. The MFS of cycle Bj4 might be represented by the burrowed, glauconitic horizon at ~910 m (Figure 4.4).

4.3. Materials

Microscope slides of palynomorphs from the Lyme Bay Borehole, the Winterborne Kingston Borehole and Horn Park Quarry were borrowed from the micropalaeontology collections of the British Geological Survey (BGS). As these samples had not been spiked with *Lycopodium* spores, absolute abundances could not be calculated. For the majority of the samples examined from the Winterborne Kingston Borehole succession, only one microscope slide was available. This means that some rare taxa may not have been recorded from these samples. However, as the Lyme Bay Borehole covers a similar stratigraphic interval to Winterborne Kingston, it is reasonable to assume that the number of taxa recorded in total is a good estimate of the total richness in the Wessex Basin.

From the Lyme Bay Borehole, ten interval samples (samples composed of material covering 0.5 to 1 m of strata), and four samples from individual horizons, were examined from an interval spanning the Lower Bajocian, *H. discites* zone to the Upper Bajocian *G. garantiana/P.parkinsoni* zone (Figure 4.3). For the Winterborne Kingston Borehole, ten samples were examined from the *W. laeviuscula/S. propinquans* to *P. parkinsoni* zones of the Bajocian (Figure 4.3). From Horn Park Quarry, two samples were examined from the Upper Aalenian *G. concavum* zone.

4.4. Palynology of the Wessex Basin

The palynological composition and stratigraphic distribution of dinoflagellate cysts is presented below for each succession studied. The taxa encountered are fully documented in Chapter 6, and the procedure followed for taxa left in open nomenclature is shown in Table 6.1.

4.4.1. Horn Park Quarry - Upper Aalenian, G. concavum *zone.*

The two samples from the *G. concavum* zone of the Inferior Oolite Group exposed at Horn Park Quarry contain abundant and well-preserved palynomorphs (data table appendix B.1). The lowermost sample (MPA 12155) is dominated by sporomorphs whilst the uppermost sample (MPA 12154) contains roughly equal proportions of marine and terrestrially-derived palynomorphs (Figure 4.5). Within both samples, the marine component is dominated by dinoflagellate cysts, whilst the majority of terrestrial palynomorphs are gymnosperm pollen (Figure 4.5).

Eleven dinoflagellate cyst taxa are present in the samples from Horn Park Quarry (Table 4.1). The gonyaulacaceans *Batiacasphaera* spp., *Dissiliodinium giganteum* and *Dissiliodinium* spp., occur in this zone. *Batiacasphaera* and *Dissiliodinium* are long-ranging with range bases in the Aalenian (Feist-Burkhardt and Wille, 1992). However, the occurrence of *Dissiliodinium giganteum* in this zone is coeval with the appearance of this taxon in Swabia (Table 3.2a). Non-gonyaulacaceans present in this zone include the long-ranging species *Mancodinium semitabulatum, Nannoceratopsis ambonis, Nannoceratopsis dictyambonis, Nannoceratopsis plegas, Nannoceratopsis spp*. and *Pareodinia ceratophora*, all of which have FADs in the Upper Pliensbachian to Aalenian (Feist-Burkhardt and Wille, 1992; Riding and Thomas, 1992). There is also a questionable occurrence (due to poor preservation) of *Phallocysta elongata.*

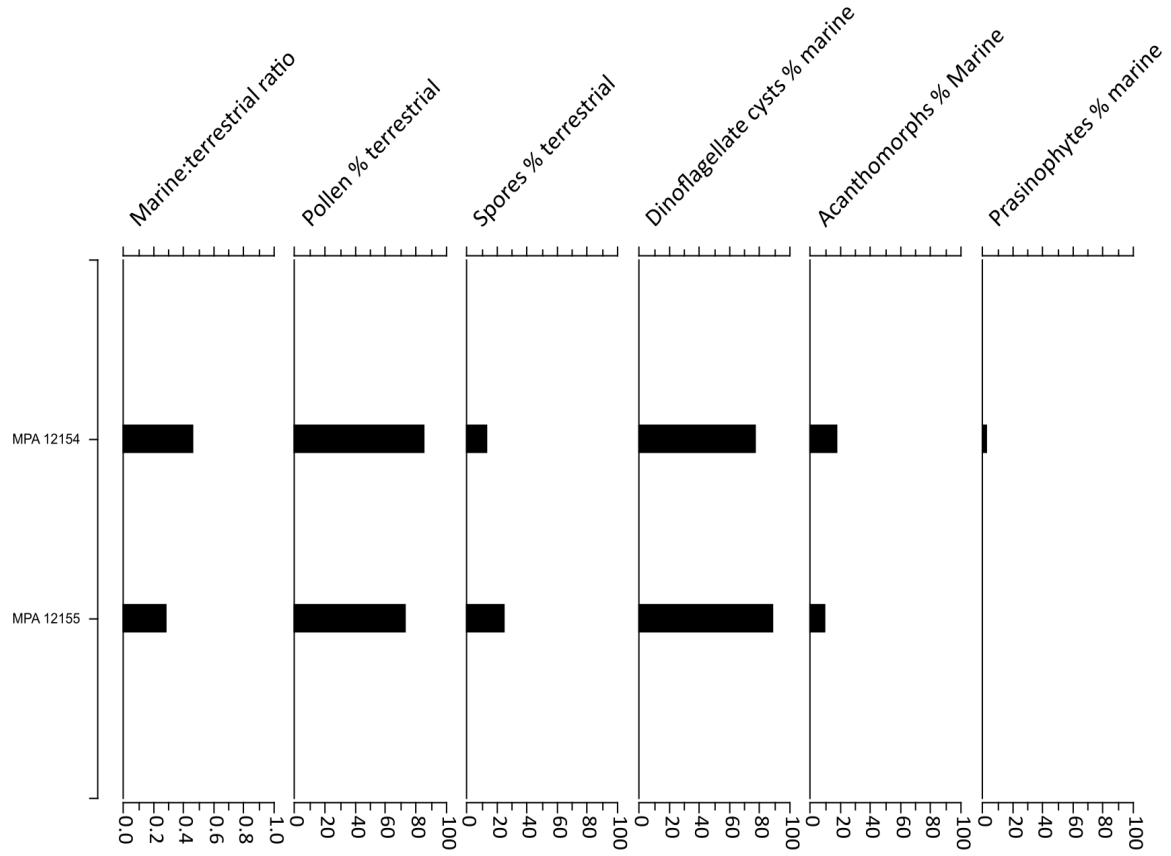

Figure 4.5. Relative abundances of main palynomorph groups from the Upper Aalenian to Horn Park Quarry.
Sporomorphs predominate, of which pollen is the main group. Within marine palynomorphs, dinoflagellate cysts are dominant.

In terms of abundances, the dinoflagellate cyst assemblages are dominated by *Nannoceratopsis gracilis*, which accounts for around 50% of the dinoflagellate cysts (Figure 4.6). *Dissiliodinium* spp. is also moderately abundant, making up 10–20% of the dinoflagellate cysts (Figure 4.6).

Sample	Ammonite zone	Total dinocysts	Dinocysts indet.	*Batiacasphaera* spp.	*Nannoceratopsis dictyyambonis*	*Phallocysta elongata*	*Dissiliodinium* spp.	*?Dissiliodinium* spp.	*Nannoceraptopsis gracilis*	*Mancodinium semitabulatum*	*Nannoceratopsis* spp.	*Nannoceratopsis plegas*	*Dissiliodinium giganteum*	*Nannoceratopsis ambonis*	*Pareodinia ceratophora*
MPA 12154	*G. concavum*	110	2	7	1		21	7	60	1		3	3	4	1
MPA 12155	*G. concavum*	78	9	6	1 ?		8	9	39	2	4				

Table 4.1. Dinoflagellate cysts recorded from the Upper Aalenian G. concavum zone of Horn Park Quarry. Grey fill denotes gonyaulacacean taxa.

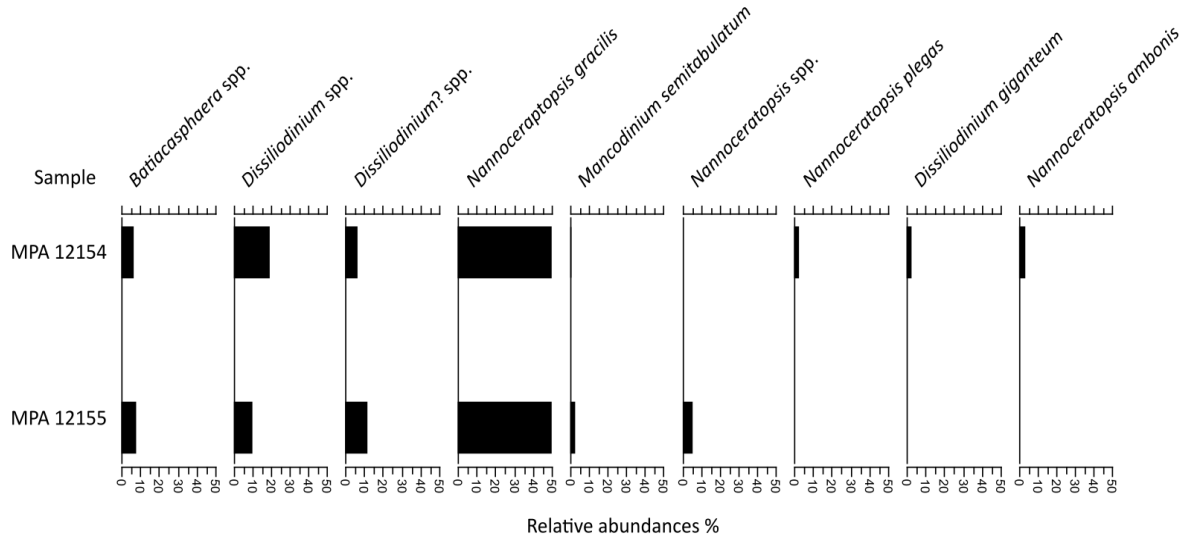

Figure 4.6. Relative abundances of dinoflagellate cysts from Horn Park Quarry. Expressed as percentage of total dinoflagellate cysts. *Nannoceratopsis gracilis* is the dominant species.

4.4.2. The Lyme Bay Borehole

The 14 samples from the Lyme Bay Borehole contain abundant, well-preserved palynomorphs, which are dominated by marine forms, the majority of which are dinoflagellate cysts (Figure 4.7; data table appendix B.1). Other marine palynomorphs include moderately abundant acanthomorph acritarchs (largely *Micrhystridium* spp.), foraminiferal test linings, and occasional prasinophytes (Figure 4.7, data table appendix B.3). Within the sporomorph component, gymnosperm pollen is the dominant group, with bisaccate pollen forming a significant component (typically 50–70%), relative to total pollen. Other palynomorphs include rare *Botryocccus* (data table appendix B.3). The marine:terrestrial ratio shows no temporal trend through the succession, and the relative abundance of dinoflagellate cysts also exhibits no trajectory (Figure 4.7).

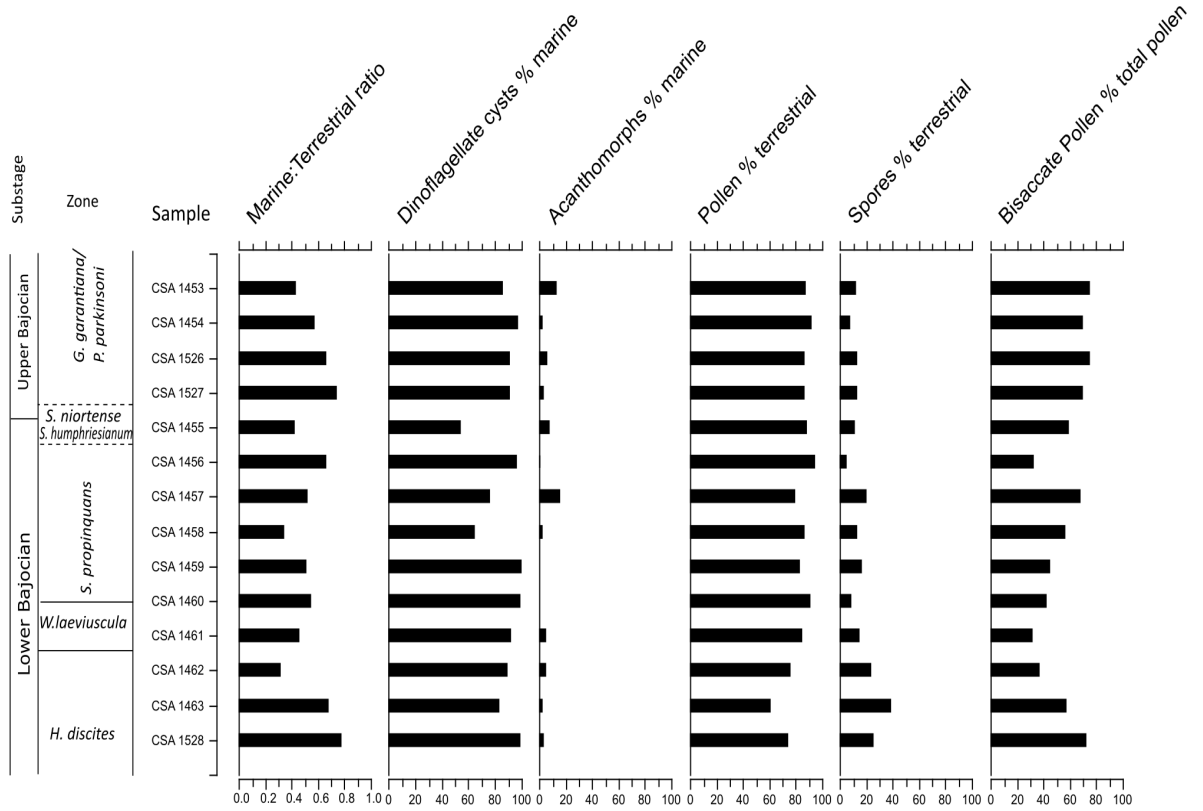

Figure 4.7. Relative abundances of main palynomorph groups from the Lyme Bay Borehole.
The marine:terrestrial ratio is variable with no systematic temporal trend. Within marine palynomorphs, dinoflagellate cysts are the dominant group. Within sporomorphs, pollen is dominant, of which bisaccate pollen forms a large proportion.

A total of 39 dinoflagellate cyst taxa were recorded from the Lyme Bay Borehole (Table 4.2). The pattern of appearances is continuous, although there are a particularly pronounced number of appearances in the *G. garantiana/P. parkinsoni* zone (Table 4.2). The stratigraphic succession of the borehole is subdivided into Lower Bajocian, Lower-Upper Bajocian transition and Upper Bajocian.

4.4.2.1. Lower Bajocian - H. discites to S. propinquans zones

Sixteen taxa appear through the Lower Bajocian *H. discites* to *S. propinquans* zones (15.24 to 7.20 m) in the Lyme Bay Borehole, and the pattern of appearances is relatively continuous (Table 4.2). In the *H. discites* zone (15.24 to 12.83 m), ten taxa appear, eight of which are gonyaulacaceans. The gonyaulacaceans *Batiacasphaera* spp., *Dissiliodinium* spp., and *Dissiliodinium giganteum* have range bases in the Middle to Upper Aalenian (Feist-Burkhardt and Wille, 1992). However, the appearance of *Durotrigia daveyi* and *Gongylodinium erymnoteichon* in the *H. discites* zone is consistent with the previously reported FADs of these species (Riding and Thomas, 1992). The occurrence of *Durotrigia* sp. cf. *D. daveyi* represents the lowest record of this taxon, which has been reported from the *W. laeviuscula* to *S. propinquans* zones in Swabia (Chapter 3, Table 2a), and from the *S. propinquans* zone of northern France (Feist-Burkhardt and Monteil, 1997). There is a questionable occurrence due to poor preservation of *Kallosphaeridium*?

Table 4.2. Quantitative dinoflagellate cyst range chart for the Lyme Bay borehole.
Grey fill denotes gonyaulacacean taxa. The depth and coverage of interval samples (*) is shown. The dashed red line signifies the unconformable nature of the Upper Inferior Oolite. Note the large number of appearances in the Upper Bajocian.

Sample	CSA 1453*	CSA 1454*	CSA 1526	CSA 1527	CSA 1455*	CSA 1456*	CSA 1457*	CSA 1458*	CSA 1459*	CSA 1460*	CSA 1461*	CSA 1462*	CSA 1463*	CSA 1528
Depth (m)	4.00-4.20	4.20-4.60	6	6.4	6.85-7.00	7.40-8.20	8.20-9.00	9.00-9.67	9.50-10.50	10.50-11.50	11.50-12.83	12.83-13.59	13.50-14.10	14.6
Lithostratigraphic unit	Upper Inferior Oolite					Middle Inferior Oolite								
Substage	Upper Bajocian					Lower Bajocian								
Ammonite zone	*G. garantiana/P. parkinsoni*				*S. humphriesianum/S. niortense*	*S. propinquans*				*W. laeviuscula/S. propinquans*	*W. laeviuscula*	*H. discites*		
Total dinocysts	112	167	179	199	67	180	108	66	153	161	125	84	170	201
Dinocysts indet.	25	21	10	24	15	33	27	21	12	31	24	28	41	20
Batiacasphaera spp.	26	8	41	34	29	99	59	27	24	49	38	28	37	139
?*Batiacasphaera* spp.	5	14	3	17	0	20	14	10	6	28	11	20	17	3
Dissiliodinium spp.	5	4	5			2	3	2	1	3	1		4	24
?*Dissiliodinium* spp.	9	7	10	4	1	3	1	1		4	2	4	11	6
Durotrigia sp. cf. *D. daveyi*											?			2
Nannoceraptopsis gracilis								1		1	5		36	1
Pareodinia halosa	1	1				3		1	4	P	14	3	7	6
Durotrigia daveyi						1			101	31	22	1	P	?
Mancodinium semitabulatum									2				1	
Dissiliodinium giganteum		1	3		2	2		2	1	4	3		14	
Pareodinia ceratophora													1	
Gongylodinium erymnoteichon			1						1	?			1	
Valvaeodinium spp.	1		2									?		
Kallosphaeridium ? hypornatum	6	3	2	2	4	14	4		1	8		?		
Durotrigia sp. 1			3			1				1	5			
Nannoceratopsis spp.						1				1				
Kallosphaeridium spp.		1						1						
Ellipsoidictyum/Valensiella complex	18	69	7	87	7	1								
Orobodinium automobile					2									
Sentusidinium spp.	2	2	2	10	2									
Valensiella ovulum		1	2	5	4									
Aldorfia aldorfensis			2		?									
Acanthaulax crispa	1	16	P	1	1									
Meiourogonyaulax spp.	5	11	63	6										
Ctenidodinium continuum	1		P	1										
Ctenidodinium cornigerum				2										
Endoscrinium asymmetricum				?										
Eodinia ? spp.		1		1										
Impletosphaeridium sp. 1	1			1										
Meiourogonyaulax sp. cf. *M. caytonensis*				1										
Meiourogonyaulax valensii		3	13	2										
Pareodinia sp. 1 of F-B & M 1997			?	1										
Nannoceratopsis spiculata	4		2											
Kalyptea sp.			1											
Korystocysta aldridgeii		P	1											
Ctenidodinium sellwoodii	1	1	3											
Kalyptea stegasta			1											
Gontaulacysta pectinigera		P	2											
Chytroeisphaeridia chytroeides		1												
Korystocysta gochtii		2												
Rhynchodiniopsis ? *regalis*	1													

hypornatum, which has a FAD in the *W. laeviuscula* zone (Feist-Burkhardt and Monteil, 1997). Non-gonyaulacaceans appearing in the *H. discites* zone include *Mancodinium semitabulatum*, *Pareodinia ceratophora*, *Pareodinia halosa* and *Nannoceratopsis gracilis*, which are long-ranging species with first appearances in the Pliensbachian to Aalenian (Prauss 1989; Riding and Thomas, 1992). In the sample CSA 1461 (12.83 to 11.50 m) from the *W. laeviuscula* zone, only *Durotrigia* sp. 1, appears. This bioevent is coeval with Swabia at a zonal level (Chapter 3, Table 2a). Sample CSA 1460 (11.50 to 10.50 m) spans

the *W. laeviuscula* and *S. propinquans* zone, where there is one appearance, *Nannoceratopsis* spp., which is a long-ranging group and was recorded throughout the Upper Aalenian to Lower Bathonian of Swabia (Chapter 3, Table 2a,b). In the *S. propinquans* zone (11.00 to 7.20 m) there are two appearances, the gonyaulacaceans *Kallosphaeridium* spp. and the *Ellipsoidictyum/Valensiella* complex. The former is long-ranging, with a FAD in the Lower Aalenian (Feist-Burkhardt and Wille, 1992). However, the *Ellipsoidictyum/Valensiella* complex has a FAD in the lowermost subzone (*D. pinguis/ D. hebridica*) of the *S. humprheisianum* zone in southern Germany. In other areas of Europe, the *D. pinguis/D. hebridica* subzone forms the uppermost subzone of the *S. propinquans* zone. In Lyme Bay, there is no subzonal control. However, given that the *Ellipsoidictyum/Valensiella* complex appears in the uppermost sample of the *S. propinquans* zone (CSA 1456, 8.20 to 7.40 m), it is possible that this corresponds to the *D. pinguis/D. hebridica* subzone and is thus coeval with southern Germany.

Dinoflagellate cyst assemblages through the Lower Bajocian in the Lyme Bay Borehole are dominated by *Batiacasphaera* spp., which comprises 20–70% of dinoflagellate cysts through this interval. There is also an acme of *Durotrigia daveyi* in the *S. propinquans* zone, where it represents around 60% of dinoflagellate cysts (Figure 4.8).

4.4.2.2. Lower-Upper Bajocian transition, S. humphriesianum and S. niortense zones

A single interval sample (CSA 1455, 7.00 to 6.85 m) spans the *S. humphriesianum* and *S. niortense* zones, both of which are stratigraphically thin and incomplete in the Lyme Bay Borehole (Penn et al., 1980). Four appearances and one questionable appearance are recorded from this sample. The appearances of the gonyaulacaceans *Acanthaulax crispa*, *Sentusidinium* spp. and *Valensiella ovulum* may be coeval with the appearance of these taxa in the *S. humphriesianum* zone in Swabia (Chapter 3). A questionable occurrence (due to poor preservation) of *Aldorfia aldorfensis* was recorded from this interval, the FAD of this species is known from the *S. humphriesianum* zone (Feist-Burkhardt and Wille, 1992). The only non-gonyaulacacean to appear in this interval is *Orobodinium automobile*, a species which has a FAD in the *W. laeviuscula/S. propinquans* zone in Swabia (Chapter 3, Table 2a).

In terms of relative abundances, dinoflagellate cyst assemblages through the Lower-Upper Bajocian transition are dominated by two groups, *Batiacasphaera* spp. and the *Ellipsoidictyum/Valensiella* complex. The former comprises ~40% of dinoflagellate cysts whilst the latter represents ~10% of the assemblage (Figure 4.8).

4.4.2.3. Upper Bajocian, G. garantiana/P. parkinsoni zones

Eighteen taxa appear through the *G. garantiana/P. parkinsoni* zone (6.85 to 3.77 m), with 13 of these belonging to the family Gonyaulacaceae. However, the majority of these taxa have FADs lower in the Bajocian in other areas of Europe. Several species of *Ctenidodinium*: *C. continuum*, *C. cornigerum* and *C. sellwoodii,* appear in this zone, these species have FADs in the *S. humphriesianum* and *S. niortense* zones in Swabia (Chapter 3; Table 2a). *Meiourogomyaulax* spp. appears in the lowermost sample CSA

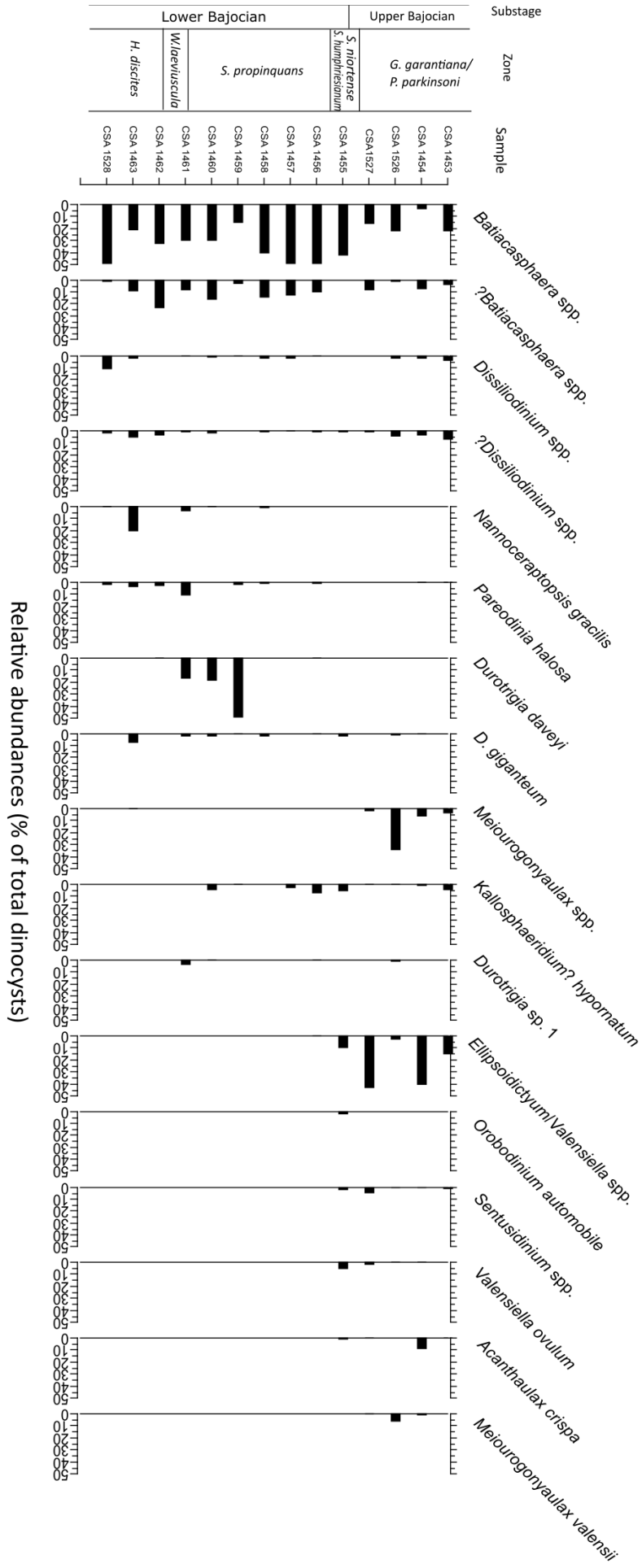

Figure 4.8. Relative abundances of dinoflagellate cysts from the Lyme Bay Borehole. *Batiacasphaera* spp. is abundant throughout the Bajocian, whilst the *Ellipsoidictyum/Valensiella* complex is abundant in the Upper Bajocian. Taxa with an abundance of <5% have been removed for clarity.

1527 (6.40 m), this group has a FAD in the *S. humphriesianum* zone of Swabia (Feist-Burkhardt and Götz, 2016). *Chytroeisphaeridia chytroeides* has a FAD in the *W. laeviuscula* zone in Swabia (Chapter 3). *Eodinia*? spp., *Rhynchodiniopsis*? *regalis*, *Korystocysta gochtii* and *Meiourogonyaulax valensii* all appear in the *S. humphriesianum* zone in Swabia. However, the occurrence of *Meiourogonyaulax* sp. cf *M. caytonensis* in sample CSA 1527 (6.40 m) appears to be the lowest record of this morphotype, which in Swabia occurs in the *Z. zigzag* zone (Chapter 3, Table 2b). *Endoscrinium asymmetricum* and *Gonyaulacysta pectinigera* appear in this zone, these species have FADs in the *S. niortense* zone in southern Germany (Feist-Burkhardt and Wille, 1992). The appearance of *Korystocysta aldridgeii* in sample CSA 1526 (5.00 m) is coeval with Swabia if this horizon corresponds to the *P. parkinsoni* zone, but would lower the FAD if it corresponds to the *G. garantiana* zone. Non-gonyaulacaceans to appear in the *G. garantiana/P. parkinsoni* zones include *Pareodinia* sp. 1 of Feist-Burkhardt and Monteil (1997), which appears in the lowermost sample (CSA 1527, 6.40 m) and has been previously been reported from the *P. parkinsoni* and *Z. zigzag* zones of France. Likewise, *Impletosphaeridium* sp. 1 appears in sample CSA 1527, and ranges from the *P. parkinsoni* to *Z. zigzag* zones in Swabia (Chapter 3, Table 2b). *Kalyptea* sp. and *K. stegasta*, both appear in sample CSA 1526 (6.00 m). The FAD of *Kalyptea stegasta* is in the *S. propinquans* zone (Feist-Burkhardt and Monteil, 1997). *Nannoceratopsis spiculata* appears in sample CSA 1526 but the FAD of this species is in the Aalenian (Riding and Thomas, 1992).

Dinoflagellate cyst assemblages in the Upper Bajocian of the Lyme Bay Borehole are dominated by two groups, *Batiacasphaera* spp. and the *Ellipsoidictyum/Valensiella* complex, which both form 10–40 % of dinoflagellate cysts. *Meiourogonyaulax* spp. is also moderately abundant in the *G. garantiana/P. parkinsoni* zone, forming up to 35% of the dinoflagellate cyst flora (Figure 4.8).

4.4.3. The Winterborne Kingston Borehole

The ten samples from the Bajocian of the Winterborne Kingston Borehole succession contain abundant palynomorphs, and preservation is generally good (Figure 4.9, data table appendix B.1). The proportion of marine to terrestrial-derived palynomorphs is variable throughout the succession (Figure 4.9). As is the case in the Lyme Bay Borehole, the marine component is dominated by dinoflagellate cysts, and the terrestrial dominated by gymnosperm pollen. Additional marine palynomorphs groups include moderately abundant acanthomorph acritarchs (predominantly *Micrhystridium* spp.), foraminiferal test linings and rare prasinophytes (Figure 4.9, data table appendix B.4). Other terrestrial palynomorph groups include trilete spores which occur in moderate abundance throughout the succession. *Botryococcus* is also present in low numbers in five samples, and the sphaeromorph acritarch *Fromea tornatilis* is present in two samples (data table appendix B.4).

The stratigraphic pattern of dinoflagellate cyst appearances seen in the Winterborne Kingston Borehole is broadly comparable to that of the Lyme Bay Borehole, with a total of 40 dinoflagellate cyst taxa recorded. There is a particularly high number of appearances in the *G. garantiana* and *P. parkisoni* zones

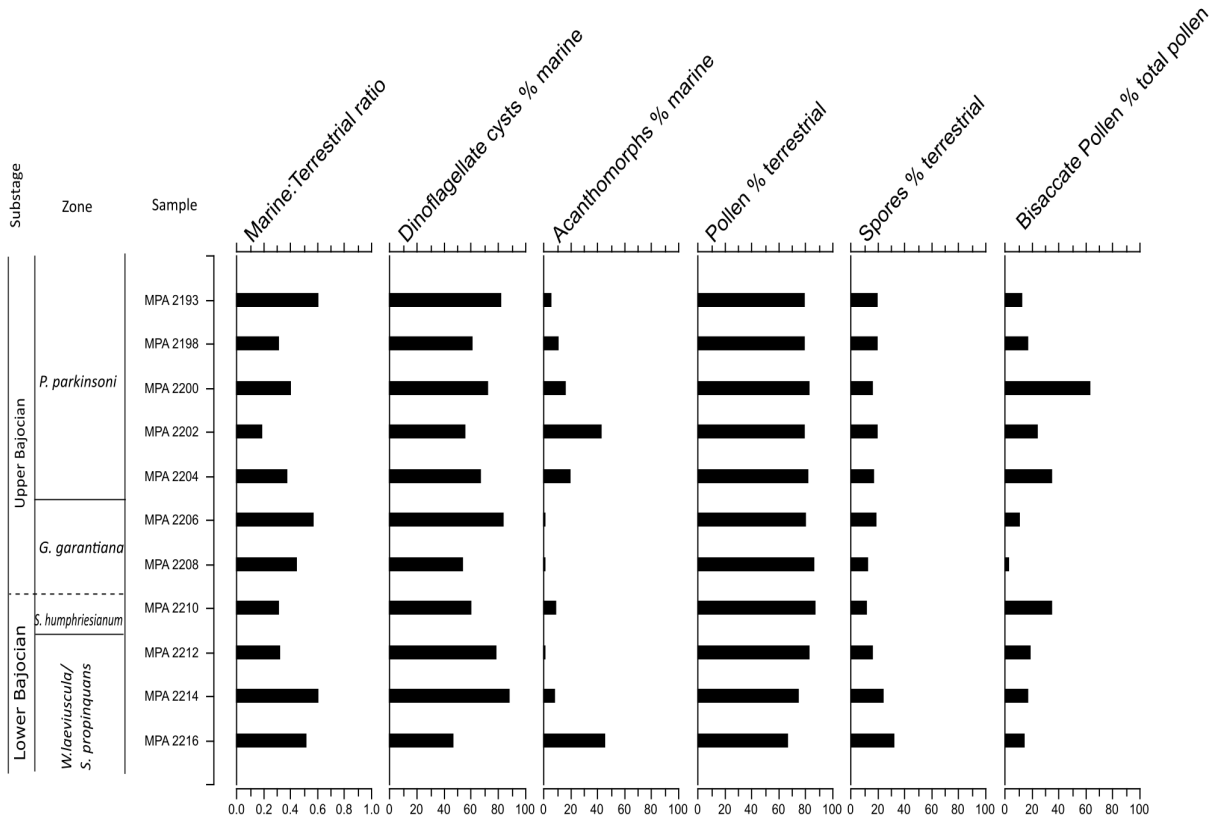

Figure 4.9. Relative abundances of main palynomorph groups for the Winterborne Kingston Borehole. The marine:terrestrial ratio is variable, with no systematic temporal trend. Within marine palynomorphs, dinoflagellate cysts dominate. Within sporomorphs, pollen dominates, of which bisaccate pollen forms a moderately abundant component.

(Table 4.3). As with Lyme Bay, the stratigraphic succession is subdivided into Lower Bajocian, Lower-Upper Bajocian transition and Upper Bajocian.

4.4.3.1. Lower Bajocian, W. laeviuscula/S. propinquans zones.

Ten dinoflagellate cyst taxa were recorded from the *W. laeviuscula/S. propinquans* zones (920.80 to 917.39 m), eight of which are gonyaulacaceans. The taxonomic composition is similar to that of the equivalent interval in the Lyme Bay Borehole, with the occurrences of gonyaulacaceans with FADs in the Aalenian such as *Batiacasphaera* spp., *Dissiliodinium* spp., and *Dissiliodinium giganteum* (Chapter 3; Feist-Burkhardt and Wille, 1992). Other taxa to occur include *Durotrigia daveyi*, *Durotrigia* sp. cf. *D. daveyi*, *Durotrigia* sp. 1 and *Gongylodinium erymnoteichon*, all of which appear in the *H. discites* and *W. laeiuscula* zones in the Lyme Bay Borehole. Non-gonyaulacaceans recorded from the *W. laeviuscula/ S. propinquans* zones include the long-ranging taxa *Mancodinium semitabulatum*, *Nannoceratopsis gracilis* and *Pareodinia halosa* which have FADs in the Pliensbachian–Toarcian (Riding and Thomas, 1992).

Within the dinoflagellate cyst assemblages, the lowermost sample of the Lower Bajocian, MPA 2216, is dominated by *Nannoceratopsis gracilis*, which forms over 50% of the dinoflagellate cyst flora (Figure

Table 4.3. Quantitative dinoflagellate cyst range chart for the Winterborne Kingston borehole.

Grey fill denotes gonyaulacacean taxa. The depth of each sample is shown. The dashed red lines denote stratigraphic breaks around the Lower–Upper Bajocian transition, particularly that of the unconformable Upper Inferior Oolite. Note the large number of appearances in the Upper Bajocian.

Sample	MPA 2216	MPA 2214	MPA 2212	MPA 2210	MPA 2208	MPA 2206	MPA 2204	MPA 2202	MPA 2200	MPA 2198	MPA 2193
Depth (m)	920.25	919.75	918	916.5	915	913.5	912	911.25	910.5	910	909
Lithostratigraphic Unite	Middle Inferior Oolite				Upper Inferior Oolite						
Substage	Lower Bajocian				Upper Bajocian						
Ammonite zone	*W. laeviuscula*			*S. humphriesianum*	*G. garantiana*		*P. parkinsoni*				
Total dinoflagellate cysts	72	159	76	58	74	145	78	33	87	58	151
Dinocysts indet.	4	8	12	6	13	24	14	5	13	8	16
Batiacasphaera spp.	1	54	22	17	7	9	11	7	31	14	5
?*Batiacasphaera* spp.	6	40	7	6	8	12	12	4		12	6
Dissiliodinium giganteum	1	22				1	1				1
Nannoceraptopsis gracilis	41	10	3								
Mancodinium semitabulatum	?	1									
Dissiliodinium spp.	9	9	1				2		4	2	3
?Dissiliodinium spp.	10	14	2	2	1	2	2		5	6	3
Durotrigia sp. 1		1									
Durotrigia sp. cf d. daveyi			18								
Durotrigia daveyi			9		?						
Gongylodinium erymnoteichon			1								
Durotrigia ? sp.			1								
Kallosphaeridium hypornatum				3			1			3	
Ellipsoididtyum/Valensiella complex				19	33	44	10	9	13	7	7
Acanthaulax crispa				4	2	30	1			?	
Meiourogonyaulax spp.				1		8		3	4	2	2
Pareodinia ceratophora					1	3	2	1			3
Ctenidodinium cornigerum					2	6	10		P		51
Meiourogonyaulax valensii					1	1	1	1	2		
Ctenidodinium sellwoodii					1				7	1	42
Rhynchodiniopsis ? spp.					2	1			1		
Impletosphaeridium sp. 1					3						
Kallosphaeridium spp.						1					
Ctenidodinium continuum						1	?			?	
Eodinia ? spp.						?					
Gontaulacysta pectinigera						1	1	?			
Rhynchodiniopsis ? *regalis*						?					
Korystocysta pachyderma						1		?			
Sentusidinium spp.							1		3	1	3
Nannoceratopsis spiculata							4	1			2
Korystocysta aldridgeii							5				
Endoscrinium luridum							?				
Korystocysta gochtii								?	1		
Lithodinia jurassica								1		1	
Korystocysta sp.2								1			1
Carpathodinium predae								?			1
Kalyptea diceras									1		
Chytroesphaeridia chytroeides									1		
Atopodinium polygonale									1	?	
Nannoceratopsis spp.										1	
Ctenidodinium combazii											4
Gonyaulacysta ? sp.											1

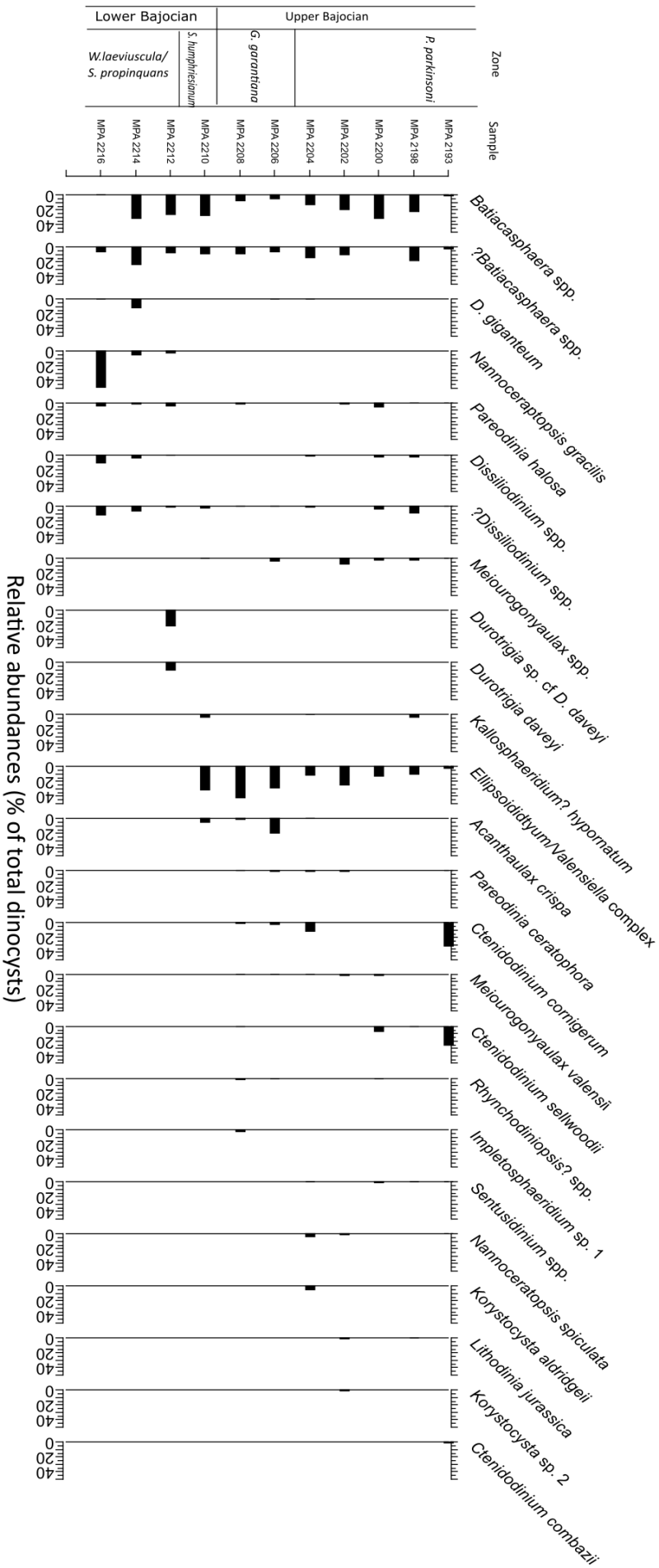

Figure 4.10. Relative abundances of dinoflagellate cysts from the Winterborne Kingston Borehole.

Batiacasphaera spp. is abundant throughout the Bajocian, whilst the *Ellipsoidictyum/Valensiella* complex is abundant in the Upper Bajocian. Taxa with an abundance of <5% have been removed for clarity.

4.10). The other two samples from the *W. laeviuscula/S. propinquans* zones (MPA 2214 and MPA 2212) are dominated by *Batiacasphaera* spp., which comprises 30% of dinoflagellate cysts (Figure 4.10). Sample MPA 2212 also contains moderate abundances (10–20%) of *Durotrigia daveyi* and *Durotrigia* sp. cf. *D. daveyi* (Figure 4.10).

4.4.3.2. Lower-Upper Bajocian transition, S. humphriesianum zone

Four dinoflagellate cyst taxa, all gonyaulacaceans, appear in sample MPA 2210 (916.5m) from the *S. humphriesianum* zone (Table 4.3). These are: *Acathaulax crispa,* the *Ellipsoidictyum/Valensiella* complex, *Meiourogonyaulax* spp. and *Kallosphaeridium*? *hypornatum*. The FADs of *A. crispa* and *Meiourogonyaulax* spp. have been widely reported from the *S. humphriesianum* zone (Chapter 3; Riding and Thomas, 1992; Feist-Burkhardt and Wille, 1992). *Kallosphaeridium*? *hypornatum* appears in the *W. laeviuscula* zone, whilst the appearance of the *Ellipsoidictyum/Valensiella* complex was recorded from the uppermost *S. propinquans* zone in the Lyme Bay Borehole (Table 4.2). The dinoflagellate cyst assemblage of sample MPA 2210 is dominated by *Batiacasphaera* spp., and the *Ellipsoidictyum/ Valensiella* complex (Figure 4.10).

4.4.3.3. Upper Bajocian, G. garantiana and P. parkinsoni zones

In the *G. garantiana* zone (915.84 to 912.45 m), ten taxa appear, eight of which are gonyaulacaceans (Table 4.3). *Ctenidodinium continuum*, *C. cornigerum* and *C. sellwoodii* appear in this zone, these taxa have FADs around the Upper-Lower Bajocian transition in Swabia (Chapter 3; Feist-Burkhardt and Wille, 1992). Other gonyaulacaceans also appear in this zone, and have FADs around the Lower-Upper Bajocian transition; these include *Gonyaulacysta pectinigera, Meiourogonyaulax valensii,* and *Korystocysta pachderma* (Chapter 3; Prauss, 1989; Riding and Thomas, 1992; Feist-Burkhardt and Wille, 1992). There are questionable appearances (due to poor preservation) of *Eodinia*? spp., and *Rhynchodiniopsis*? *regalis*, these taxa appear in the *S. humphriesianum* and *S. niortense* zones in Swabia (Chapter 3; Feist-Burkhardt and Wille, 1992). Non-gonyaulacaceans which appear in the *G. garantiana* zone include *Pareodinia ceratophora*, which is long-ranging, with a FAD in the Aalenian (Riding and Thomas, 1992; Feist-Burkhardt and Wille, 1992).

In the *P. parkinsoni* zone (912.45 to 909 m), 13 taxa appear, nine of which are gonyaulacaceans. The appearance of *Korystocysta aldridgeii* in sample MPA 2204 (912.00 m) of the *P. parkinsoni* zone is coeval with the appearance of this species in Swabia. Likewise, the appearance of *Korystocysta* sp. 2 in sample MPA 2202 (911.25 m) in this zone is consistent with the occurrence of this morphotype in the *P. parkinsoni* zone of Swabia (Table 3.2b). *Lithodinia jurassica* also occurs in sample MPA 2202; the FAD of this species is in the *S. humphriesianum* zone of Swabia (Feist-Burkhardt and Wille, 1992). *Atopodinium polygonale* appears in MPA 2200 (910.50 m), the FAD of this species is in the S. *humphriesianum* zone in Swabia (Feist-Burkhardt and Wille, 1992). Likewise, *Chytroesphaeridia chytroeides* also appears in sample MPA 2200, the FAD of this species in the *W. laeviuscula* zone in

Swabia (Chapter 3, Table 2a). The appearance of *Ctenidodinium combazii* in sample MPA 2193 (909 m) is consistent with the previously reported FAD of this species in the *P. parkinsoni* zone (Chapter 3; Feist-Burkhardt and Wille, 1992). There is a questionable occurrence (due to poor preservation) of *Endoscrinium luridum*.

The dinoflagellate cyst floras from the Upper Bajocian of the Winterborne Kingston Borehole are dominated by *Batiacasphaera* spp. and the *Ellipsoidictyum/Valensiella* complex, which both comprise 10–50% of dinoflagellate cysts through this interval (Figure 4.10).

4.4.4. The overall stratigraphic pattern

In terms of the stratigraphic pattern of dinoflagellate cyst appearances in the Wessex Basin, there is a relatively continuous pattern of appearances throughout the Upper Aalenian and Lower Bajocian, with few appearances around the Lower-Upper Bajocian transition (Table 4). There is a then a major increase in appearances in the Upper Bajocian *G. garantiana* and *P. parkinsoni* zones (Table 4). Comparison of stratigraphic data to the sequence stratigraphic record of the Bajocian in the Wessex Basin indicates that changes in relative sea level may have influenced the pattern of dinoflagellate cyst appearances, via large-scale changes in sedimentation and erosion. There are only five appearances recorded from the *S. humphriesianum*/*S. niortense* zones of the Wessex Basin, whereas there are 25 in Swabia, and 27 appearances in Normandy (Chapter 3; Feist-Bukhardt and Monteil, 1997). Only a single subzone can be recognised from each zone in the Lyme Bay and Winterborne Kingston boreholes. This is due to hiatuses associated with the development of sequence boundaries and sediment starvation in distal settings, which in turn has resulted in far fewer appearances being recorded from these zones. The most notable stratigraphic pattern in the Wessex Basin is the marked increase in appearances at the base of the *G. garantiana* zone in the Winterborne Kingston Borehole and the *G. garantiana/P. parkinsoni* zone in the Lyme Bay Borehole. Many of the taxa that appear in the *G. garantiana* and *P. parkinsoni* zones have first appearances which are lower in Swabia, and the higher appearances in the Wessex Basin are clearly a product of the transgressive nature of the *G. garantiana* zone, the lower surface of which is unconformable and corresponds to a transgressive surface of the Vesulian unconformity, which is coincident with third order sequence boundary Bj4 (section 4.2).

4.5 Dinoflagellate cyst richness patterns

A total of 51 dinoflagellate cyst taxa were recorded from the Upper Aalenian to Upper Bajocian of the Wessex Basin (Table 4.4). This means richness is lower in the Wessex Basin compared to northern France or Swabia; ~70 taxa were recorded from the Bajocian of Swabia and northern France respectively (Chapter 3; Feist-Burkhardt and Monteil, 1997). The sample rarefaction curve for Lower and Upper Bajocian of the Lyme Bay Borehole suggests that there is an increase in richness irrespective of sampling intensity in the Wessex Basin (Figure 4.11). For the purposes of rarefaction analysis, the samples covering the Lower–Upper Bajocian were included with the Upper Bajocian samples as the Lower–Upper Bajocian

Table 4.4. Composite zonal range chart for the uppermost Aalenian to Upper Bajocian of the Wessex Basin.
Grey fill denotes gonyaulacacean taxa.

Substage	Upper Aalen.	Lower Bajocian					Upper Bajocian	
Zone	*G. concavum*	*H. discites*	*W. laeviuscula*	*W. laeviuscula/S. propinquans*	*S. propinquans*	*S. humphriesianum/S. niortense*	*G. garantiana*	*P. parkinsoni*
Batiacasphaera spp.	X	X	X	X	X	X	X	X
Dissiliodinium giganteum	X	X	X	X	X	X	X	X
Dissiliodinium spp.	X	X	X	X	X	X		X
?*Dissiliodinium* spp.	X	X	X	X	X	X	X	X
Mancodinium semitabulatum	X	X	X	X	X			
Nannoceraptopsis gracilis	X	X	X	X	X			
Nannoceratopsis ambonis	X	X	X	X	X			
Nannoceratopsis dictyyambonis	X	X	X	X	X			
Nannoceratopsis plegas	X	X	X	X	X			
Nannoceratopsis spp.	X	X	X	X	X			X
Pareodinia ceratophora	X	X	X	X	X		X	X
Phallocysta elongata	?	X	X	X	X		X	X
?*Batiacasphaera* spp.		X	X	X	X		X	X
Durotrigia daveyi		X	?	X	X			
Durotrigia sp. cf. *D. daveyi*		?	X	X	X			
Kallosphaeridium ? *hypornatum*		X	X	X	X	X		X
Gongylodinium erymnoteichon		X	X	X	X		X	X
Pareodinia halosa		X	X	X	X		X	X
Valvaeodinium spp.		?		X	X		X	X
Durotrigia sp. 1			X	X	X		X	X
Durotrigia ? sp.				X	X	X	X	X
Meiourogonyaulax spp.				X	X	X	X	X
Ellipsoidictyum/Valensiella complex				X	X	X	X	
Kallosphaeridium spp.				X	X	X	X	X
Acanthaulax crispa				X	X	?	X	
Aldorfia aldorfensis				X	X	X	X	
Orobodinium automobile				X	X	X	X	
Sentusidinium spp.				X	X	X	X	X
Valensiella ovulum				X	X	X	X	
Rhynchodiniopsis? spp.				X	X	X	X	X
Ctenidodinium continuum				X	X	X	X	?
Ctenidodinium cornigerum				X	X	X	X	X
Ctenidodinium sellwoodii				X	X	X	X	X
Endoscrinium asymmetricum				X	X	X	?	?
Eodinia ? spp.				X	X	X	?	1
Gontaulacysta pectinigera				X	X	X	X	X
Impletosphaeridium sp. 1				X	X	X	X	
Kalyptea sp.				X	X	X	X	X
Kalyptea stegasta				X	X	X	X	X
Meiourogonyaulax sp. cf *M. caytonensis*				X	X	X	X	X
Meiourogonyaulax valensii				X	X	X	X	X
Pareodinia sp. 1 of F-B & M 1997				X	X	X	X	X
Rhynchodiniopsis ? regalis							X	
Lithodinia jurassica								X
Atopodinium polygonale								X
Ctenidodinium combazii								X
Gonyaulacysta ? sp.								X
Kalyptea diceras								X
Korystocysta gochtii								X
Chytroesphaeridia chytroides								X
Korystocysta aldridgeii								X
Nannoceratopsis spiculata								X
Korystocysta pachyderma								X

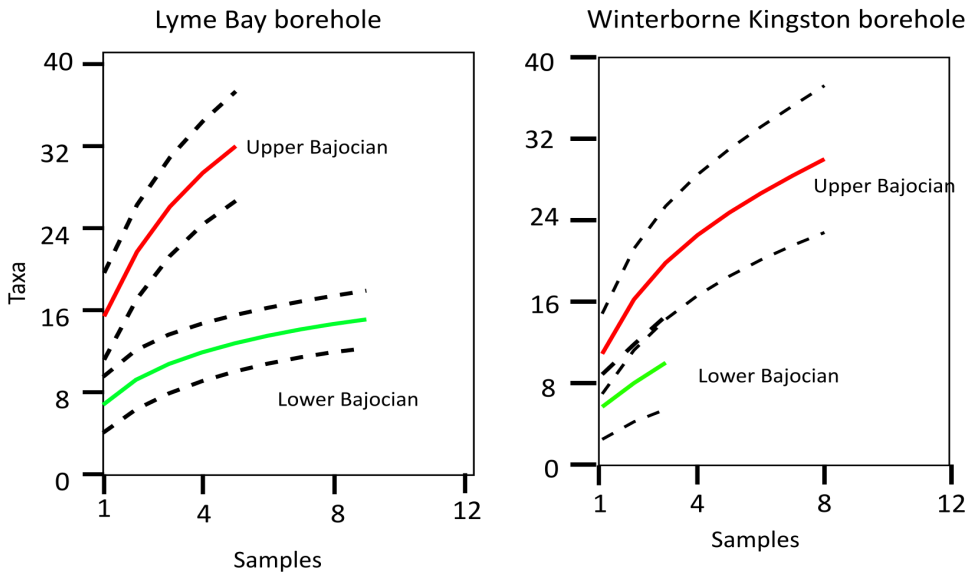

Figure 4.11. Sample rarefaction curves for the Lyme Bay and Winterborne Kingston boreholes. It can be observed that there is an increase in richness, irrespective of sampling intensity from the Lower to Upper Bajocian. The steep curves for the Upper Bajocian in both boreholes suggest an underestimate of total richness.

transition in both Lyme Bay and Winterborne Kingston is represented by a single sample. The curve for the Lower Bajocian is relatively flat, suggesting that the taxa recorded are a reliable estimate of richness. However, the curve for the Lower-Upper Bajocian transition and the Upper Bajocian is relatively steep, indicating that these intervals have been under-sampled. The patterns shown by sample rarefaction are broadly indicative of the stratigraphy of the Wessex Basin. The Lower Bajocian is relatively complete and expanded, but the extremely condensed and largely missing nature of the Lower-Upper Bajocian transition has influenced the low number of taxa recorded from this interval. Within the Lyme Bay Borehole, core loss in the Upper Bajocian hampered recovery from this interval, which has also driven an underestimate of richness. The sample rarefaction curves for the Winterborne Kingston Borehole (Figure 4.11), are also relatively steep, but this may also be due to the fact only one slide was examined for most samples, and so rare taxa may not have been recorded.

In terms of temporal richness trends, sample-based and zonal richness clearly increased throughout the Bajocian in the Wessex Basin (figures 4.12, 4.13, 4.14). In terms of raw richness, sample-based raw richness plots for the Lyme Bay Borehole (Figure 4.12) fluctuate through the Lower Bajocian, with a sudden pronounced increase in the *G. garantiana* zone. A similar pattern, although less pronounced, is seen in the Winterborne Kingston Borehole succession, with a general trend of increasing richness through the *G. garantiana* and *P. parkinsoni* zones (Figure 4.13). When richness is plotted per zone, and taxa are allowed to range through from first to last occurrence in the Wessex Basin, it can be seen that richness slightly increased through the Lower Bajocian, with a major increase (by around 50%) in the *G. garantiana* zone (Figure 4.14). It can also be observed that the proportion of gonyaulacacean

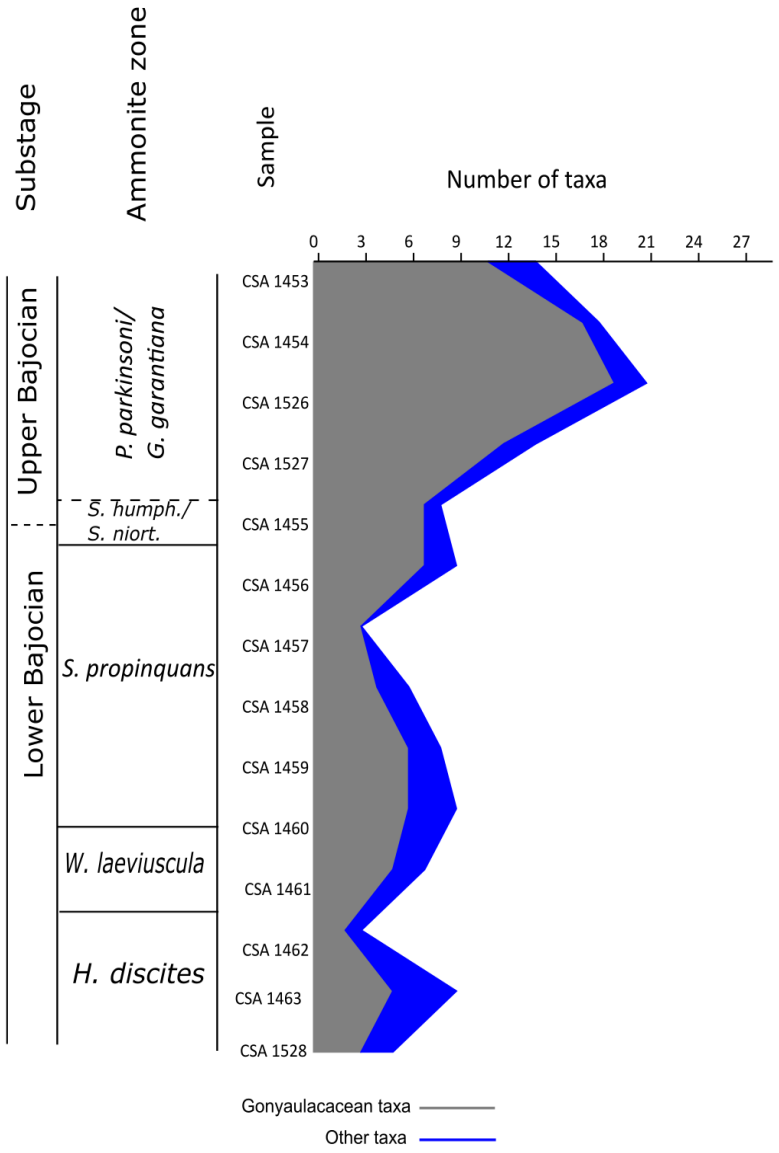

Figure 4.12. Number of dinoflagellate cyst taxa per sample for the Lyme Bay Borehole.
It can be observed that there is a significant increase in richness in the Upper Bajocian, driven by an increase in the number of gonyaulacacean taxa.

species increased from around 40% to 80% through the Upper Aalenian to Upper Bajocian in the Wessex Basin, further demonstrating that this group became the dominant dinoflagellate cyst family through the Bajocian (Figure 4.15).

4.6 Palaeoenvironmental interpretations using palynology

The samples from the Lyme Bay Borehole are dominated by microplankton and pollen (Figure 4.16), indicating deposition in an offshore environment. This is further supported by the relatively high abundances of bisaccate pollen (Figure 4.7). The low abundance of spores indicates that the succession was deposited in an environment distal to a source of terrigenous discharge. Within the microplankton assemblages, dinoflagellate cysts are the dominant group (Figure 4.15), implying deposition in a neritic environment with normal salinity conditions (Tyson, 1993), consistent with a carbonate ramp palaeoenvironment. The ternary plots also show no temporal trend in the distribution of samples from the

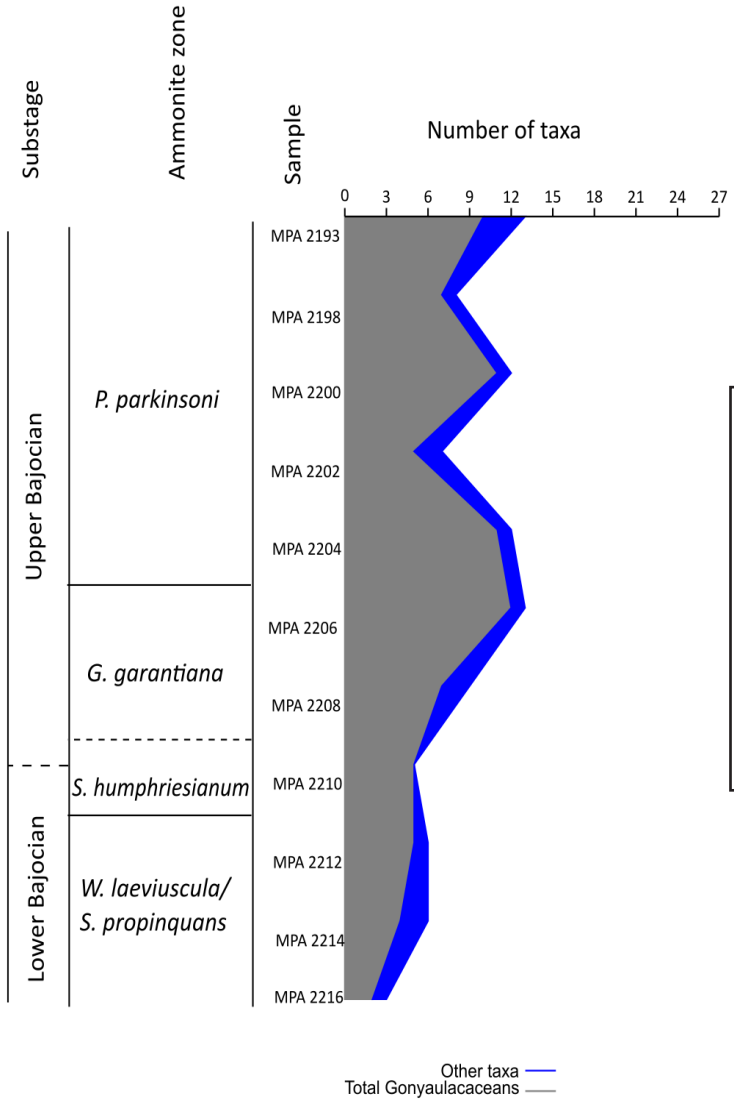

Figure 4.13. Number of dino-flagellate cyst taxa per sample for the Winterborne Kingston borehole.
There is an increase in richness in the Upper Bajocian, driven by an increase in gonyaulacacean richness.

Lower and Upper Bajocian, with samples from both substages demonstrating equally wide distributions. These data imply there was no systematic shift in the depositional environment of the Inferior Oolite Group during the Bajocian, a conclusion also reached by Penn et al. (1980) based on the prevalence of packestones throughout the succession.

The overall pattern in the palynomorph assemblages of the Winterborne Kingston Borehole (figures 4.7, 4.16), is comparable to that of the Lyme Bay Borehole in that there was no temporal trend throughout. This indicates that there was no systematic temporal change in the environment of deposition during the Bajocian. However, samples generally contain a larger proportion of sporomorphs (mainly pollen) relative to the Lyme Bay Borehole, indicating the Inferior Oolite Group in the Winterborne Kingston area was laid down in a more proximal palaeoevironment. This is also supported by the lower abundance of bisaccate pollen relative to total pollen. However, the palaeogeographic reconstruction of the Wessex basin indicates the Winterborne Kingston Borehole succession was deposited slightly more distally in relation to the Cornubian landmass compared to the Lyme Bay Borehole (Figure 4.1) and clay mineral data suggests this was the provenance area for the silicilastic material (Jones and Sellwood, 1989).

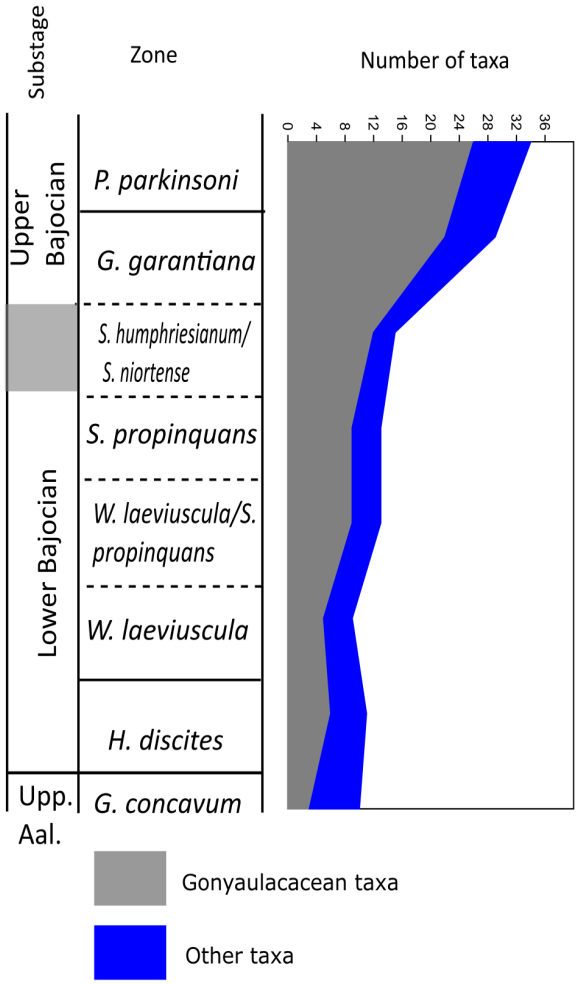

Figure 4.14. Number of dinoflagellate cyst taxa per zone in the Wessex Basin. Taxa have been allowed to range through from their first to last occurrence in the Wessex Basin. There is an increase in gonyaulacacean diversity of around 100% through the Lower–Upper Bajocian transition.

In summary palynological and sedimentological data demonstrate that, throughout the Bajocian, the Inferior Oolite Group of the Lyme Bay and Winterborne Kingston boreholes was deposited in an offshore carbonate ramp environment, and underwent little systematic change in depositional setting. Although there were significant changes in the rates of sedimentation and erosion, the depositional environment was that of a (distal) carbonate ramp throughout the Bajocian. The low abundance of spores and of *Botryoccocus*, combined with the relatively low abundance of siliciclastics implies there was relatively little terrigenous input into the areas represented by the Lyme Bay and Winterborne Kingston successions in the Wessex Basin during the Bajocian.

4.6.1 Palaeoenvironmental trends and dinoflagellate cyst appearances, richness and abundances

Palynological and sedimentological data from the Lyme Bay and Winterborne Kingston boreholes demonstrate that there was no systematic shift in palaeoenvironments throughout the Bajocian in the Wessex Basin, although changes in relative sea level have driven changes in sedimentation and erosion. Consequently, the increase in dinoflagellate cyst richness and appearances does not appear to be linked with a shift to a more offshore or distal palaeoenvironment. Moreover, dinoflagellates appear to have been the dominant organic-walled encysting phytoplankton group through the Late Aalenian to Late Bajocian in the Wessex Basin. Within the dinoflagellate abundance data, Lower Bajocian assemblages in the Lyme Bay and Winterborne Kingston horeholes are primarily dominated by *Batiacasphaera* spp.

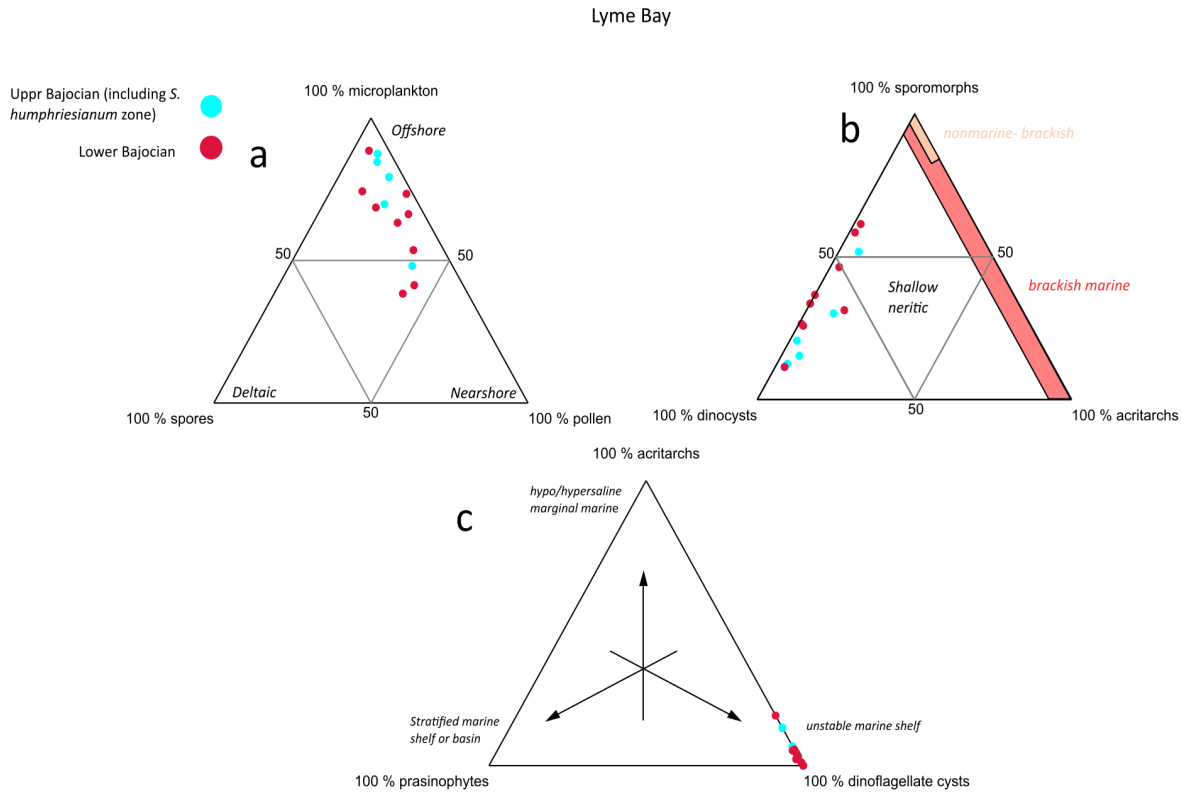

Figure 4.15. Ternary plots for the Lyme Bay borehole.
a= microplankton-spores-pollen plot, after Federova (1977), Duringer and Doubinger (1985). b= sporomorph-acritarch-dinoflagellate cyst plot, after Burger (1980). c= phytoplankton plot, after Tyson (1993).
Plot A shows that samples from the Lower and Upper Bajocian are variably dominated by microplankton and pollen. Plots B and C show that within microplankton assemblages, samples from both the Lower and Upper Bajocian are dominated by dinoflagellate cysts.

Assemblages from the Lower-Upper Bajocian transition and Upper Bajocian are mainly represented by *Batiacasphera* spp. and the *Ellipsoidictyum/Valensiella* complex. These taxa are also abundant in the Swabian Basin, indicating that they were widely distributed, and as such could tolerate a range of palaeoenvironmental conditions. The low abundances of taxa such as *Dissiliodinium giganteum*, *Acanathaulax crispa* and *Sentusidinium* spp, which are abundant in the Swabian Basin, indicate that differences in sea surface conditions, such as temperature, nutrient levels, or salinity, drove spatial and temporal trends in dinoflagellate cyst assemblage compositions during the Bajocian.

4.7 Summary

The palynological record of the Upper Aalenian and Bajocian of the Wessex Basin shows that there is a gradual increase in the appearances of taxa through the Lower Bajocian, prior to the *S. humphriesianum* zone. However, the Lower-Upper Bajocian transition in this region is largely missing, resulting in a low number of appearances. In turn, many of the taxa which occur in the overlying *G. garantiana* and *P. parkinsoni* zones have FADs around the Lower–Upper Bajocian transition. Consequently, third-order transgressive-regressive cycles have directly driven the stratigraphic pattern via changes in sedimentation and erosion. However, the palynological record demonstrates that despite changes in sea level, the

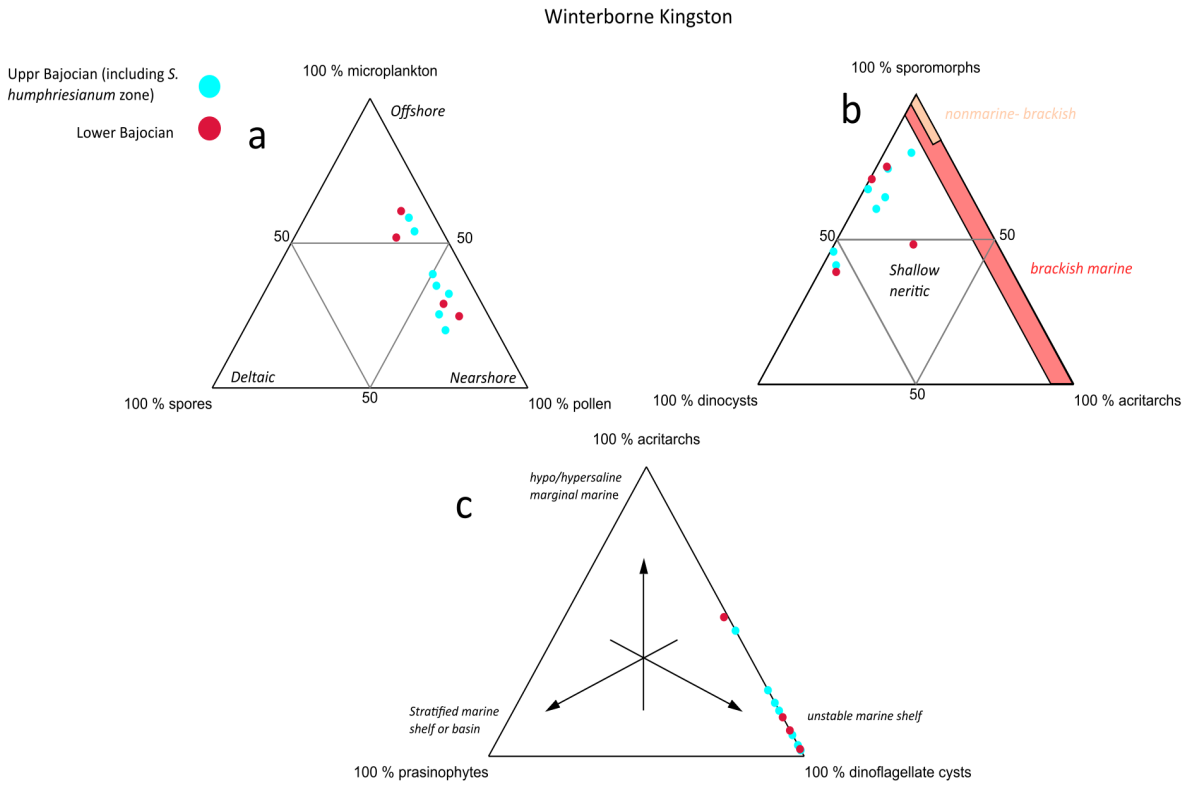

Figure 4.16. Ternary plots for the Winterborne Kingston borehole.
a= microplankton-spores-pollen plot, after Federova (1977), Duringer and Doubinger (1985). b= sporomorph-acritarch-dinoflagellate cyst plot, after Burger (1980). c= phytoplankton plot, after Tyson (1993).
Plot A shows that samples from the Lower Bajocian and Upper Bajocian are variably dominated by micro-plankton and pollen, of which pollen predominates.
Plots B and C show that within microplankton assemblages, samples from the Lower and Upper Bajocian are predominantly dominated by dinoflagellate cysts. Acritarchs are however more abundant than in the samples from Lyme Bay.

environment of deposition did not significantly change through the Bajocian. As such, the increase in dinoflagellate cyst first appearances was not associated with a systematic shift in palaeoenvironment. Within dinoflagellate cyst floras, the Lower Bajocian was dominated by *Batiacasphaera* spp. and the Upper Bajocian by *Batiacasphaera* spp. and *Ellipsoidictyum/Valensiella* complex. The abundance of these groups suggests they could tolerate a range of palaeoenvironmental conditions as they are also abundant in the Swabian Basin, whilst the suppression of abundances of other taxa may reflect differences in sea surface conditions relative to Swabia (Chapter 8).

4.8. The palynology of the Lower Bajocian of the Hebrides Basin, Isle of Skye, Scotland, UK

The palynology of the Toarcian to Bathonian of the Hebrides Basin was examined by Riding et al. (1991) who reported semi-quantitative palynological data from the Lower Bajocian. Upon examination of the slides from the Lower Bajocian used by Riding et al. (1991), I noticed numerous specimens of *Dissiliodinium giganteum,* which were not recorded by the previous authors. This prompted a restudy of the material, which is lodged in the British Geological Survey's micropalaeontology collection. However, whilst Riding et al. (1991) analysed 26 samples from the Lower Bajocian, only 11 could be

located, which severely reduced the scope of this restudy. As such, the data gathered from these samples is briefly summarised in this section.

Eleven palynological samples from the type section of the Bearreraig Sandstone Formation, originally collected and processed for Riding et al. (1991)'s study were analysed. These are from the Lower Bajocian with six samples are from the *H. discites* zone of the Udairn Shales (50 to 90 m above the base of the Beareraig Sandstone), three from the *W. laeviuscula* zone of the Holm Sandstone Member (90 to 125 m), one from the *S. propinquans* zone of the Holm Sandstone (125 to 145 m) and one from the *S. humphriesianum* zone of the Rigg Sandstone (145 to 200 m).

The palynological assemblages are shown in Figures 4.17, 4.18. Raw count data can be found in data table appendix D.1. The preservation of samples is generally fair to good (data table appendix D.1), and the palynomorph assemblages are dominated by gymnosperm pollen (Figure 4.17). This is consistent with nearshore, largely tidal depositional environment of the Bearairaig Sandstone Formation (Mellere and Steele, 1996). Within the marine component, dinoflagellate cysts are the dominant group (Figures A.1). A total of 20 dinoflagellate cyst taxa were recorded Formation (data table appendix D.1). The relative abundances of dinoflagellate cyst taxa is summarised in Figure 4.18.

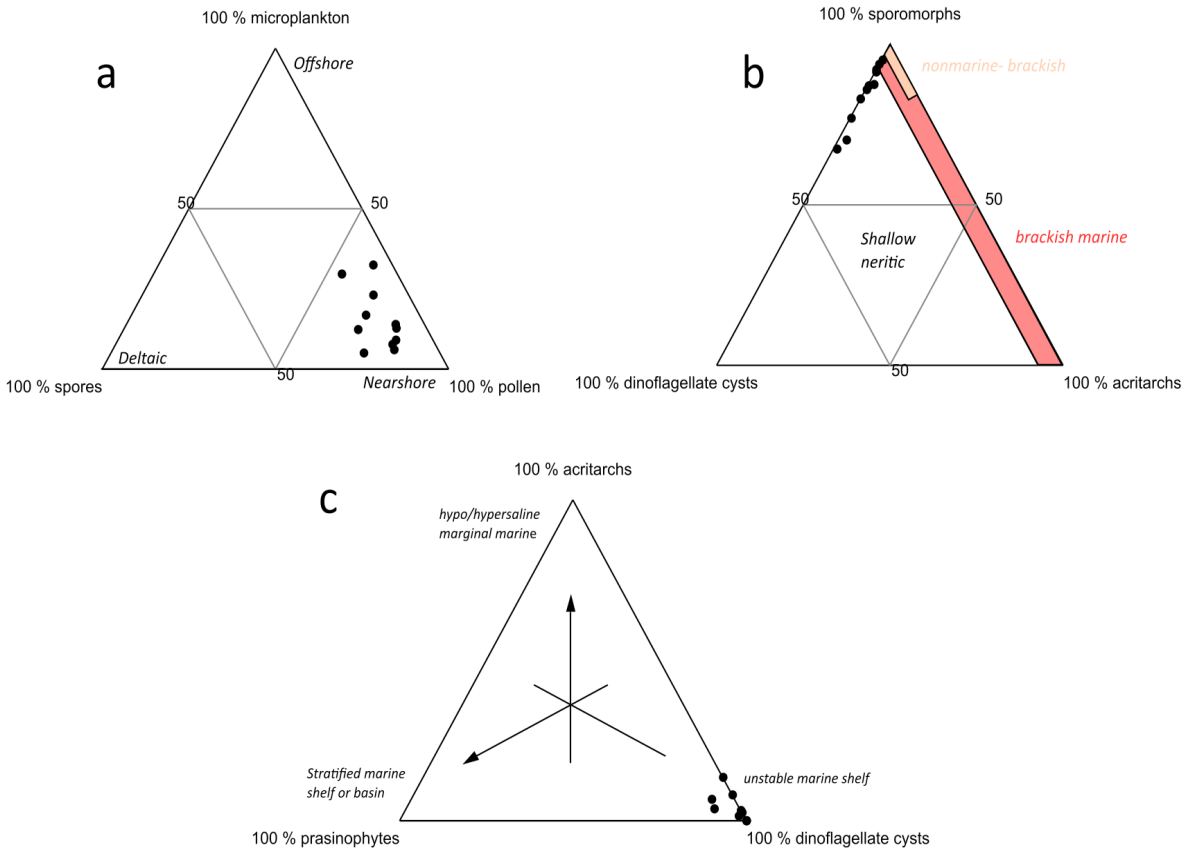

Figure 4.17. Ternary plots for Skye.
a= microplankton-spores-pollen plot, after Federova (1977), Duringer and Doubinger (1985). b= sporomorph-acritarch-dinoflagellate cyst plot, after Burger (1980). c= phytoplankton plot, after Tyson (1993).

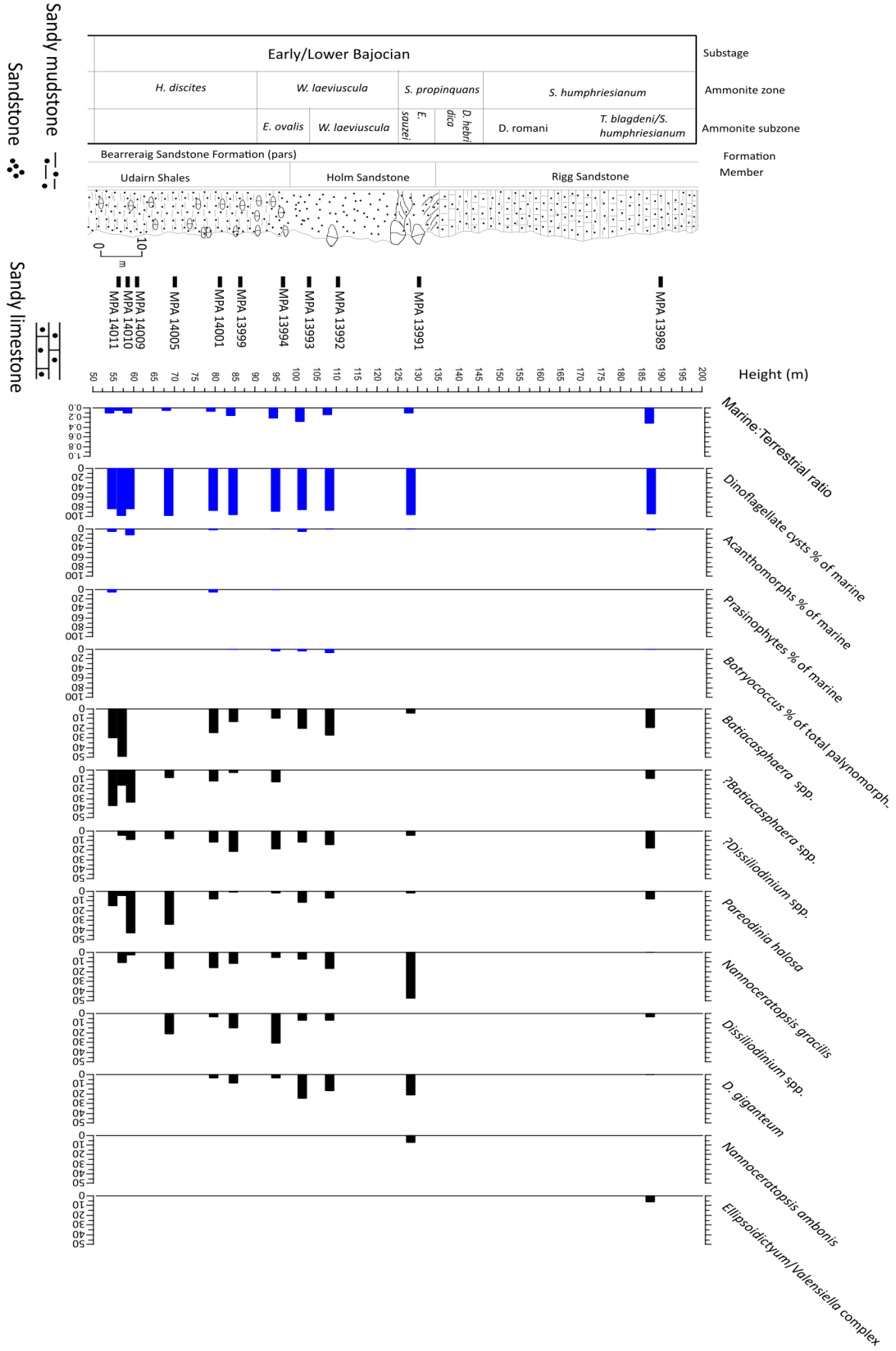

Figure 4.18. Relative abundances of palynomorph groups and dinoflagellate cysts for the Lower Bajocian of Skye.

Note the moderate abundance of *D. giganteum.* Log modified from Riding et al. (1991) fig. A. 2.

Chapter 5. The palynology of the Bajocian and lowermost Bathonian of the northwest Paris Basin, Normandy, France

5.1. Introduction

The Paris Basin of northern France contains thick Jurassic successions of primarily carbonate rocks (Brigaud et al., 2009). d'Orbigny (1842) originally described the Bajocian Stage from the Falaises des Hachettes, a seastack of Bajocian strata on the Normandy coast. This type section was sampled by Feist-Burkhardt and Monteil (1997) in their study of Bajocian dinoflagellate cysts. These authors also sampled the Bajocian–Bathonian boundary at a nearby cliff section. The samples collected by Feist-Burkhardt and Monteil (1997) yielded exceptionally well-preserved dinoflagellate cysts, however, these authors presented only an absence/presence record of dinoflagellate cyst stratigraphic distributions. Therefore, a lack of quantitative data makes it impossible to assess the palaeoecological dynamics within dinoflagellate cyst assemblages, or set the dinoflagellate cyst record within a wider palaeoenvirommental context. Consequently, I collected samples for palynological analysis from the Normandy coast. The localities sampled included Falaises des Hachettes and the Bajocian–Bathonian boundary section sampled by Feist-Burkhardt and Monteil (1997). An additional locality of Upper Bajocian strata was also sampled.

5.1.1. Geological background

The Paris Basin is located to the south and southeast of the Wessex Basin, and is structurally bounded by the Armorican Massif to the west and the London-Brabant Platform to the north and north east (Figure 5.1; Brigaud et al., 2009). Middle Jurassic carbonates were laid down in a shallow carbonate ramp environment (Brigaud et al., 2009).

The ammonite zonation, lithostratigraphy, and sequence stratigraphy of the Bajocian and Bathonian on the Normandy coast was described in detail by Rioult et al. (1991) and is shown in Figure 5.2. These authors used the presence of abundant ammonites throughout Middle Jurassic succession to provide a subzone-level zonation scheme (Rioult et al., 1991 and references therein). The stratigraphy is summarised below.

The Falaises des Hachettes section exposes four formations of mainly micritic and ferruginous limestones. The Upper Aalenian and the Lower Bajocian *H. discites* zone, are not exposed on the Normandy coast around the stratotype area (Rioult et al., 1991). The Lower Bajocian is represented by the Middle and Upper members of the Maliere Formation. The Middle Member corresponds to the *W. laeviuscula* zone and is a unit of biomicrite with chert nodules and interbeds. The Middle Member has an intensively bored upper surface which is infilled with the glauconite-rich conglomerate of the Couche Verte.

The Maliere Formation is overlain by the Oolithe ferrugineuse de Bayeux Formation, with is marked by a sharp erosional contact that has resulted in the erosion of the majority of the underlying Couche Verte

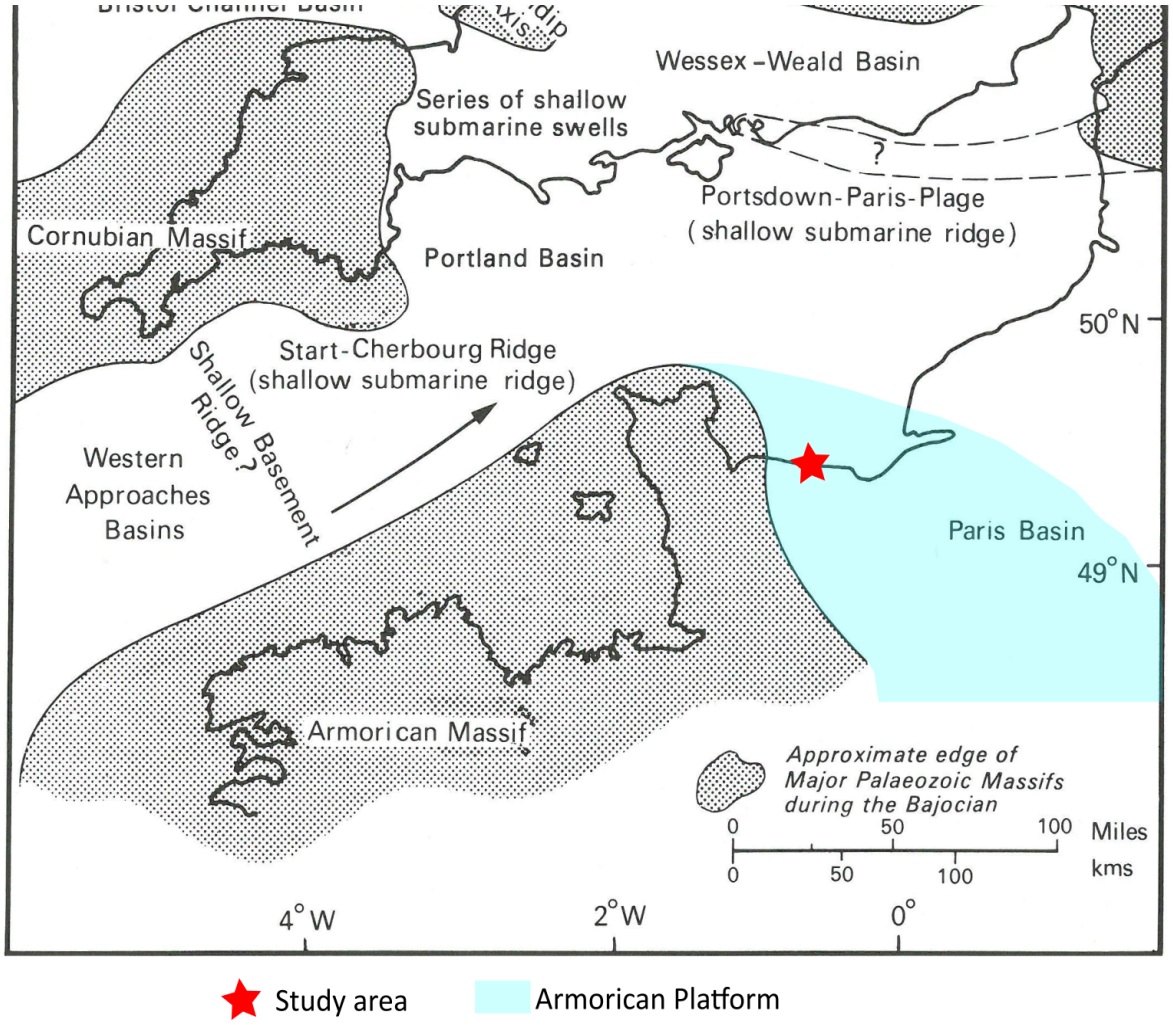

Figure 5.1. Palaeogeography of the northwest Paris Basin.
Blue fill denotes the carbonate platform on which Middle Jurassic carbonates were deposited (Brigaud et al., 2009). The location of d'Orbigny's Bajocian stratotype is shown. Modified from Penn et al. (1980).

Member. Consequently, the uppermost subzone of the *S. propinquans* zone, the *D. hebridica* subzone, is missing. The Oolithe ferrugineuse de Bayeux Formation is a condensed unit (<0.5 m) of ferruginous oolitic limestones, and corresponds to the *S. humphriesianum* to lowermost *P. parkinsoni* zones. The formation is comprised of four distinct beds. Bed A is a 25 cm thick unit of ferruginous ooids and oncoids with a stromatolitic pavement towards the upper part, and corresponds to the *S. humphriesianum* zone. Bed B is a unit of ferruginous oolitic limestone which is up to 15 cm thick and is of *S. niortense* zone age. Bed C is a <10 cm thick unit of biomicrite with abundant ferruginous ooids and pebbles at the base, and corresponds to the *G. garantiana* zone to the lowermost *P. acris* subzone of the *P. parkinsoni* zone. Bed D is a <30 cm thick bed of iron-ooids and and corresponds to the *P. densicostata* subzone of the *P. parkinsoni* zone.

The Oolithe ferrugineuse de Bayeux Formation is overlain by the Calcaire à Spongiaires Formation, a 10 to 20 m thick unit of biomicrite with abundant sponge fossils, which is referable to the *P. parkinsoni* zone, *P. bomfordi* subzone. This formation is comprised of two members: the Lower Member contains

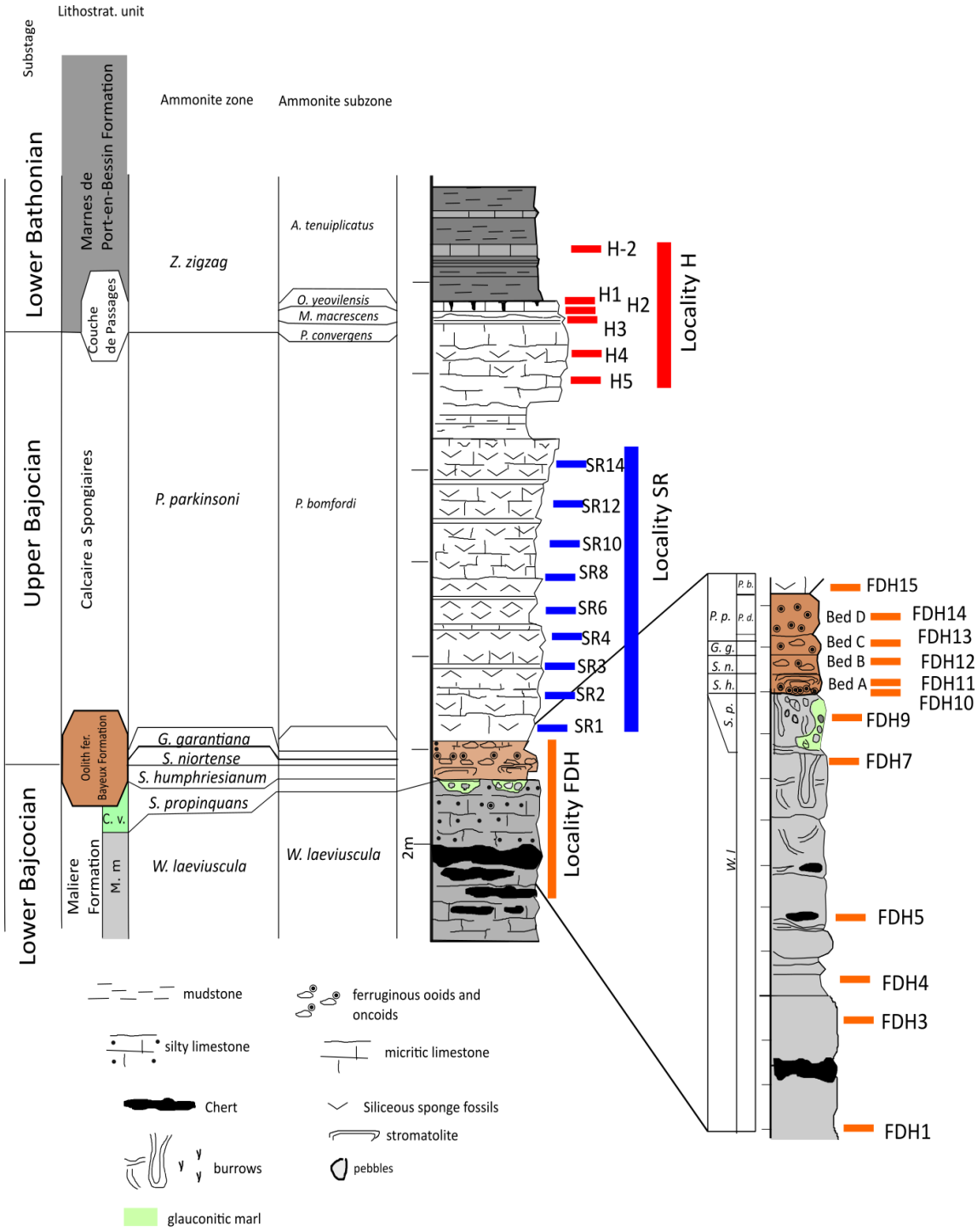

Figure 5.2. Composite lithological log through the Bajocian–Lower Bathonian of the Normandy coast. The stratigraphic coverage of each locality is shown. The distribution of palynological samples is also shown. Brown fill highlights the Oolith ferrugineuse de Bayeux Formation. The lithostratigraphy of this unit, and the underlying Maliere Formation has been expanded to show the individual beds. Green fill denotes the glauconite-rich Couche Vert (C. V.) Member of the Maliere Formation. The Couche Vert infills the bored upper surface of the Middle Member (M. M) of the Maliere Formation, and corresponds to the *S. propinquans* zone. Modified from Feist-Burkhardt and Monteil (1997) fig.1, and based on Rioult et al. (1991) fig. 9. Ammonite zone abbreviations: *P.p.= P. parkinsoni, P. d. = P. densicostata* subzone

abundant sponge beds; whilst the upper member is finer-grained has fewer sponge beds which are reduced in thickness. The Upper Member is bounded by a sharp upper contact, and is overlain by three

condensed limestone beds, termed the Couche de Passage. Each bed corresponds to one subzone of the *Z. zigzag* zone: the *P. convergens, M. macrescens* and *O. yeovilensis* subzones. The upper surface of the Couche de Passage is a bored horizon which is overlain by the Marnes de Porte-en-Bessin Formation. This unit is composed of marls and thin interbeds of limestone and represents the *A. tenuiplicatus* subzone of the *Z. zigzag* zone.

5.1.1.2. Sequence stratigraphic and depositional environmental interpretation

The sequence stratigraphic framework of the Jurassic of Normandy was documented by Rioult et al. (1991), and is shown in Figure 5.3. The Bajocian and Bathonian succession was laid down on a carbonate ramp and represents a sequence of stacked transgressive-regressive cycles, with an overall trend to more distal/deeper environments (Rioult et al., 1991). In the Lower Bajocian, the Middle Member of the Maliere Formation represents a transgressive systems tract, and the bored upper surface corresponds to the maximum flooding surface, which led to hardground development. The glauconitic Couche Verte Member, which infills the bored upper surface of the Middle Member, represents as highstand systems tract laid down under distal, sediment starved, conditions. The major erosional surface between the Maliere and Oolithe de ferrugineuse de Bayeux formations, which has eroded most of the Couche Verte, corresponds to sequence boundary Bj2, with Bed A of the Oolithe de ferrugineuse de Bayeux Formation laid down as a transgressive deposit, with the upper part of the bed representing the highstand systems tract. The overlying beds B, C, and D correspond to another transgressive pulse and are separated from bed A by a sequence boundary (Bj3) which is coincident with the transgressive surface. This corresponds to time-gap as the lowermost subzone of the *S. niortense* zone, the *T. banksi* subzone, is missing. Beds B and C correspond to the transgressive systems tract whilst bed D represents the highstand systems tract, with the maximum flooding surface (MFS) developed between beds C and D. Preat et al. (2000) reported fossilised iron-encrusted bacteria from the Oolithe ferrugineuse de Bayeux Formation and argued that deposition occurred in a distal ramp environment, at a depth which fluctuated between the base of the photic zone to around storm wave base. The bottom waters were largely dysaerobic, as indicated by the lack of a benthic macrofauna in Beds A, B and C, but the abundant bioturbation and sponge fossils of Bed D indicates a return to oxygenated conditions (Preat et al., 2000).

The overlying Calcaire à Spongiaires Formation represents a relatively complete sequence with lowstand, transgressive, and highstand systems tracts represented. The base is marked by a sharp contact, which represents a sequence boundary (Bj5) and the Lower Member corresponds to a lowstand systems tract. The Upper Member and Couche de Passage were deposited as four back-stepping parasequences in a transgressive system tract. The first parasequence is represented by the Upper Member whilst the other three are represented by each of the three beds of the Couche de Passage. The erosional surface at the base of Couche de Passage represents a ravinement surface whilst the bored hardground of the upper surface represents a maximum flooding surface. The overlying Marnes de Port-en-Bessin Formation corresponds to the highstand systems tract. The hardground surface at the top of the Couche de Passage

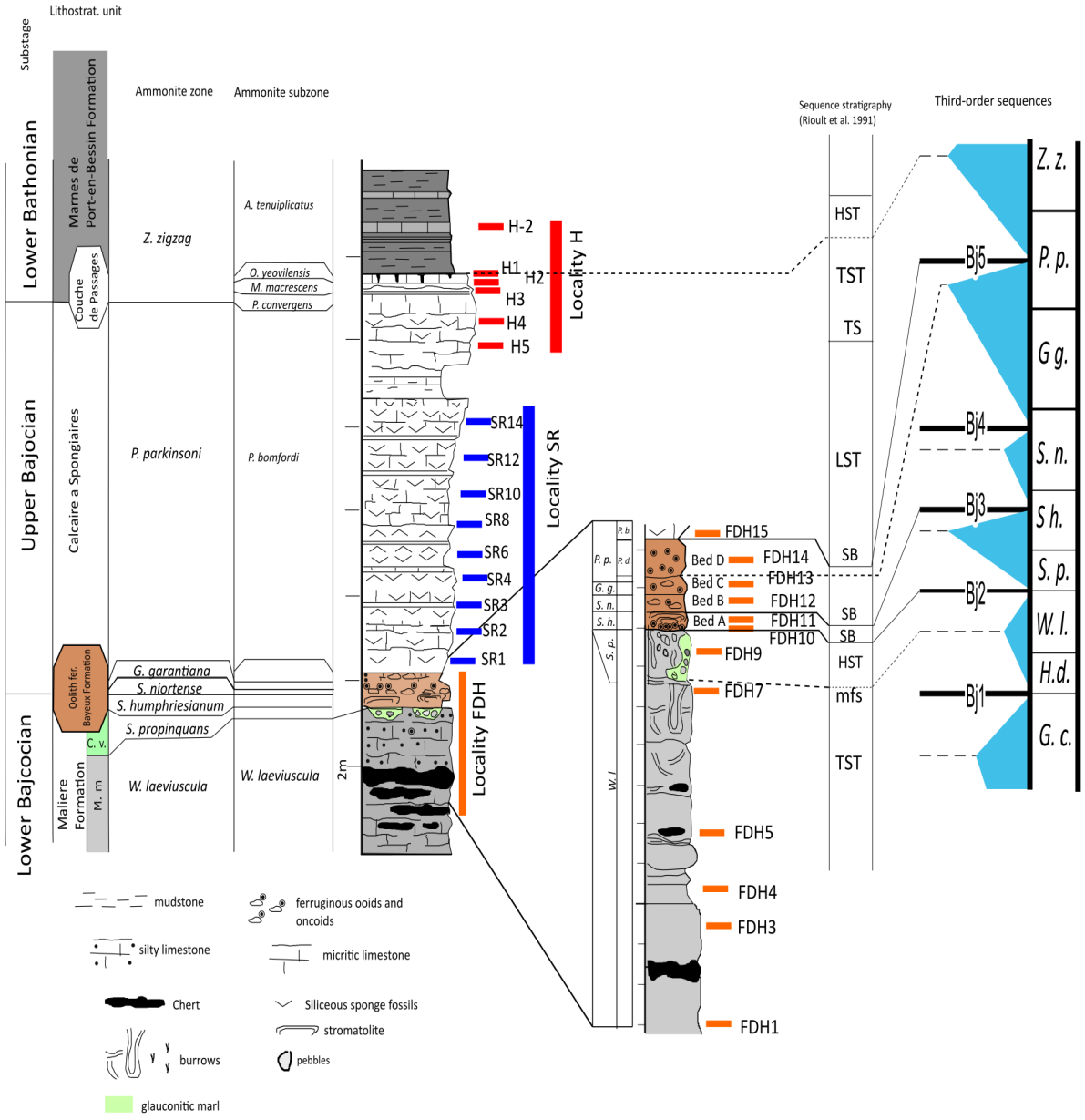

Figure 5.3. Sequence stratigraphic interpretation of Riolut et al. (1991)and correlation to Jacquin et al. (1998) third order sequences for the Bajocian–Lower Bathonian of the Normandy coast.
Sequence boundary Bj4 cannot be recognised in Normandy (Riolut et al., 1991; Jacquin et al., 1998). Maximum flooding of the T7 cycle is marked by the bored surface at the top Couche de Passage, and major lithological transition from condensed limestone beds to marls.

represents a maximum flooding surface, which marks the peak transgression of the second-order T7 transgressive cycle in Europe during the Early Bathonian (Riolut et al., 1991; Hallam, 2001). Jacquin et al. (1998) interpreted this feature as sequence boundary Bt1, however, the bored hardground surface is more consistent with sediment-starved highstand conditions, and as such the interpretation of Riolut et al. (1991) used here.

5.1.3. Previous research

Feist-Burkhardt and Monteil (1997) examined the dinoflagellate cyst record of the Bajocian of the

Normandy coast. These authors based their study on 25 samples from three localities. Thirteen samples were analysed from the *W. laeviuscula* to *P. parkinsoni* zones of the Bajocian from Falaises des Hachettes. Nine samples were studied from the Bajocian–Bathonian boundary at the western harbour wall of Port-en-Bessin. Feist-Burkhardt and Monteil (1997) reported that a sample from the stromatolitic unit of Bed A (*S. humphriesianum* zone) of the Oolithe ferrugineuse de Bayeux Formation proved barren of palynomorphs. Consequently, these authors substituted three ammonite-dated samples from an inland exposure of ferruginous oolitic limestone of *S. humphriesianum* zone age. These authors did not provide details of the locality of these samples beyond that of the village, Saint Martin de Fontenay, which is located around 40 km southeast of the Normandy coastal section.

Feist-Burkhardt and Monteil (1997) reported relatively low richness dinoflagellate cyst assemblages from the Lower Bajocian *W. laeviuscula* and *S. propinquans* zones, with a total of 13 taxa (Figure 1.2). There is a sudden increase in appearances around the *S. humphriesianum* and *S. niortense* zones, with 13 taxa and 14 taxa appearances from each zone respectively (Figure 1.2). There in one appearance in the *G. garantiana* zone, before a burst of 27 appearances in the *P. parkinsoni* zone. Five appearances were recorded from the *Z. zigzag* zone of the Lower Bathonian (Figure 1.2). These authors also noted that from the *S. humphriesianum* zone upwards, the Gonyaulaceae became the dominant dinoflagellate cyst family.

5.2. Materials

Field-outcrop rock samples were collected and processed from three localities along the Normandy coast around the village of Port-en-Bessin (Figure 5.4). The latitude/longitude and stratigraphy of each locality is summarised in Table 5.1. The lithostratigraphic coverage of each locality is shown in Figure 5.2. The *W. laeviuscula* to *P. parkinsoni* zones of the Bajocian were sampled at the historical Bajocian stratotype of Falaises des Hachettes (locality FDH), which was previously sampled by Feist-Burkardt and Monteil (1997). It is located on the coast between the villages of Port-en-Bessin and Saint Honorine des Pertes (Figure 5.4; Table 1). This section exposes the Maliere, Oolithe ferrugineuse de Bayeux, and Calcaire à Spongiaires formations. The extremely condensed nature of the Oolithe ferrugineuse de Bayeux Formation (<50 cm) meant that only one or two samples could be taken from each bed in order to collect a sufficient mass of rock for processing, as the palynomorphs are in very low abundance (see below).

The Bajocian–Bathonian boundary was sampled at a cliff located next to the western harbour wall at Porte-en-Bessin (Locality H: Figure 5.4; Table 5.1), which was also sampled by Feist-Burkhardt and Monteil (1997). A third Calcaire à Spongiaires Formation locality (SR), located on the coast between Saint Honorine des Pertes and Falaises des Hachettes (Figure 5.4; Table 5.1), was sampled to provide additional samples from the *P. parkinsoni* zone (*P. bomfordi* subzone). Locality SR is located stratigraphically between the uppermost sample of locality FDH and the lowermost beds of Locality H (Figure 5.2).

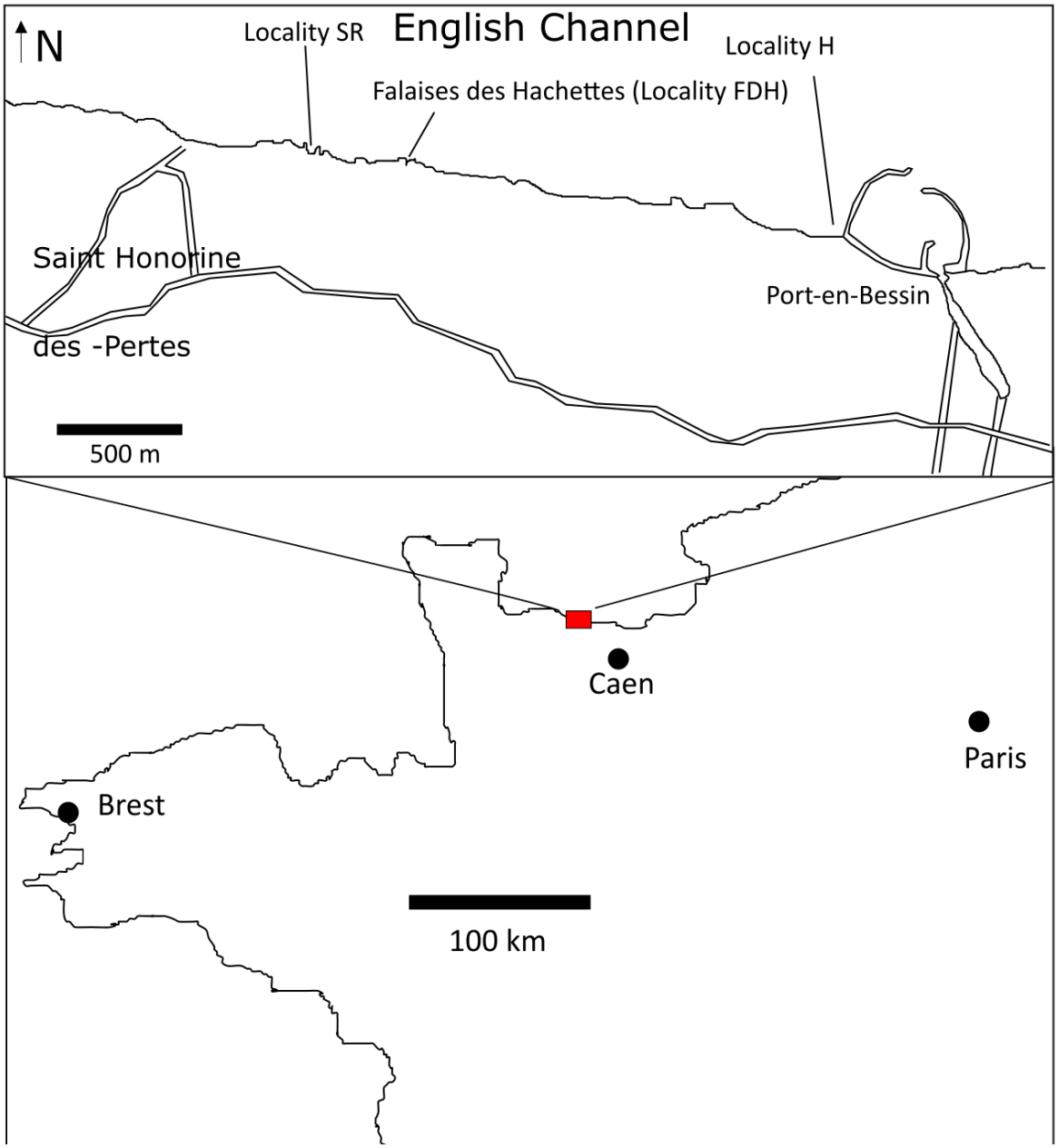

Figure 5.4. Locality map showing the location of the study area within northwestern France, the localities sampled are shown.

The number of samples processed from each locality is summarised in Table 5.2. Photographs of the sampled areas are shown in figures 5.4, 5.5 and 5.6. Samples were processed quantitatively, with two *Lycopodium* spore tablets added to the sample (data table appendices C.1, C.2, C.3).

5.3. Palynology

Of the 27 samples processed, 11 were palynologically productive (Table 5.2). The number of palynological composition of samples from each locality is described below. For absolute abundances of palynomorphs, the error is <5% for all samples examined (data table appendix C.2).

Locality	Code	Latitude and longitude (decimal degrees)	Stratigraphy
Falaises des Hachettes	FDH	49.353414°N, 0.785775°W	Bajocian- *W. laeviuscula* to *P. parkinsoni* zones
Cliff at Western Harbour Wall of Port-en-Bessin	H	49.350616°N, 0.761063°W	Bajocian-Bathonian, *P. parkinsoni* to *Z. zigzag* zones
Cliff exposure between Saint Honorine des Pertes and Port-en-Bessin	SR	49.353854°N, 0.791428°W	Bajocian- *P. parkinson* i, bomfordi subzone.

Table 5.1. Localities sampled in Normandy.

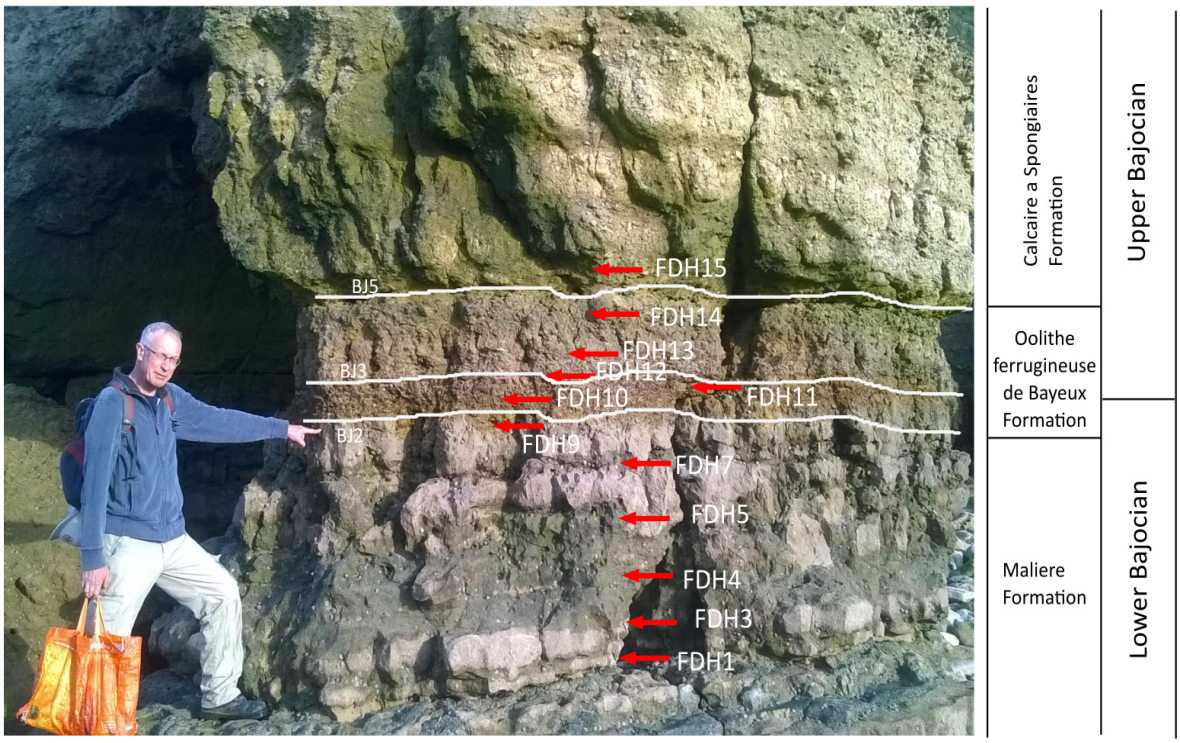

Figure 5.5. Photograph of Locality FDH- d'Orbigny's Bajocian type section.

The Maliere, Oolithe ferrugineuse de Bayeux, and Calcaire à Spongiaires formations are shown, along with sample points. The white lines denote sequence boundaries Bj2, Bj3, and Bj5. Facing south west.

5.3.1. Falaises des Hachettes

Thirteen samples were processed from Falaises des Hachettes: six from the Maliere Formation, five from the Oolith ferrugineuse de Bayeux Formation, and one from the lowermost Calcaire à Spongiaires Formation (Table 5.2). One productive sample was yielded from the *W. laeviuscula* zone of the Maliere Formation (Middle Member), one from the *S. propinquans* zone of the Couche Verte Member, and one from the *P. parkinsoni* zone of the Lower Member of the Calcaire à Spongiaires Formation (Table 5.2). All samples from the Oolithe ferrugineuse de Bayeux Formation were barren.

The palynological composition of productive samples is summarised in Figure 5.8, and data table appendix C.1. The sample from the *W. laeviuscula* zone yielded a low abundance of palynomorphs (200 palynomorphs per g). These are well preserved, and assemblages are dominated by sporomorphs, with a marine:terrestrial ratio of 0.23. Within the terrestrial component, gymnosperm pollen predominates over spores. Within the marine component, dinoflagellate cysts are the dominant group and

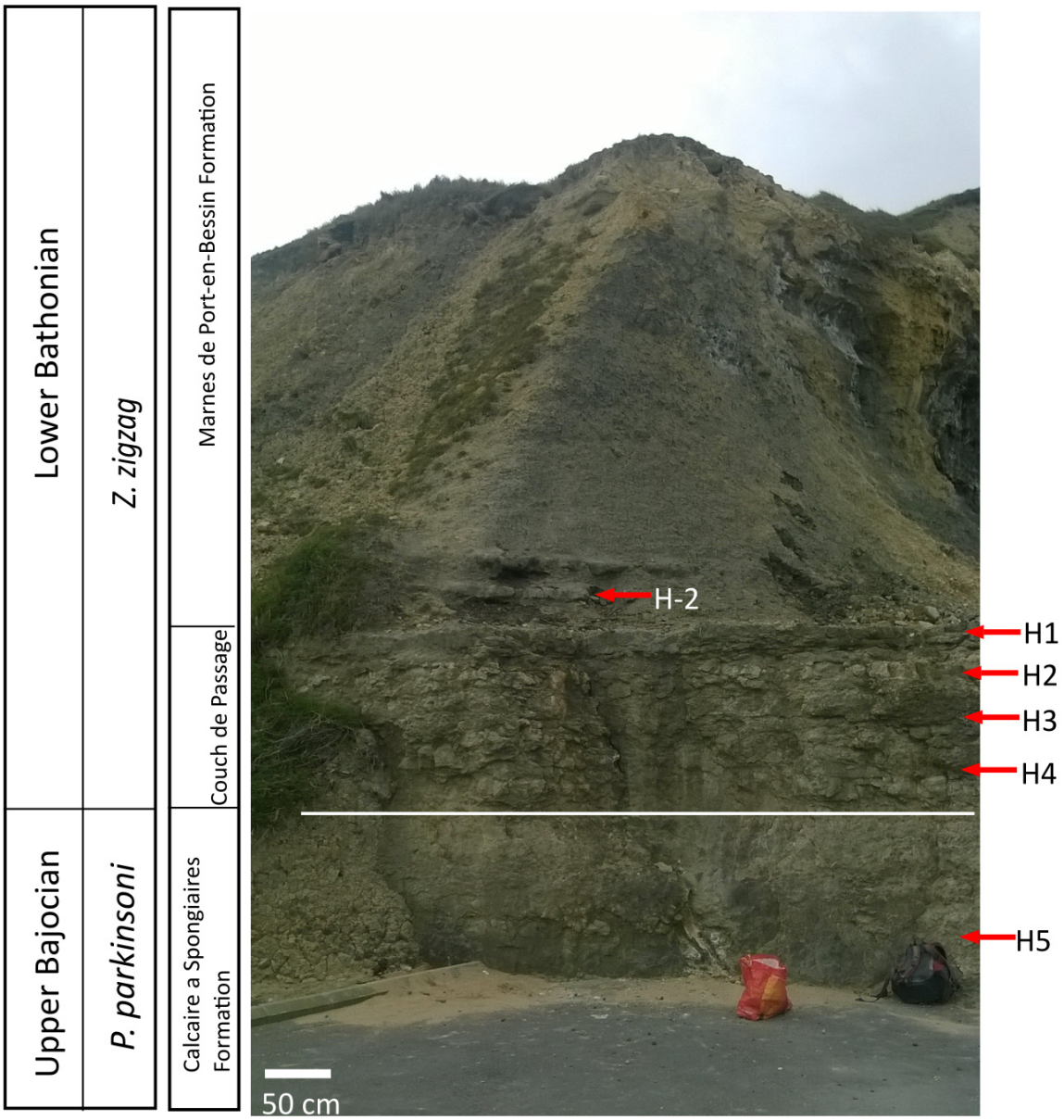

Figure 5.6. Photograph of Locality H- the Bajocian–Bathonian boundary.
Sample points are shown. Note the major lithological transition from the beds of condensed limestone of the Couche de Passage, to the marls of the Marnes de Port-en-Bessin Formation. Facing north.

acanthomorphic acritarchs, predominantly *Micrhystridium* spp., are moderately abundant. The sample from the *S. propinquans* zone contains very few palynomorphs (75 palynomorphs per g), which are well preserved. Within the assemblages, marine and terrestrially-derived palynomorphs are approximately equal in abundance, with a marine:terrestrial ratio of 0.47. As with the underlying *W. laeviuscula* zone, sporomorphs are dominated by gymnosperm pollen. Within marine palynomorphs, dinoflagellate cysts are the dominant group, with acanthomorphic acritarchs (mainly *Micrhystridium* spp.) also present in moderate abundance. The productive sample from the lowermost Calcaire à Spongiaires (*P. parkinsoni*) yielded a much higher abundance of palynomorphs relative to the two Lower Bajocian samples (1300 palynomorphs per g), and these are well preserved. The assemblage is dominated by marine palynomorphs, with a marine:terrestrial ratio of 0.70. Dinoflagellate cysts and acanthomorphs

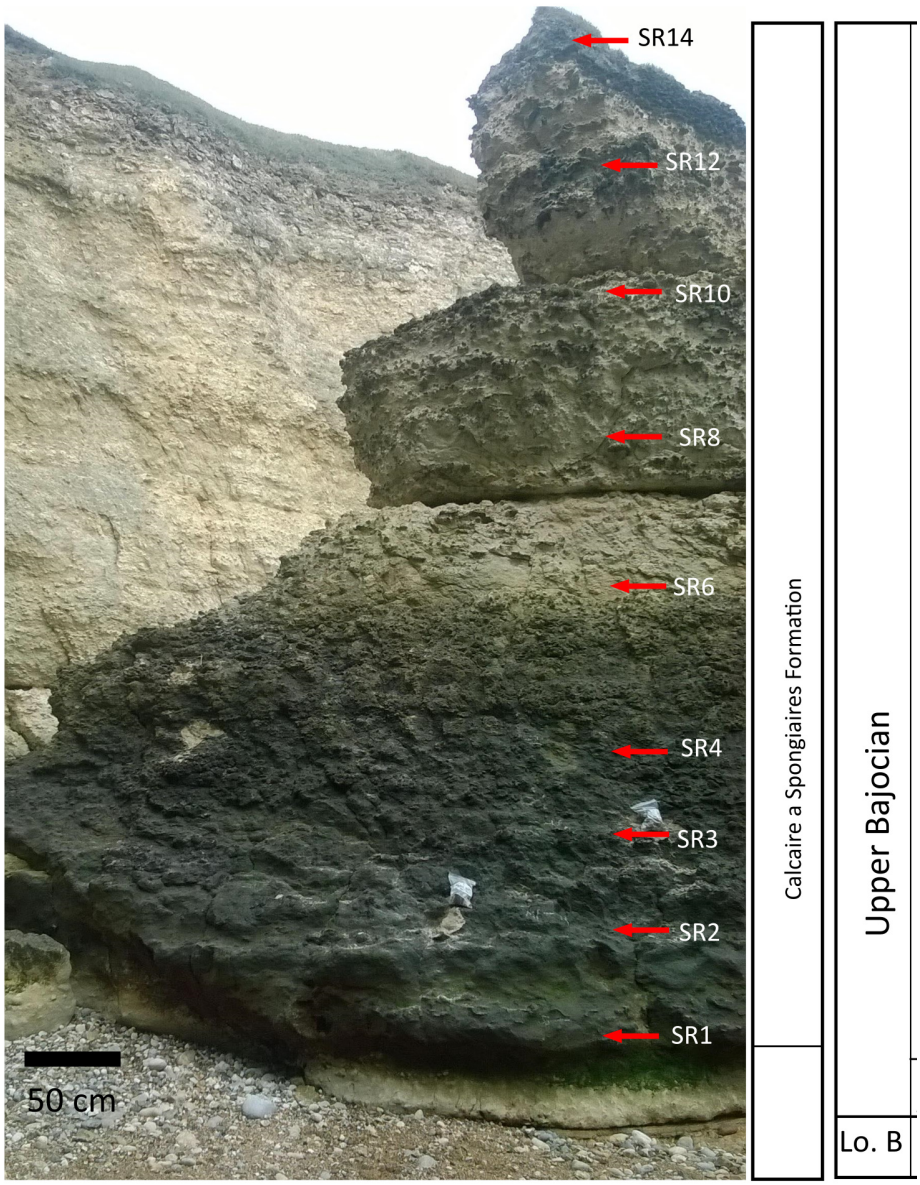

Figure 5.7. Photography of locality SR- the Calcaire à Spongiaires sample points are shown.

Facing west.

(primarily *Micrhystridium* spp.) are equally abundant. Within sporomorphs, gymnosperm pollen is the dominant component.

5.3.2. Locality SR- Calcaire à Spongiaires Formation

Of the nine samples processed from the *P. parkinsoni* zone of the Calcaire à Spongiaires Formation (Lower Member), three were productive. The palynomorph assemblages are summarised in Figures 5.10 and data table appendix C.1. The samples contain 600 to 1600 palynomorphs per gram, and the associations are well-preserved. The marine:terrestrial ratio fluctuates from 0.61 to 0.43 to 0.78 throughout the succession (Figure 5.8). Within the marine component, dinoflagellate cysts are dominant, and *Micrhystridium* spp. is also present in moderate abundances. Foraminiferal test linings and prasinophytes also present in very low abundance (data table appendix C.3). The terrestrial palynomorphs are dominated by gymnosperm pollen.

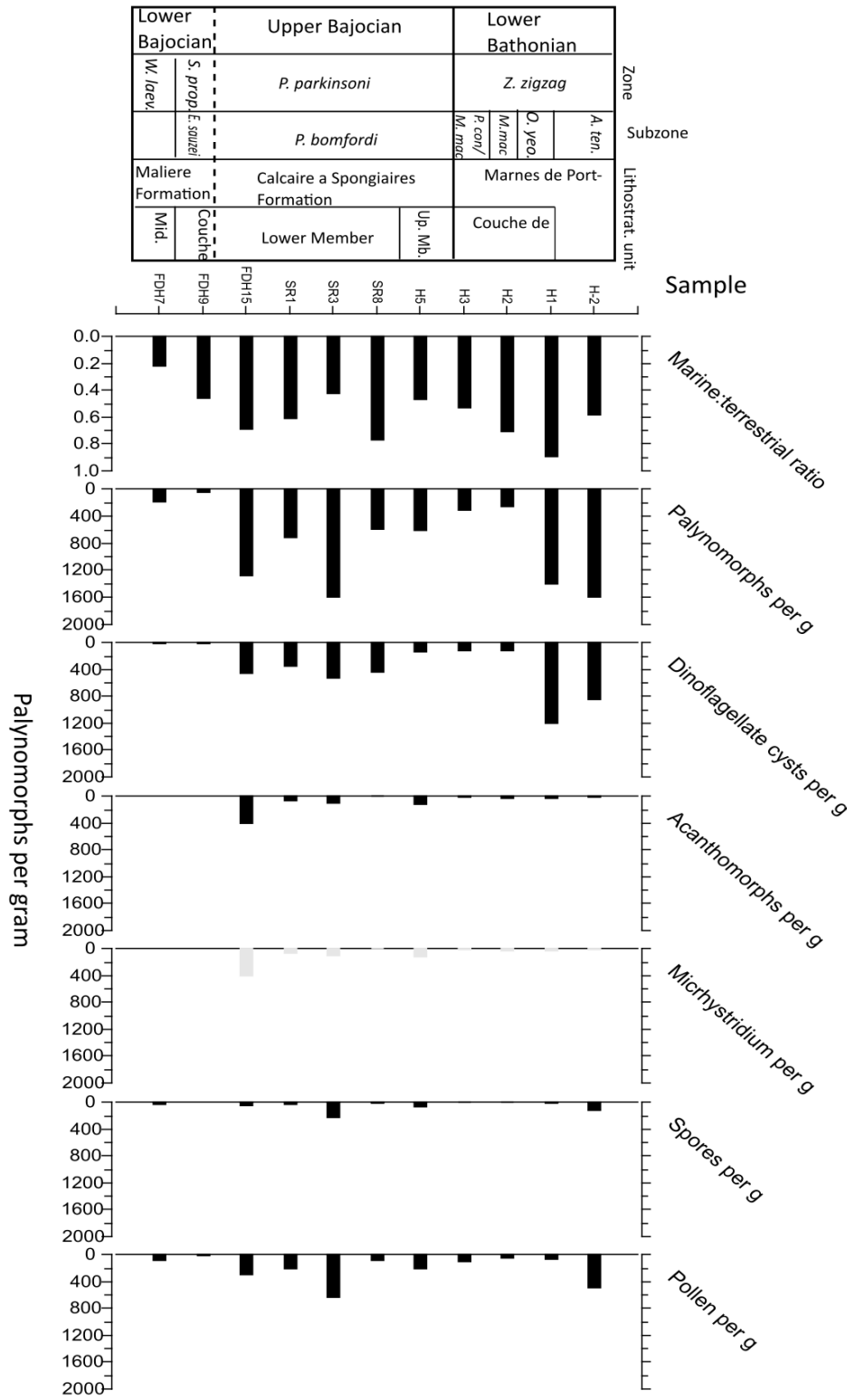

Figure 5.8. Absolute abundances of main palynomorph groups for the Bajocian–Lower Bathonian of Normandy.

It can be observed that abundances of palynomorphs from the Maliere Formation are extremely low. In contrast, abundances are higher through the Calcaire à Spongiaires and Marnes de Port-en-Bessin formations. The marine:terrestrial ratio shows generally low values in the Lower Bajocian (~0.2–0.4), and fluctuating, but generally higher values in the Upper Bajocian. Peak values can be observed in the Lower Bathonian, particularly sample H-1 which corresponds to the maximum flooding surface at the top of the Couche de Passage. *Z. zigzag* subzones: *P. con/M. mac= P. convergens/M. macrescens, M. mac= M. macrescens. A. ten= A. tenuiplicatus*

Locality	Lithostratigraphic unit	Zone
FDH		
FDH 1	Maliere Formation- Middle Member	*W. laeviuscula*
FDH 3	Maliere Formation- Middle Member	*W. laeviuscula*
FDH 4	Maliere Formation- Middle Member	*W. laeviuscula*
FDH 5	Maliere Formation- Middle Member	*W. laeviuscula*
FDH 7	Maliere Formation- Middle Member	*W. laeviuscula*
FDH 9	Maliere Formation- Couche Vert Member	*S. propinquans*
FDH 10	Oolithe ferrugineuse de Bayeux Formation- Bed A	*S. humphriesianum*
FDH 11	Oolithe ferrugineuse de Bayeux Formation- Bed A	*S. humphriesianum*
FDH 12	Oolithe ferrugineuse de Bayeux Formation- Bed B	*S. niortense*
FDH 13	Oolithe ferrugineuse de Bayeux Formation- Bed C	*G. garantiana*
FDH 14	Oolithe ferrugineuse de Bayeux Formation- Bed D	*P. parkinsoni*
FDH 15	Calcaire à Spongiaires Formation- Lower Member	*P. parkinsoni*
SR		
SR 1	Calcaire à Spongiaires Formation- Lower Member	*P. parkinsoni*
SR 2	Calcaire à Spongiaires Formation- Lower Member	*P. parkinsoni*
SR 3	Calcaire à Spongiaires Formation- Lower Member	*P. parkinsoni*
SR 4	Calcaire à Spongiaires Formation- Lower Member	*P. parkinsoni*
SR 6	Calcaire à Spongiaires Formation- Lower Member	*P. parkinsoni*
SR 8	Calcaire à Spongiaires Formation- Lower Member	*P. parkinsoni*
SR 10	Calcaire à Spongiaires Formation- Lower Member	*P. parkinsoni*
SR 12	Calcaire à Spongiaires Formation- Lower Member	*P. parkinsoni*
SR 14	Calcaire à Spongiaires Formation- Lower Member	*P. parkinsoni*
H		
H-2	Marnes de Port-en-Bessin Formation	*Z. zizag*
H1	Couche de Passage	*Z. zizag*
H2	Couche de Passage	*Z. zizag*
H3	Couche de Passage	*Z. zizag*
H4	Couche de Passage	*Z. zizag*
H5	Calcaire à Spongiaires Formation- Lower Member	*P. parkinsoni*

Table 5.2. Samples processed per locality.
Red denotes palynologically-productive samples.

5.3.3. Bajocian–Bathonian boundary, Port-en-Bessin harbour wall (Locality H)

Six samples were processed from the Bajocian–Bathonian boundary (locality H), five of which were productive (Figure 5.8; data table appendix C.1). Sample H5 of the uppermost Bajocian *P. parkinsoni* zone (Calcaire à Spongiaires Formation, Upper Member) contains well-preserved palynomorphs, with 630 palynomorphs per gram of sediment recorded. Marine and terrestrial palynomorphs occur in subequal abundances (marine:terrestrial ratio of 0.48). Dinoflagellate cysts and acritarchs occur in equal abundances in the marine component, whilst the terrestrial component is dominated by gymnosperm pollen. Sample H4 of the Couche de Passage (lowermost Bathonian, *Z. zigzag* zone, *P. convergens* subzone), proved barren of palynomorphs. Sample H3 of the *P. convergens/M. macrescens* subzones of the *Z. zigzag* zone yielded 340 palynomorphs per gram of sediment. These are well-preserved and contain marine palynomorphs and sporomorphs in approximately equal abundances (marine:terrestrial ratio of 0.54). Sample H2 yielded well preserved palynomorphs, with 280 palynomorphs per gram. The assemblage is dominated by microplankton, with a marine:terrestrial raito of 0.70. The marine

palynomorphs are dominated by dinoflagellate cysts, and *Micrhystridium* spp. is also present in moderate abundance. The sporomorphs are dominated by gymnosperm pollen. In sample H1 of the *O. yeovilensis* subzone of the *Z. zigzag* zone, there is an increase in the absolute abundance of palynomorphs, with 1430 palynomorphs per gram of sediment. The assemblages are overwhelmingly dominated by marine palynomorphs, with a marine:terrestrial ratio of 0.90. The assemblage is dominated by dinoflagellate cysts, with *Micrhystridium* spp. also present in moderate abundance. In the uppermost sample, H-2 which corresponds to the *A. tenuiplicatus* subzone of the *Z. zigzag* zone in the Marnes de Port-en-Bessin Formation, the absolute abundance of palynomorphs is around 1600 palynomorphs per gram of sediment. The marine:terrestrial ratio is 0.59, marine palynomorphs are dominated by dinoflagellate cysts whilst sporomorphs are dominated by gymnosperm pollen.

5.4. Stratigraphic palynology

The stratigraphic distributions of dinoflagellate cysts recorded from the three localities studied are described below, and are summarised in Table 3.

*5.4.1. Lower Bajocian **W. laeviuscula** and **S. propinquans** zones (Falaises des Hachettes)*

The gonyaulacacean taxa present in the sample from the *W. laeviuscula* zone are *Baticasphaera* spp., *Dissiliodinium giganteum* and *Dissiliodinium* spp. (Table 5.3). Non-gonyaulacaceans present include relatively long-ranging taxa such as *Nannoceratopsis gracilis*, *Nannoceratopsis* spp., *Mancodinium semitabulatum* and *Valvaeodinium* spp. The questionable occurrences (due to poor preservation) are *Orobodinium automobile*, the FAD of this species is in the *W. laeviuscula/S. propinquans* zone in Swabia (Table 3.2a) and *Valvaeodinium cavum*, which is a long-ranging species with a FAD in the Upper Toarcian (Feist-Burkhardt and Wille, 1992).

In sample FDH9 from the *S. propinquans* zone, there are four appearances, all of which are gonyaulacaceans. As well documented herein, *Kallosphaeridium* spp. is a long-ranging group with a FAD in the Lower Aalenian (Feist-Burkhardt and Wille, 1992). *Kallosphaeridium*? *hypornatum* is present in this sample was also recorded from the *W. laeviuscula* zone by Feist-Burkhardt and Monteil (1997). The appearance of *Durotrigia* sp. cf. *D. daveyi* is consistent with Feist-Burkhardt and Monteil (1997), although this taxon appears earlier in the Wessex and Swabian basins (Chapters 3, 4). The samples are dominated by *Batiacasphaera* spp., which represents around 50% of dinoflagellate cysts. *Batiacasphaera*? spp., *Dissiliodinium* spp., *Dissiliodinium*? spp., and *Nannoceratopsis gracilis* are also present in moderate abundances (5–10%; Figure 5.9).

*5.4.2. Upper Bajocian **P. parkinsoni** zone*

Dinoflagellate cyst floras from the Upper Bajocian, *P. parkinsoni* zone exhibit much greater richness compared to the two Lower Bajocian assemblages, with the inceptions of 42 taxa (Table 5.3).

5.4.2.1. Falaises des Hachettes

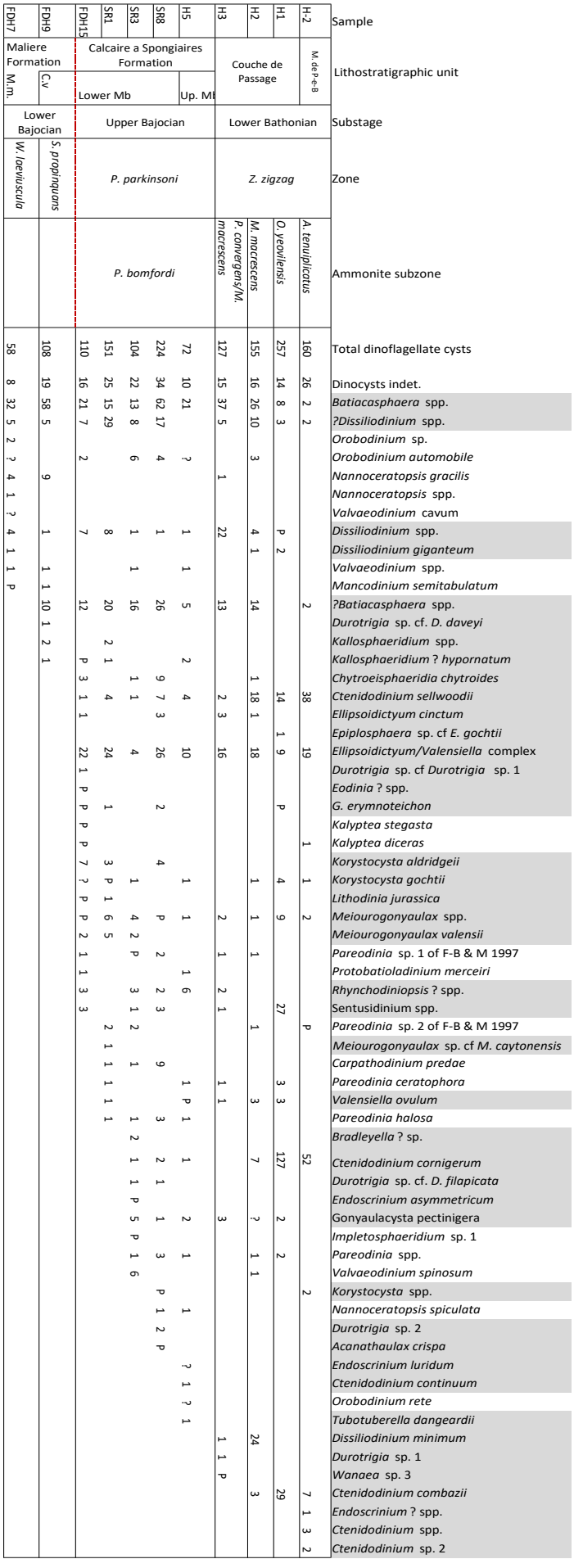

Table 5.3. Composite quantitative dinoflagellate cyst range chart for the Bajocian–Lower Bathonian of Normandy.
Grey fill denotes the gonyaulacacean taxa. The broken red line highlights the discontinuity of the composite range chart as samples from the Oolithe ferrugineuse de Bayeux formation, which spans the Upper–Lower Bajocian transition, were barren of palynomorphs.

In the uppermost sample from Falaises des Hachettes, which corresponds to the *P. parkinsoni* zone (*P. bomfordi* subzone) of the lowermost Calcaire à Spongiaires Formation, there are appearances of 18 taxa, 14 of which are gonyaulacaceans. The majority of these taxa have range bases which are lower than the *P. parkinsoni* zone. Taxa which have FADs in the *P. parkinsoni* zone include *Korystocysta aldridgeii*, the occurrence of this in the *P. parkinsoni* zone of Normandy is coeval with Swabia at a zonal level (Table 3.2b). The dinoflagellate cyst assemblage from this sample is dominated by *Batiacasphaera* spp., and the *Ellipsoidictyum/Valensiella* complex, which each comprise 20–30% of the dinoflagellate cysts (Figure 5.9).

5.4.2.2. Calcaire à Spongiaires Formation exposure (Locality SR)

In the three samples of the *P. parkinsoni* zone from Locality SR, there are 18 appearances (Table 5.3), ten of which are gonyaulacaceans. As with the underlying sample from the Falaises des Hachettes, the majority of taxa have first appearances which are lower than the *P. parkinsoni* zone. The assemblages are dominated by *Batiacasphaera* spp. and the *Ellipsoidictyum/Valensiella* complex, which each form 10–30% of dinoflagellate cyst taxa (Figure 5.9).

5.4.2.3. Port-en-Bessin harbour wall (locality H)

In the single sample (H5) from the uppermost Bajocian (*P. parkinsoni* zone, Calcaire à Spongiaires Formation) there are two appearances, both gonyaulacaceans (Table 5.3). The appearance of *Tubotuberella dangeardii* represents the FAD of this species, which lowers this from the *Z. zigzag* zone of the Bathonian (Feist-Burkhardt and Wille, 1992). In contrast, *Ctenidodinium continuum* appears in the *S. niortense* zone in Swabia (Table 3.2b). There is a questionable occurrence (due to poor preservation) of *Endoscrinium luridum*, the FAD of this species is in the *P. parkinsoni* zone in southern Germany (Feist-Burkhardt and Wille, 1992). Similarly, there is a questionable occurrence (due to poor preservation) of *Orobodinium rete*, which Feist-Burkhardt and Monteil (1997) recorded from the uppermost sample of the *P. parkinsoni* zone. As with locality SR, the dinoflagellate cyst assemblage is dominated by *Batiacasphaera* spp. and the *Ellipsoidictyum/Valensiella* complex (Figure 5.9).

Figure 5.9. Relative abundances of dinoflagellate cysts for the Bajocian–Lower Bathonian of Normandy (p.96).
Batiacasphaera spp. is abundant throughout, and the *Ellipsoidictyum/Valensiella* complex is abundant through the Upper Bajocian. There is a significant increase in the abundance of *Ctenidodinium*, particularly *C. cornigerum* in the Lower Bathonian. The increase in abundance is observed from sample H-1, which corresponds to the maximum flooding surface at the top of the Couche de Passage. *Z. zigzag* subzone abbreviations as per Figure 5.8. Taxa with an abundance of <5% have been removed for clarity.

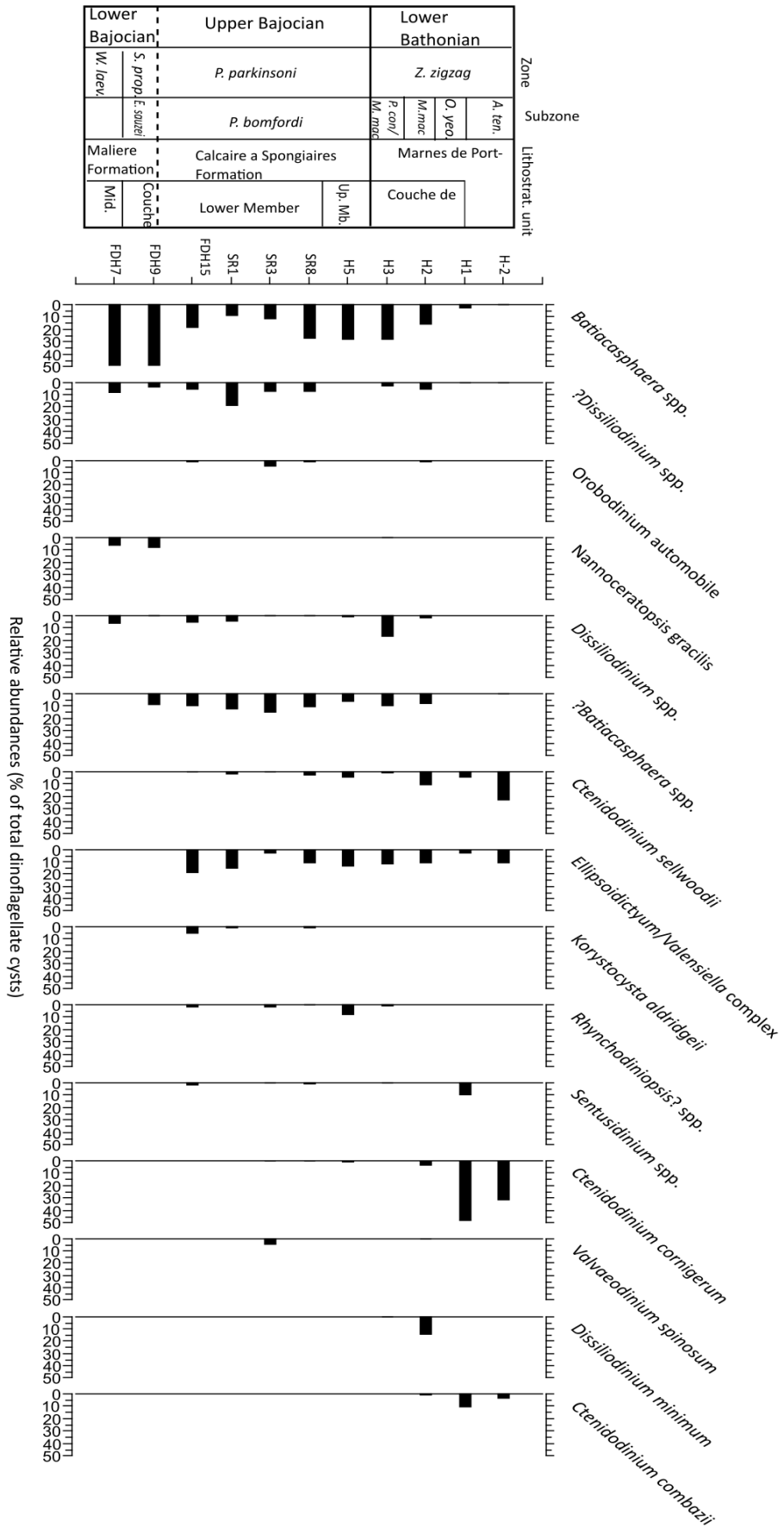

Figure 5.9. Relative abundances of dinoflagellate cysts for the Bajocian–Lower Bathonian of Normandy.
Caption on p. 95

*5.4.3. Lower Bathonian **Z. zigzag** zone*

5.4.3.1 Port-en-Bessin harbour wall (Locality H)

Five taxa, all of which are gonyaulacaceans appear in the *Z. zigzag* zone. *Ctenidodinium combazii* appears in the lowermost sample (H3), which corresponds to the *P. convergens/M. macrescens* subzones. This species has a FAD in the *P. parkinsoni* zone but Feist-Burkhardt and Monteil (1997) also recorded the local range base of this species from the lowermost *Z. zigzag* zone, *P. convergens* subzone. *Durotrigia* sp. 1 also appears in sample H3, but this species appears in the Lower Bajocian of the Swabian and Wessex basins (chapters 3, 4). The other three taxa all appear in the uppermost sample (H-2) which corresponds to the *A. tenuiplicatus* subzone. *Endoscrinium*? spp. and *Ctenidodinium* sp. 2 have range bases in the *S. humphriesianum* zone in Swabia (Table 3.2a), whilst *Ctenidodinium* spp. has been recorded from the *G. garantiana* to *Z. zigzag* zones in Swabia (Table 3.2b). The most striking pattern seen in the dinoflagellate cyst abundance data is the enormous increase in the abundance of *Ctenidodinium*, particularly *C. cornigerum* in the *Z. zigzag* zone. *Ctenidodinium cornigerum* is present in low abundances from the *P. parkinsoni* zone to sample H2 of the *Z. zigzag* zone, *M. macrescens* subzone. However, in the *O. yeovilensis* subzone, *C. cornigerum* comprises 50% of dinoflagellate cysts and in the uppermost subzone of the *Z. zigzag* zone (*A. tenuiplicatus*) it comprises 30% of dinoflagellate cysts. A similar pattern, although less pronounced, is observed in *Ctenidodinum sellwoodii* throughout the *Z. zigzag* zone. There is also an increase in the abundance of *Sentusidinium* spp. throughout the Lower Bathonian.

5.5. Comparisons with previous research

The total number of taxa recorded from the two Lower Bajocian samples of Falaises des Hachettes is similar to that recorded by Feist-Burkhardt and Monteil (1997). These authors examined three samples from the *W. laeviuscula* zone and one from the *S. propinquans* zone, and reported 13 taxa. Eleven taxa are reported herein, with questionable appearances of two taxa due to poor preservation. The quantitative data collected from this thesis demonstrate that the Lower Bajocian samples contain abundant spores and pollen, with low to moderate marine:terrestrial ratios, indicating that the Maliere Formation was deposited in a relatively proximal environment. The low richness of dinoflagellate cysts from this interval may therefore be related to the palaeoenvironmental setting. Moreover, the absolute abundances of palynomorphs is very low which may indicate that that palynomorphs were transported to more distal areas (section 5.6).

As previously mentioned, the samples from the Oolithe ferrugineuse de Bayeux Formation were palynologically barren. Feist-Burkhardt and Monteil (1997) reported negative results from the *S. humphriesianum* zone, having sampled the stromatolitic upper part of Bed A. These authors substituted samples from ammonite-dated inland exposure of ferruginous oolitic limestone from Saint-Martin-de-Fontenay, but provided no locality details or map of this exposure. For this thesis, the oncoidal lower part of Bed A, as well as the stromatolitic upper part, were sampled, but both samples proved barren

of palynomorphs. Feist-Burkhardt and Monteil (1997) recorded 14 appearances from a single sample of the *S. niortense* zone of bed B of Oolithe ferrugineuse de Bayeux Formation, but the sample processed from the same horizon herein was barren. Similarly, Feist-Burkhardt and Monteil (1997) recorded 24 taxa, and one appearance from Bed C of the *G. garantiana* zone, whilst the equivalent sample processed here was barren. The sample from Bed D which corresponds to lowermost *P. parkinsoni* zone was also barren, but Feist-Burkhardt and Monteil (1997) recorded six appearances from this unit.

The pattern observed from the overlying *P. parkinsoni* zone (*P. bomfordi* subzone) of the Calcaire à Spongiaires Formation is similar to that observed by Feist-Burkhardt and Monteil (1997). These authors recorded 20 appearances, and 54 taxa. Herein, 48 taxa were recorded. The pattern of appearances from the samples examined (Table 3) is relatively continuous throughout the Calcaire à Spongiaires Formation, and a similar pattern was recorded by Feist-Burkhardt and Monteil (1997).

The Calcaire à Spongiaires Formation is overlain by the Couche de Passage, which corresponds to the *P. convergens*, *M. macrescens* and *O. yeovilensis* subzones of the Lower Bathonian, *Z. zigzag* zone. Five appearances were recorded from samples examined herein, and Feist-Burkhardt and Monteil (1997) also reported five appearances.

The Couche de Passage is overlain by marls and limestone of the Marnes de Port-en-Bessin Formation, which corresponds to the. *A. tenuiplicatus* subzone of the *Z. zigzag* zone. Three appearances were recorded from the single sample, H-2 examined from this unit, whilst Feist-Burkhardt and Monteil (1997) recorded no appearances.

5.6. Palynomorph preservation

The large proportion of barren samples from Normandy is enigmatic, as many barren horizons herein yielded palynomorphs according to Feist-Burkhardt and Monteil (1997). However, the stratigraphic distribution of barren samples is not random, which may point towards the taphonomic processes which have driven barren recoveries. Of the six samples from the Lower Bajocian, Maliere Formation, only two were productive. In contrast, none of the five samples examined from the overlying Oolithe ferrugineuse de Bayeux Formation were productive. Eleven samples were processed from the Upper Bajocian Calcaire à Spongiaires Formation, of which five were productive. Furthermore, five samples were processed from the Lower Bathonian Couche de Passage/Marnes de Port-en-Bessin Formations, of which four were productive. Consequently, these barren recoveries are concentrated in the Maliere and Oolithe ferrugineuse de Bayeux formations.

Dinoflagellate cysts, and palynomorphs in general, are subject to various taphonomic processes. Palynomorphs behave hydrodynamically like silt particles, and are concentrated in fine-grained siliciclastic sediments (Dale, 1976; Traverse, 2007). Dinoflagellate cysts are sensitive to destruction by oxygenated bottom waters (Zonneveld et al., 2008 and references therein), whilst early-stage and long-

term diagenetic processes can alter the molecular composition of palynomorphs via sulphurisation and thermal alteration (Yule et al., 2000; Zonneveld et al., 2008). Recrystallization in carbonate rocks can result in the destruction of palynomorphs (Traverse, 2007), whilst uplift and subsequent weathering can destroy organic material.

The absolute abundance of palynomorphs in the two productive samples from the Maliere Formation is much lower than that of the Calcaire à Spongiaires or Couche de Passage/Marnes de Port-en-Bessin formations. The Maliere Formation is condensed unit, with ~4 m of sediment representing the *W. laeviuscula* and *S. propinquans* zones, which according to the cyclostratigraphic timescale of Sucheras-Marx et al. (2013) represent around 2 myr (Figure 1.11). In contrast, the Upper Bajocian Calcaire à Spongiaires Formation represents a single ammonite subzone, yet is ~20 m in thickness. Consequently, it is likely that sedimentation rates greatly increased in the Upper Bajocian of the Paris Basin (Rioult et al., 1991). If the flux of palynomorphs was constant, then it would be expected that there would be a lower abundance of palynomorphs in the Calcaire à Spongiaires Formation due to dilution. However, the opposite trend is observed. Moreover, a higher proportion of productive samples were observed from the Calcaire à Spongiaires Formation than the Maliere Formaiton. Furthermore, the Oolithe ferrugineuse de Bayeux Formation is extremely condensed, as three ammonite zones are represented by <50 cm of sediment, and no productive samples were collected from this formation.

Sedimentation rate therefore appears to be strongly correlated with palynomorph abundance and preservation. During sediment-starved condensed intervals, such as those represented by the Maliere and Oolithe ferrugineuse de Bayeux formations, the flux of sporomorphs transported in fine-grained sediments would have been low. Moreover, palynomorphs which settled through the water column, such as microplankton and windblown bisaccate pollen, would have been left exposed on the seafloor for long periods of time, due to low sedimentation rates. Consequently, bottom water currents could have easily reworked and transported palynomorph assemblages at the sediment-water interface to other areas of the basin. Productive horizons may be explained by brief fluxes of rapid sedimentation. This scenario of differential transport is supported by observations from modern carbonate environments. Traverse and Ginsburg (1966) documented pollen and associated palynomorph assemblages from the Great Bahama Bank. The distribution of palynomorphs was strongly influenced by differential transport. In areas of intense turbulence, palynomorphs were eroded and transported, whereas, in quiet water areas they were deposited. Consequently, palynomorph assemblages exhibit a high degree of lateral variability in abundance (Traverse and Ginsburg, 1966). This may explain the sporadic recovery of palynomorphs, and the differences in productivity between the samples in this study, and those of Feist-Burkhardt and Monteil (1997). It is also possible that the growth of diagenetic cements and recrystallization resulted in the patchy distribution of palynomorphs throughout the Normandy succession. Palaeoredox of bottom waters in the Paris Basin does not appear to have exerted a significant control on palynomorph preservation as all samples from the Oolithe ferrugineuse de Bayeux Formation were barren, yet this

unit was deposited under largely dysoxic bottom water conditions (section 5.1.1.2).

5.7. Palaeoenvironmental interpretations from palynology and implications for dinoflagellate cyst appearances

Given that palynomorphs were subjected to differential transport in the Paris Basin, can the composition of palynomorph assemblages still provide useful palaeoenvironmental information? From a broad perspective, samples from the Lower Bajocian Maliere Formation are dominated by sporomorphs. In contrast, samples from the Upper Bajocian to Lower Bathonian generally record higher marine:terrestrial ratios, which peak in the Lower Bathonian, Marnes de Port-en-Bessin Formation. As documented in section 5.1.1.2, sequence stratigraphic interpretations demonstrate a series of third-order transgressive-regressive cycles in the Paris Basin, which reflect the second-order T7 sea level cycle. The distinct lithological change to the fine-grained marls of the Marnes de Port-en-Bessin Formation represents the maximum transgression of the T7 sea level cycle in the Paris Basin (Rioult et al., 1991). This is reflected in the palynomorph assemblages, as peak marine:terrestrial ratios of ~0.90 were recorded in sample H1, which was taken from the maximum flooding surface which is formed by the upper contact of the Couche de Passage (Figure 5.6). Consequently, the broad shifts in the composition of palynomorph assemblages track an overall shift to a more distal environment of deposition through the Bajocian–Lower Bathonian, which is consistent with sedimentological data.

Within microplankton assemblages, acanthomorph acritarchs are moderately abundant in the Upper Bajocian, but decline in absolute abundance in the Lower Bathonian. This decline is concomitant with the increase in abundance of dinoflagellate cysts. This supports the observations from the Swabian Basin that acanthomorphs were poorly-adapted to offshore, fully-marine conditions, in comparison to dinoflagellates during the Mid Jurassic. In terms of dinoflagellate cyst assemblage compositions, the Lower Bajocian samples are dominated by *Batiacasphaera*, whilst samples from the Upper Bajocian are dominated by *Batiacasphaera* and the *Ellipsoidictyum/Valensiella* complex (Figure 5.9). This is broadly comparable to the pattern seen in dinoflagellate cyst abundances in the neighbouring Wessex Basin, indicating that dinoflagellate cyst assemblages in the Paris Basin recorded a primary palaeoecological signal. *Batiacasphaera* spp. and the *Ellipsoidictyum/Valensiella* complex may have thrived in the carbonate ramp environments of these basins (Chapter 8). A significant change occurred in the Lower Bathonian, where *Ctenidodinium*, particularly *C. cornigerum*, increases in abundance (Figure 5.9). This mirrors the pattern seen in the Swabian Basin with *C. combazii,* and as such appears to represent a primary palaeoecological signal. Given the coincidence of acme of *C. cornigerum* with maximum flooding in the Early Bathonian, this species may have been adapted to normal salinity, fully marine conditions (Chapter 8).

The increase in dinoflagellate cyst richness from the Lower Bajocian to the Upper Bajocian–Lower

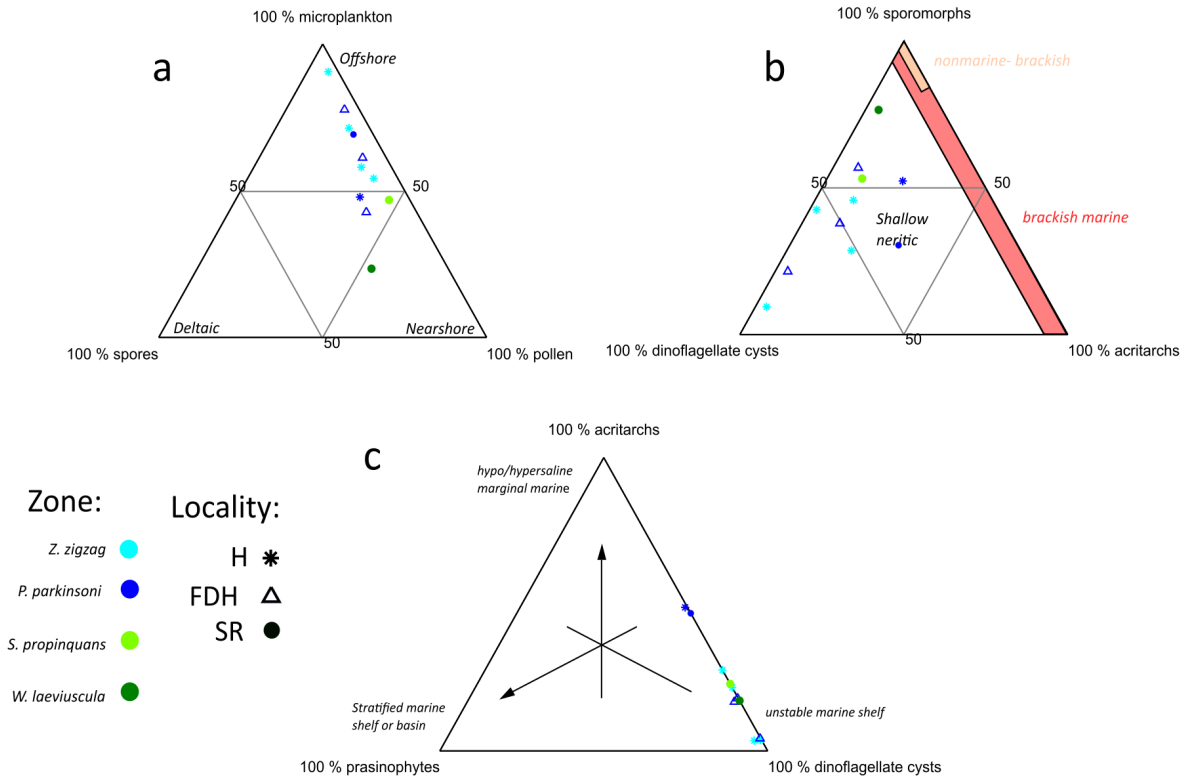

Figure 5.10. Ternary plots for Normandy.
a= microplankton-spores-pollen plot, after Federova (1977), Duringer and Doubinger (1985). b= sporomorph-acritarch-dinoflagellate cyst plot, after Burger (1980). c= phytoplankton plot, after Tyson (1993).
Plot A shows that samples from Normandy are dominated by microplankton and pollen. Samples from the Lower Bajocian are dominated by pollen, whilst samples from the Upper Bajocian *P. parkinsoni* zone and Lower Bathonian *Z. zigzag* zone contain a higher proportion of microplankton. Plots B and C show that within microplankton assemblages, dinoflagellate cysts are generally dominant.

Bathonian is therefore associated with a broad shift from a more proximal palaeoenvironment in the Maliere Formation, to a distal, offshore environment of deposition in the Marnes de Port-en-Bessin Formation. This is broadly comparable to the pattern seen in the Swabian Basin, and indicates that changes in relative sea level exerted significant control on the pattern of dinoflagellate cyst appearances in Europe during the Mid Jurassic (Chapter 8). Moreover, the burst of appearances recorded by Feist-Burkhardt and Monteil from the *S. humphriesianum* and *S. niortense* zones of the Oolithe ferrugineuse de Bayeux Formation are correlated with two major transgressive pulses, as these zones represent two third-order cycles (section 5.1.1.2).

5.8. Summary

Despite numerous barren samples, dinoflagellate cyst assemblages from the Paris Basin record an increase in richness from the Lower to Upper Bajocian–Lower Bathonian. The preservation of palynomorphs was probably driven by sedimentation rate, with extremely low sedimentation rates in the condensed parts of the succession resulting in the erosion and transport of palynomorphs. Lateral variability in water

turbulence may have driven lateral variability in the abundance and preservation of palynomorphs, which can be observed in modern carbonate environments. Palynomorph assemblages record a shift from a more proximal to a distal environment of deposition from the Lower Bajocian to the Lower Bathonian. This is supported by sedimentology, indicating that broad trends in palynomorph assemblages are reliable palaeoenvironmental indicators. Consequently, the increase in dinoflagellate cyst richness is broadly correlated with an overall shift to a more distal palaeoenvironment, which is comparable to the pattern seen in the Swabian Basin. In terms of palaeoecological patterns, Lower Bajocian dinoflagellate cyst assemblages are dominated by *Batiacasphaera* spp., whilst the Upper Bajocian is dominated by *Batiacasphaera* spp. and the *Ellipsoidictyum/Valensiella* complex. This pattern is broadly comparable to that in the Wessex Basin, and may indicate that these dinoflagellate cyst groups proliferated in the carbonate ramp environments of these depocentres. The Lower Bathonian is marked by the acme of *Ctenidodinium*, particularly *C. cornigerum*, which is coincident with maximum flooding. This pattern largely mirrors that seen in the Swabian Basin with *C. combazii,* and is fully documented in Chapter 8.

Chapter 6. Systematic palaeontology of dinoflagellate cysts

6.1 Introduction

The classification of thecate dinoflagellates and their cysts is primarily based on tabulation pattern (Chapter 1; Fensome et al., 1993). This phenotypic classification is well supported by molecular data, particularly for the Gonyaulacales (Janouškovec et al., 2017), which represent the majority of taxa recorded during this study. These, and other taxa encountered, are described below and have been arranged alphabetically within each taxonomic rank. The classification of genera and species follows that of Williams et al. (2017), except where emendations have been made. The terminology used for the description of dinoflagellate cysts follows that of Williams et al. (2000). The 'para' prefix has not been used as it is clear that this thesis deals with cysts rather than motile cells. Tabulation has been described using Kofoid terminology (Evitt, 1985). The slide number and England Finder co-ordinates of all figured specimens are included in the plate captions.

The stratigraphic occurrence for the region(s) each taxon was recorded from is given below. All measurements are in micrometers (μm). Unless otherwise stated, 'width' refers to the maximum lateral width of the dinoflagellate cyst, and 'length' refers to the total length from the antapex (posterior) to the apex (anterior). For spherical-shaped taxa, the diameter is given. Where minimum, mean and maximum measurements are stated they are given as 'minimum (mean) maximum', e.g. '60 (75) 90 μm'. The number of specimens which were measured is indicated by 'n'.

6.1.2. Use of open nomenclature

Morphotypes have been encountered during the study for this thesis of which there are too few specimens for the erection of new species, or are too poorly preserved to allow identification to species level. These have been documented as using open nomenclature (Table 6.1). Further, genera which lack tabulation such as *Batiacasphaera*, *Dissiliodinium, Sentusidinium*, and *Ellipsoidictyum*/*Valensiella* are difficult to handle taxonomically due to their lack of informative characters and highly plastic morphology. These have been grouped together as spp.. Although this is not an ideal approach, many workers (e.g. Riding et al., 1991; Feist-Burkhardt and Wille, 1992; Feist-Burkhardt and Monteil 1997; Mantle and Riding, 2012; Feist-Burkhardt and Götz, 2016) have also used these broad morphological groupings in previous Bajocian dinoflagellate cyst studies. The usage of "?" and "cf." is explained in Table 6.1. A list of the dinoflagellate cyst taxa recorded in this thesis is given in Table 6.2, along with page numbers for each taxon's description.

Symbol/Abbreviation	Explanation
sp.	A morphotype which cannot be attributed to an existing species but insufficient material is available for the erection of a new species
spp.	Morphotypes which cannot be attributed to an existing species but are too variable or morphologically plastic to separate as distinct morphotypes
"?" after genus name	Specimens questionably assigned to a genus as they do not fully exhibit generic level characteristics, or exhibit characters that are not associated with that genus.
"?" before genus name	Specimens which were too poorly preserved to confidently attribute to the genus/species
cf .	The use of *confer* denotes morphotypes which differ sufficiently in morphology that they can only be compared with an existing species, rather than attributed to it.

Table 6.1. Use of open nomenclature for dinoflagellate cyst taxa- recorded for this thesis.

Acanthaulax crispa	p. 111	*Endoscrinium* sp.	p. 118	*Nannoceratopsis ambonis*	p. 105				
Aldorfia aldorfensis	p. 111	*Endoscrinium* sp. cf. *E. luridum*	p. 118	*Nannoceratopsis dictyambonis*	p. 105				
Atopodinium polygonale	p. 126	*Endoscrinium* ? spp.	p. 119	*Nannoceratopsis gracilis*	p. 105				
Batiacasphaera spp.	p. 126	*Eodinia* ? sp.	p. 119	*Nannoceratopsis plegas*	p. 105				
?*Batiacasphaera* spp.	p. 126	*Eodinia* ? spp.	p. 119	*Nannoceratopsis spiculata*	p. 106				
Bradleyella sp.	p. 112	*Epiplosphaera* sp. cf *E. gochtii*	p. 128	*Nannoceratopsis* spp.	p. 106				
Bradleyella ? sp.	p. 112	*Gongylodinium erymnoteichon*	p. 128	*Orobodinium automobile*	p. 131				
Carpathodinium predae	p. 108	*Gonyaulacysta jurassica* subsp. *adecta*	p. 120	*Orobodinium rete*	p. 132				
Carpathodinium sp. of Riding et al. 1991	p. 108	*Gonyaulacysta pectinigera*	p. 120	*Orobodinium* sp.	p. 132				
Chytroeisphaeridia chytroeides	p. 127	*Gonyaulacysta* ? sp.	p. 120	*Orobodinium* sp. A of Gocht & Wille 1990	p. 132				
Ctenidodinium continuum	p. 113	*Impletosphaeridium* sp. 1	p. 129	*Pareodinia ceratophora*	p. 106				
Ctenidodinium cornigerum	p. 113	*Impletosphaeridium* sp. 2	p. 130	*Pareodinia halosa*	p.107				
Ctenidodinium ornatum	p. 113	*Jansonia psilata*	p. 109	*Pareodinia* sp. 1 of Feist-Burkhardt & Monteil 1997	p.107				
Ctenidodinium sp. 1	p. 114	*Jansonia* sp. 1	p. 110	*Pareodinia* sp. 2 of Feist-Burkhardt & Monteil 1997	p.107				
Ctenidodinium sp. 2	p. 114	*Jansonia* sp. 2	p. 110	*Pareodinia* spp.	p.107				
Ctenidodinium spp.	p. 114	*Kallosphaeridium* spp.	p. 123	*Phallocysta elongata*	p. 132				
Ctenidodinium ? sp.	p. 114	*Kallosphaeridium* ? *hyporatum*	p. 123	*Protobatioladinium mercieri*	p. 108				
Ctenidodinium sellwoodii	p. 113	*Kalyptea diceras*	p. 108	*Rhychodiniopsis* sp. cf. *R* ? *regalis*	p. 124				
Ctenidodonium combazii	p. 112	*Kalyptea* sp.	p. 109	*Rhychodiniopsis* ? spp.	p. 125				
Dissiliodinium giganteum	p. 115	*Kalyptea stegasta*	p. 109	*Rhynchodiniosis* ? *regalis*	p. 124				
Dissiliodinium minimum	p. 116	*Korystocysta aldridgeii*	p. 121	*Sentusidinium* spp.	p. 128				
Dissiliodinium spp.	p. 116	*Korystocysta gochtii*	p. 120	*Tubotuberella dongeardii*	p. 110				
Dissiliodinium ? *hoeneratum*	p. 116	*Korystocysta pachyderma*	p. 121	*Tubotuberella* sp.	p. 110				
?*Dissiliodinium* spp.	p. 116	*Korystocysta* sp. 1	p. 122	*Valensiella ampulla*	p. 129				
Durotrigia sp. cf. *Durotrigia* sp. 1	p. 118	*Korystocysta* sp. 2	p. 122	*Valensiella ovulum*	p. 129				
Durotrigia daveyi	p. 117	*Korystocysta* spp.	p. 122	*Valvaeodinium cavum*	p. 130				
Durotrigia sp. 1	p. 117	*Lithodinia jurassica*	p. 123	*Valvaeodinium* sp. cf. *V. spinosum*	p. 131				
Durotrigia sp. 2	p. 117	*Mancodinium semitabulatum*	p. 109	*Valvaeodinium spinosum*	p. 131				
Durotrigia sp. cf. *D. daveyi*	p. 117	*Meiourogonyaulax* sp. cf. *M. caytonensis*	p. 124	*Valvaeodinium* spp.	p. 131				
Durotrigia sp. cf. *D. filapicata*	p. 117	*Meiourogonyaulax* spp.	p. 124	*Valvaeodinium vermicylindratum*	p. 131				
Durotrigia ? sp.	p. 118	*Meiourogonyaulax valensii*	p. 123	*Wanaea acollaris*	p. 125				
Ellipsoidictyum cinctum	p. 127	*Mendicodinium* sp.	p. 130	*Wanaea* sp. 1	p. 125				
Ellipsoidictyum/Valensiella complex	p. 127	*Moesiodinium raileanui*	p. 130	*Wanaea* sp. 2	p. 125				
Endoscrinium asymmetricum	p. 118			*Wanaea* sp. 3	p. 125				

Table 6.2. List of dinoflagellate cyst taxa recorded in this thesis, with page numbers of descriptions.

Division DINOFLAGELLATA Fensome et al. 1993

Subdivision DINOPHYCEAE Fensome et al. 1993

Class DINOPHYCEAE Pascher 1914

Subclass DINOPHYSIPHYCIDAE Möhn 1984 ex Fensome et al. 1993

Order NANNOCERATOPSIALES Piel & Evitt 1980

Family NANNOCERATOPSIACEAE Gocht 1970

Nannoceratopsis Deflandre 1939 emend. Riding and Helby 2001

Nannoceratopsis ambonis Drugg1978 emend. Riding 1984 (Plate XII, 10)

Remarks: This species is similar to *N. gracilis* but is distinguished by its thickened, solid, sagittal band. *Nannocertaopsis ambonis* was encountered in samples from the *G. concavum* to the lowest part of the *S. humphriesianum* zone in Swabia and the *S. propinquans* zone in Skye.

Dimensions: dorso-ventral width: 49 (52.6) 70 µm; length: 59.4 (75) 90 µm; n= 5.

Nannoceratopsis dictyambonis Riding 1984

Remarks: *Nannoceratopsis dictyambonis* is distinguished by its distinctive reticulate sagittal band. This species was recorded from the *H. discites*, *W. laeviuscula/S. propinquans* and *S. humphriesianum* zones of Swabia and the *G. concavum* zone of Dorset.

Dimensions: dorso-ventral width: 37.8/54 µm; length: 66.6/63 µm; n= 2.

Nannoceratopsis gracilis Alberti 1961 emend. van Helden 1977 (Plate XII, 7)

Remarks: *Nannoceratopsis gracilis* has two antapical horns of unequal length and a psilate to microreticulate autophragm. The morphology is variable, particularly the development of the ventral antapical horn. In some specimens this is a distinct, pointed horn, whilst in others it is a slightly-rounded protrusion. This variability seems to reflect a continuous morphological spectrum. *Nannoceratopsis gracilis* was encountered consistently from the *G. concavum* to the lower part of the *S. humphriesianum* zone and sporadically from the *S. niortense*, *G. garantiana* and *Z. zigzag* zones in Swabia. In Dorset it occurs in the *G. concavum* to *S. propiquans* zones, it was recorded from the *W. laeviuscula* and *S. propinquans* zones of Normandy with a single specimen encountered in the *P. parkinsoni* zone. In Skye it was recorded from the *H. discites* to *S. humphriesianum* zones.

Dimensions: dorso-ventral width: 36 (43) 62 µm; length: 56 (73.5) 85 µm; n= 35.

Nannoceratopsis plegas Drugg 1978 (Plate XII, 9)

Remarks: This species has a sickle-like outline due to the prominent dorsal antapical horn. It was recorded from the *W. laeviuscula*, *S. humphriesianum* and *G. garantiana* zones in Swabia, the *G. concavum* zone of Dorset, and the *W. laeviuscula* zone of Skye.

Dimensions: dorso-ventral width: 46.8 (52.5) 57.6 µm; length: 48.6 (68.4) 77.4 µm; n= 4.

Nannoceratopsis spiculata Stover 1966 (Plate XII, 8)

Remarks: *Nannoceratopsis spiculata* is defined by its two prominent antapical horns of approximately equal length, with apparent cavation at the tips. It was recorded from the *W. laeviuscula* to *Z. zigzag* zones of Swabia, the *G. concavum*, *G. garantiana* and *P. parkinsoni* zones of Dorset, the *P. parkinsoni* zone of Normandy, and the *W. laeviuscula* zone of Skye.

Dimensions: dorso-ventral width: 44 (52) 61 µm; length: 79 (83) 88 µm; n= 4.

Nannoceratopsis spp. (Plate XII, 11–12)

Remarks: Morphotypes of *Nannoceratopsis* are often highly variable yet simple in morphology. Consequently, forms were recorded which could not be assigned to an existing species. These are grouped together as *Nannoceratopsis* spp. and vary from triangular to sub-ovoidal with a scabrate to microreticulate autophragm. The antapical horns are pointed to bulbous/globulose. They were encountered from the *W. laeviuscula* to the *Z. zigzag* zones in Swabia, the *P. parkinsoni* zone in Dorset, the *W. laeviuscula* zone in Normandy, and the *W. laeviuscula* and *S. propinquans* zones of Skye.

Dimensions: dorso-ventral width: 54 (64.4) 81 µm; length: 32.4 (40) 54 µm; n= 5.

Subclass PERIDINIPHYCIDAE Fensome et al. 1993

Order GONYAULACALES Taylor 1980

Suborder CLADOPYXIINEAE Fensome et al. 1993

Family PAREODINIACEAE Gocht 1957

Subfamily PAREODINIOIDEAE (Autonym)

Pareodinia Deflandre 1947 emend. Below 1990

Pareodinia ceratophora Deflandre 1947 emend. Gocht 1970 (Plate XII, 1–2).

Remarks*: Pareodinia ceratophora* is variable in its morphology but is distinguished by its anterior intercalary archaeopyle, apical horn and elongate body; some specimens bear a kalyptra. This species was encountered from the *H. discites* to the *Z. zigzag* zones in Swabia. It occurs in the *P. parkinsoni* and

Z. zigzag zones of Normandy, the *G. concavum*, *H. discites*, *G. garantiana* and *P. parkinsoni* zones in Dorset, and the *H. discites* zone in Skye.

Dimensions: width: 43.2 (54) 70.2 µm; length including apical horn: 59.4 (79.9) 95.4 µm; n= 5.

Pareodinia halosa (Filatoff 1975) Prauss 1989 emend. Prauss 1989 (Plate XII, 3–4)

Remarks: This distinctive species is characterised by its sub-circular shape and prominent kalyptra which is often highly variable in shape and size (which may be the result of differing preservation), a few specimens showing 'sculpting' of the kalyptra (plate XII, 4). This species occurs in the *G. concavum–Z. zigzag* zones of Swabia, the *H. discites*, *W. laeviuscula, S. propinquans*, *G. garantiana* and *P. parkinsoni* zones of Dorset, in Skye it occurs through the *H. discites* to *S. humphriesianum* zones and in Normandy it is present in *P. parkinsoni* zone.

Dimensions: width with kalyptra: 32.4 (50) 86.4 µm, width without kalyptra: 23.4 (34.4) 48.6 µm; length with kalyptra: 36 (59) 81 µm, length without kalyptra: 19.8 (41) 59.4 µm; n= 30.

Pareodinia sp. 1 of Feist-Burkhardt & Monteil 1997 (Plate XIV, 4)

Remarks: This morphotype is distinguished by its broad apical horn and rugulate wall; it was encountered in samples from the *G. garantiana* zone of Dorset and the *P. parkinsoni* to *Z. zigzag* zones of Normandy.

Dimensions: width: 26 µm; length (including apical horn): 32.5 µm; n=1.

Pareodinia sp. 2 of Feist-Burkhardt & Monteil 1997 (Plate XIV, 5)

Remarks: This form is distinguished by its reduced apical horn which imparts a semicircular outline to the cyst body. This morphotype was encountered from the *P. parkinsoni* and *Z. zigzag* zones of Normandy.

Dimensions: width: 26 µm; length: 27.5 µm; n=1.

Pareodinia spp.

Remarks: Forms not attributable to any of those described above or existing species of *Pareodinia* were encountered in low numbers from the *P. parkinsoni* and *Z. zigzag* zones of Normandy. These have apical horn, scabrate autophragms and occasionally possess small spines towards the antapex.

Dimensions: width: 28.8 (29.4) 30.6 µm; length (including apical horn): 55.8 (58.8) 63 µm; n= 3.

Protobatioladinium Nøhr-Hansen 1986

Remarks: *Protobatioladinium* is distinguished from *Pareodinia* by its archaeopyle which is formed

from a combination of the anterior intercalary plates and apical homologues, whereas *Pareodinia* has an archaeopyle formed by the loss of two to three intercalary plates.

Protobatioladinium mercieri Feist-Burkhardt & Pross 1999 (Plate XII, 5–6)

Remarks: *Protobatioladinium mercieri* has a thick, scabrate autophragm, the apical horn is elongate to conical in shape and rounded at the tip. A faint cingulum is marked by low sutural ridges. This species was recorded from the *G. garantiana* zone and *Z. zigzag* zone of Swabia and the *P. parkinsoni* zone of Normandy.

Dimensions: width: 49.9 (53.8) 56.5 µm; length (including apical horn): 74.5 (84.5) 89.8 µm; n= 3.

Subfamily BROOMEOIDEAE (Eisenack 1969) Fensome et al. 1993

Carpathodinium Drugg 1978 emend. Below 1990

Carpathodinium predae (Beju 1971) Drugg 1978 emend. Below 1990 (Plate X, 6, Plate XIV, 6)

Remarks: *Carpathodinium predae* has well-defined tabulation and is small in size; it was encountered from the *S. niortense* to *Z. zigzag* zones of Swabia and the *P. parkinsoni* zone in Dorset and Normandy.

Dimensions: width: 23.4 (29) 37.2 µm; length: 41.4 (44.8) 48.6 µm; n= 5.

Carpathodinium sp. of Riding et al. 1991

Remarks: A single specimen was recorded from the *H. discites* zone of Skye. It is squatter and wider than *C. predae* and is too poorly preserved and partially obscured to fully interpret. This form is similar in its morphology to *Carpathodinium* sp. A of Feist-Burkhardt (1990) which was reported from the Upper Aalenian and Lower Bajocian of southern Germany. However, *Carpathodinium* sp. of Riding et al. 1991 has a much thicker authophragm.

Dimensions: width: 42 µm; length: 45 µm; n= 1.

Kalyptea Cookson and Eisenack 1960 emend. Wiggins 1975

Kalyptea diceras Cookson and Eisenack 1960 emend. Fisher & Riley 1980

Remarks: The genus *Kalyptea* is distinguished by possessing apical and antapical horns. In this, the type species, the apical horn is longer than the antapical counterpart; the latter is broader and more bulbous in shape. No specimens encountered had a kalyptra. *Kalyptea diceras* was recorded from the *P. parkinsoni* and *Z. zigzag* zones of Normandy; a single specimen was recorded from the *P. parkinsoni* zone of Dorset.

Dimensions: width: 27 µm; length: 57.5 µm; n= 1.

Kalyptea stegasta (Sarjeant 1961) Wiggins 1975

Remarks: The polar horns are of roughly equal length and are pointed to rounded at the tips. *Kalyptea stegasta* was recorded the *P. parkinsoni* zone in Swabia and Normandy, and in the *G. garantiana* zone of Dorset.

Dimensions: width including kalyptra: 72 µm, without kalyptra: 48.5 µm; length including kalyptra: 102.5 µm, length without kalyptra: 95.5 µm; n= 1.

Kalyptea sp.

Remarks: This form was encountered in one sample from the *G. garantiana* zone of Dorset. It has a psilate wall and horns of approximately equal length, both of which have rounded tips. The antapical horn is slightly broader than the apical. It is distinguished from other species of *Kalyptea* by its psilate wall and horns of equal length.

Dimensions: width: 21.5 µm; length: 47 µm; n= 1.

Family MANCODINIACEAE Fensome et al. 1993

Subfamily MANCODINIOIDEAE (Autonym)

Mancodinium Morgenroth 1970 emend. Below 1987

Mancodinium semitabulatum Morgenroth 1970 emend. Below 1987 (Plate XIV, 1)

Remarks: The sulcal tab formed by the anterior sulcal plate and disintegration archaeopyle, make *M. semitabulatum* a very distinctive species. This species was recorded from the *W. laeviuscula* zone in Swabia, the *G. concavum*, *H. discites* and *S. propinquans* zones in Dorset and the *S. propinquans* zone of Normandy. There is a single questionable occurrence from the *H. discites* zone of Skye.

Dimensions: width: 32.4 (38.4) 43.9 µm; length of hypocyst: 25.2 (30.4) 42.42 µm; n= 4.

Family UNCERTAIN

Jansonia Pocock 1972 emend. Riding & Walton in Riding et al. 1991

Remarks: *Jansonia* is herein assigned to the Cladopyxiineae, as it exhibits a partiform tabulation pattern (e.g. Plate XIII, 2).

Jansonia psilata Martinez et al. 1999 (Plate XIII, 2)

Remarks: *Jansonia psilata* was recorded sporadically, and in low numbers from the *S. humphriesianum* zone to the *G. garantiana* zone of Swabia, and is distinguished by its clearly defined tabulation indicated by low sutural crests and psilate autophragm. This is the first record of this species from Europe.

Dimensions: width: 18 (21.3) 25.2 µm; length: 18 (19.3) 21.6 µm; n= 4.

Jansonia sp. 1 (Plate XIII, 3–4)

Remarks: A single specimen of *Jansonia* sp. 1 was recorded from the *H. discites* zone of Swabia. It has a rugulate autophragm and the tabulation is faintly defined on the hypocyst by low sutural ridges but the cingulum is prominent.

Dimensions: width: 30 µm; length 35 µm; n= 1.

Jansonia sp. 2 (Plate XIII, 5)

Remarks: *Jansonia* sp. 2 encountered as a single specimen from the *H. discites* zone of Swabia. It has a thick, creased autophragm, and a well-defined cingulum.

Dimensions: width: 29.5 µm; length: 34.5 µm; n= 1.

Suborder GONYAULACINEAE (autonym)

Family GONYAULACEAE Lindemann 1928 emend. Feist-Burkhardt 1995

Subfamily GONYAULACOIDEAE (autonym)

Tubotuberella Vozzhennikova 1967 emend. Dodekova 1990

Tubotuberella dangeardii (Sarjeant 1968) Stover & Evitt 1978 emend. Sarjeant 1982

Remarks: One specimen of this species was recorded from the *P. parkinsoni* zone of Normandy, the pericoel is particularly large on the hypocyst and is capped by small denticles.

Dimensions: width: 50.5 µm; length including pericoel: 93.5 µm, length excluding pericoel: 68.5 µm; n= 1.

Tubotuberella sp.

Remarks: A single specimen with prominent apical and antapical cavation was recorded from the *P. parkinsoni* zone of Swabia. Poor preservation prevented identification to species level.

Dimensions: width: 57.5 µm; length including pericoel: 86.5 µm; n= 1.

.

Subfamily LEPTODINIOIDEAE Fensome et al. 1993

Acanthaulax Sarjeant 1968 emend. Sarjeant 1982

Acanthaulax crispa (Wetzel 1967) Woollam & Riding 1983 (Plate I, 1–6).

Remarks: This species displays considerable morphological variation. Some forms are very close to the morphology of the holotype in possessing a differentiated autophragm, intratabular crests, sutural crests with small capitate and/or baculate processes and an apical horn. However, many specimens are enigmatic and difficult to interpret, but have a thick, spongy differentiated autophragm, which is covered in dense rugulate ornamentation. Tabulation is variably expressed, usually indistinctly by low sutural ridges, sometimes formed from the merging of the rugulate ornament. The development of sutural crests is highly variable. Some of these forms resemble *Aldorfia aldorfensis* (e.g. Plate I, 6), strongly suggesting that *A. crispa* and *A. aldorfensis* are closely related. However these forms fall within a continuous morphological spectrum and have thus been included within *A. crispa*. A type 1P archaeopyle was commonly observed, formed by the loss of the 3'' plate and in some specimens the archaeopyle is markedly elongate. *Acanthaulax crispa* was encountered from the *S. humphriesianum* zone to the lowermost *Z. zigzag* zone in Swabia, the (?)*S. humphriesianum* to *G. Garantiana* zones of Dorset and the *P. parkinsoni* zone of Normandy.

Dimensions: width: 43.2 (68.2) 82.8 µm; length: 54 (77) 102.6 µm; n= 50.

Aldorfia Stover & Evitt 1978

Remarks: Stover and Evitt (1978) erected *Aldorfia* to include species of the *Gonyaulacysta* complex which have two wall layers connected by dense fibrous ornament, with *Aldorfia aldorfensis* as the type species. *Aldorfia* is now monotypic and there is uncertainty regarding the precise nature of the wall layers. Fensome et al. (1993) assigned *Aldorfia* to the Cribroperidinoideae, however it has been placed the Leptodinioideae as *Aldorfia aldorfensis* clearly exhibits neutral torsion (Wiggan et al., 2017).

Aldorfia aldorfensis (Gocht 1970) Stover & Evitt 1978 (Plate I, 7–12)

Remarks: This species is distinguished by its highly distinctive wall structure, composed of two layers, a dense, spongy, differentiated autophragm and reticulate ectophragm which are connected by fibrous ornamentation. The outline is subovoidal with an apical horn; the ornamentation tends to be longer in the apical and antapical regions. The archaeopyle is type 1P, formed from the loss of the 3'' plate. *Aldorfia aldorfensis* was encountered in the *P. parkinsoni* and *Z. zigzag* zones of Swabia, and the *G. garantiana* zone of Dorset.

Dimensions: width: 63 (77) 86.4 µm; length: 63 (81) 95.4 µm; n= 10.

Bradleyella Woollam 1983

Remarks: *Bradleyella* is herein assigned to the Gonyaulacaceae, subfamily Leptodinioideae as it exhbits gonyaulacacean paratabulation, and has neutral torsion (see Woollam, 1983).

Bradleyella sp. (Plate XI, 7)

Remarks: This form is distinguished from *B. adela* as it has a thicker autophragm and more prominently defined tabulation; it also possesses fine, simple spines. Two specimens were recorded from the *P. parkinsoni* zone of Swabia.

Dimensions: width: 49 um; width: 46.5 µm; n=1.

Bradleyella? sp.

Remarks: This morphotype has prominently defined tabulation, a scabrate to rugulate autophragm and has been questionably assigned to *Bradleyella* due to its comparatively large size compared to that of *B. adela*. Two specimens from the *P. parkinsoni* zone of Normandy were recorded.

Dimensions: width: 64µm, length: 68 µm; n= 1.

Ctenidodinium Deflandre 1939 emend. Benson 1985

Ctenidodonium combazii Dupin 1968 (Plate II, 1–3, Plate IV, 8–9)

Remarks: This species is typified by its large size, prominent sutural crests which are surmounted by processes and a relatively small 1”” plate. The autophragm is scabrate and relatively thick, and the sutural crests are highly variable in height between specimens (ranging from 2–13 µm) but are typically around 5 µm and are usually best developed around the cingulum and on the hypocyst. Processes can be conical, birfurcate, trifurcate or multifurcate, often within a single specimen. The processes are frequently longest around the cingulum and the 1”” plate. Disarticulated epicysts and hypocysts are common. Some specimens show intratabular growth bands on the hypocyst. Woollam (1983) considered *C. combazii* to be a possible taxonomic junior synonym of *Ctenidodinium cornigerum*. However, it is clear that these are distinct species. The 1”” plate of *C. combazii* is notably smaller (relative to overall cyst size) than that of *C. cornigerum*, (Plate IV, 6–9). Moreover the sutural crests of *C. combazii* are generally higher than those of *C. cornigerum* and the overall cyst size is typically larger. *Ctenidodinium combazii* was recorded from the *P. parksinoni* and *Z. zigzag* zones of Swabia and the *P. parkinsoni* zone

in Dorset and Normandy.

Dimensions: width with processes: 86.4 (107.8) 135 µm; width without processes: 54 (80.1) 95.4 µm; n= 30.

Ctenidodinium continuum Gocht 1970 (Plate II, 6)

Remarks: This species is typified by distinctive sawtooth-like denticular sutural crests; it was recorded from the lower part of the *S. niortense* zone to the *Z. zigzag* zone in Swabia, the *G. garantiana* zone of Dorset and the *P. parkinsoni* zone of Normandy.

Dimensions: width including crests: 72.8 (90.4) 115.3 µm; n= 5.

Ctenidodinium cornigerum Valensi 1953 emend. Jan du Chêne et al. 1985 (Plate II, 5, Plate IV, 1–3, 6–7)

Remarks: This species is similar in morphology to *C. sellwoodii,* but is distinguished by its longer processes and generally larger size. *Ctenidodinium cornigerum* can be distinguished from *C. combazii* by its large 1”” plate, less well developed and lower sutural crests. Processes are often simple but can be bifurcate, trifurcate or multifurcate. It was recorded from the *S. niortense* to the *Z. zigzag* zones in Swabia, the *G. garantiana* and *P. parkinsoni* zones of Dorset, and *P. parkinsoni* to *Z. zigzag* zones of Normandy.

Dimensions: width with processes: 57.6 (71) 108 µm; width without processes: 45 (56.4) 82.8 µm. n= 30.

Ctenidodinium ornatum (Eisenack 1935) Deflandre 1939 (Plate II, 4)

Remarks: A single specimen of *C. ornatum* was recorded from sample S108 of the *Z. zigzag* zone of Swabia. Although similar in morphology to *C. combazii* this species has higher crests which are capped by simple processes.

Dimensions: width (including processes): 92.5 um; length (of hypocyst and epicyst, including processes): 88.5 µm; n= 1.

Ctenidodinum sellwoodii (Sarjeant 1975) Stover & Evitt 1978 (Plate III, 1–3)

Remarks: This species is highly variable and is characterised by low sutural ridges or low crests which bear short processes, typically <7 µm in length. These are predominantly distally simple, but occasional bifurcate processes are rarely present. The number of processes is highly variable with some specimens having very few processes. *Ctenidodinum sellwoodii* was recorded consistently from the uppermost sample of the *S. humphriesianum* zone to the *Z. zigzag* zone in Swabia, the *G. garantiana* and *P. parkinsoni* zones in Dorset and the *P. parkinsoni* to *Z. zigzag* zones of Normandy.

Dimensions: width: 54 (68) 93.6 µm; n= 30.

Ctenidodinium sp. 1 (Plate III, 4)

Diagnsosis: proximate, acavate dinoflagellate cyst. The autophragm is <1 µm thick, scabrate in texture and dark in colour. Tabulation is indicated by low sutural ridges and crests which are capped by very fine (<0.5 µm in width) processes which are no longer than 2 µm in length. Operculum remains attached in nearly all specimens.

Remarks*: Ctenidodinium* sp. 1 was recorded from the *W. laeviuscula* to the *S. humphriesianum* zones of Swabia. This morphotype is defined by its small size, thick, scabrate autophragm, low sutural crests and ridges which may bear short (<2 µm) spines. The cingulum is prominent. With its simple morphology, *Ctenidodinium* sp. 1 may be an early representative of the genus. This form is similar to *C. sellwoodii,* but differs by its thicker, more robust autophragm and slender spines which are more densely inserted. *Ctenidodinium* sp. 1 was recorded from *W. laeviuscula* and *W. laeviuscula/S. propinquans*, and *S. humphriesianum* zone of Swabia.

Dimensions: width: 54 (59) 61.2 µm; length: 36 (49) 57.6 µm; n= 5.

Ctenidodinium sp. 2 (Plate III, 5)

Remarks: This form resembles *C. sellwoodii,* but is distinguished by possessing anastomosing processes. Specimens of *Ctenidodinium* sp. 2 were almost always encountered as disarticulated hypocysts or epicysts and were recorded consistently from the uppermost *S. humphriesianum* zone to the *Z. zigzag* zone of Swabia and in the *Z. zigzag* zone of Normandy.

Dimensions: width with processes: 66.6 (74.2) 81 µm; width without processes 52.2 (59.8) 64.8 µm; n= 5.

Ctenidodinium spp.

Remarks: morphotypes of *Ctenidodinium* were encountered from the upper part of the *G. garantiana* zone to the *Z. zigzag* zone in Swabia and the *Z. zigzag* zone of Normandy that could not be placed within any existing species.

Dimensions: width: 61.2 (85.3) 99 µm; n= 5.

Ctenidodinium? sp. (Plate III, 9)

Remarks: This somewhat enigmatic chorate form was recorded from three samples of the *H. discites* zone of Swabia. It has long slender sutural processes which are simple or bifurcate proximally; the tabulation is marked by low sutural crests and appears to be gonyaulacacean. This form has been questionably assigned as species of *Ctenidodinium* tend to be proximochorate rather than chorate.

However the overall morphology is similar to *Ctenidodinium*. This may be an early representative or precursor to the genus.

Dimensions: width with processes: 52.3 (57.2) 59.9 µm; width without processes: 26.2 (40.5) 43.2; µm; n= 3.

Dissiliodinium Drugg 1978 emend. Feist-Burkhart & Monteil 2001

Dissiliodinium giganteum Feist-Burkhardt 1990 (Plate V, 1–6; Plate VI, 4–6, Plate VII, 1)

Remarks: *Dissiliodinium giganteum* has a thin (<0.5 µm) autophragm and is psilate, occasionally scabrate. Due to the thin wall, specimens are often folded, wrinkled or mechanically damaged. In some specimens the apical, anterior sulcal, 1", and 6" plates are folded back into the cyst. Isolated opercular pieces are also frequently found within the cyst body. Although the species is typified by its large size, specimens encountered during this study were observed to exhibit a large variation in size, ranging from 66 to 138 µm in diameter. However, it can clearly be seen from the histogram below (Figure 6.1) that the size of specimens falls on a positively-skewed unimodal distribution. Therefore, 'small' specimens, which are otherwise identical in morphology, were assigned to *D. giganteum*.

Dissiliodinium giganteum was recorded from the *G. concavum* to the *Z. zigzag* zones in Swabia, the *G. concavum* to *P. parkinsoni* zones in Dorset, and the *H. discites* to *S. humphriesianum* zones in Skye. In Normandy the species was recorded from the *W. laeviuscula* and *Z. zigzag* zones.

Dimensions: Width: 66 (92.6) 138.6 µm; n= 100.

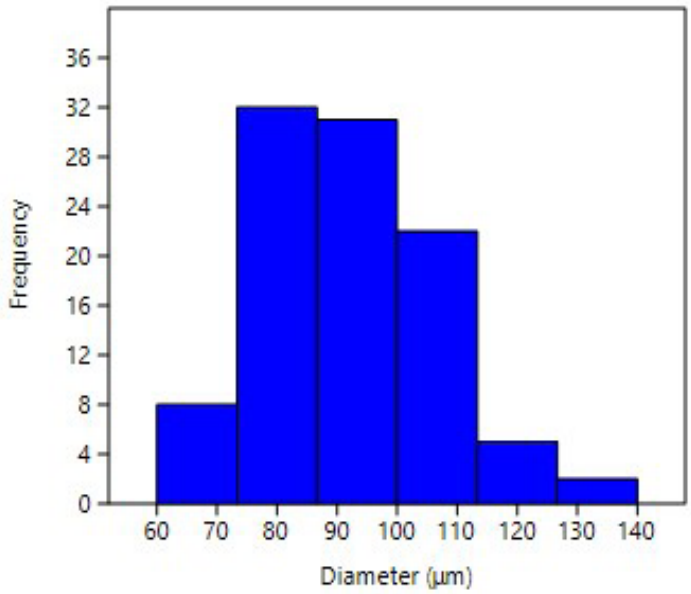

Figure 6.1. Histogram of *Dissiliodinium giganteum* sizes.
n= 100

Dissiliodinium minimum Feist-Burkhardt & Monteil 2001 (Plate VII, 4)

Remarks: This species was recorded from the *P. parkinsoni/Z. zigzag* zone boundary and the *Z. zigzag* zone of Normandy, and in the *G. garantiana* zone of Swabia. It is distinguished by its small size and scabrate to rugulate autophragm; some specimens bear small simple spines. Due to their small size and relatively robust autophragm, specimens of *D. minimum* are more-commonly well preserved than other species of *Dissiliodinium*.

Dimensions: width: 37.8 (41.4) 48.6 µm; length: n= 5.

Dissiliodinium? *hocneratum* (Fenton et al. 1980) Lentin & Williams 1993 (Plate VI, 3, Plate VII, 8)

Remarks: *Dissiliodinium*? *hocneratum* is characterised by its type 2P archaeopyle formed by the loss of the 3'' and 4'' plates, and hence is questionably assigned to *Dissiliodinium*. The autophragm is thin (<0.5 µm) and psilate to scabrate . In a few specimens the opercular plates were located inside the cyst. *Dissiliodinium*? *hocneratum* was encountered from the *W. laeviuscula* zone, and *S. humphreisianum* to *Z. zigzag* zones in Swabia,

Dimensions: width: 57.6 (66.2) 70.2 µm; length: 61.2 (67.3) 75.6 µm; n= 5.

Dissiliodinium spp. (Plate VI, 7–9, Plate VII, 2–3)

Remarks: *Dissiliodinium* spp. includes all morphotypes that could not be attributed to established species. The morphologies are highly variable; some forms have a thick (1–2 µm) autophragm which is commonly granulate, rugulate or scabrate, and rarely perforate. *Dissiliodinium* spp. was encountered throughout each section studied.

Dimensions: width: 52.2 (67.8) 90 µm; n= 30.

?*Dissiliodinium* spp.

Remarks: These are specimens which are too poorly preserved to confidently assign to *Dissiliodinium*. Specimens are often crushed, wrinkled, and otherwise poorly preserved cysts which lack tabulation and are medium to large in size.

Durotrigia Bailey 1987

Remarks: *Durotrigia* is similar in morphology to *Dissiliodinium* due to its 2P–5P archaeopyle. However, it is distinguished by its tabulation of positive-relief structures such as ridges and crests, whereas *Dissiliodinium* usually lacks tabulation and if present it is marked by negative-relief structures such as grooves (Feist-Burkhardt and Monteil 2001).

Durotrigia daveyi Bailey 1987 (Plate VI, 1–2, Plate VII, 5)

Remarks: The tabulation is demarcated by low sutural crests which bear short (2–3 µm) processes, the crests more promiment around the cingulum, the autopharagm is scabrate to rugulate. *Durotrigia daveyi* was recorded from the *W. laeviuscula* and *S. propinqauns/W.laeviuscula* zones of Swabia and the *H. discites* to *S. propinquans* zones of Dorset.

Dimensions: width: 43.2 (60.1) 79.2 µm; length: 37.8 (65.3) 84.6 µm; n= 26.

Durotrigia sp. cf. *D. daveyi* Bailey 1987

Remarks: Specimens comparable to *D. daveyi* were encountered in the *W. laeviuscula* and *S. propinquans/W. laeviuscula* zones in Swabia, the *H. discites* zone in Dorset, and the *S. propinquans* zone of Normandy. These morphotypes have low sutural ridges which lack spines except for around the cingulum in two specimens.

Dimensions: width: 59.4 (62.4) 66.6 µm; length of hypocyst: 30.6 (36) 45 µm; n= 3.

Durotrigia sp. cf *D. filapicata* (Gocht 1970) Riding & Bailey 1991

Remarks: Two specimens were encountered in the *P. parkinsoni* zone of Normandy; these differ from *D. filapicata* as there is no apical horn, which is a prominent feature of this species (Gocht 1970, pl. 1 figs. 1–4).

Dimensions: width: 48 µm; length: 57.5 µm; n= 1.

Durotrigia sp. 1 (Plate VII, 6)

Remarks: The tabulation is poorly expressed in most specimens except for the cingulum, which is marked by low ridges surmounted by short (<2 µm) spines. The archaeopyle is formed by the loss of ?5 precingular plates. The autophragm is scabrate to rugulate, and some specimens exhibit creases and folds. This species is placed within *Durotrigia* rather than *Dissiliodinium* as the tabulation is expressed by positive-relief structures in the form of low ridges. *Durotrigia* sp. 1 was encountered from the *W. laeviuscula* to *S. niortense* zones of Swabia, the *W. laeviuscula* to *G. garantiana* zones of Dorset, the *Z. zigzag* zone in Normandy, and the *H. discites* zone of Skye.

Dimensions: width: 66.6 (83.16) 95.4 µm; n= 5.

Durotrigia sp. 2. (Plate VII, 7)

Remarks: This form has a thick, scabrate autophragm, clear cingulum and faint tabulation indicated by low, discontinuous ridges. *Durotrigia* sp. 2 was recorded from the *S. humphriesianum* zone of Swabia, and the *P. parkinsoni* zone of Normandy.

Dimensions: width: 86 µm; length: 94 µm; n= 1.

Durotriga sp. cf. *Durotrigia* sp. 1

Remarks: A single specimen of this morphotype as encountered in the *P. parkinsoni* zone of Normandy. It is distinguished from *Durotrigia* sp. 1 as the wall is smoother.

Dimensions: width: 90 µm; length: 81 µm; n= 1.

Durotrigia? sp.

Remarks: This morphotype was recorded as a single specimen from the *W. laeviuscula/S. propinquans* zones of Dorset. It has been questionably assigned to *Durotrigia* as it has a thick, spongy differentiated autophragm, somewhat reminiscent of *Aldorfia.*

Dimensions: width: 75.6 µm; length: 84.6 µm; n= 1.

Endoscrinium (Klement 1960) Vozzhennikova 1967 emend. Riding & Fensome 2002

Endoscrinium asymmetricum Riding 1987 (Plate X, 4)

Remarks. This species is defined by the asymmetrical hypocystal lobes, the left lobe is wing-like whilst the two layers on the right side of the hypocyst are more closely appressed, thereby imparting an asymmetrical outline. This extremely distinctive species was recorded in the *G. garantiana* zone in Swabia and the *P. parkinsoni* zone in Normandy with a questionable occurrence from poor preservation in the *G. garantiana* zone of Dorset.

Dimensions: width: 77 µm; length: 68 µm; n= 1.

Endoscrinium sp. cf. *E. luridum* (Deflandre 1938) Gocht 1970 (Plate X, 2–3)

Remarks: This form is subspherical to subovoidal/elongate in outline, the pericoel is much narrower than *E. luridum*. Some specimens were more elongate with more pronounced antapical cavation, however these forms are apically acavate. *Endoscrinium* sp. cf. *E. luridum* was encountered from the S. *niortense* to the *P. parkinsoni* zones in Swabia with one questionable occurrence in the *Z. zigzag* zone. This morphotype has been reported from the Upper Bajocian—Lower Bathonian of offshore Australia by Mantle and Riding (2012).

Dimensions: width: 50.4 (61.92) 75.6 µm; length: 48.6 (66.2) 79.2 µm; n= 5.

Endoscrinium sp.

Remarks: One specimen was recorded outside of the count from the *Z. zigzag* zone of Swabia. This

morphotype is circumcavate, with the wall layers more widely parted at the antapex; a 1P archaeopyle is clearly visible. This form is considerably larger than *Endoscrinium* sp. cf. *E. luridum* with a wider pericoel.

Dimensions: width including pericoel: 66 µm; length including pericoel: 90 µm; n= 1.

Endoscrinium? spp. (Plate X, 1)

Remarks: These forms are morphotypes with poorly developed cavation and were encountered from the *S. humphriesianum* to *P. parkinsoni* zones in Swabia and the *Z. zigzag* zone in Normandy. They are commonly hypocavate, and in some the presence of cavation is difficult to determine as the endophragm and periphragm are closely appressed. One specimen clearly shows a 1P type archaeopyle (Plate X, 1).

Dimensions: width: 50.4 (60.8) 68.4 µm; length: 57.6 (65.1) 72 µm; n= 5.

Eodinia Eisenack 1936 emend. Berger 1986

Eodinia? spp. (Plate III, 6–8)

Remarks: Specimens of *Eodinia*? spp. are distinguished by their epicystal archaeopyle and thick, spongy autophragm. The differentiation of the autophragm varies between specimens and across individual cysts, but the outer layer is commonly rugulate. Some specimens show the development of sutural crests, commonly around the antapex, which are capped with capitate processes which often merge into ridges. Specimens were commonly encountered as disarticulated epicysts or hypocysts. One specimen displayed an apical horn, and another exhibits faint intratabular ridges. An attached operculum was found in some specimens, and the principal archaeopyle suture appears to be located along the anterior margin of the cingulum, with the operculum attached ventrally. These morphotypes are questionably assigned to *Eodinia* as the autophragm only shows partial differentiation, rather than the development of a true second wall layer. These morphotypes were observed from the *S. niortense* to *P. parkinsoni* zones of Swabia, the *P. parkinsoni* zone of Dorset and the *P. parkinsoni* zone of Normandy.

Dimensions: width: 63 (82.2) 108 µm; n= 10.

Eodinia? sp.

Remarks: Two specimens were encountered in samples S95 and S97 from the *G. garantiana* zone in Swabia. The cyst body is ovoidal in outline and longer than broad. The autophragm is scabrate to microgranulate, is differentiated, and has a partially developed fine reticulum. The archaeopyle is not clear but one specimen shows a small schism above the cingulum. The partial development of a differentiated autophragm means this morphotype has been questionably placed in *Eodinia*, and is

distinguished from *Eodinia*? spp. by its morphology and small size.

Dimensions: width: 50.8 µm; length: 60.19 µm; n= 1.

Gonyaulacysta Deflandre 1964 emend. Helenes & Lucas-Clark 1997

Gonyaulacysta jurassica (Deflandre 1938) Norris & Sarjeant 1965 subsp. *adecta* Sarjeant 1982

Remarks: One specimen was recorded from the *Z. zigzag* zone of Swabia.

Dimensions: width: 61 µm; length: 65 µm; n= 1.

Gonyaulacysta pectinigera (Gocht 1970) Fensome 1979 (Plate XV, 3–6)

Remarks: *Gonyaulacysta pectinigera* was recorded from the *S. niortense* and *Z. zigzag* zones in Swabia, the *G. garantiana* and *P. parkinsoni* zones of Dorset and the *P. parkinsoni* to *Z. zigzag* zones of Normandy. Several extremely well preserved specimens were recorded from the samples from Normandy (Plate XV, 4–7). One specimen recorded from the *Z. zigzag* of Swabia is markedly bigger than those recorded from Normandy and Dorset (Plate XV, 3)

Dimensions: width: 45 (55.6) 82.6 µm; length: 48.6 (60.6) 84.4 µm; n= 5.

Gonyaulacysta? sp. (Plate XV, 8)

Remarks: One specimen of this form was recorded from the *P. parkinsoni* zone of Dorset. This has been questionably assigned to *Gonyaulacysta* as it is weakly bicavate, however, it displays a clear L-type sulcus.

Dimensions: width: 53.5 µm; length: 76.5 µm; n=1

Korystocysta Woollam 1983 emend. Benson 1985

Remarks: *Korystocysta* was assigned to the subfamily Cribroperidinoideae by Fensome et al. (1993, p. 89). However this genus clearly exhibits neutral torsion (Sarjeant, 1976, fig. 2), and is clearly closely related to *Ctenodidinium*, hence is herein transferred to the Leptodinioideae (Wiggan et al., 2017).

Korystocysta gochtii (Sarjeant 1976) Woollam 1983 (Plate II, 7, Plate IV, 5)

Remarks: This, the type species, was encountered in the *Z. zigzag* zone of Swabia, the *P. parkinsoni* and *Z. zigzag* zones in Normandy and the *G. garantiana* to *P. parkinsoni* zones in Dorset.

Dimensions: width: 86.6 (92.9) 100.8 µm; n =3.

Korystocysta pachyderma (Deflandre 1938) Woollam 1983 (Plate II, 8)

Remarks: This species was recorded from two samples in the uppermost *S. niortense* zone of Swabia and the other in the *G. garantiana* zone of Dorset, and is distinguished from other species by its intratubular ornament.

Dimensions: width: 79.5 um; length of hypocyst: 42.5 µm, length of epicyst: 46.5 µm; n= 1.

Korystocysta aldridgeii Wiggan et al. 2017 (Plate XVI, 1–6)

Original description (Wiggan et al. 2017):

Diagnosis. A species of *Korystocysta* with faint to discontinuous sutural ridges which may be capped by short spines, a small, broad apical protuberance, and scabrate to slightly granulate autophragm; it is consistently broader than long.

Description. A species of *Korystocysta* which is primarily dorsoventrally flattened, and with a subovoidal dorsoventral outline. It is large in size. *Korystocysta aldridgeii* sp. nov. is consistently broader than it is long, and has a short, rounded apical protuberance. The species is acavate, and the autophragm is of moderate thickness and is scabrate to slightly granulate. The gonyaulacacean tabulation is indicated by low, and dominantly discontinuous sutural ridges which often bear denticles or small (<5 µm) spines. The cingulum however, is fully indicated by continuous ridges irregularly capped by denticles or small spines. The epicystal archaeopyle is normally clearly expressed.

Dimensions: width**:** 80 (99) 119 µm, n= 30.

Holotype: width: 114 µm, length: 103 µm

Paratype: width: 118 µm, length: 104 µm

Derivation of name: *Korystocysta aldridgeii* sp. nov. is named in memory of the late Richard J. Aldridge (1945–2014), who was F.W. Bennett Professor of Geology at the University of Leicester, UK.

Remarks: *Korystocysta aldridgeii* sp. nov. is a highly distinctive representative of this genus because its width is consistently greater than its length. The size, general morphology, stratigraphical extent and overall similarity to *Korystocysta gochtii* and *Korystocysta pachyderma* of this species clearly indicates that it belongs within the genus *Korystocysta.* Further to its distinctive relatively squat/stout overall shape, it is also characterised by a short, distally-rounded apical protuberance, moderately thick, scabrate to slightly granulate autophragm and discontinuous, sutural ridges which are irregularly ornamented with denticles and small spines. The sutures, despite being markedly discontinuous, clearly indicate a gonyaulacacean tabulation. The autophragm is relatively thin, and specimens are therefore susceptible to

mechanical damage, particularly the epicyst which is frequently broken, and rarely encountered intact.

Comparison. *Korystocysta aldridgeii* sp. nov. is shorter, more squat, and generally larger than the other two valid species of this genus, *Korystocysta gochtii* and *Korystocysta pachyderma.* Both the latter are longer than they are broad (Woollam, 1983). *Korystocysta gochtii*, the type, has a much more pronounced apical horn and whilst *Korystocysta pachyderma* also bears prominent intratabular ridges and is thick walled (Woollam 1983, pl. 1, fig. 9).

Stratigraphic range. *Korystocysta aldridgeii* sp. nov. ranges from the *P. parkinsoni* to *Z. zigzag* zones in Swabia, where it occurs abundantly and is a good marker for the Bajocian–Bathonian transition. There a questionable occurrence in the *G. garantiana* zone (sample S89) and the lowermost sample (S102) of the *P. parkinsoni* zone. In Normandy and Dorset the species occurs in the *P. parkinsoni* zone.

Repository. The type material is curated in the collections of the Sedgwick Museum, Department of Earth Sciences, University of Cambridge, Downing Street, Cambridge, UK. Holotype: slide S105-A, England finder co-ordinates: L48/2, museum accession number CAMSM X.50257.1. Paratype: slide S105-B, G36, museum accession number CAMSM X.50257.2.

Korystocysta sp. 1 (Plate II, 10)

Remarks: A single specimen was encountered in the lowermost *S. humphriesianum* zone of Swabia. This is an isolated hypocyst which is triangular in shape and slightly pointed at the antapex. It has a granular to rugulate autophragm with indistinct tabulation; the cingulum is marked by low ridges.

Dimensions: width: 63 µm; length: 47 µm; n= 1.

Korystocysta sp. 2 (Plate II, 9)

Remarks: Three specimens were encountered, one in the *P. parkinsoni* zone in Swabia and the others in the *G. garantiana* and *P. parkinsoni* zone in Dorset. This morphotype is distinguished by its thick (ca. 1 µm) autophragm which is scabrate, the tabulation is defined by low sutural ridges, and the 1P plate is markedly elongate.

Dimensions: width: 85 µm; length: 79 µm; n= 1.

Korystocysta spp.

Remarks: Poorly preserved specimens not attributable to any of those described above were encountered in the *P. parkinsoni* to *Z. zigzag* zones of Normandy. These have scabrate autophragms with tabulation demarcated by low sutural ridges, one specimen exhibits an apical horn.

Dimensions: width: 84.5 µm; length of hypocyst and epicyst: 81 µm; n= 1.

Kallosphaeridium de Coninck 1969 emend. Wood et al. 2016

Remarks: *Kallosphaeridium* is similar to *Batiacasphaera* and *Sentusidinium,* but differs as the operculum is attached and has 5 plates.

Kallosphaeridium? *hypornatum* Prauss 1989 emend. Wood et al. 2016 (Plate VIII, 10)

Remarks: This is a distinctive species characterised by granular ornamentation around the antapex, the rest of the cyst is psilate to scabrate. This species was questionably assigned to *Kallosphaeridium* by Wood et al. (2016) as the presence of a mid-dorsal (1a/3') plate on the operculum is yet to be confirmed. It was recorded confidently from the *S. propinquans/S.humphriesianum* zone to the *P. parkinsoni* zone Swabia, the *W. laeviuscula/S. propinquans* to *P. parkinsoni* zones of Dorset, the *S. propinquans* and *P. parkinsoni* zones of Normandy, and the *W. laeviuscula* zone of Skye.

Dimensions: width: 48.6 (61.9) 72 µm; length: 46.8 (55.4) 70.2 µm; n= 5.

Kallosphaeridium spp. (Plate VIII, 11)

Remarks: Specimens of *Kallosphaeridium* with variable morphologies were encountered from the *W. laeviuscula* to *Z. zigzag* zones in Swabia, the *S. propinquans* and *G. garantiana* zones of Dorset, the *S. propinquans* and *P. parkinsoni* zones of Normandy and the *H. discites* zone of Skye. They have been grouped together as *Kallosphaeridium* spp. and are scabrate to rugulate; one specimen from Swabia has small spines on the antapex.

Dimensions: width: 45 (58.7) 75.6 µm; length: 43.2 (61.2) 77.4 µm; n= 5.

Lithodinia Eisenack 1935 emend. Williams et al. 1993

Lithodinia jurassica Eisenack 1935 emend. Gocht 1975 (Plate VIII, 12)

Remarks: This species was recorded from the *P. parkinsoni* zone of Swabia and Normandy and the *G. garantiana* and *P. parkinsoni* zones of Dorset.

Dimensions: width: 75 µm; length 55 µm; n= 1.

Meiourogonyaulax Sarjeant 1966

Meiourogonyaulax valensii Sarjeant 1966 (Plate IX, 7–8, Plate X, 7–8)

Remarks: *Meiourogonyaulax valensii* is distinguished by its prominent sutural crests. The autophragm is scabrate, rugulate or finely reticulate, the crests also display this variation. *Meiourogonyaulax valensii* was encountered from the *S. humphriesianum* to the *Z. zigzag* zone in Swabia, the *G. garantiana* and *P. parkinsoni* zones in Dorset and the *P. parkinsoni* zone in Normandy.

Dimensions: width with crests: 54 (62.8) 77.4 µm, width without crests: 45 (55.7) 77.4 um; length with crests: 59.4 (70.6) 86.4 µm, length without crests: 50.4 (61.6) 72 µm; n= 10.

Meiourogonyaulax sp. cf. *M. caytonensis* (Sarjeant 1959) Sarjeant 1969 (Plate X, 9)

Remarks: This form is broader than long, and bears low sutural crests which are surmounted by small spines and is similar in morphology to *M. caytonensis* but lacks punctate/perforate sutural crests. This morphotype was recorded from the *Z. zigzag* zone of Swabia, the *G. garantiana* zone of Dorset and the *P. parkinsoni* zone of Normandy.

Dimensions: width: 64.5 µm; length 61 µm; n= 1.

Meiourogonyaulax spp. (Plate IX, 4–6)

Remarks: These specimens are forms with an apical archaeopyle and gonyaulacacean tabulation. The morphology of this group is highly variable and specimens are grouped together as *Meiourogonyaulax* spp. These are commonly ovoidal to subspherical in shape. The autophragm is scabrate to rugulate or very finely reticulate; some have a thick, differentiated autophragm with a luxuria composed of rugulate ornmanent that can be up to 4 µm thick. Tabulation is variably developed and is commonly demarcated by low sutural ridges. The group was recorded consistently from the *S. humpriesianum* to *Z. zigzag* zones of Germany, the (?)*S. humphriesianum* to *P. parkinsoni* zones of Dorset, and the *P. parkinsoni* to *Z. zigzag* zones of Normandy.

Dimensions: width: 36 (54) 75 µm, length: 41 (56); 75 µm; n= 20.

Rhynchodiniopsis Deflandre 1935 emend. Jan du Chêne et al. 1985

Rhynchodiniosis? *regalis* (Gocht 1970) Jan du Chêne et al. 1985 (Plate III, 10, Plate 15, 1–3)

Remarks: This species is distinguished by its prominent denticular crests with a transverse midbar. It was encountered from the *S. humphriesianum* to the *P. parkinsoni* zones in Swabia, and the *G. garantiana* zone of Dorset.

Dimensions: width: 50.4 (64) 79.2 µm; length: 59.4 (67) 75.6 µm: n= 5.

Rhychodiniopsis sp. cf. *R*? *regalis* (Gocht 1970) Jan du Chêne et al. 1985 (Plate III, 11)

Remarks: Two specimens of this form were encountered in the *S. niortense* and *G. garantiana* zones of Swabia. *Rhychodiniopsis* sp. is distinguished from *R*? *regalis* by its sutural crests which are proximally finely fenestrate and distally denticular, and thus lack a transverse mid-bar.

Dimensions: width: 64 µm; length 75 µm; n= 1.

Rhychodiniopsis? spp. (Plate XI, 8–9)

Remarks: Morphotypes placed in *Rhychodiniopsis*? spp. are small, acavate, subspherical to subovoidal, somewhat enigmatic forms bearing denticular sutural crests distinct tabulation and an L-type sulcus. All specimens lack an apical horn, the autophragm is psilate. *Rhynchodiniopsis*? spp. was encountered sporadically and in low abundance from the *S. humphriesianum* to the *Z. zigzag* zones of Swabia and the *P. parkinsoni* zone of Normandy.

Dimensions: mean width: 30.6 (37.7) 50 µm; length: 39.6 (46.3) 56 µm; n= 3.

Wanaea Cookson & Eisenack 1958 emend. Riding & Helby 2001

Wanaea acollaris Dodekova 1975 emend. Riding & Helby 2001 (Plate II, 11)

Remarks: *Wanaea acollaris* was recorded in low abundances from the *G. garantiana*, *P. parkinsoni* and *Z. zigzag* zones of Swabia. Specimens have a squat antapical horn and an autophragm which is granular to rugulate.

Dimensions: width: 84.5 µm; length of hypocyst including antapical horn: 61 µm; n= 1.

Wanaea sp. 1

Remarks: One specimen of *Wanaea* sp. 1 was recorded from the *P. parkinsoni* zone of Swabia. It is distinguished by its rugulate to microreticulate autophragm and small antapical protrusion.

Dimensions: width 75 µm; n= 1.

Wanaea sp. 2

Remarks: This form is distinguished by its psilate wall which is folded and crinkled, and its prominent antapical horn. It was recorded outside of the count from sample S105 from the uppermost *P. parkinsoni* zone of Swabia.

Dimensions: width: 81.5 µm; length of hypocyst including antapical horn: 47 µm; n= 1.

Wanaea sp. 3

Remarks: A single specimen of *Wanaea* sp. 3 was encountered from the *Z. zigzag* zone boundary of Normandy. It has a psilate wall, attached operculum and small rounded protrusion at the anapex. This form is similar to *Wanaea* sp. 1, but the antapical horn is greatly reduced in size.

Dimensions: width: 63 µm; length of hypocyst and epicyst: 52 µm; n= 1.

Subfamily UNCERTAIN

Atopodinium Drugg 1978 emend. Masure 1991

Remarks: *Atopodinium* is herein attributed to the Gonyaulacaceae as it exhibits a sexiform gonyaulacacean tabulation pattern (see Masure, 1991).

Atopodinium polygonale (Beju 1983) Masure 1991 emend. Masure 1991 (Plate X, 5)

Remarks: Two unequivocal specimens, (and one questionable specimen) of this highly distinctive species were recorded from the *P. parkinsoni* zone of Dorset and Normandy.

Dimensions: width: 71 µm; length: 54.5 µm; n= 1.

Batiacasphaera Drugg 1970 emend. Wood et al. 2016

Batiacasphaera spp. (Plate VIII, 5–9, Plate IX, 4–6)

Diagnosis: Acavate, proximate dinoflagellate cysts, subspherical to ovoidal in outline. Tabulation only shown by the apical (tA) archaeopyle. Faint cingulum sometimes present. Autophragm psilate, scabrate, rugulate and granular. Small to intermediate in size.

Remarks: Proximate dinoflagellate cysts with an apical archaeopyle, lacking tabulation, and psilate to granular wall texture were grouped together as *Batiacasphaera* spp.. Some specimens, exhibit prominent accessory archaeopyle sutures (e.g. Plate IX, 1–3). The simple, highly variable morphology makes species-level identification difficult, hence representatives were not speciated. Forms vary from smooth to granular, and can be scabrate or rugulate, the thickness of the autophragm is highly variable, and can be up to 4 µm. *Batiacasphaera* spp. was recorded consistently throughout each section studied.

Dimensions: width: 36 (48) 66 µm; length: 30 (49) 67 µm; 100 specimens measured.

?*Batiacasphaera* spp.

Remarks: Small to intermediate sized acavate dinoflagellate cysts that are poorly preserved, and spherical to subspherical/ovoidal/pentagonal cysts in shape were encountered in abundance through all the sections studied. These were questionably assigned to *Batiacasphaera* due to poor preservation.

Chytroeisphaeridia (Sarjeant 1962) Downie & Sarjeant 1965 emend. Davey 1979

Chytroeisphaeridia chytroeides (Sarjeant, 1962) Downie & Sarjeant 1965 emend. Davey 1979 (Plate XIII, 1, Plate XIV, 3)

Remarks: A small, smooth-walled species with a 1P type archaeopyle. An operculum within the cyst body was observed in a few specimens (e.g. Plate XIV, 3). *Chytroeisphaeridia chytroeides* was encountered from the *W. laeviuscula*, *P. parkinsoni* and *Z. zigzag* zones in Swabia. Four questionable occurrences, due to poor preservation, were also recorded from the *S. propinquans/W. laeviusucula*, *S. niortense* and *Z. zigzag* zones. It was recorded from the *P. parkinsoni* zone in Dorset and the *P. parkinsoni* to *Z. zigzag* zones in Normandy.

Dimensions: width: 32.4 (35) 37.2 µm; length: 41.4 (47.2) 50.5 µm; n= 4.

Ellipsoidictyum Klement 1960

Remarks: *Ellipsoidictyum*, and the closely related genus *Valensiella* are herein assigned to the family Gonyaulaceae. The overall morphology of *Ellipsoidictyum/Valensiella* is comparable to gonyaulacaceans genera such *Batiacasphaera*, *Meiourogonyaulax* and *Sentusidinium*.

Ellipsoidictyum cinctum Klement 1960 (Plate IX, 12)

Remarks: This species was recorded in four samples from the *P. parkinsoni* and *Z. zigzag* zones of Normandy; the specimens encountered are egg-shaped and have a clearly defined cingulum (e.g. Plate IX, 12).

Dimensions: width: 36 µm; length: 40 µm; n= 1.

Ellipsoidicytum/Valensiella complex (Plate IX, 9–11, Plate XI, 1–3)

Remarks: The genera *Valensiella* and *Ellipsoidictyum* are differentiated on the basis that the former possesses an ectophragm whereas the latter has an autophragm only and a cingulum. However, many specimens were encountered with a partially developed ectophragm. Some specimens had no ectophragm and others a fully developed ectophragm. These lie on a continuous morphological spectrum. Moreover, mechanical damage and degradation can result in the loss of the ectophragm. Therefore morphotypes with a reticulate ornamentation and an apical archaeopyle that could not be accommodated within existing species of *Ellipsoidictyum* or *Valensiella* were grouped together as the *Ellipsoidictyum/Valensiella* complex. The density of the reticulation is highly variable, the muri in some specimens are closely packed whilst others are widely spaced with large lumina. The lumina are scabrate to psilate. This group

was recorded from the *S. humphriesianum* zone to *Z. zigzag* zone in Swabia, the (?) *S. humphriesianum* to *P. parkinsoni* zones in Dorset and the *P. parkinsoni* to *Z. zigzag* zones of Normandy.

Dimensions: width: 36 (53.7) 81 µm; length: 36 (52.5) 77.4 µm; n= 50.

Epiplosphaera Klement 1960

Remarks: *Epiplosphaera* is herein assigned to the Gonyaulacaceae, on the basis of its overall morphology, which is comparable to gonyaulacaceans such as *Batiacasphaera, Meiourogonyaulax,* and *Sentusidinium*.

Epiplosphaera sp. cf *E. gochtii* (Fensome 1979) Brenner 1988

Remarks: A single specimen of this morphotype was encountered in the *Z. zigzag* zone of Normandy. It is elongate in shape and has irregularly development reticulate ornamentation; a sulcus and cingulum can be observed. This form differs from *E. gochtii* as the as the processes are slender and conical in shape, whereas in *E. gochtii* they are broader, buccinate or capitate, with a few bifurcating forms and one prominent hollow process (Fensome 1979, text fig. 8).

Dimensions: width: 18µm; length 25 µm; n= 1.

Gongylodinium Fenton et al. 1980 emend. Feist-Burkhardt & Monteil 1997

Gongylodinium erymnoteichon Fenton et al. 1980 emend. Feist-Burkhardt & Monteil 1997 (Plate VII, 9)

Remarks: With its 2P type archaeopyle, *Gongylodinium erymnoteichon* is similar to *Dissiliodinium*? *hocneratum* but differs in that the autophragm is thicker and covered in very short (<1 µm) spines. This species was recorded from the *W. laeviuscula* to the *Z. zigzag* zones in Swabia, the *H. discites*, *S. propinquans* and *G. garantiana* and *P. parkinsoni* zones in Dorset and the *P. parkinsoni* and *Z. zigzag* zones of Normandy. In Skye it was encountered from the *W. laeviuscula* and *S. humphriesianum* zones.

Dimensions: width: 50.4 (55.7) 66.6 µm; length: 39.6 (51.8) 63 µm; n= 5.

Sentusidinium Sarjeant and Stover 1978 emend. Wood et al. 2016

Sentusidinium spp. (Plate VIII, 1–4)

Diagnosis: Acavate, proximate to proximochorate dinoflagellate cysts. Autophragm covered in short

simple non-tabular spines, which are conical and either pointed or blunt distally. Tabulation indicated only by the apical archaeopyle. Ovoidal to subspherical in outline, commonly wider than long, small to intermediate in size.

Remarks: *Sentusidinium* spp. includes all proximate/proximochorate cysts with an apical archaeopyle and simple, non-tabular processes. The simple but variable morphology of this group makes consistent speciation difficult and hence are grouped together as *Sentusidinium* spp.. The process length and distribution density is highly variable. Most specimens are proximate as the processes are usually <10% of the width of the cyst body, but occasional proximochorate forms was observed. The intra-process areas are psilate. This group was encountered consistently in moderate to high abundances from the uppermost *S. humphriesianum* to the *Z. zigzag* zones in Swabia, the (?) *S. humphriesianum* to *P. parkinsoni* zones in Dorset, and the *P. parkinsoni* and *Z. zigzag* zones in Normandy.

Dimensions: width including processes: 34 (47) 63 µm; length including processes: 27 (42) 56 µm; n= 50.

Valensiella Eisenack 1963 emend. Courtinat 1989

Valensiella ampulla Gocht 1970 (Plate XI, 6)

Remarks: *Valensiella ampulla* is distinguished by its finely reticulate ornamentation which is comprised of discontinuous elements. It was recorded in two samples from the *P. parkinsoni* zone of Swabia.

Dimensions: width: 55.5 µm; length: 52.5 µm; n=1.

Valensiella ovulum (Deflandre 1947) Eisenack 1963 emend. Courtinat 1989 (Plate XI, 4–5)

Remarks: This, the type species of *Valensiella,* was encountered sporadically from the uppermost part of the *S. humphriesianum* to the *Z. zigzag* zones in Swabia, the (?) *S. humphriesianum* to *G. garantiana* zones of Dorset, and the *P. parkinsoni* to *Z. zigzag* zones of Normandy.

Dimensions: width: 53 (57) 61 µm; length: 56.5 (60) 68 µm; n= 5.

Suborder UNCERTAIN

Family Uncertain

Impletosphaeridium Morgenroth 1966 emend. Islam 1993

Impletosphaeridium sp. 1 (Plate XIII, 6)

Remarks: Two specimens of this small simple chorate species with dense, extremely fine (0.5 µm

wide) bifurcating processes were recorded from the *P. parkinsoni* and *Z. zigzag* zones of Swabia, five specimens were also recorded from the *G. garantiana* zone of Dorset

Dimensions: width including processes: 52/63 µm; without processes: 38/39.6 µm; n= 2.

Impletosphaeridium sp. 2 (Plate XIII, 7)

Remarks: A single specimen was recorded from sample S108 from the *Z. zigzag* zone of Swabia. This form is larger than *Impletosphaeridium* sp. 1 and has fewer processes which are conical and distally simple.

Dimensions: width including processes: 67 µm; width without processes: 48 µm; n= 1.

Mendicodinium Morgenroth 1970 emend. Bucefalo Palliani et al. 1997

Mendicodinium sp. (Plate II, 12)

Remarks: *Mendicodinium* sp. was recorded from the *G. garantiana* zone of Swabia, and has a hypocyst which is slightly larger than the epicyst and a scabrate autophragm.

Dimensions: width: 65 µm; length (hypocyst and epicysts): 59 µm; n= 1.

Order PERIDINIALES Haeckel 1894

Suborder HETEROCAPSINEAE Fensome et al. 1993

Family HETEROCAPSACEAE Fensome et al. 1993

Moesiodinium Antonesçu 1974 emend. Below 1987

Moesiodinium raileanui Antonesçu 1974 (Plate XIV, 9)

Remarks: This distinctive, small, circumcavate species was recorded from two samples (S36 and S40) from the *W. laeviuscula/ S. propinquans* zone of Swabia. The anterior intercalary archaeopyle can clearly be observed in two specimens.

Dimensions: width: 23.4 (27.3) 32.4 µm; length: 28 (31) 36 µm; n= 3.

Order UNCERTAIN

Suborder UNCERTAIN

Family COMPARODINIACEAE Vozzhennikova 1979

Valvaeodinium Morgenroth 1970 emend. Below 1987

Valvaeodinium cavum Davies 1983 emend. Below 1987

Remarks: A single specimen of a small, ovoidal dinoflagellate cyst was recovered from sample FDH7 of the *W. laeviuscula* zone of Normandy. This has capitate processes but no archaeopyle is visible and the overall preservation is poor so was recorded as a questionable occurrence of *V. cavum.*

Dimensions: width: 25 µm; length: 34 µm; n= 1.

Valvaeodinium spinosum (Fenton et al. 1980) Below 1987 (Plate XIV, 7)

Remarks: *Valvaeodium spinosum* was recorded from the *G. garantiana* to the *Z. zigzag* zone in Swabia, and from the *P. parksinoni* zone of Normandy. It is elongate in shape, and the autophragm is surmounted with small, fine spines.

Dimensions: width: 29/33.5 µm; length: 42.5/45.46 µm; n= 2.

Valvaeodinium sp. cf. *V. spinosum* (Fenton et al. 1980) Below 1987 (Plate XIII, 8)

Remarks: A single specimen was encountered sample S48 of the *S. humphriesianum* zone of Swabia. This form is larger and broader than *V. spinosum*, which is more elongate (Fenton et al., 1980, pl. 14, fig. 13). *Valvaeodinium* sp. cf. *V. spinosum* may be a precursor morphotype.

Dimensions: width: 47.2 µm; length: 57.5 µm; n= 1.

Valvaeodinium vermicylindratum Below 1987 (Plate XIII, 9)

Remarks: The distinctive vermiculate ornamentation of this species distinguishes it from *V. spinosum*. *Valvaeodinium vermicylindratum* was recorded from two samples from the *S. niortense* zone of Swabia.

Dimensions: width: 39 µm; length: 58 µm; n= 1.

Valvaeodinium spp. (Plate XIII, 10–11)

Remarks: These forms are elongate to subovoidal in shape, with a scabrate to granulate autophragm, sometimes with longitudinal folds; the autophragm is typically <1 µm thick. Specimens of *Valvaeodinium* spp. were recorded in low numbers from the *S. propinquans*/*S. humphriesianum* zone to the *Z. zigzag* zone of Swabia, the *G. garantiana* and *P. parkinsoni* zones of Dorset, the *W. laeviuscula* to *P. parkinsoni* zones of Normandy and the *S. humphriesianum* zone of Skye.

Dimensions: width: 25.2 (35.8) 54 µm; length: 21.6 (44.1) 63 µm; n= 8.

Family UNCERTAIN

Orobodinium Gocht &Wille 1990

Orobodinium automobile Gocht & Wille 1990 (Plate XIII, 12–13)

Remarks: This species has a relatively thick (1µm) autophragm which is psilate to scabrate. *Orobodinium automobile* was encountered from the *W. laeviuscula*/*S.propinquans* zone to the *Z. zigzag* zone of Swabia, the *G. concavum*, and *S.humphriesianum/S. niortense* zones of Dorset, the *P. parkinsoni* and *Z. zigzag* zones of Normandy.

Dimensions: diameter: 18 (20.3) 22.5 µm; n= 5.

Orobodinium rete Gocht & Wille 1990

Remarks: A single poorly-preserved specimen was encountered from the *P. parkinsoni* zone of Normandy; it has distinctive reticulate ornamentation but has been recorded as a questionable occurrence due to poor preservation.

Dimensions: diameter: 21.5 µm; n= 1.

Orobodinium sp. A of Gocht & Wille 1990 (Plate XIII, 14–15)

Remarks: Two specimens of *Orobodinium* sp. A were recorded, one from the *Z. zigzag* zone of Swabia and the other from the *S. propinquans* zone of Dorset. It is distinguished from *O. automobile* in by its differentiated autophragm, the outer layer of which is covered in vermiculate ornamentation; it is also larger in size.

Dimensions: diameter: 27.5 µm; n=1.

Orobodinium sp. (Plate XIV, 8)

Remarks: Two specimens were encountered in the *W. laeviuscula* zone of Normandy. These have a thick, differentiated autophragm, the luxuria is microrugulate to punctate, the overall size is very small. The texture of the autophragm and extremely-small size distinguish this morphotype from other species of the genus.

Dimensions: diameter: 15 µm; n= 1.

Phallocysta Dörhöfer & Davies 1980 emend. Below 1987

Phallocysta elongata (Beju 1971) Riding 1994 (Plate XIV, 2)

Remarks: Three specimens of *P. elongata* were recorded from two samples (G3 and G5) from the *H. discites* zone of Swabia.

Dimensions: width: 32.5 µm; length 42 µm; n= 1.

6.2. Plates.

The slide number and England Finder co-ordinates are given for each figured specimen.

Plate I after Wiggan et al. (2017) plate I.

Plate II after Wiggan et al. (2017) plate II.

Plate III modified from Wiggan et al. (2017) plate III.

Plate V after Wiggan et al. (2017) plate IV.

Plate VII after Wiggan et al. (2017) plate V.

Plate VIII after Wiggan et al. (2017) plate IX.

Plate X modified from Wiggan et al. (2017) plate VI.

Plate XI after Wiggan et al. (2017) plate XI.

Plate XII modified from Wiggan et al. (2017) plates VIII and XII.

Plate XIII modified from Wiggan et al. (2017) plate X.

Plate XVI after Wiggan et al. (2017) plate VII.

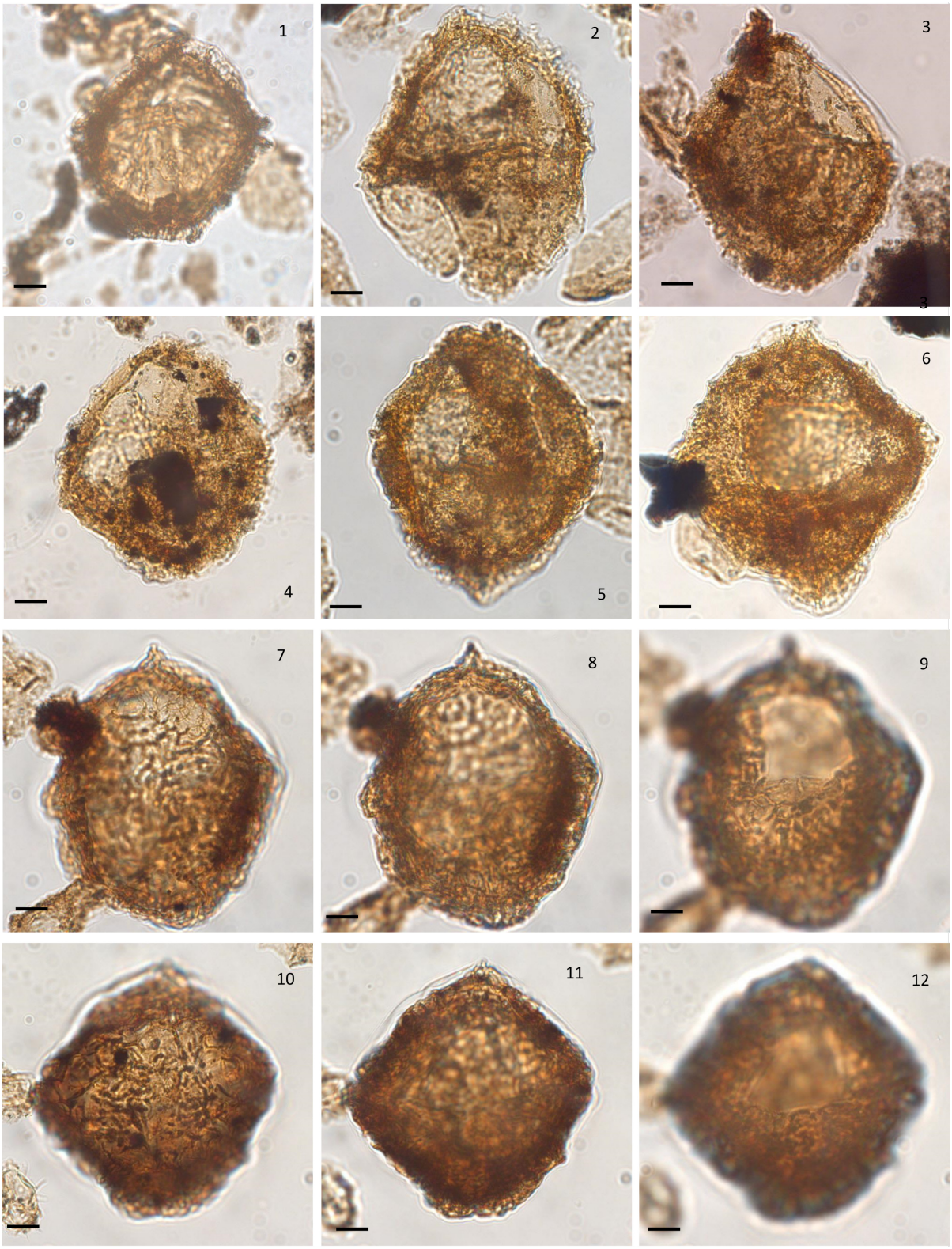

Plate I Selected dinoflagellate cysts from Swabia.

Scale bar represents 10 µm. **1–6**: *Acanthaulax crispa* (Wetzel 1967) Woollam & Riding 1983. **1**: dorsal view, low focus, slide S63-1, EF co. S71. **2**: dorsal view, median focus, slide S71-B, EF co. Q51/3. **3**: lateral view, median focus, slide S74-B, EF co. T45/3. **4**: dorso-lateral view, median focus, slide S91-C, EF co. V52/1. **5**: dorso-lateral view median focus, slide S71-B, EF co. M35. **6**: dorsal view, median focus, slide S71-B, EF co. Q43/3. **7–12**: *Aldorfia aldorfensis* (Gocht 1970) Stover & Evitt 1978.**7–9**: same specimen, dorso-ventral view. **7**: high focus, **8**: median focus, **9**: low focus, slide S105-A, EF co. F36. **10–12**: same specimen, dorso-ventral view **10**: high focus, **11**: median focus, **12**: low focus, slide S105-A, EF co. K68/1.

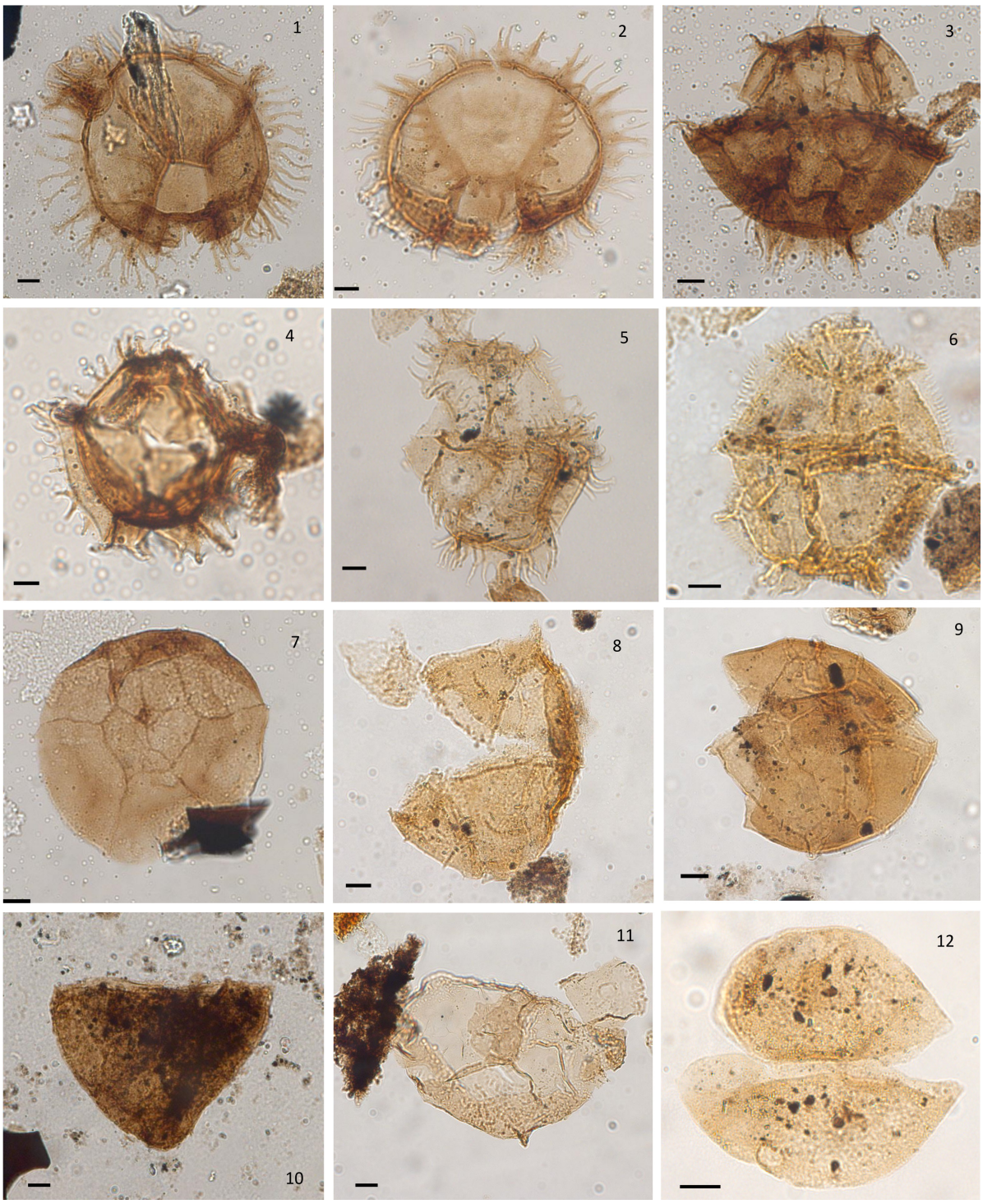

Plate II Selected dinoflagellate cysts from Swabia. Scale bar represents 10 µm.

1–3: *Ctenidodinium combazii* Dupin 1968. **1**: antapical view, median focus, slide S108-A, EF co. S48. **2**: dorsal-antapical view, median focus, S108-A, EF co. U73/2. 3: dorso-ventral view, median focus, slide S108-A, EF co. U47/2. **4**: *Ctenidodinium ornatum* (Eisenack 1935) Deflandre 1939. Dorso-ventral view, median focus, slide S108-A, EF co. V67-1. **5**: *Ctenidodinium cornigerum* Valensi 1953 emend. Jan du Chêne et al. 1985. Dorsal view, low focus, slide S108-A, EF co. V67/1. **6**: *Ctenidodinium continuum* Gocht 1970. Ventral view, median focus, slide S97-A, EF co. J50. **7**: *Korystocysta gochtii* (Sarjeant 1976) Woollam 1983. Apical view, low focus, slide S108-A, EF co. Q60/4. **8**: *Korystocysta pachyderma* (Deflandre 1938) Woollam 1983. Lateral view, median focus, slide S81-A, EF co. T43. **9**: *Korystocysta* sp. 2. Dorso-ventral view, median focus, slide S104-A, EF co. N60/1. **10**: *Korystocysta* sp. 1. Dorso-ventral view, median focus, slide S49-B, EF co. N57. **11**: *Wanaea acollaris* Dodekova 1975 emend. Riding & Helby 2001. Dorso-ventral view/apical view, median focus, slide S105-A, EF co. R47/4.

12: *Mendicodinium* sp. Dorso-ventral view, median focus, slide S97-C, P53.

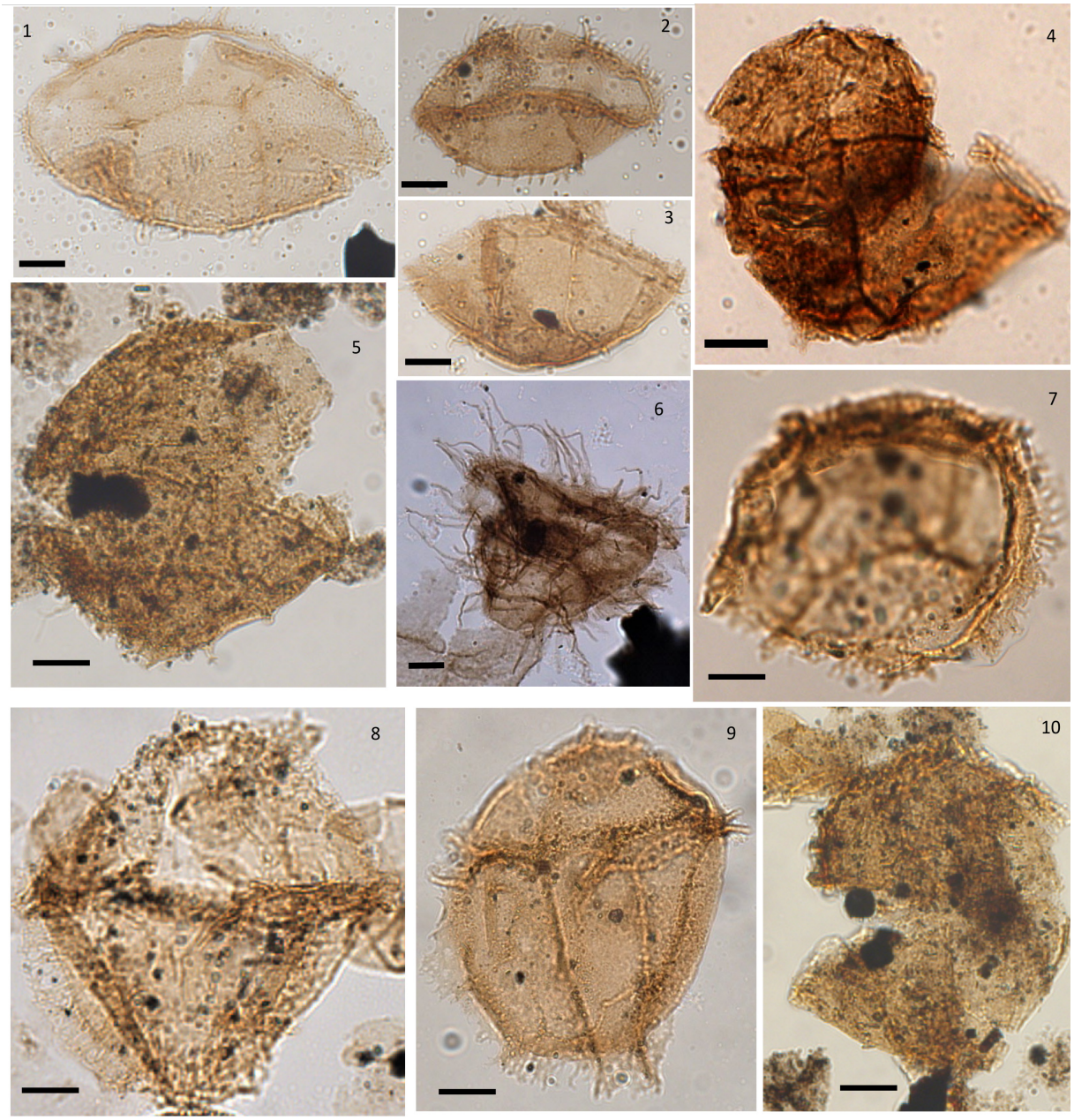

Plate III Selected dinoflagellate cysts from Swabia.

Scale bar represents 10 µm, except in 5 and 10 where it represents 20 µm., and in 8, 9 where it represents 15 µm. **1–3**: *Ctenidodinium sellwoodii* (Sarjeant 1975) Stover & Evitt 1978. **1**: dorsal view, median focus, slide S108-A, EF co. V55/3. **2**: antapical view, low focus, slide S108-B, EF co. N62/1. **3**: dorsal view, high focus, slide S108-B, EF co. M35/1. **4**: *Ctenidodinium* sp. 1 ventro-lateral view, median focus, slide S24-1, EF co. CONTROL box. **5**: *Eodinia*? spp. Ventral view, high focus, slide S101-B, EF co. J65/1. **6**: *Ctenidodinium*? sp. Ventral(?) view, median focus, slide G5-2, EF co. T53. **7**: *Ctenidodinium* sp. 2. Antapical view, median focus, slide S71-B, EF co. L62. **8**: *Rhynchodiniopsis*? *regalis* (Gocht 1970) Jan du Chêne et al. 1985. Dorso-ventral view, high focus, slide S99-A, EF co. F37/3. **9**: *Rhynchodiniopsis* sp. cf *R*? *regalis* (Gocht 1970) Jan du Chêne et al. 1985. Dorso-ventral view/lateral view, low focus, slide S95-A, EF co. W44. **10**: *Eodinia*? spp. Dorsal view, median focus, slide S74-B, EF co. P49.

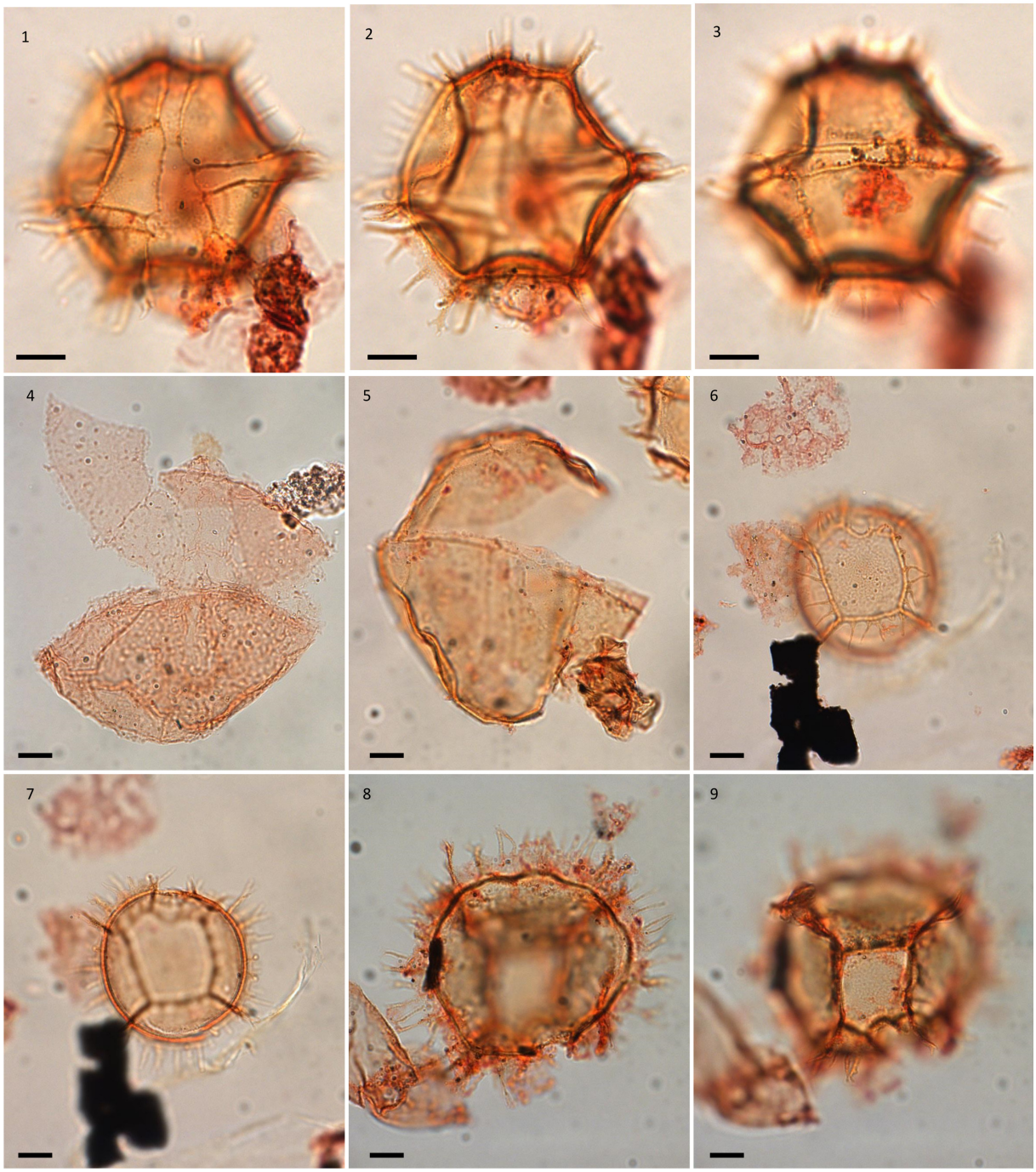

Plate IV Selected dinoflagellate cysts from Normandy.

Scale bar represents 10 µm. **1–3**: *Ctenidodinium cornigerum* Valensi 1953 emend. Jan du Chêne et al. 1985. Same specimen, slide H1-A, EF co. R66/2. The specimen has does not have a visible archaeopyle. **1**: ventral view, high focus, **2**: dorso-ventral view, median focus, **3**: dorsal view, low focus. **4**: *Korystocysta aldridgeii* Wiggan et al. 2017. Dorso-ventral view, median focus. Slide FDH15-1, EF co. Q35/3. Note the damaged epicyst, a common feature of this species. **5**: *Korystocysta gochtii* (Sarjeant 1976) Woollam 1983. Right lateral view, high focus. Slide H1-A, EF co. Q47. **6–7**: *Ctenidodinium cornigerum* Valensi 1953 emend. Jan du Chêne et al. 1985. Same specimen, antapical view. Slide H1-B, EF co. R51/4. Note the relatively large size of the 1'''' plate. **6**: high focus, **7**: median focus. **8–9**: *Ctenidodinium combazii* Dupin 1968. Same specimen, antapical view. Slide H1-B, EF co. R61. Note the relatively small size of the 1'''' plate. **8**: high focus, 9: median to low focus.

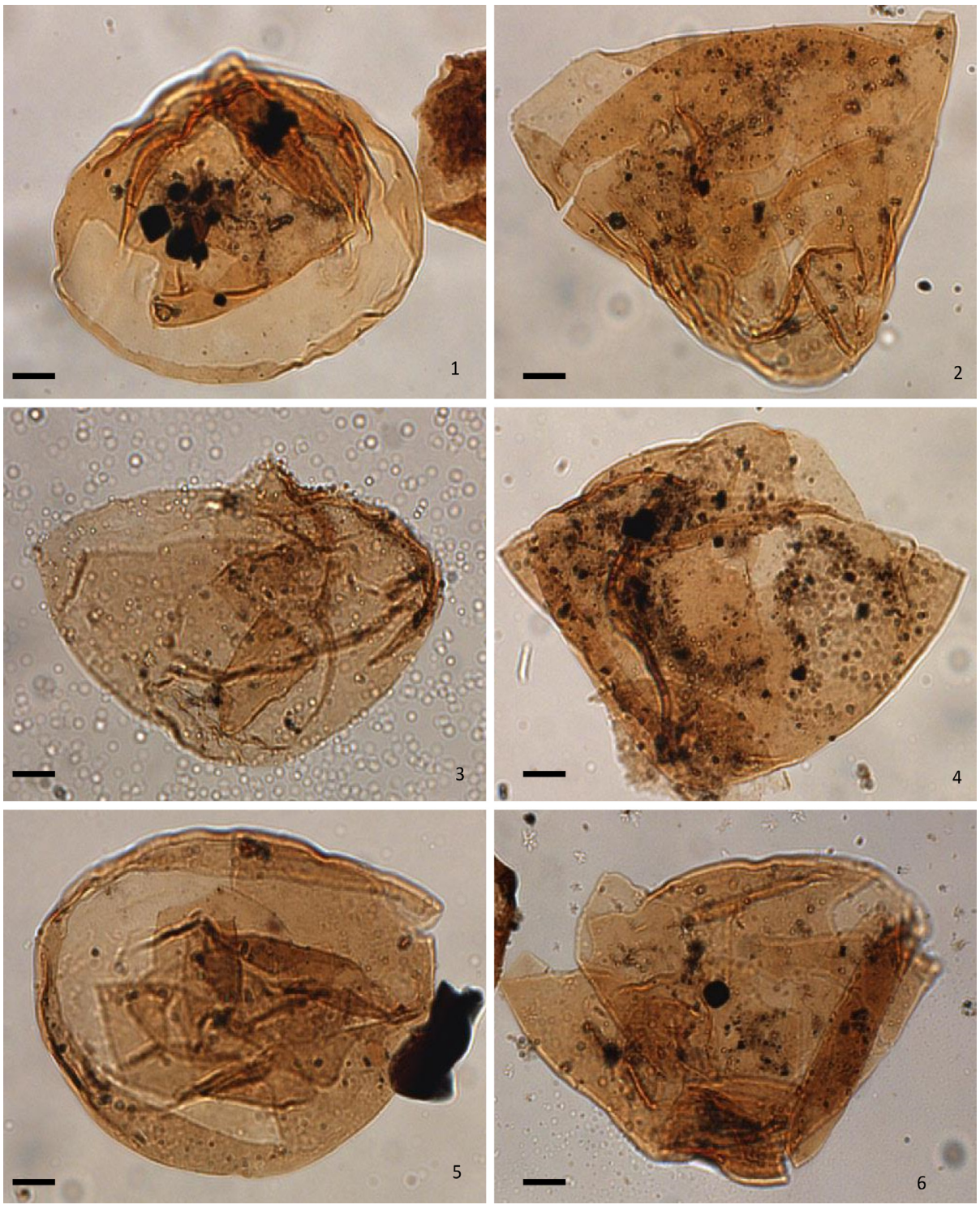

Plate V Specimens of *Dissiliodinium giganteum* from Swabia.

Scale bar represents 10 µm. **1–6**: *Dissiliodinium giganteum* Feist-Burkhardt 1990. **1**: apical view, high focus, slide S2-C, EF co. R54/1. **2**: dorso-ventral view, low focus, slide S2-C, EF co. V43/3. **3**: dorso-ventral view, median focus, slide S17-B, EF co. E45/2. **4**: dorso-ventral view, low focus, slide S17-B, EF co. L42/3. **5**: high focus, slide S18-B, EF co. C60. **6**: dorso-ventral view, high focus, slide S17-B, EF co. U65/2.

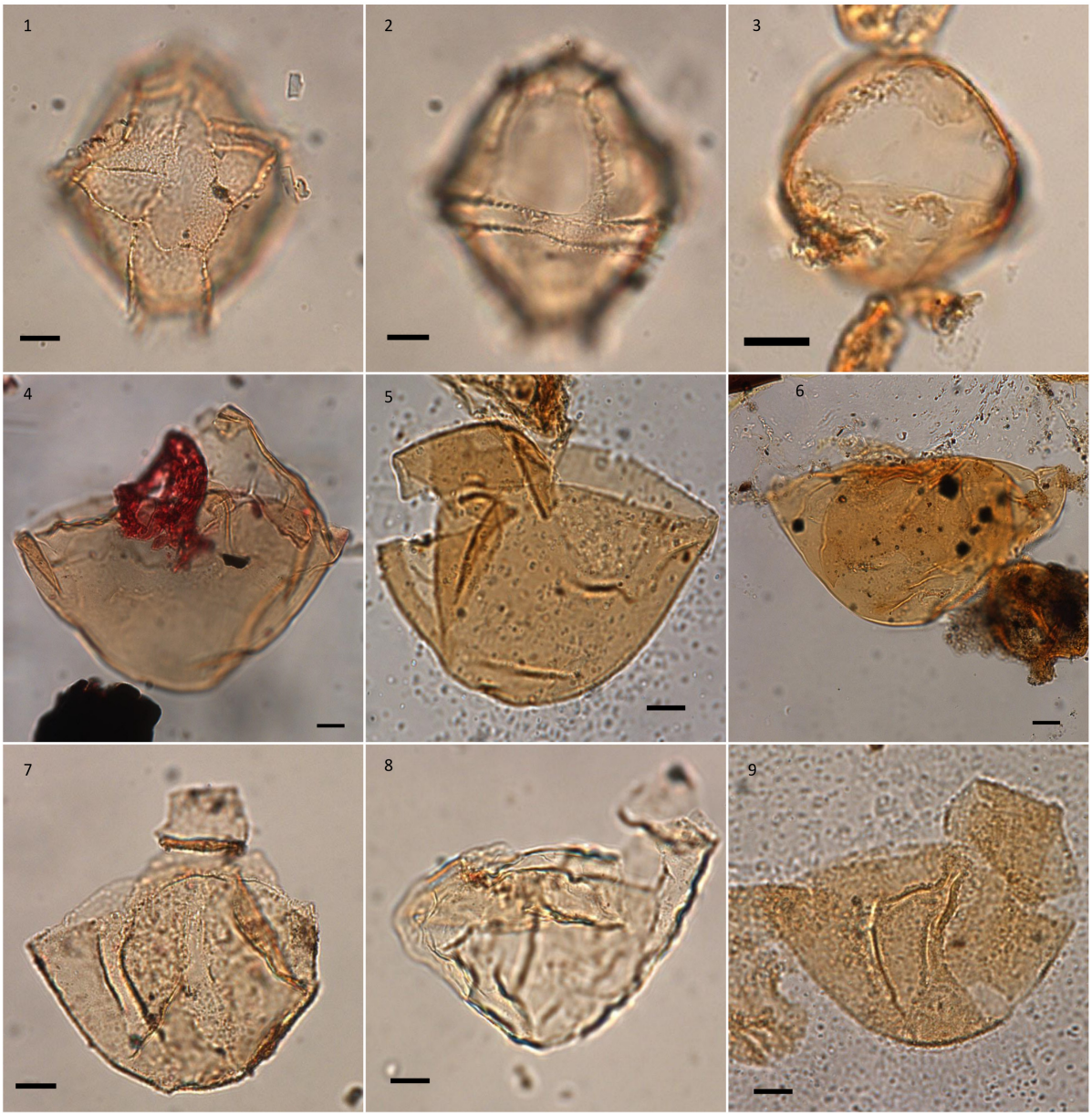

Plate VI Selected dinoflagellate cysts from Dorset and the Isle of Skye.

Scale bar represents 10 µm. **1–2**: *Durotrigia daveyi* Bailey 1987. Slide CSA 1459-4, EF co. Q49/4. **1**: ventral view, high focus, **2**: dorsal view, low focus. **3**: *Dissiliodinium*? *hocneratum* (Fenton et al. 1980) Lentin & Williams 1993. Dorsal view, high focus. Slide CSA 1526-3, EF co. C38. **4–6**: *Dissiliodinium giganteum* Feist-Burkhardt 1990. **4**: oblique lateral view, low focus, slide MPA 2214-4, EF co. U59/4. **5**: ventral view, low focus, slide MPA 13991-2(2), EF co. P52/3. **6**: ventral view, high focus, slide MPA 13999-2(2), EF co. V54/2. Note the apical tongue which has been folded back into the cyst. **7–9**: *Dissiliodinium* spp. **7**: dorsal view, high focus, slide MPA 2216-4, EF co. O39. **8**: right lateral view, median focus, slide MPA 2216-4, EF co. J49/3. **9**: dorso-ventral view, median focus, slide MPA14005-3(2), EF co. E55/2.

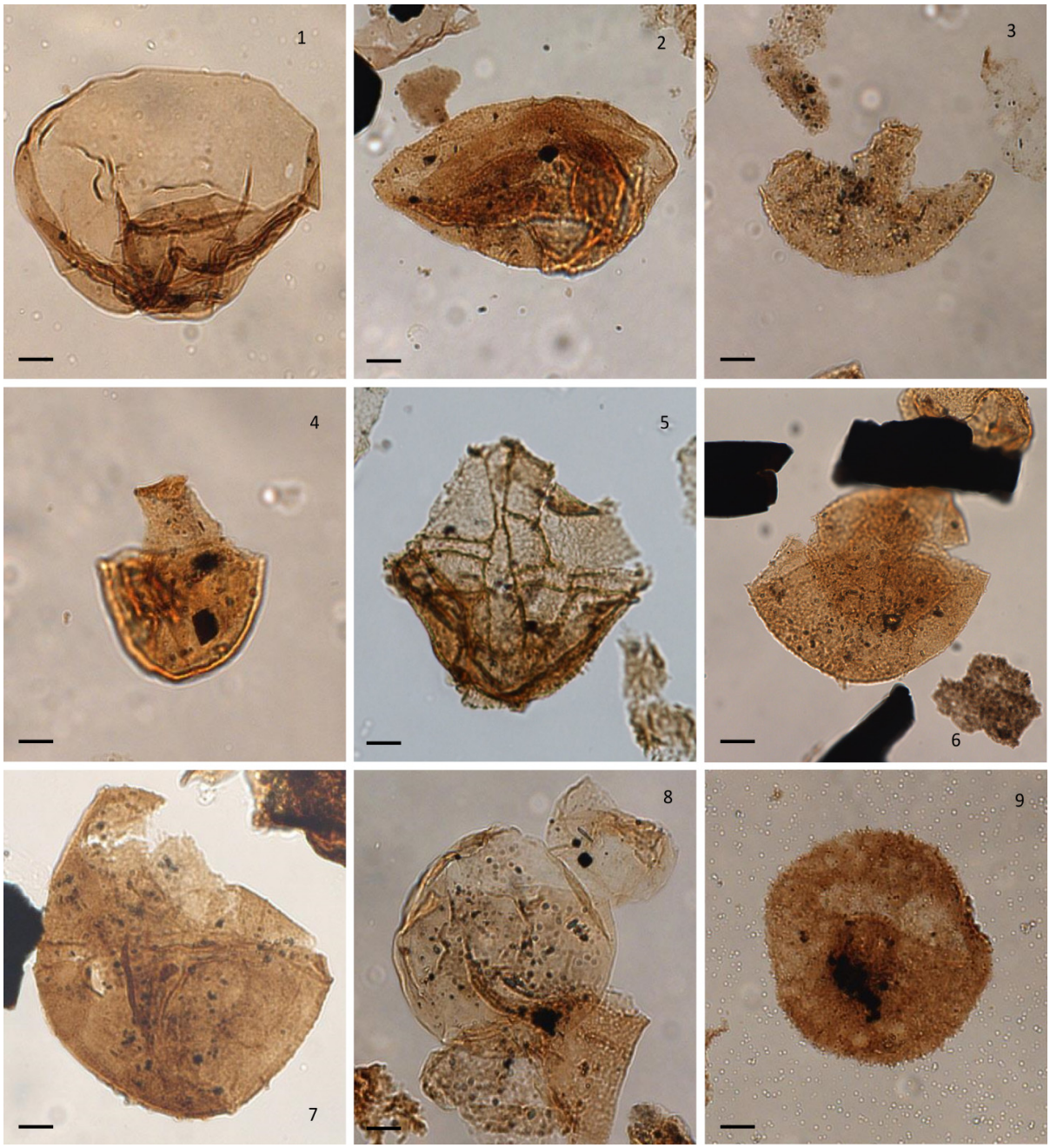

Plate VII Selected dinoflagellate cysts from Swabia.

Scale bar represents 10 µm. **1**: *Dissiliodinium giganteum* Feist-Burkhardt 1990. Apical view, low focus, slide S18-B, EF co. W56/1. **2–3**: *Dissiliodinium* spp. **2**: ventro-apical view, high focus, slide S48-5, EF co. P47/3 **3**: ventral view, slide S74-B, EF co. V48/2-4, high focus. **4**: *Dissiliodinium minimum* Feist-Burkhardt & Monteil 2001. Dorsal view, median focus, side S92-3, EF co. K55. **5**: *Durotrigia daveyi* Bailey 1987. Ventral view, high focus, slide S28-C, EF co. R59/2. **6**: *Durotrigia* sp. 1. Dorso-ventral view, high focus, slide S8-B, EF co. J/K62. **7**: *Durotrigia* sp. 2. Lateral view, median focus, slide S50-A, EF co. G48/1-3. **8**: *Dissiliodinium*? *hocneratum* (Fenton et al. 1980) Lentin & Williams 1993. Dorsal view, high focus, slide S71-B, EF co. V48/2-4. **9**: *Gongylodinium erymnoteichon* Fenton et al. 1980. Dorso-ventral view, low focus, slide S109-A, EF co. T50/2.

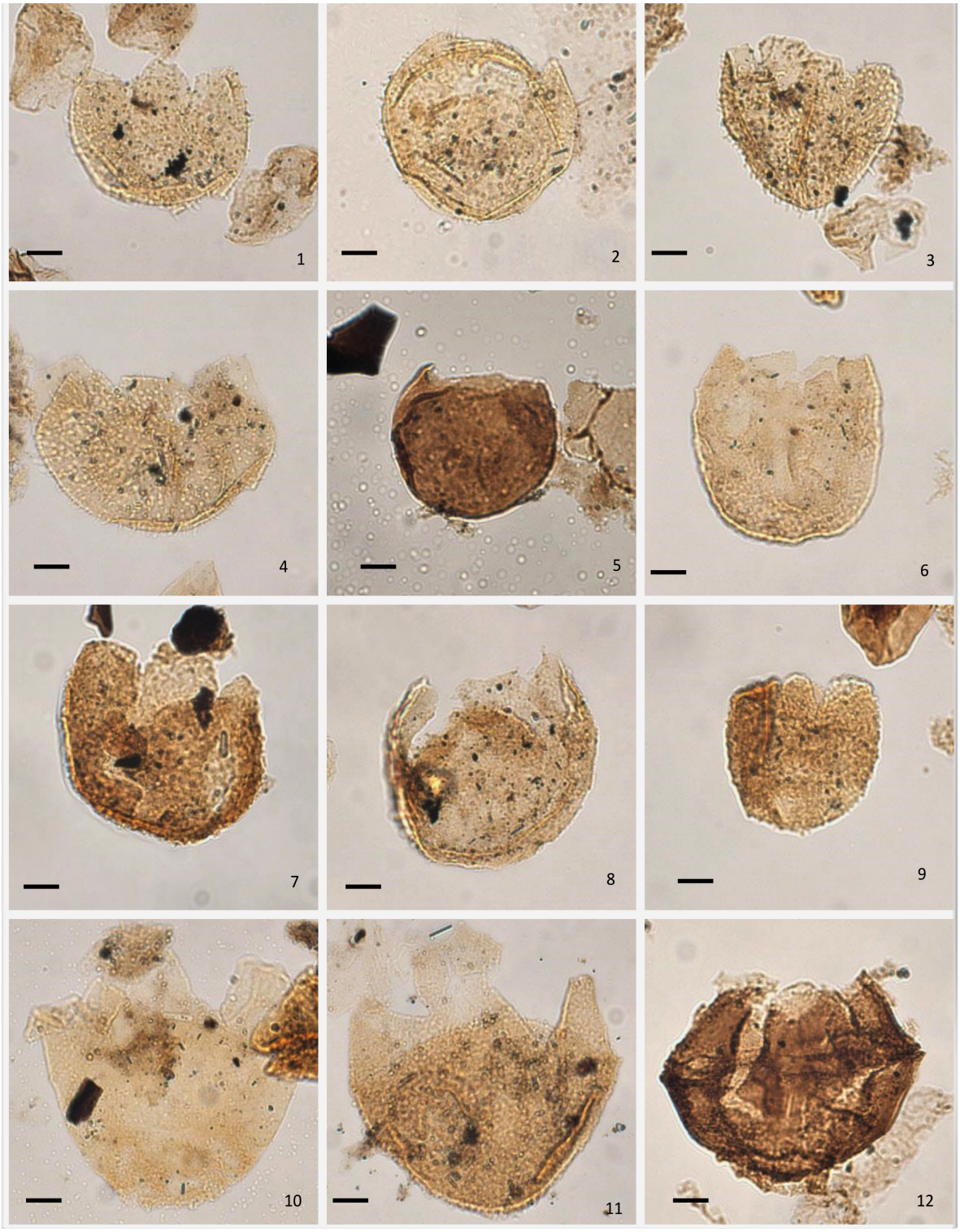

Plate VIII Selected dinoflagellate cysts from the Swabia.

Scale bar represents 10 µm. **1–4**: *Sentusidinium* spp. **1**: dorso-ventral view, median focus, slide S71-B, EF co. M68, **2**: dorso-ventral view, high focus, slide S69-2, EF co. O69, **3**: dorso-ventral view, median focus, slide S71-B, EF co. H47/3-4. Dorso-ventral view, low focus, slide S71-B, EF co. M57. **5–9**: *Batiacasphaera* spp. **5**: low focus, slide S108-B, EF co. Q55/1-2. **6**: median focus, slide S71-B, EF co. J72/1. **7**: median focus, S71-A, EF co. V45. **8**: high focus, slide S71-A, EF co. W71/1. **9**: median focus, slide S71-B, EF co. W54. **10**: *Kallosphaeridium*? *hypornatum* Prauss 1989 emend. Wood et al. 2016. Dorso-ventral view, high focus, slide S66-A, EF co. V62. **11**: *Kallosphaeridium* spp. Dorso-ventral view, median focus, slide S7-B, EF co. C55/3. **12**: *Lithodinia jurassica* Eisenack 1935 emend. Gocht 1975. Dorso-ventral view, low focus, slide S102-1, EF co. T54/3-4.

Plate IX Selected dinoflagellate cysts from Dorset, the Isle of Skye and Normandy.

(P. 143). Scale bar represents 10 µm.

1–3: *Batiacasphaera* spp.

1: dorso-ventral view, high focus, slide CSA 1528-4, EF co. L34/4.

2: low focus, slide CSA 1528-4, EF co. H46/1.

3: high focus, slide CSA 1526-3, EF co. F39/1.

4–6: *Meiourogonyaulax* spp.

1: ventral view, high focus, slide CSA 1526-4, EF co. Q33/2.

2: dorso-ventral view, median focus, slide CSA 1526-3, EF co. O39.

3: apical view, high focus, slide CSA 1526-3, EF co. O49.

7–8: *Meiourogonyaulax valensii* Sarjeant 1966. Same specimen, slide CSA 1526-3, EF co. F40/2-4.

7: ventral view, low focus.

8: doro-ventral view, median focus.

9–12: *Ellipsoidictyum/Valensiella* complex

9: high focus, slide CSA 1527-4, EF co. Y40/2

10: high focus, slide CSA 1527-4, EF co. N24

11: high focus, CSA 1527-4, EF co. S52/2

12: *Ellipsoidictyum cinctum* Klement 1960. High focus, slide H3-A, EF co. Q46. Note the prominent cingulum.

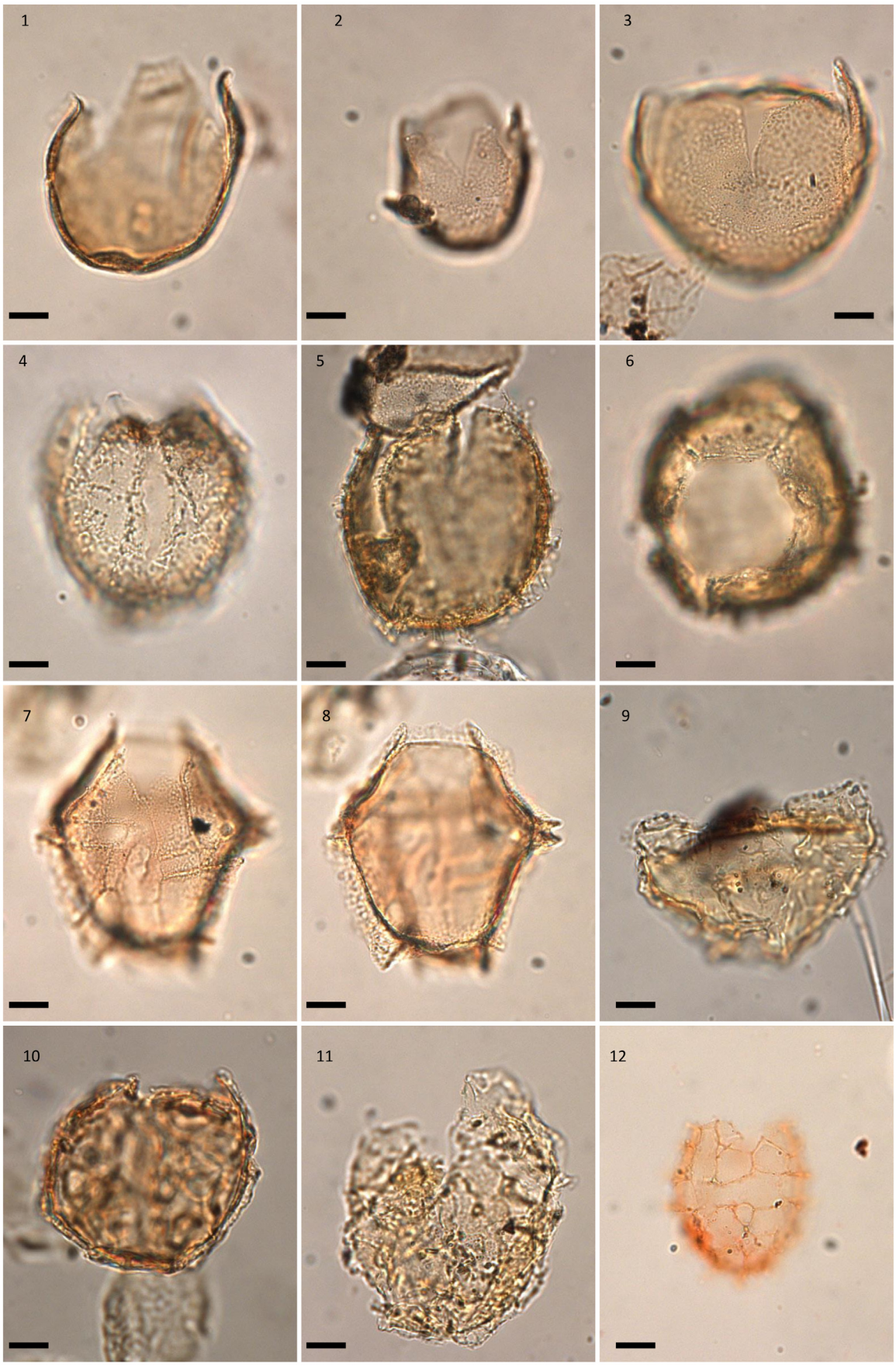

Plate IX Selected dinoflagellate cysts from Dorset, the Isle of Skye and Normandy.
Caption on p. 142

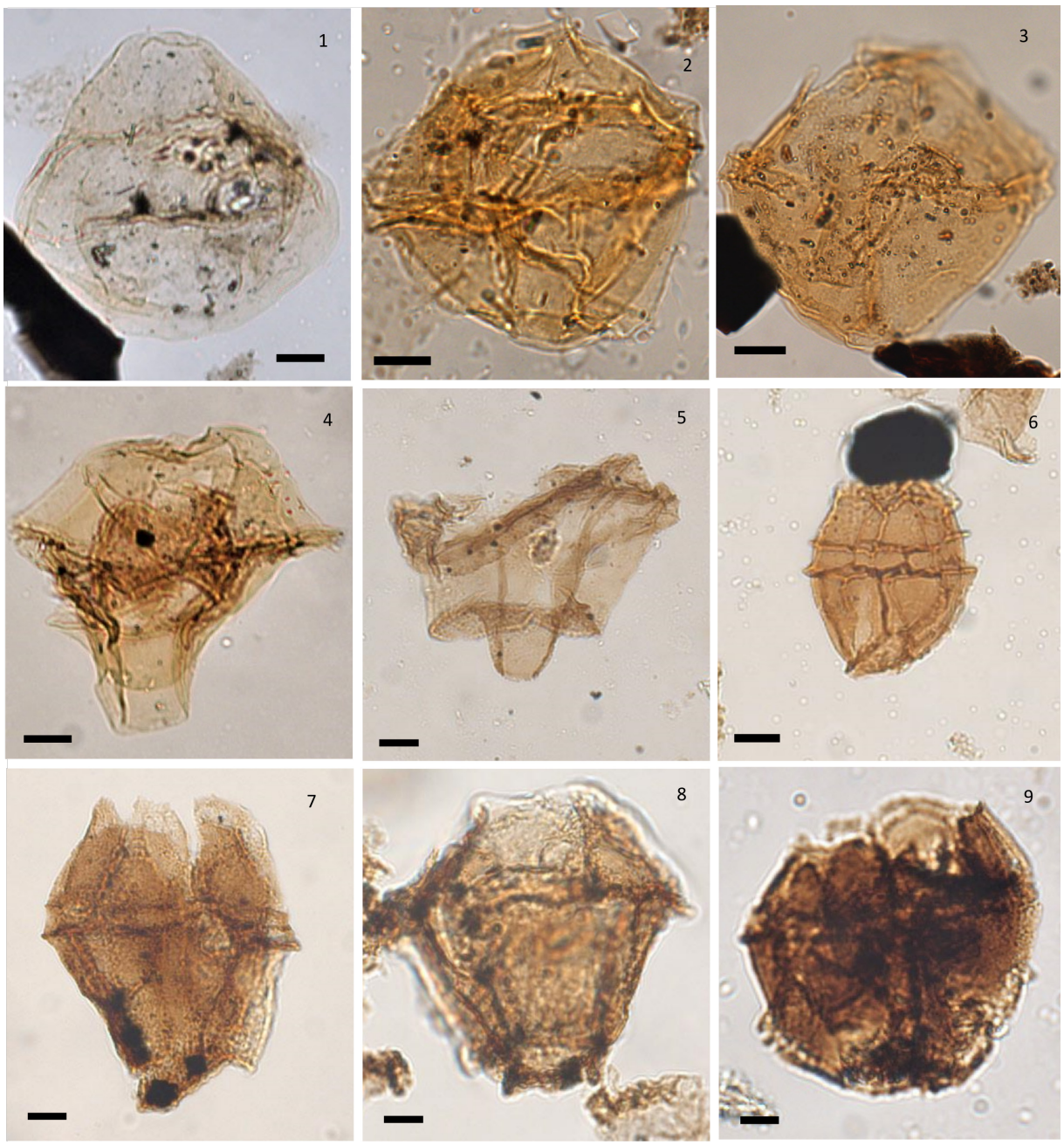

Plate X Selected dinoflagellate cysts from Swabia.

Scale bar represents 10 µm. **1**: *Endoscrinium*? spp. Dorsal view, high focus, slide S78-2, EF co. K47/3. **2–3**: *Endoscrinium* sp. cf *E. luridum*. (Deflandre 1938) Gocht 1970. **2**: dorso-ventral view, low focus, slide S69-2, EF co. U44. **3**: lateral view, median focus, slide S68-B, EF co. J37. **4**: *Endoscrinium asymmetricum* Riding 1987. Dorso-ventral view, median focus, slide S95-A, EF co. R36. **5**: *Atopodinium polygonale* (Beju 1983) Masure 1991 emend. Masure 1991. Dorso-ventral view, high focus, slide S106-B, EF co. L53/1. **6**: *Carpathodinium predae* (Beju 1971) Drugg 1978 emend. Below 1990. Dorso-ventral view, median focus, slide S108-A, EF co. L60. **7–8**: *Meiourogonyaulax valensii* Sarjeant 1966. **7**: dorso-ventral view, median focus, slide S102-1, EF co. V49/3. **8**: dorso-ventral view, high focus, slide S105-A, EF co. U62/1. **9:** *Meiourogonyaulax* sp. cf *M. caytonensis*. (Sarjeant 1959) Sarjeant 1969. Dorso-lateral view, low focus, slide S106-B, EF co. M52/2.

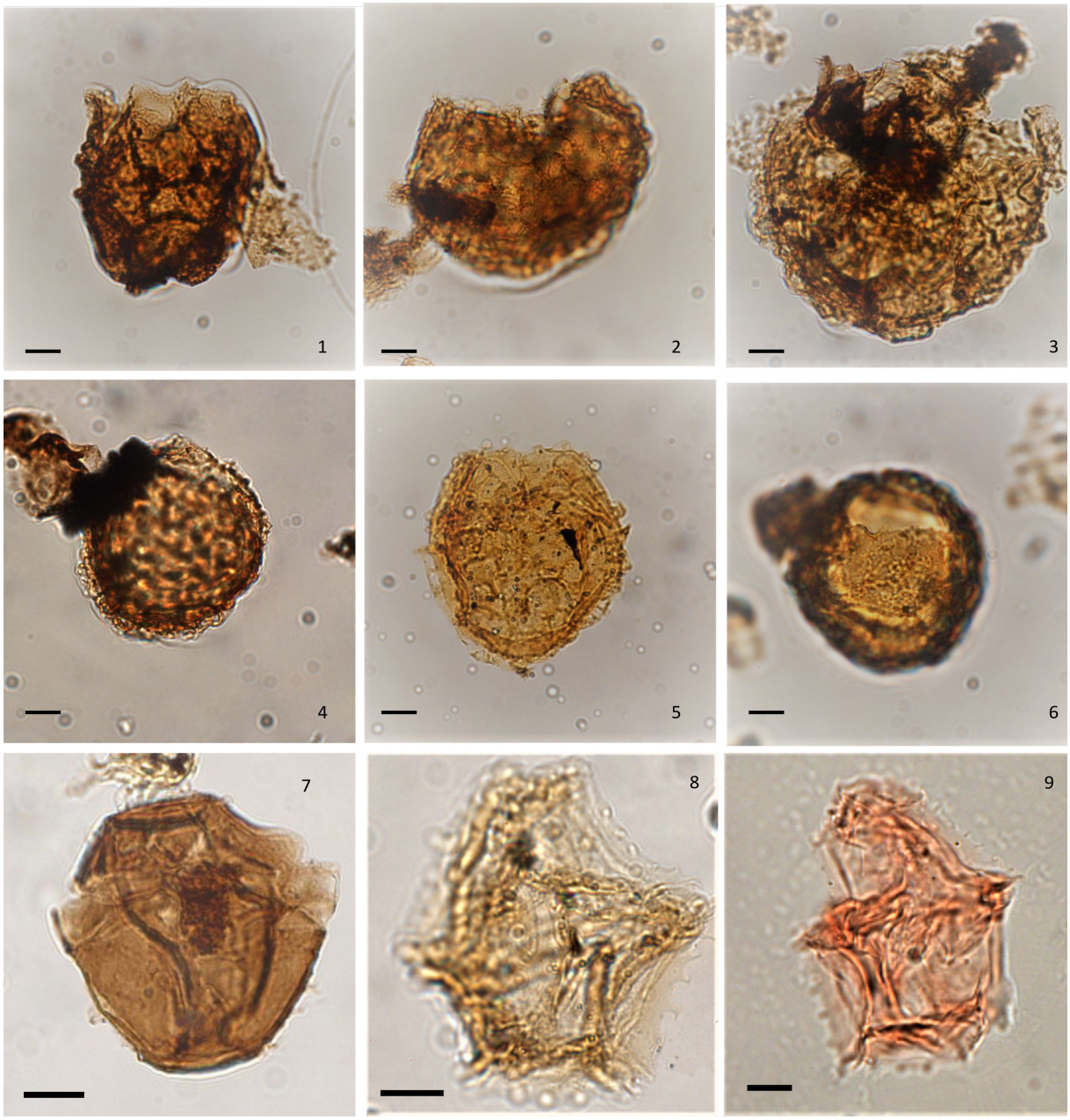

Plate XI Selected dinoflagellate cysts from Normandy and Swabia.

Scale bar represents 10 µm. **1–3**: *Ellipsoidictyum-Valensiella* complex. **1**: median focus, slide S105-A, EF co. G49/4. **2**: high focus, slide S105-A, EF co. H49. **3**: low focus, slide S105-A, EF co. M69/2. **4–5**: *Valensiella ovulum* (Deflandre 1947) Eisenack 1963 emend. Courtinat 1989. **4**: median focus, slide S105-A, EF co. J46/1. **5**: median focus, slide S66-B, EF co. S71. **6**: *Valensiella ampulla* Gocht 1970. Low focus, slide S105-A, EF co. U43/4. **7**: *Bradleyella* sp. Ventral view, median focus, slide S105-A, EF co. S59/1. **8–9**: *Rhynchodiniopsis*? spp. **8**: dorso-ventral view, high focus, slide S95-A, EF co. T59. **9**: dorso-ventral view, high focus, slide H3-B, EF co. K35/1.

Plate XII Selected dinoflagellate cysts from Swabia.

(P. 147). Scale bar represents 10 µm. **1–2**: *Pareodinia ceratophora* Deflandre 1947 emend. Gocht 1970. **1**: dorso-ventral view, normal focus, slide S105-A, EF co. H40/3. **2**: dorsal-ventral view, normal focus, slide S109-B, EF co. H54. **3–4**: *Pareodinia halosa* (Filatoff 1975) Prauss 1989 emend. Prauss 1989. **3**: dorso-ventral view, normal focus, slide S109-A, EF co. P36. **4**: with irregular, 'sculpted' kalyptra, dorso-ventral view normal focus, slide S105-A, EF co. M57/1. **5–6***: Protobatioladinium mercieri* Feist-Burkhardt & Pross 1999. **5**: lateral view, normal focus, slide S109-B, EF co. M40/1. **6**: dorso-ventral view, normal focus, slide S109-B, EF co. Q34. **7**: *Nannoceratopsis gracilis* Alberti 1961 emend. van Helden 1977. Right lateral view, median focus, slide S36-B, EF co. N40/2. **8**: *Nannoceratopsis spiculata* Stover 1966. Lateral view, low focus, slide S105-B, EF co. V39. **9**: *Nannoceratopsis plegas* Drugg 1978. Left-lateral view, high focus, slide S24-1, EF co. S62/2. **10**: *Nannoceratopsis ambonis* Drugg 1978 emend. Riding 1984. Note the thickened, solid sagittal band. Left-lateral view, median focus, slide S18-A, EF co. P57/3. **11–12**: *Nannoceratopsis* spp. **11**: right lateral view, low focus, slide S28-D, EF co. S42/2. **12**: left-lateral view, normal focus, slide S24-1, EF co. P67/3.

Plate XIII Selected dinoflagellate cysts from Swabia.

(P. 148). Scale bar represents 10 µm except in 1 where it represents 15 µm, and in 12–15 where it represents 5 µm. **1**: *Chytroeisphaeridia chytroides* (Sarjeant, 1962) Downie & Sarjeant 1965 emend. Davey 1979. Right lateral view, high focus, slide S109-B, EF co. M62/2-4. **2**: *Jansonia psilata* Martinez et al. 1999. Dorso-ventral view, median focus, slide S66-A, EF co. H72/1-3. **3–4**: *Jansonia* sp. 1. Dorsal view, slide G5-2, EF co. V70/4. 3: low focus, 4: high focus. **5**: *Jansonia* sp. 2, ventral view, high focus, slide G4-2, EF co. R58. **6**: *Impletosphaeridium* sp. 1. Apical view, median focus, slide S102-1, EF co. J71/4. **7**: *Impletosphaeridium* sp. 2. Dorso-ventral view, median focus, slide S108-B, EF co. J45/3. **8**: *Valvaeodinium* sp. cf. *V. spinosum* Fenton et al. 1980, dorso-ventral view, median focus, slide S48-2, EF co. N67-2. **9**: *Valvaeodinium vermicylindratum* Below 1987. Dorso-ventral view, median focus, slide S66-A, EF co. G45/3. **10–11**: *Valvaeodinium* spp. **10**: lateral view, median focus, slide S102-1, EF co. U68, 11: lateral view, low focus, slide S69-2, EF co. U40/1-3. **12–13**: *Orobodinium automobile* Gocht & Wille 1990. **12**: dorso-ventral view, high focus, slide S109-B, EF co. G65/2. **13**: dorso-ventral view, median focus, note the operculum which has fallen back inside the cyst body, slide S36-A, EF co. H52/3. **14–15**: *Orobodinium* sp. A of Wille & Gocht 1990. Same specimen apical view, slide S109-A, EF co. O63/1. **14**: median focus, **15**: low focus.

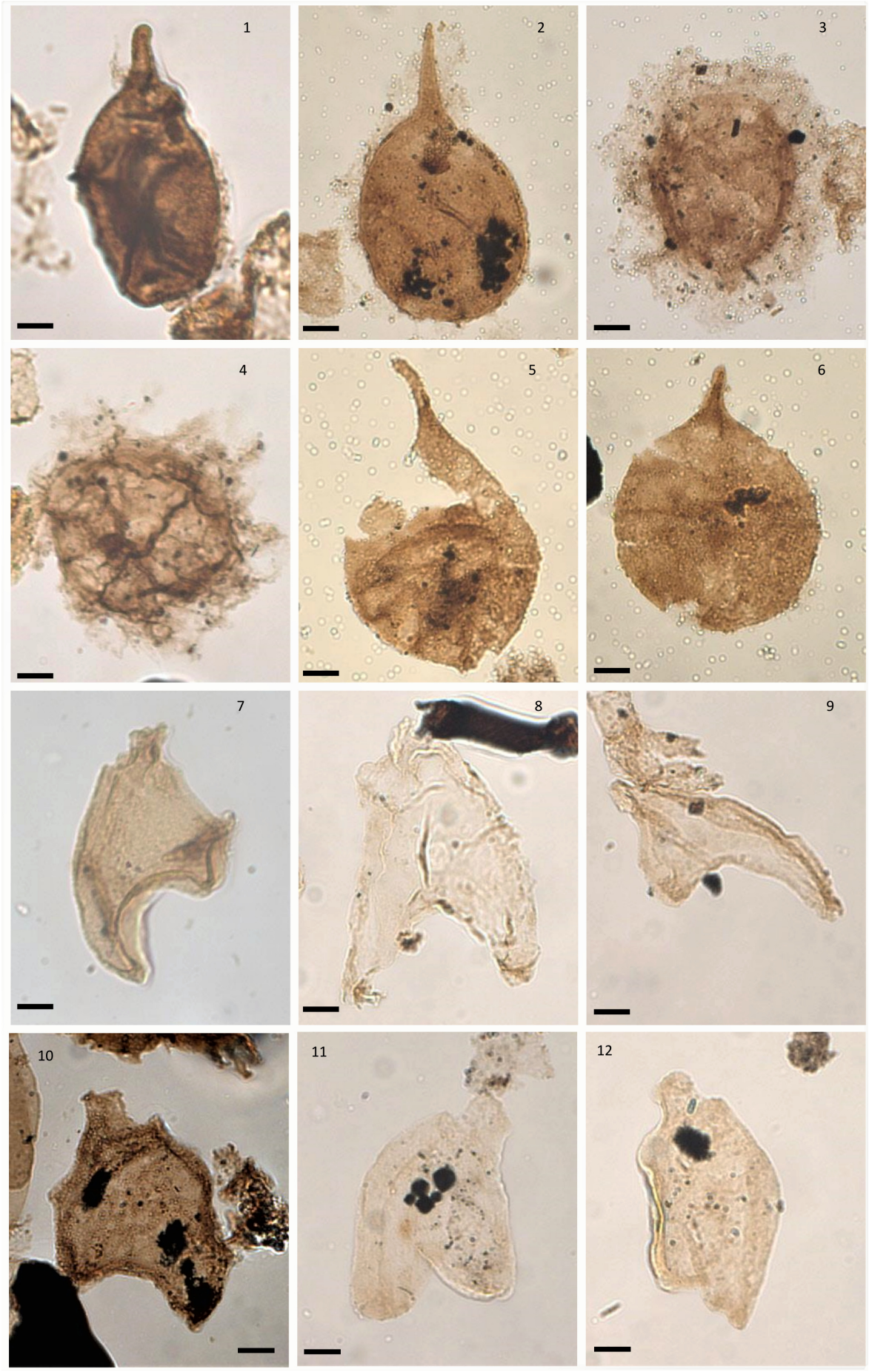

Plate XII Selected dinoflagellate cysts from Swabia. Caption on. p146.

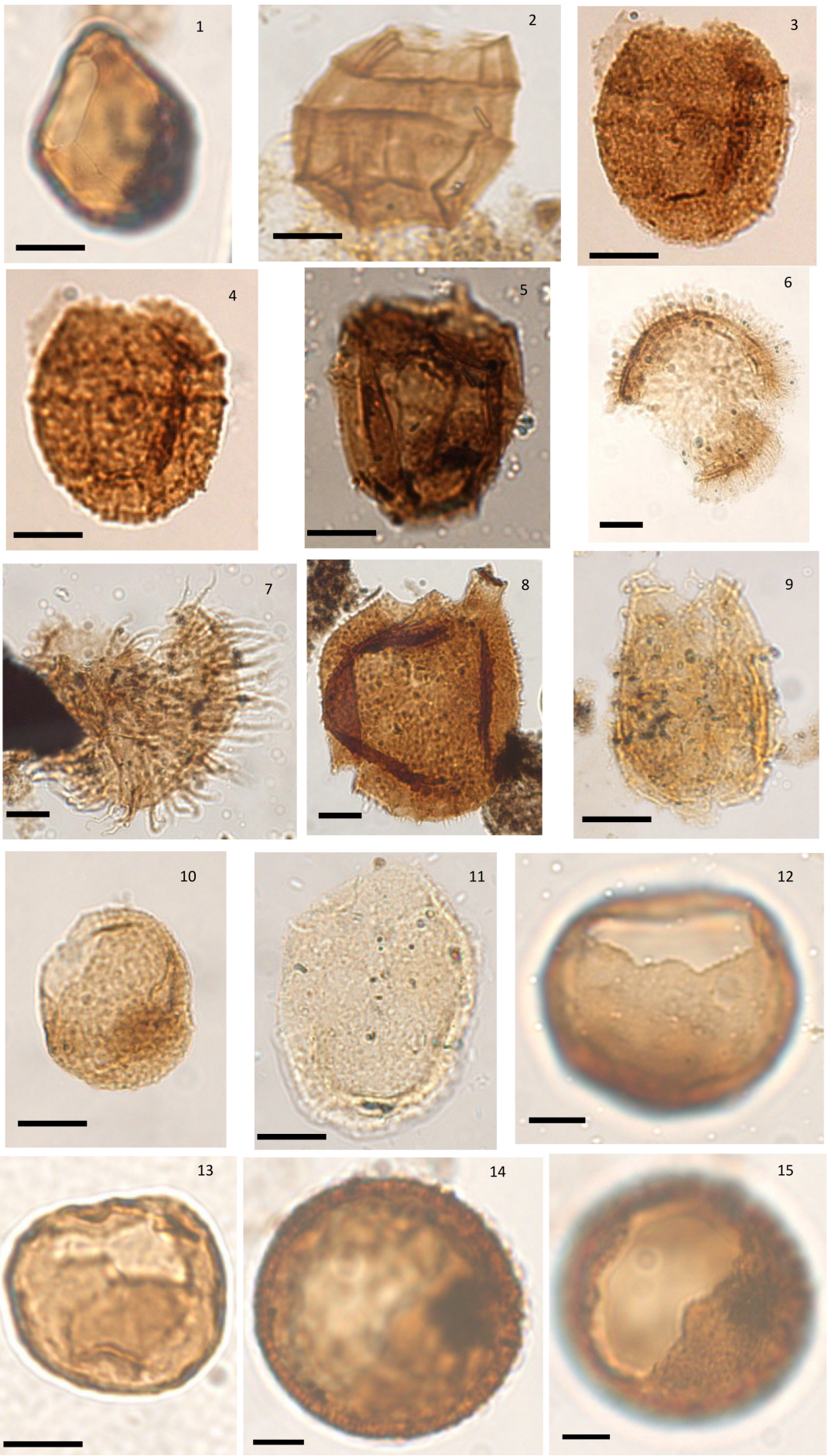

Plate XIII Selected dinoflagellate cysts from Swabia. Caption on p. 146.

Plate XIV Selected dinoflagellate cysts from Normandy and Swabia.

(P. 150). Scale bar represents 10 µm except in 8 and 9 where it represents 5 µm. **1**: *Mancodinium semitabulatum* Morgenroth 1970 emend. Below 1987, ventral view, high focus, slide FDH7-2, EF co. S72/3. Note the distinctive tab of the anterior sulcul plate and the 7'' plate. **2**: *Phallocysta elongata* (Beju 1971) Riding 1994. High focus, slightly oblique dorsal view, slide G5-2, EF co. V65/3. **3**: *Chytroeisphaeridia chytroides* (Sarjeant, 1962) Downie & Sarjeant 1965 emend. Davey 1979. Left lateral view, low focus, slide SR8-3, EF co. S37/3. Note the operculum inside the cyst. **4**: *Pareodinia* sp. 1 of Feist-Burkhardt & Monteil 1997. Dorsal view, high focus, slide FDH15-1, EF co. M62. **5**: Pareodinia sp. 2 of Feist-Burkhardt & Monteil 1997. Low focus, oblique left-lateral view, slide H2-2, EF co. P58/2-4. **6**: *Carpathodinium predae* (Beju 1971) Drugg 1978 emend. Below 1990. Dorsal view, low focus, slide SR8-3, EF co. E61. **7**: *Valvaeodinium spinosum* (Fenton et al. 1980) Below 1987. Dorso-ventral view, median focus, slide SR3-4, EF co. T48/4. **8**: *Orobodinium* sp. Median focus, slide FDH7-2, EF co. V69/4. **9**: *Moesiodinium raileanui* Antonesçu 1974. Low focus, slide S36-B, EF co. N53/1.

Plate XV Selected dinoflagellate cysts from Dorset, Normandy and Swabia.

(P. 151). Scale bar represents 10 µm. **1–2**: *Rhynchodiniopsis*? *regalis* (Gocht 1970) Jan du Chêne et al. 1985. Same specimen, slide MPA 2204-4, EF co. L62. **1**: ventral view, high focus. **2**: dorso-ventral view, median focus. **3–7**: *Gonyaulacysta pectinigera* (Gocht 1970) Fensome 1979. **3**: oblique right lateral view, low focus, slide S109-B, EF co. Q68. **4**: ventral view, high focus, slide SR3-2, EF co. K45/2. **5**: dorso-ventral view, median focus, slide H2-1, EF co. V35. **6**: dorsal view, slide SR3-2, EF co. L49/2. **7**: dorso-ventral view, median focus, slide CSA 1526-4, EF co. M54/2. **8**: *Gonyaulacysta*? sp. Ventral view, high focus, slide MPA 2193, EF co. J54.

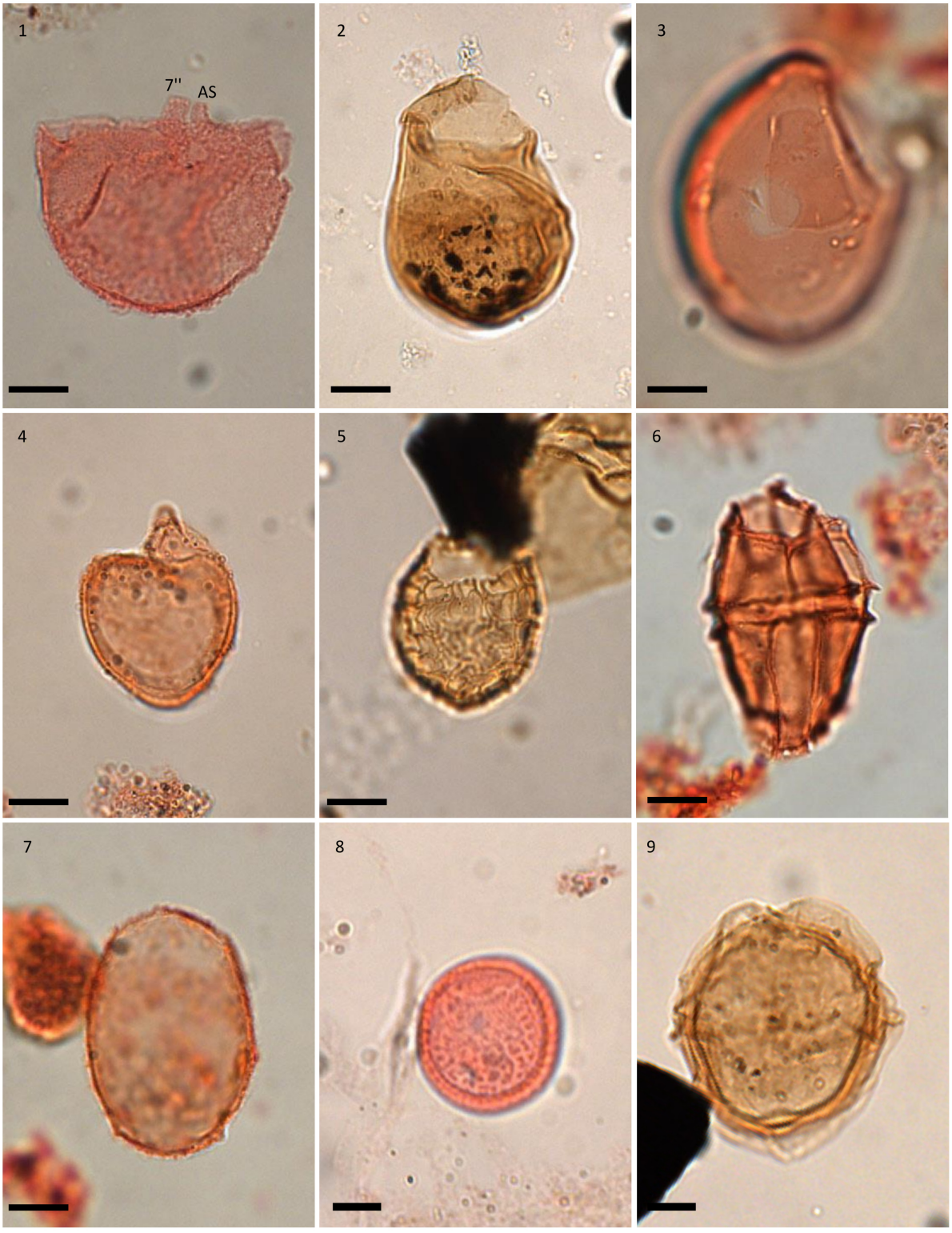

Plate XIV Selected dinoflagellate cysts from Normandy and Swabia. Caption on p. 149.

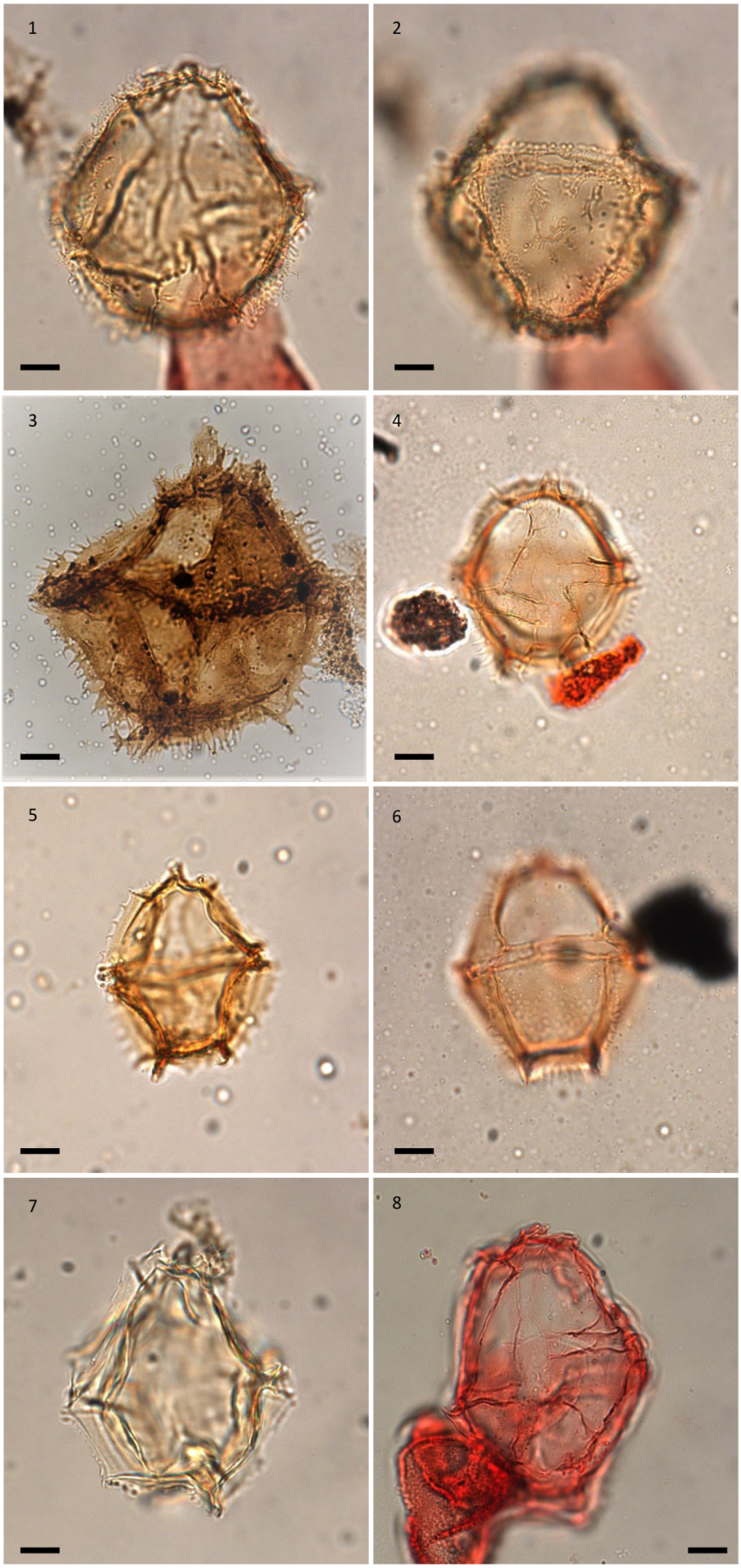

Plate XV Selected dinoflagellate cysts from Dorset, Normandy and Swabia. Caption on p. 149.

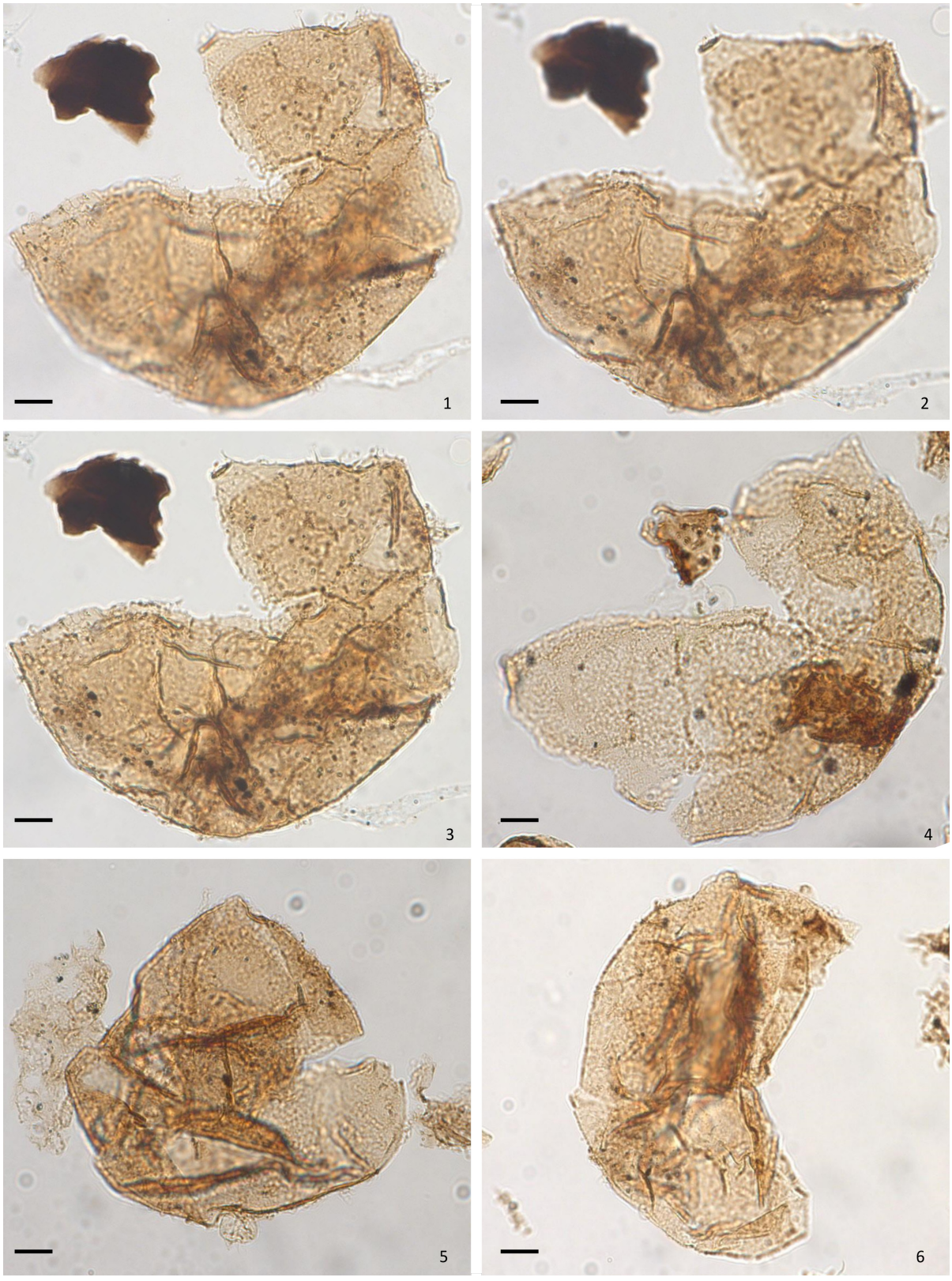

Plate XVI *Korystocysta aldridgeii*

Scale bar represents 10 µm. The slide number and England Finder co-ordinates (EF co.) of figured specimens are noted.**1–6**: *Korystocysta aldridgeii* Wiggan et al. 2017. **1–3**: holotype, right lateral view, **-**: high focus, **2**: low focus **3**: high, median and low foci stacked, slide S105-A, EF co. L48/2. **4**: paratype, right lateral view, median focus, slide S105-B, EF co. G36, **5**: ventro-lateral view, low focus, slide S105-A, EF co. U43/1. **6**: lateral view, median focus, slide S105-B, EF co. K58/1.

Chapter 7. Aalenian to Bathonian carbon isotope ($\delta^{13}C$) records: palaeoenvironmental changes during the Bajocian

7.1. Introduction.

The isotope ratio of ^{13}C to ^{12}C (expressed as $\delta^{13}C$) in carbonate minerals and organic matter can be tracked through geological time, and reflects the fluxes between sources and sinks in the global carbon cycle. The Jurassic was marked by numerous shifts in $\delta^{13}C$, which were driven by regional, and global, palaeoenvironmental changes (Jenkyns et al., 2002). Negative shifts in $\delta^{13}C$ are driven by the input of ^{12}C into the upper oceans and atmosphere, and a variety of mechanisms have been sought to explain negative $\delta^{13}C$ shifts in the Jurassic. These include volcanic outgassing, the dissociation of gas hydrates, and the widespread upwelling of ^{12}C-enriched deepwaters into the photic zone (Beerling et al., 2002; Hesselbo et al., 2003; van de Schootbrugge et al., 2005). Positive shifts in $\delta^{13}C$ primarily reflect the sequestration of ^{12}C in sedimentary organic matter, and throughout much of the Jurassic, positive $\delta^{13}C$ shifts were associated with intervals of black-shale deposition (e.g. Jenkyns et al., 2002; van de Schootbrugge et al., 2013).

To assess the relationship between the dinoflagellate cyst record and wider palaeoenvironmental changes, a $\delta^{13}C$ record based on bulk organic matter has been generated for the Upper Aalenian to Lower Bathonian of the Winterborne Kingstone borehole, Dorset, southwest England and the B404/2 borehole, Swabia, southern Germany. Organic matter was chosen for analysis as the Inferior Oolite Group of the Winterborne Kingston succession has undergone significant diagenetic recrystallisation, making bulk carbonate unsuitable for carbon isotope analysis. Bulk organic matter was analysed from the B404/2 borehole succession as this section has a low abundance of primary carbonate, and macrofossils (e.g. belemnites, bivalves) are rare. Moreover, Chapters 3 and 4 have documented the palynological record through these boreholes which allows the palynological composition to be compared to the $\delta^{13}C$ record.

7.1.1. The Bajocian carbon isotope record

Previous work has highlighted a negative carbon isotope excursion (CIE) around the Aalenian–Bajocian boundary and positive CIE in the Early Bajocian. This pattern has been reported from central Italy (Bartolini et al., 1996, 1999; Bartolini and Cecca, 1999), the Isle of Skye, Scotland, (Jenkyns et al., 2002; Korte et al., 2015), Yorkshire, northern England (Hesselbo et al., 2003), southern Spain (O'Dogherty et al., 2006), northern France (Brigaud et al., 2009), Portugal (Suchéras-Marx et al., 2012; Giraud et al., 2016), south-eastern France (Suchéras-Marx et al., 2013), and most recently, Morocco (Bodin et al., 2017). The majority of these works have documented the Middle Jurassic $\delta^{13}C$ record from bulk carbonate or calcite macrofossils. Hesselbo et al. (2003) documented the $\delta^{13}C$ of the Middle Jurassic of northern England from fossil wood and bulk organic matter. However, the bulk organic matter record

was strongly influenced by differing proportions of terrestrial and marine sources. As such, until recently, these excursions had not been documented from bulk organic matter in a marine setting. Bodin et al. (2017) examined the $\delta^{13}C$ record of the Middle Jurassic of Morocco from both bulk organic matter, and bulk carbonate. These authors recorded these excursions in the organic matter component but not the carbonate, and concluded that diagenetic overprinting, as suggested by oxygen isotopes, had distorted the carbon isotope record of the bulk carbonate. Consequently, there appears to have been perturbations in the carbon cycle during the Late Aalenian to Early Bajocian which have been recorded in numerous European successions, in both carbonate and organic matter. However, there have been no studies on the Bajocian $\delta^{13}C$ record of southern England and southern Germany or works which directly tie the palynological record to the $\delta^{13}C$ record. To date, there have been no works documenting the Bajocian $\delta^{13}C$ record outside of Europe or North Africa, making the global extent of these excursions unclear.

7.2. Methods

I collected, sub-sampled, and powdered the rock samples which were then sent to the NERC Isotope Geoscience Laboratory for $\delta^{13}C$ analysis of bulk organic matter. Fifty-nine samples with an average spacing of ~0.25 m were analysed from the Winterborne Kingston Borehole and 105 samples with an average spacing of ~0.5 m were analysed from the B404/2 borehole (data table appendices E). Samples were washed to remove any external or modern organic matter with deionised water and air dried before being powdered with an agate pestle and mortar. Around 5 g of material was powdered from the Winterborne Kingston samples whilst approximately 0.5 g of rock was powdered from the B404/2 samples. The powdered rock samples were then sent to NIGL where they were treated with 5% hydrochloric acid to remove any carbonate. $^{13}C/^{12}C$ analyses were performed by combustion in a Costech Elemental Analyser (EA) on-line to a VG TripleTrap and Optima dual-inlet mass spectrometer. $\delta^{13}C$ values were calculated to the VPDB scale using a within-run laboratory standards calibrated against the international standards NBS-18, NBS-19 and NBS-22. Replicate analysis of well-mixed samples indicated a precision of +/– <0.1‰ (1 SD). Several samples from the B404/2 borehole failed to run on the initial analysis as they were below the limit of detection, these were resampled and re-run (see data table appendix E.3).

7.3. Results

7.3.1. The Winterborne Kington, southern England

The most significant features of the $\delta^{13}C$ curve for the Winterborne Kingston borehole (Figure 1) are a negative excursion of around 0.5‰ around the Aalenian/Bajocian boundary and a positive excursion of approximately 2‰ in the Lower Bajocian. The negative $\delta^{13}C$ shift around the Aalenian–Bajocian boundary appears to begin in the lowermost part of the *H. discites* zone (921.8 m) and has a maximum amplitude of 0.5‰. The positive shift begins in the uppermost part of the *H. discites* zone with an abrupt shift of 2‰ between 921.1 and 920.94 m depth (Figure 7.1). Values then fluctuate by around 1‰ through the *W. laeviuscula/S. propinquans* zone to the *S. humphriesianum* zone. There is then an abrupt

negative shift in the *S. humphriesianum* zone between 917.24 and 916.99 m depth of 1‰, values then fall through the *S. niortense* zone by roughly 1.5‰ before fluctuating by around 1‰ through the Upper Bajocian and lowermost Bathonian.

7.3.2 The B404/2 borehole, southern Germany

There is a general trend in the $\delta^{13}C$ record of the B404/2 borehole of more positive values in the Lower Bajocian, *W. laeviuscula* to *W. laeviuscula/S. propinquans* zones and a fall to more negative values from the *S. humphriesianum* zone to the *Z. zigzag* zone, with considerable fluctuation throughout (Figure 7.1).

In the *W. laeviuscula* zone there is a negative $\delta^{13}C$ shift of around 1‰ from 195 to 190 m before a return to more positive values from 190 to 185 m. Values then remain relatively stable up to 177m, before a pronounced positive shift of around 2‰ to the most positive values seen in the succession from 175 to 170m in the *W. laeviuscula*/*S. propinquans* zone. There is then a decline through the *S. propinquans*/*S. humphriesianum* zones and lower part of the *S. humphriesianum* zone before values stabilise. There is a small positive shift towards the top of the zone around 165m. From this point there is a sharp decline of 3‰ and values then fluctuate by 1–2‰ through the Upper Bajocian and lowermost Bathonian.

7.4. Interpretation

7.4.1. Controls on the $\delta^{13}C$ composition of organic matter

The proportion of terrestrially-derived organic matter (TOM) to marine-derived organic matter (MOM) can drive changes in $\delta^{13}C$. Plants derive carbon from atmospheric CO_2 whilst phytoplankton gain their carbon primarily from dissolved bicarbonate (Burdige et al. 2005 and references therein). Although both C3 marine phytoplankton and terrestrial plants fractionate carbon in a similar way, the overall composition is different due to their use of these differing carbon sources. In the Recent, TOM from C3 fixation plants is isotopically more negative in its composition than MOM, with average $\delta^{13}C$ values of around –25 to –28‰, vs –17 to –22‰ for MOM (Burdige et al. 2005). However, several studies of organic matter from Mesozoic sediments have demonstrated that Mesozoic MOM is isotopically more negative than TOM. Arthur et al. (1985) and Dean et al. (1986) have shown that MOM from deep sea sediments of Cretaceous age exhibit lower $\delta^{13}C$ values compared to the TOM analysed from the same sediments These authors documented that Cretaceous organic matter of predominantly marine composition is ~3–4‰ lighter than mixed terrestrial-marine organic matter. Furthermore, in a study on the Middle Jurassic of Yorkshire, UK, Hesselbo et al. (2003) demonstrated that bulk organic matter with an increasing marine component showed a trend to lower $\delta^{13}C$ values. The overall $\delta^{13}C$ composition of the organic matter was also more negative than that of fossil wood sampled from the same horizons, by around 3‰. Moreover, Grice et al. (2007) demonstrated that algal-dominated organic matter from the Lower Triassic of Australia had a more negative $\delta^{13}C$ composition compared to that of terrestrially dominated organic matter from the underlying Upper Permian. Consequently, it appears that in the

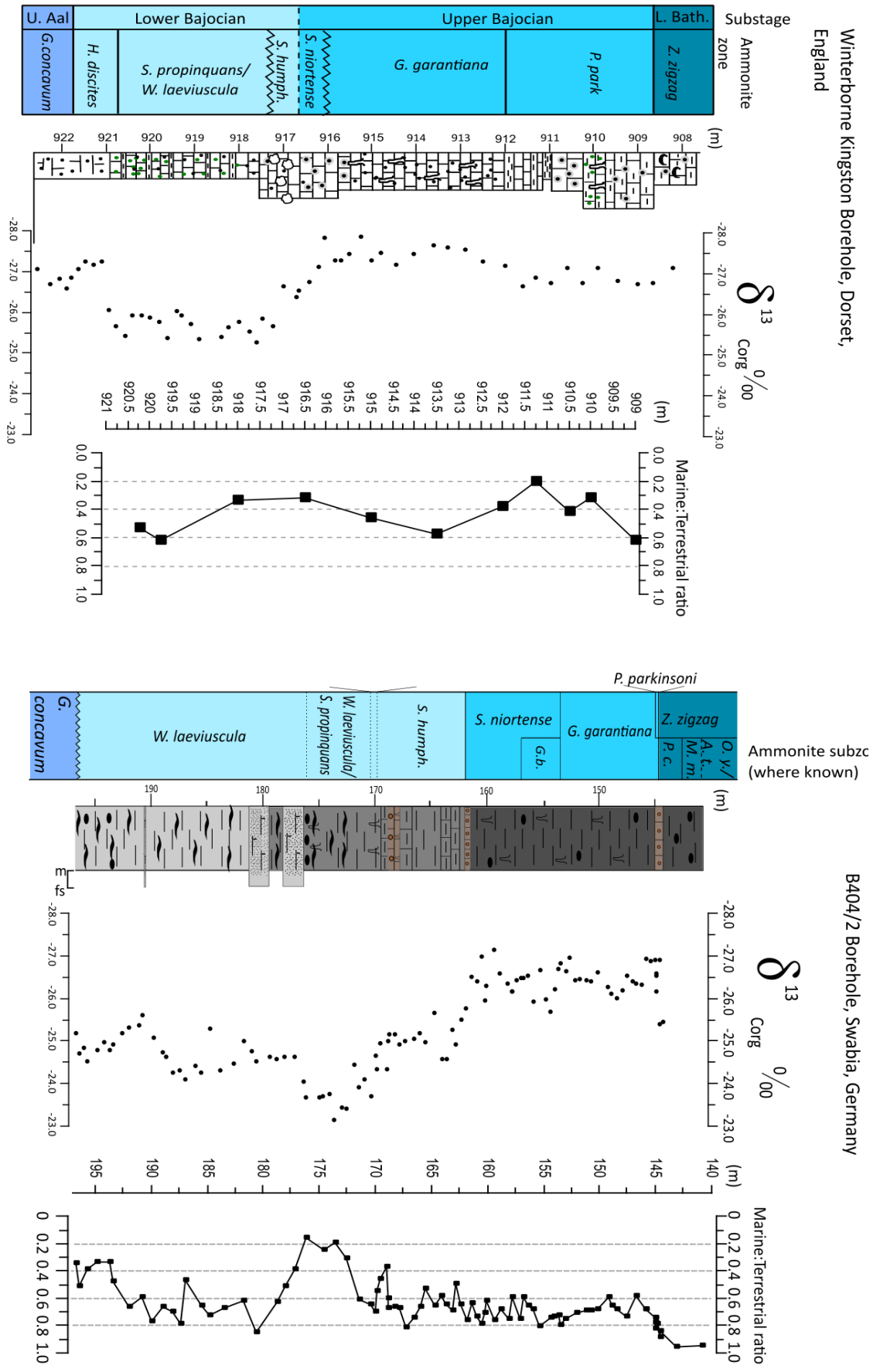

Figure 7.1. $\delta^{13}C$ curves for the Winterborne Kingston Borehole (Dorset) and the B404/2 Borehole (Swabia). Caption on p. 157.

Mesozoic the MOM is isotopically lower than TOM.

Figure 7.1. (p. 156). $\delta^{13}C$ curves for the Winterborne Kingston Borehole (Dorset) and the B404/2 Borehole (Swabia).
In Winterborne Kingston, there is a negative shift of around 0.5‰ through the Aalenian–Bajocian transition, and a positive shift of around 2‰ in the Lower Bajocian, before a negative shift of ~2% through the Lower–Upper Bajocian transition. In B404/2 there is a general trend from more positive values in the Lower Bajocian, to more negative values in the Upper Bajocian. In Winterborne Kingston the ratio of marine:terrestrial palynomorphs does not appear to strongly co-vary with the $\delta^{13}C$. In contrast, the marine:terrestrial ratio appears to negatively co-vary with the $\delta^{13}C$.

7.4.2. Influence of organic carbon source on the Winterborne Kingston and B404/2 $\delta^{13}C$ records: local controls

As the Winterborne Kingston and B404/2 successions show varying proportions of marine and terrestrial derived palynomorphs it is possible that these mixed sources of organic matter have influenced the $\delta^{13}C$ composition. However, it is important to note that as mentioned in Chapter 2, the marine:terrestrial ratio for this thesis was calculated from palynomorphs. Other sedimentary organic matter such as phytoclasts, and amorphous organic matter are not included in this ratio, and as such the palynomorph marine: terrestrial ratio may not fully portray the composition of organic matter from the sections studied. However, this ratio provides at least some insight into the changing proportions of marine and terrestrial organic matter sources, which can help interpret the changes detected in the $\delta^{13}C$.

With the Winterborne Kingston succession there is no general trend in the marine:terrestrial ratio through the succession as values fluctuates from around 0.3 to 0.6, and there is no correlation with

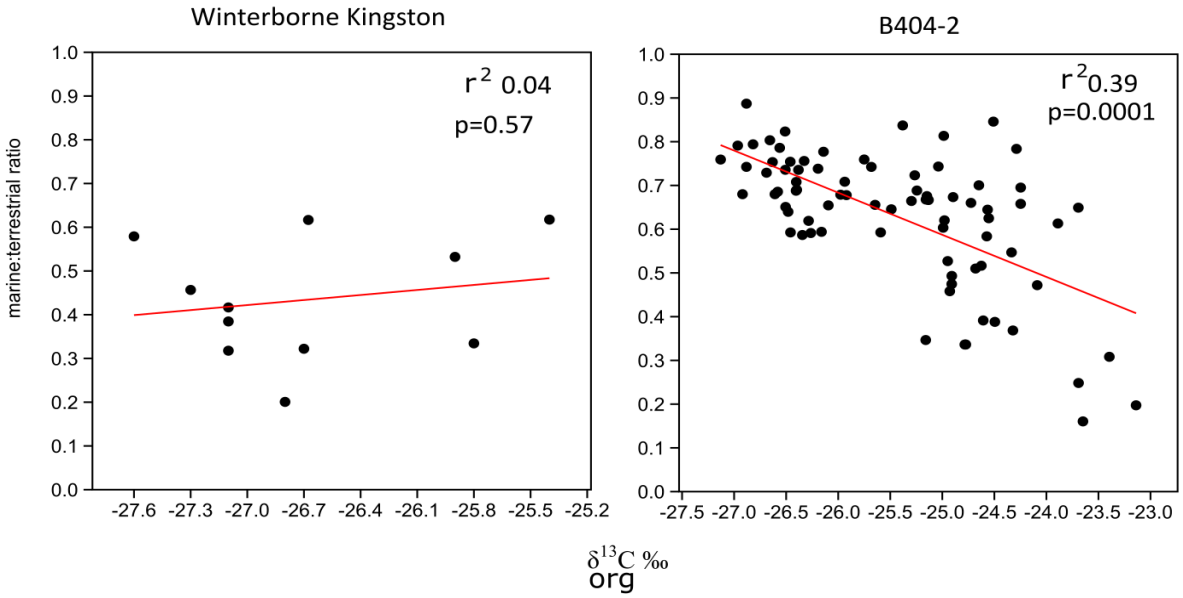

Figure 7.2. Correlation between the marine:terrestrial ratios of palynological samples and the $\delta^{13}C$ of bulk organic matter.
It can be observed that samples from Winterborne Kingston show no correlation, whilst samples from B404/2 show a moderate negative correlation.

the $\delta^{13}C$ record (Figure 7.2). As such, the changing proportions of MOM and TOM do not appear to have strongly influenced the $\delta^{13}C$ record, although the short-term (1‰) fluctuations may reflect this mixed organic carbon source and the fractionation effect of photosynthesing organisms. Moreover, the C-org $\delta^{13}C$ record from Winterborne Kingston can be correlated with the carbonate $\delta^{13}C$ curve of other European successions (section 7.4.3).

By contrast, samples from B404/2 show a moderate negative correlation between marine:terrestrial ratio and $\delta^{13}C$ (Figure 7.2). The overall upward trend of increasing marine:terrestrial ratio from the Lower-Upper Bajocian transition to the lowermost Bathonian roughly parallels the negative shift in $\delta^{13}C$ through this interval. At a finer scale, parts of the Lower Bajocian $\delta^{13}C$ curve have likely been influenced by mixed carbon sources. The ~2‰ negative $\delta^{13}C$ shift in the *W. laeviuscula* zone from 195–190 m closely correlates with an increase in the marine:terrestrial ratio. As the $\delta^{13}C$ of marine and mixed marine-terrestrial organic matter from the Mesozoic appears to differ by ~3‰ it is likely that this shift been driven by an increase in the proportion of MOM. Likewise, the huge decrease in the marine: terrestrial ratio (0.8 to 0.2) from 181 to 175 m corresponds to the pronounced 2‰ positive $\delta^{13}C$ shift to the most positive values in the succession. This is also synchronous with a facies change from mudstone, to interbedded sandstone/mudstone to mudstone. It is therefore likely that the $\delta^{13}C$ composition of this part of the record has been driven to more positive values by the huge increase in the proportion of TOM.

If the B404/2 $\delta^{13}C$ record is considered in isolation it may be assumed that the $\delta^{13}C$ composition is simply reflecting the relative inputs of terrestrial and marine organic matter. However, the shift to more negative values around the Lower-Upper Bajocian transition is also seen in carbonate sections from Spain (Figure 7.3b), but the magnitude of the shift is much smaller, around 1‰, rather than the 3‰ shift observed in B404/2. Therefore, it is possible that broad-scale $\delta^{13}C$ record is reflecting a mixed signal of both the upper water column dissolved inorganic carbon (DIC) pool associated with atmospheric changes in CO_2 or productivity, and changes in the source of organic matter. The increase in the proportion of MOM has exaggerated the magnitude of the negative shift in this region. On the other hand, parts of the Lower Bajocian record have likely been significantly influenced by changes in the proportions of TOM and MOM. Moreover, the short-term, small scale fluctuations (ca. 1‰) in $\delta^{13}C$ throughout the succession most likely reflect the mixed carbon source and the fractionation effects of photosynthesing organisms.

7.4.3. Correlation

The negative CIE around the Aalenian/Bajocian boundary in Winterborne Kingston can be clearly recognised in the Cleveland Basin of Yorkshire, England, the Hebrides Basin of western Scotland, the Lusitanian Basin of Portugal, the Umbria Basin of Italy and the Central High Atlas Rift Basin of Morocco (Figure 7.3a,b,c,d). The amplitude of this negative shift appears to be around 0.5‰ except in Yorkshire and Morocco where it is 2–3‰. This larger magnitude shift in these regions was recorded

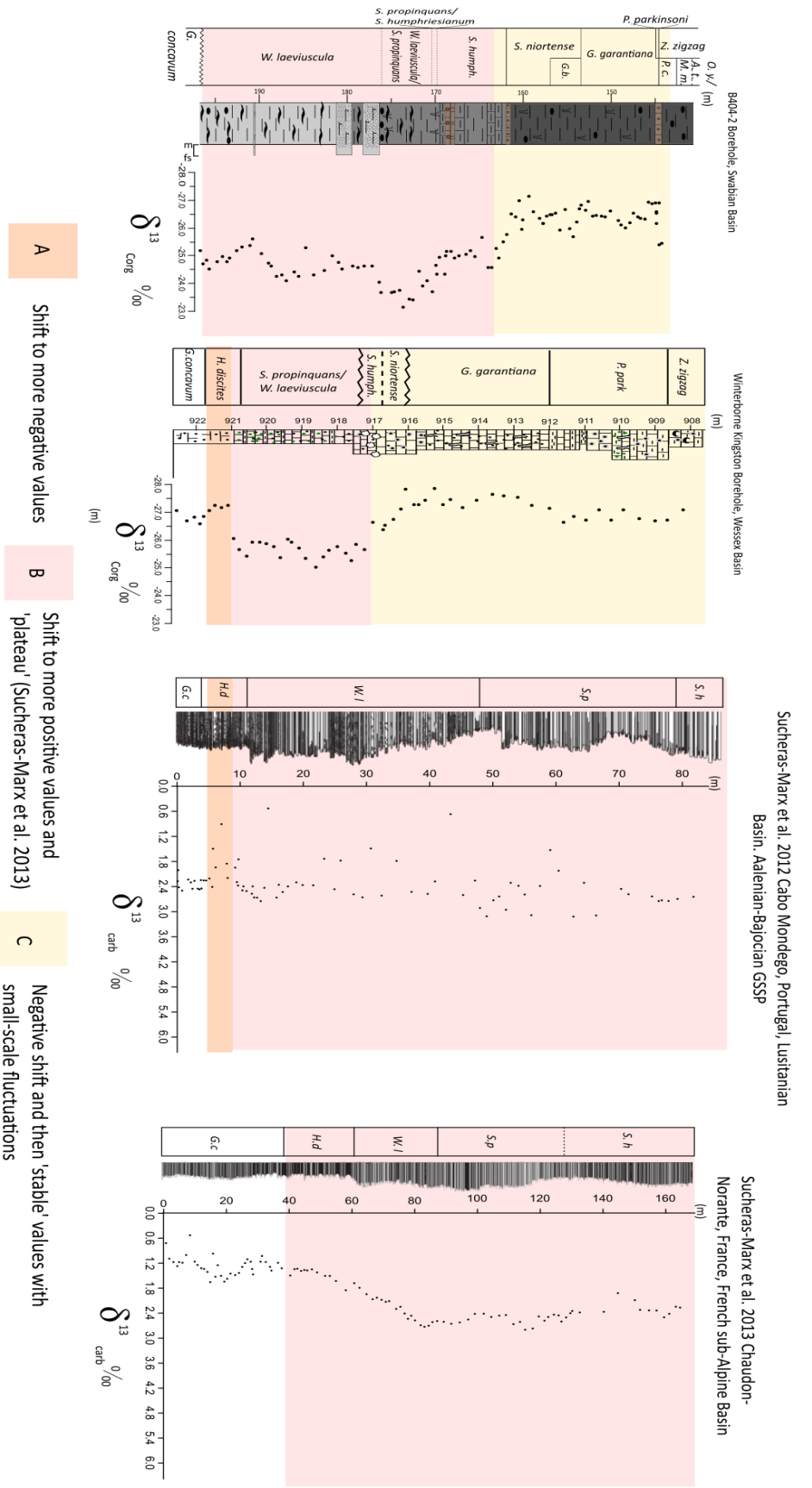

Figure 7.3a. Correlation of the $\delta^{13}C$ records from Dorset and Swabia to the French sub-Alpine Basin, and the Lusitanian Basin of Portugal.
Caption of p. 160.

Figure 7.3a. (p. 159). Correlation of the $\delta^{13}C$ records from Dorset and Swabia to bulk carbonate records from the Upper Aalenian–Lower Bajocian of the French sub-Alpine Basin, and the Lusitanian Basin of Portugal.
Logs modified from Suchéras-Marx et al. (2012, 2013), $\delta^{13}C$ data plotted from the raw data of Suchéras-Marx et al. (2012, 2013).
Zone abbreviations. Upper Aalenian: *G.c.= G. concavum*. Lower Bajocian: *H. d.= H. discites, W. l.= W. laeviuscula, S. p.= S. propinquans, S. h.= S. humphriesianum.*

in bulk organic matter. In the southern Iberian palaeomargin, O'Dogherty et al. (2006) reported a gradual decline in $\delta^{13}C$ values of bulk carbonate of around 0.5‰ through the *G. concavum* to *H. discites* zones rather than a pronounced excursion (Figure 7.3b). The timing of the CIE appears to be slightly diachronous. In Winterborne Kingston and the Lusitanian Basin, the latter of which is the Aalenian-Bajocian GSSP, the negative CIE appears to be wholly within the *H. discites* zone (Figure 7.3a). This is also the case in Yorkshire (Figure 7.3c), as the Sycarham Member in which the CIE was recorded has been dated to be of Early Bajocian, *H. discites* zone age (Hesselbo et al., 2003; Butler et al., 2005 and references therein). On Skye, the shift to more negative $\delta^{13}C$ values begins within *G. concavum* zone with the maximum amplitude in the *H. discites* zone (Figure 7.3b). However, in the Umbria Basin the shift to lower $\delta^{13}C$ begins in the Upper Aalenian with minimum values reached around the Aalenian-Bajocian boundary (Figure 7.3c). The same pattern is seen in Morocco in the Jebel Boull Kendill Section (Figure 7.3d). However, the Amellago section shows a negative shift beginning at the Aalenian/Bajocian boundary which spans the *H. discites* to *S. propinquans* zones, although the sampling resolution through this interval is relatively coarse. In the Agua Larga section of the Southern Iberian palaeomargin the shift to negative $\delta^{13}C$ values begins in the *G. concavum* zone, although the topology of this record is markedly different to the others presented (Figure 7.3b). These records indicate that there may have been a difference in the timing of this negative shift between different basins, or alternatively indicates that the ammonite zonation diachroneity in the ammonite zonation around the Aalenian/Bajocian boundary. As this negative shift appears to have affected the whole ocean-atmosphere system (section 7.4.4.) it suggests that this was a fairly synchronous event and therefore may indicate diachroneity in the ammonite zonation.

A positive shift in $\delta^{13}C$ can clearly be recognised across the Lower Bajocian of Europe and Morocco, in both bulk organic matter (this thesis, Bodin et al., 2017) and bulk carbonates (Bartolini et al., 1999; O'Dogherty et al., 2006; Suchéras-Marx et al., 2012; Korte et al., 2015). The exact timing of the shift is more difficult to assign to one ammonite zone due in part to uncertainties in the recognition of Lower Bajocian ammonite zones in several sections, including those studied herein. In Winterborne Kingston there is an abrupt positive shift in the uppermost *H. discites* zone before values then fluctuate around a stable baseline of ~ –26‰. However, the positive shift at ~921 m corresponds to a facies change from oolitic to glauconitic limestone, indicating that stratigraphic condensation from slow sedimentation rate may have exaggerated the rapidity of this shift. The most positive values recorded in the B404/2 succession occur around the *S. propinquans* zone but, as discussed above; this part of the curve may have

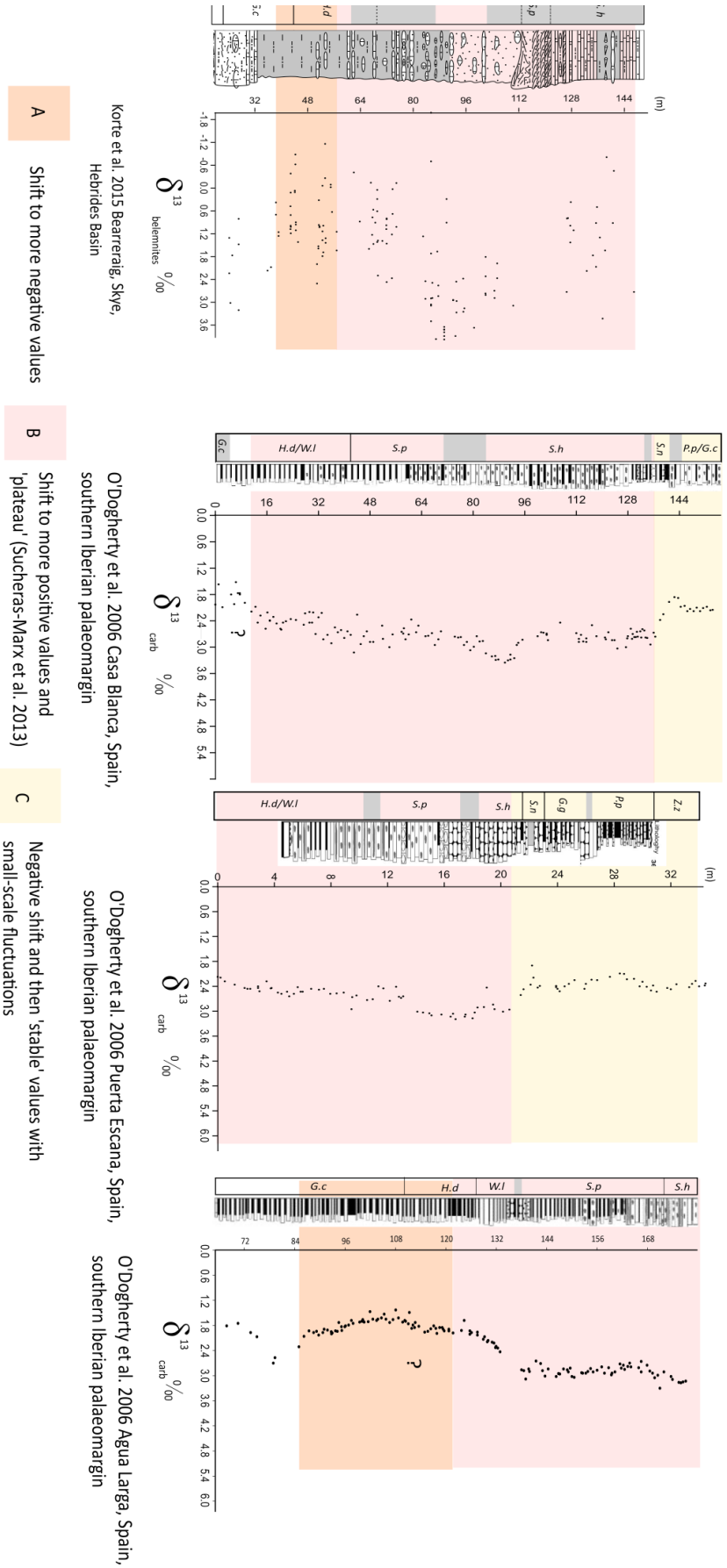

Figure 7.3b. Correlation of the $\delta^{13}C$ record to the the Isle of Skye, Scotland, and the Upper Aalenian to Lower Bathonian of southern Spain. Caption on p. 162.

Figure 7.3b. (p. 161). Correlation of the $\delta^{13}C$ record to the Upper Aalenian to Lower Bajocian of the Isle of Skye, Scotland, and the Upper Aalenian to Lower Bathonian of southern Spain.
Zone abbreviations: Upper Aalenian: *G.c= G. concavum*. Lower Bajocian: *H. d.= H. discites, W. l.= W. laeviuscula, S. p.= S. propinquans, S. h.= S. humphriesianum.* Upper Bajocian: S*. n.= S. niortense, G.g.= G. garantiana, P. p.= P. parkinsoni*, Lower Bathonian: *Z. z.= Z. zigzag*.
Logs modified from Korte et al. (2015; Skye) and O'Dogherty et al. (2006; Spain), $\delta^{13}C$ curves plotted from raw data from Korte et al. (2015) and O'Dogherty et al. (2006).

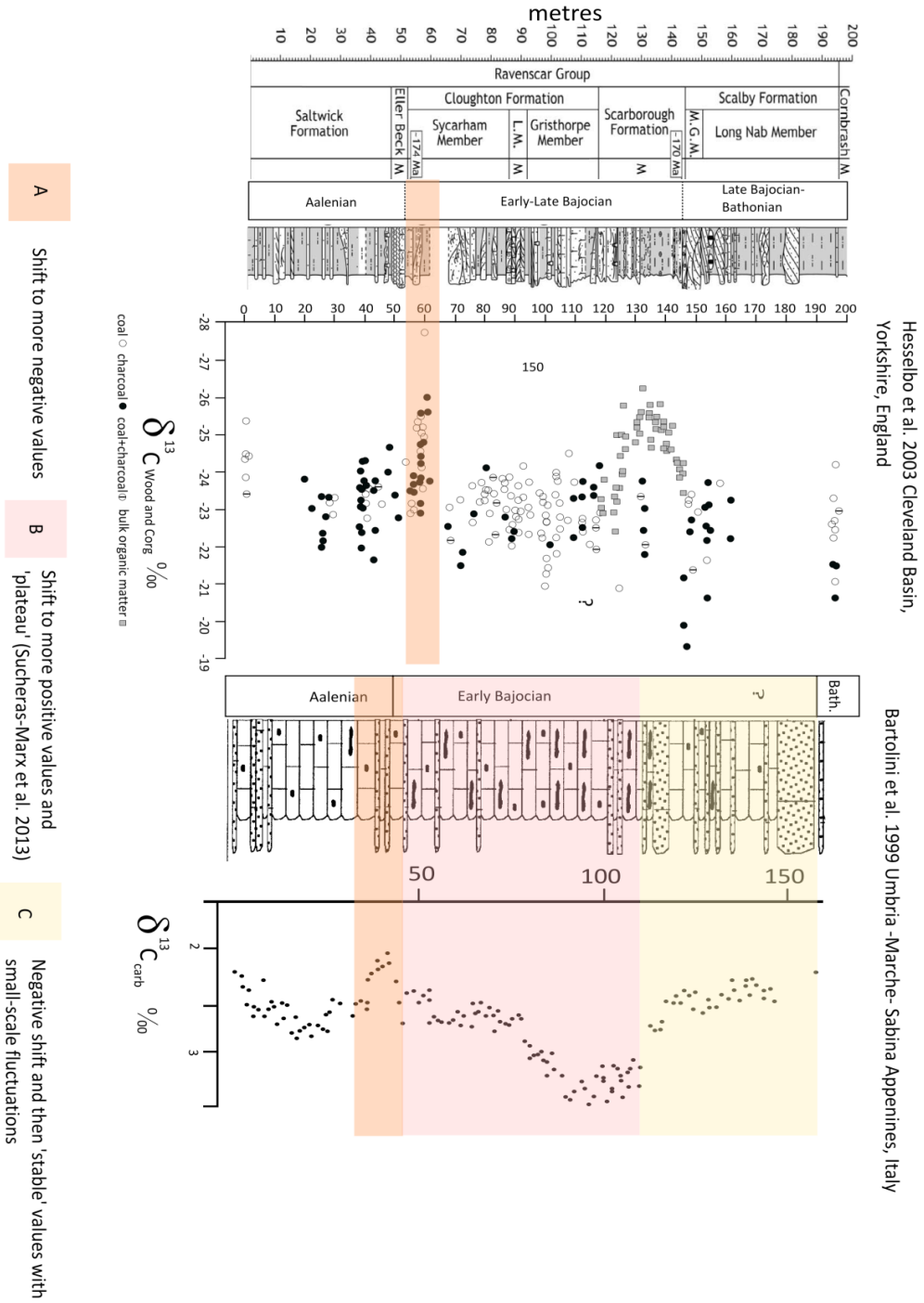

Figure 7.3c. Correlation of the $\delta^{13}C$ record to the Upper Aalenian to Bajocian of Yorkshire, England, and Umbria, Italy.
Redrawn from Hesselbo et al. (2003) (Yorkshire) and Bartolini et al. (1999) (Italy).

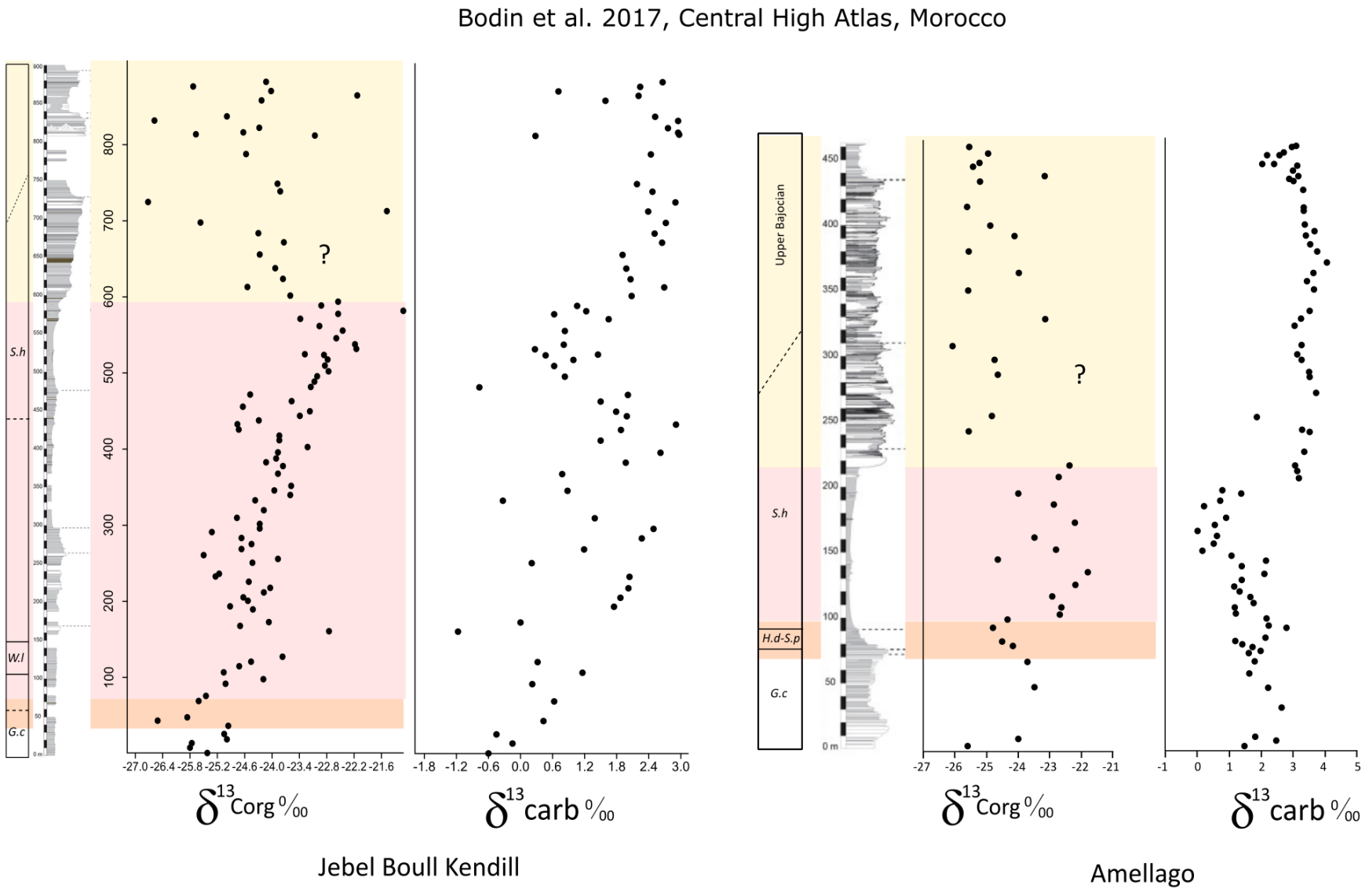

Figure 7.3d. Correlation of the $\delta^{13}C$ record to the Upper Aalenian to Upper Bajocian of Morocco.
Caption on p. 164.

Figure 7.3d. (p. 163). Correlation of the $\delta^{13}C$ record to the Upper Aalenian to Upper Bajocian of Morocco. Zone abbreviations: Upper Aalenian: *G.c= G. concavum*, Lower Bajocian: *H. d.= H. discites, W. l.= W. laeviuscula, S. p.= S. propinquans, S. h.= S. humphriesianum*. Logs after Bodin et al. (2017), $\delta^{13}C$ plotted from Bodin et al. (2017) raw data.

been influenced by the input of TOM. The general trend across Europe is a shift to more positive $\delta^{13}C$ values at around the *W. laeviuscula* zone with the most positive $\delta^{13}C$ values reached in the *S. propinquans* to *S. humphriesianum* zones (Figure 7.3a,b,c,d). The overall amplitude of the Lower Bajocian positive CIE appears to be around 1‰ in sections based on bulk carbonate and carbonate macrofossils. The amplitude is 3‰ in records based on bulk organic matter but this is probably due to the influence of a mixed source of organic carbon.

There have been few sections studied with ammonite zonal control that include the Upper Bajocian, but there is a close correlation between the Southern Iberian Palaeomargin and the pattern seen in B404/2. The decline to more negative $\delta^{13}C$ values occurs fairly synchronously towards the top of the *S. humphriesianum* zone and into the S. *niortense* zone (Figure 7a, b). In Winterborne Kingston the negative shift occurs around the same interval, but the *S. humphriesianum* and *S. niortense* zones are extremely condensed and only one subzone from each zone can be recognised (Chapter 4). Consequently the magnitude and rapidity of this negative shift may be exaggerated in Winterborne Kingston, but is broadly correlative with the southern Iberian Palaeomargin.

7.4.4. Extent of Aalenian–Bathonian carbon cycle perturbations

Hesselbo et al. (2003) demonstrated that the negative CIE occurs in fossil wood, and correlation to marine carbonates and organic matter indicates that this carbon-cycle perturbation was driven by changes in the $\delta^{13}C$ of both atmospheric CO_2, and the upper ocean DIC pool during the Late Aalenian to Early Bajocian. Although the fossil wood records of these authors study define a somewhat tenuous trend to more positive $\delta^{13}C$ values in the Lower Bajocian (Figure 3b), the positive CIE cannot be confidently recognised, making it unclear if this excursion affected the whole carbon cycle. However, the record of this positive CIE in marine carbonates and organic matter clearly indicates there were changes in the $\delta^{13}C$ of the DIC pool of the upper ocean during the Early Bajocian. Both excursions have been recorded throughout the sub-Boreal and Tethyan realms, but there are currently no $\delta^{13}C$ studies of Bajocian sections outside of Europe/North Africa, so further work is needed to assess the global extent of these carbon cycle perturbations.

7.5. Drivers behind Bajocian carbon cycle perturbations

7.5.1. Aalenian–Bajocian negative CIE

The record of the negative CIE through the Aalenian–Bajocian transiton in marine carbonates, bulk organic matter, and fossil wood indicates that this excursion reflects changes in the $\delta^{13}C$ composition of the atmosphere, and as such was likely a global event (Hesselbo et al., 2003; O'Dogherty et al., 2006). Hesselbo et al. (2003) noted that in the Cleveland Basin of Yorkshire, England, the negative CIE around

Aalenian-Bajocian boundary is coincident with an increase in plant-leaf stomatal density. These authors suggested volcanic outgassing may have driven the negative CIE, with an associated increase in pCO_2, as the Aalenian to Bajocian was marked by the birth of the Pacific Plate, subduction-related volcanism in the Pacific, and a major pulse of seafloor spreading in the Alpine Tethys (Bartolini and Larson, 2001; Bill et al., 2001). Notably however, there is little evidence from recent oxygen isotope work of warming sea surface temperatures around the Aalenian–Bajocian transition (Korte et al., 2015). This suggests that if volcanic outgassing did drive this excursion, it was not significant enough to strongly influence climate.

7.5.2. Early Bajocian positive CIE

Positive shifts in $\delta^{13}C$ can be driven by the sequestration of organic matter at the seafloor, which leaves the remaining upper water column DIC pool relatively depleted in ^{12}C. As such, for much of the Jurassic, positive CIEs were coincident with times of widespread black-shale deposition (Jenkyns et al., 2002). The Early Bajocian event is unusual in this sense as no widespread organic-rich sediments are known (Jenkyns et al., 2002; Korte et al., 2015). However, numerous authors have argued that an increase in bioproductivity from radiolarians and coccolithophores drove the Early Bajocian $\delta^{13}C$ shift (Bartolini and Cecca, 1999; Bartolini et al., 1999; Suchéras-Marx et al., 2015; Giraud et al., 2016; Aguado et al., 2017). Bartolini and Cecca (1999) noted that the Early Bajocian positive CIE was coincident with a collapse in carbonate production and the onset of biosiliceous sedimentation in the Umbria Basin of Italy, which these authors interpreted to reflect a phase of eutrophication and enhanced productivity. On the southern Iberian palaeomargin, the positive CIE is also associated with an increase in biosiliceous sediments (Figure 7.4; Aguado et al., 2017). In Morocco, the positive CIE is associated with the collapse of carbonate production and increased silicilastic deposition in the High Atlas of Morocco (Bodin et al., 2017). In the French Sub-Alpine Basin, the Lusitanian Basin of Portugal, and southern Iberian palaeomargin, the positive CIE is coincident with a major floral turnover in coccoliths, which was driven by the emergence and ecological dominance of the genus *Watznaueria* (Figures 7.4, 7.5) This genus has been interpreted as blooming in response to elevated nutrient levels during the Early Bajocian (Suchéras-Marx et al., 2015; Giraud et al., 2016; Aguado et al., 2017). Moreover, the emergence of *Watznaueria* was associated with a significant increase in the flux of coccoliths as a whole to the seafloor during the Early Bajocian (Figure 7.5; Suchéras-Marx et al., 2012). Consequently, an increase in nutrient levels and associated productivity may have driven the Early Bajocian positive CIE (Suchéras-Marx et al., 2015; Giraud et al., 2016; Aguado et al., 2017).

There are two scenarios for this increase in nutrient levels in Europe during the Early Bajocian, which were reviewed by Suchéras-Marx et al. (2015), and recently by Aguado et al. (2017). The first hypothesis is a switch to a more humid climate in the mid-palaeolatitudes during the Early Bajocian from an enhanced latitudinal temperature gradient, which lead to increased continental weathering and nutrient flux. Although the Aalenian to Bathonian was a largely cool interval of Jurassic climate, oxygen isotopes

record a shift to warmer temperatures in the *S. humphriesianum* zone of the Early Bajocian in Europe, indicating an increase in latitudinal temperature gradient between the mid and high palaeolatitudes (Figure 7.6; Suchéras-Marx et al., 2015; Korte et al., 2015). A humid climate mode in Europe during the Early Bajocian is evidenced by the switch from charcoal to coal as the dominant preservational mode of fossil wood through the Upper Aalenian to Lower Bajocian of the Cleveland Basin of Yorkshire (Hesselbo et al., 2003). Changes in clay mineral assemblages may also be indicative of a warm, humid climate. Brigaud et al. (2009) noted that clay mineral assemblages from the *S. humphrieisianum* zone of the Paris Basin contain around 20% kaolinite. In modern environments kaolinite forms in warm, humid, tropical climates from intense chemical weathering which lead Brigaud et al. (2009) to argue that there was a change to a more a warmer, more humid climate during the Early Bajocian. Rausik et al. (2001) and Raucsik and Varga (2008) documented clay mineral assemblages dominated by mixed-layer illite/smectite from the Lower Bajocian of the Mecsek mountains of Hungary. Mixed-layer illite/smectite clays form in modern environments of warm, arid conditions punctuated by short, intense wet seasons; therefore, Raucsik and Varga argued the climate of the Early Bajocian in Europe was monsoon like. Taken together, Sucheras-Marx et al. (2015) and Aguado et al. (2017) argued that these lines of geochemical, palaeontological, and mineralogical evidence are indicative of a warm, humid climate during the Early Bajocian, which enhanced chemical weathering and increased the flux of biolimiting nutrients into the European epicontinental seaway. Moreover, Phillipe et al. (2017) reported the northward spread of the low-latitude fossil wood genus *Brachyoxylon* during the Early Bajocian, which may be indicative of a warming and/or an increase in humidity in the mid-latitudes. Furthermore, O'Dogherty et al. (2006) argued that the enhanced pCO_2 levels associated with the Aalenian–Bajocian negative CIE drove the increase in weathering and nutrient flux during the Early Bajocian through climatic warming. However, evidence of warming directly associated with this excursion is lacking.

The alternative scenario is an increase in surface water productivity driven by enhanced upwelling during the Early Bajocian. Dera et al. (2014) reported a marked positive shift in neodymium isotopes during the Aalenian–Bathonian, which these authors suggested may have been forced by a stronger influence of radiogenic Tethyan waters in the European epicontinental seaway. In turn, the incursion of Tethyan waters may have been driven by thermal doming in the North Sea, which restricted the southward flow of Boreal waters through the Viking Corridor, combined with widening and deepening of the Hispanic Corridor (Dera et al. 2014 and references therein). Dera et al. (2014) suggested that on the basis of previous general circulation modelling studies, this widening and deepening may have promoted upwelling along the outer region of the European epicontinental seaway. Consequently, enhanced upwelling may have brought nutrient-rich waters into the photic zone and driven an increase in productivity.

Although these hypotheses are not mutually exclusive, both are to an extent problematic. The marked positive shift in Nd isotopes recorded by Dera et al. (2014) began in the Aalenian, with maximum values

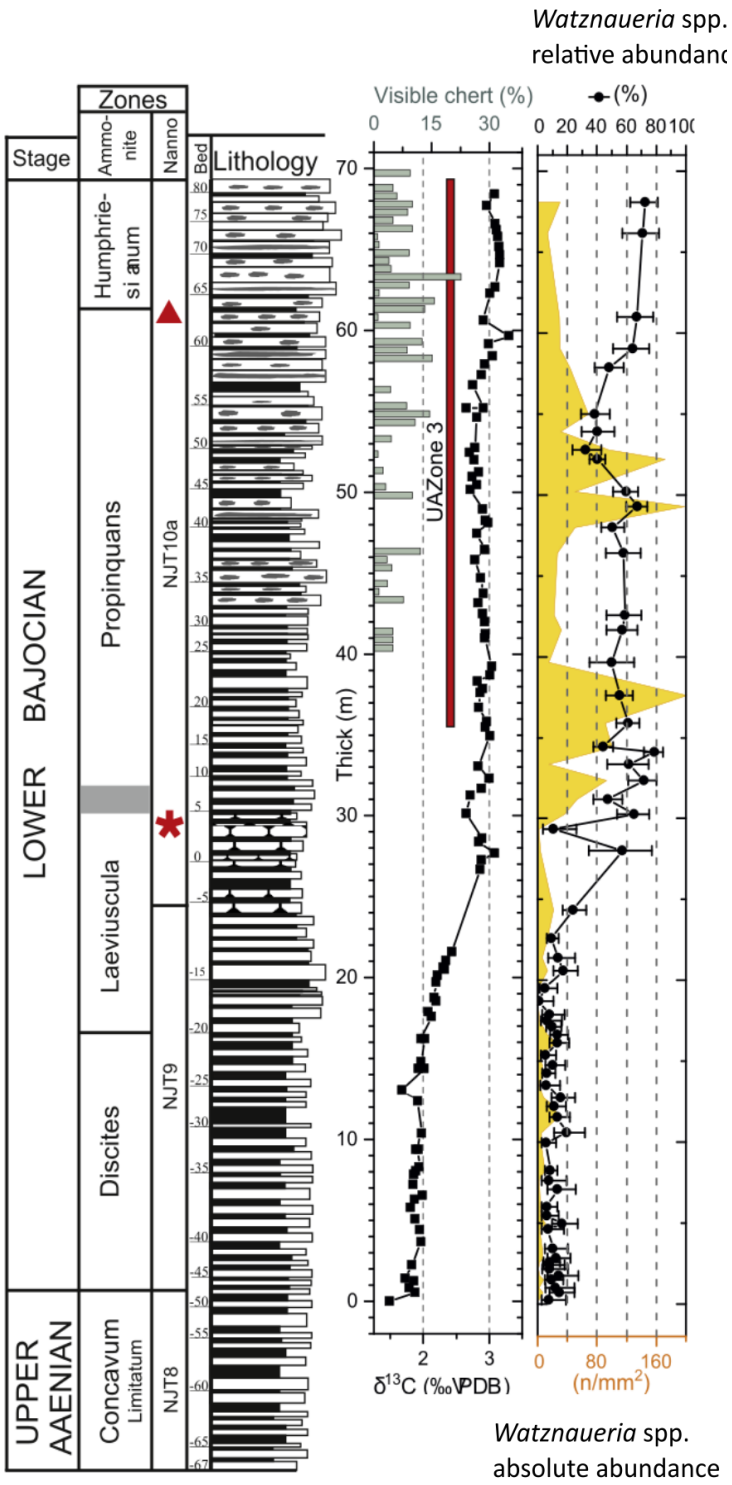

Figure 7.4. $\delta^{13}C$ and calcareous nannofossil records for the Upper Aalenian to Lower Bajocian of southern Spain. Note the increase in the absolute abundance of *Watznaueria* spp. (yellow fill) as well as the significant increase in relative abundance (black line). Also note the increase in the abundance of visible chert with the shift to more positive $\delta^{13}C$ values. Modified from Aguado et al. (2017) fig. 2.

around the Bajocian–Bathonian boundary, rather than in the Early Bajocian. Recently, Aguado et al. (2017) argued that decline in deep-dwelling calcareous nannofossil taxa through the Early Bajocian indicates a shallowing of the nutricline, which is more consistent with nutrient input from enhanced surface run-off rather than nutrients delivered from upwelling deep waters. However, the weathering hypothesis is also problematic; the negative oxygen isotope shift, and thus warmer temperatures, occurred around the *S. humphriesianum* zone. However, the shift to more positive carbon isotope values occurred during the *W. laeviuscula* zone in most sections, during an interval of positive oxygen isotope values, and thus cool

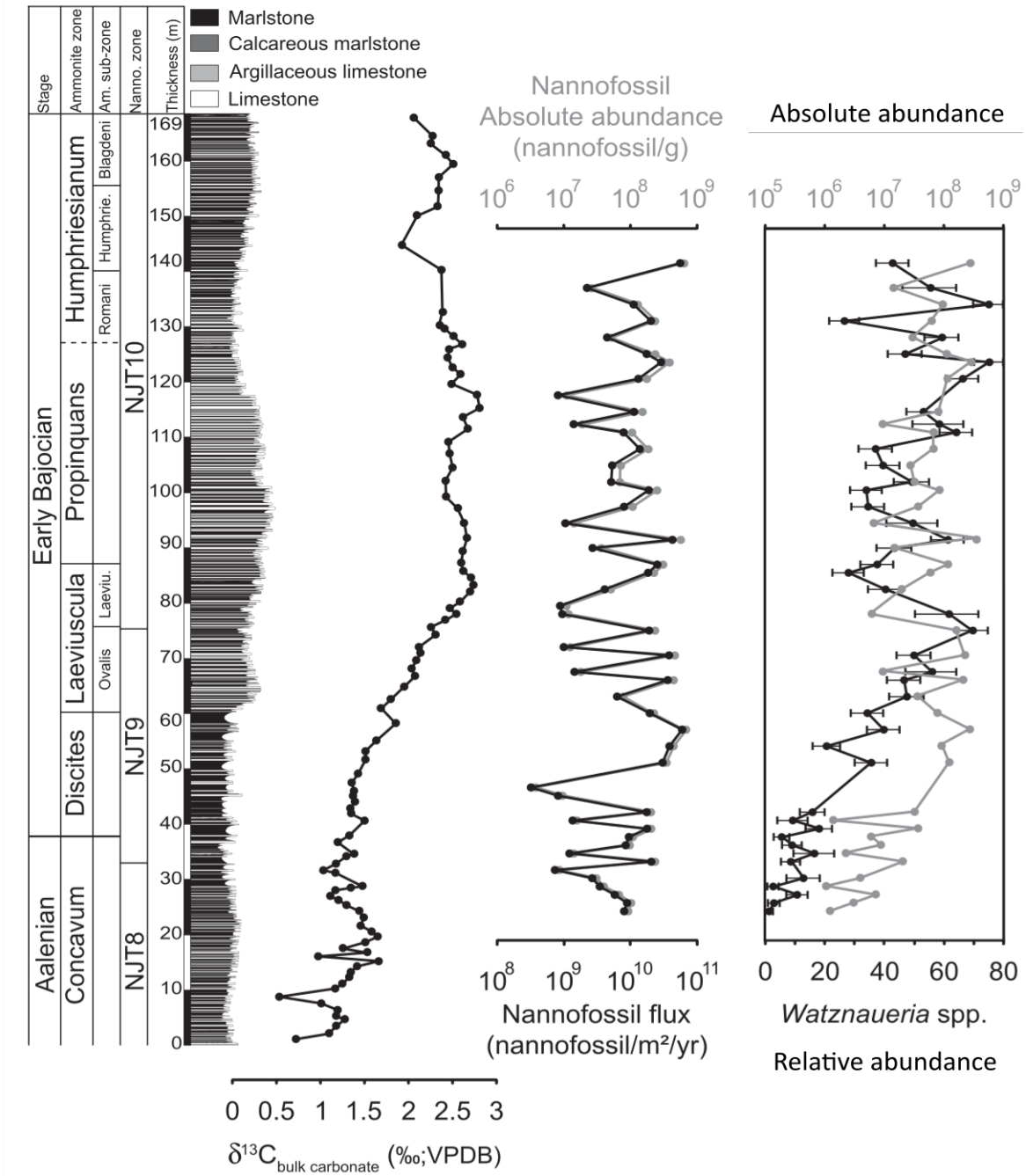

Figure 7.5. $\delta^{13}C$ and calcareous nannofossil records for the Upper Aalenian to Lower Bajocian of the French sub-Alpine Basin.
Note the relative and absolute abundance increase of *Watznaueria* spp. from the *G. concavum* zone to the *S. humphriesianum* zone, which mirrors in $\delta^{13}C$ increase. Modified from Suchéras-Marx et al. (2015; fig. 4).

temperatures. Consequently, this increase in productivity does not appear to be completely synchronous with warming temperatures, although the peak $\delta^{13}C$ values are recorded in the *S. humphriesianum* zone in several sections, coincident with the brief interval of warming. Moreover, the clay mineral assemblages from the Paris Basin and Hungary present somewhat conflicting evidence; the abundance of kaolinite in the Paris basin indicates a warm, tropical, humid climate, whilst the occurrence of mixed-layer illite/

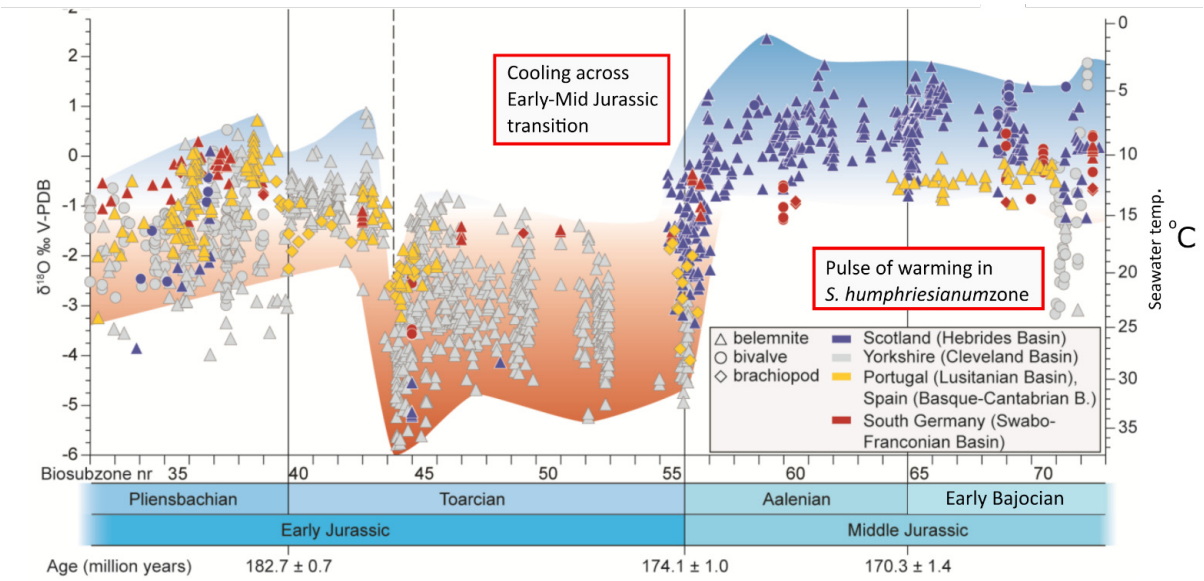

Figure 7.6. Seawater palaeotemperatures for the Early Jurassic to Early Bajocian.
Note the cooling through the Early–Mid Jurassic transition, and the brief interval of warming in the Bajocian, which corresponds to the *S. humphriesianum* zone. Modified from Korte et al. (2015, fig. 2).

smectite in Hungary indicates a monsoon-like climate, with a long dry season and short intense wet season. There is also little evidence of enhanced continental weathering in the strontium isotope record as $^{87}Sr/^{86}Sr$ isotopes show a major decline through the Bajocian (Figure 7.7; Jenkyns et al., 2002). This decline was likely driven by increased mid-ocean ridge activity in the proto-Pacific and Alpine Tethys (section 7.5.1), set within the wider tectonic context of the breakup of Pangaea. Therefore, it is possible that the input of mantle-derived ^{86}Sr may have out-weighed that of continentally-derived ^{87}Sr, even if there was a high flux of ^{87}Sr from continental weathering and run-off.

In my opinion, the Early Bajocian interval of palaeoenvironmental change remains to be fully resolved. The geochemical record of the Bajocian has been largely understudied for isotope systems other than oxygen and carbon, and in particular, there are no high-resolution strontium or osmium isotope records. On the basis of the current evidence however, it seems more likely that a switch to a more humid climate and associated increase in continental weathering drove an increase in nutrient levels during the Early Bajocian. Moreover, palaeoecological patterns seen within the Early Bajocian dinoflagellate cyst record may be consistent with enhanced weathering and continental run off (Chapter 8, section 8.5.4.)

7.5. Summary

Analysis of the $\delta^{13}C$-org record of the Wessex and Swabian basins demonstrates a negative CIE around the Aalenian-Bajocian boundary and a positive CIE in the Early Bajocian. The record from the Winterborne Kingston Borehole does not appear to have been strongly influenced by organic carbon source, whilst parts of the B404/2 record in the Lower Bajocian have been strongly influenced by changing proportions of marine and terrestrial organic matter. The $\delta^{13}C$ record is therefore a mixed signal of organic matter source and upper water column DIC composition. These CIEs can be correlated throughout Europe,

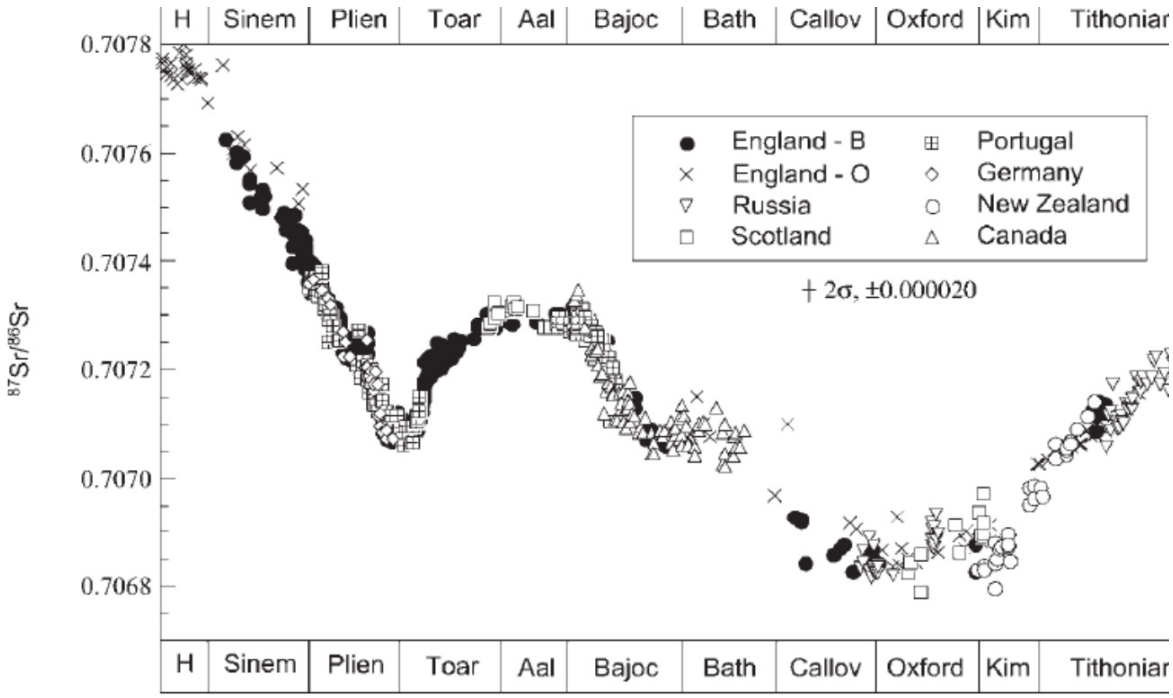

Figure 7.7. 87Sr/86Sr isotopes through the Jurassic.
Note the sharp decline in values through the Bajocian to Bathonian. Modified from Jenkyns et al. (2002) fig. 11.

from sub-Boreal to Tethyan realms. The negative $\delta^{13}C$ excursion has an amplitude of around 0.5‰ and appears to have affected the entire ocean-atmosphere system as it has been recorded from fossil wood, marine carbonates and organic matter. Therefore, there was a negative shift in the $\delta^{13}C$ composition of atmospheric CO_2 during the Late Aalenian to Early Bajocian. In contrast, the positive $\delta^{13}C$ excursion has an amplitude of 1–2 ‰ and has only been convincingly recorded from marine carbonates and marine organic matter, making it unclear if this excursion affected the whole ocean-atmosphere system or the upper ocean DIC pool. The negative CIE has been hypothesised to have been driven by volcanic activity associated with the breakup of Pangaea (Hesselbo et al., 2003), whilst the positive CIE has been related to a phase of eutrophication and high productivity in the western Tethys. In turn, an increase in nutrient levels may have been driven by a switch to a warmer, more humid climate, which increased continental weathering and the flux of biolimiting nutrients in the mid-latitudes. In Chapter 8, the patterns seen within the Early Bajocian dinoflagellate cyst record are related to this interval of palaeoenvironmental change.

Chapter 8. Resolving the pattern of the Mid Jurassic dinoflagellate radiation

8.1. Introduction

The data I documented in chapters 3 to 5 demonstrate an increase in the richness of gonyaulacacean dinoflagellate cysts through the Bajocian in the Swabian, Wessex, and Paris Basins. However, does this pattern portray a true evolutionary radiation of gonyaulacacean dinoflagellates, or simply reflect an increase in the proportion of encysting forms? Furthermore, palynological and sedimentological data from the basins I have studied record shifts in lithostratigraphic composition and palaeoenvironment that were related to sea level change in the Bajocian, indicating that fluctuations in sea level, and their expression in the sedimentological and stratigraphic record, may have influenced the pattern of dinoflagellate cyst appearances. Moreover, the dinoflagellate cyst assemblages I have documented from the Swabian, Wessex, and Paris basins record temporal and spatial changes in the relative abundances of dinoflagellate cyst taxa, which were driven by palaeoenvironmental conditions. In this chapter, I examine whether the Bajocian radiation was a true evolutionary event. To constrain the pattern of Bajocian diversification, I have compared the stratigraphic pattern from the areas I studied to sequence stratigraphic records; in turn, these have been compared to the rest of northwest Europe. Additionally, records from several other regions have been examined to assess the global extent of the Bajocian radiation. These data have been assessed within the context of wider Mid Jurassic palaeoceanographic and palaeoclimatic changes. I have used the palaeoenvironmental distribution of key dinoflagellate cyst taxa to make inferences about their palaeoecological preferences, which have been related to wider palaeoenvironmental change during the Mid Jurassic, particularly that of the Early Bajocian (Chapter 7). Finally, I summarise the findings of this thesis, and make some final remarks regarding the underlying causal mechanism of the Bajocian diversification.

8.2. The Bajocian dinoflagellate cyst record as an indicator of dinoflagellate richness: a real radiation?

The fossil record of dinoflagellates is represented by their—predominantly organic-walled—resting cysts. Only 13–16% of modern dinoflagellate species produce resting cysts, and it is not known whether this has changed through geological time (Head, 1996; Fensome et al., 1996). Cyst formation in dinoflagellates is most viable up to water depths of ~200 m, and consequently most modern encysting dinoflagellates are neritic (Wall et al., 1977; Dale and Dale, 1992; Fensome et al., 1996). As such, changes in dinoflagellate cyst richness may simply reflect changes in the proportion of encysting neritic dinoflagellates. The dinoflagellate fossil record is further complicated as it is reconstructed from morphologically-defined cyst taxa, which are a phenotypic expression of only one stage of the dinoflagellate lifecycle. Even within fossil forms that have a largely reflected tabulation, differences in morphology, such as processes length or shape, which may be considered a species-level character in fossil taxa, may be seen as intraspecific variation in Recent taxa, particularly that arising from ecophenotypic variation (Ellegaard et al., 2002;

Mertens et al., 2009a). With Quaternary taxa, cysts can be related to the motile stage and variations in morphology which arise from ecophenotypic variation are readily recognised (e.g. Ellegaard et al., 2002; Zonneveld and Susek, 2007; Mertens et al., 2009a). However, with a lack of extant representatives, the recognition of ecophenomorphs in Mid Jurassic taxa is inherently problematic, and may call into the question the reliability of the cyst record as a proxy for dinoflagellate species richness.

On a broad scale, the radiation of dinoflagellates through the early Mesozoic was characterised by the appearance of distinct tabulation types, such as suessoid, gonyaulacoid-peridinioid, and nannoceratopsoid (Fensome et. al., 1996). Moreover, tabulation-based groups such as the Gonyaulacales and Peridiniales are supported by molecular data as distinct clades (Janouškovec et al., 2017). The appearance of distinct clades, such as the Gonyaulacales and Peridiniales, as indicated by the emergence of these tabulation types, is strongly indicative of true evolutionary radiation of dinoflagellates through the Early Mesozoic (Fensome et al., 1996; Janouškovec et al., 2017). Moreover, the appearance and diversification of higher-level taxa was accompanied by a significant increase in the abundance of dinosteranes in Mesozoic sedimentary rocks (Moldowan et al., 1996). Although recent molecular analysis indicates that dinosteranes were only acquired by dinoflagellates in the Mesozoic, the concomitant increase in dinoflagellate richness and dinosterane abundance strongly suggests that dinoflagellates rose to ecological prominence through the Jurassic and Cretaceous (Janouškovec et al., 2017). However, the Bajocian is characterised by an increase in the richness of dinoflagellate cysts within one family, the Gonyaulaceae, and as such, this increase in richness may simply reflect an increase in the proportion of cyst-forming gonyaulacacean dinoflagellates.

Prior to the Bajocian, gonyaulacaceans were represented by *Batiacasphaera*, *Dissiliodinium, Kallosphaeridum* and *Sentusidinium* (Feist-Burkhardt and Pross, 2010; Feist-Burkhardt and Wille, 1992). These genera are characterised by simple, (largely) non-tabulated morphology. *Batiacasphaera*, *Kallosphaeridium* and *Sentusidinium* have apical archaeopyles whilst *Dissiliodinium* has a multi-plate precingular archaeopyle (Figure 8.1; Chapter 7). Through the Bajocian ~15 gonyaulacacean genera appeared, which exhibit a wide array of morphologies (Figure 8.1). The Early Bajocian was marked by the appearances of the first gonyaulacaceans with (more-or-less) fully reflected tabulation, such as *Durotrigia daveyi* (e.g. Chapter 4, section 4.4.2.). Morphological features such as cavation (the separation of wall layers) appeared within the Gonyaulacacae, as represented by the appearances of the genera *Cavatodissiliodinium* and *Endoscrinium* (e.g. Chapter 3, section 3.3.2.3.). Moreover, gonyaulacaceans developed ornamental features such as distally complex processes (e.g. *Ctenidodinium combazii*) and prominent sutural crests (e.g. *Meiorogonyaulax valensii*, Chapter 6, Plates II, IX). These morphological features were accompanied by an increase in the number of archaeopyle types; over the course of the Bajocian, genera with two-plate precingular, one-plate precingular, and epicystal archaeopyle-types appeared. While both fossil and Recent dinoflagellate cyst taxa can exhibit intraspecific variability within archaeopyle formation (e.g. Evitt, 1985; Harding, 1986; Ellegaard et al., 2002), the one-plate precingular

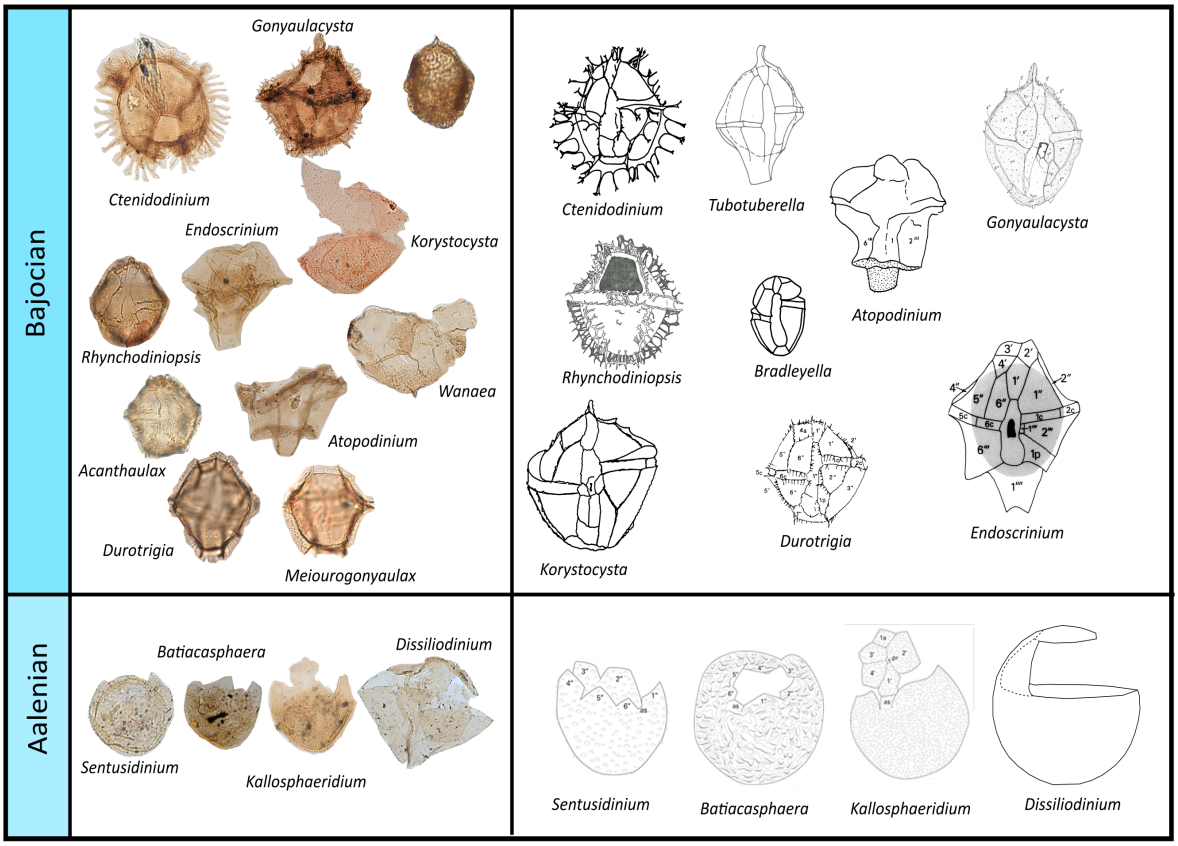

Figure 8.1. Richness and morphological variability of gonyaulacacean dinoflagellate cysts, Aalenian–Bajocian.
It can clearly be observed that Bajocian gonyaulacacean dinoflagellate cysts exhibit greater disparity than those of the Aalenian. Line drawings: *Ctenidodinium, Korystocysta*, and *Bradleyella* from Wollam (1983). Gonyaulacysta from Fensome (1979). *Atopodinium* from Beju (1983). *Tubotuberalla* from Jan du Chêne et al. (1986). *Durotrigia* from (Bailey, 1987). *Endoscrinium* from Riding (1987). *Rhynchodiniopsis* from Gocht (1970). *Batiacasphaera, Sentusidinium,* and *Kallosphaeridium* from Wood et al. (2016). *Dissiliodinium* redrawn from Feist-Burkhardt (1990).

archaeopyle appears to have been developed with the Gonyaulacacae during the Bajocian, which has remained a primary excystment strategy in gonyaulacaceans to the Recent (Feist-Burkhardt and Götz, 2016). Therefore, the increase in richness of gonyaulacacean dinoflagellate cysts through the Bajocian was accompanied by morphological innovations in archaeopyle formation, and a rapid increase in disparity. From a wider perspective, there was a major ecological transition in coccolithophores during the Early Bajocian, and the Late Bajocian was marked by the appearance of the first (mero)planktonic foraminifera, indicating that major evolutionary innovations occurred in the plankton as a whole (Chapter 1; Hart et al., 2003; Suchéras-Marx et al., 2015). The increase in the richness of gonyaulacacean dinoflagellate cysts, coupled with morphological innovations and parallel radiations of other planktonic groups, strongly suggests that the gonyaulacacean dinoflagellates underwent a true evolutionary radiation. Moreover, the richness of gonyaulacacean dinoflagellate cysts increased continuously throughout the remainder of the Jurassic (Figure 1.1), indicating that the Bajocian marks a critical interval in the evolutionary history of this group.

8.3. Constraining the stratigraphic pattern of the Bajocian dinoflagellate cyst radiation in northwest Europe

8.3.1. Swabian, Wessex and Paris basins

There is an increase in dinoflagellate cyst richness through the Bajocian of the Swabian, Wessex, and Paris basins irrespective of differences in lithostratigraphic composition, sampling frequency, palaeoenvironment, or preservation. However, fluctuations in sea level through the Bajocian have driven changes in both stratigraphic composition and palaeoenvironment through these depocentres.

The broad correlation between dinoflagellate cyst richness and sea level during the Mesozoic–Cenozoic has long been recognised (e.g. MacRae et al., 1996; van de Schootbrugge et al., 2005). Comparison of the stratigraphic data from the Swabian, Wessex, and Paris basins to sequence stratigraphic records suggests that the increase in gonyaulacacean dinoflagellate cyst richness is broadly correlated with sea level rise (Figure 8.2). In the Swabian Basin, the gradual increase in dinoflagellate cyst richness through the Bajocian largely mirrors the transgressive trend of cycle T7. However, many first appearances of gonyaulacaceans are recorded from the *S. humphriesianum* zone upwards, which corresponds to the pronounced transgressive pulse of third-order cycle BJ2, and the Late Bajocian rise in sea level (figures 8.2, 3.9). On a finer scale, appearances and richness both peak around third-order transgressive deposits and maximum flooding surfaces (Figure 8.2; Table 3.2a, 3.2b). In the Wessex Basin, the transgressive deposition of the Upper Bajocian has strongly impinged on the stratigraphic signal, as there is a significant increase in richness above the transgressive surface of the Vesulian Unconformity, which is coincident with third-order sequence boundary Bj4 (Figure 8.2; Chapter 4). Although a complete record could not be generated through the Paris Basin, the higher richness of the Upper Bajocian–Lower Bathonian *versus* the Lower Bajocian broadly mirrors the transgressive trend through this region (Figure 8.2; Chapter 5). Further, the high richness dinoflagellate cyst assemblages of the *P. parkinsoni* to *Z. zigzag* zones is correlated with the third-order transgressive-regressive cycle, which represents maximum flooding of the T7 transgression (Figure 8.2; Chapter 5). Moreover, the bursts of appearances recorded by Feist-Burkhardt and Monteil (1997) from the *S. humphriesianum* and *S. niortense* zones correspond to the third-order transgressive pulses (Figure 8.2; Chapter 5).

Figure 8.2. (p.175). Correlation of third-order sequences through the successions studied for this thesis, with number of dinoflagellate cyst taxa per sample.
In the Swabian basin, the increase in gonyaulacacean richness broadly mirrors the transgressive trend of the T7 cycle. Peaks in richness can be observed from condensed transgressive deposits such as the Subfurcaten and Parkinsoni Oolith members. In the Paris Basin, the high richness observed from the Upper Bajocian *P. parkinsoni* zone corresponds to third-order cycle Bj5, which represents the maximum flooding of the T7 transgression. In the Wessex Basin, there is a significant increase in richness above the Vesulian Unconformity, which corresponds to sequence boundary Bj4, and is coincident with the transgressive surface. Within lithostratigraphic units, grey fill denotes argillaceous units, brown fill denotes condensed ferruginous oolitic limestones/mudstones. Within the richness curves, grey fill denotes gonyaulacacean taxa, black denotes other taxa. Cross hatching in the Wessex Basin successions denotes the fact that the *S. humphriesianum* and *S. niortense* zones are prerpresented by only a single sample in both successions.

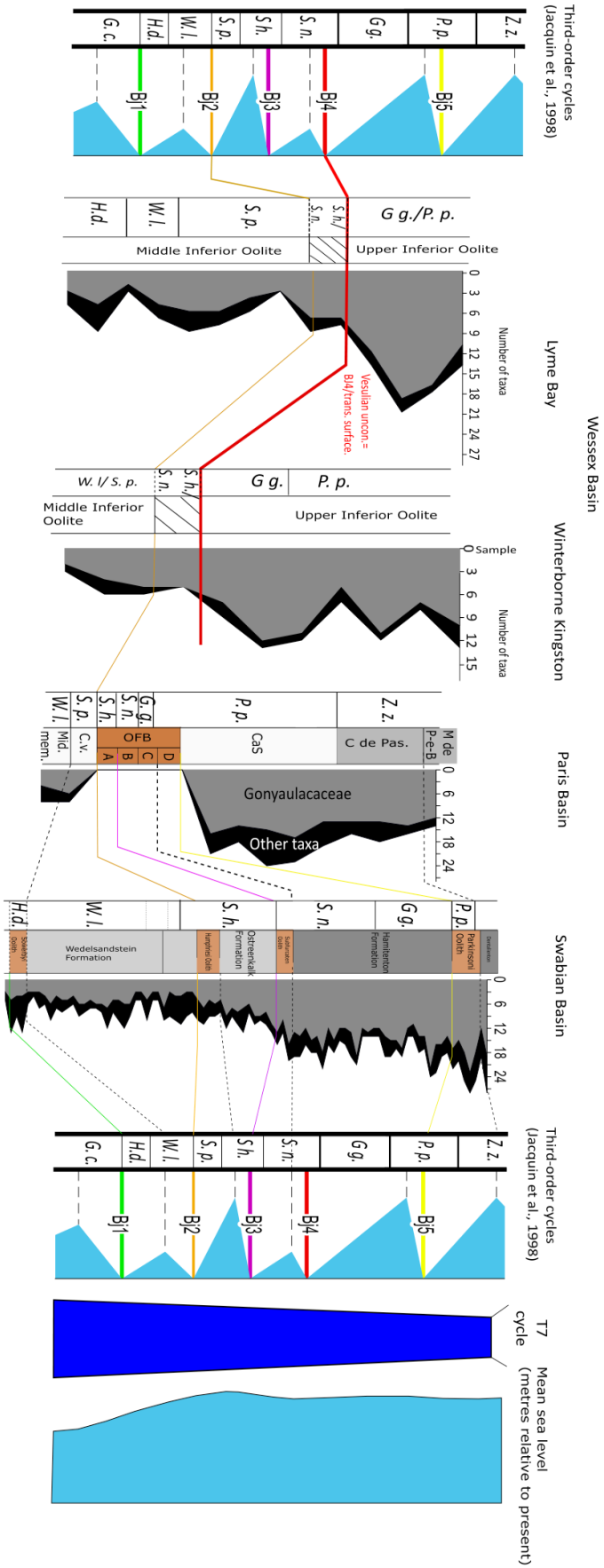

Figure 8.2. Correlation of third-order sequences through the successions studied for this thesis, with number of dinoflagellate cyst taxa per sample. Caption on p. 174.

Fluctuations in sea level also drove changes in palaeoenvironment. In the Swabian Basin, palynological and sedimentological data document a shift from a more proximal (prodelta) palaeoenvironment, to an offshore palaeoenvironment through the Bajocian–Bathonian in the B404/2 succession, with peak marine:terrestrial ratios coinciding with maximum flooding of the T7 transgression in the Lower Bathonian (Chapter 3). Similarly, a broad shift from a more proximal palaeoenvironment to a more distal palaeoenvironment is observed from palynomorph assemblages from the Lower Bajocian *versus* Lower Bathonian of the Paris Basin, with peak marine:terrestrial ratios also coinciding with maximum flooding of the T7 cycle (Chapter 5). In both the Recent oceans and in deep time, dinoflagellate cysts exhibit trends in assemblage composition and richness along inshore-offshore transects, with an increase in richness in the offshore direction, peaking at the shelf-break (Wall et al., 1977; Sluijs et al., 2005). As such, the increase in dinoflagellate cyst richness through the Swabian and Paris basins may simply be tracking an ecological trend, driven by shifting palaeoenvironments. However, palynological and sedimentological data indicate there was no systematic shift in palaeoenvironment through the Bajocian in the Wessex Basin (Chapter 4). Although fluctuation in sea level drove changes in sedimentation and erosion, the depositional environment of the Inferior Oolite Group through the Bajocian underwent little systematic change, as it was a (distal) carbonate ramp throughout (Chapter 4; Sellwood et al., 1991).

Changes in the richness of marine fossils associated with sea level fluctuations have been attributed to the 'common cause' hypothesis, whereby rising sea level drives changes in richness through a two-fold effect of increasing marine ecospace, and the increased volume of fossiliferous sedimentary rocks (Butler et al., 2011; Smith and McGowan, 2011). As such, the increase in the richness of gonyaulacaceans through the Bajocian of these regions may have been driven by this effect. However, in the Swabian Basin, the underlying Aalenian is represented by thick (~150 m) successions of shallow marine rocks (Pienkowski et al., 2008; Feist-Burkhardt and Pross, 2010). In a detailed palynological study of the Aalenian of the Swabian Basin, Feist-Burkhardt and Pross (2010) documented rich (~50 species) dinoflagellate cyst floras. However, gonyaulacaceans are of low richness, and represented by the genera *Batiacasphaera*, *Dissiliodinium* and *Kallosphaeridium* (Feist-Burkhardt and Pross, 2010). Consequently, the increase in gonyaulacacean dinoflagellate cyst richness through the Aalenian to Bajocian of the Swabian Basin does not appear to have been driven by a taphonomic megabias. Moreover, in the Wessex Basin, high dinoflagellate cyst richness is recorded from Upper Bajocian strata, whilst the Lower Bajocian is of much lower richness (figures 4.13, 4.14, 4.15), in this region, the Upper Bajocian is no thicker, or more intensively sampled than the underlying Lower Bajocian. Moreover, the Wessex Basin does not document a significant shift in palaeoenvironment associated with the increase in dinoflagellate cyst richness through the Bajocian.

8.3.2. Regional comparison

The Swabian, Wessex and Paris basins record an increase in the richness of gonyaulacacean dinoflagellate through the Bajocian which appears to be correlated with the T7 second-order transgression. However,

these basins were all shallow marine regions, located around 30–35°N in the Sub-Boreal province of the European Epicontinental Seaway (Figure 8.3; Chapter 1). To what extent is this pattern seen to the north of these areas, in the paralic palaeoenvironments of the North Sea and surrounding basins (Figure 8.3)?

The Middle Jurassic of the North Sea is primarily represented by the Brent Group, which represents deltaic and marginal-marine palaeoenvironments (Williams, 1992). Due to the marginal nature of the

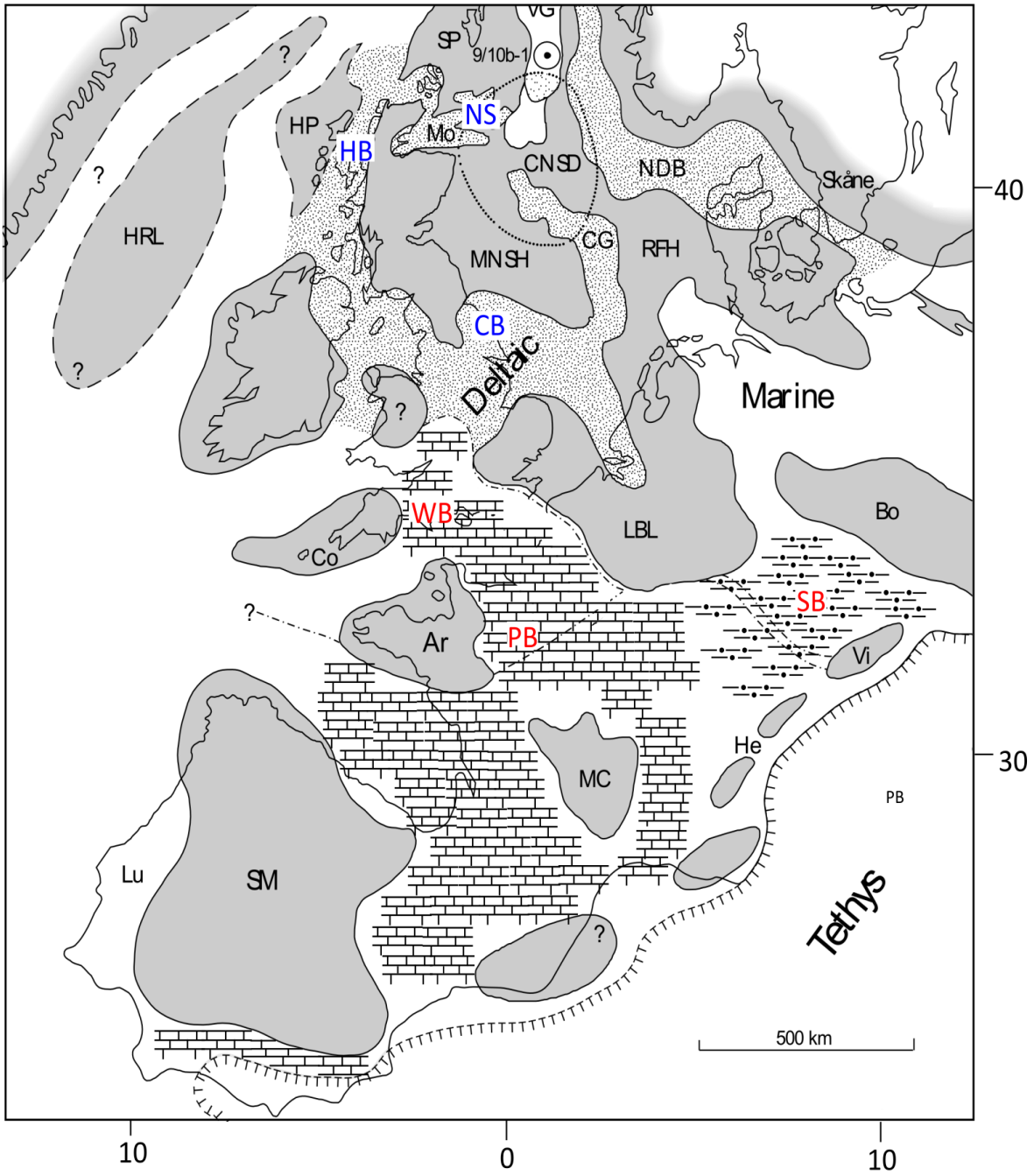

Figure 8.3. Palaeogeography of the Bajocian–Bathonian of Europe.
The marine basins studied in chapters 3–5 are shown in red. The paralic depocentres of the North Sea (NS), Cleveland Basin (CB) and the Hebrides Basin (HB) are shown in blue. Palaeolatitude/longitude is shown. Modified from Callomon (2003) fig. 1.

environment of deposition of the Brent Group, the overall dinoflagellate cyst richness is low (Whitaker et al., 1992; Williams, 1992). In the Brent province, most of the Lower Bajocian is not represented due to the unconformable nature of the base of the overlying Tarbert Formation (Figure 8.4), which represents a transgressive episode equivalent to the Vesulian event in Dorset (Chapter 4; Rioult et al. 1991, Davies et al., 2000). This transgressive event is associated with an influx of low-richness dinoflagellate cyst assemblages dominated by *Gonylodinium* sp., *Sentusidinium ringesorium* (as *S. granulatum*) and *Sentusidinium verrucosum* (Williams, 1992). The Tarbert Formation is overlain by the Heather Formation, which represents a switch to more open-marine conditions and is of Late Bajocian to Bathonian age (Figure 8.4; Williams, 1992; Butler et al., 2005). The deposition of the Heather Formation was associated with an increase in the abundance and richness of dinoflagellate cysts, although this was still relatively low (Williams, 1992; Whitaker et al., 1992). Dinoflagellate cysts which appear in the Heather Formation include *Chytroeisphaeridia chytroeides, Durotrigia aspera*, *Gonyaulacysta jurassica* and *Nannoceratopsis pellucida* (see Bailey and Partingdon, 1991; Williams, 1992; Whitaker et al., 1992). As such, appearances of dinoflagellate cyst taxa through the Bajocian in the North Sea region were strongly controlled by sea level, which drove shifts in palaeoenvironment.

A similar situation can be observed from the Cleveland Basin of northern England. In this area, the Lower Bajocian is largely represented by the marginal-marine deposits of the Cloughton Formation (Figure 8.4), which contains low richness dinoflagellate cyst floras; the only gonyaulacaceans presents are *Dissiliodinium lichenoides, Durotrigia daveyi* and *D. filapicata* (see Butler et al., 2005). The Cloughton Formation is overlain by the Scarborough Formation, which was driven by the transgressive deposition of shelfal sediments over marginal-marine facies, and represents the Lower–Upper Bajocian transition (Fogire 8.4; Gowland and Riding, 1991). The Scarborough Formation contains the appearances of gonyaulacaceans *Acanthaulax crispa*, *Ctenidodinium sellwoodii*?, *Gongylodinium erymnoteichon*, *Rhynchodiniopsis*? *regalis*?, *Valensiella ovulum* and *Wanaea acollaris* (see Gowland and Riding, 1991;

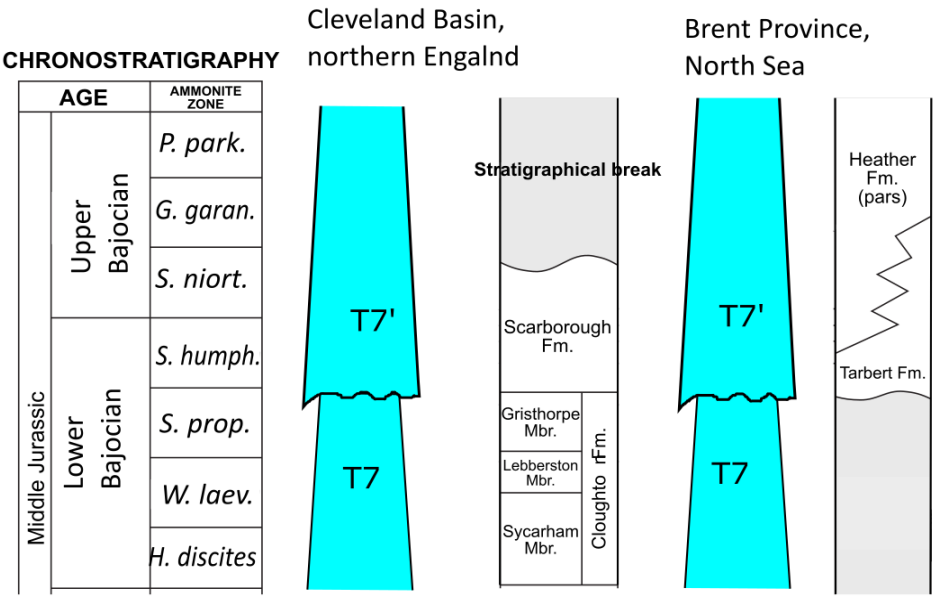

Figure 8.4. Stratigraphy of the Bajocian of the North Sea and Cleveland Basin. Grey fill denotes stratigraphic breaks. Modified from Butler et al. (2005 fig. 6).

Butler et al., 2005). With the exception of *G. erymnoteichon*, these taxa have first appearances around the Lower-Upper Bajocian transition in Swabia (Chapter 3; Feist-Burkhardt and Wille, 1992), and thus the appearances of these species in the Cleveland Basin is relatively synchronous with the Swabian Basin, and coincides with a transgressive pulse.

Moreover, a comparable pattern is seen in the Hebrides Basin of northwest Scotland. In this region, the Upper Aalenian and Lower Bajocian are represented by the Bearreraig Sandstone Formation, which was deposited in tide-dominated deltaic/estuarine palaeoenvironments (Figure 8.5; Mellere and Steel, 1996). The gonyaulacaceans from this unit are represented by *Batiacasphaera* spp., *Dissiliodinium* spp*., D. giganteum, Durotrigia daveyi Kallosphaeridium? hypornatum* and *Leptodinium* sp. cf. *L. subtile* (Figure 8.5; Riding et al., 1991). However, the Rigg Sandstone Member which corresponds to the *S. humphriesianum* zone, represents the transgressive deposition of shelfal sandstones over delta-front deposits (Mellere and Steel, 1996). The Rigg Sandstone Member includes the appearances of the *Ellipsoidictyum/Valensiella* complex and *Valensiella ovulum* (Figure 8.5; see Riding et al., 1991). Moreover, the uppermost unit of Bearrerraig Sandstone Formation is represented by the marine shales

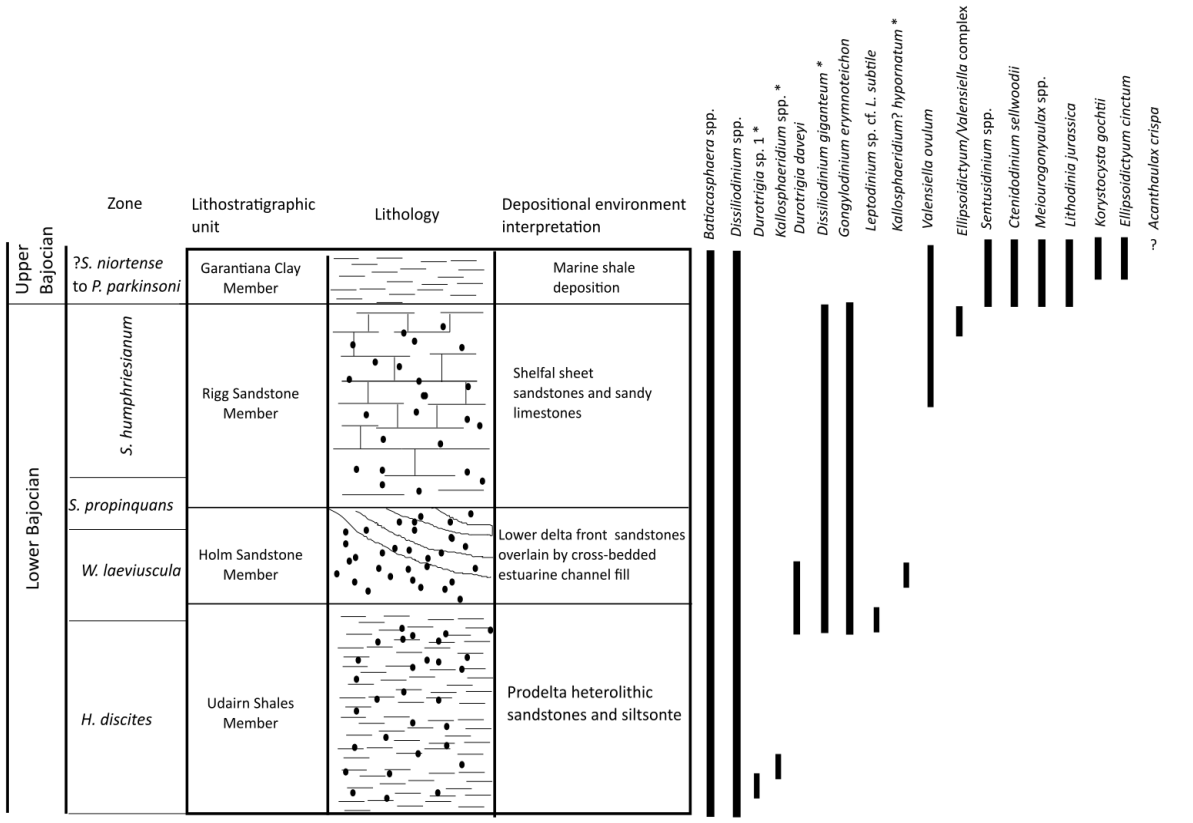

Figure 8.5. Dinoflagellate cyst range chart for the Bajocian of the Hebrides Basin, Isle of Skye, Scotland. Based on Riding et al. (1991), *denotes taxa recorded by this thesis, that were not recorded by the aforementioned authors (Chapter 4, data table appendix D.1). It can be observed that the Lower Bajocian of the Hebrides Basin is largely represented by deltaic/estuarine deposits, with a switch to marine facies through the Lower–Upper Bajocian transition. This is associated with an influx of gonyaulacacean appearances. The members all belong to the Berreraig Sandstone Formation.

of Garantiana Clay Member, which represents a major transgressive pulse and corresponds to the (?)*S. niortense–P. parkinsoni* zones (Figure 8.5; Riding et al., 1991; Mellere and Steel, 1996). This unit contains the appearances of gonyaulacaceans such as *Ctenidodinium sellwoodii*, *Korystocysta gochti*, *Meiourogonyaulax* spp., *Gonyaulacysta pectinigera*, *Sentusidinium* spp. (Figure 8.5; Riding et al., 1991). As such, transgression and the spread of marine conditions have strongly influenced the pattern of dinoflagellate cyst appearances through the Hebrides Basin during the Bajocian.

In summary, in the largely paralic palaeoenvironments of the North Sea, the Cleveland Basin and the Hebrides Basin, a marine transgression occurred around the Early–Late Bajocian transition, and Late Bajocian, and was associated with the appearances of numerous gonyaulacacean taxa. As such, sea level fluctuations appear to have exerted a regional-scale control the appearances of dinoflagellate cyst taxa through northwest Europe during the Bajocian.

8.3.3. Resolving the regional pattern of Mid Jurassic dinoflagellate cyst appearances in northwest Europe

To fully constrain the stratigraphic pattern of the dinoflagellate cyst radiation in Europe, I have integrated the stratigraphic data from this thesis with published data to create a comprehensive range chart for the Upper Aalenian to Lower Bathonian of northwest Europe (Figure 8.6a, b). It can clearly be seen that there is a continuous pattern of appearances through the Upper Aalenian to Lower Bathonian, but the highest number of first appearances are in the *S. humphriesianum* and *P. parkinsoni* zones. Moreover, from the *S. humphriesianum* zone upwards, appearances are dominated by gonyaulacacean taxa. To allow for biases arising from differences in taxonomic approaches, taxa left in open nomenclature which have only been recorded by a single study (including those I described for this thesis) have been removed in Figure 8.7a, b. However, a similar overall pattern can still be observed. Additionally, these data have been used to construct a richness curve for the Upper Aalenian to Lower Bathonian (Figure 8.8). This richness curve clearly shows a steady increase in richness, but there is a particularly pronounced increase in richness in the *S. humphriesianum* and *P. parkinsoni* zones. The curve also demonstrates that gonyaulacacean taxa comprised around 25% of dinoflagellate cyst taxa during the Late Aalenian *G. concavum* zone, but by the Early Bathonian *Z. zigzag* zone, this family represented over 60% of all dinoflagellate cyst taxa. This pattern demonstrates how the Bajocian represents a critical interval in the evolutionary history of the Gonyaulacaceae.

Comparison between the biostratigraphic data and sequence stratigraphic records demonstrates a correlation between the increase in dinoflagellate cyst richness and sea level rise through the Bajocian (figures 8.9, 8.10). Moreover, at a zonal level, the large number of appearances recorded from the *S. humphriesianum* and *P. parkinsoni* zones correspond to the major third-order transgressive pulses, the latter of which represents maximum-transgression of the T7 cycle (Figure 8.10). Appearances of taxa through the Late Aalenian–Early Bathonian in Germany, northern France, and southern England,

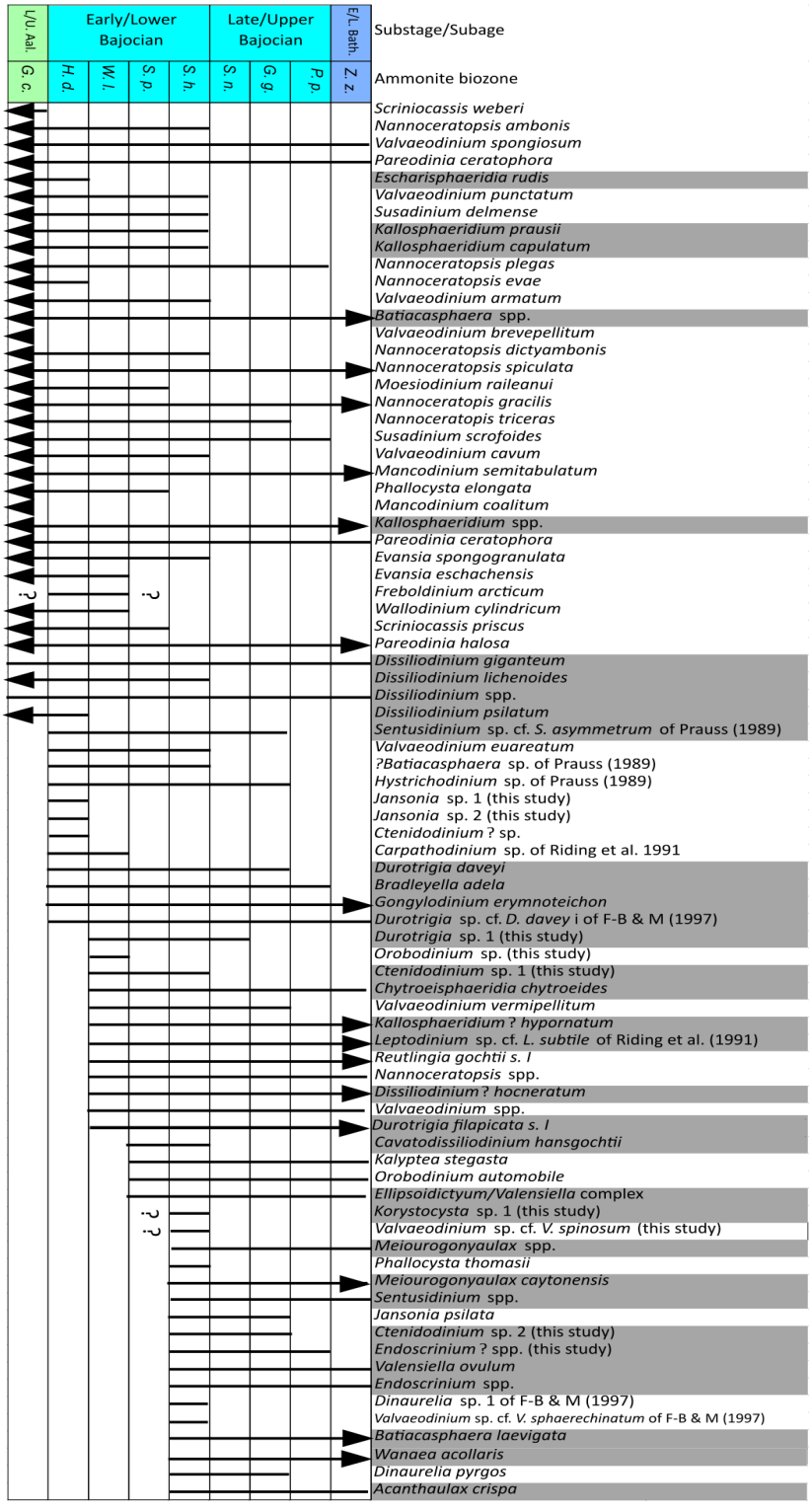

Figure 8.6a. Dinoflagellate cyst range chart showing first appearances for Late Aalenain *G. concavum* zone, to the Early Bajocian *S. humphriesianum* zone.

Grey fill denotes gonyaulacacean taxa, arrow heads indicate where a taxon ranges up/down. Based on data from this thesis, Prauss, (1989), Riding et al. (1991), Feist-Burkhardt and Wille (1992), Riding and Thomas (1992), Feist-Burkhardt and Monteil (1997; 2001), Butler et al. (2005), Feist-Burkhardt and Götz (2016). Zone abbreviations: G.*c= G. concavum, H. d.=H. discites, W. l.=W. laeviuscula, S. p.=S. propinquans, S. h.=S. humphriesianum, S. n.= S. niortense, G.g.= G. garantiana, P.p.= P. parkinsoni, Z. z.= Z. zigzag*.

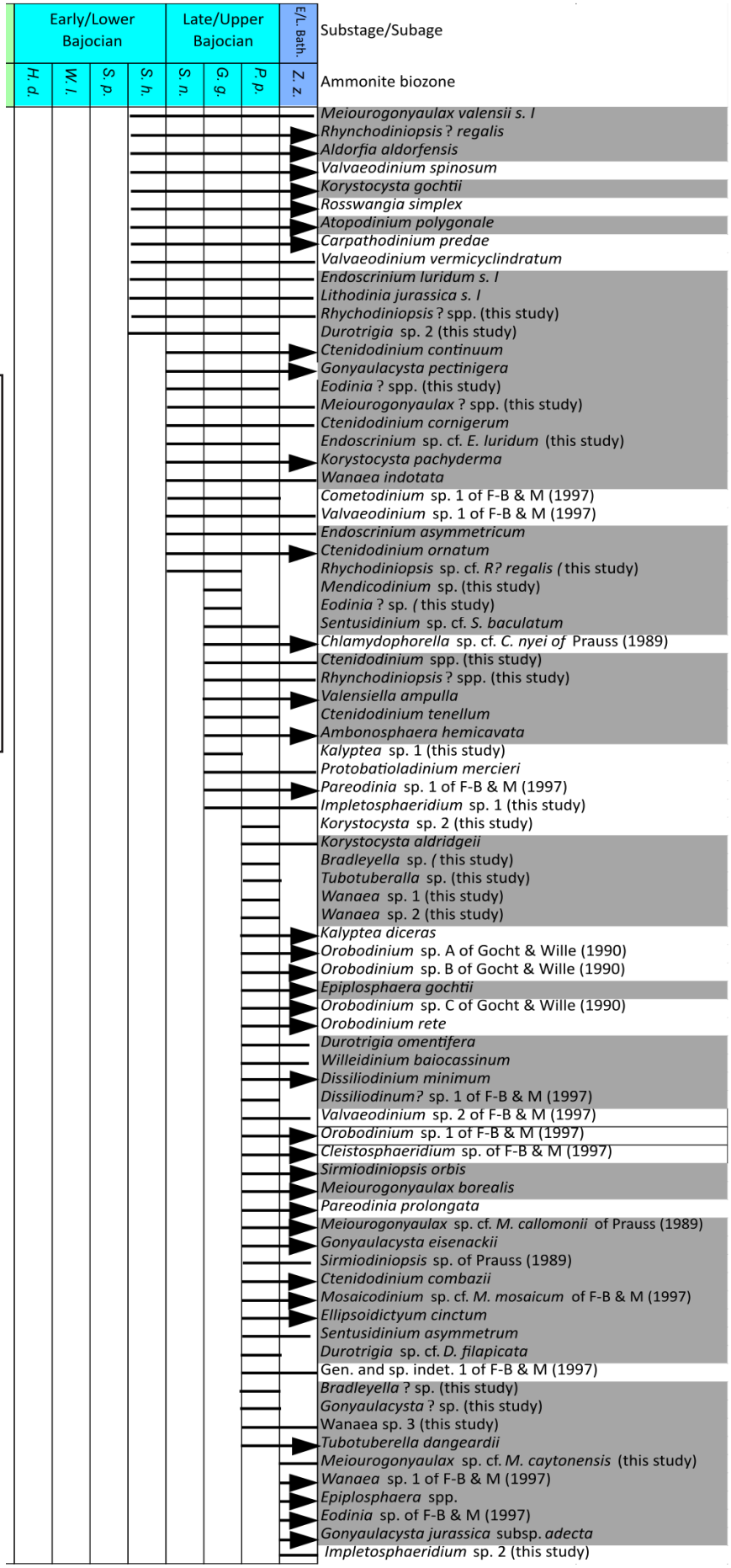

Figure 8.6b. Dinoflagellate cyst range chart showing first appearances for the Early Bajocian, *S. humphriesianum* zone, to the Early Bathonian, *Z. zigzag* zone.
Caption as per Figure 8.6a.

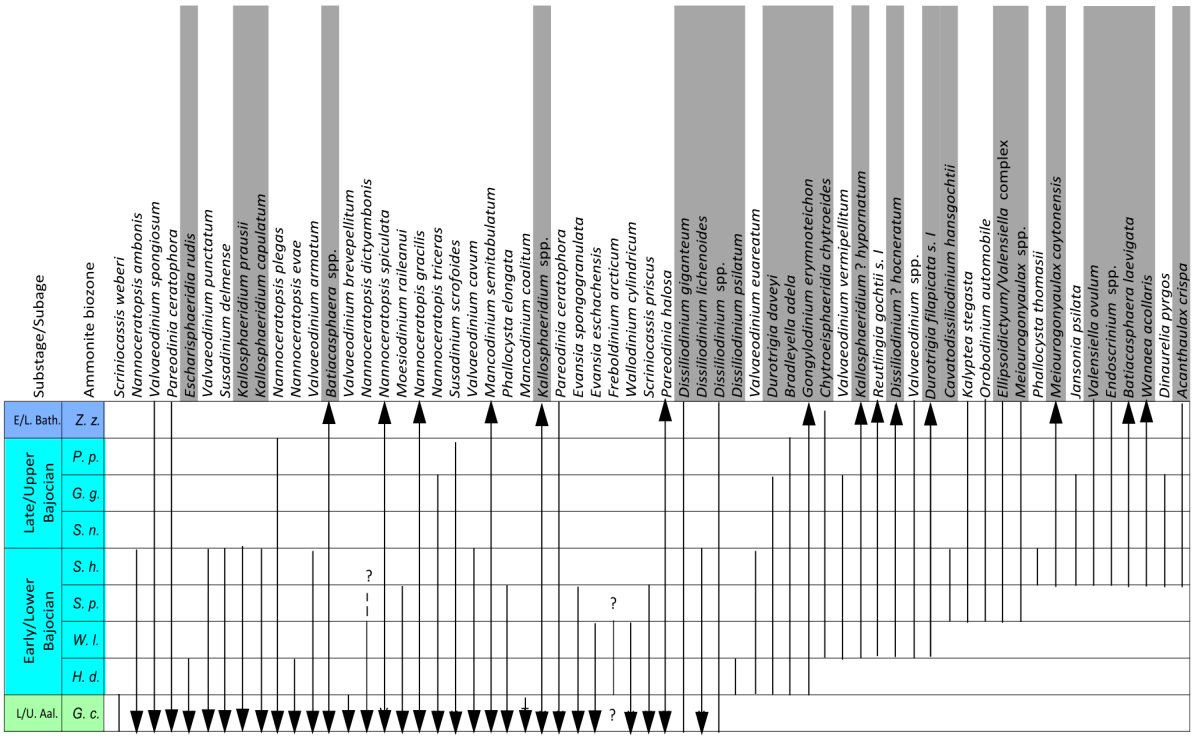

Figure 8.7a. Dinoflagellate cyst range chart for the Late Aalenian, *G. concavum* zone to the Early Bajocian, *S. humphriesianum* zone, open nomenclature removed.
Taxa left in open nomenclature which have only been recorded by a single study have been removed. Caption as per Figure 8.6.

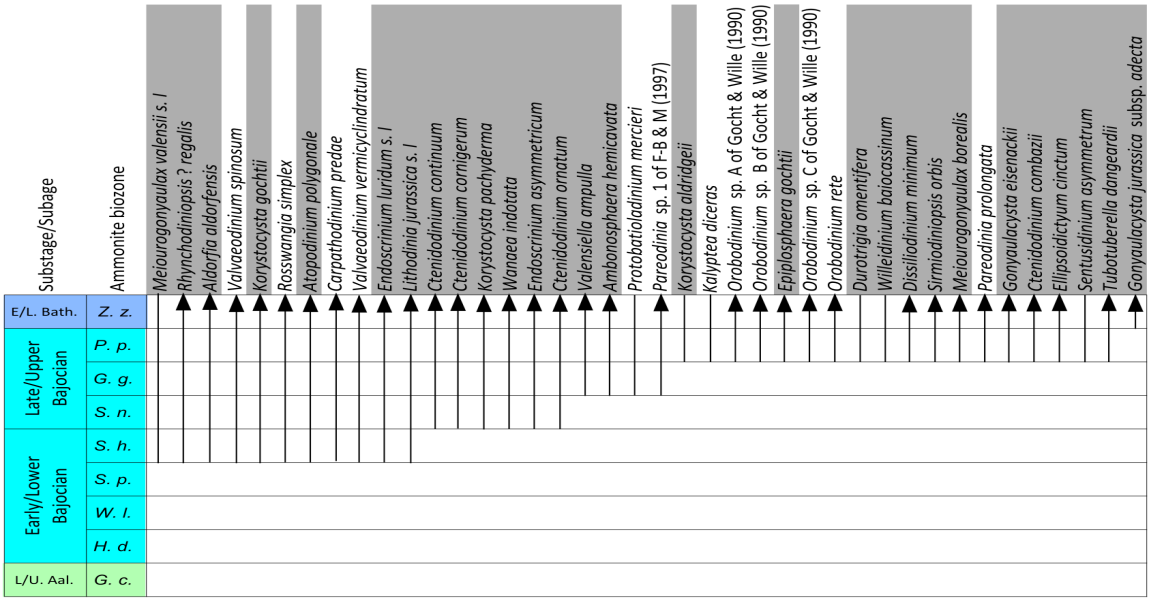

Figure 8.7b. Dinoflagellate cyst range chart showing first appearances for the Early Bajocian, *S. humphriesianum* zone, to the Early Bathonian, *Z. zigzag* zone.
Taxa left in open nomenclature which have only been recorded by a single study have been removed. Caption as per Figure 8.6.

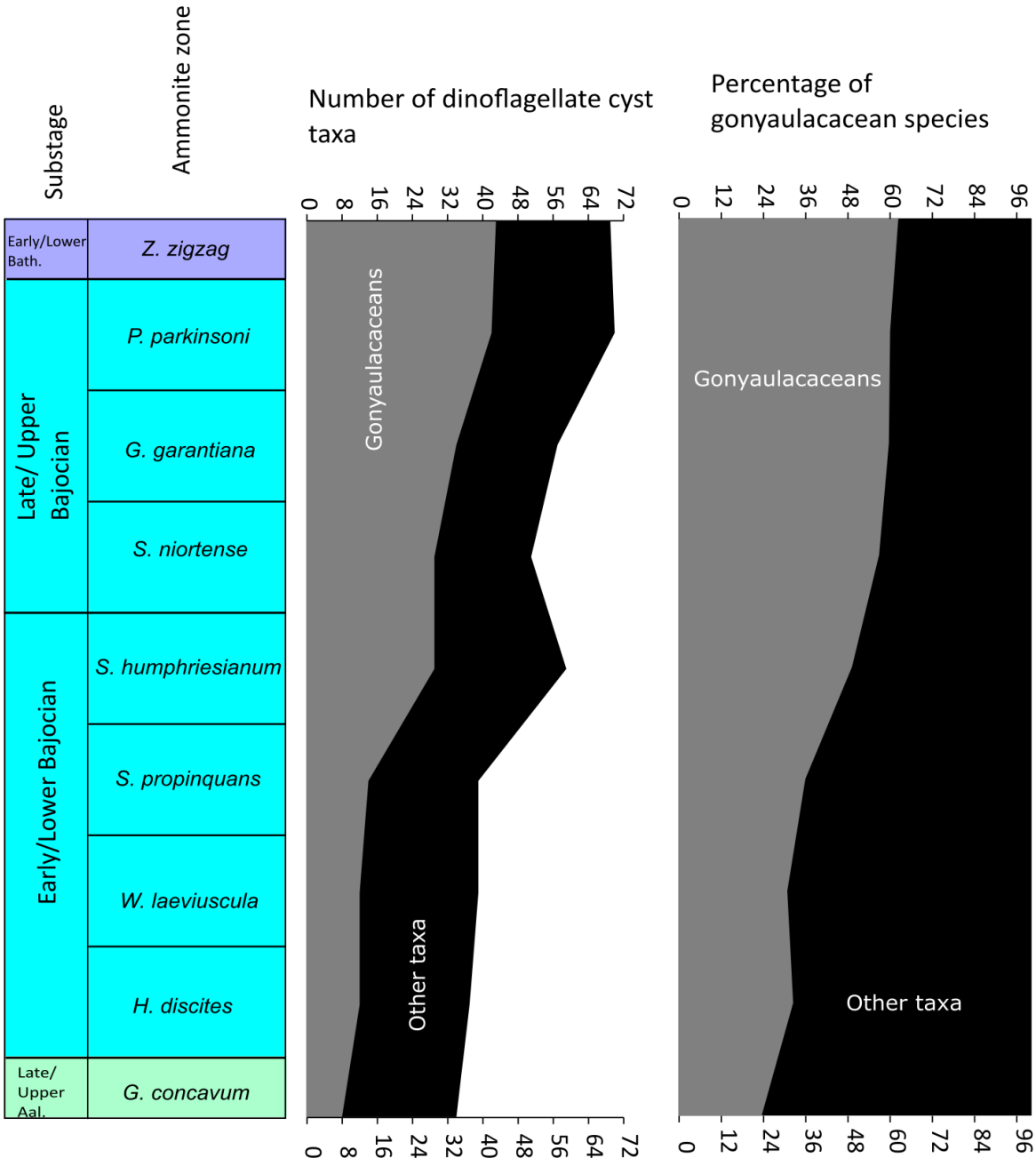

Figure 8.8. Dinoflagellate cyst richness curve and percentage of gonyaulacacean taxa for the Late Aalenian to Early Bathonian of Europe.
Based on data from Figure 8.6. There is a significant increase in gonyaulacacean richness, and the percentage of gonyaulacacean taxa also increases significantly.

could therefore have been brought into the European Epicontinental Seaway by transgressive waters, as indicated by the correlation between large numbers of appearances and transgressive pulses around the S. *humphriesianum* and *P. parkinsoni* zones. Transgression drove changes in palaeoenvironment in the paralic areas of the North Sea, northern England, and northwest Scotland, with gonyaulacaceans dispersed through these basins by the spread of marine conditions. While the driver behind this transgression remains unclear, Hallam (2001) argued that the sea level rise during the Early and Late Bajocian was eustatic, as there is evidence of this transgression in Europe, South America, and the

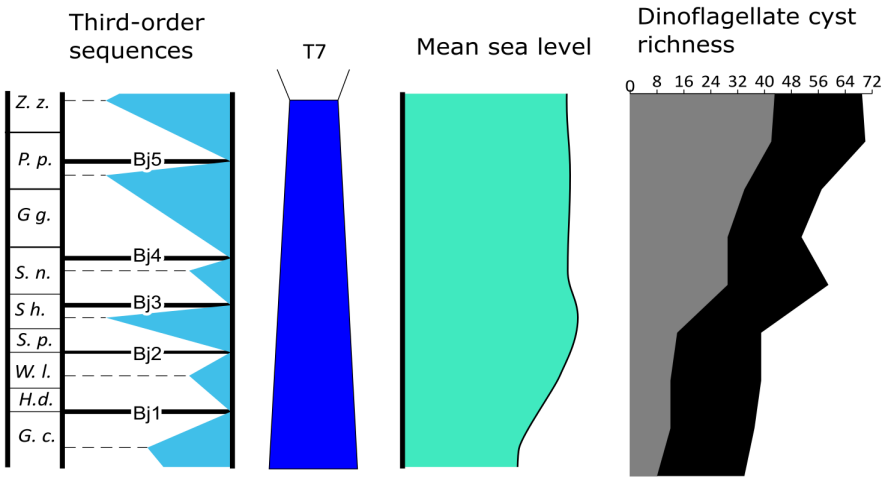

Figure 8.9. Comparison to dinoflagellate cyst richness to second order and third-order sea level cycles for the Upper Aalenian to Lower Bathonian of Europe.
It can be observed that the increase in richness through the Upper Aalenian to Lower Bathonian broadly mirrors the T7 transgression. The pronounced increase in diversity in the *S. humphriesianum* (*S. h.*) zone correlates with pronounced transgresssive pulse of Bj2. The increase through the Upper Bajocian correlated with the significant transgressive pulses of Bj4 and Bj5. Sequences after Jacquin et al. (1998), sea level after Hardenbol et al. (1998).

Himalayas. Further, in addition to sea level rise, the Bajocian was marked by changes in the tectonic configuration of ocean gateways, and ocean circulation (Chapter 1; Dera et al., 2014). Thermal doming in the North Sea during the Aalenian restricted water-mass transfer through the Viking Corridor between the European Epicontinental Seaway and the Boreal Sea (Chapter 1; Korte et al., 2015). Additionally, a major change in the direction of plate relative motion and spreading rate occurred between the African and North American plates in the Early Bajocian which drove a widening and deepening of the Hispanic Corridor (Labails et al., 2010). Neodymium isotopes record a positive shift through the Aalenian to Bathonian, which Dera et al. (2014) argued was the result of the increased influence of radiogenic Tethyan waters into the European Epicontinental Seaway. In turn, this was driven by the closing of the Viking Corridor, and the widening of the Hispanic Corridor (Dera et al., 2014). Due to the restriction of the Viking Corridor, the main path for floral dispersal would likely have been from the south, from the northwest Tethyan Ocean and the Hispanic Corridor. This given, a change in ocean circulation and rise in sea level, may have driven a rapid influx of gonyaulacacean taxa into Europe during the Bajocian, as intervals of higher sea level can promote the interconnectivity and floral interchange between ocean basins (van de Schootbrugge et al., 2005). As such, enhanced water-mass transfer may have increased floral interchange between the European Epicontinental Seaway, the northwest Tethys, and the Panthalassic Ocean (via the Hispanic Corridor), the latter of which is evidenced by the occurrence of European dinoflagellate cyst taxa in Argentina (section 8.4). Additionally, climatic factors may have also influenced the pattern of appearances in Europe. A brief interval of warming occurred in the *S. humphriesianum* zone in Europe (Figure 1.7). As this zone also corresponds to a major influx of gonyaulacacean taxa, warmer seawater temperatures, coupled with sea level rise, could have promoted

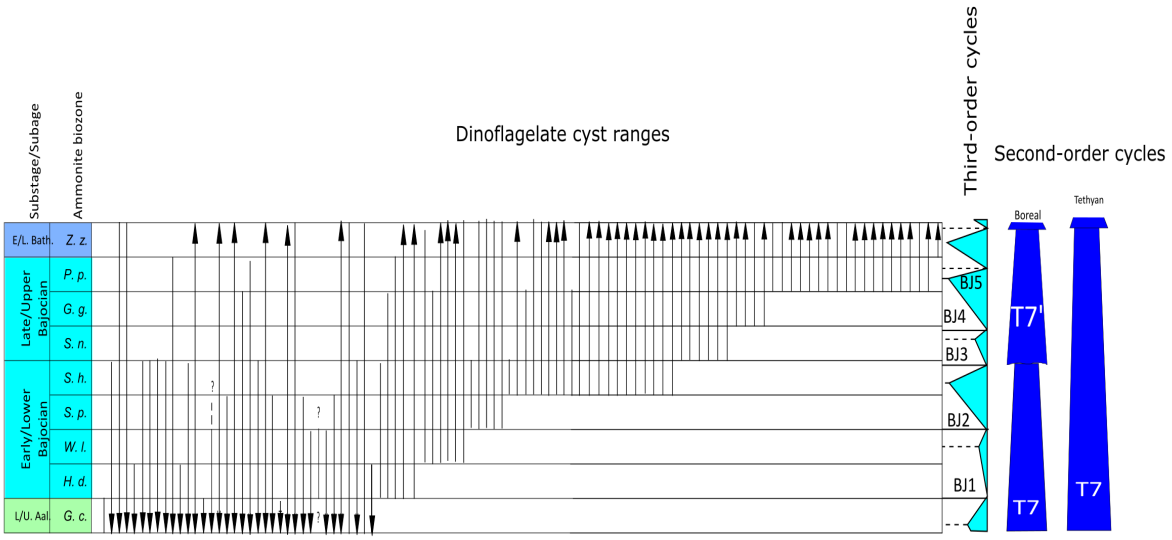

Figure 8.10. Comparison of dinoflagellate cyst ranges with sea level cycles for the Upper Aalenian to Lower Bathonian of Europe.
Ranges based on Figure 8.6. The large number of appearances in the *S. humphriesianum* (*S. h.*) zone correlates with pronounced transgressive pulse of Bj2. Similarly, the large number of appearances in the *P. parkinsoni* zone (*P. p.*) corresponds to cycles Bj4/5.

the spread of taxa from lower palaeolatitude Tethyan regions into the European Epicontinental Seaway. Further, the temporal coincidence between climatic warming and transgression in the *S. humphriesianum* zone may indicate a common cause via a glacioeustatic control on third-order sea level oscillations (cf. Dewey and Pitman, 1998).

8.4. Global comparison of the stratigraphic pattern

8.4.1. Introduction

The increase in gonyaulacacean dinoflagellate cyst richness through the Bajocian of northwest Europe appears to have been linked to sea level rise and changes in ocean circulation. However, to what extent was this increase in richness a global phenomenon, and how was it related to sea level and palaeoenvironmental change in other regions? To examine the global pattern, I have compiled dinoflagellate cyst data from various low to high palaeolatitude regions for the Bajocian–Bathonian, which is summarised in Table 8.1a, b. The palaeogeographic distribution of the regions examined is shown in Figure 8.11.

There is a clear increase in the richness of gonyaulacacean dinoflagellate cysts through the Middle Jurassic of offshore eastern Canada, but the majority of appearances are recorded from the Bathonian, rather than the Bajocian (Figure 8.12; Bujak and Williams, 1977). During the Early–Mid Jurassic, offshore Eastern Canada was located on the northern edge of the Hispanic Corridor (Figure 8.6). In this region, the Lower Jurassic to Bajocian is largely represented by marginal-marine strata, but a switch to marine conditions is observed in the Bathonian (Bujak and Williams, 1977). As such, the richness of gonyaulacaceans appears to have been closely related to shifting palaeoenvironment.

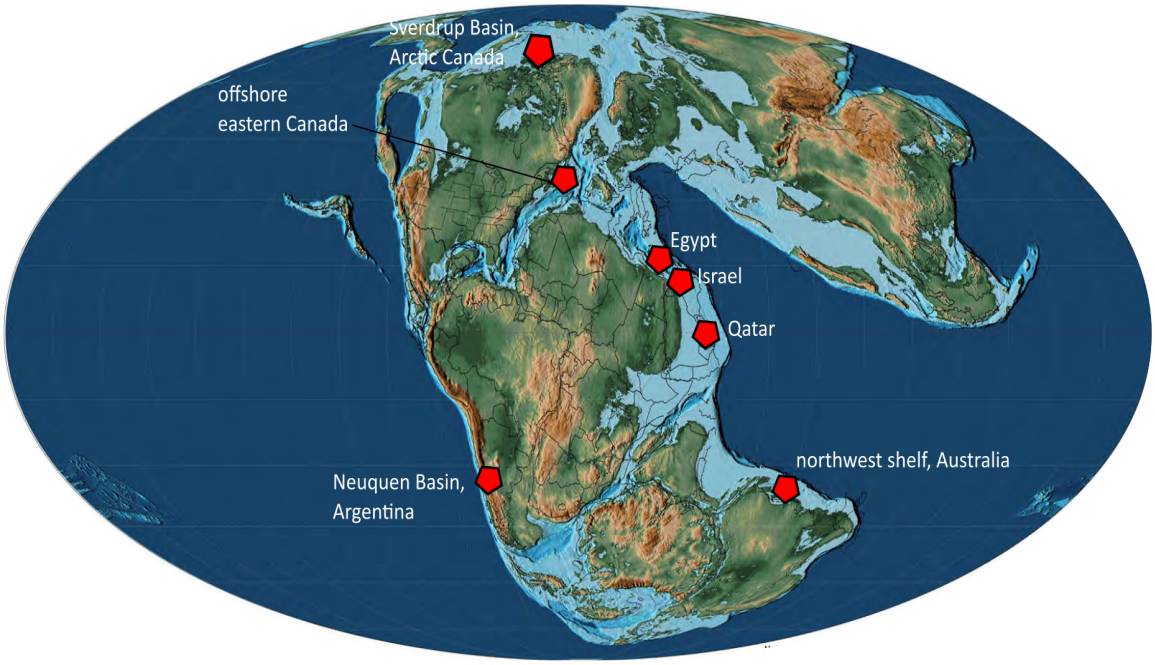

Figure 8.11. Global palaeogeography for the Bajocian showing the locations for global comparison of the dinoflagellate cyst record.
Modified from Scotese (2014).

Outside of the mid northerly palaeolatitudes, the radiation of gonyaulacaceans can clearly be seen from the Mid Jurassic of Australia, which was then located on the southern edge of the Tethyan Ocean, around 30°S (Figure 8.11). In the North Carnarvon Basin, the Bajocian is represented by the shallow marine Athol Formation, which is overlain by the fluvio-deltaic Legendre Formation (Riding et al., 2010b; Mantle and Riding, 2012). In the Bonaparte Basin the Middle Jurassic is largely represented by the deltaic Plover Formation (Riding et al., 2010a). The Bajocian to Early Bathonian is subdivided into three dinoflagellate cyst biozones, the *Dissiliodinium caddaense*, *Nannoceratopsis deflandrei* and *Wanaea verucosa* biozones. The dinoflagellate cyst taxa present through these zones is summarised in Figure 8.13.

The *Dissiliodinium caddaense* biozone was correlated by ammonites and strontium isotope stratigraphy to the *W. laeviuscula* zone (Early Bajocian) of Europe (Riding et al., 2010b). The dinoflagellate cyst assemblages of the *D. caddaense* zone are of low richness and are dominated by *Dissiliodinium caddaense* (Table 8.1a; Riding et al., 2010b). The *Dissiliodinium caddaense* zone is followed by the *Nannoceratopsis deflandrei* zone. This zone is marked by the appearances of *Acanthaulax* sp. cf. *A crispa*, *Ctenidodinium* spp. and *Durotrigia filapicata* (Riding et al., 2010a). As *Acanthaulax crispa*, and multiple species of *Ctendidodinium,* have first appearances around the Early-Late Bajocian transition in Europe, and the underlying *D. caddaense* zone is of unequivocal Early Bajocian age, Riding et al. (2010a) argued that as the *N. deflandrei* zone corresponds to the Early-Late Bajocian transition.

The *Nannoceratopsis deflandrei* zone is followed by the *Wanaea verrucosa* biozone, which is marked by

Region	Author	Age	Middle Jurassic palaeolatitude	Age control	Depositional environment		Dinoflagellate cyst taxa
Australia	Riding et al., 2010b	Early Bajocian	30°S	Ammonite and Sr isotopes	Shallow marine	*Batiacasphaera* spp. *	*Nannoceraptopsis deflandrei (N. gracilis)* *
						Dissiliodinium caddaense	*Nannoceratopsis spiculata* *
						Dissiliodinium spp. *	*Paredonia* spp. *
							Pareodinia halosa *
	Mantle and Riding, 2012	Early (?) Bajocian-Bathonian	30°s	Primarily palynozonations	Shallow marine to nearshore	*Batiacasphaera* spp. *	*Ctenidodinium* sp. A
						Mancodinium semitabulatum *	*Meiourogonyaulax* sp. B
						Dissiliodinium sp. A	*Mendicodinium* spp.
						Dissiliodinium spp.	*Pareodinia* sp. A
						Escharisphaeridia sp. A	*Bradleyella* sp. cf. *B. adela*
						Escharisphaeridia sp. B	*Jansonia* spp.
						Escharisphaeridia spp. *	*Valvaeodinium cookii*
						Leptodinium spp.	*Valvaeodinium spinosum* *
						Meiourogonyaulax spp. *	*Aldorfia* sp. A
						Nannoceraptopsis deflandrei *	*Jansoni* sp.
						Pareodinia halosa *	*Wanaea lacuna*
						Pareodinia spp.*	*Endoscrinium* sp. cf. *E. luridum* *
						Phallocysta granosa	*Ctenidodinium* sp. B
						Wanaea verrucosa	*Endoscrium kempaea*
						Egmontodinium sp. A	*Endoscrinium* spp. *
						Ctenidodinium spp.*	*Fostericysta scarffei*
						Durotrigia spp. *	*Rhynchodiniopsis* spp. *
						Evansia sp. A	*Ctenidodinium* sp. C
						Wanaea endota	*Valensiella ovulum* *
						Phallocysta spp. *	*Ternia balmei*
						Kallosphaeridium ? hypomatum	*Valensiella* spp. *
						Meiourogonyaulax strausii	*Endoscrinium luridum* *
						Nannoceratopsis senex *	*Acanathaulax crispa* *
						Sentusidinium spp.*	*Chlamydophorella* spp. *
						Meiourogonyaulax sp. A	*Leptodinium ? ancoralium*
						Meiourogonyaulax baculata *	*Lithodinia* sp. cf. *L jurassica*
						Valvaeodinium vermicylindratum	*Rhynchodiniopsis* sp. cf. *R? regalis*
						Wanaea indodata	*Ellipsoidictydum* sp.
						Gonyaulacysta ? spp	
						Dissiliodinium psilatum *	*Sentusidinium ringesoriium* (as *K. granulatum*) *
						Dissiliodinium spp. *	*Kallosphaeridium* spp. *
						Dissiliodinium sp. cf. *D. baileyi*	*Korystocysta* sp.
						Sentusidinium ? sp	*Nannoceratopsis* spp. *
Argentiana (Neuquen Basin)	Stukins et al. (2013)	Early Bajocian	30°S	Ammonites (Howell et al., 2005)	Marginal-marine/deltaic		

Table 8.1a. Dinoflagellate cysts from the Bajocian–Bathonian of the mid-palaeolatitudes of the southern Hemisphere.

Grey fill denotes gonyaulacacean taxa. *denotes taxa recorded from the Middle Jurassic of Europe.

Region	Author	Age	Middle Jurassic palaeolatitude	Age control	Depositional environment	Dinoflagellate cyst taxa	
Qatar	Ibrahim et al. (2003)	Bajocian-Bathonian	Equitorial	Strontium isotopes	Shallow marine	*Valensiella* spp. *	*Kallosphaeridium* sp.
						Chytroeisphaeridia chytroeides *	*Gonyaulacysta pectinigera* *
						Cribroperidinium spp.	*Rhynchodiniopsis* sp. cf. *R? regalis*
						Escharisphaeridia spp. *	*Prolixosphaeridium* sp.
						Mendicodinium spp.	*Barbatacysta pilosa* *
						Valensiella sp. A	*Sentusidinium rioultii* *
						Pareodinia ceratophora *	*Gonyaulacysta* spp. *
						Ctenidodinium spp. *	*Ctenidodinium continuum* *
						Ctenidodinium sellwoodii *	*Systemophora* spp. *
						Batiacasphaera spp. *	*Gonyaulacysta jurassica* *
						Korystocysta spp. *	*Acanthaulax crispa* *
						Mancodinium sp. cf. *M. semitabulatum*	*Chlamydophorella* sp.
						Valensiella sp. cf. *V. ovulum*	*Escharisphaeridia psilta*
						Sentusidinium spp. *	*Sentusidinium echinatum* *
						Korystocysta gochtii *	*Wanaea accollaris* *
						Lithodinia spp. *	*Chytroeisphaeridia* spp.
						Escharisphaeridia pocockii *	
Israel	Conway (1990)	Bajocian-Bathonian	15°N	Primarily palynozonation	Shallow marine to intertidal	*Meiourogonyaulax deflandrei*	*Meiourogonyaulax bathonica*
						Korystocysta gochtii (as *K. kettonensis*) *	*Ctenidodnium sellwoodii*
						Ellipsoidictyum spp.	*Ellipsoidictyum cinctum*
						Sentusidinium spp.	*Pareodinia prolongata*
						Valensiella ovulum	*Ellipsoidictyum gochtii*
Egypt	Ibrahim et al. (2002)	Bajocian-Bathonian	15°N	Primarily palynozonations (Keeley et al., 1990)	Shallow marine	*Pareodinia ceratophora* *	*Chlamydophorella spp.*
						Cleistosphaeridium spp.	*Rhynchodiniopsis* sp. cf. *R. gongylos*
						Carpathodinium sp. cf. *C. predae*	*Wanaea* sp.
						Korystocysta spp. *	*Sentusidinium villersense* *
						Ctenidodinium spp. *	*Escharisphaeridia pocockii* *
						Durotigia sp. cf. *D. aspera*	*Lithodinia callomanii* *
						Acathaulax sp. cf .*A. crispa*	*Systemophora* spp
						Lithodina strongylos *	*Wanaea sp. cf. W. acollaris*
						?Scriniocassis sp. B	*Sentusidinium* sp. cf. *S rioultii*
						Dissiliodinium willei *	*Ellipsoidictyum cinctum* *
						Sentusidinium spp. *	*Acanthaulax* spp
						*Chytroeishaeridia chytroeides**	*Valensiella ovulum* *
						Sentusidinium sp. A	*Rhynchodiniopsis* sp. cf. *R. cladophora*
						Lithodinia spp. *	*Mendicodinium groenlandicum* *
						Ctenidodinium ornatum *	*Meiourogonyaulax sp. cf. M. caytonensis*
						Ctenidodinium continuum *	*Apteodinium sp. A*
						Ctenidodinium sellwoodii *	*Leptodinum spp.*
						Ctenidodinium combazii *	*Adnatosphaeridium caulleryi*
						Korystocysta gochtii *	*Surculosphaeridium vestitum*
Offshore Eastern Canada	Bujak and Williams (1977)	Jurassi, including Bajocian-Bathonian	30°N	Primarily palynozonations	Shallow to marginal marine (Bajocian) marine (Bathonian)	*Mancodinium semitabulatum* *	*Lithodinia jurassica* *
						Pareodinia ceratophora *	*Valensiella ampulla* *
						Durotrigia filapicata (as G. filapicata) *	*Valensiella ovulum* *
						Korystocysta pachyderma (as C. pachydermum) *	*Valensiella vermiculata* *
						Sentusidinium rioulti (as T. rioulti) *	*Ctenidodinium ornatum* *
						Rhynchodiniopsis? regalis (as L. regale) *	*Gonyaulacysta eisenacki (as E. eisenacki)* *
						Meiourogonyaulax valensii (as *L. valensii*) *	*Systemophora areolata* *
						Aldorfia aldorfensis (as G. aldorfensis) *	*Gonyaulacysta pectinigera*
						*Leptodinium subtile**	(as *L .. subtile* ssp. *pectinigerum*) *
Sverdrup Basin, Arctic Canada	Davies, 1983	Jurassic-Cretaceous (including Bajocian-Bathonian)	60°N	Palynozonation and ammonites	Shallow marine	*Mancodinium coalitum**	*Caligodinium aceras**
						Frebolidinium serrulata *	*Microdinium opacum**
						*Valvaeodinium aquilonium**	*Opaeopsomus wapellensis**
						*Rosswangia holotabulata**	*Valvaeodinium perpunctatum**
						*Mancodinium semitabulatum**	*Valvaeodinium perpunctatum**
						*Nannoceratopsis senex**	*Scriniodinium dictyotum* *
						*Evansia evitii**	*Mendicodinium reticulatum**
						*Scriniocassis weberi**	*Phallocysta eumekes**
						*Valvaeodinium cavum**	*Chytroeisphaeridia chytroides**
						*Dingodinium minutum**	*Scriniodinium dictyotum**
						*Dodekovia syzygia**	*Reutlingia cracens**
						*Susadinium scrofoides**	*Stephanelytron membranoideum**
						*Nannoceratopsis gracilis**	*Lanterna ?cantrellii**
						*Nannoceratopsis pellucida**	*Meiourogonyaulax deflandreii**
						*Phallocysta elongata**	

Table 8.1b. Dinoflagellate cysts from the Bajocian–Bathonian of the low palaeolatitudes (both hemispheres) and the mid to high palaeolatitudes of the northern hemisphere.
Grey fill denotes gonyaulacacean taxa. *denotes taxa recorded from the Middle Jurassic of Europe.

a significant increase in dinoflagellate cyst richness, with the appearances of numerous gonyaulacaceans such as *Aldorfia*, *Endoscrinium*, *Kallosphaeridium*, *Meiourogonyaulax*, *Rhynchodiniopsis*, *Sentusidinium*, *Ellipsoidictyum*/*Valensiella* and *Wanaea* (Table 8.1a; Mantle and Riding, 2012). The dinoflagellate cyst floras through this interval are similar to those in Europe; at a generic level the only Australian

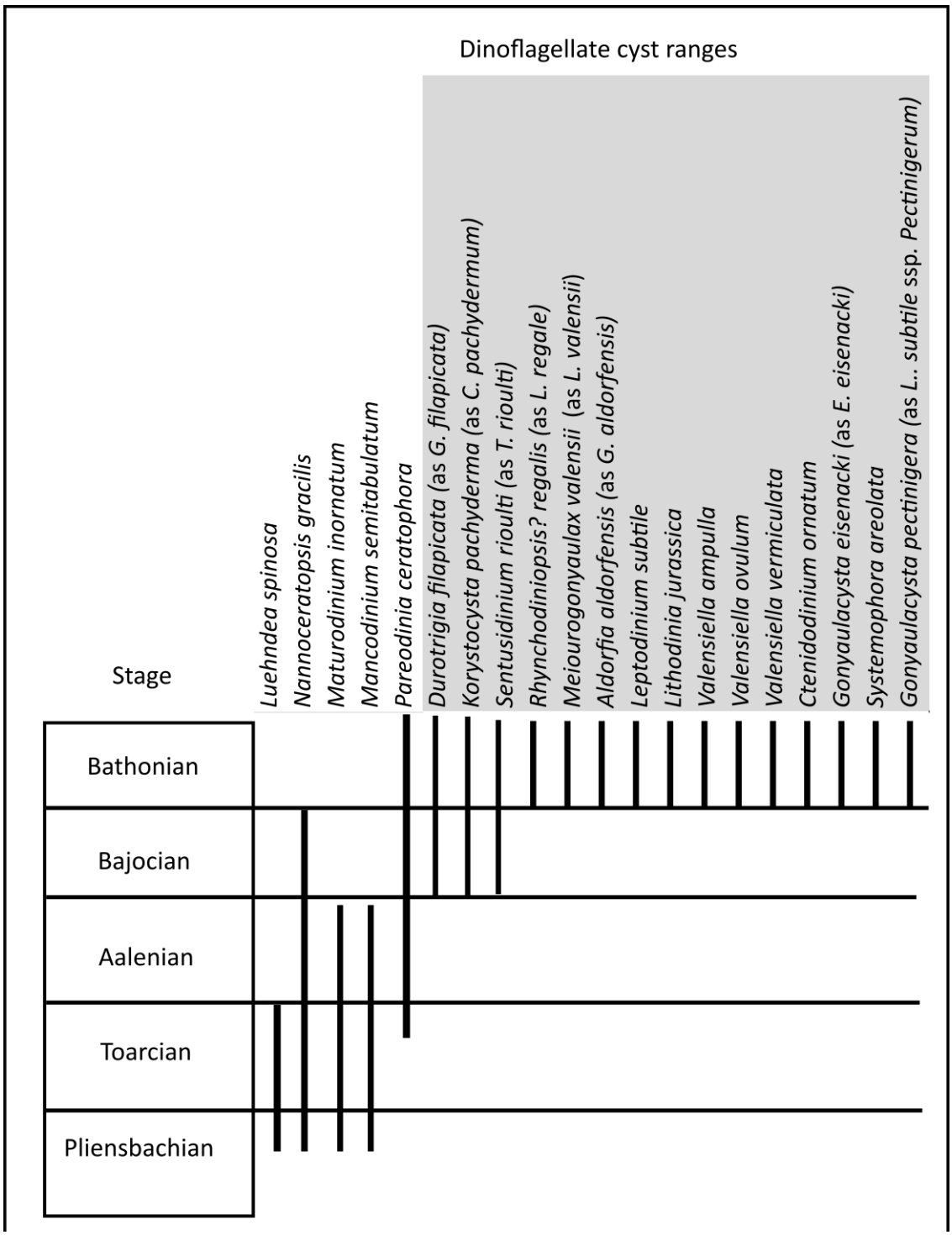

Figure 8.12. Dinoflagellate cyst range chart for the Lower to Middle Jurassic of offshore eastern Canada. Based on Bujak and Williams (1977). Grey fill denotes gonyaulacacean taxa. Note the influx of appearances in the Bathonian.

endemic genus is *Ternia* (see Mantle and Riding, 2012). At a species level, endemic species include *Ctenidodinium ancora*, *Meiourogonyaulax strausii*, *Wanaea verrucosa* and *Wanaea lacuna.* However, *C. ancora* is very similar in morphology to *Ctenidodinium sellwoodii* (Riding et al., 2010a, plate 1, figs. 3–4) and Feist-Burkhardt and Götz (2016) reported morphotypes of *Wanaea* which strongly resemble *W. verruscosa* from the Bajocian of southern Germany. Consequently, dinoflagellate cysts floras from the

Bajocian to Bathonian of Australia are of comparable taxonomic composition to those of Europe.

The pattern of dinoflagellate cyst appearances in the Northwest Shelf of Australia is also similar to that of Europe, with a significant increase in the richness of gonyaulacacean taxa. In Australia, the Early Bajocian was associated with a major marine transgression, which may correspond to the first pulse of the T7 transgression in Europe (Riding et al., 2010a). However, the Late Bajocian–Early Bathonian of Australia was regressive (Riding et al., 2010a), and as such the increase in gonyaulacacean richness through the *Nannoceratopsis deflandrei* and *Wanaea verrucosa* dinoflagellate cyst zones was not coupled to sea level rise or the spread of marine palaeoenvironments.

In terms of other mid-palaeolatitude regions from the southern Hemisphere, dinoflagellate cysts have been studied from the Bajocian of the Neuquen basin, Argentina. In this region, the Bajocian represented by marginal marine strata (Stukins et al., 2013). In a study of the Lower Bajocian Lajas Formation, Stukins et al., (2013) recorded low richness dinoflagellate cyst assemblages (Table 8.1a). The low overall richness in the Neuquen Basin is probably a consequence of the extremely marginal marine/brackish depositional environments, and thus there is no dramatic increase in richness through the Bajocian. It can however be seen that assemblages are dominated by gonyaulacacean taxa (Table 8.1a).

Within low palaeolatitude regions, it can clearly be seen that Bajocian-Bathonian dinoflagellate cyst floras are dominated by gonyaulacacean taxa, many of which are also present in Europe (Table 8.1a, b). In Egypt, the Toarcian(?) to Aalenian is represented by the shallow marine limestones of the Rajabiah Formation (Keeley et al., 1990; Keeley and Wallis, 1991; Ibrahim et al., 2002). Dinoflagellate cysts from this unit are of low richness and assemblages are comprised of *Mendicodinium, Nannoceratopsis*, *Scriniocassis* and *Valvaeodinium*; *Kallosphaeridium* is the only definitive gonyaulacacean to appear through this interval (Ibrahim et al., 2002). There is then a significant increase in the richness of gonyaulacaceans through the Bajocian to Bathonian (Figure 8.14; Ibrahim et al., 2002). The Bajocian was deposited under transgressive to highstand conditions, whilst the Bathonian was largely regressive (Keeley et al., 1990). As such, the increase in richness in dinoflagellate cysts through the Bajocian coincides with a transgressive trend; however, the appearances in Bathonian seem to have occurred during a time of sea level fall. In Israel, Pliensbachian to Lower Bajocian strata were laid down in primarily non-marine to marginal palaeoenvironments, and the only dinoflagellate cyst species recorded is *Nannoceratopsis gracilis* (see Conway, 1990). Upper Bajocian and Bathonian strata are represented by the transgressive deposition of shallow marine to intertidal limestones and marls (Conway 1990 and references therein), which was accompanied by a significant increase in the richness of gonyaulacaceans (Table 8.1b). In Qatar, the Aalenian Stage is not represented due to a depositional hiatus and the underlying Lower Jurassic deposits are largely devoid of palynomorphs due to secondary dolomitisation (Ibrahim et al., 2003). As such, it is impossible to unravel the pattern of dinoflagellate cyst appearances through the Middle Jurassic in this region, but Bajocian-Bathonian dinoflagellate cyst floras are clearly

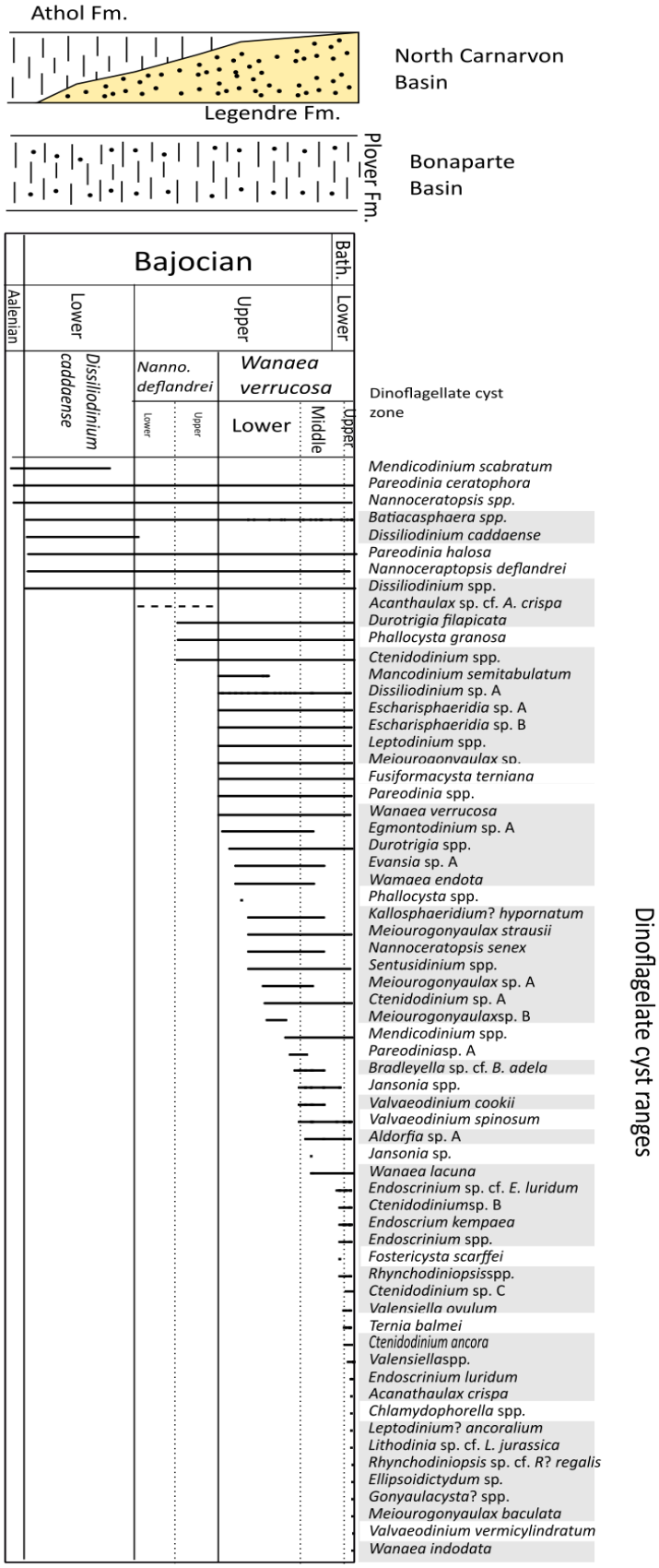

Figure 8.13. Dinoflagellate cyst range chart for the Bajocian–Lower Bathonian of the northwest shelf of Australia.

Grey fill denotes gonyaulacacean taxa. Note the large number of appearances through the *Wanaea verrucosa* dinoflagellate cyst biozone. Based on Riding et al. (2010a) and raw data from Mantle and Riding (2012).

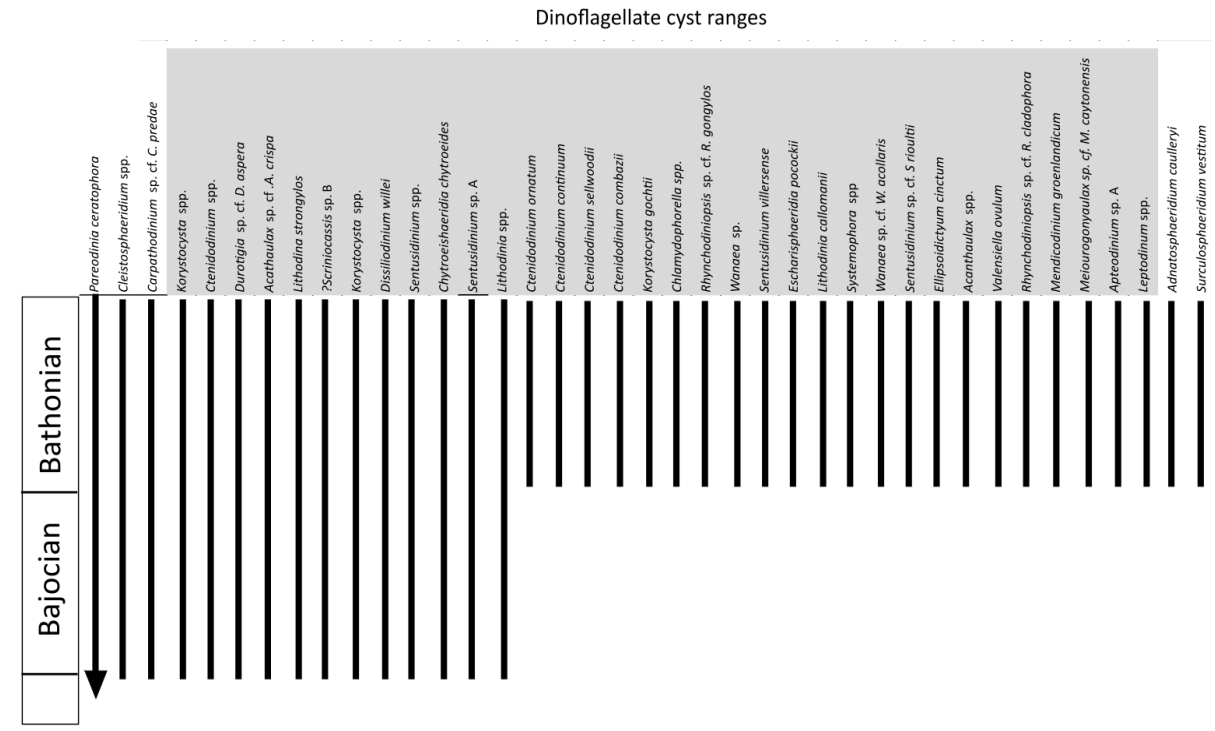

Figure 8.14. Dinoflagellate cyst range chart for the Bajocian–Bathonian of Egypt.
Grey fill denotes gonyaulacacean taxa. Note the large number of gonyaulacacean appearances through the Bajocian–Bathonian. Based on data from Ibrahim et al. (2002).

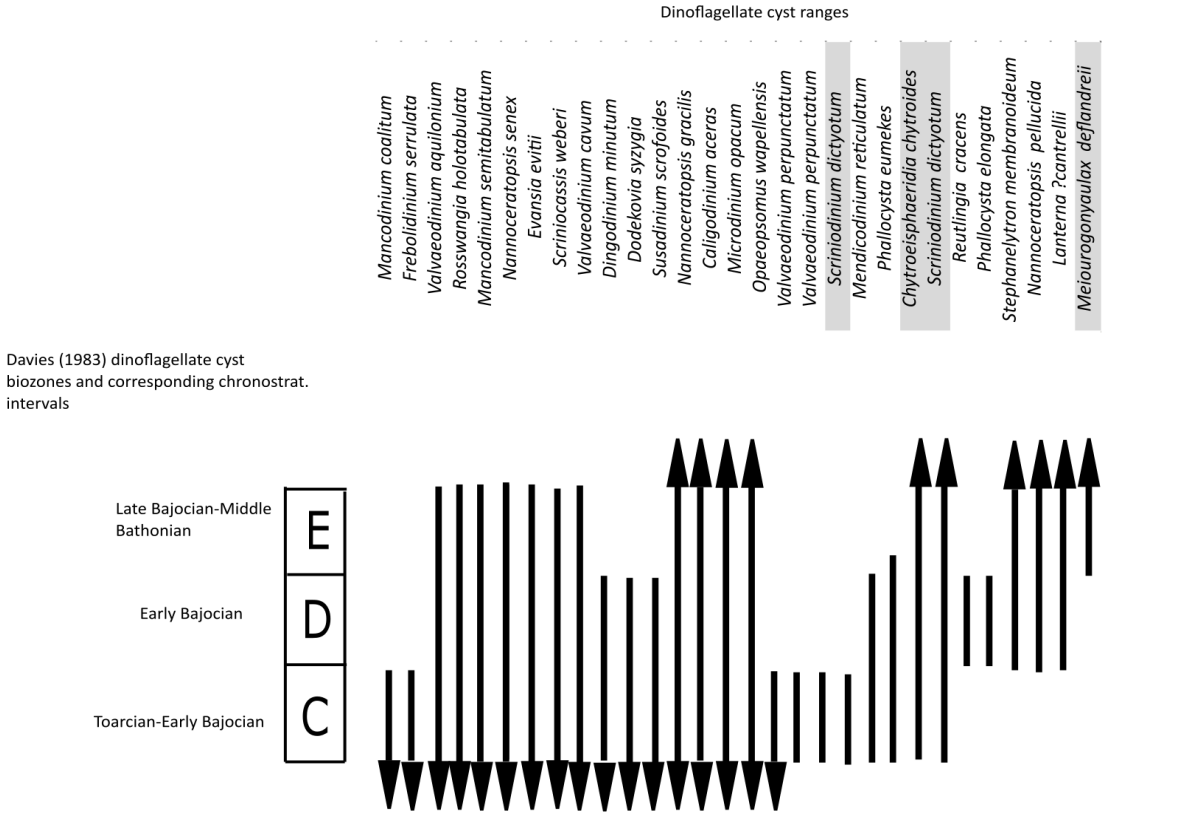

Figure 8.15. Dinoflagellate cyst range chart for the Middle Jurassic of the Sverdrup Basin, Arctic Canada.
Grey fill denotes gonyaulacacean taxa. Note the low number of gonyaulacacean appearances, and low number of dinoflagellate cyst appearances in general through the Bajocian to Bathonian.

dominated by gonyaulacaceans (Table 8.1a). Summarily, there is clearly an increase in the richness of gonyaulacacean dinoflagellate cysts through the Bajocian–Bathonian in the low palaeolatitudes.

Gonyaulacaceans do not appear to have radiated through the Bajocian in the high palaeolatitudes, as this group comprises only a minor component of dinoflagellate cyst floras from the Middle Jurassic of the Sverdrup Basin (Table 8.1b; Davies, 1983). Within dinoflagellate cyst floras from the Sverdrup Basin, there are only thirteen appearances through the Bajocian–Middle Bathonian, of which four are gonyaulacaceans (Figure 8.15). As such, the Gonyaulacacae appear to have been taxonomically and ecologically dominant in the low to mid-palaeolatitudes.

8.4.2. Controls on the global pattern: oceanographic and climatic factors

Gonyaulacacean dinoflagellate cysts increased in richness through the Bajocian–Bathonian in the low to mid palaeolatitudes of the northern and southern hemispheres. This increase in richness occured through a range of palaeoenvironments, from shallow marine and marginal marine settings in Australia to the offshore regions and carbonate ramps of the European Epicontinental Seaway. The extent to which sea level controlled the pattern of gonyaulacacean diversification during the Mid Jurassic was variable between different regions. In certain areas, transgression drove palaeoenvironmental shifts, which were associated with an increase in gonyaulacacean richness. For example, in eastern Canada, the large number of gonyaulacacean appearances in the Bathonian is linked with the spread of marine conditions. Similarly, in Israel, the increase in richness parallels a switch from marginal to shallow marine deposition. In Egypt, the appearances recorded from the Bajocian are broadly correlated with a transgressive episode, however, regressive conditions persisted through the Bathonian, and gonyaulacacean appearances and richness increased significantly through this interval (Figure 8.14). A similar decoupling between sea level rise and diversification can be observed from Australia. Low-richness gonyaulacacean dinoflagellate cyst assemblages are recorded from the Lower Bajocian shallow marine successions of the Atholl Formation, which was laid down during a major marine transgression. In contrast, Mantle and Riding (2012) recorded a significant increase in the richness of gonyaulacacean dinoflagellate cysts through Upper Bajocian–Lower Bathonian of the Plover Formation, which was laid down under widespread regressive conditions, in a nearshore depositional environment. As such, there is no simple global correlation between sea level rise and an increase in gonyaulacacean dinoflagellate cyst richness.

In Europe, the increase in gonyaulacacean richness appears to have been controlled by a combination of rising sea levels, and a change in the tectonic configuration of ocean gateways, which enhanced floral interchange, as Europe lay at the interchange between the northwest Tethys, and the Panthalassa Ocean via the Hispanic Corridor. In other regions, such as eastern Canada and North Africa, the increase in gonyaulacacean dinoflagellate cyst richness is clearly related to shifts in palaeoenvironment, controlled by sea level rise. However, in Australia, the main phase of diversification occurred during widespread

regression, suggesting that wider oceanographic factors have played a role. Mantle and Riding (2012) argued that cosmopolitan dinoflagellate cyst associations through the Bajocian–Bathonian between Europe and Australia were driven by a large-scale ocean gyre, the Tethys circumglobal current, which drove the passive dispersal of dinoflagellate cysts between the northern and southern Tethys (Chapter 1). As such, newly emerging gonyaulacaceans through the Bajocian may have been widely distributed by this ocean current between the northern and southern Tethys. The only region that does not record a significant increase in gonyaulacacean richness is the high palaeolatitudes, which may indicate that gonyaulacaceans were adapted to warmer climatic conditions, and were thus palaeoclimatically partitioned during the Bajocian–Bathonian. Conversely, the increase in richness through the low to mid-palaeolatitudes in the Mid Jurassic appears to have occurred during a 'cool mode' of the Jurassic (Chapter 1).

8.4.3. Sea level and climate as drivers of diversification

Although the Bajocian was characterised by a significant increase in gonyaulacacean dinoflagellate cyst disparity, it is still possible that this was simply an increase in the proportion of encysting dinoflagellates, driven by increased area of epicontinental seas, as the (Early) Bajocian in several regions was marked by transgression. However, while the Aalenian was largely regressive in Europe, evidence of low sea levels globally is largely lacking (Hallam, 2001). Comparison of global palaeogeographical maps from the Aalenian and Bajocian–Bathonian indicates that widespread epicontinental seas were present throughout much of the world during the Aalenian (Figure 8.16), yet gonyaulacaceans were low in richness through this interval. As such, an increase in cyst production from rising sea level is difficult to reconcile. Similarly, for these reasons, it does not appear that sea level directly drove the diversification of gonyaulacacean dinoflagellates via the creation of shallow-marine ecospace. Furthermore, the Late Pliensbachian was a critical interval of dinoflagellate evolution, yet dinoflagellates diversified at a time of widespread regression (Chapter 1; van de Schootbrugge et al., 2005). Similarly, the earliest Jurassic was marked by a widespread marine transgression during the Hettangian, yet dinoflagellate cysts were extremely low in richness through this interval (Figure 1.1; Hallam, 2001; van de Schootbrugge et al., 2013).

Dinoflagellates appear to have diversified during cool intervals of the Early–Mid Jurassic. Sea surface temperature is an important control on the ecology and biogeographical distribution of Recent dinoflagellates (e.g. Wall et al., 1977; Zonneveld et al., 2013). However, in addition to controlling sea surface temperature, climate is a major control on water column structuring within the oceans. In general, cooling climate increases the Earth's latitudinal temperature gradient, which enhances wind-driven mixing, vertical upwelling and turbulence (Falkowski and Oliver, 2007). In the past, dinoflagellates have been interpreted as preferring conditions of low turbulence, with coccolithophores and diatoms preferring moderate and high levels of turbulence respectively (Margalef, 1978). However, it has increasingly been recognised that dinoflagellates exhibit a far wider range of ecological strategies and habitats, than either

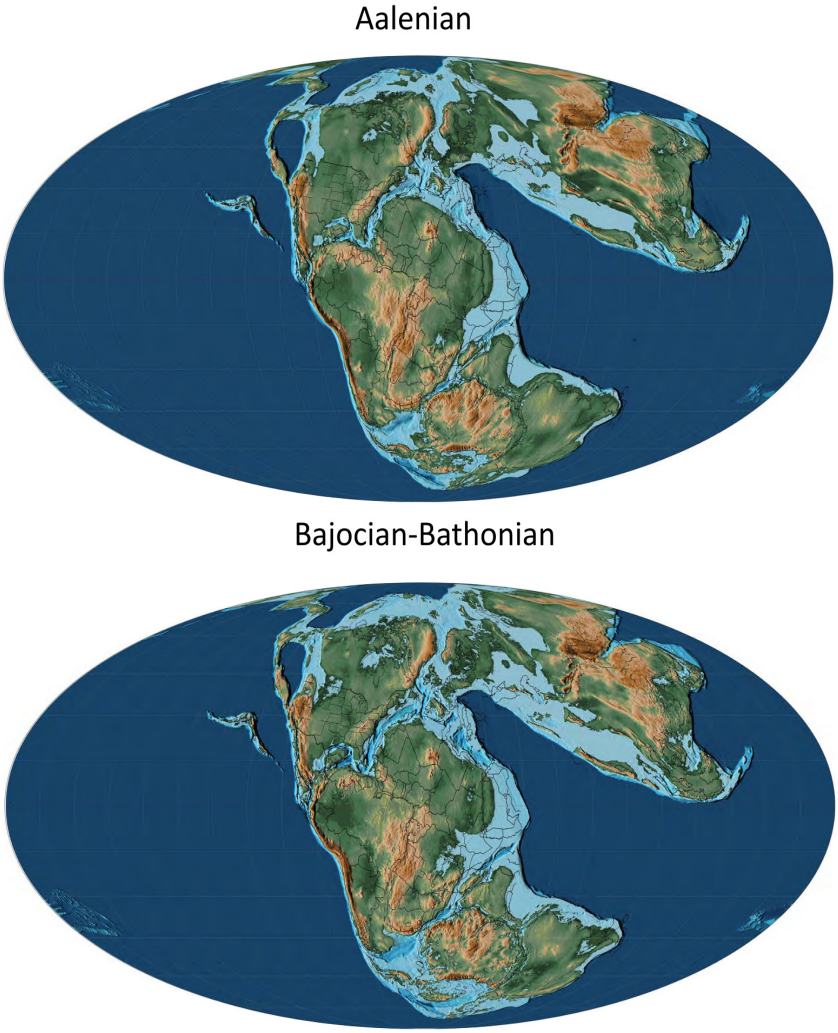

Figure 8.16. Comparison of flooded continental area for the Aalenian vs Bajocian–Bathonian.
Note that extensive epicontinental seas were present through the Aalenian, yet gonyaulacacean richness was low at this time. Modified from Scotese (2014).

the coccolithophores or the diatoms (Smayda and Reynolds, 2003). The occurrence of dinoflagellate blooms in turbulent upwelling regions challenges the supposition that the group requires low turbulence (Smayda and Reynolds, 2003; Smayda, 2010). As such, cooling climate may have driven evolutionary and ecological changes within dinoflagellates via changes in water column structure during the Jurassic. For example, the major pulse of dinoflagellate diversification during the Late Pliensbachian was linked to a phase of climatic cooling, which may have allowed Boreal taxa to spread into the mid northerly palaeolatitudes (Chapter 1; van de Schootbrugge et al., 2005). These authors argued that cooling in the mid-palaeolatitudes drove the diversification of dinoflagellates by changes in ocean ventilation, with strengthened north-easterly trade winds promoting enhanced vertical mixing and upper water column turbulence within the European Epicontinental Seaway. These conditions created ventilated bottom waters, favouring encysting dinoflagellates (van de Schootbrugge et al., 2005). Given that the Aalenian–Bathonian was a time of predominantly cool temperatures in Europe (with the possible exception of the *S. humphriesianum* zone), it is possible that a similar situation prevailed during the Bajocian. However,

the Late Pliensbachian was marked by the incursion of Boreal taxa into Europe (Bucefalo Palliani and Riding, 1997). In contrast, in the Bajocian, gonyaulacaceans appear to have formed a comparatively minor component of dinoflagellate cyst floras in the high palaeolatitudes. Moreover, marine connection through the Viking Corridor was reduced by thermal doming in the North Sea (Korte et al., 2015). These factors suggest that gonyaulacaceans did not migrate from higher palaeolatitudes into Europe during the Bajocian, and that gonyaulacaceans appear to have been poorly-adapted to cooler conditions. As such, cooling climate does not appear to form the underlying driver of diversification. Further, there is a ~5 million-year gap between cooling across through the Early–Mid Jurassic transition and the diversification of gonyaulacaceans in the Bajocian. Additionally, gonyaulacaceans reached their maximum richness in the largely warm conditions of the Cretaceous (see Fensome et al., 1996). These factors suggest that climate did not drive the diversification of gonyaulacacean dinoflagellates during the Mid Jurassic.

8.5. Palaeoecological patterns within Mid Jurassic dinoflagellate cysts from northwest Europe

8.5.1. Introduction

The relative abundances of dinoflagellate cyst taxa in the modern oceans is strongly related to sea surface conditions such as nutrient level, salinity and temperature (e.g. Wall et al., 1977; Marret and Zonneveld, 2003; Zonneveld et al., 2013). However, the palaeoecology and palaeoenvironmental distribution of Jurassic dinoflagellate cysts is relatively poorly known. Several studies have examined the responses of Early Jurassic dinoflagellate cyst floras to changing palaeoenvironmental conditions, particularly oceanic anoxic events (OAEs), most notably the Toarcian OAE (e.g. Bucefalo Palliani et al., 2002; van de Schootbrugge et al., 2005, 2013; Riding et al., 2013).

However, there has been relatively little work on the palaeoenvironmental distribution and palaeoecology of Mid Jurassic dinoflagellate cysts (Mantle, 2009), particularly for the Bajocian. Comparison of the abundance distribution of dinoflagellate cyst taxa from the Swabian, Wessex, and Paris basins, to their palaeoenvironmental and palaeogeographic distribution has allowed inferences to be made about the palaeoecological preferences of key taxa.

8.5.2. Eurytopic/cosmopolitan dinoflagellate cyst taxa

Several taxa have been recorded in moderate abundances in all areas I have studied, indicating that they were tolerant of a wide range of palaeoenvironmental conditions. *Batiacasphaera* spp. has been recorded throughout the Bajocian in all basins studied, indicating this group was tolerant of a wide-range of nutrient levels, salinities and temperatures. Similarly, the *Ellipsoidictyum/Valensiella* complex is abundant in the Upper Bajocian of all regions studied, indicating this group could tolerate a wide range environmental conditions. *Batiacasphaera* has been reported from equatorial palaeolatitude regions as well as the mid-palaeolatitudes of the southern Hemisphere (Table 8.1a, b), indicating a cosmopolitan distribution. Similarly, the *Ellipsoidictyum/Valensiella* complex has been reported from the mid to low

palaeolatitudes of the northern and southern hemispheres (Tables 1a, b). However, abundance distribution of other taxa can be observed to be more constrained, both spatially and temporally, indicating adaption to a narrower range of palaeoenvironmental conditions.

8.5.3. Palaeoenvironmentally restricted dinoflagellate cyst taxa

8.5.3.1. Dissiliodinium giganteum

A striking pattern within dinoflagellate cyst assemblages from the Swabian Basin is the dominance of *Dissiliodinium giganteum* in the prodelta deposits of the Wedelsandstein Formation (figures 3.8a, 3.9). I have also recorded *Dissiliodinium giganteum* in moderate abundances (10–25% of dinoflagellate cysts) from the Lower Bajocian (*W. laeviuscula* and S. *propinquans* zone) of the Hebrides Basin of Scotland (Figure 4.18). Elsewhere in Europe, *D. giganteum* has been reported in superabundance from the *W. laeviuscula* zone of Switzerland (Feist-Burkhardt and Götz, 2016). Gedl (2008) and Gedl and Józsa (2015) reported superabundant "blooms" of *Dissiliodinium giganteum* from the Lower Bajocian deep marine flysch and hemipelagic deposits of the Pieniny Klippen Basin of southern Poland/northern Slovakia. However, *Dissiiodinium giganteum* is present in low abundances in the Lower Bajocian of the Wessex and Paris Basins.

Based on palaeoenvironmental distribution, *Dissiliodinium giganteum* may have thrived under high-nutrient levels and could tolerate reduced salinities. In the Swabian Basin, the Lower Bajocian Wedelsandstein Formation was deposited in a prodelta environment in which the proximity to terrigenous discharge would have resulted in elevated nutrient levels (Chapter 3). Similarly, the *W. laeviuscula*/ *S. propinquans* zones in the Hebrides Basin are represented by the Holm Sandstone Member, which was deposited in a deltafront/estuarine tidal channel palaeoenvironment (Mellere and Steele, 1996). In Switzlerland, *D. giganteum* is abundant in the Lower Bajocian in facies which contain abundant sporomorphs (Hostettler et al., 2017). A similar situation pertains in the Polish Pieniny Klippen Basin, as Lower Bajocian deposits contain abundant terrigenous material (Gedl, 2008; Gedl and Józsa, 2015).

The morphology of *Dissiliodinium giganteum* further suggests an adaptation to meso-eutrophic conditions; this species is typically 90 µm in size and can reach 140 µm (Chapter 7). As most dinoflagellate cysts typically have a 1:1 ratio of cyst:motile cell size (Finkel et al., 2007), the motile cell of *D. giganteum* can be interpreted to be of an unusually large overall size. Large phytoplankton cells require higher nutrient levels due to their lower surface area to volume ratio, which limits the diffusive uptake of nutrients (Marañón, 2015). Moreover, the high abundances of *Dissiliodinium* in the Lower Bajocian suggests it formed algal blooms, which frequently form in response to elevated nutrient levels (Anderson et al., 2008).

The presence of *Dissiliodinium giganteum* from southern Germany to Scotland indicates a distribution from around 30–40°N in the European Seaway during the Bajocian. Oxygen isotopes record a temperature difference between southern Germany and Scotland during the Aalenian to Bajocian of

~5°C (Figure 1.7). Consequently, the palaeoenvironmental distribution of *D. giganteum* does not appear to have been strongly related to temperature. The moderate abundance of this taxon from nearshore deltafront/tidal channel deposits (Hebrides Basin) to superabundance in prodelta deposits (Swabian Basin) to deep marine flysch (Poland/northern Slovakia) indicates it could tolerate a range of salinities, but exhibited greatest abundance in normal salinity settings. However, the primary control on the palaeoenvironmental distribution of *D. giganteum* appears to be the availability of nutrients. The low abundance of *Dissiliodinium giganteum* in the Wessex and Paris basins may therefore indicate that these basins had relatively low nutrient levels. This is supported by the relatively low amount of siliciclastic material in these basins, indicating a low amount of terrigenous input. Assemblages from the Lower Bajocian of the Wessex and Paris basins are dominated by the cosmopolitan *Batiacasphaera* spp.. With the exception of a few specimens recorded from the Bajocian of Iran (Skupien et al., 2015), the palaeogeographic distribution of *D. giganteum* appears to be restricted to Europe.

8.5.3.2 Sentusidinium spp.

Sentusidinium spp. is moderately abundant through the Upper Bajocian of the Swabian Basin, and in the Lower Bathonian of the Paris Basin (figures 3.8b, 3.9; 5.9). The appearance, and subsequent abundance of this group in the Swabian Basin is coincident with the transition from the Ostreenakalk to Hamitenton formations (figures 3.8b, 3.9), which marks a transition to deeper, more offshore conditions (Chapter 3). Similarly, the increase in abundance of this group in the Lower Bathonian of the Paris Basin is correlated with maximum flooding of the T7 sea level cycle (Figure 5.9). Moreover, Riding et al. (1991) recorded moderate abundances (>15%) of this group from the marine shales of the Garantiana Clay Member in the Hebrides Basin, which represents a major marine incursion. These patterns strongly suggest that *Sentusidinium* spp. was adapted to normal salinity, fully-marine conditions. Additionally, the morphology of *Sentusidinium* spp. is essentially a proximochorate version of *Batiacasphaera* spp. (Chapter 6). As discussed in Chapter 1, changes in process morphology with salinity have been observed from several Recent dinoflagellate cyst taxa. Consequently, *Sentusidinium* may represent ecophenomorphs of *Batiacasphaera* produced in response to normal salinity conditions, or alternatively reflect a genus adapted to fully marine conditions. *Sentusidinium* spp. has been recorded from equatorial palaeolatitudes (Table X), and in very low abundances from nearshore facies of the Bajocian–Bathonian of Australia (Mantle and Riding, 2012). Therefore, this group had a wide palaeogeographic distribution in the Mid Jurassic, but appears to have been most abundant in normal marine palaeoenvironments.

8.5.3.3. Acanthaulax crispa

The abundant occurrence of *A. crispa* is largely restricted to the Ostreenkalk and Hamitenton formations (*S. humphriesianum–G. garantiana*) zones of the Swabian Basin. As with *Sentusidinium* spp., the abundance of this taxon may have been controlled by salinity. Butler et al. (2005) reported occasional occurrences *A. crispa* from the Scarborough Formation of the Cleveland Basin, northern England. This formation was laid down in a shelfal palaeoenvironment but the relatively low (~10%) marine

microplankton component suggests a fairly nearshore environment of deposition (Gowland and Riding, 1991). As such, the high abundance of this taxon in the offshore conditions of the Swabian Basin indicates an adaption to more normal marine salinities. Rare occurrences of *Acanathaulax crispa* were recorded by Mantle and Riding (2012) from nearshore facies of the Bajocian–Bathonian of Australia, and this taxon is also present in the equatorial palaeolatitudes (Qatar-Table X). As with *Sentusidinium* spp., this indicates a wide palaeogeographic distribution, but *A. crispa* was most abundant in palaeoenvironments with normal marine salinities.

8.5.3.4. Ctenidodinium combazii and Ctenidodinium cornigerum

In both the Swabian and Paris basins, the Lower Bathonian is marked by the acme of *Ctenidodinium* (Figure 8.17). In the Swabian Basin, *Ctendidoinium combazii* has a prominent acme in the *M. macrescens* and *A. tenuiplicatus* subzones of the *Z. zigzag* zone, where it comprises ca. 45% of dinoflagellate cysts (compared to <1% in the underlying *P. convergens* subzone - Figure 8.10). *Ctenidodinium cornigerum* and *C. sellwoodii* also increase in abundance through this interval. The abundance of *C. combazii* in the Swabian Basin is coincident with the deposition of the Dentalienton Formation, which is bounded at the base by a maximum flooding surface, marks the maximum transgression of the T7 cycle. Palynomorph assemblages from the Dentalienton Formation record the highest marine:terrestrial ratios (~0.95) seen in the Swabian succession, clearly reflecting distal, offshore conditions (Chapter 3; figures 3.5, 3.13). In the northwest Paris Basin, there is an increase in the abundance of *Ctenidodinium cornigerum* in the *O. yeovilensis* subzone, where it forms around 50% of dinoflagellate cysts (compared to <5% in the underlying *M. macrescens* subzone, Figure 8.15). Similarly, *C sellwoodii* and *C. combazii* also increase in abundance. The Lower Bathonian of the Paris Basin is largely represented by the Marnes de Port-en-Bessin Formation, which is bounded at the base by a maximum flooding surface, and also represents the maximum transgression of the T7 sea level cycle (Chapter 5; Rioult et al., 1991). Palynomorph assemblages record the highest marine:terrestrial ratio (~0.90) observed from the Paris Basin, clearly indicating offshore, distal conditions (Chapter 5, figures 5.8, 5.10).

The abundance of *Ctenidodinium* in sediments deposited under maximum flooding strongly indicates these taxa were sensitive to changes in palaeosalinity. Riding et al. (1985) noted that *C. combazii* is abundant throughout much of northwest Europe during the Bathonian, but was absent from central/ northern England until the Late Bathonian, when the transgressive Cornbrash Formation was deposited, reflecting a switch from brackish/marginal marine conditions to deeper, fully-marine conditions. Therefore, Riding et al. (1985) argued that *C. combazii* was adapted to offshore, fully-marine conditions, which is supported by the data from the Swabian Basin. However, in the Paris Basin, *C. cornigerum* is numerically superior to *C. combazii* (Figure 8.15), even though Lower Bathonian deposits were laid down under maximum transgression.

This pattern may have been driven by differences in temperature, nutrient levels or small variations in

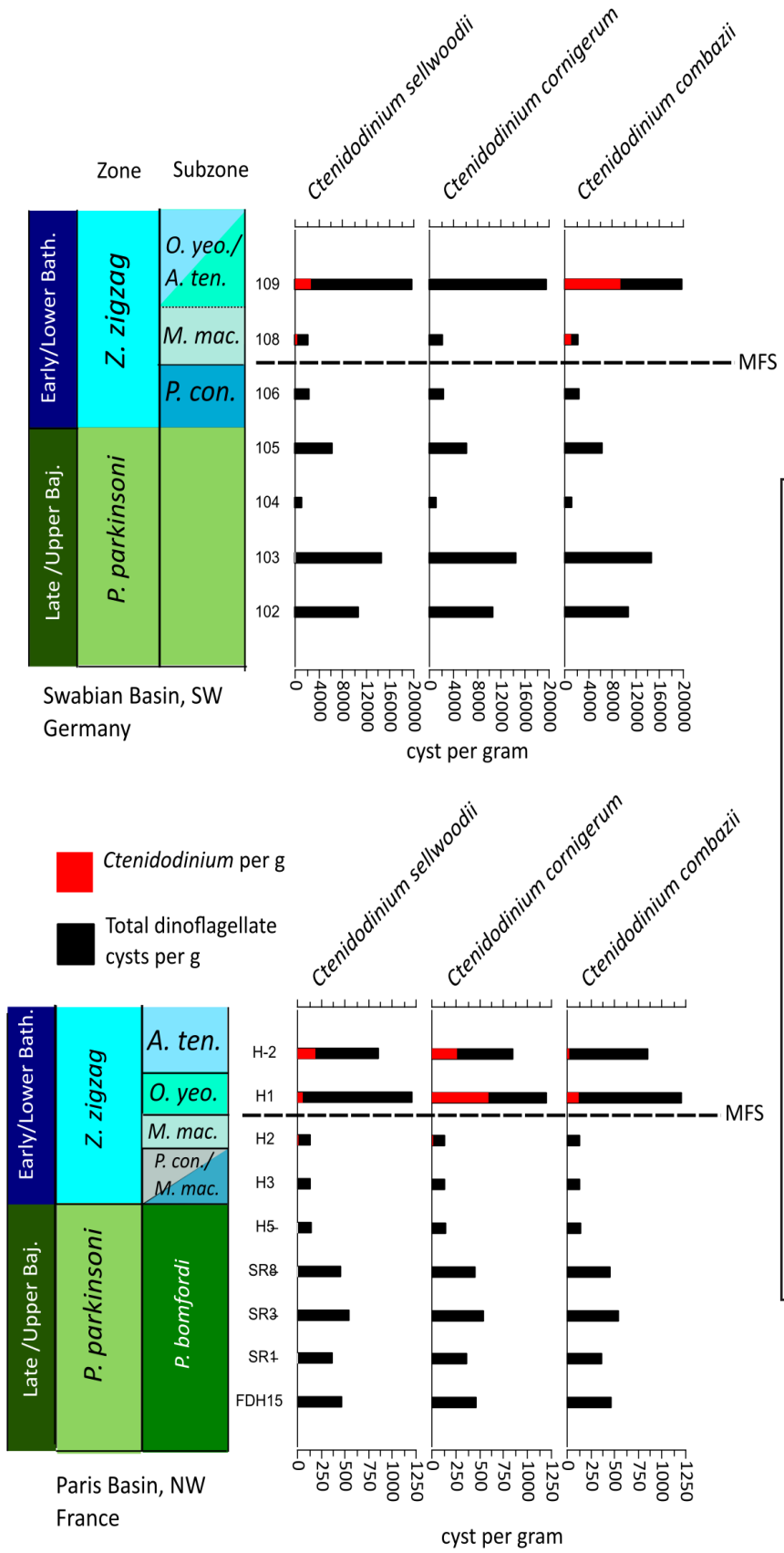

Figure 8.17. Comparison of *Ctenidodinium* absolute and relative abundances for the Bajocian–Bathonian transition of the Swabian and Paris basins. In the Swabian Basin, *C. combazii* increases in abundance to respresent around 50% of dinoflagellate cysts in the Lower Bathonian *Z. zigazag* zone, *M. macrescens* and *O. yeolvilensis/A. tenuiplicatus* subzones. In the Paris Basin, *Ctenidodinium cornigerum* increases in abundance to represent around 50% of dinoflagellate cysts through the *O. yeovilensis* and *A. tenuiplicatus* subzones. The relative location of the T7 maximum flooding surface (MFS) is shown.

salinity between the two basins. It is possible that the differences in sea surface temperature drove the different abundance patterns in *Ctenidodinium* between the Swabian and Paris basins. However, two factors argue against this. Firstly, the Swabian and Paris basins were separated by only a few degrees of palaeolatitude, and it is therefore unlikely there were significant differences in seawater temperatures

between the two depocentres. Oxygen isotopes from belemnites show comparable values for the Late Bajocian–Early Bathonian of the Paris Basin *versus* Germany (Brigaud et al., 2009 fig. 9.) Secondly, *C. combazii* migrated northwards during the Bathonian to Callovian, during an interval which was characterised by the southward spread of Boreal ammonites, and thus cooler temperatures, indicating it was not sensitive to temperature changes (Riding et al., 1985).

Gedl (2012) and Gedl et al. (2012) reported peaks in the abundance of *C. combazii* associated with terrestrial influx and higher sedimentation rates in the Middle Bathonian of central Poland. Consequently, these authors interpreted *C. combazii* as having thrived in conditions of enhanced nutrient levels and slightly reduced salinities (Wiggan et al., 2017). The coincidence of the abundance of *C. combazii* with maximum flooding in the Swabian Basin strongly indicates it was adapted to normal salinity conditions. However, the lower abundance of this species in the Paris Basin may indicate that *C. combazii* was sensitive to changes in nutrient levels. The carbonate ramp palaeoenvironment of the Paris Basin may have had lower nutrient levels in comparison to the Swabian Basin due to lower terrestrial input. The morphologies of *C. cornigerum* and *C. combazii* may also reflect adaptations to differing nutrient levels. *Ctenidodinium corgierum* is generally smaller than *C. combazii* (Chapter 6), and larger phytoplankton cells generally require higher nutrients (Marañón, 2015).

The abundance of *C. cornigerum* in deposits deposited under maximum transgression in the Paris Basin suggests that, like *C. combazii*, *C. cornigerum* was adapted to fully marine conditions. However, lower nutrient levels may have driven the dominance of *C. cornigerum* over *C. combazii* in the Swabian Basin. This is supported by data from the Wessex Basin, as *C. cornigerum* is abundant in the uppermost *P. parkinsoni* zone (Figure 4.10), indicating this species was prevalent in low-nutrient conditions of the carbonate ramp palaeoenvironments of the Paris and Wessex basins.

8.5.3.5. Summary

In summary, spatial and temporal patterns in the relative abundances of dinoflagellate cyst taxa through the successions studied can be clearly related to contrasting palaeoenvironmental conditions. In the Swabian Basin, the Lower Bajocian Wedelsandstein Formation is dominated by the abundance of *Dissiliodinium giganteum*, which thrived in high nutrient conditions. In contrast, the Ostreenkalk and Hamitenton formations are dominated by the abundances of *Acanthaulax crispa*, *Batiacasphaera* spp., the *Ellipsoidictyum/Valensiella* complex, and *Sentusidinium* spp.. The similar abundances of these groups reflects a mixture of eurytopic/cosmopolitan taxa (*Batiacasphaera* spp. and the *Ellipsoidictyum/Valensiella* complex) and taxa adapted to normal salinity conditions (*Acanthaulax crispa* and *Sentusidinium* spp.). The Lower Bathonian is marked by the acme of *Ctenidodinium combazii,* which was driven by the spread of normal salinity, fully marine conditions during maximum transgression. In contrast, assemblages from the Bajocian of the Wessex Basin exhibit less temporal variability. The Lower Bajocian is dominated by *Batiacasphaera* spp., whilst the Upper Bajocian is dominated by *Batiacasphaera* spp.

and the *Ellipsoidictyum/Valensiella* complex, indicating that restricted palaeoenvironmental conditions precluded the abundances of more stenotopic taxa, such as *Dissiliodinium giganteum*. Similarly, the Lower Bajocian of the Paris Basin is dominated by *Batiacasphaera* spp., whilst Upper Bajocian (*P. parkinsoni* zone) is dominated by *Batiacasphaera* spp., and the *Ellipsoidictyum/Valensiella* complex, demonstrating this carbonate ramp environment was also dominated by eurytopic groups. However, the Lower Bathonian is marked by the acme of *Ctenidodinium cornigerum,* which is coincident with maximum flooding, indicating the abundance of this species was driven by nomal salinity conditions. The dominance of this species over *C. combazii* in the Paris Basin may indicate an adaption to lower nutrient levels.

8.5.4. The Early Bajocian acme of **Dissiliodinium** *and the Early Bajocian positive carbon isotope excursion (CIE)*

During the Early Bajocian in Europe, there was a positive shift in $\delta^{13}C$ recorded from marine carbonate and organic matter (Chapter 7). This carbon-cycle perturbation has been related to a brief interval of intensified run-off and nutrient flux from enhanced continental weathering, driven by a shift to a more humid climate in Europe, or enhanced upwelling (Chapter 7; Suchéras-Marx et al., 2015). Previous work has argued that enhanced nutrient levels drove increased productivity of coccolithophores and radiolarians (e.g. Aguado et al., 2017); my work indicates that a similar pattern may be seen within dinoflagellate cyst floras. During the Early Bajocian in Europe, *Dissiliodinium giganteum* was abundant in southern Germany, Poland/northern Slovakia, Switzerland, and northwest Scotland, and appears to have thrived in palaeoenvironments which had elevated nutrient levels. Further, the acme of *D. giganteum* is broadly coincident with the Early Bajocian positive carbon isotope shift (Figure 8.18; Chapter 7). Given the abundance of *D. giganteum* in areas close to terrigenous input, the short-lived acme of *Dissiliodinium* during the Early Bajocian may have been driven by enhanced run-off, as the abundance of this species in areas close to the proximity of terrestrial discharge is inconsistent with a regime of nutrients delivered from upwelling. Intriguingly, *Dissiliodinium* appears to have also been abundant in the mid-palaeolatitudes of the southern Hemisphere during the Early Bajocian (figures 8.19, 8.20). The Lower Bajocian of offshore Western Australia is marked by an acme of *Dissiliodinium caddaense* (Figure 8.19; Riding et al, 2010b). The *D. caddaense* dinoflagellate cyst biozone has been correlated by ammonites and strontium isotopes to be coeval with the *W. laeviuscula* ammonite zone of Europe (section 8.4; Riding et al., 2010b). Consequently, the acme of *D. caddaense* is synchronous with the acme of *D. giganteum* in Europe. Moreover, *D. caddaense* is typified by large size (~150 μm; Helby et al., 1987) and is recorded in abundance from the Athol Formation, which was deposited in a nearshore depostional environment (Riding et al., 2010b). These data suggest that like *D. giganteum*, *D. caddaense* was adapted to high nutrient levels and could tolerate lowered salinities. Furthermore, *Dissiliodinium* is also abundant in the Lower Bajocian of the Neuquén Basin of Argentina (Figure 8.19; Stukins et al., 2013). In this region, *D. psilatum* dominates assemblages in the marginal/deltaic palaeoenvironments of

the Neuquén Basin (Stukins et al., 2013). *Dissiliodinium psilatum* is of comparable morphology to *D. giganteum* and, although slightly smaller, is still relatively large with an average width of 80 µm (Prauss, 1989). The abundance of this species in nearshore and deltaic deposits indicates it could tolerate reduced salinities, and the proximity to terrigenous discharge and relatively large size indicate an adaption to high nutrient levels.

The synchronous acme of *Dissiliodinium* in the mid-palaeolatitudes of the northern and southern hemispheres, and the coincidence between this pattern and Early Bajocian positive carbon isotope excursion (CIE), may indicate that a humid climate drove enhanced run-off in mid-palaeolatitudes of both the northern and southern hemispheres. Alternatively, this pattern could simply reflect that this genus was prevalent in high nutrient palaeoenvironments during the Early Bajocian. However, the acme of *Dissiliodinium* broadly parallels the diversification and ecological expansion of the coccolith genus *Watznaueria.* During the Late Aalenian to Early Bajocian, coccolith floras became overwhelmingly dominated by the genus *Watznaueria* (see Suchéras-Marx et al., 2015). Prior to the Early Bajocian, this genus was only a minor component of coccolith assemblages, but through the Early Bajocian *Watznaueria* diversified and expanded to become the dominant coccolith genus, and remained so for the for the rest of Mesozoic (Suchéras-Marx et al., 2015). Similarly, *Dissiliodinium* appeared in the Mid Aalenian as *D. lichenoides* (Feist-Burkhardt and Pross, 2010), but diversified in the Late Aalenian to Early Bajocian

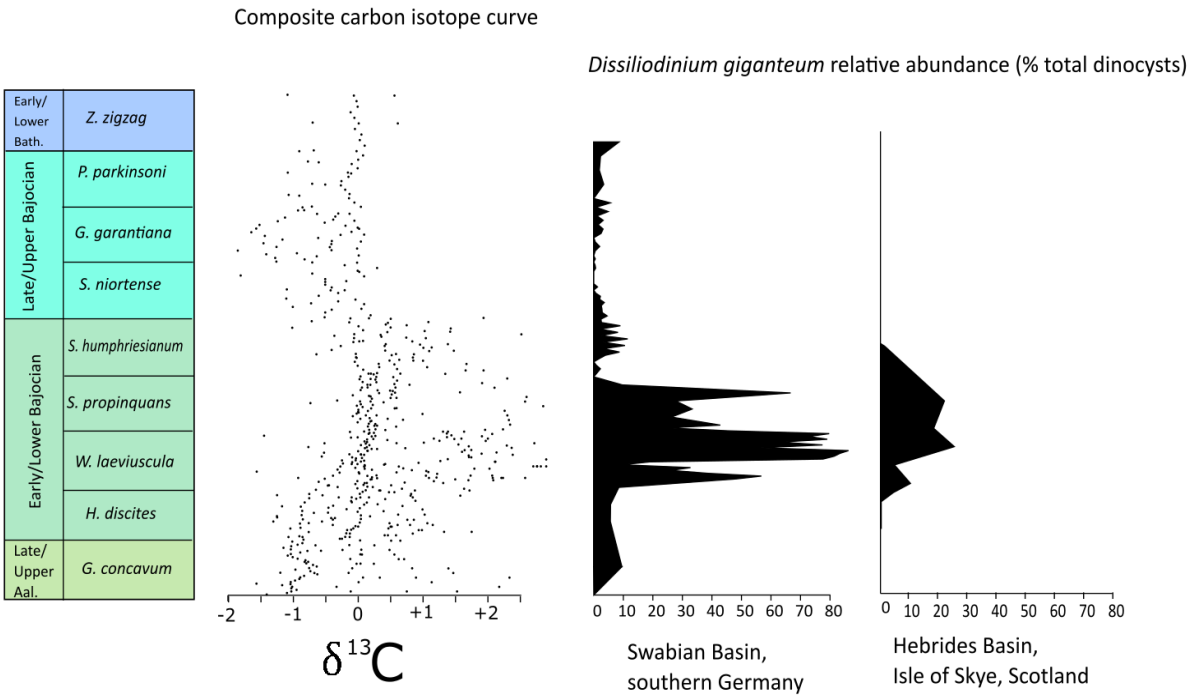

Figure 8.18. Relative abundances of *Dissiliodinium giganteum* through the Lower Bajocian, with comparison to $\delta^{13}C$ records.
Note the synchronous increase in the abundance of *D. giganteum* and the shift to more positive $\delta^{13}C$ values. Composite $\delta^{13}C$ curve based on raw data from figure 7.4. *Dissiliodinium* abundances from chapters 3 and 4.

with appearances of *D. giganteum*, *D*? *hocneratum*, *D psilatum* (Chapter 3; Table 3.2a; Prauss, 1989). At the same time, *Dissiliodinium* became ecologically prominent in several areas or Europe, and the Northwest Shelf of Australia, but formed a comparatively minor component of dinoflagellate cyst floras through the Late Bajocian in these regions (figures 8.8b, 8.9; Mantle and Riding, 2012, fig. 4). The decline in the abundance of *Dissiliodinium* in the Hebrides and Swabian basins is synchronous with a shift to a more distal palaeoenvironment, driven by transgression (section 8.3; Chapter 3). However, the fact that this genus comprised a relatively minor component of dinoflagellate cyst floras through the Late Bajocian–Early Bathonian in both Europe and Australia may indicate that it was out-competed by newly emerging gonyaulacacean taxa.

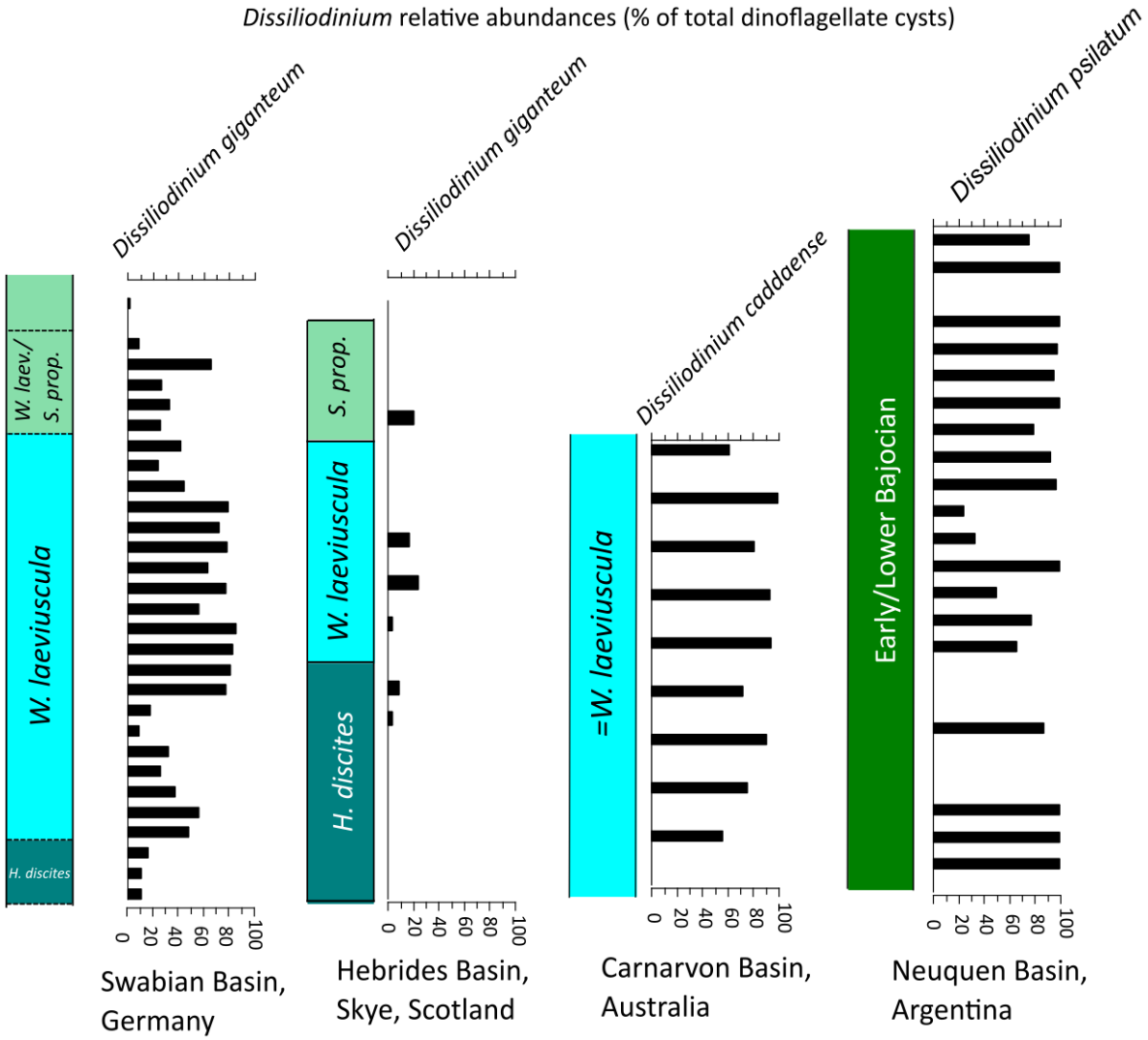

Figure 8.19. Relative abundances of *Dissiliodinium* for southern Germany, Skye, Australia, and Argentina. *Dissiliodinium* was abundant in several regions through the Early Bajocian. Abundances of *D. caddaense* based on raw data from Riding et al. (2010b). Abundances of *D. psilatum* from Stukins et al. (2013) raw data. Abundances plotted per sample (with no true vertical scale) for Germany, Australia and Argentina, plotted against section high for Skye.

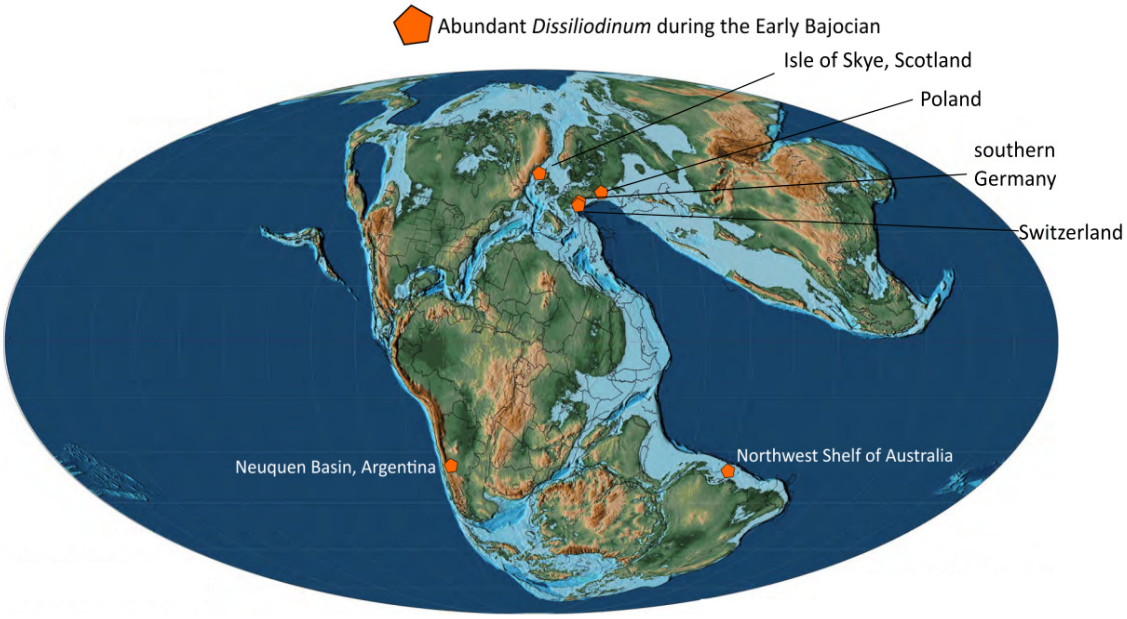

Figure 8.20. Palaeogeographic distribution of abundant *Dissiliodinium* during the Early Bajocian. *Dissiliodinium* was abundant in the mid-palaeolatitudes of the Northern and Southern hemispheres.. Palaeogeography modified from Scotese (2014)

In summary, there was an acme of *Dissiliodinium* during the Early Bajocian in the mid-palaeolatitudes of the northern and southern hemispheres. This pattern could simply reflect that this genus was prevalent in high nutrient palaeoenvironments during the Early Bajocian. Until such a time as this excursion, and accompanying palaeoenvironmental changes, can be fully documented from other regions, it remains unclear as to whether there was a wider climatic mechanism controlling the ecological prevalence of *Dissiliodinium* during the Early Bajocian. However, the temporal coincidence between the acme of *Dissiliodinium,* the positive CIE, and the ecological expansion of *Watznaueria* in Europe suggests that a brief interval of enhanced continental weathering and run-off could account for the acme of *Dissiliodinium* during the Early Bajocian.

8.6. Summary and final remarks

In this thesis, I have demonstrated that there was a significant increase in the richness of gonyaulacacean dinoflagellate cysts during the Bajocian in northwest Europe, which appears to reflect a true radiation of dinoflagellates. The basins I have studied record lithostratigraphic and palaeoenvironmental trends associated with sea level fluctuations, with an increase in gonyaulacacean richness broadly paralleling a second-order transgression. On a regional scale, the correlation between an increase in gonyaulacacean appearances and transgression indicates that sea level exerted significant control on the stratigraphic pattern, as many gonyaulacacean appearances coincide with pronounced third-order transgressive pulses. A rise in sea level, coupled with tectonic changes in ocean gateways, may have increased the water-mass transfer and floral interchange between the European Epicontinental Seaway,

the northwest Tethys and the Hispanic Corridor. Moreover, a spread of marine palaeoenvironments dispersed gonyaulacaceans through the European Epicontinental Seaway. Comparison to global records demonstrates that gonyaulacaceans increased in richness through the Mid Jurassic in the low to mid palaeolatitudes, and that dinoflagellate cyst floras were largely cosmopolitan. Sea level influenced the pattern of appearances through large-scale palaeoenvironmental shifts in several regions. In eastern Canada, numerous appearances are recorded from the Bathonian, which corresponds to a switch from marginal to fully marine conditions. Similarly, in Israel and Egypt the appearances of gonyaulacaceans in the Bajocian correspond to a transgressive phase and the spread of shallow marine palaeoenvironments. However, in Australia the main phase of diversification occurred during widespread regression, and gonyaulacaceans radiated through nearshore palaeoenvironments, indicating that sea level did not exert a global-scale control on the Bajocian diversification. Instead, the largely cosmopolitan associations of the low to mid-palaeolatitudes were likely driven by the Tethyan circumglobal current, which dispersed taxa between the northern and southern Tethys.

Within dinoflagellate cyst assemblages from northwest Europe, the temporal and spatial abundance distribution of taxa can be related to palaeoecological preferences arising from differing palaeoenvironmental settings from the areas I have studied. Further, large-scale palaeoceanographical and palaeoclimatic changes seem to have influenced these patterns on a regional, and possibly, global scale. Regionally, the acme of *Ctenidodinium* in the Early Bathonian appears to be related to oceanographic factors, as the acme of this genus is coincident with maximum transgression of the T7 cycle, and was driven by the spread of fully marine conditions. On a wider scale, the acme of *Dissiliodinium* during the Early Bajocian may have a global extent, as this genus appears to have been ecologically prominent in the mid-palaeolatitudes of the northern and southern hemispheres. The dominance of this genus may have been driven by an interval of intensified run-off, and corresponding nutrient increase, from enhanced continental weathering. On the basis of current data, this pattern cannot yet be fully resolved, but future work examining chemostratigraphic records from other regions, particularly the Northwest Shelf of Australia, would be able to demonstrate whether the Early Bajocian CIE was a global phenomenon. However, the acme of *Dissiliodinium* broadly parallels the ecological expansion of the coccolithophore *Watznaueria*, which represents a critical ecological transition within the evolutionary history of coccolithophores. In contrast, the ecological dominance of *Dissiliodinium* was relatively short-lived. However, the acme of *Dissiliodinium* was in turn a smaller component of the ecological expansion of the family Gonyaulacaceae. Viewed in this light, this ecological transition parallels that of the coccolithophores, but rather than one genus rising to ecological prominence, one family did instead.

Palaeoceanographic and palaeoclimatic changes appear to have controlled the stratigraphic pattern of the Bajocian radiation, as well as influencing palaeoecological patterns seen within dinoflagellate cyst floras, yet these factors do not appear to form the underlying driver of diversification. Although the

Bajocian was transgressive in several regions, extensive epicontinental seas were present throughout the preceding Aalenian, yet gonyaulacaceans were low in richness. Moreover, the pattern of diversification is not directly correlated with transgression on a global scale. Similarly, palaeoclimatic factors do not appear to have driven the diversification of this group. There is a ~5 myr gap between cooling in Europe through the Toarcian–Aalenian transition, and the radiation of gonyaulacaceans in the Bajocian. Additionally, the palaeobiogeographic distribution of gonyaulacaceans indicates that the group formed a relatively minor component of dinoflagellate cyst floras at high palaeolatitudes. As such, unlike the Late Pliensbachian, it does not appear that the Bajocian was marked by the southward migration of high palaeolatitude taxa. Consequently, climate does not appear to form an underlying driver of the radiation of gonyaulacaceans during the Mid Jurassic.

It is notable, however, that the richness of dinoflagellates and coccolithophores through the Early–earliest Mid Jurassic broadly mirrors that of pelagic and benthic metazoans, thereby suggesting a coupling between phytoplankton and metazoan evolution (Figure 1.9). The Mesozoic oceans were characterised by the escalatory evolution of predators and their prey, encapsulated in the concept of the Mesozoic Marine Revolution (Vermeij, 1977, 1987, 2008). Although the concept of the Mesozoic Marine Revolution was originally applied to the Cretaceous, it has since been realised that many of the escalation-related adaptions appeared through the Late Triassic–Early Jurassic (Harper et al., 1998; Vermeij, 2008). Notably, during the Mid Jurassic, important evolutionary and ecological changes occurred in planktivorous metazoans. The trophic guild of giant suspension feeding fishes, for example, first appeared in the Mid Jurassic, and the earliest fossil evidence of this group comes from the Bajocian (Friedman et al., 2010). Within other nekton, the Late Aalenian to Early Bajocian was characterised by the extinction of ammonite families which dominated Early Jurassic ammonite faunas, and their replacement by families which dominated through the Mid Jurassic (Sandoval et al., 2001). Moreover, the Bajocian was marked by the first appearance of heteromorph ammonites (O'Dogherty et al., 2006). Evidence from buccal morphology and fossilised food remains indicates that diet of both planispiral and heteromorph ammonites included mesozooplankton (Jäger and Fraaye, 1997; Kruta et al., 2011). Given the turnover within ammonites, and the appearance of giant suspension feeding fishes, these patterns may indicate that there were important evolutionary and ecological changes within mesozooplankton communities. Although the fossil record of mesozooplankton is extremely sparse (Selden et al., 2010), it is notable that many of the gonyaulacacean dinoflagellate cyst taxa which appeared through the Bajocian were characterised by thick walls and/or an ornament of sutural crests/spines e.g. *Acanthaulax*, *Aldorfia*, *Ctenidodinium, Gonyaulacysta* and *Meiourogonyaulax* (e.g. Chapter 6, plates I, II, and IX), and, there is a case for recognising the thick walls and ornaments as defensive adaptations (e.g. Sarjeant et al., 1987). Additionally, the presence of dinoflagellate cysts in zooplankton fecal pellets suggests that their predation might be a little-considered, but possibly important component of dinoflagellate ecology (Persson, 2000; Montresor et al., 2003). Given the temporal coincidence between phytoplankton diversification, and

groups of planktivorous cephalopods and fishes, these phenomena may indicate an underlying ecological driver to the Bajocian radiation, with connecting links provided by the mesozooplankton. Viewed in this light, the Mid Jurassic dinoflagellate radiation might represent a largely-overlooked component of the Mesozoic Marine Revolution.

8.7. Future directions

This thesis has demonstrated that there was a significant increase in the richness of gonyaulacacean dinoflagellate cysts through the Bajocian. However, the driver behind this radiation remains to be resolved, but could be related to the Mesozoic Marine Revolution. In order to further investigate the radiation of dinoflagellates in the Bajocian and accompanying palaeoecological changes, and to examine how this might be related to the Mesozoic Marine Revolution, the following ideas for future work are suggested:

1) Quantitative documentation of dinoflagellate cyst **diversity** through the Bajocian. The palynological data presented in chapters 3–5 have been used to assess species richness through the examined successions. However, as both species richness and the relative/absolute abundances of dinoflagellate cyst taxa have been documented, these data can be used to quantitatively assess dinoflagellate cyst *diversity*. This could be accomplished using diversity indices e.g. Simpson Index, Shannon Index etc. Moreover, the quantitative dinoflagellate cyst data presented by Mantle and Riding (2012) from the Bajocian of Australia could be used to provide a comparison from an area outside of Europe.

2) Assessment of the richness/diversity of other marine groups with comparison to dinoflagellates and other plankton. In order to assess how the radiation of dinoflagellates might be related to the wider Mesozoic Marine Revolution, the richness/diversity of dinoflagellates and other plankton through the Early–Mid Jurassic could be more closely compared with that of other pelagic groups such as ammonites and fishes. Moreover, at a finer temporal scale, species richness and diversity data for ammonites exists at an ammonite zonal level for much of the Jurassic (e.g. Sandoval et al., 2001), which could be compared directly to dinoflagellate cyst richness data through the Bajocian.

3) Investigation of Bajocian successions for Small Carbonaceous Fossils (SCFs). The mesozooplankton represent the most important trophic link between the phytoplankton and higher trophic levels, and as such it is likely this group played a crucial ecological role in the Mesozoic Marine Revolution. Unfortunately, this group has extremely sparse fossil record. However, 'zooclasts', fragments of metazoans, particularly arthropods, are relatively common in palynological samples from the Phanerozoic (e.g. Tyson, 1993). Whilst these small carbonaceous fossils (SCFs) have provided a wealth of palaeobiological insight into the Proterozoic–Phanerozoic transition (e.g. Butterfield and Harvey, 2012), including the first record of the

mesozooplankton group, the copepods (Harvey et al., 2012; Harvey and Pedder, 2013), they are a more-or-less unexplored source of micropaleontological data for the Phanerozoic. In part, this is because traditional palynological processing methods may destroy these comparatively delicate organic microfossils (Butterfield and Harvey, 2012). Future work may examine Jurassic and, in particular, the Bajocian for SCFs, in order to link the phytoplankton record to that of the zooplankton, which in turn could be linked to higher trophic levels.

4) High-resolution geochemical work. There is a lack of high-resolution geochemical records through the Bajocian, making it difficult to assess palaeoenvironmental changes. In particular, the Early Bajocian positive carbon isotope shift, and accompanying palaeoenvironmental changes remain poorly documented, particularly outside of Europe. Documenting the carbon isotope record of the Bajocian from regions with well-researched lithostratigraphic and biostratigraphic frameworks such as Australia and Argentina would allow the global extent of this $\delta^{13}C$ shift to be evaluated. The generation of high-resolution Sr and Os isotope records through the Bajocian would allow changes in continental weathering to be properly assessed; this has been carried outside extensively and successfully for the Toarcian Oceanic Anoxic Event.

References

Aberhan, M., 2001. Bivalve palaeobiogeography and the Hispanic Corridor: time of opening and effectiveness of a proto-Atlantic seaway. Palaeogeogr. Palaeoclimatol. Palaeoecol. 165, 375–394.

Aguado, R., O'Dogherty, L., Sandoval, J., 2017. Calcareous nannofossil assemblage turnover in response to the Early Bajocian (Middle Jurassic) palaeoenvironmental changes in the Subbetic Basin. Palaeogeogr. Palaeoclimatol. Palaeoecol. 472, 128–145.

d´Orbigny, A.1842: Paléontologie française. 1. Terrains oolitiques ou jurassiques, 642 pp., Bertrand, Paris.

Anderson, D., Kulis, D., Sullivan, J., Hall, S., 1990. Toxin composition variations in one isolate of the dinoflagellate *Alexandrium fundyense*. Toxicon 28, 885–893.

Anderson, D.M., Burkholder, J.M., Cochlan, W.P., Glibert, P.M., Gobler, C.J., Heil, C.A., Kudela, R.M., Parsons, M.L., Rensel, J.E.J., Townsend, D.W., Trainer, V.L., Vargo, G.A., 2008a. Harmful algal blooms and eutrophication: examining linkages from selected coastal regions of the United States. Harmful Algae, HABs and Eutrophication 8, 39–53.

Anderson, D.M., Burkholder, J.M., Cochlan, W.P., Glibert, P.M., Gobler, C.J., Heil, C.A., Kudela, R.M., Parsons, M.L., Rensel, J.E.J., Townsend, D.W., Trainer, V.L., Vargo, G.A., 2008b. Harmful algal blooms and eutrophication: Examining linkages from selected coastal regions of the United States. Harmful Algae, HABs and Eutrophication 8, 39–53.

Anderson, D.M., Kulis, D.M., Binder, B.J., 1984. Sexuality and cyst formation in the dinoflagellate *Gonyaulax tamarensis*: cyst yield in batch cultures1. J. Phycol. 20, 418–425.

Arkhipkin, A.I., 2014. Getting hooked: the role of a U-shaped body chamber in the shell of adult heteromorph ammonites. J. Molluscan Stud. 80, 354–364.

Arthur, M.A., Dean, W.E., Claypool, G.E., 1985. Anomalous $\delta^{13}C$ enrichment in modern marine organic carbon. Nature 315, 216–218.

Bailey, D., 1987. Durotrigia daveyi gen. et sp. nov., an Early Bajocian dinocyst with a variable precingular archaeopyle. J. Micropalaeontology 6, 89–96.

Bailey, D.A., Partingdon, M., 1991. Some Middle Jurassic dinocysts from the Brent Group of the northern North Sea. J. Micropalaeontology 9, 245–252.

Barski, M., Matyja, B.A., Segit, T., Wierzbowski, A., 2012. Early to Late Bajocian age of the "black flysch" (Szlachtowa Fm.) deposits: implications for the history and geological structure of the Pieniny Klippen Belt, Carpathians. Geol. Q. Vol. 56, No 3, 391–410.

Bartolini, A., Baumgartner, P., Hunziker, J., 1996. Middle and Late Jurassic carbon stable-isotope stratigraphy and radiolarite sedimentation of the Umbria-Marche Basin (Central Italy). Eclogae Geol. Helvetiae 89, 811–844.

Bartolini, A., Baumgartner, P.O., Guex, J., 1999. Middle and Late Jurassic radiolarian palaeoecology versus carbon-isotope stratigraphy. Palaeogeogr. Palaeoclimatol. Palaeoecol. 145, 43–60.

Bartolini, A., Cecca, F., 1999. 20 My hiatus in the Jurassic of Umbria-Marche Apennines (Italy): carbonate crisis due to eutrophication. Comptes Rendus Académie Sci. - Ser. IIA - Earth Planet. Sci. 329, 587–595.

Bartolini, A., Larson, R.L., 2001. Pacific microplate and the Pangea supercontinent in the Early to Middle Jurassic. Geology 29, 735–738.

Beerling, D.J., Lomas, M.R., Gröcke, D.R., 2002. On the nature of methane gas-hydrate dissociation during the Toarcian and Aptian Oceanic anoxic events. Am. J. Sci. 302, 28–49.

Beju, D., 1983. Burtonia polygonalis, a new dinoflagellate from the Bathonian of southern England. J. Paleontol. 57, 106–111.

Below, R., 1987. Evolution und Systematik von Dinoflagellaten-Zysten aus der Ordnung Peridiniales. II. Cladopyxiaceae und Valvaeodiniaceae. Palaeontogr. Abt. B 1–115.

Bill, M., O'Dogherty, L., Guex, J., Baumgartner, P.O., Masson, H., 2001. Radiolarite ages in Alpine-Mediterranean ophiolites: Constraints on the oceanic spreading and the Tethys-Atlantic connection. Geol. Soc. Am. Bull. 113, 129–143.

Bodin, S., Hönig, M.R., Krencker, F.-N., Danisch, J., Kabiri, L., 2017. Neritic carbonate crisis during the Early Bajocian: Divergent responses to a global environmental perturbation. Palaeogeogr. Palaeoclimatol. Palaeoecol. 468, 184–199.

Bogus, K., Mertens, K.N., Lauwaert, J., Harding, I.C., Vrielinck, H., Zonneveld, K.A., Versteegh, G.J., 2014. Differences in the chemical composition of organic-walled dinoflagellate resting cysts from phototrophic and heterotrophic dinoflagellates. J. Phycol. 50, 254–266.

Bown, P.R., 2005. Calcareous nannoplankton evolution: a tale of two oceans. Micropaleontology 51, 299–308.

Brett, C.E., 1995. Sequence Stratigraphy, Biostratigraphy, and Taphonomy in Shallow Marine Environments. Palaios 10, 597–616.

Brigaud, B., Durlet, C., Deconinck, J.-F., Vincent, B., Pucéat, E., Thierry, J., Trouiller, A., 2009. Facies and climate/environmental changes recorded on a carbonate ramp: A sedimentological and geochemical approach on Middle Jurassic carbonates (Paris Basin, France). Sediment. Geol. 222, 181–206.

Bucefalo Palliani, R., Riding, J., 1997. The influence of palaeoenvironmental change on dinoflagellate cyst distribution-An example from the Lower and Middle Jurassic of Quercy, southwest France. Bull. Cent. Rech. Explor.-Prod. Elf Aquitaine 21, 107–123.

Bucefalo Palliani, R., Mattioli, E., 1998. High resolution integrated microbiostratigraphy of the Lower Jurassic (late Pliensbachian–early Toarcian) of central Italy. J. Micropalaeontology 17, 153–172.

Bucefalo Palliani, R., Mattioli, E., Riding, J.B., 2002. The response of marine phytoplankton and sedimentary organic matter to the early Toarcian (Lower Jurassic) oceanic anoxic event in northern England. Mar. Micropaleontol. 46, 223–245.

Bujak, J.P., Williams, G.L., 1977. Jurassic palynostratigraphy of offshore eastern Canada. Dev. Palaeontol. Stratigr. 6, 321–339.

Burger, D. (1980): Palynological studies in the Lower Cretaceous of the Surat Basin, Australia. Bureau of Mineral Resources Geology and Geophysics Bull. 189, 1-106.

Butler, N., Charnock, M.A., Hager, K.O., Watkins, C.A., 2005. The Ravenscar Group: a coeval analogue for the Middle Jurassic reservoirs of the North Sea and offshore Mid-Norway. Recent Dev. Appl. Biostratigraphy Geol. Soc. Lond. Micropaleontol. Soc. Spec. Publ. Lond. 43–53.

Butler, R.J., Benson, R.B.J., Carrano, M.T., Mannion, P.D., Upchurch, P., 2011. Sea level, dinosaur diversity and sampling biases: investigating the 'common cause' hypothesis in the terrestrial realm. Proc. R. Soc. Lond. B Biol. Sci. 278, 1165–1170.

Butterfield, N., Harvey, T., 2012. Small carbonaceous fossils (SCFs): A new measure of early Paleozoic paleobiology. Geology 40, 71–74.

Callomon, J.H., 2003. The Middle Jurassic of western and northern Europe: its subdivisions, geochronology and correlations. Geol. Surv. Den. Greenl. Bull. 1, 61–73.

Coats, D., Tyler, M., 1985. Encystment of the dinoflagellate Gyrodinium uncatenum: temperature and nutrient effects. J Phycol 21, 200–206.

Conway, B.H., 1990. Palynostratigraphy of the Jurassic succession in the subsurface of Israel. Geological Survey of Israel Bulletin 82, 1–39 pp.

Correia, V.F., Riding, J.B., Fernandes, P., Duarte, L.V., Pereira, Z., 2017. The palynology of the lower and middle Toarcian (Lower Jurassic) in the northern Lusitanian Basin, western Portugal. Rev. Palaeobot. Palynol. 237, 75–95.

Dale, B., 1976. Cyst formation, sedimentation, and preservation: factors affecting dinoflagellate assemblages in recent sediments from trondheimsfjord, Norway. Rev. Palaeobot. Palynol. 22, 39–60.

Dale, B., Dale, A.L., 1992. Dinoflagellate contributions to the deep sea. Ocean Biocoenosis Series 5, 45–73.

Davey, R.J., 1980. Palynology. In: Penn, I.E., Dingwall, R.G., Knox, R.W.O.'.B. (eds), The Inferior Oolite (Bajocian) sequence from a borehole in Lyme Bay, Dorset. Inst. Geol. Sci. 79, 53–76., Dorset, pp. 6–11.

Davies, S.J., Dawers, N.H., McLeod, A.E., Underhill, J.R., 2000. The structural and sedimentological evolution of early synrift successions: the Middle Jurassic Tarbert Formation, North Sea. Basin Res. 12, 343–365.

De Vains, G., 1988. Etude palynologique prèliminaire de l'Hettangien à l'Aalènien du Quercy (France). Bull. Cent. Rech. Explor. Elf-Aquitaine 12, 451–469.

de Vernal, A., Marret, F., 2007. Chapter Nine Organic-Walled Dinoflagellate Cysts: Tracers of Sea-Surface Conditions, in: Vernal, C.H. and A.D. (Ed.), Developments in Marine Geology, Proxies in Late Cenozoic Paleoceanography. Elsevier, pp. 371–408.

Dean, W.E., Arthur, M.A., Claypool, G.E., 1986. Depletion of 13C in Cretaceous marine organic matter: Source, diagenetic, or environmental sigal? Mar. Geol. 70, 119–157.

Delwiche, C.F., 2007. The origin and evolution of dinoflagellates. In: Falkowski, P.G., Knoll, A.H. (eds), Evolution of Primary Producers in the Sea. Academic Press, Burlington, pp. 191–205.

Dera, G., Brigaud, B., Monna, F., Laffont, R., Pucéat, E., Deconinck, J.-F., Pellenard, P., Joachimski, M.M., Durlet, C., 2011. Climatic ups and downs in a disturbed Jurassic world. Geology 39, 215–218.

Dera, G., Prunier, J., Smith, P.L., Haggart, J.W., Popov, E., Guzhov, A., Rogov, M., Delsate, D., Thies, D., Cuny, G., Pucéat, E., Charbonnier, G., Bayon, G., 2014. Nd isotope constraints on ocean circulation, paleoclimate, and continental drainage during the Jurassic breakup of Pangea. Gondwana Res. 27, 1599–1615.

Dera, G., Toumoulin, A., De Baets, K., 2016. Diversity and morphological evolution of Jurassic belemnites from South Germany. Palaeogeogr. Palaeoclimatol. Palaeoecol. 457, 80–97.

Dewey, J.F., Pitman, W.C., 1998. Sea-level changes: mechanisms, magnitudes and rates. J.L Pindell, S Drake (Eds.), Paleogeographic evolution and non-glacial eustasy, SEPM Special Publication, 58 (1998), pp. 1-16.

Dietl, G., 1988. Der Hamitenton (Ober-Bajocium, Mittl. Jura) in Bauaufschlüssen der neuen Bundesautobahn A8, Streckenabschnitt Aichelberg-Gruibingen. Jahr. Ges. Naturk. Württemberg 143, 59–77. Dietl, G., 2013. Der Braunjura am Fuß der Schwäbischen Alb. Fossilien. Special ed. Quelle & Meyer, Wiebelsheim, pp. 1–62.

Dietze, V., Kutz, M., Franz, M., Bosch, K., 2009. Stratigraphy of the Kahlenberg near Ringsheim (Upper Rhine Valley, SW Germany) with emphasis on the Laeviuscula and Sauzei zones (Lower Bajocian, Middle Jurassic). Palaeodiversity 2, 19–65.

Dodsworth, P., 1995. A note of caution concerning the application of quantitative palynological data from oxidized preparations. J. Micropalaeontology 14, 6–6.

Duringer, P., Doubinger, J., 1985. La palynologie: un outil de caractérisation des faciès marins et continentaux à la limite Muschelkalk supérieur Lettenkohle. Sci Géol Bull 38, 19–34.

Ellegaard, M., 2000. Variations in dinoflagellate cyst morphology under conditions of changing salinity during the last 2000 years in the Limfjord, Denmark. Rev. Palaeobot. Palynol. 109, 65–81.

Ellegaard, M., Lewis, J., Harding, I., 2002. Cyst–Theca Relationship, Life Cycle, and Effects of Temperature and Salinity on the Cyst Morphology of Gonyaulax Baltica Sp. Nov. (dinophyceae) from the Baltic Sea Area1. J. Phycol. 38, 775–789.

Evitt, W.R., 1985. Sporopollenin dinoflagellate cysts: their morphology and interpretation. Amer Assn of Stratigraphic, Dallas, Tex. pp 1–333.

Falkowski, P.G., Oliver, M.J., 2007. Mix and match: how climate selects phytoplankton. Nat. Rev. Microbiol. 5, 813–819.

Falkowski, P.G., Katz, M.E., Knoll, A.H., Quigg, A., Raven, J.A., Schofield, O., Taylor, F.J.R., 2004. The evolution of modern eukaryotic phytoplankton. Science 305, 354–360.

Federova, V., 1977. The significance of the combined use of microphytoplankton, spores, and pollen for differentiation of multi-facies sediments. Quest. Phttostratigraphy Tr. Neft. Nauchno-Issledovatelskii Geol.-Razvedochnyi Inst. VNIGRI Leningr. 398, 70–88.

Feist-Burkhardt, S., 1990. Dinoflagellate cyst assemblages of the Hausen coreholes (Aalenian to early Bajocian), southwest Germany. Bull. Cent. Rech. Explor.-Prod. Elf-Aquitaine 14, 611–632.

Feist-Burkhardt, S., 2009. Palynology of the Sinemurian/Pliensbachian boundary (Lower Jurassic) in the Wutach area, SW Germany: dinoflagellate cyst systematics, biostratigraphy and heterotrophic character of Liasidium variabile. Neues

Jahrb. Für Geol. Paläontol.-Abh. 254, 293–313.

Feist-Burkhardt, S., Wille, W., 1992. Jurassic palynology in southwest Germany — state of the art. Cah. Micropaléontologie Nouv. Sér. 7, 141–156.

Feist-Burkhardt, S., Monteil, E., 1997. Dinoflagellate cysts from the Bajocian stratotype (Calvados, Normandy, western France). Bull. Cent. Rech. Explor.-Prod. Elf-Aquitaine 21, 31–105.

Feist-Burkhardt, S., Pross, J., 1999. Morphological analysis and description of Middle Jurassic dinoflagellate cyst marker species using confocal laser scanning microscopy, digital optical microscopy, and conventional light microscopy. Bull. Cent. Rech. Elf Explor. Prod. 22, 103–145.

Feist-Burkhardt, S., Monteil, E., 2001. Gonyaulacacean dinoflagellate cysts with multi-plate precingular archaeopyle. Neues Jahrb. Geol. Palaontologie-Abh. 219, 33–81.

Feist-Burkhardt, S. & Götz, A.E., 2002: Palynofazies und Sequenzstratigraphie (K1). In: Hüssner, H. et al. (Eds.): SEDIMENT 2002 – 17. Sedimentologen-Treffen, Frankfurt a. M. – Darmstadt, 29.-31.5.2002. Schriftenreihe der Deutschen Geologischen Gesellschaft 18, 57-72.

Feist-Burkhardt, S., Pross, J., 2010. Dinoflagellate cyst biostratigraphy of the Opalinuston Formation (Middle Jurassic) in the Aalenian type area in southwest Germany and north Switzerland. Lethaia 43, 10–31.

Feist-Burkhardt, S., Götz, A.E., 2016. Ultra-High-Resolution Palynostratigraphy of the Early Bajocian Sauzei and Humphriesianum Zones (Middle Jurassic) from Outcrop Sections in the Upper Rhine Area, Southwest Germany, in: Stratigraphy & Timescales. Elsevier, pp. 325–392.

Fensome, R.A., 1979. Dinoflagellate cysts and acritarchs from the Middle and Upper Jurassic of Jameson Land, east Greenland. Grønlands geologiske undersøgelse bulletin, 132, 1–98.

Fensome, R.A., MacRae, R.A., Moldowan, J.M., Taylor, F.J.R., Williams, G.L., 1996. The early Mesozoic radiation of dinoflagellates. Paleobiol. 22, 329–338.

Fensome, R.A., Saldarriaga, J.F., Taylor, “Max” F. J. R., 1999. Dinoflagellate phylogeny revisited: reconciling morphological and molecular based phylogenies. Grana 38, 66–80.

Fensome, R.A., Taylor, F., Norris, G., Sarjeant, W., Wharton, D., Williams, G., 1993. A classification of living and fossil dinoflagellates. Micropaleontology Press Special Paper, no.7, 351 pp.

Fenton, J.P.G., Neves, R., Piel, K.M., 1980. Dinoflagellate cysts and acritarchs from Upper Bajocian to Middle Bathonian strata of central and southern England. Palaeontology 23, 151–170.

Finkel, Z.V., Sebbo, J., Feist-Burkhardt, S., Irwin, A.J., Katz, M.E., Schofield, O.M.E., Young, J.R., Falkowski, P.G., 2007. A universal driver of macroevolutionary change in the size of marine phytoplankton over the Cenozoic. Proc. Natl. Acad. Sci. 104, 20416–20420.

Friedman, M., Shimada, K., Martin, L.D., Everhart, M.J., Liston, J., Maltese, A., Triebold, M., 2010. 100-Million-Year Dynasty of Giant Planktivorous Bony Fishes in the Mesozoic Seas. Science 327, 990–993.

Gast, R., Caron, D., 1996. Molecular phylogeny of symbiotic dinoflagellates from planktonic foraminifera and radiolaria.

Mol. Biol. Evol. 13, 1192–1197.

Gedl, P., 2008. Organic-walled dinoflagellate cyst stratigraphy of dark Middle Jurassic marine deposits of the Pieniny Klippen Belt, West Carpathians. Stud. Geol. Polon. 131, 7–227.

Gedl, P., 2012. Organic-walled dinoflagellate cysts from the Bathonian ore-bearing clays at Gnaszyn, Kraków-Silesia Homocline, Poland — a palaeoenvironmental approach. Acta Geol. Pol. 62, 439–461.

Gedl, P., 2013. Dinoflagellate cysts fromthe Szlachtowa Formation (Jurassic) and adjacent deposits (Jurassic-Cretaceous) of the Grajcarek Unit at Szczawnica-Zabaniszcze (Pieniny Klippen Belt, Carpathians, Poland). Geol. Quart. 57, 485–502.

Gedl, P., Józsa, S., 2015. Early?-Middle Jurassic dinoflagellate cysts and foraminifera from the dark shale of the Pieniny Klippen belt between Jarabina and Litmanova (Slovakia): age and palaeonvironment. Ann. Soc. Geol. Pol. 85, 91–122.

Gedl, P., Kaim, A., Leonowicz, P., Boczarowski, A., Dudek, T., Kędzierski,M., Rees, J., Smoleń,J., Szczepanik, P., Sztajner, P., Witkowska, M., Ziaja, J., 2012. Palaeoenvironmental reconstruction of Bathonian (Middle Jurassic) ore-bearing clays at Gnaszyn, Krakow-Silesia Homocline, Poland. Acta Geol. Pol. 62, 463–484.

Germeraad, J.H., Hopping, C.A., Muller, J., 1968. Palynology of Tertiary sediments from tropical areas. Rev. Palaeobot. Palynol. 6, 189–348.

Giraud, F., Mattioli, E., López-Otálvaro, G.E., Lécuyer, C., Suchéras-Marx, B., Alméras, Y., Martineau, F., Arnaud-Godet, F., de Kænel, E., 2016. Deciphering processes controlling mid-Jurassic coccolith turnover. Mar. Micropaleontol. 125, 36–50.

Gocht, H., 1970. Dinoflagellaten-Zysten aus dem Bathonium des Erdölfeldes Alsdorf (NW-Deutschland). Palaeontogr. Abt. B 129, 125–165.

Gowland, S., Riding, J.B., 1991. Stratigraphy, sedimentology and palaeontology of the Scarborough Formation (Middle Jurassic) at Hundale Point, North Yorkshire. Proc. Yorks. Geol. Polytech. Soc. 48, 375–392.

Gradstein, F.M., Ogg, J.G., Schmitz, M., Ogg, G., 2012. The geologic time scale 2012. elsevier.1–1129 pp.

Grice, K., Nabbefeld, B., Maslen, E., 2007. Source and significance of selected polycyclic aromatic hydrocarbons in sediments (Hovea-3 well, Perth Basin, Western Australia) spanning the Permian–Triassic boundary. Org. Geochem. 38, 1795–1803.

Guinot, G., Cavin, L., 2015. ‘Fish’ (Actinopterygii and Elasmobranchii) diversification patterns through deep time: ‘Fish’ diversification patterns through deep time. Biol. Rev. 91, 950–981.

Hallam, A., 2001. A review of the broad pattern of Jurassic sea-level changes and their possible causes in the light of current knowledge. Palaeogeogr. Palaeoclimatol. Palaeoecol. 167, 23–37.

Hallam, A., 1976. Stratigraphic distribution and ecology of European Jurassic bivalves. Lethaia 9, 245–259.

Hammer, Ø., Harper, D.A.T., and P. D. Ryan, 2001. PAST: Paleontological Statistics Software Package for Education and Data Analysis. Pal aeontologia Electronica 4, 9pp.

Haq, B.U., Hardenbol, J., Vail, P.R., 1987. Chronology of Fluctuating Sea Levels Since the Triassic. Science 235, 1156–1167.

Hardenbol, J., Thierry, J., Farley, M.B., Jacquin, T., De Graciansky, P.-C., Vail, P.R. (eds) 1998. Mesozoic and Cenozoic sequence chronostratigraphic framework of European basins. SEP Special publication no. 60.

Harding, I.C., 1986. Archaeopyle variability in Early Cretaceous dinocysts of the partiform gonyaulacoid genus Druggidium Habib. J. Micropalaeontology 5, 17–26.

Harding, I.C., Lewis, J., 1994. Siliceous dinoflagellate thecal fossils from the Eocene of Barbados. Palaeontology 37, 825–840.

Harper, E.M., Forsythe, G.T., Palmer, T., 1998. Taphonomy and the Mesozoic marine revolution; preservation state masks the importance of boring predators. Palaios 13, 352–360.

Harvey, T.H., Pedder, B.E., 2013. Copepod mandible palynomorphs from the Nolichucky Shale (Cambrian, Tennessee): Implications for the taphonomy and recovery of small carbonaceous fossils. Palaios 28, 278–284.

Harvey, T.H., Vélez, M.I., Butterfield, N.J., 2012. Exceptionally preserved crustaceans from western Canada reveal a cryptic Cambrian radiation. Proc. Natl. Acad. Sci. 109, 1589–1594.

Harris, A.J., Tocher, B.A., 2003. Palaeoenvironmental analysis of Late Cretaceous dinoflagellate cyst assemblages using high-resolution sample correlation from the Western Interior Basin, USA. Mar. Micropaleontol. 48, 127–148.

Hart, M.B., Hylton, M.D., Oxford, M.J., Price, G.D., Hudson, W., Smart, C.W., 2003. The search for the origin of the planktic Foraminifera. J. Geol. Soc. 160, 341–343.

Head,M., 1996. Modern dinoflagellate cysts and their biological affinities. In: Jansonius, J., McGregor, D.C. (Eds.), Palynology: Principles and Applications 3. American Association of Stratigraphic Palynologists, Dallas, Texas, pp. 1197–1248.

Helby, R., Morgan, R., Partridge, A., 1987. A palynological zonation of the Australian Mesozoic. Mem. Assoc. Australas. Palaeontol. 4, 1–94.

Hesselbo, S.P., Morgans-Bell, H.S., McElwain, J.C., Rees, P.M., Robinson, S.A., Ross, C.E., 2003. Carbon-cycle perturbation in the Middle Jurassic and accompanying changes in the terrestrial paleoenvironment. J. Geol. 111, 259–276.

Hostettler, B., Reisdorf, A.G., Jaeggi, D., Deplazes, G., Bläsi, H., Morard, A., Feist-Burkhardt, S., Waltschew, A., Dietze, V., Menkveld-Gfeller, U., 2017. Litho- and biostratigraphy of the Opalinus Clay and bounding formations in the Mont Terri rock laboratory (Switzerland). Swiss J. Geosci. 110, 23–37.

Ibrahim, M., Kholeif, S., Al-Saad, H., 2003. Dinoflagellate cyst biostratigraphy and paleoenvironment of the Lower-Middle Jurassic succession of Qatar, Arabian Gulf. Rev. Esp. Micropaleontol. 35, 171–194.

Ibrahim, M.I., Aboul Ela, N.M., Kholeif, S.E., 2002. Dinoflagellate cyst biostratigraphy of Jurassic-Lower Cretaceous formations of the North Eastern Desert, Egypt. Neues Jahrb. Für Geol. Paläontol.-Abh. 224, 255–319.

Ichimi, K., Yamasaki, M., Okumura, Y., Suzuki, T., 2001. The growth and cyst formation of a toxic dinoflagellate,

Alexandrium tamarense, at low water temperatures in northeastern Japan. J. Exp. Mar. Biol. Ecol. 261, 17–29.

Jacquin, T., Dardeau, G., Durlet, C., de Graciansky, P.-C., Hantzpergue, P., 1998. The North Sea cycle: an overview of 2nd-order transgressive/regressive facies cycles in western Europe. In: de Graciansky, P.C., Hardenbol, J., Jacquin, T., Vail, P.R. (Eds.), Mesozoic and Cenozoic Sequence Stratigraphy of European Basins. SEPM Special Publication. 60, pp. 445–466.

Jäger, M., Fraaye, R., 1997. The diet of the Early Toarcian ammonite Harpoceras falciferum. Palaeontology 40, 557–574.

Jan du Chêne, R., Masure, E., Becheler, I., Biffi, U., De Vains, G., Fauconnier, D., Ferrario, R., Foucher, J.-C., Gaillard, M., Hochuli, P., 1986. Guide pratique pour la détermination de kystes de dinoflagellés fossiles. Le complexe *Gonyaulacysta*. Bull. Cent. Rech. Explor.-Prod. Elf-Aquitaine Mém. 12, 1–479.

Janouškovec, J., Gavelis, G.S., Burki, F., Dinh, D., Bachvaroff, T.R., Gornik, S.G., Bright, K.J., Imanian, B., Strom, S.L., Delwiche, C.F., Waller, R.F., Fensome, R.A., Leander, B.S., Rohwer, F.L., Saldarriaga, J.F., 2017. Major transitions in dinoflagellate evolution unveiled by phylotranscriptomics. Proc. Natl. Acad. Sci. 114, E171–E180.

Jenkyns, H.C., Jones, C.E., GrÖcke, D.R., Hesselbo, S.P., Parkinson, D.N., 2002. Chemostratigraphy of the Jurassic System: applications, limitations and implications for palaeoceanography. J. Geol. Soc. 159, 351–378.

Jones, L.E., Sellwood, B.W., 1989. Palaeogeographic significance of clay mineral distributions in the Inferior Oolite Group (Mid Jurassic) of southern England. Clay Miner. 24, 91–105.

Keeley, M.L., Dungworth, G., Floyd, C.S., Forbes, G.A., King, C., McGarva, R.M., Shaw, D., 1990. The Jurassic System in northern Egypt: I. Regional stratigraphy and implications for hydrocarbon prospectivity. J. Pet. Geol. 13, 397–420.

Keeley, M.L., Wallis, R.J., 1991. The Jurassic system in northern Egypt: II. Depositional and tectonic regimes. J. Pet. Geol. 14, 49–64.

Kodrans-Nsiah, M., de Lange, G.J., Zonneveld, K.A.F., 2008. A natural exposure experiment on short-term species-selective aerobic degradation of dinoflagellate cysts. Rev. Palaeobot. Palynol. 152, 32–39

Korte, C., Hesselbo, S.P., 2011. Shallow marine carbon and oxygen isotope and elemental records indicate icehouse-greenhouse cycles during the Early Jurassic: Early Jurassic climatic/eustatic cycles. Paleoceanography 26. PA4129.

Korte, C., Hesselbo, S.P., Ullmann, C.V., Dietl, G., Ruhl, M., Schweigert, G., Thibault, N., 2015. Jurassic climate mode governed by ocean gateway. Nat. Commun. 6, 10015.

Kruta, I., Landman, N., Rouget, I., Cecca, F., Tafforeau, P., 2011. The role of ammonites in the Mesozoic marine food web revealed by jaw preservation. Science 331, 70–72.

Labails, C., Olivet, J.-L., Aslanian, D., Roest, W.R., 2010. An alternative early opening scenario for the Central Atlantic Ocean. Earth Planet. Sci. Lett. 297, 355–368.

Lake, S.D., Karner, G.D., 1987. The structure and evolution of the Wessex Basin, southern England: an example of inversion tectonics. Tectonophysics 137, 347358–356378.

Lignum, J., Jarvis, I., Pearce, M.A., 2008. A critical assessment of standard processing methods for the preparation of

palynological samples. Rev. Palaeobot. Palynol. 149, 133–149.

MacRae, R.A., Fensome, R.A., Williams, G.L., 1996. Fossil dinoflagellate diversity, originations, and extinctions and their significance. Can. J. Bot. 74, 1687–1694.

Mantle, D.J., 2009. Palynology, sequence stratigraphy, and palaeoenvironments of Middle to Upper Jurassic strata, Bayu-Undan Field, Timor Sea region. Palaeontogr. Abt. B 87–212.

Mantle, D.J., Riding, J.B., 2012. Palynology of the Middle Jurassic (Bajocian–Bathonian) Wanaea verrucosa dinoflagellate cyst zone of the North West Shelf of Australia. Rev. Palaeobot. Palynol. 180, 41–78.

Marañón, E., 2015. Cell Size as a Key Determinant of Phytoplankton Metabolism and Community Structure. Annu. Rev. Mar. Sci. 7, 241–264.

Margalef, R., 1978. Life-forms of phytoplankton as survival alternatives in an unstable environment. Oceanol. Acta 1, 493–509.

Marret, F., Zonneveld, K.A.F., 2003. Atlas of modern organic-walled dinoflagellate cyst distribution. Rev. Palaeobot. Palynol. 125, 1–200.

Masure, E., 1991. Morphology of the dinoflagellate genus *Atopodinium* Drugg emend., senior synonym of Maghrebinia below and Bejuia Stover & Williams. Palynology 15, 63–80.

Medlin, L., Fensome, R., 2013. Dinoflagellate macroevolution: some considerations based on an integration of molecular, morphological and fossil evidence. Biol. Geol. Perspect. Dinoflag. 255–266.

Mellere, D., Steel, R.J., 1996. Tidal sedimentation in Inner Hebrides half grabens, Scotland: the Mid-Jurassic Bearreraig Sandstone Formation. Geol. Soc. Lond. Spec. Publ. 117, 49–79.

Mertens, K.N., Ribeiro, S., Bouimetarhan, I., Caner, H., Combourieu Nebout, N., Dale, B., De Vernal, A., Ellegaard, M., Filipova, M., Godhe, A., Goubert, E., Grøsfjeld, K., Holzwarth, U., Kotthoff, U., Leroy, S.A.G., Londeix, L., Marret, F., Matsuoka, K., Mudie, P.J., Naudts, L., Peña-Manjarrez, J.L., Persson, A., Popescu, S.-M., Pospelova, V., Sangiorgi, F., van der Meer, M.T.J., Vink, A., Zonneveld, K.A.F., Vercauteren, D., Vlassenbroeck, J., Louwye, S., 2009a. Process length variation in cysts of a dinoflagellate, *Lingulodinium machaerophorum*, in surface sediments: Investigating its potential as salinity proxy. Mar. Micropaleontol. 70, 54–69.

Mertens, K.N., Verhoeven, K., Verleye, T., Louwye, S., Amorim, A., Ribeiro, S., Deaf, A.S., Harding, I.C., De Schepper, S., González, C., 2009b. Determining the absolute abundance of dinoflagellate cysts in recent marine sediments: the *Lycopodium* marker-grain method put to the test. Rev. Palaeobot. Palynol. 157, 238–252.

Moldowan, J.M., Dahl, J., Jacobson, S.R., Huizinga, B.J., Fago, F.J., Shetty, R., Watt, D.S., Peters, K.E., 1996. Chemostratigraphic reconstruction of biofacies: Molecular evidence linking cyst-forming dinoflagellates with pre-Triassic ancestors. Geology 24, 159–162.

Moldowan, J.M., Talyzina, N.M., 1998. Biogeochemical evidence for dinoflagellate ancestors in the Early Cambrian. Science 281, 1168–1170.

Montresor, M., Nuzzo, L., Mazzocchi, M.G., 2003. Viability of dinoflagellate cysts after the passage through the copepod gut. J. Exp. Mar. Biol. Ecol. 287, 209–221.

Morales, C., Rogov, M., Wierzbowski, H., Ershova, V., Suan, G., Adatte, T., Föllmi, K.B., Tegelaar, E., Reichart, G.-J., Lange, G.J. de, Middelburg, J.J., Schootbrugge, B. van de, 2017. Glendonites track methane seepage in Mesozoic polar seas. Geology 45, 503–506.

Morbey, S.J., 1975. The Palynostratigraphy of the Rhaetian Stage, Upper Triassic in the Kendelbachgraben, Austria. Palaeontogr. Abt. B. 152, 1–75.

Morgenroth, P., 1970. Dinoflagellate cysts from the Lias delta of Lühnde/Germany. Neues Jahrb. Für Geol. Paläontol. Abh. 136, 345–359.

O'Dogherty, L., Sandoval, J., Bartolini, A., Bruchez, S., Bill, M., Guex, J., 2006. Carbon–isotope stratigraphy and ammonite faunal turnover for the Middle Jurassic in the Southern Iberian palaeomargin. Palaeogeogr. Palaeoclimatol. Palaeoecol. 239, 311–333.

Penn, I., 1982. Middle Jurassic stratigraphy and correlation of the Winterborne Kingston borehole. Winterborne Kingston Boreh. Dorset Engl. Rep. Inst. Geol. Sci. 81, 53–76.

Penn, I.E., Dingwall, R.G., Robert William, O., Knox, B., 1980. The inferior Oolite (Bajocian) sequence from a borehole in Lyme Bay, Dorset. Inst. Geol. Sci. Rep. 79/3.

Persson, A., 2000. Possible predation of cysts—a gap in the knowledge of dinoflagellate ecology? J. Plankton Res. 22, 803–809.

Pienkowski, G., Schudack, M.E., Bosak, P., Enay, R., Feldman-Olszewska, A., Golonka, J., Gutowski, J., Herngreen, G.F.W., Jordan, P., Krobicki, M., Lathuiliere, B., Leinfelder, R.R., Michalik, J., Moennig, E., Noe-Nygaard, N., Palfy, J., Pint, A., Rasser, M.W., Reisdorf, A.G., Schmid, D.U., Schweigert, G., Surlyk, F., Wetzel, A., Wong, T.E., 2008. Jurassic. In: McCann, T. (Ed.), The Geology of Central Europe Volume 2: Mesozoic and Cenozoic. The Geological Society of London, London, pp. 823–922.

Poulsen, N.E., 1996. Dinoflagellate cysts from marine Jurassic deposits of Denmark and Poland. American Association of Stratigraphic Palynologists Contributions Series. 31, 1-227

Poulsen, N., 1998. Upper Bajocian to Callovian (Jurassic) dinoflagellate cysts from central Poland. Acta Geol. Pol. 237–245.

Poulsen, N.E., Riding, J.B., 2003. The Jurassic dinoflagellate cyst zonation of subboreal Northwest Europe. Geol. Surv. Den. Greenl. Bull. 1, 115–144.

Prauss, M., 1989. Dinozysten-Stratigraphie und Palynofazies im Oberen Lias und Dogger von NW-Deutschland. Palaeontogr. Abt. B. 214, 1–124.

Preat, A., Mamet, B., De Ridder, C., Boulvain, F., Gillan, D., 2000. Iron bacterial and fungal mats, Bajocian stratotype (Mid-Jurassic, northern Normandy, France). Sediment. Geol. 137, 107–126.

Price, G.D., 1999. The evidence and implications of polar ice during the Mesozoic. Earth-Sci. Rev. 48, 183–210.

Quattrocchio, M.E., Volkheimer, W., 1990. Jurassic and Lower Cretaceous dinocysts from Argentina: their biostratigraphic significance. Rev. Palaeobot. Palynol. 65, 319–330.

Raucsik, B., and A. Varga. 2008. Climato-environmental controls on clay mineralogy of the Hettangian-Bajocian successions of the Mecsek Mountains, Hungary: an evidence for extreme continental weathering during the early Toarcian oceanic anoxic event. Palaeogeog. Palaeoclim. Palaeoecol. 265, 1–13.

Raucsik, B., A. Demény, I. Borbély Kiss, and G. Szabó. 2001. Monsoon-like climate during the Bajocian. Clay mineralogical and geochemical study on a limestone/marl alternation (Komló Calcareous Marl Formation, Mecsek Mountains, Southern Hungary). Hantkeniana 3, 149–176.

Riding, J.B., 1984a. A palynological investigation of Toarcian to early Aalenian strata from the Blea Wyke area, Ravenscar, North Yorkshire. Proc. Yorks. Geol. Soc. 45, 109–122.

Riding, J.B., 1984b. Observations on the Jurassic dinoflagellate cyst Nannoceratopsis ambonis Drugg, 1978. J. Micropalaeontology 3, 75–79.

Riding, J.B., 1987. Dinoflagellate cyst stratigraphy of the Nettleton Bottom Borehole (Jurassic: Hettangian to Kimmeridgian), Lincolnshire, England. Proc. Yorks. Geol. Soc. 46, 231–266.

Riding, J.B., 1994. A taxonomic study of the Mesozoic dinoflagellate cysts *Phallocysta elongata* (Beju 1971) comb. nov., emend. nov. and *Wallodinium cylindricu*m (Habib 1970) Duxbury 1983 emend. nov. Palynology 18, 11–22.

Riding, J.B., 2012. A compilation and review of the literature on Triassic, Jurassic, and earliest Cretaceous dinoflagellate cysts. American Association of Stratigraphic Palynologists Contributions Series Vol. 46. AASP Foundation, Dallas, Texas (119 pp.).

Riding, J.B., 2013. The literature on Triassic, Jurassic and earliest Cretaceous dinoflagellate cysts: supplement 1. Palynology 37, 345–354.

Riding, J.B., 2014. The literature on Triassic, Jurassic and earliest Cretaceous dinoflagellate cysts: supplement 2. Palynology 38, 334–347.

Riding, J.B., Thomas, J.E., 1992. Dinoflagellate cysts of the Jurassic System, in: In: Powell, A.J. A Stratigraphic Index of Dinoflagellate Cysts. Chapman and Hall, London, pp. 7–97.

Riding, J.B., Walton, W., Shaw, D., 1991. Toarcian to Bathonian (Jurassic) palynology of the Inner Hebrides, Northwest Scotland. Palynology 15, 115–179.

Riding, J.B., Federova, V.A., Ilyina, V.I., 1999. Jurassic and lowermost Cretaceous dinoflagellate cyst biostratigraphy of the Russian Platform and northern Siberia, Russia. American Association of Stratigraphic Palynologists Foundation Contribution Series, 36 pp 1–179.

Riding, J.B., Mantle, D.J., Backhouse, J., 2010a. A review of the chronostratigraphical ages of Middle Triassic to Late Jurassic dinoflagellate cyst biozones of the North West Shelf of Australia. Rev. Palaeobot. Palynol. 162, 543–575.

Riding, J.B., Westermann, G.E.G., Darbyshire, D.P.F., 2010b. New evidence for the age of the Athol Formation (Middle Jurassic; Bajocian) in the Tusk-1 and Tusk-2 wells, offshore Carnarvon Basin, Western Australia. Alcheringa Australas. J. Palaeontol. 34, 21–35.

Riding, J.B., Leng, M.J., Kender, S., Hesselbo, S.P., Feist-Burkhardt, S., 2013. Isotopic and palynological evidence for a new Early Jurassic environmental perturbation. Palaeogeogr. Palaeoclimatol. Palaeoecol. 374, 16–27.

Rioult, M., Dugué, O., Duchene, R.J., Ponsot, C., Fily, G., Moron, J., Vail, P., 1991. Outcrop sequence stratigraphy of the Anglo-Paris Basin, Middle to Upper Jurassic (Normandy, Maine, Dorset). Bull. Cent. Rech. Explor.-Prod. Elf Aquitaine. 15, 101–194.

Sandoval, J., O'Dogherty, L., Guex, J., 2001. Evolutionary Rates of Jurassic Ammonites in Relation to Sea-Level Fluctuations. Palaios 16, 311.

Sarjeant, W.A.S., 1976. Dinoflagellate cysts and acritarchs from the Great Oolite Limestone (Jurassic: Bathonian) of Lincolnshire, England. Geobios 9, 5–46.

Sarjeant, W.A.S., Lacalli, T., Gaines, G., 1987. The Cysts and Skeletal Elements of Dinoflagellates: Speculations on the Ecological Causes for Their Morphology and Development. Micropaleontology 33, 1–36.

Scotese, C.R., 2014. Atlas of Jurassic Paleogeographic Maps, PALEOMAP Atlas for ArcGIS, volume 4, The Jurassic and Triassic, Maps 32-42, Mollweide Projection, PALEOMAP Project, Evanston, IL.

Selden, P.A., Huys, R., Stephenson, M.H., Heward, A.P., Taylor, P.N., 2010. Crustaceans from bitumen clast in Carboniferous glacial diamictite extend fossil record of copepods. Nat. Commun. 1, 50.

Sellwood, B.W., Wilson, R.C.L., 1990. Jurassic sedimentary environments of the Wessex Basin. In: 13th International Sedimentological Congress, Nottingham, UK, 1990. Field Guide No. 7, 89 pp.

Simmons, M., BouDagher-Fadel, M., Banner, F., Whittaker, J., 1997. The Jurassic Favusellacea, the earliest Globigerinina, in: The Early Evolutionary History of Planktonic Foraminifera. Springer, pp. 17–51.

Skupien, P., Pavluš, J., Falahatgar, M., Javidan, M., 2015. Middle Jurassic organic-walled dinoflagellate cysts and palynofacies from Telma-Dareh, south of Sari, northern Iran. Rev. Palaeobot. Palynol. 223, 128–137.

Slater, S.M., Wellman, C.H., 2016. Middle Jurassic vegetation dynamics based on quantitative analysis of spore/pollen assemblages from the Ravenscar Group, North Yorkshire, UK. Palaeontology 59, 305–328.

Sluijs, A., Pross, J., Brinkhuis, H., 2005. From greenhouse to icehouse; organic-walled dinoflagellate cysts as paleoenvironmental indicators in the Paleogene. Earth-Sci. Rev. 68, 281–315.

Smith, A.B., McGowan, A.J., 2011. The ties linking rock and fossil records and why they are important for palaeobiodiversity studies. Geol. Soc. Lond. Spec. Publ. 358, 1–7.

Smayda, T.J., 2010. Adaptations and selection of harmful and other dinoflagellate species in upwelling systems. 2. Motility and migratory behaviour. Prog. Oceanogr. 85, 71–91.

Smayda, T.J., Reynolds, C.S., 2003. Strategies of marine dinoflagellate survival and some rules of assembly. J. Sea Res. 49, 95–106.

Stat, M., Morris, E., Gates, R.D., 2008. Functional diversity in coral–dinoflagellate symbiosis. Proc. Natl. Acad. Sci. 105, 9256–9261.

Stockmarr, J., 1971. Tablets with spores used in absolute pollen analysis. Pollen Spores. Pollen et Spore. VIII, 615–619.

Suchéras-Marx, B., Giraud, F., Fernandez, V., Pittet, B., Lecuyer, C., Olivero, D., Mattioli, E., 2013. Duration of the Early Bajocian and the associated δ ^{13} C positive excursion based on cyclostratigraphy. J. Geol. Soc. 170, 107–118.

Suchéras-Marx, B., Mattioli, E., Giraud, F., Escarguel, G., 2015. Paleoenvironmental and paleobiological origins of coccolithophorid genus *Watznaueria* emergence during the late Aalenian–early Bajocian. Paleobiology 41, 415–435.

Suchéras-Marx, B., Guihou, A., Giraud, F., Lécuyer, C., Allemand, P., Pittet, B., Mattioli, E., 2012. Impact of the Middle Jurassic diversification of *Watznaueria* (coccolith-bearing algae) on the carbon cycle and δ13C of bulk marine carbonates. Glob. Planet. Change 86–87, 92–100.

Taylor, P.D., Ernst, A., 2008. Bryozoans in transition: The depauperate and patchy Jurassic biota. Palaeogeogr. Palaeoclimatol. Palaeoecol., 263, 9–23.

Traverse, A., 1988. Paleopalynology. Unvin Hyman Boston. 600 pp.

Traverse, A., 2007. The Natural History of Palynomorphs. In: Traverse. Paleopalynology 2nd ed. Topics in Geobiology 28. pp. 55–76. Springer.

Traverse, A., Ginsburg, R.N., 1966. Palynology of the surface sediments of Great Bahama Bank, as related to water movement and sedimentation. Mar. Geol. 4, 417–459.

Tyson, R.V., 1993. Palynofacies analysis, in: Jenkyns (eds) Applied Micropalaeontology. Springer, pp. 153–191.

van de Schootbrugge, B., Bachan, A., Suan, G., Richoz, S., Payne, J.L., 2013. Microbes, mud and methane: cause and consequence of recurrent Early Jurassic anoxia following the end-Triassic mass extinction. Palaeontology 56, 685–709.

van de Schootbrugge, B., Bailey, T.R., Rosenthal, Y., Katz, M.E., Wright, J.D., Miller, K.G., Feist-Burkhardt, S., Falkowski, P.G., 2005a. Early Jurassic climate change and the radiation of organic-walled phytoplankton in the Tethys Ocean. Paleobiology 31, 73–97.

van de Schootbrugge, B., McArthur, J.M., Bailey, T.R., Rosenthal, Y., Wright, J.D., Miller, K.G., 2005b. Toarcian oceanic anoxic event: An assessment of global causes using belemnite C isotope records. Paleoceanography 20, PA3008.

van de Schootbrugge, B., Tremolada, F., Rosenthal, Y., Bailey, T.R., Feist-Burkhardt, S., Brinkhuis, H., Pross, J., Kent, D.V., Falkowski, P.G., 2007. End-Triassic calcification crisis and blooms of organic-walled 'disaster species.' Palaeogeogr. Palaeoclimatol. Palaeoecol., Triassic-Jurassic Boundary events: problems, progress, possibilities 244, 126–141.

Vermeij, G.J., 1977. The Mesozoic marine revolution: evidence from snails, predators and grazers. Paleobiology 3, 245–258.

Vermeij, G.J., 1987. Evolution and escalation: an ecological history of life. Princeton University Press. pp 521.

Vermeij, G.J., 2008. Escalation and its role in Jurassic biotic history. Palaeogeogr. Palaeoclimatol. Palaeoecol., Jurassic Marine Palaeobiology 263, 3–8.

Wall, D., 1965. Microplankton, Pollen, and Spores from the Lower Jurassic in Britain. Micropaleontology 11, 151–190.

Wall, D., Dale, B., Lohmann, G.P., Smith, W.K., 1977. The environmental and climatic distribution of dinoflagellate cysts in modern marine sediments from regions in the North and South Atlantic Oceans and adjacent seas. Mar. Micropaleontol. 2, 121–200.

Whitaker, M., Giles, M., Cannon, S., 1992. Palynological review of the Brent Group, UK sector, North Aea. Geol. Soc. Lond. Spec. Publ. 61, 169–202.

Wiggan, N.J., Riding, J.B., Franz, M., 2017. Resolving the Middle Jurassic dinoflagellate radiation: The palynology of the Bajocian of Swabia, southwest Germany. Rev. Palaeobot. Palynol. 238, 55–87.

Williams, G., 1992. Palynology as a palaeoenvironmental indicator in the Brent Group, northern North Sea. Geol. Soc. Lond. Spec. Publ. 61, 203–212.

Williams, G., Fensome, R., Miller, M., Sarjeant, W., 2000. A glossary of the terminology applied to dinoflagellates, acritarchs and prasinophytes, with emphasis on fossils. Contrib. Ser.-Am. Assoc. Stratigr. Palynol. 37, pp. 370.

Williams, G.L., Fensome, R.A., and MacRae, R.A., 2017. DINOFLAJ3. American Association of Stratigraphic Palynologists, Data Series no. 2**.** http://dinoflaj.smu.ca/dinoflaj3

Wood, G., Gabriel, A., Lawson, J., 1996. Palynological techniques—processing and microscopy. In: Jansonius, J., McGregor, D.C. (Eds.), Palynology: Principles and Applications Vol. 1. American Association of Stratigraphic Palynologists Foundation, Dallas, Texas, pp. 29–50.

Wood, S.E.L., Riding, J.B., Fensome, R.A., Williams, G.L., 2016. A review of the *Sentusidinium* complex of dinoflagellate cysts. Rev. Palaeobot. Palynol. 234, 61–93.

Woollam, R., 1983. A review of the Jurassic dinocyst genera *Ctenidodinium* Deflandre 1938 and *Dichadogonyaulax* Sarjeant 1966. Palynology 7, 183–196.

Woollam, R., Rhys, G., Lott, G., Calver, M., 1982. Early and Middle Jurassic dinocysts in the Winterborne Kingston borehole, Dorset. Winterborne Kingston Boreh. Dorset Engl. Inst. Geol. Sci. Rep. 89–90.

Woollam, R., Riding, J., 1983. Dinoflagellate Cyst Zonation of the English Jurassic. Inst. Geol. Sci. Rep. 83/2, 1–42.

Yule, B., Roberts, S., Marshall, J., 2000. The thermal evolution of sporopollenin. Org. Geochem. 31, 859–870.

Ziegler, P.A., 1990. Geological Atlas of Western and Central Europe vol. 1. Europe. second ed. Shell Internationale Petroleum Maatschappij B.V., The Hague pp. 239.

Zonneveld, K.A.F., Susek, E., 2007. Effects of temperature, light and salinity on cyst production and morphology of *Tuberculodinium vancampoae* (the resting cyst of *Pyrophacus steinii*). Rev. Palaeobot. Palynol. 145, 77–88.

Zonneveld, K.A.F., Brummer, G.A., 2000. (Palaeo-)ecological significance, transport and preservation of organic-walled dinoflagellate cysts in the Somali Basin, NW Arabian Sea. Deep Sea Res. Part II Top. Stud. Oceanogr. 47, 2229–2256.

Zonneveld, K.A., Versteegh, G.J., de Lange, G.J., 1997. Preservation of organic-walled dinoflagellate cysts in different oxygen regimes: a 10,000 year natural experiment. Mar. Micropaleontol. 29, 393–405.

Zonneveld, K.A., Versteegh, G., Kodrans-Nsiah, M., 2008. Preservation and organic chemistry of Late Cenozoic organic-

walled dinoflagellate cysts: a review. Mar. Micropaleontol. 68, 179–197.

Zonneveld, K.A.F., Marret, F., Versteegh, G.J.M., Bogus, K., Bonnet, S., Bouimetarhan, I., Crouch, E., de Vernal, A., Elshanawany, R., Edwards, L., Esper, O., Forke, S., Grøsfjeld, K., Henry, M., Holzwarth, U., Kielt, J.-F., Kim, S.-Y., Ladouceur, S., Ledu, D., Chen, L., Limoges, A., Londeix, L., Lu, S.-H., Mahmoud, M.S., Marino, G., Matsouka, K., Matthiessen, J., Mildenhal, D.C., Mudie, P., Neil, H.L., Pospelova, V., Qi, Y., Radi, T., Richerol, T., Rochon, A., Sangiorgi, F., Solignac, S., Turon, J.-L., Verleye, T., Wang, Y., Wang, Z., Young, M., 2013. Atlas of modern dinoflagellate cyst distribution based on 2405 data points. Rev. Palaeobot. Palynol., Atlas of modern dinoflagellate cyst distribution based on 2405 data points 191, 1–197.

Data Table Appendicies

Sample no.	Lithostrat. unit	Substage	Weight (g)	Lithology	HF	HCL	ZnCL2	HN03	Palynomorph preservation
62	Ostreenkalk Formation	Lower Bajocian	20.03	Mudstone	1	1	1	1	Fair to good
61	Ostreenkalk Formation	Lower Bajocian	20.02	Mudstone	1	1	1	1	Good to very good
60	Ostreenkalk Formation	Lower Bajocian	20.04	Mudstone	1	1	1	0	Fair to good
59	Ostreenkalk Formation	Lower Bajocian	20.04	Mudstone	1	1	1	1	Good to very good
58	Ostreenkalk Formation	Lower Bajocian	20.41	Mudstone	1	1	1	0	Fair to good
57	Ostreenkalk Formation	Lower Bajocian	20.04	Mudstone	1	1	1	0	Very good
56	Ostreenkalk Formation	Lower Bajocian	20.09	Mudstone	1	1	1	1	Poor to fair
55	Ostreenkalk Formation	Lower Bajocian	20.08	Mudstone	1	1	1	1	Good
54	Ostreenkalk Formation	Lower Bajocian	20.05	Mudstone	1	1	1	1	Very good
53	Ostreenkalk Formation	Lower Bajocian	20.45	Mudstone	1	1	1	1	Fair to good
52	Humphresi oolith Member	Lower Bajocian	20.02	Marl/mudstone w. Fe ooids	1	1	1	1	Very good
51	Humphresi oolith Member	Lower Bajocian	20.07	Marl/mudstone w. Fe ooids	1	1	1	1	Fair to good
50	Humphresi oolith Member	Lower Bajocian	20	Fe oolitic/micritic limestone	1	1	1	0	Fair to good
49	Humphresi oolith Member	Lower Bajocian	20.01	Mudstone	1	1	1	0	Fair to good
48	Ostreenkalk Formation	Lower Bajocian	20.02	Mudstone	1	1	1	1	Good
47	Ostreenkalk Formation	Lower Bajocian	20.46	Mudstone	1	1	1	0	Fair to good
46	Ostreenkalk Formation	Lower Bajocian	20.07	Mudstone	1	1	1	0	Fair to good
45	Ostreenkalk Formation	Lower Bajocian	20.02	Mudstone	1	1	1	0	Good
44	Ostreenkalk Formation	Lower Bajocian	20.006	Mudstone	1	1	1	1	Very good
42	Ostreenkalk Formation	Lower Bajocian	20.02	Mudstone	1	1	1	1	Very good
40	Wedelsandstein Formation	Lower Bajocian	20.09	Sandy mudstone	1	1	1	0	Good to very good
38	Wedelsandstein Formation	Lower Bajocian	20.03	Sandy mudstone	1	1	1	1	Very good
36	Wedelsandstein Formation	Lower Bajocian	10.05	Mudstone+ nodule	1	1	1	0	Excellent
34	Wedelsandstein Formation	Lower Bajocian	20.06	Mudstone	1	1	1	1	Good to very good
34	Wedelsandstein Formation	Lower Bajocian	20.9	Mudstone	1	1	1	0	Good to very good
32	Wedelsandstein Formation	Lower Bajocian	20.55	Calcareous sandy mudstone	1	1	1	0	Good
31	Wedelsandstein Formation	Lower Bajocian	20.04	Calcareous sandy mudstone	1	1	1	1	Very good
30	Wedelsandstein Formation	Lower Bajocian	20.19	Mudstone	1	1	1	1	Very good
28	Wedelsandstein Formation	Lower Bajocian	20.01	Calcareous sandy mudstone	1	1	1	0	Very good
26	Wedelsandstein Formation	Lower Bajocian	20.08	Calcareous sandy mudstone	1	1	1	0	Good to very good
24	Wedelsandstein Formation	Lower Bajocian	20.04	Nodule	1	1	1	0	Very good to excellent
22	Wedelsandstein Formation	Lower Bajocian	20	Mudstone	1	1	1	0	Very good
21	Wedelsandstein Formation	Lower Bajocian	20.06	Mudstone	1	1	Swill.	0	Very good
19	Wedelsandstein Formation	Lower Bajocian	20.07	Mudstone	1	1	1	1	Very good
18	Wedelsandstein Formation	Lower Bajocian	20.02	Mudstone	1	1	1	0	Very good
17	Wedelsandstein Formation	Lower Bajocian	20.3	Mudstone	1	1	1	0	Very good
15	Wedelsandstein Formation	Lower Bajocian	20.02	Mudstone	1	1	1	1	Very good
13	Wedelsandstein Formation	Lower Bajocian	20.1	Mudstone	1	1	1	0	Very good
12	Wedelsandstein Formation	Lower Bajocian	20.09	Mudstone	1	1	1	0	Fair
10	Wedelsandstein Formation	Lower Bajocian	20.2	Mudstone	1	1	1	1	Very good
8	Wedelsandstein Formation	Lower Bajocian	20.06	Mudstone	1	1	1	1	Very good
7	Wedelsandstein Formation	Lower Bajocian	20.07	Mudstone	1	1	1	1	Good
5	Wedelsandstein Formation	Lower Bajocian	20.1	Mudstone	1	1	1	1	Very good
4	Wedelsandstein Formation	Lower Bajocian	20.14	Mudstone	1	1	1	0	Very good
3	Wedelsandstein Formation	Lower Bajocian	20.14	Mudstone	1	1	1	1	Very good
2	Wedelsandstein Formation	Lower Bajocian	20.06	Mudstone	1	1	1	1	Very good
1	Eisensandstein Formation	Upper Aalenian	20.3	Sandy mudstone	1	1	1	0	Fair to good
G5	Sowerbyi Ooilith	Lower Bajocian	21.78	Fe micritic limestone	1	1	1	0	Fair to good
G4	Sowerbyi Ooilith	Lower Bajocian	20.59	Fe micritic limestone	1	1	1	0	Fair to good
G3	Sowerbyi Ooilith	Lower Bajocian	20.17	Fe micritic limestone	1	1	1	0	Good

Data table appendix A.1 (a). Processing procedures and preservation of samples from the Upper Aalenian to Lower Bajocian of Swabia.

For processing procedures 1=was required on sample, 0=was not required.

Sample no.	Lithostrat unit	Substage	Weight (g)	Lithology	HF	HCL	ZnCL2	HN03	Schulze	Palynomorph preservation
109	Dentalienton Formation	Lower Bathonian	9	Phosphorite nodule	1	1	1	0	0	Excellent
108	Dentalienton Formation	Lower Bathonian	20.04	Phosphorite nodule	1	1	1	0	0	Excellent
106	Parkinsoni Ooilth	Lower Bathonian	20	Fe oolitcc/micritic limestone	1	1	1	0	0	Fair to good
105	Parkinsoni Ooilth	Upper Bajocian	20.02	Fe oolitcc/micritic limestone	1	1	1	0	0	Fair to good
104	Parkinsoni Ooilth	Upper Bajocian	20.53	Fe oolitcc/micritic limestone	1	1	1	0	0	Fair to good
103	Parkinsoni Ooilth	Upper Bajocian	20.04	Fe oolitcc/micritic limestone	1	1	1	0	0	Good to very good
102	Parkinsoni Ooilth	Upper Bajocian	20.02	Fe oolitcc/micritic limestone	1	1	1	1	0	Good to very good
101	Hamitenton Formation	Upper Bajocian	20.02	Mudstone	1	1	1	1	1	Good to very good
100	Hamitenton Formation	Upper Bajocian	20.5	Mudstone	1	1	1	0	1	Very poor+ extremely abundant AOM, excluded
99	Hamitenton Formation	Upper Bajocian	20.14	Mudstone	1	1	1	0	0	Very good
98	Hamitenton Formation	Upper Bajocian	20.67	Mudstone	1	1	1	0	1	Very poor+ extremely abundant AOM, excluded
97	Hamitenton Formation	Upper Bajocian	20.12	Mudstone	1	1	1	1	0	Very good
95	Hamitenton Formation	Upper Bajocian	20.27	Mudstone	1	1	1	0	0	Very good
94	Hamitenton Formation	Upper Bajocian	20.02	Mudstone	1	1	1	1	1	Very poor+ extremely abundant AOM, excluded
93	Hamitenton Formation	Upper Bajocian	20	Mudstone	1	1	1	0	1	Fair to good
92	Hamitenton Formation	Upper Bajocian	20	Mudstone	1	1	1	0	1	Good
91	Hamitenton Formation	Upper Bajocian	20.01	Mudstone	1	1	1	1	0	Good
90	Hamitenton Formation	Upper Bajocian	20.01	Mudstone	1	1	1	0	1	Fair to good
89	Hamitenton Formation	Upper Bajocian	20.68	Mudstone	1	1	1	0	0	Good to very good
88	Hamitenton Formation	Upper Bajocian	20.89	Mudstone	1	1	1	0	1	Good to very good
87	Hamitenton Formation	Upper Bajocian	20	Mudstone	1	1	1	1	0	Very poor+ extremely abundant AOM, excluded
86	Hamitenton Formation	Upper Bajocian	20.68	Mudstone	1	1	1	0	1	Good to very good
84	Hamitenton Formation	Upper Bajocian	20.42	Mudstone	1	1	1	0	1	Good to very good
83	Hamitenton Formation	Upper Bajocian	20.04	Mudstone	1	1	1	1	0	Good
82	Hamitenton Formation	Upper Bajocian	20.05	Mudstone	1	1	1	1	0	Good
81	Hamitenton Formation	Upper Bajocian	20.22	Mudstone	1	1	1	0	1	Good to very good
80	Hamitenton Formation	Upper Bajocian	20.02	Mudstone	1	1	1	0	0	Good to very good
78	Hamitenton Formation	Upper Bajocian	20	Mudstone	1	1	1	0	1	Good
77	Hamitenton Formation	Upper Bajocian	20.02	Mudstone	1	1	1	1	0	Very good
76	Hamitenton Formation	Upper Bajocian	20.04	Mudstone	1	1	1	0	0	Good to very good
75	Hamitenton Formation	Upper Bajocian	20.17	Mudstone	1	1	1	0	1	2.5
74	Hamitenton Formation	Upper Bajocian	20.04	Mudstone	1	1	1	0	1	3.5
72	Hamitenton Formation	Upper Bajocian	20.4	Mudstone	1	1	1	0	1	2.5
71	Hamitenton Formation	Upper Bajocian	20.06	Mudstone	1	1	1	0	0	Very good
70	Hamitenton Formation	Upper Bajocian	20.02	Mudstone	1	1	1	0	1	Fair to good
69	Hamitenton Formation	Upper Bajocian	20.02	Mudstone	1	1	1	1	0	Good to very good
68	Hamitenton Formation	Upper Bajocian	20.17	Mudstone	1	1	1	0	1	Good
67	Hamitenton Formation	Upper Bajocian	20.01	Mudstone	1	1	1	1	1	Good
66	Hamitenton Formation	Upper Bajocian	20.67	Mudstone	1	1	1	1	0	Good
65	Subfurcaten Ooilth	Upper Bajocian	20.04	Fe oolitcc/micritic limestone	1	1	1	0	0	Very good
64	Subfurcaten Ooilth	Upper Bajocian	20.6	Fe oolitcc/micritic limestone	1	1	1	0	1	Very good
63	Subfurcaten Ooilth	Upper Bajocian	20.02	Fe oolitcc/micritic limestone	1	1	1	0	0	Fair to good

Data table appendix A.1(b). Processing procedures and preservation of samples from the Upper Bajocian to Lower Bathonian of Swabia.

As per A.1(a).

							Sporomorphs					Sphaeromorphic acritarchs					Acanthomorphic acritarchs			Prasinophytes												
Sample	Depth (B404-2)	Ammonite Zone		Total lycopodium	Net Weight	Lycopodium Counted	Monolete spores	Trilete spores	Bisaccate pollen	Other pollen	*Botryococcus* spp.	*Froomea tornatlis*	*Froomea glabella*	*Froomea senilis*	*Froomea grandis*	Sphaeromorphs indet.	*Micrhystridium* spp.	*Veryhachium* spp.	*Baltisphaeridium* spp.	*Cymatiosphaera* spp.	*Tasmanites* spp.	Foramaniferal test lining	Scolecodont	Dinocysts indet.	Total dinocysts	Total Marine	Total Terrestrial	Total acanthomorphs	Total prasinophytes	Total spores	Total pollen	Total Palynormpohs
62	162.35	*S. humphriesianum*	Ostreenkalk Formation	18583	20.03	11	1	75	10	20	1						39				1	14		24	139	193	106	39	1	76	30	300
61	162.8	*S. humphriesianum*	Ostreenkalk Formation	19332	18.87	35	0	100	5	42							71				2	4		19	66	143	147	71	2	100	47	290
60	163.1	*S. humphriesianum*	Ostreenkalk Formation	38664	14.34	164	3	78	1	9						4	23				5	9		60	164	201	91	23	5	81	10	296
59	163.62	*S. humphriesianum*	Ostreenkalk Formation	19332	20.04	32	1	68	0	33	1				1		58	2			1	8		34	116	185	102	60	1	69	33	289
58	164.07	*S. humphriesianum*	Ostreenkalk Formation	38664	20.41	18	3	95	3	21							46			2	1	11		43	111	171	122	46	3	98	24	293
57	164.74	*S. humphriesianum*	Ostreenkalk Formation	19332	16.07	51	2	78	6	18	1						42	2			2	16		34	136	198	104	44	2	80	24	303
56	165.55	*S. humphriesianum*	Ostreenkalk Formation	38664	19.25	25	13	69	3	55	1						21	1	1		3	8		43	122	156	140	23	3	82	58	297
55	166	*S. humphriesianum*	Ostreenkalk Formation	19332	18.5	32	5	74	3	16	2						66				4	12		45	115	197	98	66	4	79	19	297
54	166.56	*S. humphriesianum*	Ostreenkalk Formation	19332	16.45	40	0	54	7	15							128				P	5		23	87	220	76	128	0	54	22	296
53	167.31	*S. humphriesianum*	Ostreenkalk Formation	38664	18.9	46	3	41	4	5	5				1		36				1	4		77	190	231	53	36	1	44	9	290
52	167.89	*S. humphriesianum*	Humphresi oolith Member	18583	19.8	16	6	69	8	15	1						42	1			6	11		48	142	202	98	43	6	75	23	301
51	168.26	*S. humphriesianum*	Humphresi oolith Member	38664	18.53	35	3	68	8	19	1						40				2	5		34	149	196	98	40	2	71	27	295
50	168.79	*S. humphriesianum*	Humphresi oolith Member	19332	13.45	308	4	81	5	7		1					26				2	2		52	172	202	97	26	2	85	12	300
49	168.83	*S. humphriesianum*	Humphresi oolith Member	38664	19.51	249	7	92	12	8	2					2	16				2	9		91	154	181	119	16	2	99	20	304
48	169	*S. humphriesianum*	Ostreenkalk Formation	18583	16.92	45	2	150	20	20	2						15				8	35		16	54	112	192	15	8	152	40	306
47	169.56	*S. humphriesianum*	Ostreenkalk Formation	19332	20.46	435	12	106	3	41	1					1	26				7	17		18	87	137	162	26	7	118	44	301
46	169.84	*S. humphriesianum*	Ostreenkalk Formation	19332	17.27	49	3	112	7	18							41				5	6		20	117	169	140	41	5	115	25	309
45	170	*opinquans/S. humphriesiar*	Ostreenkalk Formation	18583	13.37	39	0	68	8	13	1					3	18				8	4		30	178	208	89	18	8	68	21	301
44	170.41	*opinquans/S. humphriesiar*	Ostreenkalk Formation	19332	19.48	280	3	83	5	12	P					13	20			2	19	5	1	14	150	197	103	20	21	86	17	313
42	171.42	*S. propinquans/Leviuscula*	Ostreenkalk Formation	18583	19.37	27	0	78	21	19	1	P					111				1	13		13	62	187	118	111	1	78	40	306
40	172.59	*S. propinquans/Leviuscula*	Wedelsandstein Formation	19332	18.83	118	0	153	2	56	6						37				6	0		2	51	94	211	37	6	153	58	311
38	173.63	*S. propinquans/Leviuscula*	Wedelsandstein Formation	19332	15.58	82	1	160	4	75	4						26				13	2		1	18	59	240	26	13	161	79	303
36	174.64	*S. propinquans/Leviuscula*	Wedelsandstein Formation	19332	6.85	366	1	165	0	61							34				2	0		6	39	75	227	34	2	166	61	302
34	176.15	*S. propinquans/Leviuscula*	Wedelsandstein Formation	38664	19.18	18		136	18	97	2	2				1	25		P		3	1		1	19	48	251	25	3	136	115	304
32	177.23	*W. laeviuscula*	Wedelsandstein Formation	19332	20.55	227	4	117	7	40	1					24	25				2	4		23	77	108	168	25	2	121	47	301
31	178.11	*W. laeviuscula*	Wedelsandstein Formation	19332	19.66	51	3	93	19	32						3	119	2			P	4		4	32	157	147	121	0	96	51	307
30	178.83	*W. laeviuscula*	Wedelsandstein Formation	38664	20.19	66	4	80	11	19						4	27		10	3	5	2		2	143	190	114	37	8	84	30	308
28	180.65	*W. laeviuscula*	Wedelsandstein Formation	18583	20.01	83	1	27	1	16						13	16		2		6	1		19	222	247	45	18	6	28	17	305
26	181.75	*W. laeviuscula*	Wedelsandstein Formation	19332	19.74	94	3	96	1	9							37				1	0		12	140	178	109	37	1	99	10	287
24	183.5	*W. laeviuscula*	Wedelsandstein Formation	19332	16.41	166	1	46	15	35	P	P					27				2	1		7	172	202	97	27	2	47	50	299
22	184.77	*W. laeviuscula*	Wedelsandstein Formation	19332	20.01	32	2	52	9	17						16	26				4	2		15	177	209	80	26	4	54	26	305
21	185.58	*W. laeviuscula*	Wedelsandstein Formation	19332	19.98	32	1	64	8	31							52				3	2	1	1	142	200	104	52	3	65	39	304
19	186.95	*W. laeviuscula*	Wedelsandstein Formation	19332	19.57	24	4	97	16	43	1						28				1	4		3	110	143	160	28	1	101	59	304
18	187.43	*W. laeviuscula*	Wedelsandstein Formation	19332	17.22	88	2	41	8	15						6	27				7	1		4	204	239	66	27	7	43	23	311
17	188.07	*W. laeviuscula*	Wedelsandstein Formation	19332	20.3	24	6	56	13	18							24				2	0		8	186	212	93	24	2	62	31	305
15	189	*W. laeviuscula*	Wedelsandstein Formation	18583	20.02	32	1	82	8	13							27				3	0		4	172	202	104	27	3	83	21	306
13	190	*W. laeviuscula*	Wedelsandstein Formation	19332	20.1	190	0	58	0	13							65	3	2		1	2		7	161	234	71	70	1	58	13	305
12	190.76	*W. laeviuscula*	Wedelsandstein Formation	19332	19.94	59	15	65	9	32						3	19				P	3		44	154	176	121	19	0	80	41	300
10	191.94	*W. laeviuscula*	Wedelsandstein Formation	19332	19.95	29	12	66	11	13	P					3	78	1	1	1	3	12	1	35	105	202	102	80	4	78	24	307
8	193.4	*W. laeviuscula*	Wedelsandstein Formation	19332	19.59	49	5	96	15	49							31	1				0	1	3	116	149	165	32	0	101	64	314
7	193.73	*W. laeviuscula*	Wedelsandstein Formation	38664	20.05	37	34	142	12	35							44	1			1	2		21	65	113	223	45	1	176	47	336
5	194.78	*W. laeviuscula*	Wedelsandstein Formation	19332	19.76	20	32	129	36	30							52	3	4	2	1	1		1	52	115	227	59	3	161	66	342
4	195.7	*W. laeviuscula*	Wedelsandstein Formation	19332	19.56	33	22	118	11	54		P				1	48		1	1	1	5		2	74	130	205	49	2	140	65	336
2	196.4	*W. laeviuscula*	Wedelsandstein Formation	18583	20.06	33	9	80	4	54							39	1	3	4	8	10	1	15	87	153	147	43	12	89	58	300
G3		*H. discites*	Sowerbyi Oolith Member	38664	12.46	352	4	87	18	##		1				8	13				5	2		3	53	73	219	13	5	91	128	301
G4		*H. discites*	Sowerbyi Oolith Member	38664	20.59	149	1	94	4	##		1				20	8				7	4			44	63	217	8	7	95	122	301
G5		*H. discites*	Sowerbyi Oolith Member	38664	21.78	121	2	91	4	92						1	55				4	1		3	54	114	189	55	4	93	96	304

Data table appendix A.2(a). Raw palynology count data for the Upper Aalenian to Lower Bajocian of Swabia.

							Sporomorphs				Sphaeromorphic acritarchs						Acanthomorphic acritarchs			Prasinophytes												
Sample	Depth (B404-2)	Ammonite Zone	Lithostrat unit.	Total lycopodium	Net Weight	Lycopodium Counted	Monolete spores	Trilete spores	Bisaccate pollen	Other pollen	*Botryococcus* spp.	*Froomea tornatlis*	*Froomea glabella*	*Froomea senilis*	*Froomea grandis*	Sphaeromorphs indet.	*Micrhystridium* spp.	*Veryhachium* spp.	*Baltisphaeridium* spp.	*Cymatiosphaera* spp.	*Tasmanites* spp.	Foramaniferal test lining	Scolecodont	Dinocysts indet.	Total dinocysts	Total Marine	Total Terrestrial	Total acanthomorphs	Total prasinophytes	Total spores	Total pollen	Total Palynormpohs
109	140.8	*Z. zigzag*	Dentalienton Fm.	19332	6.96	36	0	6	4	7		P					15				P	0		23	272	287	17	15	0	6	11	304
108	143.1	*Z. zigzag*	Dentalienton Fm.	19332	10.4	203	0	10	1	2							9				2	2		16	277	290	13	9	2	10	3	303
106	144.61	*Z. zigzag*	Parkinsoni Oolith Mb.	19332	20.01	84	1	33	0	15							17		1			0	1	38	233	252	49	18	0	34	15	301
105	144.66	*P. parkinsoni*	Parkinsoni Oolith Mb.	18583	20.02	33	0	11	8	14		P					25			P		1		23	233	259	33	25	0	11	22	292
104	144.91	*P. parkinsoni*	Parkinsoni Oolith Mb.	19332	20.53	143	0	44	8	12						2	10				7	0		49	218	235	64	10	7	44	20	301
103	144.96	*P. parkinsoni*	Parkinsoni Oolith Mb.	19332	10.56	26	0	28	13	25						6	11				6	1		34	212	230	66	11	6	28	38	302
102	144.97	*P. parkinsoni*	Parkinsoni Oolith Mb.	18583	15.32	23	1	36	7	9							34					6		26	207	247	53	34	0	37	16	300
101	145.05	*G. garantiana*	Hemitenton Fm.	19332	13.14	26	0	59	8	10						2	24				11	0		54	187	222	77	24	11	59	18	301
99	145.88	*G. garantiana*	Hemitenton Fm.	38664	19.54	28		62	15	19						1	18				7	2		5	177	204	96	18	7	62	34	301
97	146.71	*G. garantiana*	Hemitenton Fm.	19332	19.55	11	2	65	38	19						1	36			5	7	2		24	126	176	124	36	12	67	57	301
95	147.55	*G. garantiana*	Hemitenton Fm.	38664	19.09	14	0	44	12	23		P					25		1		7	3		17	184	220	79	26	7	44	35	299
93	148.41	*G. garantiana*	Hemitenton Fm.	19332	20.01	5	1	57	16	23							15		1		5	1		33	183	205	97	16	5	58	39	302
92	148.9	*G. garantiana*	Hemitenton Fm.	19332	20.01	11	1	64	15	24	1					2	33				7	1		26	156	197	104	33	7	65	39	304
91	149.2	*G. garantiana*	Hemitenton Fm.	18583	20.02	6	2	70	23	26							29				5	6		30	135	175	121	29	5	72	49	296
90	150.14	*G. garantiana*	Hemitenton Fm.	38664	20.01	29		77	2	17							8				4	2		38	190	204	96	8	4	77	19	300
89	150.74	*G. garantiana*	Hemitenton Fm.	38664	20.18	29		64	21	8							37				5	4		18	161	207	93	37	5	64	29	300
88	151.15	*G. garantiana*	Hemitenton Fm.	38664	20.89	25		56	10	27						4	22			9	8	3		26	163	205	93	22	17	56	37	302
86	152.12	*G. garantiana*	Hemitenton Fm.	38664	20.68	21	3	54	6	24						1	27				3	2		39	179	211	87	27	3	57	30	299
84	153	*G. garantiana*	Hemitenton Fm.	38664	20.42	42	2	52	1	19						1	16				8	3		39	199	226	74	16	8	54	20	301
83	153.5	*G. garantiana*	Hemitenton Fm.	18583	20.04	14	4	29	12	17	1						18				7	13		29	201	239	62	18	7	33	29	302
82	153.71	*S. niortense*	Hemitenton Fm.	19332	20.05	41	3	47	18	13		P				1	23				6	18		55	171	218	81	23	6	50	31	300
81	154	*S. niortense*	Hemitenton Fm.	38664	20.22	39	1	55	8	14							14				10	4		33	192	220	78	14	10	56	22	298
80	154.4	*S. niortense*	Hemitenton Fm.	19332	20.02	47	7	46	3	20			1			4	48				5	6		15	160	219	76	48	5	53	23	300
78	155.32	*S. niortense*	Hemitenton Fm.	19332	20.01	10	1	33	13	12	P					1	13			1	3	2		33	222	241	59	13	4	34	25	301
77	155.91	*S. niortense*	Hemitenton Fm.	18583	20.02	18	0	62	22	12			1			2	31				8	4	1	20	158	202	96	31	8	62	34	301
76	156.4	*S. niortense*	Hemitenton Fm.	19332	20.04	42	6	68	15	14						2	28				9	7		23	148	192	103	28	9	74	29	297
75	156.82	*S. niortense*	Hemitenton Fm.	38664	20.17	33	2	87	10	22						2	20	1			7	0	P	43	148	176	121	21	7	89	32	299
74	157.03	*S. niortense*	Hemitenton Fm.	19332	20.04	20	0	56	9	8						2	21				15	2		16	186	224	73	21	15	56	17	299
72	157.78	*S. niortense*	Hemitenton Fm.	38664	20.04	24	3	86	12	20							30				8	0		15	139	177	121	30	8	89	32	298
71	158.16	*S. niortense*	Hemitenton Fm.	18583	20.06	6	1	45	11	15		P				3	27				7	3		14	186	223	72	27	7	46	26	298
70	158.88	*S. niortense*	Hemitenton Fm.	38664	20.02	22	3	74	2	15							34		2		7	6		24	156	205	94	36	7	77	17	299
69	159.4	*S. niortense*	Hemitenton Fm.	19332	20.02	35	0	57	5	10							28		1		6	3		30	189	227	72	29	6	57	15	299
68	160.09	*S. niortense*	Hemitenton Fm.	38664	20.17	28	6	75	11	20						4	23				2	9		36	148	182	112	23	2	81	31	298
67	160.18	*S. niortense*	Hemitenton Fm.	19332	20.01	19	0	45	17	24							14				14	3		29	178	209	86	14	14	45	41	295
66	160.53	*S. niortense*	Hemitenton Fm.	19332	20.67	30	2	38	8	13						1	28	2			1	0		36	200	231	61	30	1	40	21	293
65	160.9	*S. niortense*	Subfurcaten Oolith Mb.	19332	20.04	22	54	3	5	16							47				P	2		21	168	217	78	47	0	57	21	295
64	161.4	*S. niortense*	Subfurcaten Oolith Mb.	38664	19.4	67	4	84	3	16							68		1			3		24	118	190	107	69	0	88	19	297
63	161.87	*S. niortense*	Subfurcaten Oolith Mb.	18583	20.02	41	6	49	12	4							93				3	19		42	109	224	71	93	3	55	16	295

Data table appendix A.2(b). Raw palynology count data for the Upper Bajocian to Lower Bathonian of Swabia.

	Percentage error						Absolute abundances						Absolute abundance error					
Sample (B404/2)	Total dinocysts	Total acanthomorphs	*Michrystridium spp.*	Total prasinophytes	Total spores	Total pollen	Total dinocysts per g	Total acanthomorphs per g	*Micrhystridium* per g	Total prasinophytes per g	Total spores per g	Total pollen per g	Dinocysts per g +/-	Acanthomorphs per g +/-	Micrhystridium per g +/-	Prasinophytes per g +/-	Spores per g +/-	Pollen per g +/-
109	6.9423	6.9468	6.9468		6.954	6.9485	21063	1157.3	1157.3	0	462.93	848.7069	1462.3	80.397	80.397	0	32.192	58.973
108	6.9406	6.9484	6.9484	6.9763	6.9476	6.9643	2527.3	82.412	82.412	18.314	91.569	27.470633	175.41	5.7263	5.7263	1.2776	6.3618	1.9131
106	6.9412	6.9449	6.9451		6.943	6.9457	2679.8	207.03	195.52	0	391.05	172.52088	186.01	14.378	13.579	0	27.15	11.983
105	4.1042	4.1086	4.1086		4.1148	4.1092	6553.8	703.2	703.2	0	309.41	618.81452	268.98	28.891	28.891	0	12.731	25.429
104	6.9408	6.9477	6.9477	6.9508	6.9421	6.9441	1435.5	65.849	65.849	46.095	289.74	131.69879	99.637	4.575	4.575	3.2039	20.114	9.1453
103	6.9431	6.9493	6.9493	6.9548	6.9453	6.9447	14927	774.52	774.52	422.47	1971.5	2675.6119	1036.4	53.824	53.824	29.381	136.93	185.81
102	4.1059	4.1089	4.1089		4.1086	4.1129	10917	1793.1	1793.1	0	1951.3	843.81882	448.24	73.677	73.677	0	80.172	34.705
101	6.9432	6.9458	6.9458	6.9493	6.944	6.9468	10582	1358.1	1358.1	622.44	3338.6	1018.5458	734.69	94.328	94.328	43.256	231.83	70.756
99	3.476	3.4831	3.4831	3.4956	3.4775	3.4794	12508	1272	1272	494.68	4381.4	2402.7197	434.78	44.306	44.306	17.292	152.36	83.6
97	6.9471	6.9485	6.9485	6.9525	6.9476	6.9478	11327	3236.2	3236.2	1078.7	6023	5124.0363	786.89	224.87	224.87	75	418.45	356.01
95	3.4811	3.4858	3.486	3.5007	3.4835	3.4844	26619	3761.4	3616.7	1012.7	6365.4	5063.384	926.62	131.11	126.08	35.451	221.74	176.43
93	6.9548	6.9589	6.9592	6.9688	6.9556	6.9562	35360	3091.6	2898.4	966.12	11207	7535.7121	2459.2	215.14	201.7	67.326	779.51	524.2
92	6.947	6.9487	6.9487	6.9568	6.9477	6.9484	13701	2898.4	2898.4	614.8	5708.9	3425.3237	951.83	201.4	201.4	42.771	396.63	238
91	4.1212	4.1245	4.1245	4.1445	4.122	4.1228	20885	4486.4	4486.4	773.52	11139	7580.4779	860.71	185.04	185.04	32.058	459.13	312.52
90	3.4757	3.4929	3.4929	3.5108	3.4768	3.4825	12659	533.03	533.03	266.52	5130.4	1265.9463	440.01	18.618	18.618	9.3567	178.38	44.087
89	3.4759	3.4789	3.4789	3.5036	3.4772	3.4799	10637	2444.5	2444.5	330.34	4228.3	1915.9564	369.72	85.04	85.04	11.574	147.03	66.674
88	3.4766	3.4823	3.4823	3.4842	3.4783	3.4796	12067	1628.7	1628.7	1258.6	4145.9	2739.2398	419.54	56.717	56.717	43.851	144.21	95.316
86	3.4777	3.4822	3.4822	3.5245	3.4794	3.4816	15936	2403.8	2403.8	267.09	5074.7	2670.9036	554.21	83.705	83.705	9.4135	176.57	92.991
84	3.4742	3.4824	3.4824	3.4914	3.4761	3.4806	8971.3	721.31	721.31	360.65	2434.4	901.63705	311.68	25.119	25.119	12.592	84.623	31.383
83	4.1093	4.1155	4.1155	4.126	4.1124	4.1129	13313	1192.2	1192.2	463.65	2185.8	1920.8262	547.08	49.066	49.066	19.13	89.887	79.002
82	6.9422	6.9449	6.9449	6.9538	6.9432	6.9441	4021.4	540.89	540.89	141.1	1175.8	729.02135	279.17	37.564	37.564	9.8118	81.641	50.624
81	3.4744	3.484	3.484	3.4881	3.4763	3.4802	9413.7	686.42	686.42	490.3	2745.7	1078.6578	327.08	23.915	23.915	17.102	95.447	37.54
80	6.942	6.943	6.943	6.9559	6.9429	6.9447	3287.3	986.18	986.18	102.73	1088.9	472.54448	228.2	68.471	68.471	7.1456	75.602	32.817
78	6.9475	6.9527	6.9527	6.9652	6.9493	6.9501	21448	1256	1256	386.45	3284.8	2415.2924	1490.1	87.323	87.323	26.917	228.27	167.86
77	4.1075	4.1107	4.1107	4.122	4.1087	4.1103	8147.7	1598.6	1598.6	412.54	3197.2	1753.3078	334.67	65.714	65.714	17.005	131.36	72.067
76	6.9422	6.9443	6.9443	6.9497	6.9427	6.9442	3399.3	643.11	643.11	206.72	1699.7	666.08212	235.99	44.66	44.66	14.366	118	46.254
75	3.4753	3.4812	3.4816	3.4949	3.476	3.4789	8597	1219.8	1161.8	406.62	5169.8	1858.8182	298.78	42.466	40.447	14.211	179.7	64.666
74	6.944	6.947	6.947	6.9484	6.9449	6.9478	8971.4	1012.9	1012.9	723.5	2701.1	819.97006	622.98	70.367	70.367	50.272	187.59	56.97
72	3.477	3.4808	3.4808	3.4939	3.4776	3.4805	11174	2411.7	2411.7	643.11	7154.6	2572.4551	388.53	83.945	83.945	22.47	248.81	89.534
71	4.1209	4.1248	4.1248	4.1376	4.1229	4.1249	28717	4168.7	4168.7	1080.8	7102.2	4014.2738	1183.4	171.95	171.95	44.718	292.82	165.59
70	3.4775	3.4805	3.4808	3.497	3.4784	3.485	13694	3160.3	2984.7	614.49	6759.4	1492.344	476.22	109.99	103.89	21.489	235.12	52.008
69	6.9424	6.9445	6.9446	6.9541	6.9433	6.9469	5214.4	800.1	772.51	165.54	1572.6	413.8433	362.01	55.563	53.648	11.512	109.19	28.749
68	3.4761	3.4814	3.4814	3.5464	3.4769	3.4798	10132	1574.6	1574.6	136.92	5545.3	2122.2891	352.21	54.818	54.818	4.8557	192.81	73.851
67	6.9442	6.9489	6.9489	6.9489	6.9454	6.9455	9051	711.88	711.88	711.88	2288.2	2084.7787	628.52	49.468	49.468	49.468	158.92	144.8
66	6.9428	6.9448	6.945	7.0141	6.9442	6.9458	6235.1	935.27	872.92	31.176	1247	654.68795	432.89	64.953	60.624	2.1867	86.596	45.474
65	6.9437	6.9448	6.9448		6.9445	6.9467	7366.6	2060.9	2060.9	0	2499.4	920.82199	511.51	143.12	143.12	0	173.57	63.967
64	3.4734	3.4742	3.4743		3.4738	3.4797	3510	2052.5	2022.7	0	2617.7	565.17618	121.92	71.308	70.275	0	90.932	19.667
63	4.1041	4.1043	4.1043	4.1434	4.1052	4.1106	2467.7	2105.5	2105.5	67.919	1245.2	362.23289	101.28	86.415	86.415	2.8141	51.117	14.89
62	4.1119	4.1142	4.1142	4.2309	4.1127	4.1151	11723	3289.3	3289.3	84.342	6410	2530.2501	482.06	135.33	135.33	3.5685	263.62	104.12
61	6.9431	6.9431	6.9431	6.978	6.9428	6.9436	1931.9	2078.2	2078.2	58.542	2927.1	1375.7347	134.13	144.29	144.29	4.085	203.22	95.525
60	3.4718	3.4771	3.4771	3.4996	3.4727	3.4853	2696.2	378.13	378.13	82.202	1331.7	164.40453	93.607	13.148	13.148	2.8767	46.245	5.7299
59	6.9429	6.9435	6.9435	7.0139	6.9433	6.9444	3496.9	1808.8	1748.5	30.146	2080.1	994.81662	242.79	125.59	121.4	2.1144	144.43	69.084
58	3.4793	3.4811	3.4811	3.5256	3.4795	3.484	11682	4841.2	4841.2	315.73	10314	2525.8207	406.45	168.53	168.53	11.131	358.86	87.999
57	6.9419	6.943	6.9431	6.9773	6.9423	6.9444	3208	1037.9	990.7	47.176	1887	566.1115	222.7	72.06	68.785	3.2916	131	39.313
56	3.4769	3.482	3.4826	3.5234	3.4775	3.4782	9801.6	1847.8	1687.2	241.02	6587.9	4659.7652	340.79	64.342	58.757	8.4921	229.1	162.08
55	6.9429	6.9433	6.9433	6.9602	6.9432	6.946	3755.4	2155.3	2155.3	130.62	2579.8	620.4527	260.73	149.65	149.65	9.0916	179.12	43.097
54	6.9426	6.9424	6.9424		6.9431	6.9451	2556.1	3760.6	3760.6	0	1586.5	646.35866	177.46	261.08	261.08	0	110.15	44.89
53	3.4739	3.4771	3.4771	3.6142	3.4764	3.4891	8449.7	1601	1601	44.472	1956.8	400.24845	293.53	55.669	55.669	1.6073	68.025	13.965
52	4.1085	4.1104	4.1105	4.1279	4.1092	4.1129	8329.5	2522.3	2463.7	351.95	4399.4	1349.1446	342.22	103.68	101.27	14.528	180.78	55.489
51	3.4751	3.4777	3.4777	3.5453	3.4761	3.4794	8882.8	2384.6	2384.6	119.23	4232.7	1609.6338	308.68	82.931	82.931	4.2272	147.14	56.006
50	6.9407	6.943	6.943	6.9762	6.9411	6.9462	802.66	121.33	121.33	9.3333	396.66	55.999614	55.71	8.4241	8.4241	0.6511	27.533	3.8899
49	3.4715	3.4796	3.4796	3.5419	3.472	3.4778	1225.7	127.34	127.34	15.918	787.93	159.17694	42.549	4.4309	4.4309	0.5638	27.357	5.5358
48	4.105	4.1108	4.1108	4.1179	4.1035	4.1058	1317.9	366.1	366.1	195.25	3709.8	976.25427	54.101	15.05	15.05	8.0403	152.23	40.083
47	6.941	6.9429	6.9429	6.9505	6.9408	6.9418	188.97	56.475	56.475	15.205	256.31	95.572859	13.117	3.921	3.921	1.0568	17.79	6.6345
46	6.9421	6.9432	6.9432	6.9559	6.9421	6.9444	2672.8	936.64	936.64	114.22	2627.2	571.12133	185.55	65.033	65.033	7.9453	182.38	39.661
45	4.1038	4.1099	4.1099	4.1183	4.1049	4.1089	6343.7	641.49	641.49	285.11	2423.4	748.40918	260.33	26.365	26.365	11.742	99.479	30.752
44	6.9407	6.9439	6.9439	6.9437	6.9411	6.9445	531.64	70.886	70.886	77.974	304.81	74.430185	36.9	4.9222	4.9222	5.4143	21.157	5.1688
42	4.1065	4.1056	4.1056	4.2246	4.1061	4.1076	2203	3944.1	3944.1	35.532	2771.5	1421.2891	90.466	161.93	161.93	1.5011	113.8	58.38
40	6.942	6.9426	6.9426	6.9526	6.9411	6.9419	443.73	321.92	321.92	52.203	1331.2	504.62929	30.804	22.349	22.349	3.6295	92.398	35.031
38	6.9449	6.9436	6.9436	6.9464	6.9413	6.9418	272.38	393.43	393.43	196.72	2436.2	1195.4257	18.916	27.318	27.318	13.665	169.11	82.984
36	6.942	6.9423	6.9423	6.9761	6.9406	6.9414	300.73	262.17	262.17	15.422	1280	470.36496	20.876	18.201	18.201	1.0758	88.841	32.65
34	4.1132	4.1116	4.1116	4.1472	4.1077	4.1078	2127.8	2799.8	2799.8	335.97	15231	12879.041	87.522	115.12	115.12	13.933	625.63	529.05
32	6.9413	6.9432	6.9432	6.9762	6.9409	6.9419	319.1	103.6	103.6	8.2884	501.45	194.77668	22.15	7.1935	7.1935	0.5782	34.805	13.521
31	6.9437	6.942	6.942		6.9422	6.9428	616.98	2333	2294.4	0	1850.9	983.31638	42.841	161.95	159.28	0	128.5	68.27
30	3.4732	3.4761	3.4775	3.4901	3.4739	3.477	4149.2	1073.6	783.41	232.12	2437.3	870.45792	144.11	37.318	27.243	8.1014	84.669	30.266
28	4.102	4.1082	4.1091	4.1217	4.1058	4.1086	2484	201.4	179.02	67.134	313.29	190.21272	101.89	8.2741	7.3562	2.7671	12.863	7.8151
26	6.9413	6.9427	6.9427	7.0124	6.9415	6.948	1458.6	385.48	385.48	10.418	1031.4	104.18418	101.24	26.763	26.763	0.7306	71.596	7.2387
24	6.9409	6.9431	6.9431	6.9764	6.942	6.9419	1220.6	191.61	191.61	14.194	333.55	354.838	84.723	13.304	13.304	0.9902	23.155	24.632
22	6.9427	6.945	6.945	6.9602	6.9436	6.945	5343.8	784.97	784.97	120.76	1630.3	784.97001	371	54.516	54.516	8.4055	113.2	54.516
21	6.9428	6.9436	6.9436	6.9662	6.9434	6.9441	4293.6	1572.3	1572.3	90.709	1965.4	1179.223	298.09	109.17	109.17	6.319	136.46	81.886
19	6.9437	6.9456	6.9456	7.0146	6.9437	6.9442	4527.6	1152.5	1152.5	41.16	4157.2	2428.4364	314.38	80.046	80.046	2.8872	288.66	168.64
18	6.9412	6.9435	6.9435	6.9511	6.9425	6.944	2602.5	344.45	344.45	89.302	548.57	293.41939	180.64	23.917	23.917	6.2074	38.084	20.375
17	6.9434	6.946	6.946	6.9789	6.9442	6.9453	7380.4	952.32	952.32	79.36	2460.1	1230.0739	512.45	66.148	66.148	5.5384	170.84	85.433
15	4.1045	4.1083	4.1083	4.1442	4.1053	4.1096	4989.2	783.19	783.19	87.021	2407.6	609.14554	204.78	32.176	32.176	3.6063	98.838	25.033
13	6.9408	6.9414	6.9415	7.0121	6.9416	6.9459	814.99	354.34	329.03	5.0621	293.6	65.806756	56.567	24.596	22.84	0.355	20.381	4.5709
12	6.9417	6.945	6.945		6.9421	6.943	2530.6	312.21	312.21	0	1314.6	673.72626	175.67	21.683	21.683	0	91.26	46.777
10	6.9432	6.9434	6.9434	6.9605	6.9434	6.9455	3508.5	2673.2	2606.3	133.66	2606.3	801.9497	243.6	185.61	180.97	9.3032	180.97	55.699
8	6.9421	6.9437	6.9438		6.9422	6.9426	2336.2	644.46	624.32	0	2034.1	1288.9208	162.18	44.75	43.352	0	141.21	89.485
7	3.4761	3.4771	3.4772	3.615	3.4747	3.477	3387.7	2345.3	2293.2	52.118	9172.8	2449.5626	117.76	81.549	79.739	1.8841	318.73	85.17
5	6.945	6.9448	6.945	6.9676	6.944	6.9447	2543.7	2886.1	2543.7	146.75	7875.6	3228.5223	176.66	200.43	176.66	10.225	546.89	224.21
4	6.9432	6.9437	6.9437	6.9781	6.9427	6.9433	2216.3	1467.5	1437.6	59.9	4193	1946.7373	153.88	101.9	99.822	4.1799	291.11	135.17
2	4.1051	4.1065	4.1068	4.1138	4.1051	4.1058	2442.3	1207.1	1094.8	336.86	2498.4	1628.167	100.26	49.569	44.962	13.858	102.56	66.849
1	3.4789	3.4713	3.491	3.4789	3.4713	3.4807	377.33	41.926	41.926	101.82	1000.2	83.851659	13.127	1.4554	1.4636	3.5422	34.721	2.9186
min.	3.4715	3.4713	3.4743	3.4789	3.4713	3.477												
max.	6.9548	6.9589	6.9592	7.0146	6.9556	6.9643												

Data table appendix A. 3a. Absolute abundance errors for main palynomorph groups from Swabia.

	Percentage error							Absolute abundance							Percentage error of absolute abundance						
Sample (B404/2)	*Dissiliodinium giganteum*	*Batiacasphaera* spp.	*Ctenidodinium* spp.	*Ellipsoidictyum/Valensiella* complex	*Acanthaulax crispa*	*Sentusidinium* spp.	*Ctenidodinium combazii*	*D. giganteum* per g	*Batiacasphaera* spp. per g	*Ctenidodinium* per g	*Ellipsoidictyum/Valensiella* complex per g	*Acanthaulax crispa* per g	*Sentusidinium* spp. per g	*Ctenidodinium combazii* per g	*D. giganteum* per g +/-	*Batiacasphaera* per g +/-	*Ctenodinium* per g +/-	*Ellipsoidictyum/Valensiella complex* per g +/-	*A. crispa* per g +/-	*Sentusidinium* per g +/-	*C. combazii* per g +/-
109	6.96	6.9523	6.9425	6.96	0	6.966	6.9426	617.24	540.09	13734	308.62	0	231.47	9567.2	42.96	37.548	953.45	21.48	0	16.124	664.21356
108	0	7.1227	6.9468	6.9484	0	0	6.9492	0	9.1569	223.67	27.471	0	0	1162.9	0	0.6522	15.538	1.9088	0	0	80.8141254
106	7.1252	6.9469	6.9588	6.9433	6.9768	6.9454	7.1252	11.501	138.02	46.557	345.04	23.278	184.22	11.514	0.8195	9.5878	3.2398	23.957	1.6241	12.795	0.82039553
105	4.1978	4.1159	4.1216	4.1777	4.2238	4.1189	0	562.56	281.28	196.9	815.71	28.128	225.23	0	23.615	11.577	8.1153	34.078	1.1881	9.2772	0
104	6.9549	6.9435	7.1217	6.9495	6.9549	6.9426	0	32.925	158.04	6.5849	52.68	32.925	223.89	0	2.2899	10.973	0.469	3.661	2.2899	15.544	0
103	6.9675	6.9454	6.9535	6.9484	6.9787	6.944	7.1442	281.64	1901.1	492.88	844.93	14.822	4154.2	7.4184	19.624	132.04	34.272	58.709	1.0344	288.47	0.52998334
102	4.1227	4.1114	4.2253	4.116	4.1457	4.1888	0	369.17	1054.8	52.739	896.56	158.22	1793.1	0	15.22	43.366	2.2284	36.902	6.5592	75.11	0
101	0	6.9462	6.9488	6.9675	6.9548	6.9443	0	0	1188.3	679.36	226.34	339.52	3225.4	0	0	82.542	47.207	15.771	23.612	223.98	0
99	3.4896	3.4789	3.4871	3.4882	3.4836	3.4814	0	706.68	2685.4	848.19	777.35	121.36	1625.4	0	24.66	93.423	29.577	27.116	4.2277	56.585	0
97	7.1816	6.9495	6.9693	6.9528	6.9585	6.9495	0	89.895	2157.5	449.48	1168.6	539.37	2157.5	0	6.4559	149.94	31.325	81.253	37.532	149.94	0
95	3.4962	3.4839	3.5747	3.4862	3.4933	3.4863	0	1302	5786.7	112.68	3327.4	1591.3	3472.3	0	45.521	201.6	4.0279	116	55.591	121.06	0
93	6.9925	6.9586	6.9624	6.9577	6.9559	6.9634	0	386.45	3284.8	1739.1	3864.5	981.5	1545.8	0	27.022	228.58	121.09	268.88	68.272	107.64	0
92	6.9693	6.9492	6.9585	6.9517	6.9488	6.9525	0	439.14	2371.4	526.97	1053.9	281.52	153.95	0	30.605	164.79	36.67	73.267	19.562	10.703	0
91	4.1851	4.1338	4.1653	4.1313	4.1279	4.1267	0	309.41	1856.4	464.12	1701.7	2475.3	2939.4	0	12.949	76.741	19.332	70.304	102.18	121.3	0
90	3.4989	3.4872	3.5362	3.4796	3.4797	3.4862	0	399.77	1665.7	333.14	2065.5	2332.6	866.17	0	13.987	58.086	11.781	71.872	81.17	30.196	0
89	3.5175	3.4793	3.5175	3.4849	3.4799	3.4882	0	264.27	2180.2	264.27	1651.7	1916	726.74	0	9.2958	75.857	9.2958	57.56	66.674	25.35	0
88	0	3.4842	3.4962	3.4837	3.4796	3.4872	0	0	1258.6	518.23	1332.6	2739.2	2147	0	0	43.851	18.119	46.424	95.316	74.868	0
86	3.6179	3.4896	3.5747	3.4822	3.4848	3.4837	0	89.03	3116.1	534.19	2403.8	162.54	1869.6	0	3.221	108.74	19.096	83.705	5.6643	65.132	0
84	3.5923	3.4771	3.4973	3.4837	3.4778	3.4784	0	180.33	1758.2	27.491	631.15	1487.7	137.37	0	6.4779	61.134	0.9615	21.987	51.739	4.7784	0
83	4.2286	4.1159	4.133	4.114	4.1144	4.1151	0	66.235	1126	331.18	1523.4	4636.5	1258.5	0	2.8009	46.345	13.687	62.673	190.76	51.788	0
82	0	6.9473	6.9657	6.9473	6.9436	6.9453	0	0	305.72	7.5545	258.68	94.673	517.37	0	0	21.239	0.5262	17.972	6.5737	35.933	0
81	3.6148	3.4794	3.4976	3.4916	3.4757	3.4854	0	49.03	1225.7	294.18	392.24	3579.2	129.63	0	1.7723	42.649	10.289	13.696	124.4	4.5181	0
8	0	6.9535	6.9655	6.9495	6.9422	6.9488	0	0	123.27	61.636	184.91	2239.4	226	0	0	8.5718	4.2933	12.85	155.47	15.704	0
78	7.1883	6.9492	6.9532	6.958	6.9499	6.9493	0	96.612	3478	1159.3	1835.6	268.52	3284.8	0	6.9448	241.69	80.611	127.72	18.661	228.27	0
77	4.2268	4.1144	4.1155	4.1197	4.1197	4.1135	0	51.568	825.09	721.95	1392.3	1495.5	1753.4	0	2.1797	33.947	29.712	57.359	61.608	72.125	0
76	0	6.9456	6.9483	6.9469	6.9434	6.9469	0	0	436.4	252.65	252.65	987.64	321.56	0	0	30.31	17.555	17.551	68.576	22.338	0
75	0	3.4863	3.4887	3.4833	3.4833	3.4816	0	0	697.06	58.887	929.41	929.49	1161.8	0	0	24.302	2.0544	32.375	32.377	40.447	0
74	0	6.9463	6.9491	6.9463	6.9455	6.9478	0	0	1302.3	627.36	1302.3	1832.9	819.98	0	0	90.462	43.596	90.462	127.3	56.971	0
72	0	3.4828	3.4919	3.4896	3.4813	3.4832	0	0	1688.2	723.53	2170.5	217.59	167.78	0	0	58.796	25.265	75.741	7.575	5.8442	0
71	0	4.1267	4.1267	4.1249	4.1258	4.1234	0	0	2933.5	2933.6	2470.3	3396.7	6175.9	0	0	121.06	121.06	101.9	140.14	254.65	0
7	3.5477	3.4815	3.4945	3.4876	3.4812	3.485	0	175.57	2545.8	72.28	790.06	2721.3	1492.3	0	6.2287	88.631	2.5258	27.554	94.735	52.008	0
69	0	6.9446	6.9476	6.9458	6.9448	6.9446	0	0	772.51	358.66	413.84	717.33	993.22	0	0	53.648	24.919	28.745	49.817	68.975	0
68	3.6162	3.4836	3.4994	3.4841	3.4798	3.4956	0	68.461	1163.8	41.766	1026.9	2122.3	479.23	0	2.4757	40.543	1.4616	35.779	73.851	16.752	0
67	6.9618	6.9462	6.9493	6.9467	6.9468	6.9469	0	203.39	1525.4	661.27	1271.2	122.36	1169.6	0	14.16	105.96	45.954	88.307	8.5	81.251	0
66	6.9638	6.9439	6.9496	6.9454	6.9489	6.9489	0	124.7	1465.3	311.76	592.34	342.93	342.93	0	8.6841	101.75	21.666	41.14	23.83	23.83	0
65	6.9553	6.9448	6.9484	6.9476	6.9484	6.9478	0	263.09	2104.7	613.88	526.18	613.88	71.579	0	18.299	146.17	42.655	36.557	42.655	4.9731	0
64	3.5198	3.4763	3.5434	3.4914	3.4881	0	0	89.238	1041.1	59.492	237.97	267.72	0	0	3.141	36.192	2.1081	8.3084	9.3382	0	0
63	4.1434	4.1119	4.1635	4.1635	4.1859	4.2238	0	67.919	339.59	45.279	45.279	498.72	22.64	0	2.8141	13.964	1.8852	1.8852	20.876	0.9562	0
62	4.1414	4.1146	4.1514	4.1262	4.1192	4.1514	0	337.37	2867.6	253.26	674.73	1265.1	253.26	0	13.972	117.99	10.514	27.841	52.113	10.514	0
61	6.9663	6.9523	0	6.9663	6.9486	0	0	87.813	204.9	0	29.271	351.25	0	0	6.1173	14.245	0	2.0391	24.407	0	0
6	3.5678	3.4774	0	3.5678	3.4757	0	0	65.762	361.69	0	65.762	493.21	0	0	2.3462	12.577	0	2.3462	17.143	0	0
59	6.9662	6.9476	0	6.9542	6.9439	0	0	90.438	452.19	0	180.88	1356.6	0	0	6.3001	31.416	0	12.579	94.198	0	0
58	3.4923	3.4829	0	3.4959	3.5187	0	0	1052.4	3052	0	841.94	631.46	0	0	36.754	106.3	0	29.434	22.219	0	0
57	6.9654	6.9439	0	6.9459	6.947	0	0	70.764	684.05	0	377.41	36.644	0	0	4.929	47.5	0	26.214	2.5456	0	0
56	3.4911	3.4816	0	3.4888	3.4997	0	0	803.41	2008.5	0	883.75	482.45	0	0	28.048	69.928	0	30.832	16.884	0	0
55	6.9662	6.9474	0	6.9483	6.9525	0	0	97.966	457.18	0	391.86	293.9	0	0	6.8245	31.762	0	27.228	20.433	0	0
54	6.949	6.958	0	6.9473	0	0	0	293.8	235.04	0	352.56	0	0	0	20.416	16.354	0	24.493	0	0	0
53	3.4974	3.4763	0	3.4797	0	0	0	266.83	2045.7	0	978.39	0	0	0	9.3323	71.114	0	34.045	0	0	0
52	4.1157	4.1148	0	4.1144	0	0	0	879.88	997.19	0	1055.9	0	0	0	36.213	41.032	0	43.442	0	0	0
51	3.5279	3.479	0	3.5991	0	0	0	298.08	1788.5	0	238.46	0	0	0	10.516	62.221	0	8.5827	0	0	0
5	6.9454	6.9442	0	6.9546	0	0	0	70	83.999	0	23.333	0	0	0	4.8617	5.8331	0	1.6227	0	0	0
49	3.4946	3.4794	0	3.492	0	0	0	47.753	135.3	0	55.712	0	0	0	1.6688	4.7077	0	1.9455	0	0	0
48	4.2228	4.1632	0	0	0	0	0	24.406	48.813	0	0	0	0	0	1.0306	2.0322	0	0	0	0	0
47	0	6.944	0	0	0	0	0	0	41.27	0	0	0	0	0	0	2.8658	0	0	0	0	0
46	7.1313	6.9466	0	0	0	0	0	22.845	319.83	0	0	0	0	0	1.6291	22.217	0	0	0	0	0
45	4.1335	4.1526	0	0	0	0	0	142.55	2031.4	0	0	0	0	0	5.8924	84.357	0	0	0	0	0
44	0	6.9523	0	0	0	0	0	0	21.266	0	0	0	0	0	0	1.4785	0	0	0	0	0
42	4.1248	4.1197	4.165	0	0	0	0	213.19	284.26	71.645	0	0	0	0	8.7937	11.711	2.984	0	0	0	0
4	6.9427	0	0	0	0	0	0	295.82	0	0	0	0	0	0	20.538	0	0	0	0	0	0
38	6.9553	0	0	0	0	0	0	75.66	0	0	0	0	0	0	5.2623	0	0	0	0	0	0
36	6.9457	6.9642	0	0	0	0	0	100.24	23.133	0	0	0	0	0	6.9625	1.611	0	0	0	0	0
34	4.1315	0	0	0	0	0	0	559.96	0	0	0	0	0	0	23.135	0	0	0	0	0	0
32	6.9425	6.9455	0	0	0	0	0	136.76	58.019	0	0	0	0	0	9.4945	4.0297	0	0	0	0	0
31	6.9542	0	0	0	0	0	0	154.25	0	0	0	0	0	0	10.726	0	0	0	0	0	0
3	3.4744	3.4914	0	0	0	0	0	1886	232.12	0	0	0	0	0	65.527	8.1042	0	0	0	0	0
28	4.1216	4.142	0	0	0	0	0	1980.5	33.567	0	0	0	0	0	81.626	1.3903	0	0	0	0	0
26	6.9415	6.9498	0	0	0	0	0	1062.7	83.347	0	0	0	0	0	73.766	5.7924	0	0	0	0	0
24	6.9496	6.9524	7.1216	0	0	0	0	965.16	42.581	7.9676	0	0	0	0	67.075	2.9604	0.5674	0	0	0	0
22	6.9429	6.9465	0	0	0	0	0	3381.4	513.25	0	0	0	0	0	234.77	35.653	0	0	0	0	0
21	6.943	6.9782	7.1394	0	0	0	0	3326	60.473	3.2365	0	0	0	0	230.92	4.2199	0.2311	0	0	0	0
19	6.9442	6.952	0	0	0	0	0	2551.9	329.28	0	0	0	0	0	177.21	22.892	0	0	0	0	0
18	6.9412	6.9648	6.9767	0	0	0	0	2245.3	38.272	25.515	0	0	0	0	155.85	2.6656	1.7801	0	0	0	0
17	6.9435	6.96	0	0	0	0	0	6150.4	357.12	0	0	0	0	0	427.05	24.855	0	0	0	0	0
15	4.1468	4.1247	0	0	0	0	0	4061	174.04	0	0	0	0	0	168.4	7.1786	0	0	0	0	0
13	6.9496	0	6.9764	0	0	0	0	632.76	0	1.1241	0	0	0	0	43.974	0	0.0784	0	0	0	0
12	6.9437	6.9436	0	0	0	0	0	476.54	492.97	0	0	0	0	0	33.09	34.23	0	0	0	0	0
1	6.9497	0	0	0	0	0	0	334.15	0	0	0	0	0	0	23.222	0	0	0	0	0	0
8	6.9434	6.944	0	0	0	0	0	765.3	584.04	0	0	0	0	0	53.137	40.556	0	0	0	0	0
7	3.4823	3.4944	0	0	0	0	0	886.01	364.83	0	0	0	0	0	30.854	12.749	0	0	0	0	0
5	6.9473	6.9795	0	0	0	0	0	978.34	97.834	0	0	0	0	0	67.968	6.8283	0	0	0	0	0
4	6.9439	6.9617	0	0	0	0	0	1257.9	119.8	0	0	0	0	0	87.347	8.34	0	0	0	0	0
2	4.1659	4.128	0	0	0	0	0	1179	140.36	0	0	0	0	0	49.117	5.794	0	0	0	0	0
1	3.4944	3.4864	0	0	0	0	0	35.936	53.946	0	0	0	0	0	1.2558	1.8808	0	0	0	0	0

Data table appendix A. 3b. Absolute abundance errors for dinocyst groups shown in Figure 3.8.

Locality	Sample	Preservation
Winterborne Kingston	MPA 2193	Very good
Winterborne Kingston	MPA 2198	Very good
Winterborne Kingston	MPA 2200	Very good
Winterborne Kingston	MPA 2202	Good
Winterborne Kingston	MPA 2204	Good
Winterborne Kingston	MPA 2206	Good
Winterborne Kingston	MPA 2208	Good
Winterborne Kingston	MPA 2210	Good to very good
Winterborne Kingston	MPA 2212	Good to very good
Winterborne Kingston	MPA 2214	Good to very good
Winterborne Kingston	MPA 2216	Good to very good
Lyme Bay borehole	CSA 1453	Very good
Lyme Bay borehole	CSA 1454	Very good
Lyme Bay borehole	CSA 1526	Very good
Lyme Bay borehole	CSA 1527	Very good
Lyme Bay borehole	CSA 1455	Very good
Lyme Bay borehole	CSA 1456	Very good
Lyme Bay borehole	CSA 1457	Very good
Lyme Bay borehole	CSA 1458	Very good
Lyme Bay borehole	CSA 1459	Very good
Lyme Bay borehole	CSA 1460	Very good
Lyme Bay borehole	CSA 1461	Very good
Lyme Bay borehole	CSA 1462	Very good
Lyme Bay borehole	CSA 1463	Good
Lyme Bay borehole	CSA 1528	Very good
Horn Park Quarry	MPA 12154	Very good
Horn Park Quarry	MPA 12155	Very good

Data table appendix B.1. Preservation of samples from Dorset.
Key as per data table appendix A.1.

		Sporomorphs				Acanthomorphs		Prasinophytes											
Sample	Ammonite zone	Monolete spores	Trilete spores	Bisaccate pollen	Other pollen	*Micrhystridium* spp.	*Baltisphaeridium* spp.	*Cymatiosphaera* spp.	*Tasmanites* spp.	Dinocysts indet.	Total dinocysts	Total marine	Total terrestrial	Total acanthomorphs	Total prasinophytes	Total spores	Total pollen	Total palynomorphs
MPA 12154	*G. concavum*	2	21	73	63	27		3	2	2	110	142	159	27	5	23	136	301
MPA 12155	*G. concavum*	1	54	43	113	8	1			9	78	87	211	9	0	55	156	298

Data table appendix B.2. Raw palynology count data from Horn Park Quarry of Dorset.

			Sporomorphs							Prasinophytes											
Sample	Depth (m)	Ammonite zone	Monolete spores	Trilete spores	Bisaccate pollen	Other pollen	*Botryococcus* spp.	Sphaeromorphs indet.	*Micrhystridium* spp.	*Cymatiosphaera* spp.	*Tasmanites* spp.	Foram test lining	Dinocysts indet.	Total dinocysts	Total palynomorphs	Total marine	Total terrestrial	Total acanthomorphs	Total prasinophytes	Total spores	Total pollen	Total palynomorphs
CSA 1453	4.00-4.20	*G. garantiana/P. parkinsoni*		20	111	36			17			1	25	112	297	130	167	17	0	20	147	297
CSA 1454	4.20-4.60	*G. garantiana/P. parkinsoni*	3	7	82	35			5				21	167	299	172	127	5	0	10	117	299
CSA 1526	6	*G. garantiana/P. parkinsoni*		13	66	22			13			5	10	179	298	197	101	13	0	13	88	298
CSA 1527	6.4	*G. garantiana/P. parkinsoni*		10	47	20	3		8			11	24	199	298	218	77	8	0	10	67	298
CSA 1455	6.85-7.00	*S. humphriesianum/S. niortense*	1	19	89	64			10			47	15	67	297	124	173	10	0	20	153	297
CSA 1456	7.40-8.20	*S. propinquans*	1	4	30	62	4	6	2			5	33	180	294	187	97	2	0	5	92	294
CSA 1457	8.20-9.00	*S. propinquans*	4	23	70	34			23			10	27	108	272	141	131	23	0	27	104	272
CSA 1458	9.00-9.67	*S. propinquans*	1	25	95	73			3			32	21	66	295	101	194	3	0	26	168	295
CSA 1459	9.50-10.50	*S. propinquans*		24	54	66							12	153	297	153	144	0	0	24	120	297
CSA 1460	10.50-1..50	*W. laeviuscula/S. propinquans*	1	11	51	70						1	31	161	295	162	133	0	0	12	121	295
CSA 1461	11.50-12.83	*W. laeviuscula*	2	22	43	96			7		1	3	24	125	299	136	163	7	1	24	139	299
CSA 1462	12.83-13.59	*H. discites*		48	56	99			5			5	28	84	297	94	203	5	0	48	155	297
CSA 1463	13.50-14.10	*H. discites*	2	35	33	26			4	1	1	27	41	170	299	203	96	4	2	37	59	299
CSA 1528	14.6	*H. discites*		15	32	13			7			35	20	201	303	243	60	7	0	15	45	303

Data table appendix B.3. Raw palynology count data from the Lyme Bay Borehole of Dorset.

			Sporomorphs						Acanthomorphs		Prasinophytes										
Sample	Ammonite zone	Depth (m)	Monolete spores	Trilete spores	Bisaccate pollen	Other pollen	*Botryococcus spp.*	*Froomea tornatlis*	*Micrhystridium* spp.	*Baltisphaeridium* spp.	*Cymatiosphaera* spp.	*Tasmanites* spp.	Foram test lining	Scolecodont	Dinocysts indet.	Total dinocysts	Total marine	Total acantomorphs	Total prasinophytes	Total spores	Total pollen	Total palynomorphs
MPA 2193	*P. parkinsoni*	909		23	12	80			12				20		16	151	185	12	0	23	92	300
MPA 2198	*P. parkinsoni*	910		42	28	134			11				25		8	58	96	11	0	42	162	300
MPA 2200	*P. parkinsoni*	910.5		30	92	53			20	1			11		13	87	125	21	0	30	145	300
MPA 2202	*P. parkinsoni*	911.3	1	47	48	143		1	26						5	33	60	26	0	48	191	300
MPA 2204	*P. parkinsoni*	912		32	54	98		1	23				14		14	78	115	23	0	32	152	300
MPA 2206	*G. garantiana*	913.5	1	23	12	89	3		3				24		24	145	172	3	0	24	101	300
MPA 2208	*G. garantiana*	915		21	5	137			3				58		13	74	137	3	0	21	142	300
MPA 2210	*S. humphriesianu*	916.5		25	63	114	2		9				29		6	58	96	9	0	25	177	300
MPA 2212	*W. laeviuscula*	918		34	32	133	1		2				18		12	76	100	2	0	34	165	300
MPA 2214	*W. laeviuscula*	919.8		28	15	71	2		16				4		8	159	184	16	0	28	86	300
MPA 2216	*W. laeviuscula*	920.3	1	44	14	79	3		72		1	1	7		4	72	157	72	2	45	93	298

Data table appendix B.4. Raw palynology count data from the Winterborne Kingston borehole of Dorset.

Sample	Lithology	Lithostrat. unit	Substage	Zone	Weight (g)	HCl	HF	ZnCl2	Preservation
FDH 1	Micritic limestone	Maliere Formaiton- Middle Member	Lower Bajocian	*W. laeviuscula*	60	1	1	1	Barren
FDH 3	Micritic limestone	Maliere Formaiton- Middle Member	Lower Bajocian	*W. laeviuscula*	60	1	1	1	Barren
FDH 4	Micritic limestone	Maliere Formaiton- Middle Member	Lower Bajocian	*W. laeviuscula*	60	1	1	1	Barren
FDH 5	Micritic limestone	Maliere Formaiton- Middle Member	Lower Bajocian	*W. laeviuscula*	60	1	1	1	Barren
FDH 7	Micritic limestone	Maliere Formaiton- Middle Member	Lower Bajocian	*W. laeviuscula*	60.5	1	0	1	Very good
FDH 9	Limestone- intramicrite/floatstone	Maliere Formation- Couche Vert Member	Lower Bajocian	*S. propinquans*	60	1	0	1	Good to Very good
FDH 10	Fe oncoidal limestone	Oolithe de Ferrugineuse de Bayeux Formation- Bed A	Lower Bajocian	*S. humphriesianum*	60	1	1	1	Barren
FDH 11	Stromatolitic Limestone	Oolithe de Ferrugineuse de Bayeux Formation- Bed A	Lower Bajocian	*S. humphriesianum*	40	1	0	1	Barren
FDH 12	Fe oncoidal limestone	Oolithe de Ferrugineuse de Bayeux Formation- Bed B	Upper Bajocian	*S. niortense*	81	1	0	1	Barren
FDH 13	Fe oolitic limestone	Oolithe de Ferrugineuse de Bayeux Formation- Bed C	Upper Bajocian	*S. niortnense/G. garantiana*	81	1	0	1	Barren
FDH 14	Oolitic limestone	Oolithe de Ferrugineuse de Bayeux Formation- Bed D	Upper Bajocian	*P. parkinsoni*	101	1	0	1	Barren
FDH 15	Oolitic/Micritic limestone	Calcaire a Spongiaires Formation- Lower Member	Upper Bajocian	*P. parkinsoni*	60	1	0	1	Very good
SR 1	Micritic limestone	Calcaire a Spongiaires Formation- Lower Member	Upper Bajocian	*P. parkinsoni*	60	1	0	1	Good
SR 2	Micritic limestone	Calcaire a Spongiaires Formation- Lower Member	Upper Bajocian	*P. parkinsoni*	60	1	1	1	Barren
SR 3	Micritic limestone	Calcaire a Spongiaires Formation- Lower Member	Upper Bajocian	*P. parkinsoni*	60	1	0	1	Good
SR 4	Micritic limestone	Calcaire a Spongiaires Formation- Lower Member	Upper Bajocian	*P. parkinsoni*	60	1	1	1	Barren
SR 6	Micritic limestone	Calcaire a Spongiaires Formation- Lower Member	Upper Bajocian	*P. parkinsoni*	40	1	1	1	Barren
SR 8	Micritic limestone	Calcaire a Spongiaires Formation- Lower Member	Upper Bajocian	*P. parkinsoni*	60	1	0	1	Good to Very good
SR 10	Micritic limestone	Calcaire a Spongiaires Formation- Lower Member	Upper Bajocian	*P. parkinsoni*	60	1	0	1	Barren
SR 12	Micritic limestone	Calcaire a Spongiaires Formation- Lower Member	Upper Bajocian	*P. parkinsoni*	80	1	0	1	Barren
SR 14	Micritic limestone	Calcaire a Spongiaires Formation- Lower Member	Upper Bajocian	*P. parkinsoni*	80	1	0	1	Barren
H-2	Sparry micritic limestone	Marnes des Port-en-Bessin Formation	Lower Bathonian	*Z. zizag*	80	1	1	1	Good to Very good
H1	Micritic limestone	Couche de Passage	Lower Bathonian	*Z. zizag*	50.5	1	0	1	Very good
H2	Micritic limestone	Couche de Passage	Lower Bathonian	*Z. zizag*	81	1	0	1	Good to Very good
H3	Micritic limestone	Couche de Passage	Lower Bathonian	*Z. zizag*	51	1	0	1	Good to Very good
H4	Micritic limestone	Couche de Passage	Lower Bathonian	*Z. zizag*	50.5	1	0	1	Good to Very good
H5	Micritic limestone	Calcaire a Spongiaires Formation- Lower Member	Upper Bajocian	*P. parkinsoni*	60.2	1	1	1	Good to Very good

Data table appendix C.1. Processing procedures and preservation of palynology samples from Normandy. Key as per appendix A.1.

			Percentage errors						Total error				Absolute abundances			Absolute abundances w. errors				
		Sample	Total lycopodium error	Counted Lycopodium error	Counted palynomorphs error	Counted dinoflagellate cyst error	Counted acanthomorphs error	Counted spores error	Counted spores error	Total error- palynomorphs	Total error- dinoflagellate cysts	Total error- acathomorphs	Total error- spores	Total error- pollen	Palynomorphs per g	Dinoflagellate cysts per g	Acanthomorphs per g	Spores per g	Pollen per g	Palynomorhs per g +/-	Dinoflagellate cysts per g +/-	Acanthomorphs per g +/-	Spores per g +/-	Pollen per g+/-
H-2	H	Sample	4.91	0.15	0.06	0.08	0.41	0.19	0.1	4.91	4.91	4.93	4.92	4.91	1611	859.2	32.22	144.99	515.52	79.142	42.2116	1.58819	7.12775	25.3292
H1	H	4.91	4.91	0.11	0.06	0.06	0.32	0.33	0.23	4.91	4.91	4.92	4.92	4.92	1428.69	1215.8	47.3076	42.5768	89.8844	70.1714	59.7161	2.32821	2.09587	4.41927
H2	H	4.91	4.91	0.06	0.06	0.08	0.13	0.23	0.12	4.91	4.91	4.91	4.92	4.91	281.89	145.643	55.4383	17.853	62.9554	13.8429	7.15261	2.7232	0.87761	3.09232
H3	H	4.91	4.91	0.05	0.06	0.09	0.17	0.21	0.09	4.91	4.91	4.91	4.91	4.91	340.673	144.701	39.8781	25.0662	131.028	16.7292	7.1064	1.9593	1.23199	6.43504
H5	H	4.91	4.91	0.08	0.06	0.12	0.12	0.15	0.09	4.91	4.91	4.91	4.91	4.91	629.039	150.969	146.776	92.259	234.841	30.8921	7.41573	7.2098	4.53267	11.5344
SR8	SR	4.91	4.91	0.08	0.06	0.07	0.3	0.28	0.14	4.91	4.91	4.92	4.92	4.91	622.199	463.032	22.7382	26.8724	109.557	30.5562	22.74	1.1187	1.32171	5.38205
SR3	SR	4.91	4.91	0.13	0.06	0.1	0.21	0.15	0.09	4.91	4.91	4.92	4.91	4.91	1605.38	556.532	117.728	240.807	663.558	78.8569	27.3406	5.78789	11.8332	32.5974
SR1	SR	4.91	4.91	0.09	0.06	0.08	0.17	0.22	0.1	4.91	4.91	4.91	4.92	4.91	739.839	372.386	83.8485	51.7887	231.816	36.3344	18.2896	4.12013	2.54574	11.3865
FDH15	FDH	4.91	4.91	0.12	0.06	0.1	0.1	0.24	0.12	4.91	4.91	4.91	4.92	4.91	1302.96	477.752	425.633	73.8343	321.397	63.9976	23.4686	20.9089	3.6307	15.7894
FDH9	FDH	4.91	4.91	0.03	0.06	0.1	0.18	0.23	0.08	4.91	4.91	4.91	4.92	4.91	75.902	27.3247	8.09621	4.80713	35.4209	3.72711	1.34192	0.39779	0.23629	1.73945
FDH7	FDH	4.91	0.05	0.06	0.06	0.13	0.29	0.12	0.08	4.91	4.91	4.92	4.91	4.91	209.808	40.6986	8.4204	49.119	111.57	10.3028	1.99911	0.41417	2.41257	5.47906

Data table appendix C.2. Absolute abundance errors for main palynomorph groups from Normandy.

	Sample	Locality	Zone	Net Weight	Total lycopodium	lycopodium counted	Sporomorphs				Acanthomorphs		Prasinophytes		Foram test lining	Dinocysts indet.	Total dinoflagellate cysts	Total marine	Total terrestrial	Total acanthomorphs	Total prasinophytes	Total spores	Total pollen	Total palynomorphs
							Monolete spores	Trilete spores	Bisaccate pollen	Other pollen	*Froomea tornatlis*	*Micrhystridium* spp.	*Baltisphaeridium* spp.	*Cymatiosphaera* spp.	*Tasmanites* spp.										
	H-2	H	*Z. zigzag*	80	19332	45		27	5	91		6			4	7	26	160	177	123	6	4	27	96	300
	H1	H	*Z. zigzag*	50.45	19332	81		9		19	1	10			1	5	14	257	273	28	10	1	9	19	302
	H2	H	*Z. zigzag*	81	19332	254		19	14	53		58	1				16	155	214	86	59	0	19	67	300
	H3	H	*Z. Z. zigzag*	50.8	19332	334		22	16	99		35					15	127	162	137	35	0	22	115	299
	H5	H	*P. parkinsoni*	60.26	19332	153		44	25	87		70			1	1	10	72	144	156	70	1	44	112	300
	SR8	SR	*P. parkinsoni*	59.95	19332	156	1	12		53		11					34	224	235	66	11	0	13	53	301
	SR3	SR	*P. parkinsoni*	60.21	19332	60	1	44	18	106		22		P	2	1	22	104	129	169	22	2	45	124	298
	SR1	SR	*P. parkinsoni*	60.3	19332	130		21	21	73		34					25	151	185	115	34	0	21	94	300
	FDH15	FBH	*P. parkinsoni*	60.15	19332	74	1	16	14	60		98					16	110	208	91	98	0	17	74	299
	FDH9	FDH	*S. propinquans*	60.07	19332	1272	1	18	12	128		32				1	19	108	141	159	32	0	19	140	300
	FDH7	FDH	*W. laeviuscula*	60.55	19332	455		70	46	113		12				P	8	58	70	229	12	0	70	159	299

Data table appendix C. 3. Raw palynology count data for Normandy.

Data table appendix D.1. Raw palynology count data for Skye.

Group	Sample	MPA 13989	MPA 13991	MPA 13992	MPA 13993	MPA 13994	MPA 13999	MPA 14001	MPA 14005	MPA 14009	MPA 14010	MPA 14011
	Ammonite zone	*S. humphriesianum*	*S. propinquans*	*W. laeviuscula*	*W. laeviuscula*	*W. laeviuscula*	*H. discites*	*H. discites*	*H. discites*	*H. discites*	*H. discites*	*H. discites*
	Preservation	Poor to fair	Fair to good	Good	Good	Good	Good	Good	Good	Fair to good	Good	Fair to good
Sporomorphs	Monolete spores			1	1				1			
Sporomorphs	Trilete spores	15	25	22	45	29	45	31	35	59	37	65
Sporomorphs	Bisaccate pollen	16	166	87	61	7	77	7	28	24	19	17
Sporomorphs	Other pollen	165	70	138	100	191	126	235	213	181	226	204
	Botryococcus spp.	1		4	4	4	1					
	Froomea tornatlis				1							
	Sphaeromorphs indet.	6									1	
Acanthomorphs	*Micrhystridium* spp.	3		1	7	1				2		
Acanthomorphs	*Baltisphaeridium* spp.		1					1		3		
Prasinophytes	*Cymatiosphaera* spp.					1						
Prasinophytes	*Tasmanites* spp.							2	P			1
	Foram test lining			6	3	1					3	
	Scolecodont											
Dinoflagellate cysts	Dinocysts indet.	24	2	1	10	5	8	4	2	2		2
Dinoflagellate cysts	*Batiacasphaera* spp.	18	2	11	17	7	7	6			11	4
Dinoflagellate cysts	?*Batiacasphaera* spp.	9				9	2	3	2	11	3	5
Dinoflagellate cysts	?*Dissiliodinium* spp.	17	2	6	10	13	11	3	2	3	1	P
Dinoflagellate cysts	*Pareodinia halosa*	8	1	3	10	2	1	2	8	14	1	2
Dinoflagellate cysts	*Nannoceratopsis gracilis*	1	18	7	6	4	6	4	4	1	2	
Dinoflagellate cysts	*Durotrigia* sp. 1										P	
Dinoflagellate cysts	*Mancodinium semitabulatium*										?	
Dinoflagellate cysts	*Kallosphaeridium* spp			?						1	?	
Dinoflagellate cysts	*Dissiliodinium* spp.	4		3	6	21	8	1	5			
Dinoflagellate cysts	*Pareodinia ceratophora*		P			1			?			
Dinoflagellate cysts	*Dissiliodinium giganteum*	1	8	7	20	3	5	1				
Dinoflagellate cysts	*Carpathodinium* sp. 1 of Riding et al. 1991						1					
Dinoflagellate cysts	*Pareodinia ceratophora*						1					
Dinoflagellate cysts	*Nannoceratopsis* spp.		1			1						
Dinoflagellate cysts	*Kallosphaeridium? hypornatum*				P							
Dinoflagellate cysts	*Nannoceratopsis spiculata*				1							
Dinoflagellate cysts	*Gongylodinium erymnoteichon*	1		1								
Dinoflagellate cysts	*Nannoceratopsis plegas*				P							
Dinoflagellate cysts	*Nannoceratopsis ambonis*		3									
Dinoflagellate cysts	*Ellipsoidictyum/Valensiella complex*	6										
Dinoflagellate cysts	*Valensiella ovulum*	1										
Dinoflagellate cysts	*Valvaeodinium* sp.	1										
	Total palynomorphs	297	299	298	302	300	299	300	300	301	304	300
	Total marine	94	38	46	90	69	50	27	23	37	21	14
	Total terrestrial	196	261	248	207	227	248	273	277	264	282	286
	Total dinocysts	91	37	39	80	66	50	24	23	32	18	13
	Total acanthomorphs	3	1	1	7	1	0	1	0	5	0	0
	Total prasinophytes	0	0	0	0	1	0	2	0	0	0	1
	Total spores	15	25	23	46	29	45	31	36	59	37	65
	Total pollen	181	236	225	161	198	203	242	241	205	245	221

Depth (M)	Stage/Substage	Ammonite Zone	Lithology	Lithostratigraphic unit	d13C
908.2	Lower Bathonian	*Z. zigag*	Marl	Inferior Oolite Group	-27.1
908.65	Bathonian/Bajocian boundary	*Z. zigzag/P. parkinsoni*	Marl	Inferior Oolite Group	-26.7
909	Upper Bajocian	*P. parkinsoni*	Marl	Inferior Oolite Group	-26.7
909.45	Upper Bajocian	*P. parkinsoni*	Marl	Inferior Oolite Group	-26.8
909.9	Upper Bajocian	*P. parkinsoni*	Marl	Inferior Oolite Group	-27.1
910.26	Upper Bajocian	*P. parkinsoni*	Marl	Inferior Oolite Group	-26.7
910.6	Upper Bajocian	*P. parkinsoni*	Marl	Inferior Oolite Group	-27.1
910.95	Upper Bajocian	*P. parkinsoni*	Marl	Inferior Oolite Group	-26.7
911.3	Upper Bajocian	*P. parkinsoni*	Marl	Inferior Oolite Group	-26.8
911.6	Upper Bajocian	*P. parkinsoni*	Marl	Inferior Oolite Group	-26.6
912	Upper Bajocian	*P. parkinsoni*	Marl	Inferior Oolite Group	-27.1
912.5	Upper Bajocian	*G. garantiana*	Marl	Inferior Oolite Group	-27.2
912.9	Upper Bajocian	*G. garantiana*	Marl	Inferior Oolite Group	-27.5
913.3	Upper Bajocian	*G. garantiana*	Marl	Inferior Oolite Group	-27.6
913.6	Upper Bajocian	*G. garantiana*	Marl	Inferior Oolite Group	-27.6
914.05	Upper Bajocian	*G. garantiana*	Marl	Inferior Oolite Group	-27.4
914.45	Upper Bajocian	*G. garantiana*	Marl	Inferior Oolite Group	-27.2
914.8	Upper Bajocian	*G. garantiana*	Marl	Inferior Oolite Group	-27.5
915	Upper Bajocian	*G. garantiana*	Marl	Inferior Oolite Group	-27.3
915.24	Upper Bajocian	*G. garantiana*	Marl	Inferior Oolite Group	-27.8
915.5	Upper Bajocian	*G. garantiana*	Marl	Inferior Oolite Group	-27.4
915.7	Upper Bajocian	*G. garantiana*	Marl	Inferior Oolite Group	-27.3
915.84	Upper Bajocian	*S. niortense*	Marl	Inferior Oolite Group	-27.3
916.06	Upper Bajocian	*S. niortense*	Marl	Inferior Oolite Group	-27.8
916.2	Upper Bajocian	*S. niortense*	Marl	Inferior Oolite Group	-27.1
916.4	Upper Bajocian	*S. niortense*	Marl	Inferior Oolite Group	-26.7
916.66	Lower Bajocian	*S. humphriesianum*	Marl	Inferior Oolite Group	-26.5
916.7	Lower Bajocian	*S. humphriesianum*	Marl	Inferior Oolite Group	-26.4
916.99	Lower Bajocian	*S. humphriesianum*	Marl	Inferior Oolite Group	-26.6
917.24	Lower Bajocian	*W. laeviuscula/S. propinquans*	Marl	Inferior Oolite Group	-25.7
917.47	Lower Bajocian	*W. laeviuscula/S. propinquans*	Marl	Inferior Oolite Group	-25.8
917.6	Lower Bajocian	*W. laeviuscula/S. propinquans*	Marl	Inferior Oolite Group	-25.2
917.75	Lower Bajocian	*W. laeviuscula/S. propinquans*	Marl	Inferior Oolite Group	-25.5
918	Lower Bajocian	*W. laeviuscula/S. propinquans*	Marl	Inferior Oolite Group	-25.8
918.25	Lower Bajocian	*W. laeviuscula/S. propinquans*	Marl	Inferior Oolite Group	-25.6
918.4	Lower Bajocian	*W. laeviuscula/S. propinquans*	Marl	Inferior Oolite Group	-25.4
918.62	Lower Bajocian	*W. laeviuscula/S. propinquans*	Marl	Inferior Oolite Group	-25.0
918.9	Lower Bajocian	*W. laeviuscula/S. propinquans*	Marl	Inferior Oolite Group	-25.3
919.08	Lower Bajocian	*W. laeviuscula/S. propinquans*	Marl	Inferior Oolite Group	-25.7
919.3	Lower Bajocian	*W. laeviuscula/S. propinquans*	Marl	Inferior Oolite Group	-25.9
919.4	Lower Bajocian	*W. laeviuscula/S. propinquans*	Marl	Inferior Oolite Group	-26.0
919.62	Lower Bajocian	*W. laeviuscula/S. propinquans*	Marl	Inferior Oolite Group	-25.4
919.8	Lower Bajocian	*W. laeviuscula/S. propinquans*	Marl	Inferior Oolite Group	-25.7
920	Lower Bajocian	*W. laeviuscula/S. propinquans*	Marl	Inferior Oolite Group	-25.9
920.2	Lower Bajocian	*W. laeviuscula/S. propinquans*	Marl	Inferior Oolite Group	-25.9
920.4	Lower Bajocian	*W. laeviuscula/S. propinquans*	Marl	Inferior Oolite Group	-25.9
920.56	Lower Bajocian	*W. laeviuscula/S. propinquans*	Marl	Inferior Oolite Group	-25.4
920.77	Lower Bajocian	*W. laeviuscula/S. propinquans*	Marl	Inferior Oolite Group	-25.7
920.94	Lower Bajocian	*H. discites*	Marl	Inferior Oolite Group	-26.0
921.1	Lower Bajocian	*H. discites*	Marl	Inferior Oolite Group	-27.2
921.29	Lower Bajocian	*H. discites*	Marl	Inferior Oolite Group	-27.2
921.47	Lower Bajocian	*H. discites*	Marl	Inferior Oolite Group	-27.2
921.62	Lower Bajocian	*H. discites*	Marl	Inferior Oolite Group	-27.0
921.77	Upper Aalenian	*G. concavum*	Marl	Inferior Oolite Group	-26.8
921.9	Upper Aalenian	*G. concavum*	Marl	Inferior Oolite Group	-26.6
922.04	Upper Aalenian	*G. concavum*	Marl	Inferior Oolite Group	-26.8
922.26	Upper Aalenian	*G. concavum*	Marl	Inferior Oolite Group	-26.7
922.55	Upper Aalenian	*G. concavum*	Marl	Inferior Oolite Group	-27.0

Data table appendix E.1. Raw carbon isotope data for Dorset.

NIGL Standard	d13C	%C	%N	C/N
BROC2	-27.4	41.6	5.4	7.7
BROC2	-27.4	41.8	5.2	8.0
BROC2	-27.3	41.4	5.2	8.0
BROC2	-27.3	41.7	5.6	7.5
BROC2	-27.4	40.9	5.0	8.3
BROC2	-27.4	41.1	5.0	8.2
BROC2	-27.4	40.9	5.0	8.2
BROC2	-27.4	40.8	4.9	8.4
BROC2	-27.4	40.8	4.9	8.3
BROC2	-27.4	40.9	4.8	8.5
BROC2	-27.4	41.0	4.9	8.4
Standard dev.	0.014242697	0.382585	0.244278	0.310998
NIGL Standard	**d13C**	**%C**	**%N**	**C/N**
SOILA	-25.9	9.6	0.8	12.1
SOILA	-25.9	9.5	0.8	11.9
SOILA	-25.9	9.8	0.9	11.4
SOILA	-25.9	9.9	0.9	10.8
Standard dev.	0.014218227	0.194677	0.058461	0.57522

Data table appendix E.2. NIGL internal standards used for carbon isotope analysis of Dorset samples.

Sample No.	Lithology	Depth (M)	Lithostratigraphic Unit	Ammonite Zone	Stage/sub Stage	δ13C ‰ VPDB
107	Marly limestone	144.34-36	P. parkinsoni oolite Member	*Z. zigzag*	Low. Bathonian	-25.4
106	Marly limestone	144.61-64	P. parkinsoni oolite Member	*Z. zigzag*	Low. Bathonian	-25.4
105	Marly limestone	144.66-72	P. parkinsoni oolite Member	*P. parkinsoni*	Upper Bajocian	-26.9
104	Marly limestone	144.91	P. parkinsoni oolite Member	*P. parkinsoni*	Upper Bajocian	-26.6
103	Marly limestone	144.96	P. parkinsoni oolite Member	*P. parkinsoni*	Upper Bajocian	-26.1
102	Marly limestone	144.97-99	P. parkinsoni oolite Member	*P. parkinsoni*	Upper Bajocian	-26.5
101	Mudstone	145.05-08	Hamitenton Formation	*G. garantiana*	Upper Bajocian	-26.9
100	Mudstone	145.42-45	Hamitenton Formation	*G. garantiana*	Upper Bajocian	-26.9
99	Mudstone	145.88-91	Hamitenton Formation	*G. garantiana*	Upper Bajocian	-26.9
98	Mudstone	146.22-25	Hamitenton Formation	*G. garantiana*	Upper Bajocian	-26.3
97	Mudstone	146.71-73	Hamitenton Formation	*G. garantiana*	Upper Bajocian	-26.3
96	Mudstone	147.03-05	Hamitenton Formation	*G. garantiana*	Upper Bajocian	-26.4
95	Mudstone	147.55-57	Hamitenton Formation	*G. garantiana*	Upper Bajocian	-26.5
94	Mudstone	147.96-98	Hamitenton Formation	*G. garantiana*	Upper Bajocian	-26.2
93	Mudstone	148.41-43	Hamitenton Formation	*G. garantiana*	Upper Bajocian	-26.0
92	Mudstone	148.90 DI	Hamitenton Formation	*G. garantiana*	Upper Bajocian	-26.1
91	Mudstone	149.20-22	Hamitenton Formation	*G. garantiana*	Upper Bajocian	-26.3
90	Mudstone	150.14-16	Hamitenton Formation	*G. garantiana*	Upper Bajocian	-26.6
89	Mudstone	150.74-76	Hamitenton Formation	*G. garantiana*	Upper Bajocian	-26.4
88	Mudstone	151.15-17	Hamitenton Formation	*G. garantiana*	Upper Bajocian	-26.4
87	Mudstone	151.79-81	Hamitenton Formation	*G. garantiana*	Upper Bajocian	-26.4
86	Mudstone	152.12-14	Hamitenton Formation	*G. garantiana*	Upper Bajocian	-26.4
85	Mudstone	152.67-69	Hamitenton Formation	*G. garantiana*	Upper Bajocian	-26.9
84	Mudstone	153-153.03	Hamitenton Formation	*G. garantiana*	Upper Bajocian	-26.6
83	Mudstone	153.50-52	Hamitenton Formation	*G. garantiana*	Upper Bajocian	-26.8
82	Mudstone	153.71-73	Hamitenton Formation	*S. niortense- Garantina baculata subzone*	Upper Bajocian	-26.7
81	Mudstone	154-154.03	Hamitenton Formation	*S. niortense- Garantina baculata subzone*	Upper Bajocian	-26.2
80	Mudstone	154.40-42	Hamitenton Formation	*S. niortense- Garantina baculata subzone*	Upper Bajocian	-25.7
79	Mudstone	154.74-76	Hamitenton Formation	*S. niortense- Garantina baculata subzone*	Upper Bajocian	-26.0
78	Mudstone	155.32-34	Hamitenton Formation	*S. niortense- Garantina baculata subzone*	Upper Bajocian	-26.7
77	Mudstone	155.91-93	Hamitenton Formation	*S. niortense- Garantina baculata subzone*	Upper Bajocian	-25.9
76	Mudstone	156.40-43	Hamitenton Formation	*S. niortense- Garantina baculata subzone*	Upper Bajocian	-26.5
75	Mudstone	156.82-84	Hamitenton Formation	*S. niortense- Garantina baculata subzone*	Upper Bajocian	-26.5
74	Mudstone	157.03-05	Hamitenton Formation	*S. niortense- Garantina baculata subzone*	Upper Bajocian	-26.5
73	Mudstone	157.37-39	Hamitenton Formation	*S. niortense*	Upper Bajocian	-26.4
72	Mudstone	157.78-80	Hamitenton Formation	*S. niortense*	Upper Bajocian	-26.2
71	Mudstone	158.16-19	Hamitenton Formation	*S. niortense*	Upper Bajocian	-26.3
70	Mudstone	158.88-90	Hamitenton Formation	*S. niortense*	Upper Bajocian	-26.6
69	Mudstone	159.40-43	Hamitenton Formation	*S. niortense*	Upper Bajocian	-27.1
68	Mudstone	160.09-10 DI	Hamitenton Formation	*S. niortense*	Upper Bajocian	-26.3
67	Mudstone	160.18-20	Hamitenton Formation	*S. niortense*	Upper Bajocian	-25.9
66	Mudstone	160.53-56	Hamitenton Formation	*S. niortense*	Upper Bajocian	-27.0
65	Marl	160.90-92	Subfurcatum oolite Member	*S. niortense*	Upper Bajocian	-26.4
64	Marl	161.40-50 DI	Subfurcatum oolite Member	*S. niortense*	Upper Bajocian	-26.5
63	Marl	161.87-96 DI	Subfurcatum oolite Member	*S. niortense*	Upper Bajocian	-25.8
62	Mudstone	162.35-37	Ostreenkalk Formation	*S. humphriesianum*	Lower Bajocian	-25.5
61	Mudstone	162.80-82	Ostreenkalk Formation	*S. humphriesianum*	Lower Bajocian	-24.9
60	Mudstone	163.10-13	Ostreenkalk Formation	*S. humphriesianum*	Lower Bajocian	-25.2
59	Mudstone	163.62-65	Ostreenkalk Formation	*S. humphriesianum*	Lower Bajocian	-24.6
58	Mudstone	164.07-09	Ostreenkalk Formation	*S. humphriesianum*	Lower Bajocian	-24.6
57	Mudstone	164.74-77	Ostreenkalk Formation	*S. humphriesianum*	Lower Bajocian	-25.6
56	Mudstone	165.55-57	Ostreenkalk Formation	*S. humphriesianum*	Lower Bajocian	-24.9
55	Mudstone	166-166.04	Ostreenkalk Formation	*S. humphriesianum*	Lower Bajocian	-25.2
54	Mudstone	166.56-59	Ostreenkalk Formation	*S. humphriesianum*	Lower Bajocian	-25.0
53	Mudstone	167.31-33	Ostreenkalk Formation	*S. humphriesianum*	Lower Bajocian	-25.0
52	Marl	167.89-92	Humphresi oolite Member	*S. humphriesianum*	Lower Bajocian	-24.9
51	Marl	168.26-29	Humphresi oolite Member	*S. humphriesianum*	Lower Bajocian	-25.1
50	Marly shelly limestone	168.79-82	Humphresi oolite Member	*S. humphriesianum*	Lower Bajocian	-25.1
49	Marly shelly limestone	168.83-95- DI	Humphresi oolite Member	*S. humphriesianum*	Lower Bajocian	-25.0
48	Mudstone	169-169.03	Ostreenkalk Formation	*S. humphriesianum*	Lower Bajocian	-24.3
47	Mudstone	169.56-60	Ostreenkalk Formation	*S. humphriesianum*	Lower Bajocian	-24.9
46	Mudstone	169.84-86	Ostreenkalk Formation	*S. humphriesianum?*	Lower Bajocian	-24.3
45	Mudstone	170-170.05	Ostreenkalk Formation	*S. propinquans/S. humphriesianum*	Lower Bajocian	-24.6
44	Mudstone	170.41-45	Ostreenkalk Formation	*S. propinquans/S. humphriesianum*	Lower Bajocian	-23.7
43	Mudstone	170.98-171	Ostreenkalk Formation	*S. propinquans/W. laeviuscula*	Lower Bajocian	-24.1
42	Mudstone	171.42-45	Ostreenkalk Formation	*S. propinquans/W. laeviuscula*	Lower Bajocian	-23.9
41	Sandy mudstone	171.90-92	Ostreenkalk Formation	*S. propinquans/W. laeviuscula*	Lower Bajocian	-24.4
40	Sandy mudstone	172.59-61	Wedelsandstein Formation	*S. propinquans/W. laeviuscula*	Lower Bajocian	-23.4
39	Mudstone	173-173.02	Wedelsandstein Formation	*S. propinquans/W. laeviuscula*	Lower Bajocian	-23.4
38	Mudstone	173.63-65	Wedelsandstein Formation	*S. propinquans/W. laeviuscula*	Lower Bajocian	-23.1
37	Mudstone	174.03-05	Wedelsandstein Formation	*S. propinquans/W. laeviuscula*	Lower Bajocian	-23.7
36	Mudstone	174.64-67	Wedelsandstein Formation	*S. propinquans/W. laeviuscula*	Lower Bajocian	-23.7
35	Mudstone	174.96-98	Wedelsandstein Formation	*S. propinquans/W. laeviuscula*	Lower Bajocian	-23.7
34	Mudstone	176.15-17	Wedelsandstein Formation	*S. propinquans/W. laeviuscula*	Lower Bajocian	-23.6
33	Sandy marl	176.38-42	Wedelsandstein Formation	*W. laeviuscula*	Lower Bajocian	-24.0
32	Sandy marl	177.23-31	Wedelsandstein Formation	*W. laeviuscula*	Lower Bajocian	-24.6
31	Sandy marl	178.11-16	Wedelsandstein Formation	*W. laeviuscula*	Lower Bajocian	-24.6
30	Mudstone	178.83-85	Wedelsandstein Formation	*W. laeviuscula*	Lower Bajocian	-24.6
29	Mudstone	179.42-45	Wedelsandstein Formation	*W. laeviuscula*	Lower Bajocian	-24.6
28	Mudstone	180.65-68	Wedelsandstein Formation	*W. laeviuscula*	Lower Bajocian	-24.5
27	Mudstone	181-181.03	Wedelsandstein Formation	*W. laeviuscula*	Lower Bajocian	-24.7
26	Mudstone	181.75-77	Wedelsandstein Formation	*W. laeviuscula*	Lower Bajocian	-25.0
25	Mudstone	182.60-63	Wedelsandstein Formation	*W. laeviuscula*	Lower Bajocian	-24.4
23	Mudstone	183.83-85	Wedelsandstein Formation	*W. laeviuscula*	Lower Bajocian	-24.3
22	Mudstone	184.77-79	Wedelsandstein Formation	*W. laeviuscula*	Lower Bajocian	-25.3
21	Mudstone	185.58-60	Wedelsandstein Formation	*W. laeviuscula*	Lower Bajocian	-24.2
20	Mudstone	186.03-06	Wedelsandstein Formation	*W. laeviuscula*	Lower Bajocian	-24.4
19	Mudstone	186.95-96	Wedelsandstein Formation	*W. laeviuscula*	Lower Bajocian	-24.1
18	Mudstone	187.43-46	Wedelsandstein Formation	*W. laeviuscula*	Lower Bajocian	-24.3
17	Mudstone	188.07-09	Wedelsandstein Formation	*W. laeviuscula*	Lower Bajocian	-24.2
16	Mudstone	188.66-68	Wedelsandstein Formation	*W. laeviuscula*	Lower Bajocian	-24.6
15	Mudstone	189-189.02	Wedelsandstein Formation	*W. laeviuscula*	Lower Bajocian	-24.7
14	Mudstone	189.77-78	Wedelsandstein Formation	*W. laeviuscula*	Lower Bajocian	-25.1
12	Mudstone	190.76-77	Wedelsandstein Formation	*W. laeviuscula*	Lower Bajocian	-25.6
11	Mudstone	191.11-13	Wedelsandstein Formation	*W. laeviuscula*	Lower Bajocian	-25.4
10	Mudstone	191.94-95	Wedelsandstein Formation	*W. laeviuscula*	Lower Bajocian	-25.3
9	Mudstone	192.53-54	Wedelsandstein Formation	*W. laeviuscula*	Lower Bajocian	-25.2
8	Mudstone	193.40-43	Wedelsandstein Formation	*W. laeviuscula*	Lower Bajocian	-24.9
7	Mudstone	193.73-74	Wedelsandstein Formation	*W. laeviuscula*	Lower Bajocian	-24.8
6	Mudstone	194.21-23	Wedelsandstein Formation	*W. laeviuscula*	Lower Bajocian	-24.9
5	Mudstone	194.78-79	Wedelsandstein Formation	*W. laeviuscula*	Lower Bajocian	-24.8
4	Mudstone	195.7-195.71	Wedelsandstein Formation	*W. laeviuscula*	Lower Bajocian	-24.5
3	Mudstone	196-196.015	Wedelsandstein Formation	*W. laeviuscula*	Lower Bajocian	-24.8
2	Mudstone	196.40-43	Wedelsandstein Formation	*W. laeviuscula*	Lower Bajocian	-24.7
1	Mudstone	196.7	Eisensandstein Formation	*Concavum*	Upper Aalenian	-25.2
	below limit of detection on first analysis, were resampled					

Data table appendix E.3. Raw carbon isotope data for Swabia.

NIGL standard	%C	%N	C/N	δ13C ‰ VPDB
BROC2	40.8	4.8	8.4	-27.4
BROC2	40.8	4.8	8.4	-27.3
BROC2	40.7	5.1	8.0	-27.3
BROC2	40.4	4.4	9.1	-27.4
BROC2	40.7	4.5	9.1	-27.4
BROC2	40.6	4.4	9.2	-27.3
BROC2	40.8	4.0	10.3	-27.4
BROC2	41.0	4.4	9.3	-27.4
BROC2	40.7	4.4	9.3	-27.6
BROC2	40.8	4.8	8.4	-27.3
BROC2	40.8	4.8	8.4	-27.3
BROC2	41.0	4.9	8.3	-27.3
BROC2	41.2	4.9	8.4	-27.4
BROC2	41.3	4.9	8.4	-27.4
BROC2	41.0	5.0	8.2	-27.4
BROC2	41.1	5.0	8.2	-27.4
BROC2	40.8	4.8	8.4	-27.4
BROC2	40.8	4.8	8.4	-27.4
BROC2	40.5	4.8	8.4	-27.4
BROC2	40.9	4.7	8.8	-27.4
BROC2	40.8	4.7	8.7	-27.4
BROC2	40.8	4.7	8.7	-27.4
BROC2	40.4	4.6	8.7	-27.4
BROC2	40.8	4.6	8.9	-27.4
BROC2	41.0	4.6	8.9	-27.3
BROC2	41.8	4.4	9.6	-27.3
BROC2	41.3	3.7	11.2	-27.5
XBROC2	40.8	4.8	8.4	-27.2
XBROC2	40.8	4.8	8.4	-27.2
BROC2	40.8	4.8	8.4	-27.4
BROC2	40.8	4.8	8.4	-27.4
BROC2	41.3	4.9	8.5	-27.4
BROC2	41.1	4.9	8.4	-27.3
BROC2	41.6	4.9	8.5	-27.4
BROC2	40.6	4.8	8.4	-27.4
BROC2	40.8	4.8	8.4	-27.3
BROC2	40.9	4.8	8.5	-27.3
BROC2	41.0	4.9	8.4	-27.4
Standard dev.	**0.28**	**0.28**	**0.60**	**0.07**
NIGL standard	**%C**	**%N**	**C/N**	**δ13C ‰ VPDB**
SOILB	3.0	0.1	22.6	-24.2
SOILB	3.1	0.1	27.6	-24.1
SOILB	3.1	0.2	14.6	-24.1
SOILB	3.0	0.2	16.4	-24.1
SOILB	3.0	0.2	16.0	-24.1
SOILB	3.1	0.2	15.2	-24.1
SOILB	3.0	0.2	15.0	-24.1
Standard dev.	0.051863	0.037804	4.937108	0.033872728

Data table appendix E.4. NIGL internal standards used for carbon isotope analysis of Swabian samples.